NEONATAL BRAIN INJURY AND THE SEARCH FOR NEW THERAPIES

EDITED BY: Daniel Alonso-Alconada, Silvia Carloni and Francisco J. Alvarez

PUBLISHED IN: Frontiers in Pediatrics, Frontiers in Cellular Neuroscience and Frontiers in Neurology

frontiers Research Topics

ISSN 1664-8714
ISBN 978-2-88976-492-1
DOI 10.3389/978-2-88976-492-1

About Frontiers

Frontiers is more than just an open-access publisher of scholarly articles: it is a pioneering approach to the world of academia, radically improving the way scholarly research is managed. The grand vision of Frontiers is a world where all people have an equal opportunity to seek, share and generate knowledge. Frontiers provides immediate and permanent online open access to all its publications, but this alone is not enough to realize our grand goals.

Frontiers Journal Series

The Frontiers Journal Series is a multi-tier and interdisciplinary set of open-access, online journals, promising a paradigm shift from the current review, selection and dissemination processes in academic publishing. All Frontiers journals are driven by researchers for researchers; therefore, they constitute a service to the scholarly community. At the same time, the Frontiers Journal Series operates on a revolutionary invention, the tiered publishing system, initially addressing specific communities of scholars, and gradually climbing up to broader public understanding, thus serving the interests of the lay society, too.

Dedication to Quality

Each Frontiers article is a landmark of the highest quality, thanks to genuinely collaborative interactions between authors and review editors, who include some of the world's best academicians. Research must be certified by peers before entering a stream of knowledge that may eventually reach the public - and shape society; therefore, Frontiers only applies the most rigorous and unbiased reviews.
Frontiers revolutionizes research publishing by freely delivering the most outstanding research, evaluated with no bias from both the academic and social point of view. By applying the most advanced information technologies, Frontiers is catapulting scholarly publishing into a new generation.

What are Frontiers Research Topics?

Frontiers Research Topics are very popular trademarks of the Frontiers Journals Series: they are collections of at least ten articles, all centered on a particular subject. With their unique mix of varied contributions from Original Research to Review Articles, Frontiers Research Topics unify the most influential researchers, the latest key findings and historical advances in a hot research area! Find out more on how to host your own Frontiers Research Topic or contribute to one as an author by contacting the Frontiers Editorial Office: frontiersin.org/about/contact

NEONATAL BRAIN INJURY AND THE SEARCH FOR NEW THERAPIES

Topic Editors:
Daniel Alonso-Alconada, University of the Basque Country, Spain
Silvia Carloni, University of Urbino Carlo Bo, Italy
Francisco J. Alvarez, Hospital de Cruces, Spain

Citation: Alonso-Alconada, D., Carloni, S., Alvarez, F. J., eds. (2022). Neonatal Brain Injury and the Search for New Therapies. Lausanne: Frontiers Media SA. doi: 10.3389/978-2-88976-492-1

Table of Contents

frontiers | Frontiers in Pediatrics

EDITORIAL
published: 09 June 2022
doi: 10.3389/fped.2022.933917

Editorial: Neonatal Brain Injury and the Search for New Therapies

Silvia Carloni[1], *Francisco J. Álvarez*[2] *and Daniel Alonso-Alconada*[3]*

[1] Department of Biomolecular Sciences, University of Urbino Carlo Bo, Urbino, Italy, [2] Biocruces Bizkaia Health Research Institute, Cruces University Hospital, Barakaldo, Spain, [3] Department of Cell Biology and Histology, School of Medicine and Nursing, University of the Basque Country (UPV/EHU), Leioa, Spain

Keywords: hypoxia-ischemia (HI), newborn, neonatal encephalopathy (NE), brain injury, therapies, neuroprotection

Editorial on the Research Topic

Neonatal Brain Injury and the Search for New Therapies

Hypoxia-ischemia is largely recognized as a major cause of brain injury in the perinatal period that can lead to neonatal encephalopathy (1, 2). When this occurs, it frequently leads to neonatal mortality or to severe long-term neurological deficits in newborns with devastating consequences both for the baby and its family, contributing to over 50 million disability-adjusted life years worldwide each year (3). Therefore, the study of the complex relationship among the different mechanisms/factors involved in the injury of the developing brain and the finding of new pharmacological approaches are a high priority in perinatal care. Accordingly, the characterization of peripheral markers would help to predict the development of putative damage, and their modulation after pharmacological treatments may anticipate its efficacy as a potential therapeutic intervention for translation to the clinical practice.

The Research Topic "*Neonatal Brain Injury and the Search for New Therapies*" includes novel and original contributions in the study of neonatal encephalopathy with the aim to give a comprehensive and groundbreaking overview of the pathophysiology and treatment of this disease. Original reports that explore and clarify the prognostic value of biomarkers and specific diagnostic interventions are included. This collection also highlights the most recent evidences of new targets for therapeutic intervention. In this Research Topic issue of Frontiers, we bring together a special collection of 15 articles contributing sound evidence for the key concepts outlined.

Some papers analyzed relevant peculiarities of preterm infants as a sensible population of patients at risk of brain injury. Ma et al. studied the dynamic functional connectivity in both term and late preterm infants and observed that the latter preferred to stay in a state with general weak connectivity between networks; authors also found that this preference declined as maturity increased. Shaw et al. highlighted that the poor long-term neurodevelopmental and behavioral outcomes observed in preterm births could be associated to an impaired oligodendrocyte development; authors concluded that promoting GABAergic action might improve outcomes. In an exhaustive review, Shandley et al. focused on the key role of nutrition for brain development in neonatal life, providing a wide-range synopsis regarding the role of nutritive and non-nutritive feeding in the neonate outcomes, the underlying mechanisms involved in neurophysiology, and the relationship of abnormal activity with brain injury in preterm and term infants. Terrin et al. evaluated how protein intake can affect the early cerebral growth in very low birth weight newborns, showing that several cerebral structures' measurements were affected by high protein intake when administered by parental nutrition, encouraging the administration mainly by enteral nutrition.

Three original studies focused on the important topic of the identification of prognostic factors that could correlate with the ongoing brain damage. Zheng et al. showed that perfusion magnetic resonance imaging could have an important role in the identification of hypoxic-ischemic

OPEN ACCESS

Edited and reviewed by:
Arjan Te Pas,
Leiden University, Netherlands

Correspondence:
Daniel Alonso-Alconada
daniel.alonsoa@ehu.eus

Specialty section:
This article was submitted to Neonatology, a section of the journal Frontiers in Pediatrics

Received: *01 May 2022*
Accepted: *25 May 2022*
Published: *09 June 2022*

Citation:
Carloni S, Álvarez FJ and Alonso-Alconada D (2022) Editorial: Neonatal Brain Injury and the Search for New Therapies. Front. Pediatr. 10:933917. doi: 10.3389/fped.2022.933917

encephalopathy, regardless of findings on conventional magnetic resonance imaging, and in the prediction of language and motor outcomes. Zhu et al., in addition, revealed that multi-slice radiomic analysis based on apparent diffusion coefficients metrics could provide more quantitative information on brain development in neonates with congenital heart diseases, suggesting that these measurements may be more clinically helpful to identify atypical brain development in patients. In an original study, Sweetman et al. investigated the connection between high cytokines levels observed after innate immune cell activation, brain injury and the outcome in infants with neonatal encephalopathy. Authors found that moderate or severe encephalopathy and mortality were associated with elevated interleukin-8 and granulocyte-macrophage-colony-stimulating-factor, pointing out that these cytokines may predict early outcomes in neonatal brain injury.

Several papers provided new evidence of neuroprotective strategies. Fernández et al. found that methylene blue, a guanylyl cyclase inhibitor with free-radical scavenger properties, reduced the retinal damage induced by perinatal asphyxia in the neonatal rat. Authors concluded that methylene blue could regulate key players of inflammation, matrix remodeling, gliosis and angiogenesis in the eye, whose treatment may prevent the deleterious visual consequences of perinatal asphyxia. Yu et al. demonstrated that the intranasal administration of exogenous interleukin-4 improved myelination and attenuated the functional deficits in a hypoxia-induced periventricular leukomalacia model. Kollareth et al. demonstrated that the acute injection of docosahexaenoic acid triglyceride emulsion provided a very similar protection as hypothermia in a neonatal mouse model of hypoxic-ischemic brain injury, indicating an advantageous treatment in providing a feasible and effective strategy in patients after hypoxia-ischemia injury. Purohit et al. demonstrated that the use of human cord blood derived from unrestricted somatic stem cells restored aquaporin channel expression, reduced inflammation and inhibited the development of hydrocephalus after experimentally induced perinatal intraventricular hemorrhage in rabbit. Kasala et al. analyzed the effects of the simultaneous use of morphine and caffeine on brain development. Authors revealed that the concurrent use of morphine, administered to premature neonates for pain control, and caffeine, used for apnea treatment, induced apoptosis and mitochondrial dysfunction in the developing brain compared to the individual use of the compounds. Chan et al. discussed in an appropriate review the links between the respiratory support of the preterm neonate and the brain injury patterns. Authors pointed that the use of animal models are essential resources for studying the pathophysiology of ventilation-induced brain injury, with important translational implications that can be helpful to outline the way to care preterm neonates, with the aim to improve their neurodevelopmental outcomes.

As of today, advances toward new neuroprotective interventions in hypoxic-ischemic encephalopathy have been limited by incomplete understanding of secondary processes. Alonso-Alconada et al. described that the subventricular zone could be affected by neonatal asphyxia. In their work, hypoxic-ischemic piglets showed a decrease in cellularity together with a reduction in both cell proliferation and neurogenesis in this neurogenic niche, suggesting that asphyxia could compromise the replacement of the lost neurons and the achievement of global repair. In a comprehensive review article, Kleuskens et al. provided an overview on the pathophysiology of cerebral hyperperfusion, commonly observed during the first 1–5 days in asphyctic neonates. Authors highlighted the gaps in current understanding in term animals and neonates, analyzing data from both the hemodynamic changes and the endogenous pathways involved. They concluded that these findings should be simultaneously considered together with the brain imagining techniques, becoming a valuable resource in assessing the impact in neurodevelopmental outcome.

In summary, this Research Topic provides original articles and reviews that, together collected, may add new information on the epidemiology, pathophysiology, diagnosis and management of brain injury in the neonate, also identifying relevant treatments for testing in future clinical trials.

AUTHOR CONTRIBUTIONS

SC wrote the draft. FÁ and DA-A critically reviewed the manuscript. All authors contributed to the article and approved the submitted version.

FUNDING

DA-A was supported by EITB Maratoia-BIOEF (BIO18/IC/003) and the Spanish Ministry of Science and Innovation (MINECOR20/P66/AEI/10.13039/501100011033).

ACKNOWLEDGMENTS

We would like to thank Frontiers for the opportunity to develop this topic and to the contributors for their time and effort on this project. We specially thank all the reviewers who provided useful suggestions to improve the manuscripts.

REFERENCES

1. Gunn AJ, Thoresen M. Neonatal encephalopathy and hypoxic-ischemic encephalopathy. *Handb Clin Neurol.* (2019) 162:217–37. doi: 10.1016/B978-0-444-64029-1.00010-2
2. Volpe JJ. Neonatal encephalopathy: an inadequate term for hypoxic-ischemic encephalopathy. *Ann Neurol.* (2012) 72:156–66. doi: 10.1002/ana.23647
3. Lee AC, Kozuki N, Blencowe H, Vos T, Bahalim A, Darmstadt GL, et al. Intrapartum-related neonatal encephalopathy incidence and impairment at regional and global levels for 2010 with trends from

1990. *Pediatr Res.* (2013) 74(Suppl 1):50–72. doi: 10.1038/pr.2013.206

Conflict of Interest: The authors declare that the research was conducted in the absence of any commercial or financial relationships that could be construed as a potential conflict of interest.

Publisher's Note: All claims expressed in this article are solely those of the authors and do not necessarily represent those of their affiliated organizations, or those of the publisher, the editors and the reviewers. Any product that may be evaluated in this article, or claim that may be made by its manufacturer, is not guaranteed or endorsed by the publisher.

frontiers in Cellular Neuroscience

ORIGINAL RESEARCH
published: 04 June 2020
doi: 10.3389/fncel.2020.00157

Methylene Blue Prevents Retinal Damage Caused by Perinatal Asphyxia in the Rat

Juan Carlos Fernández[1,2†], Rafael Peláez[3†], Manuel Rey-Funes[1†], Manuel Soliño[1], Daniela S. Contartese[1], Verónica B. Dorfman[4], Juan José López-Costa[1], Ignacio M. Larrayoz[3‡], César F. Loidl[1‡] and Alfredo Martínez[3‡]*

[1]Instituto de Biología Celular y Neurociencia "Prof. E. de Robertis", Facultad de Medicina, Universidad de Buenos Aires, Buenos Aires, Argentina, [2]Primera Cátedra de Farmacología, Facultad de Medicina, Universidad de Buenos Aires, Buenos Aires, Argentina, [3]Center for Biomedical Research of La Rioja (CIBIR), Logroño, Spain, [4]Centro de Estudios Biomédicos, Biotecnológicos, Ambientales y Diagnóstico (CEBBAD), Universidad Maimónides, Buenos Aires, Argentina

OPEN ACCESS

Edited by:
Daniel Alonso-Alconada, University of the Basque Country, Spain

Reviewed by:
Enrique Hilario, University of the Basque Country, Spain
Kenji Sakamoto, Teikyo University, Japan

***Correspondence:**
Alfredo Martínez
amartinezr@riojasalud.es

[†]These authors have contributed equally to this work and share first authorship

[‡]These authors have contributed equally to this work and share last authorship

Specialty section:
This article was submitted to Cellular Neuropathology, a section of the journal Frontiers in Cellular Neuroscience

Received: *14 January 2020*
Accepted: *12 May 2020*
Published: *04 June 2020*

Citation:
Fernández JC, Peláez R, Rey-Funes M, Soliño M, Contartese DS, Dorfman VB, López-Costa JJ, Larrayoz IM, Loidl CF and Martínez A (2020) Methylene Blue Prevents Retinal Damage Caused by Perinatal Asphyxia in the Rat. Front. Cell. Neurosci. 14:157. doi: 10.3389/fncel.2020.00157

Perinatal asphyxia (PA) is responsible for a large proportion of neonatal deaths and numerous neurological sequelae, including visual dysfunction and blindness. In PA, the retina is exposed to ischemia/reoxygenation, which results in nitric oxide (NO) overproduction and neurotoxicity. We hypothesized that methylene blue (MB), a guanylyl cyclase inhibitor, and free-radical scavenger currently used in the clinic, may block this pathway and prevent PA-induced retinal degeneration. Male rat pups were subjected to an experimental model of PA. Four groups were studied: normally delivered (CTL), normally delivered treated with 2 mg Kg-1 MB (MB), exposed to PA for 20 min at 37°C (PA), and exposed to PA and, then, treated with MB (PA-MB). Scotopic electroretinography performed 45 days after birth showed that PA animals had significant defects in the a- and b-waves and oscillatory potentials (OP). The same animals presented a significant increase in the thickness of the inner retina and a large number of TUNEL-positive cells. All these physiological and morphological parameters were significantly prevented by the treatment with MB. Gene expression analysis demonstrated significant increases in iNOS, MMP9, and VEGF in the eyes of PA animals, which were prevented by MB treatment. In conclusion, MB regulates key players of inflammation, matrix remodeling, gliosis, and angiogenesis in the eye and could be used as a treatment to prevent the deleterious visual consequences of PA. Given its safety profile and low cost, MB may be used clinically in places where alternative treatments may be unavailable.

Keywords: angiogenesis, apoptosis, electroretinography, inner retinal thickness, methylene blue, perinatal asphyxia

INTRODUCTION

Perinatal asphyxia (PA) is the most severe perinatological problem across the world (World Health Organization, 1991) and is associated with approximately one-quarter of global neonatal deaths (Liu et al., 2015). PA generates a transient global ischemic status which could damage the central nervous system, including the retina (Ferriero, 2004). Depending on the length and intensity of the ischemic episode, PA sequelae may include attention-deficit hyperactivity disorder, spasticity, epilepsy,

mental retardation (Herrera et al., 2018), and hearing or visual dysfunctions, including blindness (Hill, 1991). In 2010, there were an estimated 1.15 million cases of neonatal encephalopathy, of which 96% were from low- and middle-income countries (Mukhtar-Yola et al., 2018). Therapeutic hypothermia is currently the standard of care for newborns exposed to PA (Rivero-Arias et al., 2019), but this treatment may require expensive devices to be properly applied (Dingley et al., 2015) that could be prohibitive for some developing regions of the world. Our long-term goal is to investigate and promote the use of safe and affordable drugs in the prevention of visual loss associated with PA.

Exposure of the retina to hypoxia/ischemia-reoxygenation induces the expression of hypoxia-inducible factor-1α (HIF1α) and its target genes such as vascular endothelial growth factor (VEGF), adrenomedullin (AM), and inducible nitric oxide synthase (iNOS), among others (Rey-Funes et al., 2011). VEGF and AM are angiogenic factors that contribute to the thickening of the inner layers of the retina (Rey-Funes et al., 2013), whereas iNOS produces nitric oxide (NO) which reacts with the free radical superoxide resulting in elevated levels of peroxynitrites and extensive protein nitration, leading to neuronal cell death (Rodrigo et al., 2005). Excessive NO formation induces cytotoxic effects in the retina and is postulated as a key neurotoxic factor in retinal ischemia (Osborne et al., 2004). Therefore, inhibitors of NO activity may constitute valuable drugs for preventing retinal damage in the context of PA.

Most physiological actions of NO are mediated by the formation of the second messenger cGMP, which is produced by the action of guanylyl cyclase (Ding and Weinberg, 2007). Methylene blue (MB) is a guanylyl cyclase inhibitor (Hwang et al., 1998) which is also able to inhibit NADPH oxidase and myeloperoxidase enzymes (Heydrick et al., 2007) by either acting as a free radical scavenger or competing for oxygen (Atamna et al., 2008). MB exhibits a high safety profile (Bewick and Pfleiderer, 2014; Landoni et al., 2014) and is approved for clinical use as an antidote of poison-induced methemoglobinemia (Wright et al., 1999), in norepinephrine-refractory hypotension (Sparicio et al., 2004), and for the surgical management of hyperparathyroidism (Bewick and Pfleiderer, 2014), among others. MB is on the World Health Organization's List of Essential Medicines, the most effective and safe medicines needed in a health system (World Health Organization, 2017). Also, MB has been shown to prevent retinal damage induced by rotenone (Zhang et al., 2006) or optic neuropathy (Rojas et al., 2009) in animal models. In a previous article, we showed that MB was able to significantly reduce morphological and molecular hallmarks of retinal damage caused by PA when applied preventively to the pregnant dams before delivery (Rey-Funes et al., 2016). The risks of suffering PA are well known (Martinez-Biarge et al., 2013) and the application of MB to high-risk mothers may reduce vision loss in their children. Nevertheless, we understand that an efficacious treatment that is applied after PA has been diagnosed would be better received by patients and the medical staff. In consequence, this report aimed to demonstrate the beneficial effects of treating asphyctic newborns with MB on physiological, morphological, and molecular markers of retinal damage.

MATERIALS AND METHODS

PA Animal Model

Severe PA was induced using a noninvasive model of hypoxia-ischemia as described (Loidl et al., 2000). Sprague–Dawley albino rats with genetic quality and sanitary certification from the animal facility of our Institution were cared for following the guidelines published in the ARVO Statement for the Use of Animals in Ophthalmic and Vision Research. The procedures described below were approved by the Ethical Committee of CICUAL (Comité Institucional para el Uso y Cuidado de Animales de Laboratorio, Resolution N° 2079/07), Facultad de Medicina, Universidad de Buenos Aires, Argentina. Appropriate proceedings were performed to minimize the number of animals used and their suffering, pain, and discomfort. Animals were kept under standard laboratory conditions at 24°C, with light/dark cycles of 12/12 h, and food and water were provided *ad libitum*. Thirty timed-pregnant Sprague–Dawley rats were sacrificed by decapitation and immediately hysterectomized after their first pups were delivered vaginally. These normally delivered, non-manipulated pups were used as controls. Full-term fetuses, still inside the uterus, were subjected to asphyxia performed by transient immersion of both uterine horns in a water bath for 20 min at 37°C. After asphyxia, the uterine horns were opened, pups were removed, dried of delivery fluids, stimulated to breathe, and their umbilical cords were ligated. Pups were then placed for recovery under a heating lamp and given to surrogate mothers. To avoid the influence of hormonal variations due to the female estrous cycle, only male pups were included in this study. One hour after birth, control newborns were randomly divided into two groups, which received a 50 μl subcutaneous injection of either saline solution (CTL group, $n = 30$) or a dose of 2 mg Kg^{-1} methylene blue in saline solution (Sigma, St. Louis, MO, USA; MB group, $n = 30$). The same procedure was implemented with asphyctic newborns to generate the other two experimental groups: asphyctic animals that received saline (PA group, $n = 30$) or methylene blue treatment (PA-MB group, $n = 30$).

Electroretinograms

Forty-five days after birth, young rats ($n = 10$ per experimental group) were subjected to scotopic electroretinography, as described (Rey-Funes et al., 2017). Briefly, after overnight adaptation in the dark, rats were anesthetized with 40 mg/Kg ketamine (Ketamine 50®, Holiday-Scott SA, Beccar, Argentina) + 5 mg/Kg xylazine (Kensol®, Laboratorios Köning SA, Buenos Aires, Argentina) under dim red illumination. An ophthalmic solution of 5% phenylephrine hydrochloride and 0.5% tropicamide (Fotorretin, Poen, Buenos Aires, Argentina) was used to dilate the pupils. Rats were placed facing the stimulus at a distance of 25 cm in a highly reflective environment. A reference electrode was placed through the ear, a grounding electrode was attached to the tail, and a gold electrode was placed in contact with the central cornea. Scotopic electroretinograms

TABLE 1 | Antibodies used in this study.

Primary antibodies				
Target	**Species**	**Dilution**	**Source**	**Reference**
GFAP	Rabbit polyclonal	1:500	Dako	Z0334
HNEJ-2	Mouse monoclonal	1:25	Abcam	ab48506
8-OHdG	Mouse monoclonal	1:50	Santa Cruz	sc-66036
Secondary antibodies				
Specificity	**Label**	**Dilution**	**Source**	**Reference**
Donkey anti-rabbit	Alexa Fluor® 555	1:200	Invitrogen	A31572
Donkey anti-mouse	Alexa Fluor® 488	1:600	Invitrogen	A21202

(ERG) were recorded from both eyes simultaneously and 20 responses were collected to flashes of unattenuated white light (1 ms, 1 Hz) from a photic stimulator (light-emitting diodes) set at maximum brightness. The registered response was amplified (9 cd s/m^2 without filter), filtered (1.5-Hz low-pass filter, 500 Hz high-pass filter, notch activated), and averaged (Akonic BIO-PC, Buenos Aires, Argentina). The a-wave was measured as the difference in amplitude between the recording at onset and the trough of the negative deflection and the b-wave amplitude was measured from the trough of the a-wave to the peak of the b-wave. Values from each eye were averaged, and the resultant mean value was used to compute the group's mean a- and b-wave amplitudes ± SEM. To calculate oscillatory potentials (OP), the same photic stimulator was used with filters of high (300 Hz) and low (100 Hz) frequency. The amplitudes of the OP were estimated by using the peak-to-trough method. The sum of three OP was used for statistical analysis.

Tissue Processing, Histology, and TUNEL

Rats on the four experimental groups were sacrificed 6 days postpartum (n = 4 per experimental group). Animals were decapitated. After enucleating, anterior segments of the eyes, including the lens, were discarded, and the posterior segments of the eyes containing the retinas were fixed in 4% paraformaldehyde in 0.1 M pH 7.4 phosphate buffer at 4°C for 48 h. Tissues were dehydrated and paraffin-embedded. Tissue sections (5 μm-thick) were stained for terminal deoxynucleotidyl transferase dUTP nick end labeling (TUNEL) with the in situ Cell Death Detection POD Kit (Roche, Basel, Switzerland), following manufacturer's instructions. Visualization of immunoreactivity was performed with 0.03% 3,3′diaminobenzidine (Sigma Co, St. Louis, MO, USA), 3% nickel ammonium sulphate and 0.01% hydrogen peroxide diluted in 0.1 M buffer acetate, yielding a black product.

The animals used for electroretinography were intraperitoneally anesthetized with ketamine/xylazine and intracardially perfused with the same fixative. The posterior segments of the eyes were paraffin-embedded, sectioned, and stained with hematoxylin-eosin to count the number of ganglion cells and to measure the thickness of the most inner layers of the retina (IR), which includes the internal limiting membrane, the retinal optic nerve fiber layer, and the ganglion cell layer (GCL), as reported (Rey-Funes et al., 2013).

Immunofluorescence and Confocal Microscopy

Additional tissue sections were dewaxed, rehydrated, and subjected to antigen retrieval (10 mM sodium citrate, 0.5% Tween 20, pH 6.0, 30 min at 95°C). Non-specific binding was blocked by exposure to 10% normal donkey serum (Jackson Immunoresearch Laboratories, West Grove, PA, USA) for 30 min, and then tissue sections were incubated with primary antibodies (**Table 1**), overnight at 4°C. The following day, the presence of the primary antibody was detected by incubation with fluorescent secondary antibodies (**Table 1**) and counterstained with DAPI (Molecular Probes, Eugene, OR, USA). These slides were analyzed with a confocal microscope (TCS SP5, Leica, Badalona, Spain).

Image Analysis

The eyes of four animals of each experimental group were analyzed. Care was taken on selecting anatomically matched areas of retina among animals before assays. The central area of the sagittal plane was chosen for each retina. The thickness of all layers in the retina was measured in 10 fields using Scion Image software. Special attention was paid to the inner retina (IR), which includes the internal limiting membrane, the optic retinal nerve fiber layer, and the GCL.

TUNEL-positive cells were counted on the retinas of four eyes per experimental group. Fields were chosen in the central region of retinal cross-sections and the number of positive cells in ten fields, 500 μm in length, was recorded.

RNA Extraction and Quantitative Real-Time PCR

Animals from all experimental groups (n = 4 per experimental group) were sacrificed at different times after MB treatment (4, 6, 12, 24 h). The posterior chambers of the eyes were homogenized with TRIzol (Invitrogen, Madrid, Spain) and RNA was isolated with RNeasy Mini kit including a DNAse I on-column digestion (Qiagen, Germantown, MD, USA). One microgram of total RNA was reverse-transcribed into first-strand cDNA using random primers and the SuperScript III kit (Invitrogen) in a total volume of 20 μl according to the manufacturer's instructions. Reverse transcriptase was omitted in control reactions, where the absence of PCR-amplified DNA confirmed the lack of contamination from genomic DNA. Resulting cDNA was mixed with SYBR

Green PCR Master Mix (Applied Biosystems, Carlsbad, CA, USA) for quantitative real-time polymerase chain reaction (qRT-PCR) using 0.3 μM forward and reverse oligonucleotide primers (**Table 2**). Quantitative measures were performed using a 7300 Real-Time PCR System (Applied Biosystems). Cycling conditions were an initial denaturation at 95°C for 10 min, followed by 40 cycles of 95°C for 15 s and 60°C for 1 min. In the end, a dissociation curve was implemented from 60 to 95°C to validate amplicon specificity. Gene expression was calculated using relative quantification by interpolation into a standard curve. All values were divided by the expression of the housekeeping gene 18S.

Statistical Analysis

All data were analyzed with GraphPad Prism 5 software and were considered statistically significant when $p < 0.05$. Values are expressed as means ± SEM. Normally distributed data were evaluated by ANOVA followed by either Holm-Sidak or Newman–Keuls *post hoc* test.

RESULTS

MB Treatment Prevents Asphyxia-Induced Modifications of the a- and b-Waves and the Oscillatory Potentials of the Electroretinogram

Animals were divided into four experimental groups and treated as explained in the "Materials and Methods" section. The overall mortality rate for the asphyctic group was 40%, similar to previous reports (Loidl et al., 2000). Injection of MB, a well-known dye (Li et al., 2018), left a blue area under the skin of treated animals but this stain disappeared 2 or 3 days after injection. Scotopic ERG performed 45 days after birth showed that those animals that had suffered PA had a significant ($p < 0.001$) reduction of the a- and b-wave amplitude (**Figures 1C,E**, **2C,E**) compared to those who were born uneventfully (**Figures 1A,E**, **2A,E**). Treatment of the control animals with MB resulted in a mild reduction ($p < 0.05$) in the amplitude of both waves (**Figures 1B,E**, **2B,E**). Notably, MB treatment of asphyctic pups resulted in a- ($p < 0.05$) and b- ($p < 0.001$) waves more similar to the controls than to the PA animals (**Figures 1D,E**, **2D,E**).

Similar observations were made when studying the OP (**Figure 3**). PA-induced a strong loss of complexity ($p < 0.0001$) in the OP patterns (**Figures 3C,E**) whereas MB treatment significantly ($p < 0.001$) restored the control pattern (**Figures 3D,E**).

TABLE 2 | Primers used for quantitative real-time polymerase chain reaction (qRT-PCR) in this study.

Target gene	Forward primer	Reverse primer
iNOS	AGGCCACCTCGGATATCTCT	GCTTGTCTCTGGGTCCTCTG
IL1β	CCTCTGCCAAGTCAGGTCTC	GAATGTGCCACGGTTTTCTT
TNFα	GAGAGATTGGCTGCTGGAAC	TGGAGACCATGATGACCGTA
MMP2	ACCGTCGCCCATCATCAA	CCTTCAGCACAAAGAGGTTGC
MMP9	TGTCCAGACCAAGGGTACAGC	GAAGAATGATCTAAGCCCAGCG
GFAP	GAAGAAAACCGCATCACCAT	GGCACACCTCACATCACATC
VEGF	GCCAGCACATAGGAGAGATGAGC	CAAGGCTCACAGTGATTTTCTGG
PEDF	ACCCTCGCATAGACCTTCAG	GGCATTTCCCTTGTAGACCG
18S	ATGCTCTTAGCTGAGTGTCCCG	ATTCCTAGCTGCGGTATCCAGG

The annealing temperature was 60°C for all primers. 18S was used as a housekeeping gene.

MB Treatment Reduces Asphyxia-Induced Thickening of the Inner Retina and GFAP Immunoreactivity

It has been previously reported that PA results in morphological changes of the retina, including a thicker inner retina (IR), and an increased number of GFAP-positive cellular processes (Rey-Funes et al., 2016). This was also the case in the present study. The eyes of the PA group had a significantly ($p < 0.0001$) thicker IR (**Figures 4C,E**) than those of the CTL group (**Figures 4A,E**). Treatment of the control newborns with MB did not change this parameter (**Figures 4B,E**) but the treatment of the asphyctic pups significantly ($p < 0.0001$) prevented this morphological manifestation of the pathology (**Figures 4D,E**). The thickness of all other layers of the retina was measured and compared but no statistically significant differences were found among experimental groups (results not shown). The number of ganglion cells in a specified length (500 μm) was also compared among experimental groups (**Figure 4F**). There was a very significant reduction in the number of ganglion cells in the PA animals ($p < 0.0001$) compared to the control groups. In the PA-MB group, the number of ganglion cells was significantly higher ($p < 0.0001$) than in the PA group (**Figure 4F**).

Furthermore, GFAP immunostaining showed a marked increase in GFAP signal in the PA group (**Figure 5C**) compared with either the CTL (**Figure 5A**) or MB (**Figure 5B**) groups. Application of MB (**Figure 5D**) reduced GFAP expression to levels similar to those observed in the controls.

MB Treatment Reduces Asphyxia-Induced Apoptosis in the Ganglion Cell Layer

TUNEL analysis of the retinas (**Figure 6**) showed that exposure to PA results in a very significant ($p < 0.0001$) increase in the number of apoptotic cells (arrows) in the GCL (**Figures 6C,E**), whereas control animals have a very low number of labeled cells (**Figures 6A,E**). Postnatal treatment with MB significantly ($p < 0.0001$) reduced the number of apoptotic cells in the retina of asphyctic animals (**Figures 6D,E**) whereas it had no significant effect on non-asphyctic retinas (**Figures 6B,E**). A large number of apoptotic cells was observed among the neuroblasts that would develop into the inner (black arrowheads in **Figure 6C**) and outer (white arrowheads in **Figure 6C**) nuclear layers of the retina of PA animals. These were not seen in control animals (**Figures 6A,B**) and were very scarce in MB-treated rats (**Figure 6D**).

Also, retina sections were exposed to antibodies against 4-hydroxynonenal (HNEJ-2; **Figures 7A–D**) and 8-hydroxy-

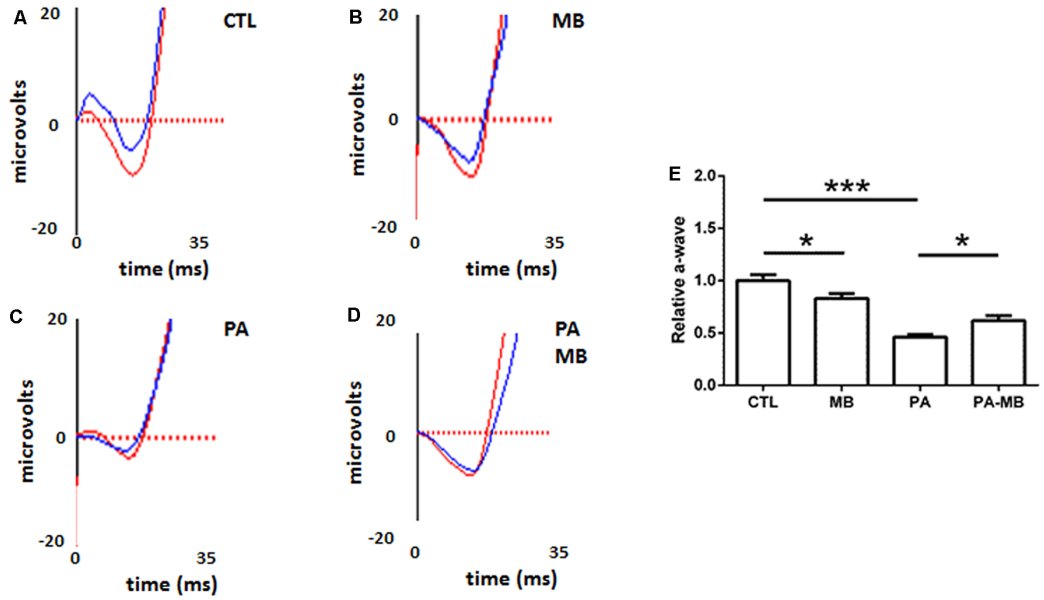

FIGURE 1 | Representative scotopic electroretinograms (ERG) showing the a-waves on the four experimental groups: CTL **(A)**, methylene blue (MB; **B**), perinatal asphyxia (PA; **C**), and PA-MB **(D)**. The response of the right eye is represented by red lines and that of the left one by blue lines. Quantification of the a-wave amplitude, relativized to the CTL group, is represented as a histogram **(E)**. Bars represent the mean ± SEM of all samples (n = 10 animals per group). Asterisks represent statistically significant differences. $^{*}p < 0.05$; $^{***}p < 0.001$. Statistical test: ANOVA followed by Holm-Sidak *post hoc* test.

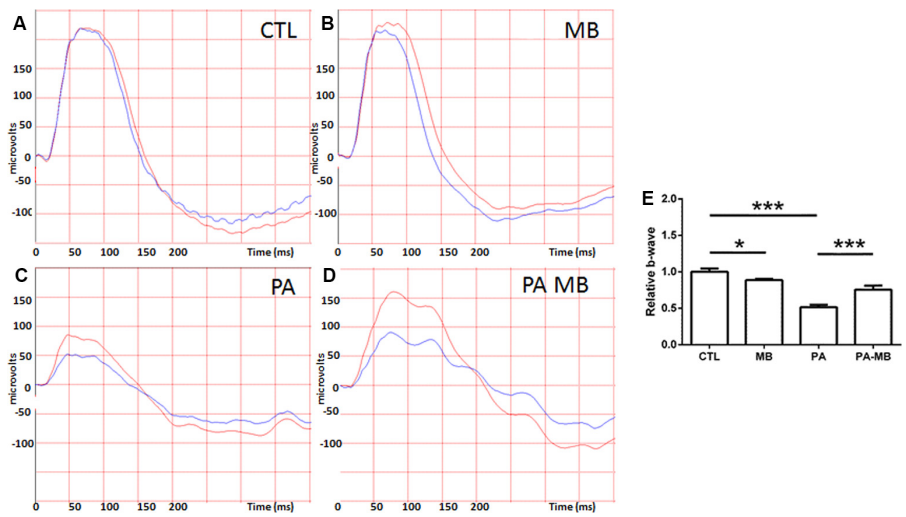

FIGURE 2 | Representative scotopic ERG showing the b-waves on the four experimental groups: CTL **(A)**, MB **(B)**, PA **(C)**, and PA-MB **(D)**. The response of the right eye is represented by red lines and that of the left one by blue lines. Quantification of the b-wave amplitude, relativized to the CTL group, is represented as a histogram **(E)**. Bars represent the mean ± SEM of all samples (n = 10 animals per group). Asterisks represent statistically significant differences. $^{*}p < 0.05$; $^{***}p < 0.001$. Statistical test: ANOVA followed by Holm-Sidak *post hoc* test.

2'-deoxyguanosine (8-OHdG; **Figures 7E–H**) to further study tissue damage due to asphyxia. For both markers, there was a signal increase in the retinas of the PA group (**Figures 7C,G**) when compared to the CTL (**Figures 7A,E**) and the MB group (**Figures 7B,F**). Also, in both cases, the application of MB post-asphyxia resulted in a decrease in the damage markers (**Figures 7D,H**).

MB Treatment Modulates Gene Expression of Key Players in Inflammation, Gliosis, Matrix Remodeling, and Angiogenesis

Gene expression was studied in the retina for several markers (**Table 2**) at different times after MB injection. There was a clear time-specific modulation that was different for each gene.

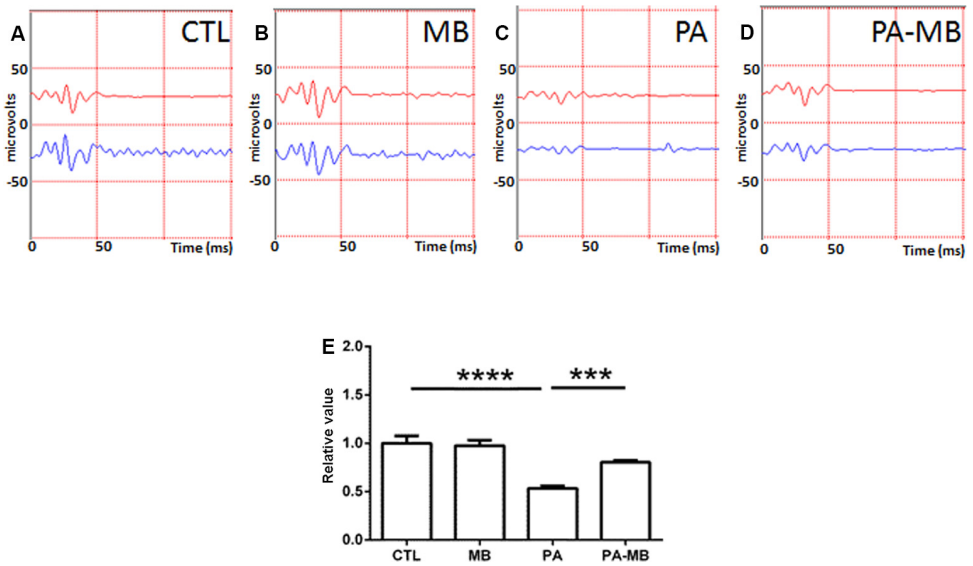

FIGURE 3 | Representative scotopic ERG showing the oscillatory potentials (OP) on the four experimental groups: CTL **(A)**, MB **(B)**, PA **(C)**, and PA-MB **(D)**. The response of the right eye is represented by a red line and that of the left one by a blue line. Quantification of the relative OP sums, relativized to the CTL group, is represented as a histogram **(E)**. Bars represent the mean ± SEM of all samples (n = 10 animals per group). Asterisks represent statistically significant differences. ***$p < 0.001$; ****$p < 0.0001$. Statistical test: ANOVA followed by Holm-Sidak *post hoc* test.

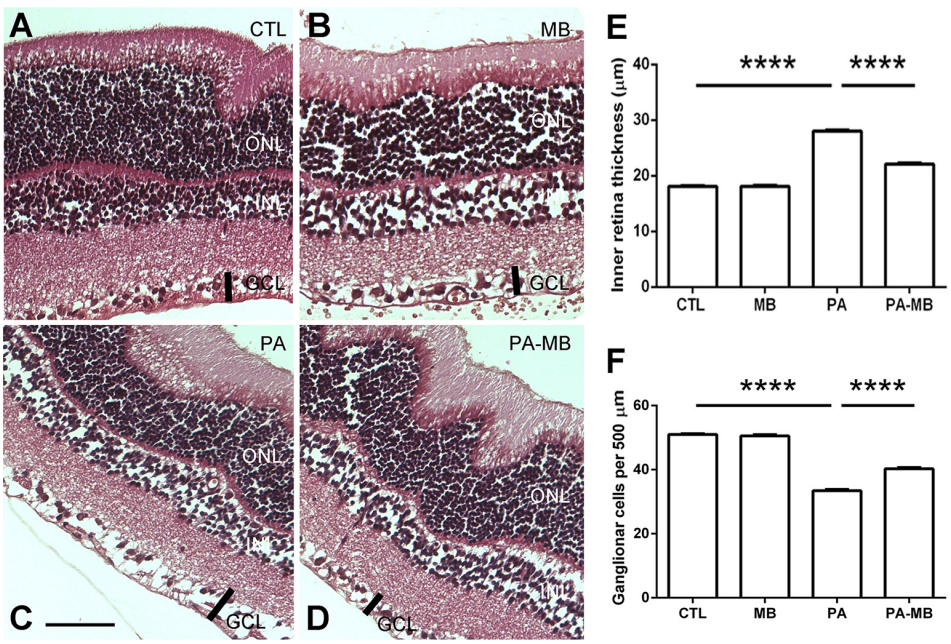

FIGURE 4 | Representative histological images of the retina of animals of the four experimental groups: CTL **(A)** MB **(B)**, PA **(C)**, and PA-MB **(D)** taken 45 days after birth. Three layers of the retina are labeled in the pictures for reference: outer nuclear layer (ONL), inner nuclear layer (INL), and ganglion cell layer (GCL). The thick black bar demarcates the inner retina (IR). Horizontal bar = 50 µm. Quantification of the IR thickness **(E)** and the number of ganglion cells per 500 µm **(F)** are shown as histograms. Bars represent the mean ± SEM of all samples (n = 4 animals per group, five measurements per animal). Asterisks represent statistically significant differences, ****$p < 0.0001$. Statistical test: ANOVA followed by Holm-Sidak *post hoc* test.

The earliest significant change occurred for iNOS expression (**Figure 8A**). At 4 h after treatment, there was a significant ($p < 0.05$) increase of iNOS in the PA animals when compared to CTL and MB groups. Treatment of PA animals with MB completely prevented iNOS overexpression ($p < 0.05$). Other inflammation markers whose expression was modulated by MB

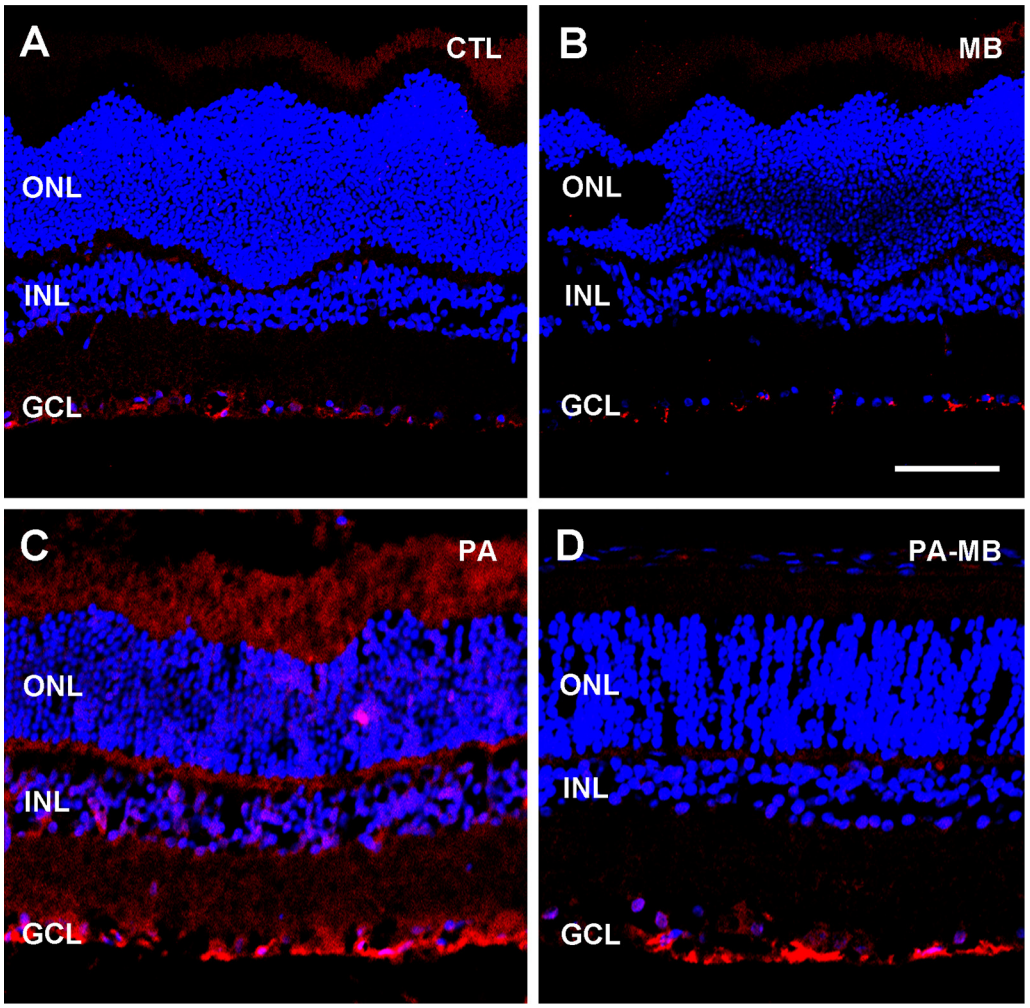

FIGURE 5 | Representative confocal microscopy images, labeled for GFAP (red), of the retina of animals of the four experimental groups: CTL **(A)**, MB **(B)**, PA **(C)**, and PA-MB **(D)**, taken 45 days after birth. Three layers of the retina are labeled in the pictures for reference: ONL, INL, and GCL. Nuclei are counterstained with DAPI (blue). GFAP staining is more intense in the PA group than in all the others. Horizontal bar = 50 μm.

included IL1β at 12 h (**Figure 8B**) and TNFα at 24 h (**Figure 8C**). In both cases, there was no significant increase of expression in the PA group over controls but there was a significant ($p < 0.05$) decrease in the PA-MB group when compared to the PA animals.

Matrix metalloproteinases (MMP) are key enzymes on tissue remodeling. We did not see any significant modulation of MMP2 at any time by either asphyxia or MB treatment (**Figure 8D**). On the other hand, MMP9 expression was significantly ($p < 0.05$) increased on the PA group at 12 h and this pathological increase was fully prevented ($p < 0.05$) by MB treatment (**Figure 8E**). Coinciding with these MMP9 changes, we also found a significant decrease of GFAP expression, a marker of gliosis, on the PA-MB group when compared to the PA animals at 12 h (**Figure 8F**).

Increased angiogenesis is a typical response to hypoxia/ischemia in the retina (Rey-Funes et al., 2013) and we studied the expression of a positive regulator, VEGF, and a negative regulator of angiogenesis, PEDF. At 6 h there was a significant ($p < 0.05$) increase of VEGF expression in the retinas of asphyctic rats, and this increase was significantly counteracted ($p < 0.05$) by MB treatment (**Figure 8G**). Also, although the expression of PEDF did not change in the PA group, there was a very significant ($p < 0.001$) increase in the PA-MB group when compared to all other experimental groups (**Figure 8H**). This PEDF behavior was observed both at 6 h and at 24 h.

DISCUSSION

In this study, we have shown that MB applied to newborns that have suffered PA has very significant advantages in retinal electrophysiology, morphological markers of retinal pathology, and gene expression modulation, suggesting that this treatment may be useful in preventing retinal damage and visual loss associated to PA.

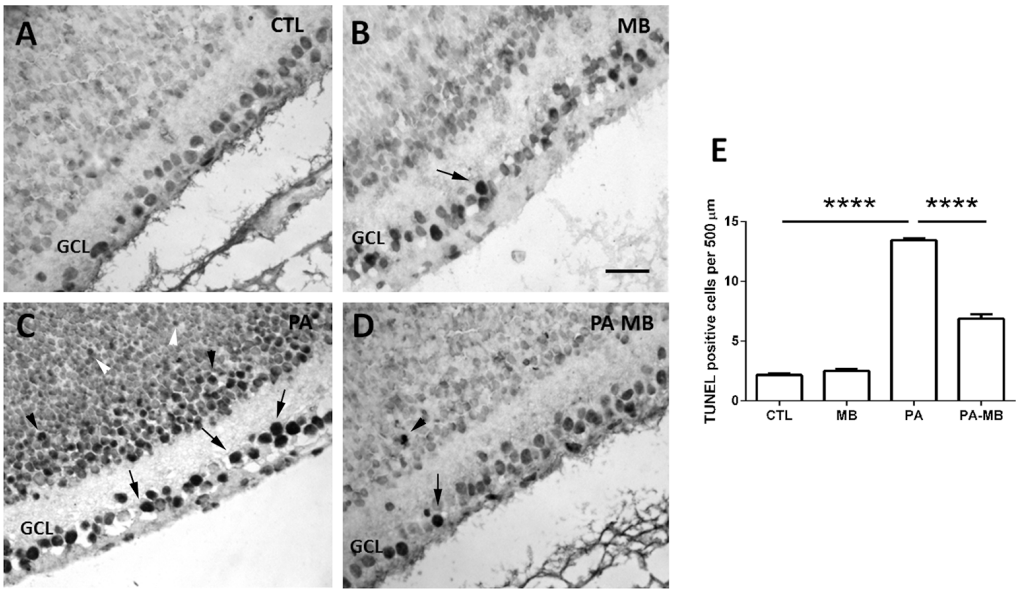

FIGURE 6 | TUNEL positive cells in the four experimental groups 6 days post-treatment. Representative images of retinas from CTL **(A)**, MB **(B)**, PA **(C)**, and PA-MB **(D)** animals. TUNEL positive cells were found mainly in the GCL (arrows), in the precursors of the INL (black arrowheads), and of the ONL (white arrowheads). Bar = 20 μm. Quantification of the results is shown as a histogram **(E)**. Bars represent the mean ± SEM of all samples (n = 4 animals per group, five measurements per animal). Asterisks represent statistically significant differences, ****$p < 0.0001$. Statistical test: ANOVA followed by Holm-Sidak *post hoc* test.

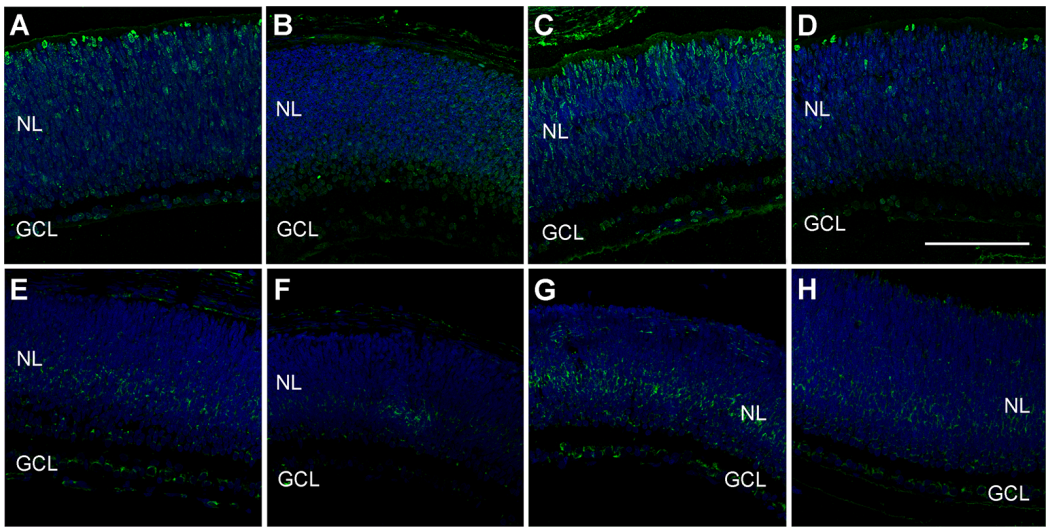

FIGURE 7 | Representative confocal microscopy images, labeled in green for HNEJ-2 **(A–D)** or 8-OHdG **(E–H)**, of the retina of animals of the four experimental groups: CTL **(A,E)**, MB **(B,F)**, PA **(C,G)**, and PA-MB **(D,H)**, taken 6 days after birth. Two layers of the retina are labeled in the pictures for reference: nuclear layer (NL; animals are too young to distinguish the ONL and the INL yet), and GCL. Nuclei are counterstained with DAPI (blue). Increased staining is found for both HNEJ-2 and 8-OHdG in the PA samples compared to the other groups. Horizontal bar = 100 μm.

This study follows our previous work where we showed that MB injected into pregnant dams before delivery had a beneficial impact on the retinal health of the newborns (Rey-Funes et al., 2016). However, although the risks for developing PA are well known (Martinez-Biarge et al., 2013; Bogdanovic et al., 2014), it is difficult to convince the mothers and the medical staff to apply a preventative treatment just before delivery. Our current data show that MB treatment is, at least, as efficient when applied to newborns a few hours after delivery, once the asphyxia episode has occurred and it is evident to everyone involved that an intervention is needed.

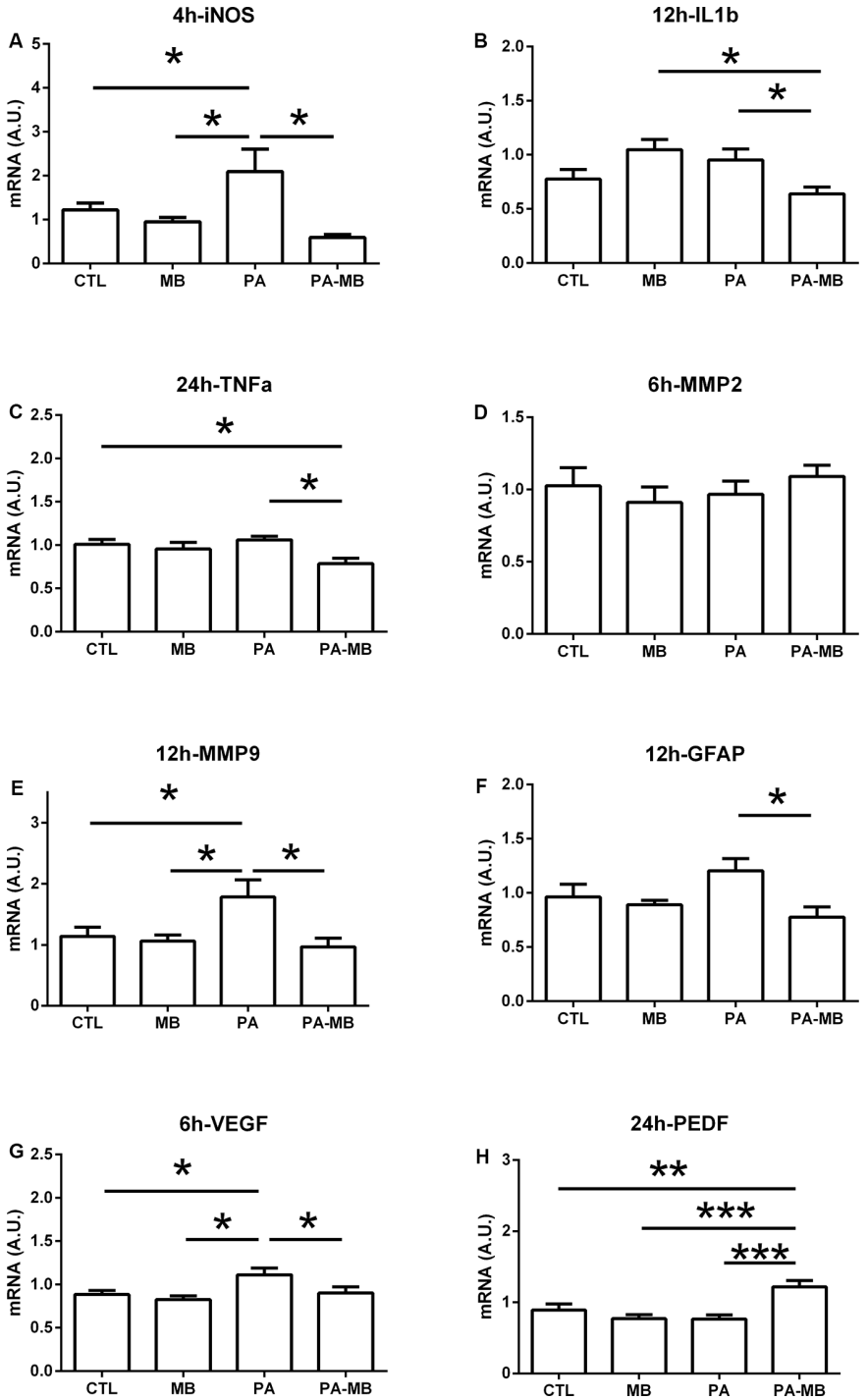

FIGURE 8 | Relative gene expression in the retina of the four experimental groups for iNOS **(A)**, IL1β **(B)**, TNFα **(C)**, MMP2 **(D)**, MMP9 **(E)**, GFAP **(F)**, VEGF **(G)**, and PEDF **(H)**. Samples were collected at the indicated times after treatment. All data represent the quotient between the gene of interest and the expression of the housekeeping gene 18S. Bars represent the mean ± SEM of all measurements (n = 6–8). Asterisks represent statistically significant differences as indicated. *$p < 0.05$, **$p < 0.01$; ***$p < 0.001$. Statistical test: ANOVA followed by the Newman–Keuls *post hoc* test.

Scotopic ERG showed that PA resulted in a significant reduction of the amplitude for both a- and b-waves, as well as a loss of complexity in the OP patterns. It is recognized that the a-wave is generated by the photoreceptors, the OP by the cells in the inner nuclear layer (INL), and the b-wave by the ganglion cells (Jung et al., 2015; Matei et al., 2020;

Zhai et al., 2020). Different animal models of retinal damage influence ERG in a model-specific fashion. For instance, models of blunt ocular trauma (Blanch et al., 2014) or chemical intoxication (Chen et al., 2013) induce photoreceptor apoptosis and a-wave disruption. Conversely, ischemic retinopathy models (Osborne et al., 2004) or optic nerve injury (Rey-Funes et al., 2017) are characterized by impaired inner retinal function, showing changes in the b-wave. Therefore, we can conclude that PA affects all the components of the retinal visual axis. This was confirmed by the observation of TUNEL-positive cells in the three anatomical demarcations in the retina and overexpression of the damage markers NHEJ-2 and 8-OHdG in rats exposed to PA. Interestingly, the application of MB was able to normalize the physiological patterns as well as the morphological telltales of retinal pathology, indicating that this could constitute a new treatment to prevent visual loss in children affected by PA.

A common morphological feature observed in all models of ocular hypoxia/ischemia-reperfusion is the thickening of the inner layer of the retina due to a pathological increase in gliosis and angiogenesis (Rey-Funes et al., 2013; Luo et al., 2018). Gliosis is due to a proliferation of the GFAP-positive processes of Müller cells (Pekny et al., 2014) whereas the excessive number of blood vessels reflects a lost balance between proangiogenic and antiangiogenic factors within the eye environment (Friedlander, 2007). In the present study, both the immunoreactivity and RNA expression of GFAP was significantly downregulated by the treatment with MB. The proliferation of reactive astrocytes, or Müller cells in the case of the retina, is considered an obstacle for the proper physiological communication among neighboring neurons (Pekny et al., 2014), so we can consider that it may contribute to the compromised electrophysiological recordings we found in PA animals and, perhaps, to the excessive apoptosis of ganglion cells detected by direct counting and corroborated by TUNEL. The contribution of MB treatment to the reduction of retinal gliosis can thus be considered a very desirable outcome.

Our initial hypothesis was that MB can modulate NO production and function in the eye and, as a consequence, could provide neuroprotection for ischemic injuries of the retina, including PA. Our qRT-PCR results confirm this hypothesis and show a fast expression of the inducible form of NOS just 4 h after PA, which was prevented by MB. iNOS is a Ca^{2+} independent isoform of NOS whose expression rises rapidly in response to inflammatory signals and other injuries, including ischemia-reperfusion of the retina (Rodrigo et al., 2005). iNOS produces large amounts of NO which acts as a free radical and contributes to tissue damage (Toda and Nakanishi-Toda, 2007). The complete blocking of iNOS induction by MB treatment points to a mechanistic explanation for the beneficial effects of MB on preserving retinal function even after suffering the ischemic insult. Other inflammatory mediators that are regulated by MB are IL1β and TNFα. The mechanism by which MB reduces expression of these inflammatory markers is unknown but it may follow the earlier lowering on iNOS expression and a general reduction on the inflammatory milieu of the eye.

Eye angiogenesis must be very tightly controlled to avoid pathological blood vessel overproduction, which is the cause of many retinal and choroidal chronic diseases (Lau et al., 2018). The main proangiogenic factor of the eye is VEGF (Virgili et al., 2018) whereas the major antiangiogenic factor is PEDF (Farnoodian et al., 2017). Furthermore, there is a mutually opposite regulation between these two factors: VEGF can induce MMP expression, which in turn will degrade retinal PEDF (Notari et al., 2005). In our analysis, we found a fast upregulation of VEGF expression within 6 h of PA. This was to be expected since VEGF is transactivated by HIF-1 transcription factor, which rapidly signals to the nucleus under hypoxic conditions (Kurihara et al., 2014). That this upregulation was prevented by MB treatment suggests a preventive antiangiogenic effect for MB in the retina. Also, PEDF did not change in the PA animals but its expression was very significantly elevated in the PA animals that were treated with MB. This elevation of an antiangiogenic molecule, together with the downregulation of VEGF, may partly explain the protective effect of MB on retinal morphology and physiology.

Another aspect needed for angiogenesis and retinal thickening is extracellular matrix remodeling. Dynamic changes in the connective tissue depend on the activity of many proteases, including MMPs and, in particular, gelatinases (Jabłońska-Trypuć et al., 2016). Interestingly, MMP2 did not respond to either PA or the treatment with MB but MMP9 expression increased following PA. It has been shown that hypoxia (Li and Zheng, 2017) and iNOS (Anavi et al., 2015) can upregulate MMP9 expression under some conditions, and that MMP9 is a proangiogenic factor (Djordjevic et al., 2018), so the increased expression of MMP9 following PA may contribute to enhanced angiogenesis and the thickening of the IR we observed in these animals. Also, MMP9 has been implicated in the degradation of PEDF in the retina (Notari et al., 2005), thus further implicating this protease in angiogenesis regulation. The fact that MB was able to completely prevent MMP9 overexpression, probably through blockade of excessive NO availability, further supports the protective role of this chemical.

In summary, MB represents an effective treatment to reduce the physiological, morphological, and molecular telltales of retinal degeneration following episodes of PA and, given its safety profile and low cost, it could be used as an alternative therapy to hypothermia in regions of the world where that intervention may be unavailable.

DATA AVAILABILITY STATEMENT

The raw data supporting the conclusions of this article will be made available by the authors, without undue reservation, to any qualified researcher.

ETHICS STATEMENT

The animal study was reviewed and approved by Ethical Committee of CICUAL (Comité Institucional para el Uso y Cuidado de Animales de Laboratorio).

AUTHOR CONTRIBUTIONS

JF, RP, MR-F, MS, DC, VD, and JL-C: acquisition, analysis, and interpretation of data. IML, CFL, and AM: conception and design, analysis and interpretation of data. AM: wrote the article. All authors revised the original manuscript and agreed on its contents.

FUNDING

CFL is supported by UBACyT 20020160100150BA. IML is supported by a Miguel Servet contract (CP15/00198) from the Instituto de Salud Carlos III-FEDER (Fondo Europeo de Desarrollo Regional, a way to build Europe) and by FRS.

ACKNOWLEDGMENTS

We want to thank Andrea Pecile, Marianela Ceol Retamal, and Manuel Antonio Ponce for excellent assistance at the animal facility; Ing. Lisandro Antón for electroretinography setup; and Nicolás Spada for histological assistance (University of Buenos Aires). We also gratefully acknowledge Ms. Judit Narro for histological assistance and Dr. Josune García-Sanmartín for immunofluorescence staining (CIBIR).

REFERENCES

Anavi, S., Eisenberg-Bord, M., Hahn-Obercyger, M., Genin, O., Pines, M., and Tirosh, O. (2015). The role of iNOS in cholesterol-induced liver fibrosis. *Lab. Invest.* 95, 914–924. doi: 10.1038/labinvest.2015.67

Atamna, H., Nguyen, A., Schultz, C., Boyle, K., Newberry, J., Kato, H., et al. (2008). Methylene blue delays cellular senescence and enhances key mitochondrial biochemical pathways. *FASEB J.* 22, 703–712. doi: 10.1096/fj.07-9610com

Bewick, J., and Pfleiderer, A. (2014). The value and role of low dose methylene blue in the surgical management of hyperparathyroidism. *Ann. R. Coll. Surg. Engl.* 96, 526–529. doi: 10.1308/003588414x13946184903883

Blanch, R. J., Ahmed, Z., Thompson, A. R., Akpan, N., Snead, D. R., Berry, M., et al. (2014). Caspase-9 mediates photoreceptor death after blunt ocular trauma. *Invest. Ophthalmol. Vis. Sci.* 55, 6350–6357. doi: 10.1167/iovs.13-13708

Bogdanovic, G., Babovic, A., Rizvanovic, M., Ljuca, D., Grgic, G., and Djuranovic-Milicic, J. (2014). Cardiotocography in the prognosis of perinatal outcome. *Med. Arch.* 68, 102–105. doi: 10.5455/medarh.2014.68.102-105

Chen, J. M., Zhu, G. Y., Zhao, Z. Q., and Xia, W. T. (2013). Electroretinogram and histopathologic changes of the retina after methanol intoxication. *Fa Yi Xue Za Zhi* 29, 5–11, 16. doi: 10.3969/j.issn.1004-5619.2013.01.002

Ding, J. D., and Weinberg, R. J. (2007). Distribution of soluble guanylyl cyclase in rat retina. *J. Comp. Neurol.* 502, 734–745. doi: 10.1002/cne.21206

Dingley, J., Liu, X., Gill, H., Smit, E., Sabir, H., Tooley, J., et al. (2015). The feasibility of using a portable xenon delivery device to permit earlier xenon ventilation with therapeutic cooling of neonates during ambulance retrieval. *Anesth. Analg.* 120, 1331–1336. doi: 10.1213/ane.0000000000000693

Djordjevic, B., Cvetkovic, T., Stoimenov, T. J., Despotovic, M., Zivanovic, S., Basic, J., et al. (2018). Oral supplementation with melatonin reduces oxidative damage and concentrations of inducible nitric oxide synthase, VEGF and matrix metalloproteinase 9 in the retina of rats with streptozotocin/nicotinamide induced pre-diabetes. *Eur. J. Pharmacol.* 833, 290–297. doi: 10.1016/j.ejphar.2018.06.011

Farnoodian, M., Wang, S., Dietz, J., Nickells, R. W., Sorenson, C. M., and Sheibani, N. (2017). Negative regulators of angiogenesis: important targets for treatment of exudative AMD. *Clin. Sci.* 131, 1763–1780. doi: 10.1042/cs20170066

Ferriero, D. M. (2004). Neonatal brain injury. *N. Engl. J. Med.* 351, 1985–1995. doi: 10.1056/NEJMra041996

Friedlander, M. (2007). Fibrosis and diseases of the eye. *J. Clin. Invest.* 117, 576–586. doi: 10.1172/JCI31030

Herrera, T. I., Edwards, L., Malcolm, W. F., Smith, P. B., Fisher, K. A., Pizoli, C., et al. (2018). Outcomes of preterm infants treated with hypothermia for hypoxic-ischemic encephalopathy. *Early Hum. Dev.* 125, 1–7. doi: 10.1016/j.earlhumdev.2018.08.003

Heydrick, S. J., Reed, K. L., Cohen, P. A., Aarons, C. B., Gower, A. C., Becker, J. M., et al. (2007). Intraperitoneal administration of methylene blue attenuates oxidative stress, increases peritoneal fibrinolysis, and inhibits intraabdominal adhesion formation. *J. Surg. Res.* 143, 311–319. doi: 10.1016/j.jss.2006.11.012

Hill, A. (1991). Current concepts of hypoxic-ischemic cerebral injury in the term newborn. *Pediatr. Neurol.* 7, 317–325. doi: 10.1016/0887-8994(91)90060-x

Hwang, T. L., Wu, C. C., and Teng, C. M. (1998). Comparison of two soluble guanylyl cyclase inhibitors, methylene blue and ODQ, on sodium nitroprusside-induced relaxation in guinea-pig trachea. *Br. J. Pharmacol.* 125, 1158–1163. doi: 10.1038/sj.bjp.0702181

Jabłońska-Trypuć, A., Matejczyk, M., and Rosochacki, S. (2016). Matrix metalloproteinases (MMPs), the main extracellular matrix (ECM) enzymes in collagen degradation, as a target for anticancer drugs. *J. Enzyme Inhib. Med. Chem.* 31, 177–183. doi: 10.3109/14756366.2016.1161620

Jung, S., Polosa, A., Lachapelle, P., and Wintermark, P. (2015). Visual impairments following term neonatal encephalopathy: do retinal impairments also play a role? *Invest. Ophthalmol. Vis. Sci.* 56, 5182–5193. doi: 10.1167/iovs.15-16407

Kurihara, T., Westenskow, P. D., and Friedlander, M. (2014). Hypoxia-inducible factor (HIF)/vascular endothelial growth factor (VEGF) signaling in the retina. *Adv. Exp. Med. Biol.* 801, 275–281. doi: 10.1007/978-1-4614-3209-8_35

Landoni, G., Pasin, L., Di Prima, A. L., Dossi, R., Taddeo, D., and Zangrillo, A. (2014). Methylene blue: between scylla (meta-analysis) and charybdis (propensity). *J. Cardiothorac. Vasc. Anesth.* 28, e12–e13. doi: 10.1053/j.jvca.2013.12.012

Lau, C. M. L., Yu, Y., Jahanmir, G., and Chau, Y. (2018). Controlled release technology for anti-angiogenesis treatment of posterior eye diseases: current status and challenges. *Adv. Drug. Deliv. Rev.* 126, 145–161. doi: 10.1016/j.addr.2018.03.013

Li, J., Chen, X., Qi, M., and Li, Y. (2018). Sentinel lymph node biopsy mapped with methylene blue dye alone in patients with breast cancer: a systematic review and meta-analysis. *PLoS One* 13:e0204364. doi: 10.1371/journal.pone.0204364

Li, Y. Y., and Zheng, Y. L. (2017). Hypoxia promotes invasion of retinoblastoma cells *in vitro* by upregulating HIF-1α/MMP9 signaling pathway. *Eur. Rev. Med. Pharmacol. Sci.* 21, 5361–5369. doi: 10.26355/eurrev_201712_13921

Liu, L., Oza, S., Hogan, D., Perin, J., Rudan, I., Lawn, J. E., et al. (2015). Global, regional, and national causes of child mortality in 2000–13, with projections to inform post-2015 priorities: an updated systematic analysis. *Lancet* 385, 430–440. doi: 10.1016/S0140-6736(14)61698-6

Loidl, C. F., Gavilanes, A. W., Van Dijk, E. H., Vreuls, W., Blokland, A., Vles, J. S., et al. (2000). Effects of hypothermia and gender on survival and behavior after perinatal asphyxia in rats. *Physiol. Behav.* 68, 263–269. doi: 10.1016/s0031-9384(99)00125-0

Luo, H., Zhuang, J., Hu, P., Ye, W., Chen, S., Pang, Y., et al. (2018). Resveratrol delays retinal ganglion cell loss and attenuates gliosis-related inflammation from ischemia-reperfusion injury. *Invest. Ophthalmol. Vis. Sci.* 59, 3879–3888. doi: 10.1167/iovs.18-23806

Martinez-Biarge, M., Diez-Sebastian, J., Wusthoff, C. J., Mercuri, E., and Cowan, F. M. (2013). Antepartum and intrapartum factors preceding neonatal hypoxic-ischemic encephalopathy. *Pediatrics* 132, e952–e959. doi: 10.1542/peds.2013-0511

Matei, N., Leahy, S., Auvazian, S., Thomas, B., Blair, N. P., and Shahidi, M. (2020). Relation of retinal oxygen measures to electrophysiology and survival indicators after permanent, incomplete ischemia in rats. *Transl. Stroke Res.* doi: 10.1007/s12975-020-00799-9 [Epub ahead of print].

Mukhtar-Yola, M., Audu, L. I., Olaniyan, O., Akinbi, H. T., Dawodu, A., and Donovan, E. F. (2018). Decreasing birth asphyxia: utility of statistical process control in a low-resource setting. *BMJ Open Qual.* 7:e000231. doi: 10.1136/bmjoq-2017-000231

Notari, L., Miller, A., Martínez, A., Amaral, J., Ju, M., Robinson, G., et al. (2005). Pigment epithelium-derived factor is a substrate for matrix metalloproteinase

type 2 and type 9: implications for downregulation in hypoxia. *Invest. Ophthalmol. Vis. Sci.* 46, 2736–2747. doi: 10.1167/iovs.04-1489

Osborne, N. N., Casson, R. J., Wood, J. P., Chidlow, G., Graham, M., and Melena, J. (2004). Retinal ischemia: mechanisms of damage and potential therapeutic strategies. *Prog. Retin. Eye Res.* 23, 91–147. doi: 10.1016/j.preteyeres.2003.12.001

Pekny, M., Wilhelmsson, U., and Pekna, M. (2014). The dual role of astrocyte activation and reactive gliosis. *Neurosci. Lett.* 565, 30–38. doi: 10.1016/j.neulet.2013.12.071

Rey-Funes, M., Dorfman, V. B., Ibarra, M. E., Peña, E., Contartese, D. S., Goldstein, J., et al. (2013). Hypothermia prevents gliosis and angiogenesis development in an experimental model of ischemic proliferative retinopathy. *Invest. Ophthalmol. Vis. Sci.* 54, 2836–2846. doi: 10.1167/iovs.12-11198

Rey-Funes, M., Ibarra, M. E., Dorfman, V. B., Serrano, J., Fernández, A. P., Martínez-Murillo, R., et al. (2011). Hypothermia prevents nitric oxide system changes in retina induced by severe perinatal asphyxia. *J. Neurosci. Res.* 89, 729–743. doi: 10.1002/jnr.22556

Rey-Funes, M., Larrayoz, I. M., Contartese, D. S., Soliño, M., Sarotto, A., Bustelo, M., et al. (2017). Hypothermia prevents retinal damage generated by optic nerve trauma in the rat. *Sci. Rep.* 7:6966. doi: 10.1038/s41598-017-07294-6

Rey-Funes, M., Larrayoz, I. M., Fernández, J. C., Contartese, D. S., Rolón, F., Inserra, P. I., et al. (2016). Methylene blue prevents retinal damage in an experimental model of ischemic proliferative retinopathy. *Am. J. Physiol. Regul. Integr. Comp. Physiol.* 310, R1011–R1019. doi: 10.1152/ajpregu.00266.2015

Rivero-Arias, O., Eddama, O., Azzopardi, D., Edwards, A. D., Strohm, B., and Campbell, H. (2019). Hypothermia for perinatal asphyxia: trial-based resource use and costs at 6-7 years. *Arch. Dis. Child. Fetal Neonatal Ed.* 104, F285–F292. doi: 10.1136/archdischild-2017-314685

Rodrigo, J., Fernandez, A. P., Serrano, J., Peinado, M. A., and Martinez, A. (2005). The role of free radicals in cerebral hypoxia and ischemia. *Free Radic Biol. Med.* 39, 26–50. doi: 10.1016/j.freeradbiomed.2005.02.010

Rojas, J. C., John, J. M., Lee, J., and Gonzalez-Lima, F. (2009). Methylene blue provides behavioral and metabolic neuroprotection against optic neuropathy. *Neurotox. Res.* 15, 260–273. doi: 10.1007/s12640-009-9027-z

Sparicio, D., Landoni, G., and Zangrillo, A. (2004). Angiotensin-converting enzyme inhibitors predispose to hypotension refractory to norepinephrine but responsive to methylene blue. *J. Thorac. Cardiovasc. Surg.* 127:608. doi: 10.1016/j.jtcvs.2003.01.001

Toda, N., and Nakanishi-Toda, M. (2007). Nitric oxide: ocular blood flow, glaucoma, and diabetic retinopathy. *Prog. Retin. Eye Res.* 26, 205–238. doi: 10.1016/j.preteyeres.2007.01.004

Virgili, G., Parravano, M., Evans, J. R., Gordon, I., and Lucenteforte, E. (2018). Anti-vascular endothelial growth factor for diabetic macular oedema: a network meta-analysis. *Cochrane Database Syst. Rev.* 10:CD007419. doi: 10.1002/14651858.cd007419.pub6

World Health Organization. (1991). *Consultation on Birth Asphyxia and Thermal Control of the Newborn.* Geneva, Switzerland: World Health Organization.

World Health Organization. (2017). *WHO Model List of Essential Medicines.* Available online at: http://apps.who.int/iris/bitstream/handle/10665/273826/EML-20-eng.pdf.

Wright, R. O., Lewander, W. J., and Woolf, A. D. (1999). Methemoglobinemia: etiology, pharmacology, and clinical management. *Ann. Emerg. Med.* 34, 646–656. doi: 10.1016/s0196-0644(99)70167-8

Zhai, W., Gao, L., Qu, L., Li, Y., Zeng, Y., Li, Q., et al. (2020). Combined transplantation of olfactory ensheathing cells with rat neural stem cells enhanced the therapeutic effect in the retina of RCS rats. *Front. Cell. Neurosci.* 14:52. doi: 10.3389/fncel.2020.00052

Zhang, X., Rojas, J. C., and Gonzalez-Lima, F. (2006). Methylene blue prevents neurodegeneration caused by rotenone in the retina. *Neurotox. Res.* 9, 47–57. doi: 10.1007/bf03033307

Conflict of Interest: The authors declare that the research was conducted in the absence of any commercial or financial relationships that could be construed as a potential conflict of interest.

frontiers in Pediatrics

ORIGINAL RESEARCH
published: 23 July 2020
doi: 10.3389/fped.2020.00412

Changes of Dynamic Functional Connectivity Associated With Maturity in Late Preterm Infants

Xueling Ma[1,2,3], *Xiushuang Wu*[4,5] *and Yuan Shi*[1,2,3,6*]

[1] Department of Neonatalogy, Children's Hospital of Chongqing Medical University, Chongqing, China, [2] National Clinical Research Center for Child Health and Disorders, Chongqing, China, [3] Key Laboratory of Child Development and Disorders, Ministry of Education, Chongqing, China, [4] Department of Pediatrics, Daping Hospital, Army Medical University, Chongqing, China, [5] Department of Pediatrics, Yunnan Provincial Crops of Chinese People's Armed Police Force, Langfang, China, [6] Chongqing Key Laboratory of Child Infection and Immunity, Chongqing, China

Objective: To investigate the changes of dynamic functional connectivity (DFC) in late preterm infants, and assess whether these changes are associated with the indicators measuring the maturity of neonates.

Methods: Resting-state fMRI (rs-fMRI) data of eligible neonates was acquired with a 3.0-T MRI scanner in the Department of Radiology, Daping Hospital, Army Medical University (Chongqing, China). After the selection of functional connectivity networks obtained by independent component analysis (ICA), a sliding-window approach was used to cluster all the windows into different states. Then the differences of temporal properties of DFC between groups were compared, and the association between these temporal properties and the degree of maturity was also explored in each state.

Results: Eventually, 34 late preterm and 37 term neonates were included in the final analysis. Based on their data, 5 components were located in 5 networks: default-mode (DMN), dorsal attention (DAN), auditory (AUD), sensorimotor (SMN), and visual (VN). Then four reoccurring state patterns of functional connectivity were identified with the k-means clustering method. The late preterm group dwelled significantly longer in State III (late preterm: 33.57 ± 37.64 s, term: 18.50 ± 11.71 s; $P = 0.03$), which was characterized by general weaker connectivity between networks. Also, the correlation analysis shows the degree of maturity is negatively correlated to the dwell time and fractional windows in State III.

Conclusion: Our findings suggested that compared with term infants, late preterm infants preferred to stay in a state with general weak connectivity between networks, but this preference declined as maturity increased.

Keywords: late preterm infants, premature brain injury, fMRI, independent component analysis, dynamic functional connectivity

OPEN ACCESS

Edited by:
Silvia Carloni,
University of Urbino Carlo Bo, Italy

Reviewed by:
Anna Tarocco,
University of Ferrara, Italy
Qianshen Zhang,
University of Hong Kong, China

****Correspondence:***
Yuan Shi
shiyuan@hospital.cqmu.edu.cn

Specialty section:
This article was submitted to Neonatology, a section of the journal Frontiers in Pediatrics

Received: *01 March 2020*
Accepted: *15 June 2020*
Published: *23 July 2020*

Citation:
Ma X, Wu X and Shi Y (2020) Changes of Dynamic Functional Connectivity Associated With Maturity in Late Preterm Infants. Front. Pediatr. 8:412. doi: 10.3389/fped.2020.00412

INTRODUCTION

Preterm birth accounts for 11% of all live-births worldwide, and their survival rate has remarkably increased in recent few years (1, 2). Preterm infants, even late preterm infants (born between 34^{+0} and 36^{+6} weeks of gestation), are still at risk for neurodevelopmental impairment. Accounting for about 75% of all preterm births, late preterm infants are the largest group of preterm newborns. Severe brain injuries such as cerebral palsy seldom happen in late preterm infants, but mild to moderate injuries often occur in this group. According to recent studies, mild injuries may also lead to developmental and emotional-behavioral problems in adolescence, involving language disorder, attention deficit hyperactivity disorder, developmental coordination disorder, autism spectrum disorder, and so on (3, 4).

A series of characteristic alterations in the structural and functional connectivity of brain were identified in many neurological disorders. By observing these alterations, the associations across many brain disorders may be revealed (5). As for neurodevelopmental problems caused by premature birth, both commonalities and differences in clinical characteristics have been noticed. Therefore, exploring characteristic alterations of the connectivity networks in preterm infants may help reveal mechanisms of various disorders related to premature brain injury. For instance, lesions in different locations can cause similar symptoms if these lesions affect the same brain network. For this reason, we chose to analyze the functional network connectivity in late preterm neonates.

A recent technique called dynamic functional connectivity (DFC), assesses temporal variations of functional connectivity during MRI acquisition by dividing resting-state functional MRI (rs-fMRI) scans into a series of "sliding windows" (6, 7) and clustering these windows into several states by k-means method (6, 8).

We hypothesized that the temporal properties of DFC between term and late preterm infants were different, and there were associations between these properties and indicators measuring maturity.

MATERIALS AND METHODS

Participants

A total of 155 neonates were initially recruited from the Department of Pediatrics, Daping Hospital, Army Medical University (Chongqing, China), including 58 term and 97 late preterm infants. Enrolled patients were initially chosen following these criteria: neonates without unstable medical condition or contraindication to MRI, gestational age more than 34 weeks, no acute or chronic diseases, no resuscitation history at birth, no major congenital malformations, and no congenital infections. After the acquisition of MRI data, two experienced experts reviewed the imaging and reported the result together, infants with definite or suspicious intracranial hemorrhage or other major structural abnormalities were also excluded in the following analysis. This step excluded 32 preterm and 3 term infants, remaining 120 infants in the dataset.

This study was approved by the Ethics Committee of Daping Hospital, Army Medical University (Chongqing, China). All study procedures followed the Declaration of Helsinki. Written informed consent was obtained from every infant's parents.

Data Acquisition

Scans were collected using a 3.0-T MRI scanner (Siemens, Germany) during natural sleep in the Department of Radiology, Daping Hospital, Army Medical University (Chongqing, China). Infants were transported to MRI scanner, accompanied by a nurse and a neonatologist. Scanning was immediately done after the infant was fed to induce drowsiness. Neonatal ear muffs were used to block out MRI noise. During the examination, each participant was continuously monitored by an electrocardiogram and a pulse oximeter and closely observed by the accompanied neonatologist. Structural images were collected with a turbo-spin echo (TSE), T2-weighted sequence, TR/TE/flip angle = 3,200/393 ms/150°, voxel size = 1.25 × 1.25 × 1.95 mm^3; 96 transversal slices, bandwidth = 751 Hz/pixel. Rs-fMRI scans were collected using a T2-weighted echo-planar imaging (EPI) sequence, field of view = 220 × 220 mm^2, TR/TE/flip angle = 2,000/30 ms/90°, voxel size = 3.4 × 3.4 × 3.0 mm^3 with no gap, number of slices = 33. For each neonate, 240 volumes were obtained across the whole brain.

Preprocessing

The rs-fMRI data was preprocessed using Gretna2.0 (9) implemented in MATLAB (version R2013b)/SPM12. At the beginning of preprocessing, the first 10 volumes were removed to reach a steady state, leaving 230 volumes for each infant. Slice timing (middle slice as reference slice) was carried out for correction of acquisition time delay between slices, and realignment (register to mean) was carried out for correction of head motion between volumes. Since excessive head motion can affect DFC analysis (10), conservative inclusion criteria were chosen to minimize head-motion bias, which means acquisitions with frame wise displacement (FD) >0.5 mm would be removed (11), as well as the ones with translational movement more than 2 mm or rotational movement more than 2°. According to these criteria, we excluded 31 late preterm infants and 18 term infants, and 34 late preterm and 37 term infants were included in the final analysis. The following steps included reorientation manually, spatial normalization with EPI template (12), spatially smoothing with a Gaussian kernel (full width at half-maximum of 4 mm). The flow chart of data processing is shown in **Figure 1**.

Group Independent Component Analysis

After data preprocessing, a data-driven technique called spatial independent component analysis (ICA) was performed with GIFT (version 3.0b) (13, 14) to decompose the data into spatial independent components. Two steps for data reductions were run during the analysis, that is, the subject-level and group-level principal component analysis. ICA was performed under the component number from 14 to 30 to obtain stable infant networks (the number estimated by minimum description length criteria is 14), and at last the component number of 25 was chosen for its relatively stable and intact network profiles. To

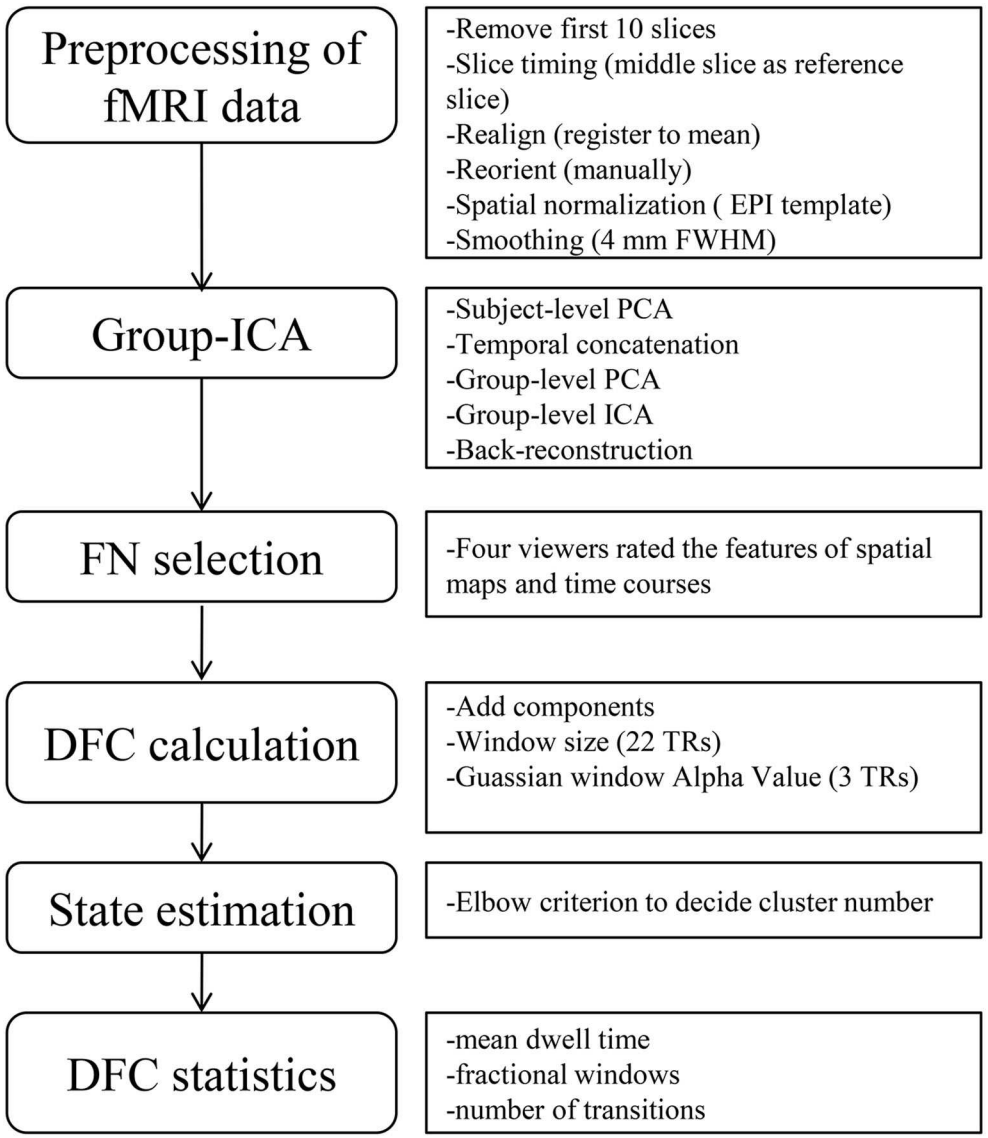

FIGURE 1 | Flow chart of data processing. The left part shows the overall steps of data processing, and the right part is the detailed sub-steps, including some important parameters in each step. ICA, independent component analysis; FN, functional networks; DFC, dynamic functional connectivity; FWHM, full width at half-maximum; PCA, principal component analysis; TRs, times of repetition.

replicate the decomposed independent components, the Infomax ICA algorithm was repeated for 20 times in ICASSO (15, 16) and the aggregate spatial maps were generated. With the group ICA back reconstruction method (17), the subject-specific spatial maps and their corresponding time courses were then generated.

Functional Networks Selection

To differentiate between resting-state functional networks (FN) and physiological components, a previously described procedure was applied (18). Four viewers visually inspected the spatial maps and average power spectra, and scores from 0 (definite artifact) to 1 (certain functional network) were given by them based on these expectations: (1) RSNs should exhibit peak activation in gray matter, low spatial overlap with vascular, ventricular, and susceptibility artifacts; (2) Time course should be dominated by low-frequency fluctuations, with ratio of the integral of spectral power below 0.10 Hz to the integral of power between 0.15 and 0.25 Hz (19). Following these criteria, components were divided into 3 categories: artifact (score $= 0$), mixed ($0 <$ score < 3), functional network (score ≥ 3). This procedure resulted in 5 components located in 5 networks, default-mode (DMN), dorsal attention (DAN), auditory (AUD), sensorimotor (SMN), and visual (VN), shown in **Figure 2**.

Additional postprocessing of the selected components was performed following a previous research (6) to remove remaining noise sources. Briefly, steps included detrending, filtering with

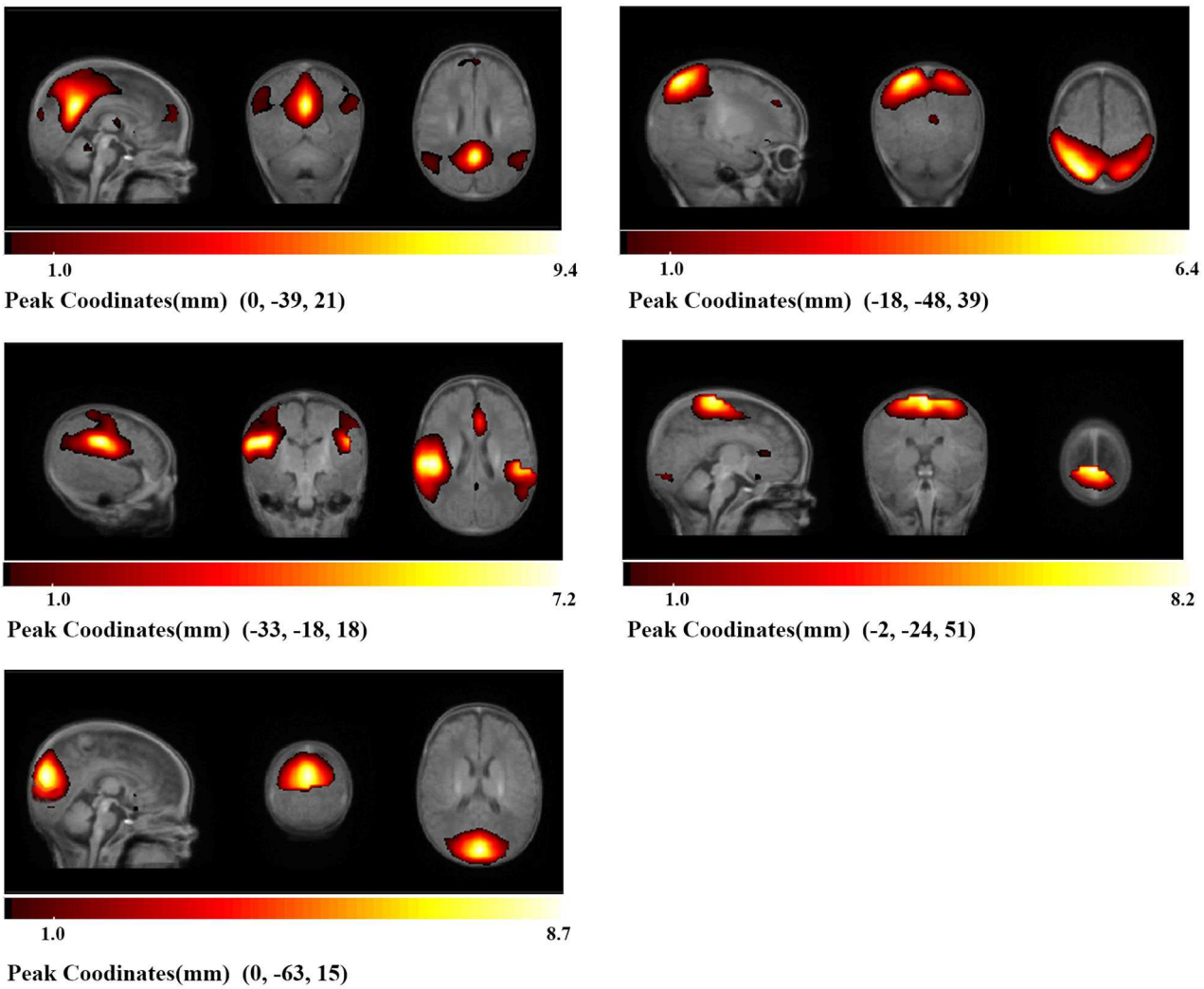

FIGURE 2 | Identified networks. Based on the anatomical and functional properties, five components were located in five networks (DMN, DAN, AUD, SMN, VN). Brighter parts indicate stronger local activity, and under each part is its color bar and peak coordinates.

a cut-off value of low frequency fluctuation set as 0.15 Hz, and despiking.

DFC Analysis

DFC was calculated based on a sliding window approach using GIFT toolbox. A sliding window length of 22 times of repetition (TRs) with a Gaussian window Alpha Value of 3 TRs was set, since this length could provide a good compromise between the quality of correlation matrix estimation and the ability to resolve dynamics (6). By sliding the window in a step length of 1 TR along the 230 TRs length scan, we obtained 208 consecutive windows across the entire scans. After computing DFC, all the functional connectivity matrices were transformed to z-score using Fisher's z-transformation for further analysis.

K-means method with sqEuclidean distance was used to regroup similar functional matrices of the different windows into different states, and the analysis was repeated 150 times to obtain a relatively stable result. The number of optimal clusters was calculated following the elbow criterion (6), and the number was set to be 4.

We investigated the temporal properties of DFC states derived from the state vector of every infant. Three measures in subjects were assessed, including: (1) Mean dwell time, defined as the average number of consecutive windows belonging to one state before changing to the other state; (2) fractional windows, defined as the number of total windows belonging to one state; (3) number of transitions, defined as the number of times that the state switched from one to the other.

Statistical Comparisons and Correlations Analysis

The demographic and clinical data of all initially enrolled infants were recorded. Statistical analysis was performed

TABLE 1 | Demographic and clinical data of all initial enrolled patients.

	Preterm		t/χ^2	*P*	Term		t/χ^2	*P*
	Included	Excluded			Included	Excluded		
Demographic data								
Number	34	63			37	31		
Gestational age (weeks)	35.93 ± 1.34	35.64 ± 0.95	1.11	0.27	40.29 ± 1.06	40.00 ± 0.80	1.04	0.30
Birth weight (kg)	2.03 ± 0.41	2.03 ± 0.23	−0.05	0.96	3.27 ± 0.38	3.29 ± 0.39	−0.19	0.85
SGA infants	11/23	16/47	0.53	0.49	2/35	2/19	0.35	0.62
Delivery method (CS/VD)	9/25	15/48	0.08	0.81	13/24	5/16	0.80	0.40
Twins or triplets	2/32	2/61	0.41	0.61	2/35	0/21	1.18	0.53
Gender (male/female)	15/19	32/31	0.39	0.67	19/18	11/10	0.00	1.00
Days of birth (days)	9.47 ± 2.02	9.48 ± 2.06	−0.01	0.99	9.62 ± 2.30	9.62 ± 1.96	0.00	1.00
PMA (weeks)	37.28 ± 1.34	36.99 ± 0.95	1.10	0.28	41.66 ± 1.13	41.38 ± 0.92	0.96	0.34
Maternal factors								
Antenatal steroid	6/28	4/59	3.05	0.16	0	0		
PROM	1/33	2/61	0.00	1.00	3/34	1/20	0.23	1.00
DM, GDM, GH or PE	2/32	2/61	0.41	0.61	0/37	1/20	1.79	0.36
Clinical data after birth								
Apgar-1min	9.00 ± 1.07	9.24 ± 1.00	−1.09	0.28	9.38 ± 0.86	9.48 ± 0.51	−0.47	0.64
Apgar-5min	9.68 ± 0.48	9.83 ± 0.38	−1.57	0.12	10.00 ± 0.00	9.95 ± 0.22	1.00	0.32
Breast milk/mixed/formula	1/23/10	1/40/22	0.46	0.84	24/10/3	12/8/1	0.88	0.7
Ventilation time (hours)	25.76 ± 28.36	15.81 ± 25.67	1.76	0.08	0.00 ± 0.00	2.29 ± 10.47	−1.00	0.33
Apnea	2/32	2/61	0.41	0.61	0	0		
Sepsis	0	0			0	0		
Convulsions	0	0			0	0		
Hypothermia	1/33	1/62	0.20	1.00	0	0		

Student's t-test or Mann-Whitney U-test was used for continuous variables, while Pearson's chi-square test was used for categorical variables. SGA, small for gestational age; CS, cesarean section; VD, vaginal delivery; PMA, postmenstrual age; PROM, premature rupture of the membranes; DM, diabetes mellitus; GDM, gestational diabetes mellitus; GH, gestational hypertension; PE, preeclampsia.

using Statistical Package for Social Science 24.0 (SPSS 24.0). Differences in the demographic and clinical data were compared between the final included and excluded infants, and differences in maturity and temporal properties of DFC were compared between the late preterm and term infants. For continuous variables, we used Student's *t*-test for parametric data and Mann-Whitney *U*-test for nonparametric data. Pearson's chi-square test was used to compare categorical variables. We also carried out Pearson's correlation analysis between altered temporal properties and indicators measuring the maturity (birth weight, gestational age, postmenstrual age) for all participants. Significance was set at a $P < 0.05$ in all tests.

TABLE 2 | Demographic characteristics.

	Late preterm	Term	t/χ^2	*P*-value
Number	34	37		
Gestational age (weeks)	35.93 ± 1.34	40.29 ± 1.06	−15.27	0.00*
Days after birth (days)	9.47 ± 2.02	9.62 ± 2.30	−0.29	0.77
Postmenstrual age (weeks)	37.28 ± 1.34	41.66 ± 1.13	−14.88	0.00*
Birth Weight (kg)	2.03 ± 0.41	3.27 ± 0.38	−13.38	0.00*

*Student's t-test or Mann-Whitney U-test was used for continuous variables, while Pearson's chi-square test was used for categorical variables. Significant results are marked with a *.*

RESULTS

Demographic and Clinical Characteristics

Recorded characteristics of all initially recruited infants were compared between the final included and excluded infants, including demographic characteristics such as gestational age, days of birth, and postmenstrual age when scanned, some maternal factors during pregnancy, and clinical data during hospitalization. No significant differences were found between them, as shown in **Table 1**. These results indicated that characteristics of the final included and excluded infants were roughly balanced. Then we compared the indicators measuring maturity between final included late term and term infants, which were significantly different between groups, including gestational age (preterm:35.93 ± 1.34, term:40.29 ± 1.06; $P = 0.00$), postmenstrual age when scanned (preterm: 37.28 ± 1.34, term:41.66 ± 1.13, $P = 0.00$), and birth weight (preterm: 2.03 ± 0.41, term: 3.27 ± 0.38, $P = 0.00$), as shown in **Table 2**.

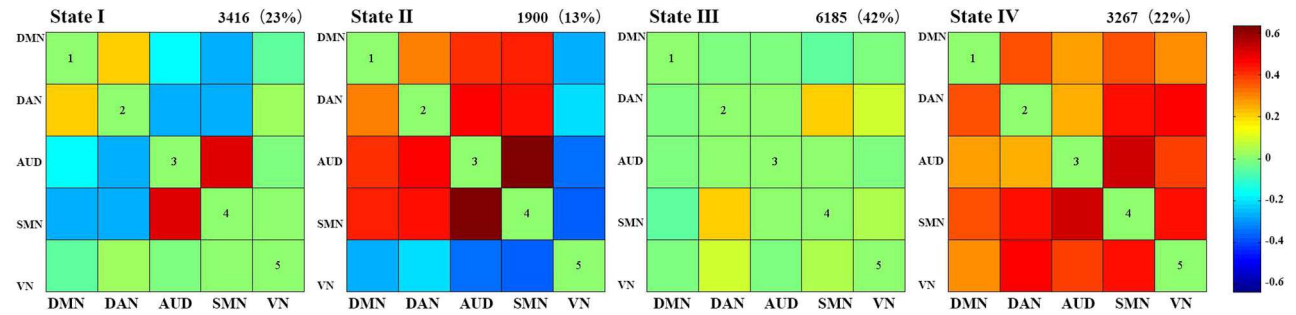

FIGURE 3 | Cluster centroids of each state. The total number of occurrences and percentage of total occurrences of each state are listed above each cluster. State I was dominated by weak connections except the connection between SMN and AUD, State II was characterized by relatively strong positive and negative connectivity, State III was characterized by general weak connectivity between networks, State IV demonstrated relatively strong positive connections across nearly all networks.

TABLE 3 | Temporal properties.

	Preterm	Term	*t*	*P*
Dwell time (State I)	10.36 ± 12.67	25.43 ± 33.07	−2.49	0.02*
Dwell time (State II)	14.83 ± 15.96	13.75 ± 34.18	0.17	0.87
Dwell time (State III)	33.57 ± 37.64	18.50 ± 11.71	2.24	0.03*
Dwell time (State IV)	22.12 ± 35.76	21.98 ± 47.00	0.01	0.99
Fractional windows (State I, %)	12.51 ± 17.24	32.89 ± 26.26	−3.89	0.00*
Fractional windows (State II, %)	13.05 ± 12.59	12.69 ± 20.56	0.09	0.93
Fractional windows (State III, %)	48.11 ± 25.69	36.16 ± 23.96	2.02	0.04*
Fractional windows (State IV, %)	26.33 ± 25.17	18.26 ± 26.34	1.32	0.19
Number of transitions	8.21 ± 3.91	8.57 ± 4.32	−0.37	0.71

*For continuous variables, student's t-test was used for parametric data and Mann-Whitney U-test was used for non-parametric data, significant results are marked with a *.*

Temporal Properties of Dynamic Connectivity in Each State

We identified four reoccurring state patterns of functional connectivity based on the k-means clustering method. As illustrated in **Figure 3**, State III, which was characterized by general weak connectivity, occurred most frequently in all states (42%), while State II, which was characterized by relatively strong positive and negative connectivity, occurred least frequently (13%). More specifically, State III portrayed wide-spread weak between-network connectivity among all identified networks, including DMN, DAN, AUD, SMN, and VN, suggesting a rather static functional activity in State III. Additionally, State I occurred in 23% and State IV in 22% of all the windows. State IV demonstrated relatively strong positive connections across nearly all networks, whereas State I was dominated by weak connections except the connection between SMN and AUD.

As shown in **Table 3**, the mean dwell time in State I and State III was significantly different between groups. Specifically, the late preterm group showed a significantly shorter mean dwell time in State I (preterm: 10.36 ± 12.67, term: 25.43 ± 33.07, $P = 0.02$), while a significantly longer mean dwell time in state III (preterm: 33.57 ± 37.64, term: 18.50 ± 11.71; $P = 0.03$). Notably, as shown in the violin plot in **Figure 5B**, some infants in the late preterm group spent extremely long time in State III, while no one in the term group did. As for the fractional windows, significant differences between groups were also identified in State I and State III. No significant group differences were identified in the mean dwell time or fractional windows in State II and State IV. The number of transitions was not significantly different between groups, either.

In summary, these changes indicated that the late preterm group switched states as frequently as the term infants, but they stay longer in State III than term infants. Since State III was characterized by general weak functional connectivity among all networks, it seemed that late preterm group preferred to stay in a more inactive state, compared with term neonates. Between-group comparison of cluster centroids of each state and the temporal properties of DFC were presented in **Figures 4**, **5**, respectively.

Correlation Between Clinical Data and DFC Properties

Correlation analysis was carried out to test whether the temporal properties of DFC were associated with the indicators measuring the maturity of included infants (gestational age, postmenstrual age, birth-weight). In line with our hypothesis, the mean dwell time and fractional time in State III showed a significant negative correlation with all these maturity indicators, whereas a positive correlation was found in state I, as shown in **Table 4**.

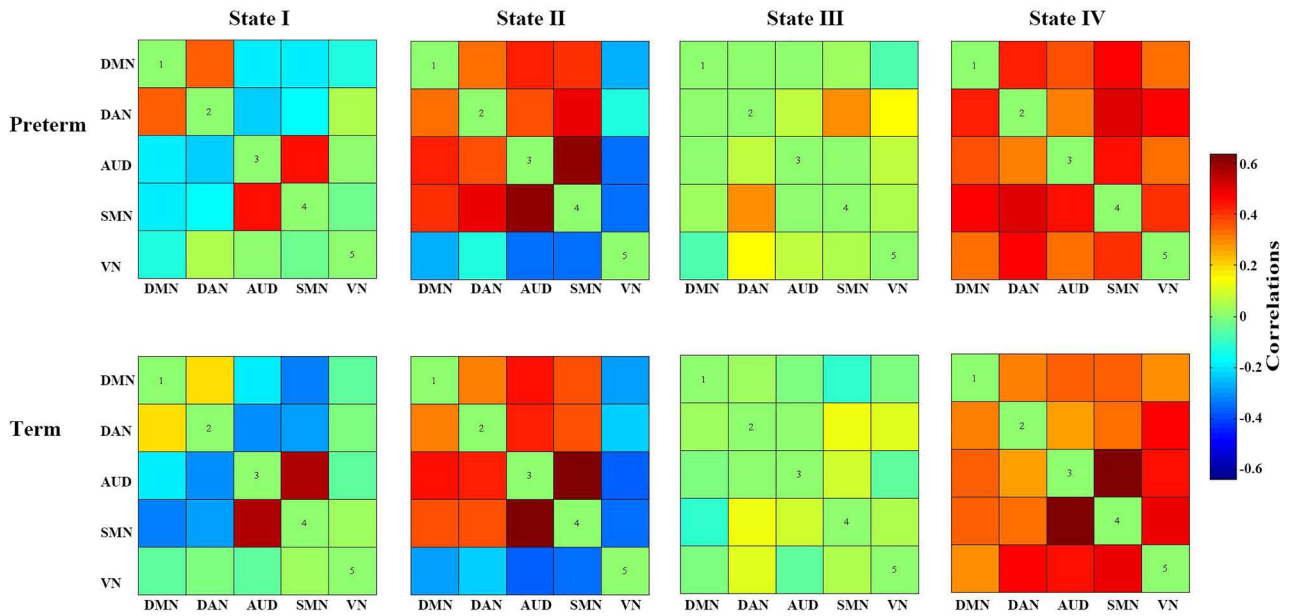

FIGURE 4 | Between-group comparison of cluster centroids of each state.

DISCUSSION

With increasing evidence emphasizing the neurodevelopmental problems faced by late preterm children (20), there is an increasing need to explore the possible underlying changes in their brains. Conventional brain MRI has the potential to detect even minor structural changes and help clinicians to make early diagnosis about premature brain injury. However, some late preterm infants without obvious structural changes also have developmental and emotional-behavioral problems in childhood and adolescence. Previous study has provided evidence for an aberrant structural and functional connectivity in preterm infants and a long-lasting impact of preterm birth on the organization of resting-state networks in school-aged children and adolescents (21, 22). Nonetheless, previous rs-fMRI studies of premature infants were mostly performed when they reached term equivalent age (23–25). As for the rapidly developing newborn brains, the best window for observing abnormalities may be missed. As far as we know, this is the first study that applied a DFC method to identify differences in the DFC properties between late preterm and term neonates, and the scanning time of all infants was from 34^{+6} to 43^{+2} weeks of postmenstrual age. Results demonstrated that a DFC approach can capture functional dynamics and reveal DFC characteristics in both term and late preterm brains across time.

In this study, we mainly focused on the temporal properties of the DFC, including the mean dwell time, fractional windows and the number of transitions. Besides, we investigated the association between these temporal properties and indicators measuring the maturity. Five networks (DMN, DAN, AUD, SMN, and VN) were found in included neonates, which demonstrates a much simpler constitution than the functional networks in adults. Based on identified networks, four connectivity states were found across all participants. Significant differences existed between groups in the time staying in State III, which was characterized by general weak connectivity. The result indicated the preference for a weak connectivity state in late preterm infants. In addition, the correlation analysis showed the degree of maturation was negatively correlated to the dwell time and fractional time in state III, whereas state I showed the opposite result. The late preterm group spent less time in State I, which was dominated by weak connectivity but relatively strong connectivity between SMN and AUD. However, cautions are needed when explaining the result about State I, since it contains negative connections, and the retest reliability of negative connections was questioned by a previous research (26).

Since functional connectivity of premature infants of different gestational age demonstrates different development stages out of the uterus, it is worth noting that in both groups, SMN shows a strong connectivity with AUD in all states except State I, which is in line with the regular sequence of neurodevelopment of this period. Previous studies have identified multiple RSNs incorporating cortical and subcortical gray matter regions, including those located in primary motor and sensory cortices (e.g., SMN, VN, AUD) and those involving association cortices (e.g., DMN, DAN, frontoparietal control) (23, 27, 28). It was reported that networks located in primary sensory and motor regions are established by term, and these networks demonstrate less variability between subjects (29). Our findings show that the connections between SMN and VN are strong in most of states in both late preterm and term group, which is consistent with the sequence of networks development identified by previous studies.

The causes and mechanisms of premature brain injury are so complex, so this study chose strict inclusion criteria to

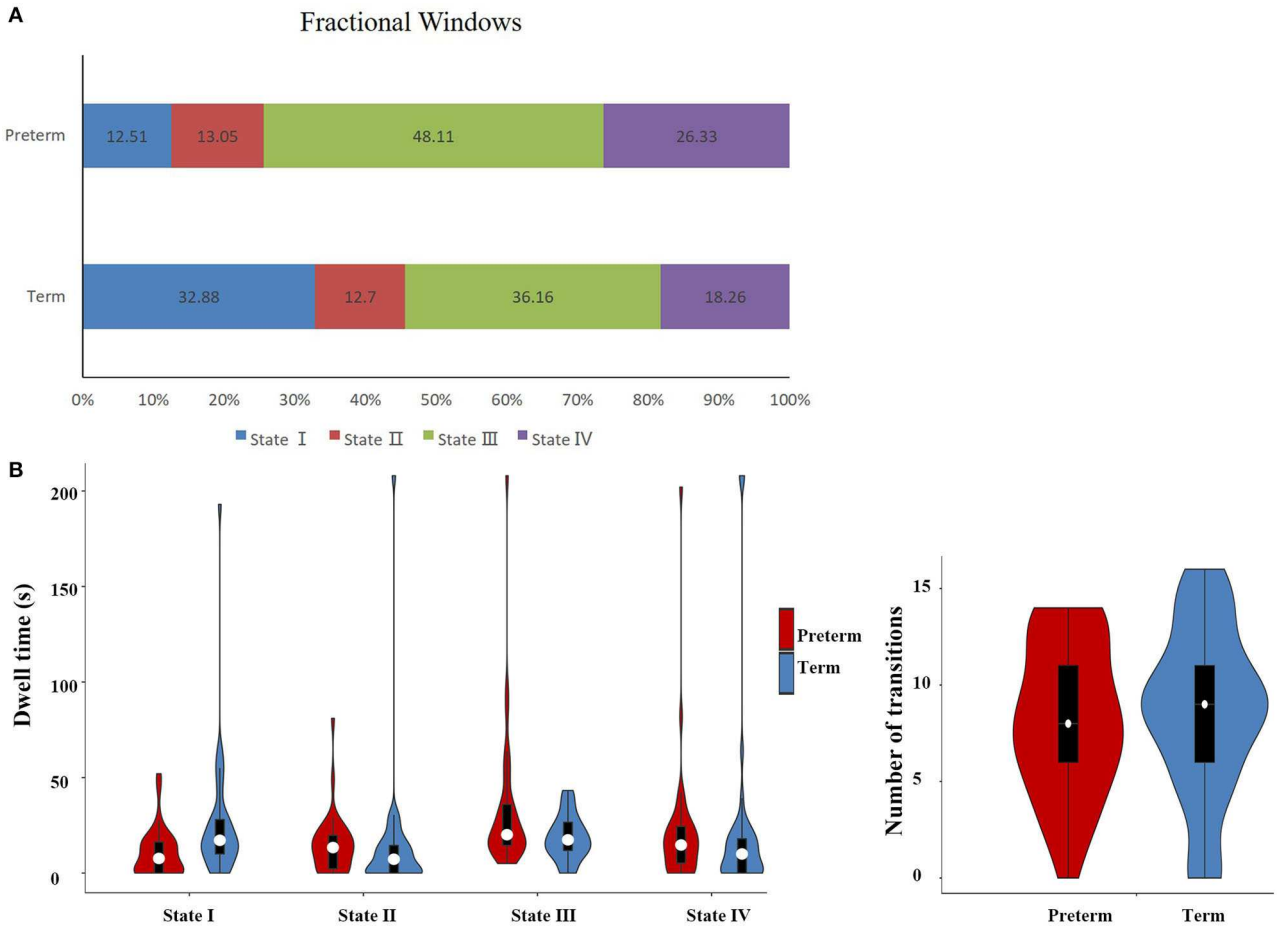

FIGURE 5 | Temporal properties of DFC states for the late preterm and term neonates. **(A)** Percentage of total time that all subjects spent in each state. **(B)** Mean dwell time and number of transitions between states were plotted using violin plots. The fractional windows and mean dwell time in State I and State III were significantly different between groups. It is worth noting that some infants in the late preterm group spent very long time in State III, while no one in the term group did.

make it possible to investigate one of the possible mechanisms. In addition, this study excluded infants with hemorrhage to simplify the research condition and facilitate the spatial normalization process. At the same time, this inclusion criteria may cause bias for the analysis, since preterm infants have a significantly higher chance of intracranial hemorrhage than term infants, which usually occurs within 72 h after birth and can lead to long-term neurological sequelae (30). Besides, a unique challenge was placed in image registration in infants, especially in those with brain injury. Specifically, due to the rapid changes in the size and cortical folding of brain in early life, notable heterogeneity exists in the registration process when we process data from neonates of different maturity. Our study included patients whose postmenstrual age is between 34^{+6} weeks and 43^{+2} weeks, and used the neonatal atlas for both term and late preterm infants. A narrower period for gestational-age specific atlas, such as 2–4 weeks, might make the spatial normalization more precise. In addition, we found some infants in the late preterm group spent extremely long time in State III, so the follow-up of neurodevelopment in these infants is very meaningful for they might have a higher chance of neurodevelopmental problems. But our study failed to perform reliable statistical analysis of the follow-up data due to the low completion rate of follow-up. However, though there is a lack of direct evidences to support the view that the length of time in State III is positively associated with neurodevelopment in the future, indirect evidences provided by previous studies of static functional connectivity indicate that preterm birth has persisting developmental effects on functional connectivity and motor performance in children, and altered static functional connectivity is related to motor development in childhood (31, 32). In addition, studies of DFC in adults have shown that the dwell time in a weakly connected state is associated with cognitive and intellectual impairment in a variety of neuropsychiatric disorders such as Parkinson's disease, autism and depression (33–35).

To conclude, this is the first study to assess dynamic connectivity properties in neonates. Compared to term neonates, the late preterm group shows a preference for

TABLE 4 | Correlations between DFC temporal properties and clinical characteristics.

		GA	PMA	BW
Dwell time (State I)	*r*	0.370	0.406	0.383
	P	0.001*	0.000*	0.001*
Dwell time (State II)	*r*	−0.109	−0.109	−0.079
	P	0.367	0.367	0.511
Dwell time (State III)	*r*	−0.338	−0.327	−0.292
	P	0.004*	0.005*	0.014*
Dwell time (State IV)	*r*	0.043	0.015	−0.049
	P	0.724	0.898	0.685
Fractional windows (State I, %)	*r*	0.529	0.558	0.508
	P	0.000*	0.000*	0.000*
Fractional windows (State II, %)	*r*	−0.114	−0.120	−0.059
	P	0.343	0.319	0.623
Fractional windows (State III, %)	*r*	−0.279	−0.285	−0.219
	P	0.018*	0.016*	0.067
Fractional windows (State IV, %)	*r*	−0.151	−0.169	−0.227
	P	0.209	0.158	0.057
Number of transitions	*r*	0.059	0.045	0.084
	P	0.627	0.712	0.485

*Pearson's correlation test was used, significant results are marked with a *. GA, gestational age; PMA, postmenstrual age; BW, birth-weight.*

a state with general weak connectivity and the length of time in that state is negatively correlated to the degree of maturity. We believe these findings provide new perspectives for understanding the state-dependent neurophysiological mechanisms in premature brain injury. However, due to unique challenges associated with neonatal neuroimaging acquisition and analysis, further targeted studies were needed in this high-risk population.

DATA AVAILABILITY STATEMENT

The datasets generated for this study are available on request to the corresponding author.

ETHICS STATEMENT

The studies involving human participants were reviewed and approved by Ethics Committee of Daping Hospital, Army Medical University (Chongqing, China). Written informed consent to participate in this study was provided by the participants' legal guardian/next of kin.

AUTHOR CONTRIBUTIONS

YS and XM: study design, analysis, interpretation of data, drafting, and revising the article. XW: acquisition of data. YS final approval of the version to be published and providing funding for the study. All authors: contributed to the article and approved the submitted version.

FUNDING

This study was supported by National Natural Science Foundation of China (Grant No. 81741065 to YS).

ACKNOWLEDGMENTS

We are grateful to all of the study participants and their families for their cooperation.

REFERENCES

1. Blencowe H, Cousens S, Oestergaard MZ, Chou D, Moller AB, Narwal R, et al. National, regional, and worldwide estimates of preterm birth rates in the year 2010 with time trends since 1990 for selected countries: a systematic analysis and implications. *Lancet.* (2012) 379:2162–72. doi: 10.1016/S0140-6736(12)60820-4
2. Salmaso N, Jablonska B, Scafidi J, Vaccarino FM, Gallo V. Neurobiology of premature brain injury. *Nat Neurosci.* (2014) 17:341–6. doi: 10.1038/nn.3604
3. Palumbi R, Peschechera A, Margari M, Craig F, Cristella A, Petruzzelli MG, et al. Neurodevelopmental and emotional-behavioral outcomes in late-preterm infants: an observational descriptive case study. *BMC Pediatr.* (2018) 18:318. doi: 10.1186/s12887-018-1293-6
4. Walsh BH, Inder TE. MRI as a biomarker for mild neonatal encephalopathy. *Early Hum Dev.* (2018) 120:75–9. doi: 10.1016/j.earlhumdev.2018.02.006
5. van den Heuvel MP, Sporns O. A cross-disorder connectome landscape of brain dysconnectivity. *Nat Rev Neurosci.* (2019) 20:435–46. doi: 10.1038/s41583-019-0177-6
6. Allen EA, Damaraju E, Plis SM, Erhardt EB, Eichele T, Calhoun VD. Tracking whole-brain connectivity dynamics in the resting state. *Cereb Cortex.* (2014) 24:663–76. doi: 10.1093/cercor/bhs352
7. Damaraju E, Allen EA, Belger A, Ford JM, McEwen S, Mathalon DH, et al. Dynamic functional connectivity analysis reveals transient states of dysconnectivity in schizophrenia. *Neuroimage Clin.* (2014) 5:298–308. doi: 10.1016/j.nicl.2014.07.003
8. Yang Z, Craddock RC, Margulies DS, Yan CG, Milham MP. Common intrinsic connectivity states among posteromedial cortex subdivisions: insights from analysis of temporal dynamics. *Neuroimage.* (2014) 93(Pt 1):124–37. doi: 10.1016/j.neuroimage.2014.02.014
9. Wang J, Wang X, Xia M, Liao X, Evans A, He Y. GRETNA: a graph theoretical network analysis toolbox for imaging connectomics. *Front Hum Neurosci.* (2015) 9:386. doi: 10.3389/fnhum.2015.00458
10. Hutchison RM, Womelsdorf T, Allen EA, Bandettini PA, Calhoun VD, Corbetta M, et al. Dynamic functional connectivity: promise, issues, and interpretations. *Neuroimage.* (2013) 80:360–78. doi: 10.1016/j.neuroimage.2013.05.079
11. Power JD, Barnes KA, Snyder AZ, Schlaggar BL, Petersen SE. Spurious but systematic correlations in functional connectivity MRI networks arise from subject motion. *Neuroimage.* (2012) 59:2142–54. doi: 10.1016/j.neuroimage.2011.10.018
12. Shi F, Yap P-T, Wu G, Jia H, Gilmore JH, Lin W, et al. Infant brain atlases from neonates to 1- and 2-year-olds. *PLoS ONE.* (2011) 6:e18746. doi: 10.1371/journal.pone.0018746
13. Calhoun VD, Adali T, Pearlson GD, Pekar JJ. A method for making group inferences from functional MRI data using independent component analysis. *Hum Brain Mapp.* (2001) 14:140–51. doi: 10.1002/hbm.1048

14. Erhardt EB, Rachakonda S, Bedrick EJ, Allen EA, Adali T, Calhoun VD. Comparison of multi-subject ICA methods for analysis of fMRI data. *Hum Brain Mapp.* (2011) 32:2075–95. doi: 10.1002/hbm.21170
15. Bell AJ, Sejnowski TJ. An information-maximization approach to blind separation and blind deconvolution. *Neural Comput.* (1995) 7:1129–59. doi: 10.1162/neco.1995.7.6.1129
16. Himberg J, Hyvärinen A, Esposito F. Validating the independent components of neuroimaging time series via clustering and visualization. *NeuroImage.* (2004) 22:1214–22. doi: 10.1016/j.neuroimage.2004.03.027
17. Calhoun VD, Adali T, Pearlson GD, Pekar JJ. Spatial and temporal independent component analysis of functional MRI data containing a pair of task-related waveforms. *Hum Brain Mapp.* (2001) 13:43–53. doi: 10.1002/hbm.1024
18. Allen EA, Erhardt EB, Damaraju E, Gruner W, Segall JM, Silva RF, et al. A baseline for the multivariate comparison of resting-state networks. *Front Syst Neurosci.* (2011) 5:2. doi: 10.3389/fnsys.2011.00002
19. Cordes D, Haughton VM, Arfanakis K, Wendt GJ, Turski PA, Moritz CH, et al. Mapping functionally related regions of brain with functional connectivity MR imaging. *Am J Neuroradiol.* (2000) 21:1636–44. Available online at: http://www.ajnr.org/content/ajnr/21/9/1636.full.pdf
20. Cheong JLY, Thompson DK, Olsen JE, Spittle AJ. Late preterm births: new insights from neonatal neuroimaging and neurobehaviour. *Semin Fetal Neonatal Med.* (2019) 24:60–5. doi: 10.1016/j.siny.2018.10.003
21. Rogers CE, Lean RE, Wheelock MD, Smyser CD. Aberrant structural and functional connectivity and neurodevelopmental impairment in preterm children. *J Neurodev Disord.* (2018) 10:38–38. doi: 10.1186/s11689-018-9253-x
22. Wehrle FM, Michels L, Guggenberger R, Huber R, Latal B, O'Gorman RL, et al. Altered resting-state functional connectivity in children and adolescents born very preterm short title. *NeuroImage Clin.* (2018) 20:1148–56. doi: 10.1016/j.nicl.2018.10.002
23. Smyser CD, Snyder AZ, Shimony JS, Mitra A, Inder TE, Neil JJ. Resting-state network complexity and magnitude are reduced in prematurely born infants. *Cereb Cortex.* (2016) 26:322–33. doi: 10.1093/cercor/bhu251
24. Weinstein M, Ben-Sira L, Moran A, Berger I, Marom R, Geva R, et al. The motor and visual networks in preterm infants: an fMRI and DTI study. *Brain Res.* (2016) 1642:603–11. doi: 10.1016/j.brainres.2016.04.052
25. Tortora D, Severino M, Di Biase C, Malova M, Parodi A, Minghetti D, et al. Early pain exposure influences functional brain connectivity in very preterm neonates. *Front Neurosci.* (2019) 13:899. doi: 10.3389/fnins.2019.00899
26. Fox MD, Snyder AZ, Vincent JL, Corbetta M, Van Essen DC, Raichle ME. The human brain is intrinsically organized into dynamic, anticorrelated functional networks. *Proc Natl Acad Sci USA.* (2005) 102:9673–8. doi: 10.1073/pnas.0504136102
27. Smyser CD, Snyder AZ, Shimony JS, Blazey TM, Inder TE, Neil JJ. Effects of white matter injury on resting state fMRI measures in prematurely born infants. *PLoS ONE.* (2013) 8:e68098. doi: 10.1371/journal.pone.0068098
28. Smyser CD, Wheelock MD, Limbrick DD Jr, Neil JJ. Neonatal brain injury and aberrant connectivity. *NeuroImage.* (2019) 185:609–23. doi: 10.1016/j.neuroimage.2018.07.057
29. Gao W, Elton A, Zhu H, Alcauter S, Smith JK, Gilmore JH, et al. Intersubject variability of and genetic effects on the brain's functional connectivity during infancy. *J Neurosci.* (2014) 34:11288–96. doi: 10.1523/JNEUROSCI.5072-13.2014
30. Su B-H, Lin H-Y, Huang F-K, Tsai M-L, Huang Y-T. Circulatory management focusing on preventing intraventricular hemorrhage and pulmonary hemorrhage in preterm infants. *Pediatr Neonatol.* (2016) 57:453–62. doi: 10.1016/j.pedneo.2016.01.001
31. Damaraju E, Phillips JR, Lowe JR, Ohls R, Calhoun VD, Caprihan A. Resting-state functional connectivity differences in premature children. *Front Syst Neurosci.* (2010) 4:23. doi: 10.3389/fnsys.2010.00023
32. Wheelock MD, Austin NC, Bora S, Eggebrecht AT, Melzer TR, Woodward LJ, et al. Altered functional network connectivity relates to motor development in children born very preterm. *Neuroimage.* (2018) 183:574–83. doi: 10.1016/j.neuroimage.2018.08.051
33. Díez-Cirarda M, Strafella AP, Kim J, Peña J, Ojeda N, Cabrera-Zubizarreta A, et al. Dynamic functional connectivity in Parkinson's disease patients with mild cognitive impairment and normal cognition. *Neuroimage Clin.* (2018) 17:847–55. doi: 10.1016/j.nicl.2017.12.013
34. Fiorenzato E, Strafella AP, Kim J, Schifano R, Weis L, Antonini A, et al. Dynamic functional connectivity changes associated with dementia in Parkinson's disease. *Brain.* (2019) 142:2860–72. doi: 10.1093/brain/awz192
35. Yao Z, Shi J, Zhang Z, Zheng W, Hu T, Li Y, et al. Altered dynamic functional connectivity in weakly-connected state in major depressive disorder. *Clin Neurophysiol.* (2019) 130:2096–104. doi: 10.1016/j.clinph.2019.08.009

Conflict of Interest: The authors declare that the research was conducted in the absence of any commercial or financial relationships that could be construed as a potential conflict of interest.

frontiers in Neurology

REVIEW
published: 14 August 2020
doi: 10.3389/fneur.2020.00862

Respiratory Support of the Preterm Neonate: Lessons About Ventilation-Induced Brain Injury From Large Animal Models

Kyra Y. Y. Chan[1,2], *Suzanne L. Miller*[1,2], *Georg M. Schmölzer*[3,4], *Vanesa Stojanovska*[1,2†] *and Graeme R. Polglase*[1,2*†]

[1] The Ritchie Centre, Hudson Institute of Medical Research, Clayton, VIC, Australia, [2] Department of Obstetrics and Gynecology, Monash University, Clayton, VIC, Australia, [3] Neonatal Research Unit, Centre for the Studies of Asphyxia and Resuscitation, Royal Alexandra Hospital, Edmonton, AB, Canada, [4] Department of Pediatrics, University of Alberta, Edmonton, AB, Canada

OPEN ACCESS

Edited by:
Francisco J. Alvarez,
Hospital de Cruces, Spain

Reviewed by:
Ting Guo,
Hospital for Sick Children, Canada
Donna M. Ferriero,
University of California, San Francisco, United States

***Correspondence:**
Graeme R. Polglase
graeme.polglase@monash.edu

[†]These authors have contributed equally to this work

Specialty section:
This article was submitted to Pediatric Neurology, a section of the journal Frontiers in Neurology

Received: 10 February 2020
Accepted: 07 July 2020
Published: 14 August 2020

Citation:
Chan KYY, Miller SL, Schmölzer GM, Stojanovska V and Polglase GR (2020) Respiratory Support of the Preterm Neonate: Lessons About Ventilation-Induced Brain Injury From Large Animal Models. Front. Neurol. 11:862. doi: 10.3389/fneur.2020.00862

Many preterm neonates require mechanical ventilation which increases the risk of cerebral inflammation and white matter injury in the immature brain. In this review, we discuss the links between ventilation and brain injury with a focus on the immediate period after birth, incorporating respiratory support in the delivery room and subsequent mechanical ventilation in the neonatal intensive care unit. This review collates insight from large animal models in which acute injurious ventilation and prolonged periods of ventilation have been used to create clinically relevant brain injury patterns. These models are valuable resources in investigating the pathophysiology of ventilation-induced brain injury and have important translational implications. We discuss the challenges of reconciling lung and brain maturation in commonly used large animal models. A comprehensive understanding of ventilation-induced brain injury is necessary to guide the way we care for preterm neonates, with the goal to improve their neurodevelopmental outcomes.

Keywords: ventilation, respiratory support, ventilation-induced brain injury, neurodevelopment, preterm

INTRODUCTION

Respiratory support is a necessary life-saving intervention which has been associated with brain injury, especially in preterm neonates. Preterm birth, defined as birth prior to 37 completed weeks of gestation, is a major cause of perinatal mortality and morbidity (1, 2). Almost 1 million preterm infants who survive the neonatal period suffer adverse neurodevelopmental outcomes (1) which, in addition to an individual burden, imposes enormous financial and social costs to their families and society. Many complications associated with prematurity are due to an interruption of normal organ development that would otherwise proceed to term *in utero*. For this reason, the distinction of babies by gestational age (GA) at birth—extremely preterm (<28 weeks), very preterm (28–<32 weeks), and moderate to late preterm (32–<37 weeks)—helps to identify infant populations which are most at risk of complications related to preterm birth (3). Notably, the lungs of very and extremely preterm infants are often too immature to provide adequate respiratory function required to sustain extrauterine life.

The lower the GA of the infant at birth, the less mature the lungs are, and the higher the requirement for respiratory support. An estimated 2.4 million babies are born very and extremely preterm worldwide each year (3) and ∼60–95% of these infants will require respiratory support during their neonatal period (2, 4–7). At the same time, the brains of these infants who require respiratory support are at a vulnerable stage of development and prone to injury. It is this combination of high requirements for respiratory support and the heightened vulnerability of their immature brains that increases the risk of ventilation-induced brain injury (VIBI) in extremely preterm infants.

Importantly, VIBI is likely to ensue as early as when respiratory support commences in the delivery room. Depending on GA, ∼34–85% of preterm infants require intubation and positive pressure ventilation (PPV) to establish lung aeration immediately after birth (2, 8–10). These statistics exclude non-invasive forms of ventilation, meaning the total percentage of preterm infants who need respiratory support immediately after birth is substantially higher. Despite this high requirement, the limitations of equipment used in delivery suites mean that a significant proportion of babies receive inappropriate pressures or tidal volumes (V_T) (11, 12), which can initiate pathways leading to VIBI (13). Subsequent to this, the duration of ventilatory support in the neonatal intensive care unit (NICU) is proportional to the risk of neurodevelopmental impairment and disorders (5, 14).

Respiratory support exacerbates key pathways of preterm brain injury: (1) cerebral inflammation and (2) cerebral hemodynamic instability (13, 15, 16), meaning ventilated preterm infants are in the unfortunate position of double jeopardy and are at an increased risk of brain injury. The nature of VIBI is not fully understood because it is difficult to determine clinically if brain injury is attributed solely or predominantly to ventilation. It is in this background that large animal models have played a vital role in improving our understanding of the pathogenesis of VIBI and to aid development of therapies.

In this review we will explore the issue of VIBI, how large animal models have been utilized to investigate VIBI, and the value of these models to develop much-needed therapies.

PRETERM BIRTH, THE REQUIREMENT FOR RESPIRATORY SUPPORT, AND HOW THIS MAY BE INJURIOUS

Prematurity is the key contributor to the need for respiratory support in newborns. The majority of extremely preterm newborns will require respiratory support due to inadequate alveolarization, insufficient surfactant production, and impaired lung liquid clearance, together with reduced respiratory drive, weak chest muscles and flexible ribs (16, 17).

Our improved understanding of respiratory transition and lung function from fetal to newborn life has led to significant advances in neonatal respiratory care, many of which aim to reduce the risk of chronic lung diseases and adverse neonatal outcomes. Despite this, a significant proportion of preterm infants still develop long-term pulmonary and neurodevelopmental morbidities due to ventilation-induced injury. Various methods of respiratory support (e.g., nasal continuous positive airway pressure, PPV via face mask or endotracheal tube) have been linked to cerebral inflammation and neuropathologies in preterm infants, including cystic periventricular leukomalacia, diffuse white matter injury and intraventricular hemorrhage (IVH) (14, 18–21). It is essential to clarify and address the effect ventilation has on the preterm infant.

Positive Pressure Ventilation in the Delivery Room

Most infants can independently transition from a fetus to a newborn, but many preterm infants will require assistance for this physiologically challenging process. Neonatal transition involves cardiovascular adaptations and, more importantly, respiratory adaptations since the newborn is no longer supported by the placenta for oxygenation (17). Infants who cannot spontaneously breathe at birth will require PPV which is usually first delivered non-invasively via a facemask, and infants who are still unable to initiate stable respiration are intubated (22, 23). Extremely preterm infants may be electively intubated in the delivery room in some centers although it has been suggested that individualized intubation strategies after establishing respiratory failure may be better to reduce morbidities (24, 25), given that the process of intubation may itself be injurious and is associated with neurodevelopmental impairments (26).

A significant proportion of very and extremely infants require intubation in the delivery room. Despite decreasing percentages of infants requiring intubation in the delivery room over the past decades (7, 10), a staggering 31.6–77.7% of very low birth weight (VLBW) and/or extremely preterm infants continue to require this invasive intervention (2, 7, 9, 10). Early PPV in the delivery room has been associated with the development of severe IVH (20, 21). VLBW infants, mostly born extremely preterm, who received PPV in the delivery room had a nearly 3-fold increased likelihood of severe IVH (grades III and IV) than infants who did not receive PPV (20). However, it could be that the infants who require higher levels of intervention are sicker and more vulnerable to brain injury to begin with, hence it is challenging to accurately determine the extent to which advanced resuscitation is causal in the progression of brain injury in these infants.

Importantly, despite the high requirement of PPV in the delivery room, it is likely the least controlled respiratory support a neonate will ever receive, and this has proven to be inadvertently injurious to the immature brain (11, 13, 21). Current neonatal resuscitation guidelines in the delivery room rely on visual assessment of chest rise to deliver an adequate V_T during PPV where pressure monitoring is unavailable (23, 27, 28). Besides being subjective, the ability to observe changes in chest wall movement is reduced when a preterm infant is covered to maintain body temperature during delivery room resuscitation, stabilization, and transportation (27). It is challenging even for experienced clinicians to accurately estimate the V_T delivered (11, 28) and a noticeably expanded chest wall from PPV may itself be a sign of lung overdistension. Excessively high V_T causes

volutrauma—a major cause of lung inflammation and injury (16, 29–32). Together, these factors contribute to a suboptimal ventilation situation that leads to injury of the lung and, consequently, the brain. Indeed, the use of excessive V_T has dire consequences on the immature brain. Preterm infants <29 weeks GA who received unintentional high V_T ventilation (>6 ml/kg, where median normal V_T is 4.2–5.8 ml/kg) in the delivery room had a nearly 4-fold higher incidence of IVH than infants who received normal V_T (<6 ml/kg; 51% vs. 13%) (21, 33).

Other mechanisms by which PPV leads to lung injury are barotrauma (e.g., high airway pressure), atelectrauma (e.g., repeated opening and closing of collapsed airways), and biotrauma (30–32, 34). Systemic inflammation secondary to lung injury can also initiate cerebral inflammation which is a major cause of brain injury. Inappropriate ventilation pressures and volumes can also trigger the hemodynamic pathway of injury to cause hemorrhagic brain injury (13).

Mechanical Ventilation in the Neonatal Intensive Care Unit

Preterm infants often continue to require respiratory support after transfer to the NICU. In Australia and New Zealand, up to 95.0% of very and extremely preterm babies (<32 weeks GA) and 91.3% of moderate to late preterm infants (32–36 weeks GA) needed assisted ventilation in the NICU, with each baby receiving on average 8.8 days of assisted ventilation (2). A cohort study in South Korea reported that 38.5% of VLBW preterm infants received >7 days of mechanical ventilation (35). Importantly, the trends for long-term respiratory support in preterm infants do not seem to be decreasing (2, 36).

Prolonged periods of mechanical ventilation increases the risks of IVH (4, 22), periventricular leukomalacia or white matter injury (4, 6, 19, 35, 37), cerebral palsy (14), and attention deficit hyperactivity disorder (14) in preterm infants. In a retrospective analysis of extremely low birth weight infants, most of whom were extremely preterm, only 24% of infants who were ventilated for ≥60 days and 7% of those ventilated for ≥90 days survived without neurodevelopmental impairments (5). All infants who had been ventilated for ≥120 days and survived suffered some form of neurodevelopmental impairment (5).

Compared to the initiation of PPV in the delivery room, PPV in the NICU is much more controlled with sophisticated equipment and vigilant monitoring of ventilation parameters (38). The precise cause of VIBI in this setting has not been thoroughly investigated, with additional confounding factors such as analgesia and anesthetics (39–41), oxygenation (19), and a plethora of other NICU interventions for a range of primary and/or secondary complications that need to be considered. However, it is known that the duration of ventilation is an important determinant of neurodevelopmental morbidities (5, 19, 42).

Attempts to shift management encouraging earlier extubation or less invasive ventilation strategies have not translated to improved neurological outcomes in preterm infants (43). Furthermore, limiting the duration of mechanical ventilation to reduce complications is not always feasible with preterm infants. Therefore, it is imperative to devise treatments for unavoidable brain injury from prolonged respiratory support.

USING ANIMAL MODELS TO INVESTIGATE VENTILATION-INDUCED BRAIN INJURY

Clinical observations discussed above underpin the need to understand mechanisms through which respiratory support causes brain injury, to allow focused clinical strategies or new therapies aimed at improving outcomes. However, such investigations are not necessarily achievable in preterm infants since respiratory support cannot be studied in isolation. Herein lies the value of using animals for comprehensive characterization of VIBI through imaging, physiological, immunohistochemical, and molecular techniques. Animals can also be used to model various conditions such as growth restriction and chorioamnionitis to more closely interrogate VIBI under conditions of compromised pregnancies.

Studies using large animals, most often sheep, to model ventilation-induced injury can be categorized by experimental technique (fetal [head-out or *in utero* ventilation] or neonatal ventilation) and period/duration of ventilation (acute or chronic) (**Figure 1**). These different experimental techniques enable replication of specific scenarios of preterm respiratory support, including the initial resuscitation in the delivery room and prolonged care in the NICU. However, with all models, an understanding of the strengths and limitations is essential for appropriate interpretation of the findings and potential replication in clinical trials.

Balance Between Lung and Brain Development in Large Animal Models

An inevitable limitation to using large animals to model neonatal conditions is the difference in developmental milestones of major organ systems and physiology compared to humans. The animal's age cannot be chosen based on gestation duration alone since an animal at 0.65 gestation is not necessarily developmentally equivalent to a human at 0.65 gestation. Instead, the crucial factor is the stage of development of the organ of interest. This proves challenging for models of VIBI as the developmental milestones of both the brain and lungs must be considered. Detailed comparisons of species-specific lung development and anatomical features have previously been compiled (44–46) and comparisons for brain development are summarized in **Table 1**. This presents a conundrum: how do we balance desired stage of brain development with lung maturation?

Non-human primate studies have used baboons (*Papio papio*; *Papio cynocephalus*) delivered at 125 days (term is 185 days; 0.68 gestation) which have similar lung development to an infant born at 26 weeks preterm age (44). At this stage, brain development is comparable to that of a 26–28 week-old extremely preterm human infant (51). While these developmental stages are congruent, there are significant technical challenges as well as practical, financial and ethical concerns associated with the use of non-human primates (62). Thus, even though they are the closest animal models to humans and offer vital insights to

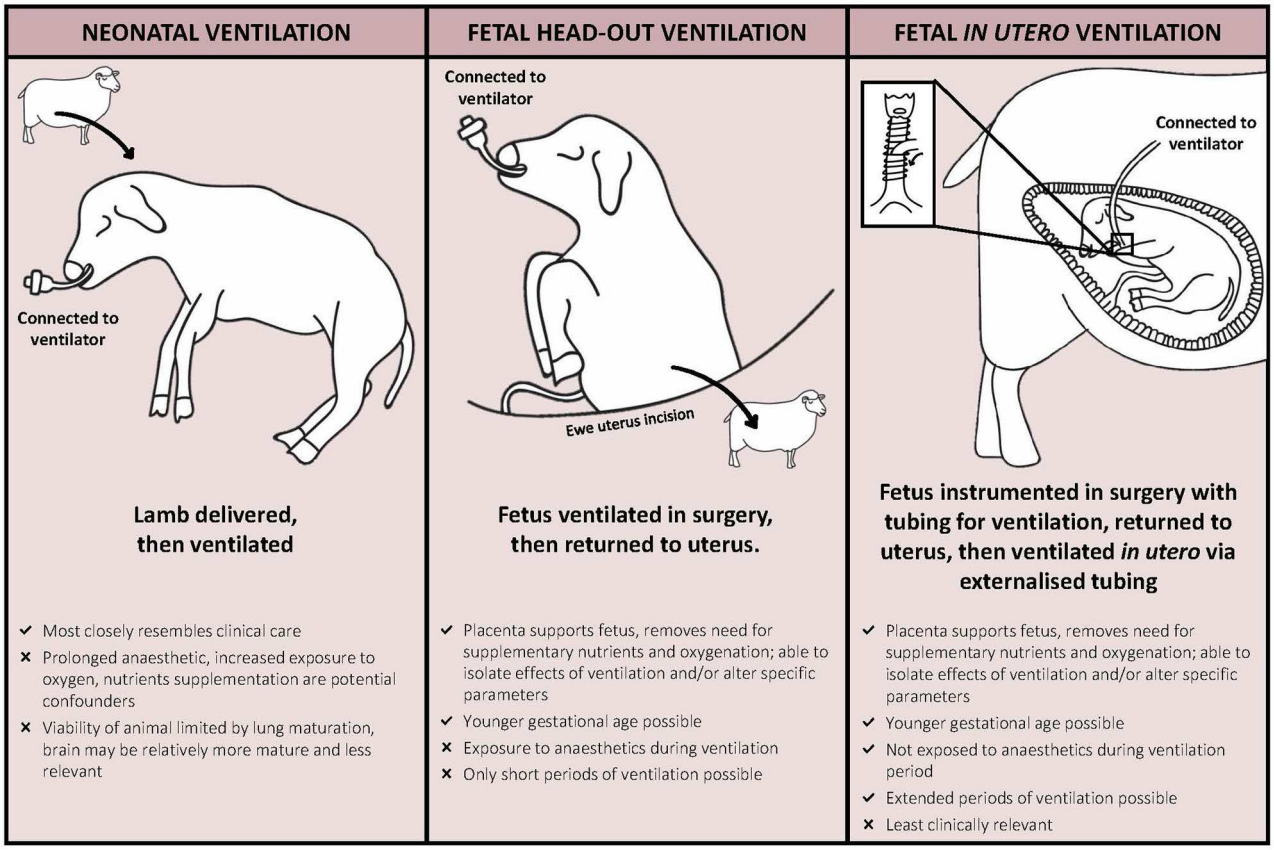

FIGURE 1 | Experimental models of ventilation-induced injury in sheep outlining the major advantages and disadvantages of each model.

developmental studies (62), non-human primate models of VIBI are relatively less commonly pursued.

Piglets (*Sus scrofa*) have been proposed to be suitable for studying neurodevelopment and cerebral consequences of early life insults (63). A piglet at 91–94 days gestation (term is 115 days; 0.8 gestation) is physiologically similar to a 23–25 week extremely preterm infant in terms of lung development and the requirement for respiratory support for survival (64). Neurodevelopment of the piglet at this GA is slightly more mature, comparable instead to a moderate to late preterm human infant (63, 65). Besides this developmental mismatch, there are significant challenges in performing fetal surgery and chronic instrumentation in pigs due to relatively large litters and the large size of the sow. Hence, piglets have not been widely used in VIBI studies that require these techniques. The suitability of piglets in postnatal ventilation studies for VIBI has not been extensively explored.

Similarly, brain maturation in sheep (*Ovies aries)* advances more rapidly in late gestation than development of the lungs, relative to humans. Previous studies in preterm lambs that have investigated VIBI were performed at the earliest GA at which the lambs were viable with respiratory support [125 days where term is 148 days; 0.85 gestation; structural lung development comparable to a 26–28 week human infant (46, 66)]. However, a limitation is that the fetal sheep brain development at 125 days gestation is comparable to a late preterm or term human fetus on the basis of white matter maturation (60, 61). Studies using lambs at this gestation have investigated the effect of respiratory support for up to 4 weeks on chronic lung injury (67), but have only looked at VIBI up to 24 h of ventilation (68).

Modeling of Acute VIBI

Animal studies to date have focused on VIBI downstream of lung injury resulting from volutrauma in the delivery room. The rationale behind these studies is that clinical findings have shown that variable V_T during delivery room resuscitation can be outside recommended limits (11, 12, 69).

Observed V_T during mask ventilation can range from 0 to 31 ml/kg (11, 12, 69) and V_T during endotracheal tube ventilation has been reported to be 3.9–9.6 ml/kg (12). The upper ranges of these V_T are higher than the recommended 4–8 ml/kg for very and extremely preterm infants (11). This is critical as we have known for decades that as few as six manual inflations of high V_T (35–40 ml/kg) are enough to induce injury in immature, surfactant-deficient lungs of preterm lambs (70). Sheep studies that have investigated acute VIBI have similarly found that brief periods of high V_T ventilation resulted in detectable brain injury as early as 90 min after ventilation onset (13, 15, 16, 71–73). Importantly, even if recommended V_T is delivered, the act of

TABLE 1 | Comparative gestational ages for key brain development processes in the human, baboon, and sheep.

Developmental process	Human (term 40 weeks)	Baboon (term 185 days)	Sheep (term 148 days)
Weight			
Growth spurt	26–28 wk	125–140 d	85–100 d
Cortical folding			
Primary	*ev* 26–28 wk	*ev* 125 d	*ev* 71–89 d
Secondary	*ev* 32–34 wk	*ev* 140 d	n.d.
Tertiary	*ev* 40–44wk	*ev* 160 d	n.d.
Six distinct cortical layers	ev 28 wk	*ev* 125 d	*ev* 89 d
Neurogenesis and Gliogenesis			
Main neuronal multiplication	10–15 wk	n.d.	40–80 d
Main glial multiplication	36–40 wk	n.d.	95–130 d
Myelination			
Periventricular white matter (preOL predominant)	23–28 wk	n.d.	93–99 d
Internal capsule	*ev* 32 wk	*ev* 125 d	*ev* 78–96 d
Superior temporal gyrus	Mature at 48 wk	Moderate at 160 d	n.d.
Cerebellum	*ev* 28 wk	*ev* 125 d	*ev* 80 d

d, days; ev. evident at; n.d., not determined; OL, oligodendrocytes; wk. weeks.
Note that there is often heterogeneity in development not just between different regions in the brain, but within each region. Compiled from refs human and cross-species comparisons (19, 47–50), baboon (51–53), sheep (54–61).

respiratory support in itself can activate an immune response in immature respiratory units (30, 31, 34).

To isolate this initial period of injurious respiratory support, akin to poorly regulated V_T in the delivery room, sheep studies have employed an acute high V_T ventilation strategy: 15 min injurious ventilation with stepwise increments of V_T to achieve a high target V_T of 10–15 ml/kg, which is 2–3 times the normal V_T of lambs for that GA (125 days of term 148 days; ∼5–7 ml/kg) (13, 15, 16, 71–73). Thereafter, lambs are sustained on appropriate respiratory support (neonatal model) or returned to the uterus (head-out model) to allow for the inflammation and injury pathways to manifest into gross lung/brain injury. These studies have provided valuable information on the pathology and mechanisms of acute VIBI (discussed in section Understanding VIBI From Injurious Respiratory Support in the Delivery Room).

Chronic Models of VIBI

The majority of animal models used to model VIBI are acute, focusing on the initial hours after birth. This is mainly due to inherent problems with maintaining animals for long periods of time. In particular, the problem with maintaining respiratory support for long periods of time in newborn animal models is the inability to control for specific factors, due to the need to introduce increasing levels of neonatal intensive care—akin to that of looking after a chronically ventilated preterm infant. To get around this problem, animal models have utilized respiratory support via a head-out approach or entirely *in utero* (**Figure 1**). Using these techniques, the intact placental circulation manages nutrition and gas exchange of the fetus, allowing subtle mechanisms of respiratory support to be examined. In the head-out approach, the fetal head and chest are exteriorized, the fetus is intubated and ventilation with various strategies altering delivered volume, pressures, respiratory frequencies, or oxygen content, and then returned to the uterus (74–78). *In utero* ventilation (IUV) studies require the fetus to be exteriorized and instrumented with ventilation tubes and equipment required for monitoring prior to being returned to the uterus. After a recovery period for the ewe and fetus, the fetus is ventilated via the externalized ventilation tubes for various times, although to date the longest has been 12 h (79–81). IUV has been used in fetal sheep to study cardiopulmonary physiology (82, 83), lung mechanics (84), and ventilation-induced lung injury (79, 81, 85). While cerebral physiological responses to IUV have been investigated previously (86), histopathology of brain injury after IUV has not been reported.

It is obvious that these *in utero* models are not designed with the intention to replicate clinical situations given that prolonged neonatal studies are more reflective of current clinical care. Instead, they provide the opportunity to manipulate specific ventilatory parameters in isolation so that we can better understand the contribution of a sole variable to lung and brain injury. Importantly, the IUV model allows ventilation of a fetus at a younger gestation than would be viable postnatally. This is advantageous, especially in ovine models, as the stage of brain development will be more comparable to that of extremely preterm infants.

UNDERSTANDING VIBI FROM INJURIOUS RESPIRATORY SUPPORT IN THE DELIVERY ROOM

Animal Studies That Investigate Pathology of VIBI

Studies in preterm lambs have characterized acute white matter changes following 15 min of injurious high V_T ventilation

(13, 15, 16, 71–73, 87, 88). High V_T ventilation causes a robust pulmonary inflammatory response which increases systemic and cerebral inflammation, characterized by elevated IL-6 and IL-8 messenger ribonucleic acid (mRNA) levels in the periventricular and subcortical white matter of the brain in ventilated preterm lambs (15, 73, 87). Increased microglial activation and aggregation, and a higher incidence of vascular protein extravasation (indicative of a compromised blood-brain barrier) and cerebral hemorrhage in the same regions were also observed (15, 73, 88). Injurious ventilation did not alter expression of myelin basic protein (MBP; oligodendrocyte marker) in the internal capsule or neuronal nuclei (NeuN; neuron marker) in the thalamus (89) and did not increase inflammation or injury in gray matter (90).

Importantly, pathology resultant from injurious ventilation can be visualized using non-invasive imaging such as magnetic resonance imaging (MRI) (72, 77, 91) and correlated with histopathology (89). Magnetic resonance spectroscopy (MRS) detected acute changes in brain metabolite peak-area ratios (Lactate/Creatine and Lactate/Choline) in preterm lambs that received high V_T although macroscopic injury was absent in structural MR images (T1, T2) (72). Alterations in MRS-detected metabolite levels relate to neuronal damage and potentially predict subsequent neurodevelopmental impairments (92, 93). Notably, these MRS changes were observed within 90 min of ventilation onset (72). Recent findings suggest that MRS-detectable changes persist 24 h after injurious ventilation (77). Diffusion tensor imaging (DTI) perhaps offers the most sensitive measures of early brain injury. DTI detected decreased diffusivity measures in the frontal white matter (axial, radial, and mean) and internal capsule (axial) in preterm lambs 24 h after injurious ventilation (77). These parameters have been suggested to correlate with myelination deficits (77).

Mechanistic Insight From Animal Studies

Several explanations have been put forward to link ventilation and brain injury. Studies in ventilated preterm lambs have identified two major pathways of acute VIBI: cerebral inflammation and hemodynamic instability (13, 15, 16, 77). Both pathways are proposed to be downstream effects of the pulmonary consequences following ventilation (13, 15, 16). Incidentally, these key VIBI pathways mirror those of preterm brain injury—suggesting compounded risk of injury in preterm infants. These mechanisms have been reviewed previously (13).

Briefly, the inflammatory pathway of VIBI involves upregulation of pro-inflammatory cytokines (e.g., IL-6, IL-8) and activation of microglia and astrocytes within the developing white matter of the brain (94). Injurious ventilation initiates a profound pulmonary inflammatory response caused by volutrauma, barotrauma, atelectrauma, and/or biotrauma (30–32, 34). This inflammatory cascade is associated with systemic inflammation and subsequent localized inflammation and injury in the white matter involving glia cells (13, 15, 16). Activated microglia and astrocytes are thought to mediate the destruction of cells in the oligodendrocyte lineage, contributing to hypomyelination and diffuse white matter injury that can underlie long-term neurological sequelae such as cerebral palsy (94, 95).

The hemodynamic pathway of injury refers to significant alterations, caused by PPV and atypical to hemodynamic changes during the transition at birth, to pulmonary blood flow and consequently cardiac output and cerebral blood flow (CBF) (15, 16). During PPV, applying a high pressure into the airways decreases pulmonary capillary transmural pressure, causing compression of intra-alveolar capillaries, hence increasing capillary resistance and decreasing pulmonary blood flow (13, 16). This reduces pulmonary venous return, left ventricular output, and accordingly alters CBF (13, 15, 16). Arterial blood pressure variability within a physiological range is not usually a problem because it is compensated by pressure-flow autoregulation to sustain a stable CBF. This involves constriction and dilation of arteries to alter cerebral vasculature resistance in response to changing perfusion pressures (96). The autoregulatory plateau, bounded by lower and upper limits of arterial pressure, has been postulated to be narrower in preterm infants with decreasing GA (96–98). Moreover, it has been suggested that preterm delivery or treatments reflective of clinical care of the preterm infant, including mechanical ventilation, affects cerebral autoregulation (99). Prolonged CBF fluctuations for more than 10 to 20 s has been defined as cerebral hemodynamic instability (100). The initiation of ventilation in preterm lambs caused CBF instability in the initial 15 min, even when a gentle strategy was used (71); the variability in CBF amplified when an injurious high V_T strategy was used (15). Clinically, 91% of babies with respiratory distress syndrome who had fluctuating CBF after 12 h of life subsequently had an IVH (101), highlighting the critical importance of preventing fluctuations in hemodynamics immediately after birth.

The relative contribution of each pathway toward the progression of white matter injury discussed in section Animal Studies That Investigate Pathology of VIBI is unknown although a recent study suggests that the hemodynamic pathway has an additive effect on the inflammatory pathway on injury progression, but the inflammatory pathway seems to dominate (77).

UNDERSTANDING VIBI FROM VENTILATION IN THE NEONATAL INTENSIVE CARE UNIT

Ventilation studies in preterm baboons and lambs suggest that the brain injury underlying neurodevelopmental impairments in chronically ventilated preterm infants involves subtle diffuse white and gray matter lesions, often without intraventricular or germinal matrix hemorrhage and overt lesions or infarcts (19, 51, 102–104). This indicates a potentially distinct mechanism of injury to acute VIBI sustained in delivery room settings.

Preterm baboons have been used extensively to study the impact of prolonged mechanical ventilation (2–4 weeks) on the

lungs (105–107) and, more recently, the brain (103, 107, 108). In these studies, preterm baboons (125 days of term 185 days; 0.68 gestation) are cared for with similar interventions to that of preterm infants in the NICU, including mechanical ventilation using a gentle strategy to maintain V_T at 4–6 ml/kg with adequate chest motion (51, 106). While not investigating injury from ventilation *per se*, the brain injury observed in these animals is not from any direct insult or influenced by potentiating conditions associated with preterm birth or an adverse uterine environment. The subtle neuropathologies from preterm birth and subsequent intensive care alone closely resemble what is observed clinically (51, 102, 103, 109). After 14 days of ventilator support, preterm baboon brains had delayed gyrification (102, 104), reduced brain weight (102–104), reduced white and gray matter volumes (103, 104), increased white and gray matter injury (51), increased astrogliosis in the forebrain (103), increased ramified microglia (103), and a reduction of oligodendrocytes (103, 104) compared to gestation-matched controls. These histopathological indices correlated with microstructural and macrostructural changes detected by *ex vivo* MRI (109).

Additionally, the effects of shorter durations of controlled NICU respiratory support have been investigated in sheep. Preterm lambs (125 days of term 148 days; 0.85 gestation) ventilated with a non-injurious strategy (V_T at 5–7 ml/kg) had increased IL-8 and connective tissue growth factor (CTGF) mRNA levels and decreased vascular occludin protein density in the white matter after 2 h (110). When the length of ventilation was extended to 24 h, ventilated lambs had increased astrogliosis within cortical gray matter but otherwise no apparent neuropathology or changes in glial cell populations compared to unventilated control lambs (68).

Both the preterm baboon and lamb models discussed are neonatal ventilation models. However, as mentioned above, a disadvantage of the neonatal ventilation model is the intensive care requirements of maintaining a preterm animal for significant periods of time, making them more akin to human studies where individual parameters cannot be teased apart unless large numbers of animals are used, which is financially unviable. This is where the IUV model may be advantageous if used for extended periods beyond 24 h.

INFLUENCE OF THE ANTENATAL ENVIRONMENT ON RESPIRATORY SUPPORT AND VIBI

Work explored in the previous sections have studied the pathology and mechanisms of VIBI in preterm but otherwise healthy animals. The ability to isolate effects of respiratory support with minimal confounding factors is vital and these findings provide a foundation to explore therapeutic options to minimize VIBI which will be discussed in section Bench to Bedside of this review. However, it is important to consider that the clinical situation is much more complex—many preterm infants will have been exposed to adverse uterine environments which may increase their risk of VIBI.

Adverse Antenatal Conditions Alter Responses to Postnatal Respiratory Support

Adverse antenatal conditions such as fetal growth restriction (FGR) and intrauterine inflammation have independently been associated with adverse neurodevelopmental outcomes in preterm infants (111, 112). Further, these infants often require respiratory support after birth, increasing the risk of brain injury. Yet, there is a paucity of information on how these antenatal conditions alter the response these infants have to ventilation and if this contributes to VIBI.

Fetal Growth Restriction and VIBI

FGR is a condition where the fetus fails to reach its projected growth potential, often due to placenta insufficiency (112). FGR fetuses are sometimes delivered preterm to prevent deterioration in an adverse *in utero* environment (112), thus many will require respiratory support due to prematurity. FGR fetuses have altered cardiovascular and vascular function, most notably the characteristic "brain-sparing" phenomenon by redirecting blood flow and oxygen delivery to important organs including the heart, adrenals, and brain. These adaptations persist to early postnatal life and may affect how a growth-restricted infant responds to ventilation. Preterm growth-restricted lambs ventilated with a gentle non-injurious strategy for 24 h had disrupted interaction of astrocyte end-feet with cerebral blood vessels, increased microgliosis, and increased oxidative stress compared to their unventilated counterparts and to ventilated preterm appropriately-grown lambs (68). Notably, differences between growth-restricted and appropriately grown lambs were evident after 2 h of ventilation (110). This suggests that growth restricted infants may be at increased risk of VIBI, perhaps in part due to differences in the neurovascular unit and blood-brain barrier properties (68, 110).

Intrauterine Inflammation and VIBI

Intrauterine inflammation, which most commonly presents as chorioamnionitis, is a major cause of preterm birth (113). Antenatal inflammation alters the vulnerability and response of the immature brain to ventilation (71, 91, 114). Lipopolysaccharide(LPS)-mediated inflammation *in utero* amplified cerebral hemodynamic instability during the initiation of ventilation in preterm lambs (71). Compared to saline controls, these lambs that had been exposed to LPS 2 or 4 days before preterm delivery had increased inflammation, vascular extravasation, and microhemorrhages in cerebral white matter regions after ventilation (71). Further, injurious ventilation increased the number of apoptotic cells ($TUNEL^+$ cells) in the subcortical white matter of LPS-exposed lambs, compared to their unventilated counterparts (114). Injurious ventilation had no obvious acute detrimental effects on white matter (89) and gray matter (90) compared to injuriously ventilated healthy preterm lambs and to LPS-exposed lambs that received gentle ventilation. Brain macro- and microstructure as assessed by MRI and DTI were similarly not different (89, 91). However, a novel DTI color map threshold technique detected lower diffusivity indices in white matter regions of the brain, indicative

of subtle brain injury in the ventilated lambs that were exposed to inflammation prior to delivery (91). Importantly, using a non-injurious ventilation strategy did not mitigate VIBI in the LPS-exposed lambs (114). Clinically, histologic chorioamnionitis is associated with a longer cumulative duration of mechanical ventilation in VLBW infants (35), thereby increasing the risk of VIBI. However, the combination of chorioamnionitis and prolonged ventilation has not been investigated in large animals and the potential cerebral effects are unknown.

Cerebral Effects of Antenatal Medical Interventions

Corticosteroid administration is a common antecedent to preterm birth, where antenatal glucocorticoids (betamethasone and dexamethasone) are given to accelerate fetal lung maturation before preterm labor (115). Clinically, antenatal glucocorticoid administration is suggested to reduce the incidence and severity of IVH (115) and does not affect subsequent development of subsequent childhood mental and behavioral disorders in preterm infants (116). However, information on its interaction with respiratory support is scant. A recent study found that antenatal betamethasone improved cerebral hemodynamic instability in preterm lambs that received 15 min of high V_T injurious ventilation followed by 75 min non-injurious ventilation (88). However, there was an increase in the percentage of amoeboid microglia in the periventricular white matter, the number of vessel profiles with protein extravasation in the subcortical white matter, and malondialdehyde levels in cerebrospinal fluid, suggesting increased inflammation and oxidative stress in betamethasone-treated animals than their saline-treated counterparts ventilated with the same protocol (88). This potential increased risk of VIBI following antenatal betamethasone administration may lie in the increased lung compliance and hence susceptibility of the lungs to volutrauma rather than a direct cerebral effect (88).

It is crucial to consider that antenatal glucocorticoid administration may have additional interactions with the conditions mentioned above; for example, growth restricted fetuses have different hemodynamic responses to antenatal glucocorticoids compared to appropriately grown fetuses (117). Maternal betamethasone administration increased fetal cardiac output and blood flow to major organs whereas cardiac output was decreased and blood flow to major organs remained unchanged in control fetuses (118). Furthermore, there were transient decreases in carotid blood flow, an index for CBF, in both control and FGR fetuses. While CBF of control fetuses were stable after returning to baseline levels, FGR fetuses displayed a persistent rebound increase in carotid blood flow from 10 h after treatment (119). Whether these altered responses are beneficial or harmful in the context of VIBI needs to be ascertained. Indeed, little is known about the combined effects of adverse antenatal conditions, antenatal glucocorticoid administration, and postnatal respiratory support on brain injury in the preterm infant. Large animal models of VIBI may provide a means to address this.

BENCH TO BEDSIDE

Establishing reliable animal models with reproducible neuropathology that is reflective of injury seen clinically expedites efforts to test novel potential interventions and/or therapeutic candidates. Potential treatments for VIBI and their mechanisms of actions have recently been discussed in detail by Barton et al. (120) and this remains an active area of research.

In the delivery room setting, physiological-based cord clamping (PBCC) can stabilize pulmonary, systemic, and cerebral circulation in preterm (121, 122) and near-term lambs (123), essentially mitigating the hemodynamic pathway of injury, but it is unlikely to prevent VIBI resultant from the inflammatory pathway. PBCC refers to delaying umbilical cord clamping until respiration has been initiated and established in the newborn or providing respiratory support prior to umbilical cord clamping (121–123). Thus, a therapy that targets both pathways of VIBI, with a focus on modulating inflammation, is required. To date, animal experiments have investigated short-term effects of erythropoietin (EPO) and human amnion epithelial cells (hAECs) as prophylactic postnatal treatments for VIBI resultant from acute volutrauma (73, 87, 124). These treatments have proposed mechanisms of action that make them ideal candidates for neuroprotection. EPO has anti-inflammatory, anti-apoptotic, and neurotrophic properties while hAECs are anti-inflammatory and reparative (120).

When administered to preterm lambs that received 15 min of injurious high V_T ventilation, single early low doses of 300 IU/kg and 1,000 IU/kg human recombinant EPO did not reduce or exacerbate lung and brain injury (124, 125), suggesting that EPO doses presently used in clinical trials appear to be safe for preterm infants receiving respiratory support. However, they appear to not be efficacious as a therapy for VIBI given the lack of therapeutic potential observed. High doses of EPO of 3,000 IU/kg and 5,000 IU/kg increased cerebrospinal fluid EPO levels to "neuroprotective levels" [>100 mU/ml (126)] within 2 h of administration (73, 124). These high doses, respectively, had a protective effect on blood-brain barrier integrity (124) and differential regional effects on white matter (73) despite both doses amplifying lung inflammation and injury (125, 127). Together, these data highlight a complex dose response with distinct effects on the lungs and brain, indicating that further investigation is required to elucidate the efficacy of EPO in the context of a preterm infant requiring respiratory support.

In a similar study, preterm lambs that received high V_T ventilation were administered an intratracheal infusion of 9×10^7 hAECs before ventilation onset and an additional intravenous dose of 9×10^7 hAECs within 5 min of delivery (total 1.8×10^8 hAECs) (87, 128). The cells were able to enter the brain within 2 h of administration, as detected by fluorescent cell labeling in the frontal and parietal periventricular and subcortical white matter of the brain (87). Cell administration reduced microgliosis and vascular protein extravasation (87), potentially as a downstream effect of reduced pulmonary inflammation (128). However, hAECs did not stabilize hemodynamic transition or modulate systemic inflammation within the brief period of the experiment, and conversely they induced an increase in

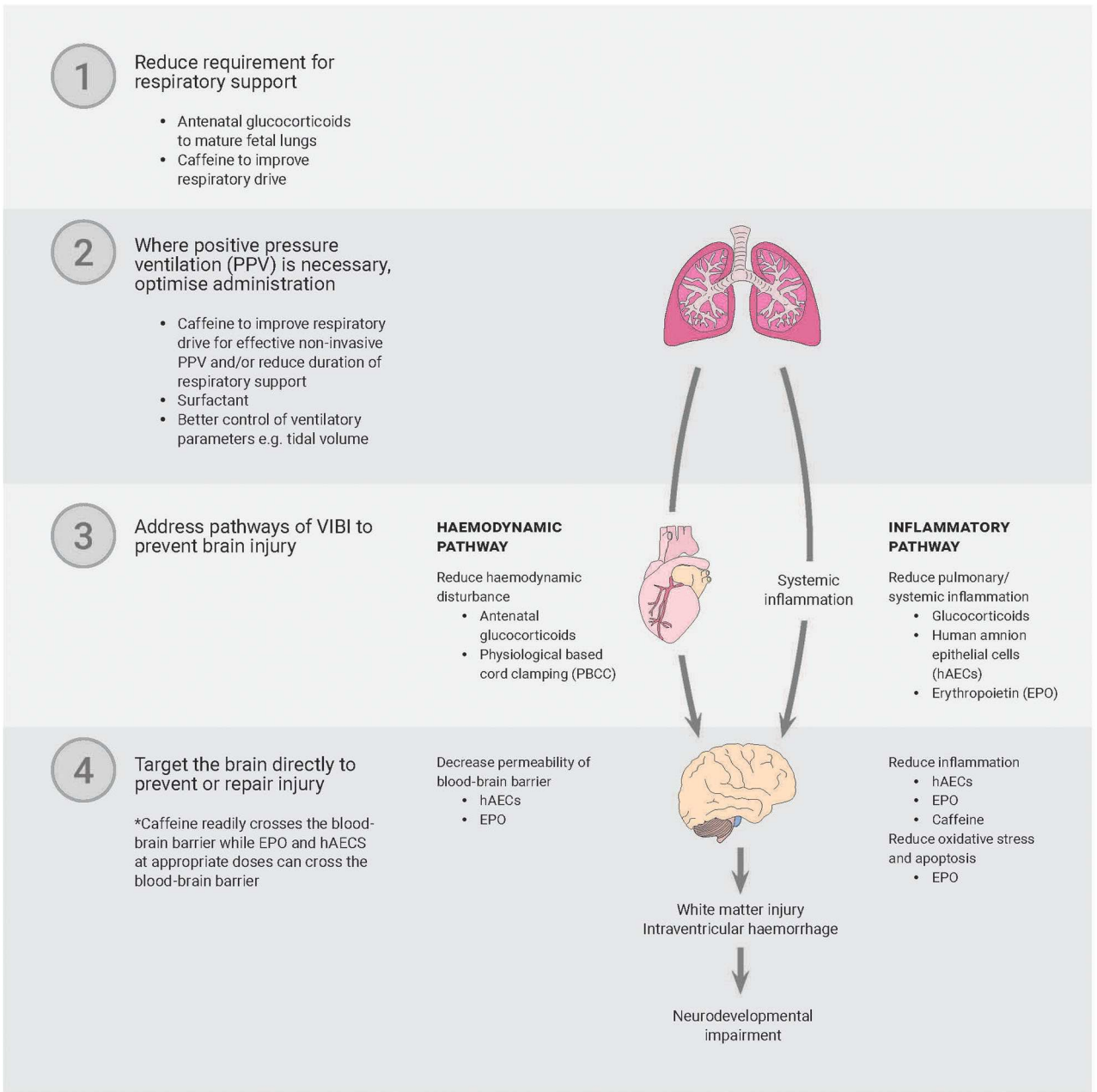

FIGURE 2 | A multipronged approach is likely necessary to prevent or reduce ventilation-induced brain injury. Only strategies discussed in-text have been included in the diagram. PPV, positive pressure ventilation; PBCC, physiological-based cord clamping; hAECs, human amnion epithelial cells; EPO, erythropoietin.

pro-inflammatory cytokine mRNA levels within the brain (87, 128). Further long-term effects of hAECs on acute VIBI have not been investigated to accurately determine the interaction of hAECs and ventilation on the preterm brain.

Chronic ventilation studies in animals have so far focused on treatments to reduce lung rather than brain injury. Sheep fetuses ventilated *in utero* for 12 h and administered intratracheal infusion of 3×10^7 hAECs and an intravenous dose of 3×10^7 hAECs at 3 h and 6 h after ventilation onset (total 1.2×10^8 hAECs) demonstrated a reduction in ventilation-induced lung injury (81), and as such may have the potential to reduce VIBI but this remains a speculation.

While the above strategies have some promise, it is unlikely that a single strategy will prevent or reduce VIBI. The key might lie in a multipronged approach that involves reducing the requirement for or duration of respiratory support, optimizing how PPV is administered to avoid adverse effects, and reducing the sequelae of unpreventable adverse effects of PPV (**Figure 2**).

In this regard, researchers in The Netherlands have investigated the use of caffeine in the delivery room, showing improved respiratory efforts of preterm infants (24–30 weeks GA), potentially reducing the need for invasive respiratory support in this setting (129). Further, spontaneous respiratory drive is a determinant of effective use of gentle non-invasive respiratory support (130). However, caffeine administration to mechanically ventilated preterm infants (23–30 weeks GA) in the first 5 days of life did not encourage early extubation or decrease ventilation duration in the NICU (130, 131). The trial was terminated due to safety concerns, making it difficult to interpret results and secondary outcome findings of morbidities including BPD and IVH (130, 131). In contrast, caffeine had neuroprotective effects in very preterm infants when assessed at 18 months' corrected age (132, 133), in part attributed to earlier discontinuation of PPV and decreased rates of bronchopulmonary dysplasia (134, 135). The treatment benefits of caffeine administered in the first 10 days of life on neurobehavioral and functional cognitive outcomes were less pronounced at 5- and 11-years follow-up, with only slight but statistically significant improvements to motor outcomes observed (136–138). Earlier administration of caffeine within the first 2 days of life has been associated with improved neurodevelopmental outcomes at 18 to 24 months' corrected age compared to late administration (133) but whether these benefits persist have not been reported. Certainly, these contradictory findings highlight the need to better understand the interaction of caffeine, respiratory support, and neurodevelopmental outcomes. Independently, caffeine has been postulated to have neuroprotective properties by reducing inflammation, reducing periventricular white matter injury, and stabilizing hemodynamics in preterm infants (133).

Correspondingly, protective ventilation strategies have reduced brain inflammation and vascular protein extravasation but do not completely mitigate injury in preterm lambs (15, 16, 72, 114). Together, these indicate that our current efforts to minimize the need for respiratory support and, where respiratory support is necessary, improve the way PPV is administered are inadequate to prevent VIBI. Large animal models will likely play a key role in studies focusing on stimulating respiratory function at birth and optimizing the delivery of non-invasive respiratory support to minimize lung and brain inflammation and injury. Additionally, there is an apparent need to devise treatments and large animal models of VIBI provide a means to address this.

SUMMARY

This review highlights the necessity of large animal models when investigating the relationship between invasive respiratory support, the lungs, and the brain in the preterm infant. These models provide a powerful research tool; a combination of physiological, histological, molecular and imaging techniques provides an integrated picture of the interactions between respiratory support and the immature brain which is difficult to obtain in a clinical setting.

Recognizing the consequences of respiratory support on the immature brain will encourage development of effective therapies to prevent or treat VIBI in otherwise healthy preterm infants. VIBI should also be considered when investigating treatments for other conditions such as FGR, chorioamnionitis, and hypoxic injury where the compromised infant will often receive respiratory support.

AUTHOR CONTRIBUTIONS

KC contributed to the conception of the review and created the table. KC and GS conceptualized and created the figures. KC, SM, GS, VS, and GP contributed to structuring, drafting, revising, and the final approval of the version to be published. All authors contributed to the article and approved the submitted version.

FUNDING

This work was supported by the National Health and Medical Research Council (NHMRC) and/or National Heart Foundation of Australia and/or NHMRC Fellowships (VS: 1165935 and GP: 1105526) and the Victorian Government's Operational Infrastructure Support Program.

REFERENCES

1. Blencowe H, Lee ACC, Cousens S, Bahalim A, Narwal R, Zhong N, et al. Preterm birth-associated neurodevelopmental impairment estimates at regional and global levels for 2010. *Pediatr Res.* (2013) 74(Suppl. 1):17–34. doi: 10.1038/pr.2013.204
2. Chow SSW, Creighton P, Chambers G, Lui K. *Report of the Australian and New Zealand Neonatal Network 2017*. Sydney, NSW: ANZNN (2019).
3. Blencowe H, Cousens S, Oestergaard MZ, Chou D, Moller AB, Narwal R, et al. National, regional, and worldwide estimates of preterm birth rates in the year 2010 with time trends since 1990 for selected countries: a systematic analysis and implications. *Lancet.* (2012) 379:2162–72. doi: 10.1016/S0140-6736(12)60820-4
4. Serenius F, Ewald U, Farooqi A, Holmgren PÅ, Håkansson S, Sedin G. Short-term outcome-after active perinatal management at 23-25 weeks of gestation. A study from two Swedish perinatal centres. Part 3: neonatal morbidity. *Acta Paediatr Int J Paediatr.* (2004) 93:1090–7. doi: 10.1111/j.1651-2227.2004.tb02722.x
5. Walsh MC, Morris BH, Wrage LA, Vohr BR, Poole WK, Tyson JE, et al. Extremely low birthweight neonates with protracted ventilation: mortality and 18-month neurodevelopmental outcomes. *J Pediatr.* (2005) 146:798–804. doi: 10.1016/j.jpeds.2005.01.047
6. Gagliardi L, Bellù R, Zanini R, Dammann O. Bronchopulmonary dysplasia and brain white matter damage in the preterm infant: a complex relationship. *Paediatr PerinatEpidemiol.* (2009) 23:582–90. doi: 10.1111/j.1365-3016.2009.01069.x
7. Soll RF, Edwards EM, Badger GJ, Kenny MJ, Morrow KA, Buzas JS, et al. Obstetric and neonatal care practices for infants 501 to 1500 g from 2000 to 2009. *Pediatrics.* (2013) 132:222–8. doi: 10.1542/peds.2013-0501
8. Serenius F, Ewald U, Farooqi A, Holmgren PÅ, Håkansson S, Sedin G. Short-term outcome after active perinatal management at 23-25 weeks of gestation. A study from two Swedish tertiary care centres.

Part 2: infant survival. *Acta Paediatr Int J Paediatr.* (2004) 93:1081–9. doi: 10.1111/j.1651-2227.2004.tb02721.x
9. Cho SJ, Shin J, Namgung R. Initial resuscitation at delivery and short term neonatal outcomes in very-low-birth-weight infants. *J Korean Med Sci.* (2015) 30:S45–51. doi: 10.3346/jkms.2015.30.S1.S45
10. Stoll BJ, Hansen NI, Bell EF, Walsh MC, Carlo WA, Shankaran S, et al. Trends in care practices, morbidity, and mortality of extremely preterm Neonates, 1993-2012. *J Am Med Assoc.* (2015) 314:1039–51. doi: 10.1001/jama.2015.10244
11. Schmölzer GM, Kamlin OCOF, O'Donnell CPF, Dawson JA, Morley CJ, Davis PG. Assessment of tidal volume and gas leak during mask ventilation of preterm infants in the delivery room. *Arch Dis Child Fetal Neonatal Ed.* (2010) 95:1–4. doi: 10.1136/adc.2009.174003
12. van Vonderen JJ, Hooper SB, Krabbe VB, Siew ML, te Pas AB. Monitoring tidal volumes in preterm infants at birth: mask versus endotracheal ventilation. *Arch Dis Child Fetal Neonatal Ed.* (2015) 100:F43–6. doi: 10.1136/archdischild-2014-306614
13. Barton SK, Tolcos M, Miller SL, Roehr CC, Schmölzer GM, Davis PG, et al. Unraveling the links between the initiation of ventilation and brain injury in preterm infants. *Front Pediatr.* (2015) 3:97. doi: 10.3389/fped.2015.00097
14. Tsai W, Hwang Y, Hung T, Weng S, Lin S-J, Chang W-T. Association between mechanical ventilation and neurodevelopmental disorders in a nationwide cohort of extremely low birth weight infants. *Res Dev Disabil.* (2014) 35:1544–50. doi: 10.1016/j.ridd.2014.03.048
15. Polglase GR, Miller SL, Barton SK, Baburamani AA, Wong FY, Aridas JDS, et al. Initiation of resuscitation with high tidal volumes causes cerebral hemodynamic disturbance, brain inflammation and injury in preterm lambs. *PLoS ONE.* (2012) 7:e39535. doi: 10.1371/journal.pone.0039535
16. Polglase GR, Miller SL, Barton SK, Kluckow M, Gill AW, Hooper SB, et al. Respiratory support for premature neonates in the delivery room: effects on cardiovascular function and the development of brain injury. *Pediatr Res.* (2014) 75:682–8. doi: 10.1038/pr.2014.40
17. Hillman NH, Kallapur SG, Jobe AH. Physiology of transition from intrauterine to extrauterine life. *Clin Perinatol.* (2012) 39:769–83. doi: 10.1016/j.clp.2012.09.009
18. Rees S, Inder T. Fetal and neonatal origins of altered brain development. *Early Hum Dev.* (2005) 81:753–61. doi: 10.1016/j.earlhumdev.2005.07.004
19. Albertine KH. Brain injury in chronically ventilated preterm neonates. *Clin Perinatol.* (2012) 39:727–40. doi: 10.1016/j.clp.2012.06.017
20. Aly H, Hammad TA, Essers J, Wung JT. Is mechanical ventilation associated with intraventricular hemorrhage in preterm infants? *Brain Dev.* (2012) 34:201–5. doi: 10.1016/j.braindev.2011.04.006
21. Mian Q, Cheung P-Y, O'Reilly M, Barton SK, Polglase GR, Schmölzer GM. Impact of delivered tidal volume on the occurrence of intraventricular haemorrhage in preterm infants during positive pressure ventilation in the delivery room. *Arch Dis Child Fetal Neonatal Ed.* (2019) 104:F57–62. doi: 10.1136/archdischild-2017-313864
22. Aly H. Is it safer to intubate premature infants in the delivery room? *Pediatrics.* (2005) 115:1660–5. doi: 10.1542/peds.2004-2493
23. Australian and New Zealand Committee on Resuscitation. *ANZCOR Guideline 13. 4 – Airway Management and Mask Ventilation of the Newborn Infant* (2016).
24. Lindner W, Vossbeck S, Hummler H, Pohlandt F. Delivery room management of extremely low birth weight infants: spontaneous breathing or intubation? *Pediatrics.* (1999) 103:961–7. doi: 10.1542/peds.103.5.961
25. Bajaj M, Natarajan G, Shankaran S, Wyckoff M, Laptook AR, Bell EF, et al. Delivery room resuscitation and short-term outcomes in moderately preterm infants. *J Pediatr.* (2018) 195:33–38.e2. doi: 10.1016/j.jpeds.2017.11.039
26. Wallenstein MB, Birnie KL, Arain YH, Yang W, Yamada NK, Huffman LC, et al. Failed endotracheal intubation and adverse outcomes among extremely low birth weight infants. *J Perinatol.* (2016) 36:112–5. doi: 10.1038/jp.2015.158
27. Tracy M, Downe L, Holberton J. How safe is intermittent positive pressure ventilation in preterm babies ventilated from delivery to newborn intensive care unit? *Arch Dis Child Fetal Neonatal Ed.* (2004) 89:F84–7. doi: 10.1136/fn.89.1.F84
28. Poulton DA, Schmölzer GM, Morley CJ, Davis PG. Assessment of chest rise during mask ventilation of preterm infants in the delivery room. *Resuscitation.* (2011) 82:175–9. doi: 10.1016/j.resuscitation.2010.10.012
29. Parker JC, Hernandez LA, Peevy KJ. Mechanisms of ventilator-induced lung injury. *Crit Care Med.* (1993) 21:131–43. doi: 10.1097/00003246-199301000-00024
30. Jobe AH, Ikegami M. Mechanisms initiating lung injury in the preterm. *Early Hum Dev.* (1998) 53:81–94. doi: 10.1016/S0378-3782(98)00045-0
31. Attar MA, Donn SM. Mechanisms of ventilator-induced lung injury in premature infants. *Semin Neonatol.* (2002) 7:353–60. doi: 10.1053/siny.2002.0129
32. Schmölzer GM, Te Pas AB, Davis PG, Morley CJ. Reducing lung injury during neonatal resuscitation of preterm infants. *J Pediatr.* (2008) 153:741–5. doi: 10.1016/j.jpeds.2008.08.016
33. Mian QN, Pichler G, Binder C, O'Reilly M, Aziz K, Urlesberger B, et al. Tidal volumes in spontaneously breathing preterm infants supported with continuous positive airway pressure. *J Pediatr.* (2014) 165:702–706.e1. doi: 10.1016/j.jpeds.2014.06.047
34. Curley GF, Laffey JG, Zhang H, Slutsky AS. Biotrauma and ventilator-induced lung injury: clinical implications. *Chest.* (2016) 150:1109–17. doi: 10.1016/j.chest.2016.07.019
35. Choi Y-B, Lee J, Park J, Jun YH. Impact of prolonged mechanical ventilation in very low birth weight infants: results from a national cohort study. *J Pediatr.* (2018) 194:34–9.e3. doi: 10.1016/j.jpeds.2017.10.042
36. Lundqvist P, Källén K, Hallström I, Westas LH. Trends in outcomes for very preterm infants in the southern region of Sweden over a 10-year period. *Acta Paediatr Int J Paediatr.* (2009) 98:648–53. doi: 10.1111/j.1651-2227.2008.01155.x
37. Barnett ML, Tusor N, Ball G, Chew A, Falconer S, Aljabar P, et al. Exploring the multiple-hit hypothesis of preterm white matter damage using diffusion MRI. *NeuroImage Clin.* (2018) 17:596–606. doi: 10.1016/j.nicl.2017.11.017
38. Vento M, Aguar M, Leone TA, Finer NN, Gimeno A, Rich W, et al. Using intensive care technology in the delivery room: a new concept for the resuscitation of extremely preterm neonates. *Pediatrics.* (2008) 122:1113–6. doi: 10.1542/peds.2008-1422
39. Kumar P, Denson SE, Mancuso TJ. Premedication for nonemergency endotracheal intubation in the neonate. *Pediatrics.* (2010) 125:608–15. doi: 10.1542/peds.2009-2863
40. Andropoulos DB. Effect of anesthesia on the developing brain: infant and fetus. *Fetal Diagn Ther.* (2018) 43:1–11. doi: 10.1159/000475928
41. Lee J, Loepke AW. Does pediatric anesthesia cause brain damage? – Addressing parental and provider concerns in light of compelling animal studies and seemingly ambivalent human data. *Korean J Anesthesiol.* (2018) 71:255–73. doi: 10.4097/kja.d.18.00165
42. Vliegenthart RJS, van Kaam AH, Aarnoudse-Moens CSH, van Wassenaer AG, Onland W. Duration of mechanical ventilation and neurodevelopment in preterm infants. *Arch Dis Child Fetal Neonatal Ed.* (2019) 104:F631–5. doi: 10.1136/archdischild-2018-315993
43. Behnke J, Lemyre B, Czernik C, Zimmer K-P, Ehrhardt H, Waitz M. Non-invasive ventilation in neonatology. *Dtsch Arztebl Int.* (2019) 116:177–83. doi: 10.3238/arztebl.2019.0177
44. Yoder BA, Coalson JJ. Animal models of bronchopulmonary dysplasia. The preterm baboon models. *Am J Physiol Lung Cell Mol Physiol.* (2014) 307:L970–7. doi: 10.1152/ajplung.00171.2014
45. Albertine KH. Utility of large-animal models of BPD: chronically ventilated preterm lambs. *Am J Physiol Lung Cell Mol Physiol.* (2015) 308:L983–1001. doi: 10.1152/ajplung.00178.2014
46. Schittny JC. Development of the lung. *Cell Tissue Res.* (2017) 367:427–44. doi: 10.1007/s00441-016-2545-0
47. Chi JG, Dooling EC, Gilles FH. Gyral development of the human brain. *Ann Neurol.* (1977) 1:86–93. doi: 10.1002/ana.410010109
48. Hagberg H, Peebles D, Mallard C. Models of white matter injury: comparison of infectious, hypoxic-ischemic, and excitotoxic insults. *Ment Retard Dev Disabil Res Rev.* (2002) 8:30–8. doi: 10.1002/mrdd.10007
49. Counsell SJ, Rutherford MA, Cowan FM, Edwards AD. Magnetic resonance imaging of preterm brain injury. *Arch Dis Child Fetal Neonatal Ed.* (2003) 88:F269–74. doi: 10.1136/fn.88.4.F269
50. Workman AD, Charvet CJ, Clancy B, Darlington RB, Finlay BL. Modeling transformations of neurodevelopmental sequences

across mammalian species. *J Neurosci.* (2013) 33:7368–83. doi: 10.1523/JNEUROSCI.5746-12.2013
51. Dieni S, Inder T, Yoder B, Briscoe T, Camm E, Egan G, et al. The pattern of cerebral injury in a primate model of preterm birth and neonatal intensive care. *J Neuropathol Exp Neurol.* (2004) 63:1297–309. doi: 10.1093/jnen/63.12.1297
52. Inder T, Neil J, Yoder B, Rees S. Patterns of cerebral injury in a primate model of preterm birth and neonatal intensive care. *J Child Neurol.* (2005) 20:965–7. doi: 10.1177/08830738050200120601
53. Rees SM, Loeliger MM, Munro KM, Shields A, Dalitz PA, Dieni S, et al. Cerebellar development in a baboon model of preterm delivery. *J Neuropathol Exp Neurol.* (2009) 68:605–15. doi: 10.1097/NEN.0b013e3181a39b3f
54. Romanes GJ. The prenatal medullation of the sheep's nervous system. *J Anat.* (1947) 81:64–81.
55. Åarström K-E. on the early development of the isocortex in fetal sheep. *Prog Brain Res.* (1967) 26:1–59. doi: 10.1016/S0079-6123(08)61418-1
56. Patterson DSP, Sweasey D, Hebert CN. Changes occurring in the chemical composition of the central nervous system during foetal and post-natal development of the sheep. *J Neurochem.* (1971) 18:2027–40. doi: 10.1111/j.1471-4159.1971.tb05062.x
57. McIntosh GH, Baghurst KI, Potter BJ, Hetzel BS. Foetal brain development in the sheep. *Neuropathol Appl Neurobiol.* (1979) 5:103–14. doi: 10.1111/j.1365-2990.1979.tb00664.x
58. Back SA, Riddle A, Dean J, Hohimer AR. The instrumented fetal sheep as a model of cerebral white matter injury in the premature infant. *Neurotherapeutics.* (2012) 9:359–70. doi: 10.1007/s13311-012-0108-y
59. Riddle A. Spatial heterogeneity in oligodendrocyte lineage maturation and not cerebral blood flow predicts fetal ovine periventricular white matter injury. *J Neurosci.* (2006) 26:3045–55. doi: 10.1523/JNEUROSCI.5200-05.2006
60. Barlow RM. The foetal sheep: morphogenesis of the nervous system and histochemical aspects of myelination. *J Comp Neurol.* (1969) 135:249–62. doi: 10.1002/cne.901350302
61. Back SA, Riddle A, Hohimer AR. Role of instrumented fetal sheep preparations in defining the pathogenesis of human periventricular white-matter injury. *J Child Neurol.* (2006) 21:582–9. doi: 10.1177/08830738060210070101
62. Phillips KA, Bales KL, Capitanio JP, Conley A, Czoty PW, 't Hart BA, et al. Why primate models matter. *Am J Primatol.* (2014) 76:801–27. doi: 10.1002/ajp.22281
63. Conrad MS, Johnson RW. The domestic piglet: an important model for investigating the neurodevelopmental consequences of early life insults. *Annu Rev Anim Biosci.* (2015) 3:245–64. doi: 10.1146/annurev-animal-022114-111049
64. Eiby YA, Wright LL, Kalanjati VP, Miller SM, Bjorkman ST, Keates HL, et al. A pig model of the preterm neonate: anthropometric and physiological characteristics. *PLoS ONE.* (2013) 8:e68763. doi: 10.1371/journal.pone.0068763
65. Sweasey D, Patterson DSP, Glancy EM. Biphasic myelination and the fatty acid composition of cerebrosides and cholesterol esters in the developing central nervous system of the domestic pig. *J Neurochem.* (1976) 27:375–80. doi: 10.1111/j.1471-4159.1976.tb12256.x
66. Alcorn DG, Adamson TM, Maloney JE, Robinson PM. A morphologic and morphometric analysis of fetal lung development in the sheep. *Anat Rec.* (1981) 201:655–67. doi: 10.1002/ar.1092010410
67. Albertine KH, Jones GP, Starcher BC, Bohnsack JF, Davis PL, Cho SC, et al. Chronic lung injury in preterm lambs. Disordered respiratory tract development. *Am J Respir Crit Care Med.* (1999) 159:945–58. doi: 10.1164/ajrccm.159.3.9804027
68. Malhotra A, Castillo-Melendez M, Allison BJ, Sutherland AE, Nitsos I, Pham Y, et al. Neuropathology as a consequence of neonatal ventilation in premature growth-restricted lambs. *Am J Physiol Integr Comp Physiol.* (2018) 315:R1183–94. doi: 10.1152/ajpregu.00171.2018
69. Schilleman K, Van Der Pot CJM, Hooper SB, Lopriore E, Walther FJ, Te Pas AB. Evaluating manual inflations and breathing during mask ventilation in preterm infants at birth. *J Pediatr.* (2013) 162:457–63. doi: 10.1016/j.jpeds.2012.09.036
70. Björklund LJ, Ingimarsson J, Curstedt T, John J, Robertson B, Werner O, et al. Manual ventilation with a few large breaths at birth compromises the therapeutic effect of subsequent surfactant replacement in immature lambs. *Pediatr Res.* (1997) 42:348–55. doi: 10.1203/00006450-199709000-00016
71. Polglase GR, Nitsos I, Baburamani AA, Crossley KJ, Slater MK, Gill AW, et al. Inflammation *in utero* exacerbates ventilation-induced brain injury in preterm lambs. *J Appl Physiol.* (2012) 112:481–9. doi: 10.1152/japplphysiol.00995.2011
72. Skiöld B, Wu Q, Hooper SB, Davis PG, McIntyre R, Tolcos M, et al. Early detection of ventilation-induced brain injury using magnetic resonance spectroscopy and diffusion tensor imaging: an *in vivo* study in preterm lambs. *PLoS ONE.* (2014) 9:e95804. doi: 10.1371/journal.pone.0095804
73. Barton SK, McDougall ARA, Melville JM, Moss TJM, Zahra VA, Lim T, et al. Differential short-term regional effects of early high dose erythropoietin on white matter in preterm lambs after mechanical ventilation. *J Physiol.* (2016) 594:1437–49. doi: 10.1113/JP271376
74. Hillman NH, Moss TJM, Kallapur SG, Bachurski C, Pillow JJ, Polglase GR, et al. Brief, large tidal volume ventilation initiates lung injury and a systemic response in fetal sheep. *Am J Respir Crit Care Med.* (2007) 176:575–81. doi: 10.1164/rccm.200701-051OC
75. Hillman NH, Kallapur SG, Pillow JJ, Moss TJM, Polglase GR, Nitsos I, et al. Airway injury from initiating ventilation in preterm sheep. *Pediatr Res.* (2010) 67:60–5. doi: 10.1203/PDR.0b013e3181c1b09e
76. Hillman NH, Polglase GR, Pillow JJ, Saito M, Kallapur SG, Jobe AH. Inflammation and lung maturation from stretch injury in preterm fetal sheep. *Am J Physiol Lung Cell Mol Physiol.* (2011) 300:L232–41. doi: 10.1152/ajplung.00294.2010
77. Alahmari DM, Chan KYY, Stojanovska V, LaRosa D, Barton SK, Nitsos I, et al. Diffusion tensor imaging detects ventilation-induced brain injury in preterm lambs. *PLoS ONE.* (2017) 12:e0188737. doi: 10.1371/journal.pone.0188737
78. Kothe TB, Royse E, Kemp MW, Schmidt A, Salomone F, Saito M, et al. Effects of budesonide and surfactant in preterm fetal sheep. *Am J Physiol Cell Mol Physiol.* (2018) 315:L193–201. doi: 10.1152/ajplung.00528.2017
79. Allison BJ, Crossley KJ, Flecknoe SJ, Davis PG, Morley CJ, Harding R, et al. Ventilation of the very immature lung *in utero* induces injury and BPD-like changes in lung structure in fetal sheep. *Pediatr Res.* (2008) 64:387–92. doi: 10.1203/PDR.0b013e318181e05e
80. Allison BJ, Crossley KJ, Flecknoe SJ, Morley CJ, Polglase GR, Hooper SB. Pulmonary hemodynamic responses to *in utero* ventilation in very immature fetal sheep. *Respir Res.* (2010) 11:1–11. doi: 10.1186/1465-9921-11-111
81. Hodges RJ, Jenkin G, Hooper SB, Allison B, Lim R, Dickinson H, et al. Human amnion epithelial cells reduce ventilation-induced preterm lung injury in fetal sheep. *Am J Obstet Gynecol.* (2012) 206:448.e8–448.e15. doi: 10.1016/j.ajog.2012.02.038
82. Iwamoto HS, Teitel DF, Rudolph AM. Effects of lung distension and spontaneous fetal breathing on hemodynamics in sheep. *Pediatr Res.* (1993) 33:639–44. doi: 10.1203/00006450-199306000-00021
83. Giraud G, Morton M, Reid D, Reller M, Thornburg K. Effects of ductus arteriosus occlusion on pulmonary artery pressure during *in utero* ventilation in fetal sheep. *Exp Physiol.* (1995) 80:129–39. doi: 10.1113/expphysiol.1995.sp003828
84. Blanco CE, Martin CB, Hanson MA, McCooke HB. Breathing activity in fetal sheep during mechanical ventilation of the lungs *in utero*. *Eur J Obstet Gynecol Reprod Biol.* (1987) 26:175–82. doi: 10.1016/0028-2243(87)90054-2
85. O'Reilly M, Hooper SB, Allison BJ, Flecknoe SJ, Snibson K, Harding R, et al. Persistent bronchiolar remodeling following brief ventilation of the very immature ovine lung. *Am J Physiol Lung Cell Mol Physiol.* (2009) 297:992–1001. doi: 10.1152/ajplung.00099.2009
86. Gleason CA, Jones MD, Traystman RJ, Notter RH. Fetal cerebral responses to ventilation and oxygenation *in utero*. *Am J Physiol Integr Comp Physiol.* (1988) 255:R1049–54. doi: 10.1152/ajpregu.1988.255.6.R1049
87. Barton SK, Melville JM, Tolcos M, Polglase GR, McDougall AR, Azhan A, et al. Human amnion epithelial cells modulate ventilation-induced white matter pathology in preterm lambs. *Dev Neurosci.* (2015) 37:338–48. doi: 10.1159/000371415
88. Stojanovska V, Barton SK, Tolcos M, Gill AW, Kluckow M, Miller SL, et al. The effect of antenatal betamethasone on white matter inflammation and

injury in fetal sheep and ventilated preterm lambs. *Dev Neurosci.* (2018) 40:497–507. doi: 10.1159/000496466
89. Alahmari DM, Barton SK, Galinsky R, Nitsos I, Atik A, Farrell M, et al. Correlation between diffusion tensor imaging and histological brain injury in ventilated preterm lambs. *Imaging Med.* (2017) 9:67–76. doi: 10.14303/Imaging-Medicine.1000061
90. Stojanovska V, Atik A, Nitsos I, Skiöld B, Barton SK, Zahra VA, et al. Effects of Intrauterine inflammation on cortical gray matter of near-term lambs. *Front Pediatr.* (2018) 6:145. doi: 10.3389/fped.2018.00145
91. Alahmari DM, Skiöld B, Barton SK, Nitsos I, McDonald C, Miller SL, et al. Diffusion tensor imaging colour mapping threshold for identification of ventilation-induced brain injury after intrauterine inflammation in preterm lambs. *Front Pediatr.* (2017) 5:70. doi: 10.3389/fped.2017.00070
92. Bapat R, Narayana PA, Zhou Y, Parikh NA. Magnetic resonance spectroscopy at term-equivalent age in extremely preterm infants: association with cognitive and language development. *Pediatr Neurol.* (2014) 51:53–9. doi: 10.1016/j.pediatrneurol.2014.03.011
93. Hyodo R, Sato Y, Ito M, Sugiyama Y, Ogawa C, Kawai H, et al. Magnetic resonance spectroscopy in preterm infants: association with neurodevelopmental outcomes. *Arch Dis Child Fetal Neonatal Ed.* (2018) 103:F238–44. doi: 10.1136/archdischild-2016-311403
94. Khwaja O, Volpe JJ. Pathogenesis of cerebral white matter injury of prematurity. *Arch Dis Child Fetal Neonatal Ed.* (2007) 93:F153–61. doi: 10.1136/adc.2006.108837
95. Back SA, Rosenberg PA. Pathophysiology of glia in perinatal white matter injury. *Glia.* (2014) 62:1790–815. doi: 10.1002/glia.22658
96. Greisen G. Autoregulation of cerebral blood flow in newborn babies. *Early Hum Dev.* (2005) 81:423–8. doi: 10.1016/j.earlhumdev.2005.03.005
97. Verma PK, Panerai RB, Rennie JM, Evans DH. Grading of cerebral autoregulation in preterm and term neonates. *Pediatr Neurol.* (2000) 23:236–42. doi: 10.1016/S0887-8994(00)00184-3
98. du Plessis AJ. The role of systemic hemodynamic disturbances in prematurity-related brain injury. *J Child Neurol.* (2009) 24:1127–40. doi: 10.1177/0883073809339361
99. Czynski AJ, Terry MH, Deming DD, Power GG, Buchholz JN, Blood AB. Cerebral autoregulation is minimally influenced by the superior cervical ganglion in two-week-old lambs, and absent in preterm lambs immediately following delivery. *PLoS ONE.* (2013) 8:e82326. doi: 10.1371/journal.pone.0082326
100. Gilmore MM, Stone BS, Shepard JA, Czosnyka M, Easley RB, Brady KM. Relationship between cerebrovascular dysautoregulation and arterial blood pressure in the premature infant. *J Perinatol.* (2011) 31:722–9. doi: 10.1038/jp.2011.17
101. Perlman JM, McMenamin JB, Volpe JJ. Fluctuating cerebral blood-flow velocity in respiratory-distress syndrome. *N Engl J Med.* (1983) 309:204–9. doi: 10.1056/NEJM198307283090402
102. Rees SM, Camm EJ, Loeliger M, Cain S, Dieni S, McCurnin D, et al. Inhaled nitric oxide: effects on cerebral growth and injury in a baboon model of premature delivery. *Pediatr Res.* (2007) 61:552–8. doi: 10.1203/pdr.0b013e318045be20
103. Loeliger M, Inder TE, Shields A, Dalitz P, Cain S, Yoder B, et al. High-frequency oscillatory ventilation is not associated with increased risk of neuropathology compared with positive pressure ventilation: a preterm primate model. *Pediatr Res.* (2009) 66:545–50. doi: 10.1203/PDR.0b013e3181bb0cc1
104. Loeliger M, Inder TE, Dalitz PA, Cain S, Camm EJ, Yoder B, et al. Developmental and neuropathological consequences of ductal ligation in the preterm baboon. *Pediatr Res.* (2009) 65:209–14. doi: 10.1203/PDR.0b013e31818d6d0b
105. Coalson JJ, Winter VT, Siler-Khodr T, Yoder BA. Neonatal chronic lung disease in extremely immature baboons. *Am J Respir Crit Care Med.* (1999) 160:1333–46. doi: 10.1164/ajrccm.160.4.9810071
106. Yoder BA, Siler-Khodr T, Winter VT, Coalson JJ. High-frequency oscillatory ventilation: effects on lung function, mechanics, and airway cytokines in the immature baboon model for neonatal chronic lung disease. *Am J Respir Crit Care Med.* (2000) 162:1867–76. doi: 10.1164/ajrccm.162.5.9912145
107. Loeliger M, Inder T, Cain S, Ramesh RC, Camm E, Thomson MA, et al. Cerebral outcomes in a preterm baboon model of early versus delayed nasal continuous positive airway pressure. *Pediatrics.* (2006) 118:1640–53. doi: 10.1542/peds.2006-0653
108. Verney C, Rees S, Biran V, Thompson M, Inder T, Gressens P. Neuronal damage in the preterm baboon: impact of the mode of ventilatory support. *J Neuropathol Exp Neurol.* (2010) 69:473–82. doi: 10.1097/NEN.0b013e3181dac07b
109. Griffith JL, Shimony JS, Cousins SA, Rees SE, McCurnin DC, Inder TE, et al. MR imaging correlates of white-matter pathology in a preterm baboon model. *Pediatr Res.* (2012) 71:185–91. doi: 10.1038/pr.2011.33
110. Allison BJ, Hooper SB, Coia E, Jenkin G, Malhotra A, Zahra V, et al. Does growth restriction increase the vulnerability to acute ventilation-induced brain injury in newborn lambs? Implications for future health and disease. *J Dev Orig Health Dis.* (2017) 8:556–65. doi: 10.1017/S204017441700037X
111. Miller SL, Huppi PS, Mallard C. The consequences of fetal growth restriction on brain structure and neurodevelopmental outcome. *J Physiol.* (2016) 594:807–23. doi: 10.1113/JP271402
112. Sharma D, Shastri S, Sharma P. Intrauterine growth restriction: antenatal and postnatal aspects. *Clin Med Insights Pediatr.* (2016) 10:67–83. doi: 10.4137/CMPed.S40070
113. Goldenberg RL, Culhane JF, Iams JD, Romero R. Epidemiology and causes of preterm birth. *Lancet.* (2008) 371:75–84. doi: 10.1016/S0140-6736(08)60074-4
114. Barton SK, Moss TJM, Hooper SB, Crossley KJ, Gill AW, Kluckow M, et al. Protective ventilation of preterm lambs exposed to acute chorioamnionitis does not reduce ventilation-induced lung or brain injury. *PLoS ONE.* (2014) 9:e112402. doi: 10.1371/journal.pone.0112402
115. Roberts D, Brown J, Medley N, Dalziel SR. Antenatal corticosteroids for accelerating fetal lung maturation for women at risk of preterm birth. *Cochrane Database Syst Rev.* (2017) 3:CD004454. doi: 10.1002/14651858.CD004454.pub3
116. Räikkönen K, Gissler M, Kajantie E. Associations between maternal antenatal corticosteroid treatment and mental and behavioral disorders in children supplemental content. *JAMA.* (2020) 323:1924–33. doi: 10.1001/jama.2020.3937
117. Miller SL, Wallace EM. Effect of antenatal steroids on haemodynamics in the normally grown and growth restricted fetus. *Curr Pediatr Rev.* (2013) 9:67–74. doi: 10.2174/1573396311309010014
118. Miller SL, Supramaniam VG, Jenkin G, Walker DW, Wallace EM. Cardiovascular responses to maternal betamethasone administration in the intrauterine growth-restricted ovine fetus. *Am J Obstet Gynecol.* (2009) 201:613.e1–613.e8. doi: 10.1016/j.ajog.2009.07.028
119. Miller SL, Chai M, Loose J, Castillo-Meléndez M, Walker DW, Jenkin G, et al. The effects of maternal betamethasone administration on the intrauterine growth-restricted fetus. *Endocrinology.* (2007) 148:1288–95. doi: 10.1210/en.2006-1058
120. Barton SK, Tolcos M, Miller SL, Christoph-Roehr C, Schmölzer GM, Moss TJM, et al. Ventilation-induced brain injury in preterm neonates: a review of potential therapies. *Neonatology.* (2016) 110:155–62. doi: 10.1159/000444918
121. Bhatt S, Alison BJ, Wallace EM, Crossley KJ, Gill AW, Kluckow M, et al. Delaying cord clamping until ventilation onset improves cardiovascular function at birth in preterm lambs. *J Physiol.* (2013) 591:2113–26. doi: 10.1113/jphysiol.2012.250084
122. Polglase GR, Dawson JA, Kluckow M, Gill AW, Davis PG, Te Pas AB, et al. Ventilation onset prior to umbilical cord clamping (physiological-based cord clamping) improves systemic and cerebral oxygenation in preterm lambs. *PLoS ONE.* (2015) 10:e0117504. doi: 10.1371/journal.pone.0117504
123. Polglase GR, Blank DA, Barton SK, Miller SL, Stojanovska V, Kluckow M, et al. Physiologically based cord clamping stabilises cardiac output and reduces cerebrovascular injury in asphyxiated near-term lambs. *Arch Dis Child Fetal Neonatal Ed.* (2018) 103:F530–8. doi: 10.1136/archdischild-2017-313657
124. Chan KYY, LaRosa DA, Tolcos M, Li A, Zahra VA, Polglase GR, et al. Optimizing the dose of erythropoietin required to prevent acute ventilation-induced cerebral white matter injury in preterm lambs. *Dev Neurosci.* (2017) 39:298–309. doi: 10.1159/000459620
125. Allison BJ, LaRosa DA, Barton SK, Hooper S, Zahra V, Tolcos M, et al. Dose-dependent exacerbation of ventilation-induced lung injury by

erythropoietin in preterm newborn lambs. *J Appl Physiol.* (2019) 126:44–50. doi: 10.1152/japplphysiol.00800.2018
126. Juul SE, McPherson RJ, Farrell FX, Jolliffe L, Ness DJ, Gleason CA. Erythropoietin concentrations in cerebrospinal fluid of nonhuman primates and fetal sheep following high-dose recombinant erythropoietin. *Biol Neonate.* (2004) 85:138–44. doi: 10.1159/000074970
127. Polglase GR, Barton SK, Melville JM, Zahra V, Wallace MJ, Siew ML, et al. Prophylactic erythropoietin exacerbates ventilation-induced lung inflammation and injury in preterm lambs. *J Physiol.* (2014) 592:1993–2002. doi: 10.1113/jphysiol.2013.270348
128. Melville JM, McDonald CA, Bischof RJ, Polglase GR, Lim R, Wallace EM, et al. Human amnion epithelial cells modulate the inflammatory response to ventilation in preterm lambs. *PLoS ONE.* (2017) 12:e0173572. doi: 10.1371/journal.pone.0173572
129. Dekker J, Hooper SB, Van Vonderen JJ, Witlox RSGM, Lopriore E, Te Pas AB. Caffeine to improve breathing effort of preterm infants at birth: a randomized controlled trial. *Pediatr Res.* (2017) 82:290–6. doi: 10.1038/pr.2017.45
130. Amaro CM, Bello JA, Jain D, Ramnath A, D'Ugard C, Vanbuskirk S, et al. Early caffeine and weaning from mechanical ventilation in preterm infants: a randomized, placebo-controlled trial. *J Pediatr.* (2018) 196:52–7. doi: 10.1016/j.jpeds.2018.01.010
131. Jain VG, Saroha V, Patel RM, Jobe A. Is early caffeine therapy safe and effective for ventilated preterm infants? *J Perinatol.* (2019) 39:754–7. doi: 10.1038/s41372-019-0336-7
132. Schmidt B, Roberts RS, Davis P, Doyle LW, Barrington KJ, Ohlsson A, et al. Long-term effects of caffeine therapy for apnea of prematurity. *N Engl J Med.* (2007) 357:1893–902. doi: 10.1056/NEJMoa073679
133. Lodha A, Entz R, Synnes A, Creighton D, Yusuf K, Lapointe A, et al. Early caffeine administration and neurodevelopmental outcomes in preterm infants. *Pediatrics.* (2019) 143:e20181348. doi: 10.1542/peds.2018-1348
134. Schmidt B, Roberts RS, Davis P, Doyle LW, Barrington KJ, Ohlsson A, et al. Caffeine therapy for apnea of prematurity. *N Engl J Med.* (2006) 354:2112–21. doi: 10.1056/NEJMoa054065
135. Lodha A, Seshia M, McMillan DD, Barrington K, Yang J, Lee SK, et al. Association of early caffeine administration and neonatal outcomes in very preterm neonates. *JAMA Pediatr.* (2015) 169:33–8. doi: 10.1001/jamapediatrics.2014.2223
136. Schmidt B, Anderson PJ, Doyle LW, Dewey D, Grunau RE, Asztalos EV, et al. Survival without disability to age 5 years after neonatal caffeine therapy for apnea of prematurity. *JAMA.* (2012) 307:275–82. doi: 10.1001/jama.2011.2024
137. Schmidt B, Roberts RS, Anderson PJ, Asztalos EV, Costantini L, Davis PG, et al. academic performance, motor function, and behavior 11 years after neonatal caffeine citrate therapy for apnea of prematurity. *JAMA Pediatr.* (2017) 171:564. doi: 10.1001/jamapediatrics.2017.0238
138. Mürner-Lavanchy IM, Doyle LW, Schmidt B, Roberts RS, Asztalos EV, Costantini L, et al. Neurobehavioral outcomes 11 years after neonatal caffeine therapy for apnea of prematurity. *Pediatrics.* (2018) 141:e20174047. doi: 10.1542/peds.2017-4047

Conflict of Interest: The authors declare that the research was conducted in the absence of any commercial or financial relationships that could be construed as a potential conflict of interest.

frontiers in Neurology

ORIGINAL RESEARCH
published: 26 August 2020
doi: 10.3389/fneur.2020.00885

Early Protein Intake Influences Neonatal Brain Measurements in Preterms: An Observational Study

Gianluca Terrin[1], Maria Chiara De Nardo[1], Giovanni Boscarino[1], Maria Di Chiara[1], Raffaella Cellitti[1], Simona Ciccarelli[1], Corinna Gasparini[1], Pasquale Parisi[2], Matteo Urna[2], Benedetta Ronchi[1], Alessia Russo[1], Giulia Sabatini[1] and Mario De Curtis[1]*

[1] Department of Maternal and Child Health, University of Rome La Sapienza, Rome, Italy, [2] Child Neurology, NESMOS Department, Faculty of Medicine & Psychology, Sapienza University, Rome, Italy

Introduction: To limit extrauterine growth restriction, recent guidelines on nutrition of preterm neonates recommended high protein intake since the first day of life (DOL). The impact of this nutritional strategy on the brain is still controversial. We aimed to evaluate the effects of protein intake on early cerebral growth in very low birth weight newborns.

Materials and Methods: We performed serial cranial ultrasound (cUS) scans at 3–7 DOL and at 28 DOL in very low birth weight newborns consecutively observed in the neonatal intensive care unit. We analyzed the relation between protein intake and cerebral measurements at 28 DOL performed by cUS.

Results: We enrolled 100 newborns (gestational age 29 ± 2 weeks, birth weight 1,274 ± 363 g). A significant ($p < 0.05$) positive correlation between enteral protein intake and biparietal diameter ($r = 0.490$**), occipital–frontal diameter ($r = 0.608$**), corpus callosum (length $r = 0.293$*, genu $r = 0.301$*), caudate head (right $r = 0.528$**, left $r = 0.364$**), and cerebellum (transverse diameter $r = 0.440$**, vermis height $r = 0.356$**, vermis width $r = 0.377$**) was observed at 28 DOL. Conversely, we found a significant negative correlation of protein intake given by parenteral nutrition (PN) with biparietal diameter ($r = -0.524$**), occipital–frontal diameter ($r = -0.568$**), body of corpus callosum ($r = -0.276$*), caudate head (right $r = -0.613$**, left $r = -0.444$**), and cerebellum (transverse diameter $r = -0.403$**, vermis height $r = -0.274$*, vermis width $r = -0.462$**) at 28 DOL. Multivariate regression analysis showed that measurements of occipital–frontal diameter, caudate head, and cerebellar vermis at 28 DOL depend positively on protein enteral intake ($r = 0.402$*, $r = 0.305$*, and $r = 0.271$*) and negatively by protein parenteral intake ($r = -0.278$*, $r = -0.488$*, and $r = -0.342$*).

Conclusion: Brain development in neonatal life depends on early protein intake. High protein intake affects cerebral structures' measurements of preterm newborn when administered by PN. Positive impact on brain development encourages the administration of recommended protein intake mainly by enteral nutrition.

Keywords: newborn, VLBW, enteral nutrition, parenteral nutrition, nutrition, amino-acids solution, cranial ultrasound, cerebral growth

OPEN ACCESS

Edited by:
Francisco J. Alvarez, Hospital de Cruces, Spain

Reviewed by:
Rosa Marotta, University of Magna Graecia, Italy
Andrea Domenico Praticò, University of Catania, Italy

****Correspondence:***
Gianluca Terrin
gianluca.terrin@uniroma1.it

Specialty section:
This article was submitted to Pediatric Neurology, a section of the journal Frontiers in Neurology

Received: *17 April 2020*
Accepted: *10 July 2020*
Published: *26 August 2020*

Citation:
Terrin G, De Nardo MC, Boscarino G, Di Chiara M, Cellitti R, Ciccarelli S, Gasparini C, Parisi P, Urna M, Ronchi B, Russo A, Sabatini G and De Curtis M (2020) Early Protein Intake Influences Neonatal Brain Measurements in Preterms: An Observational Study. Front. Neurol. 11:885. doi: 10.3389/fneur.2020.00885

INTRODUCTION

Extrauterine growth restriction (EUGR) frequently occurs in preterm neonates during the first weeks after birth (1). The growth failure in early life is, in turn, associated with an increased risk of neurological impairment (1). A number of studies demonstrated that high protein intake may limit EUGR (2). Thus, current guidelines for preterm newborns recommend the administration of high macronutrient doses since the first hours of life, through parenteral route (3, 4). The effect of this nutritional strategy on brain growth is widely debated. A limited number of studies investigated the impact of different nutritional practices on brain volume, using magnetic resonance imaging (MRI) at term equivalent age (TEA) (5). Considering inconclusive results of these studies, further research has been advocated (6). However, MRI is not easy to perform during the first weeks of life when clinical conditions of newborns are critical, even if this technique is considered the gold standard for the study of cerebral structures' measurements (7). Recently, it has been demonstrated that cranial ultrasound (cUS) can be reliably used to monitor cerebral growth in preterm infants (6, 8–11). The cUS is a low-cost bedside technique, repeatable as often as necessary, available, and widely used in the neonatal intensive care unit (NICU) (8). Starting from these considerations, we aimed to study the effects of high protein supply on early cerebral volume, through serial cUS examinations in preterm neonates.

MATERIALS AND METHODS

Study Design and Population

We designed a prospective observational study to assess the effects of protein intake on brain measures by using two-dimensional cUS in preterm neonates. All newborns with gestational age (GA) <32 weeks or body birth weight (BW) <1,500 g, consecutively admitted to the NICU of Policlinico Umberto I, La Sapienza University of Rome, were prospectively included between May 2017 and August 2019. We excluded infants with major congenital malformations, inborn errors of metabolism, congenital infections, intraventricular hemorrhage (IVH) stage ≥3, death, or transfer to other hospital before 72 h of life (12–15).

Collection Data

Prenatal, perinatal, and postnatal data were prospectively collected for each patient in specific data form. In particular, GA, BW, gender, type of delivery, twin pregnancy, antenatal steroid administration, Apgar score at the 1st and 5th min after birth, pH on cord blood at birth, body temperature at the 1st h of life, Clinical Risk Index for Babies II score (CRIB II), death, and need of invasive mechanical ventilation were recorded (16). Diagnosis of the major morbidities associated with prematurity, such as necrotizing enterocolitis (Bell stage ≥2), bronchopulmonary dysplasia, IVH, PVL, retinopathy of prematurity, and sepsis proven by positive cultures, were

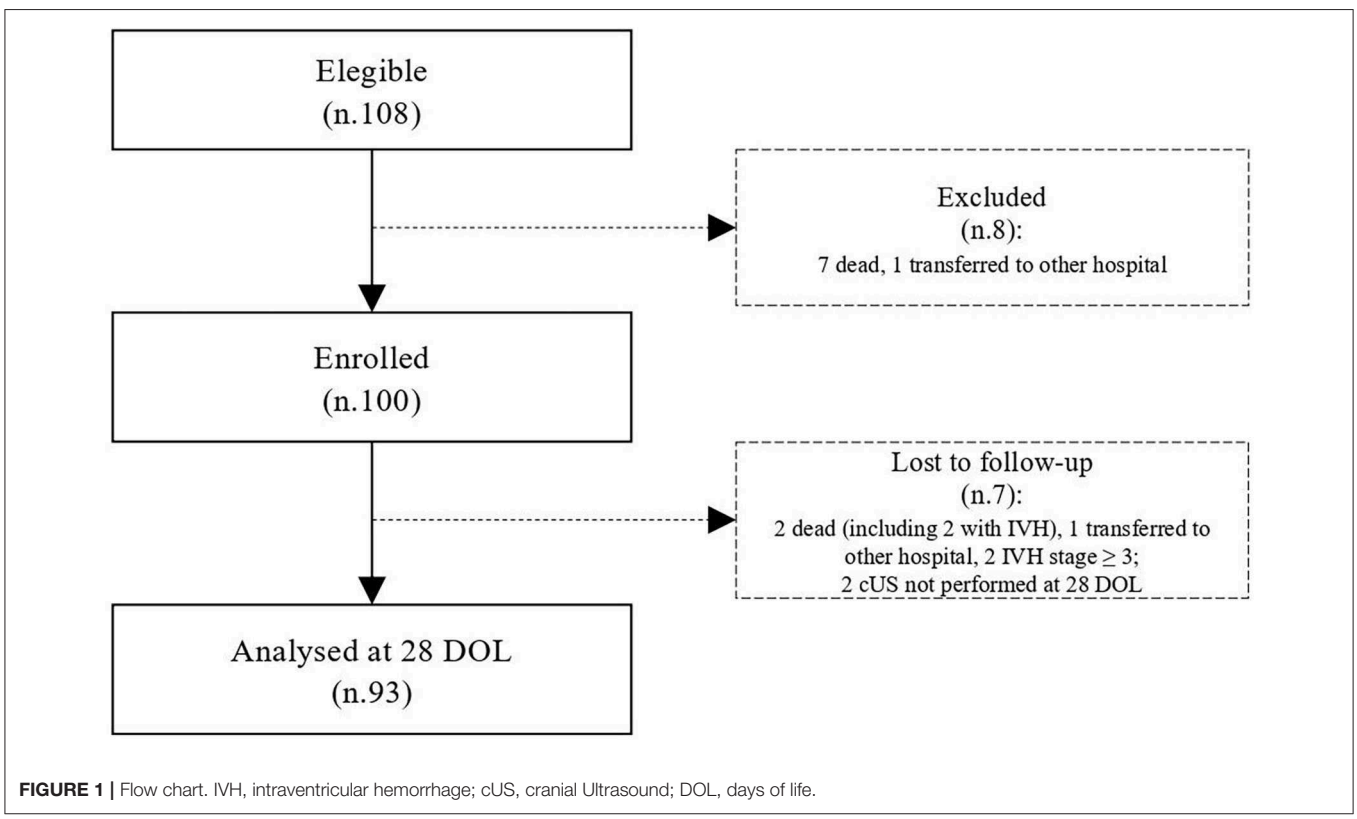

FIGURE 1 | Flow chart. IVH, intraventricular hemorrhage; cUS, cranial Ultrasound; DOL, days of life.

performed according to the standard criteria and recorded in the reporting form, as previously described (17, 18). Data on daily enteral and parenteral nutritional intake were collected during the first week of life. We collected data on parenteral nutrition (PN) complications. We measured head circumference of the newborns with a tape measure. We wrapped the tape, holding it above the eyebrows and the ears and the occipital prominence at the back of the skull, around the widest possible circumference of the head.

Nutritional Protocol

Enteral nutrition (EN) was commenced as soon as possible after birth in a stable newborn. Minimal enteral feeding was started within 24–48 h after birth at 10–20 mL/kg per day. The amount was increased by 20–30 mL/kg every day if EN was tolerated. Maternal milk (MM) without fortifications if available has been given fresh. Whether MM was not available or sufficient, a formula specifically for preterm newborns and routinely given in our NICU was used. Donor breast milk during the study period was not available. When signs or symptoms of feeding intolerance such as emesis, vomiting, severe abdominal distension associated with ileus with visible intestinal loops, blood in the stools, or systemic disorders (i.e., apnea, bradycardia, inadequate perfusion, and hemodynamic instabilities) were observed, the EN was withheld for at least 24 h (19, 20). Preterm MM was assumed to contain 65 kcal/100 mL, 1.5 g of protein/100 mL, 3.5 g of fat/100 mL, and 6.9 g of carbohydrate/100 mL. Macronutrient contents of formula and parenteral solutions were calculated based on the published manufacturers' recordings (Pre-nidina Nestlè®: proteins 2.9 g/dL, lipids 4.0 g/dL, energy 8.1 g/dL, sodium 51 mg/dL, potassium 119 mg/dL, calcium 116 mg/dL, phosphorus 77 mg/dL, iron 1.8 mg/dL, zinc 1.2 mg/dL). Parenteral nutrition was administered at birth in order to maintain adequate fluid, electrolyte, and nutrient intakes until exclusive enteral feeding (120 kcal/kg per day) was achieved. The overall fluid intake administered with enteral and PN started with 70–90 mL/kg per day and slowly increased by 10–20 mL/kg per day until reaching 150–180 mL kg per day. In PN, we administered 2 g of amino acids (TrophAmine® 6% Braun Medical Inc., Irvine, CA, USA) in the first day of life (DOL), and then we increased protein intake of 1 g/kg per day up to 4 g/kg per day, with 25 kcal per 1 g of proteins (**Table S1**). Glucose intake (dextrose injection 10%; Fresenius Kabi, USA) was started at 6 to 7 g/kg per day and increased of 0.5–1 g/kg per day up to 14 g/kg per day. Lipid (Smoflipd®; Fresenius Kabi, USA) intake was started at 1 g/kg per day and increased of 0.5–1 g/kg up to 3.5 g/kg per day. Total energy intake was calculated based on the cumulative amount of PN and EN in kcal/kg over the early 7 days. Target dose refers to enteral plus PN; thus, we adjusted intake from PN according to the amount of EN tolerated.

Cranial Ultrasonography Examination

The transducer frequency of sector probe (Philips EPIQ, Amsterdam, the Netherlands) was set at 5–10 MHz. Images were recorded in coronal and sagittal planes, according to standard procedure. We considered the anterior fontanel the optimal acoustic window for visualization of the supratentorial structures, whereas we used mastoid fontanel to evaluate the cerebellum and cerebellar vermis.

TABLE 1 | Clinical characteristics of study population.

***N* = 100**	
Gestational age, weeks	29 ± 2
Birth weight, g	1,274 ± 363
Male sex, *n* (%)	55 (55)
Cesarean section, *n* (%)	88 (88)
Twins, *n* (%)	30 (30)
Antenatal steroids,[a] *n* (%)	78 (78)
1-min Apgar score	6 ± 2
5-min Apgar score	8 ± 1
pH at birth	7.3 ± 0.1
Temperature at the 1st hour, °C	36.2 ± 0.5
Mortality, *n* (%)	3 (3)
Invasive mechanical ventilation, *n* (%)	22 (22)
NEC, *n* (%)	4 (4)
BPD, *n* (%)	4 (4)
IVH, *n* (%)	5 (5)
PLV, *n* (%)	1 (1)
ROP, *n* (%)	6 (6)
Sepsis proven by positive cultures, *N* (%)	10 (10)
Anemia of prematurity, *n* (%)	22 (22)
Full enteral feeding, days of life	15 ± 13
Star of enteral nutrition, days of life	1 ± 1
Duration of parenteral nutrition, days	15 ± 14

Data were expressed as mean ± standard deviation, when not specified. [a]Intramuscular steroids cycle in two doses of 12 mg over a 24-h period. NEC, necrotizing enterocolitis Bell stage ≥2); BPD, bronchopulmonary dysplasia; IVH intraventricular hemorrhage; PLV, periventricular leukomalacia; ROP, retinopathy of prematurity).

The cUS scans were obtained in enrolled newborns, at 3 to 7 DOL (T0) and at 28 DOL (T1), by two examiners with high training in cUS, unaware of the nutrition protocol and study aims. Each measurement was confirmed after an agreement between the two sonographers. They performed each measurement three times and then reported the mean value in a specific data form.

Cerebral structures were measured as previously described (6, 21–24). Scanning was performed at the bedside with the infant's head in supine position. With the anterior fontanel used as an acoustic window, standard views were obtained in the coronal and sagittal planes. In brief, intracranial biparietal diameter was measured in a coronal plane at the level of the foramen of Monro, and maximum intracranial occipital–frontal diameter was measured in the midsagittal plane. Maximum length of corpus callosum was measured in the midsagittal plane tracing a horizontal line between the extreme margins of the genu and the splenium. Maximum width of corpus callosum was measured in the midsagittal plane, separately for genu, body, and splenium. We visualized caudate nucleus below the floor of the frontal horn of the lateral ventricle, as a hypoechoic area located anteriorly to the caudothalamic groove. Width of the caudate head was measured in the parasagittal plane as the maximum

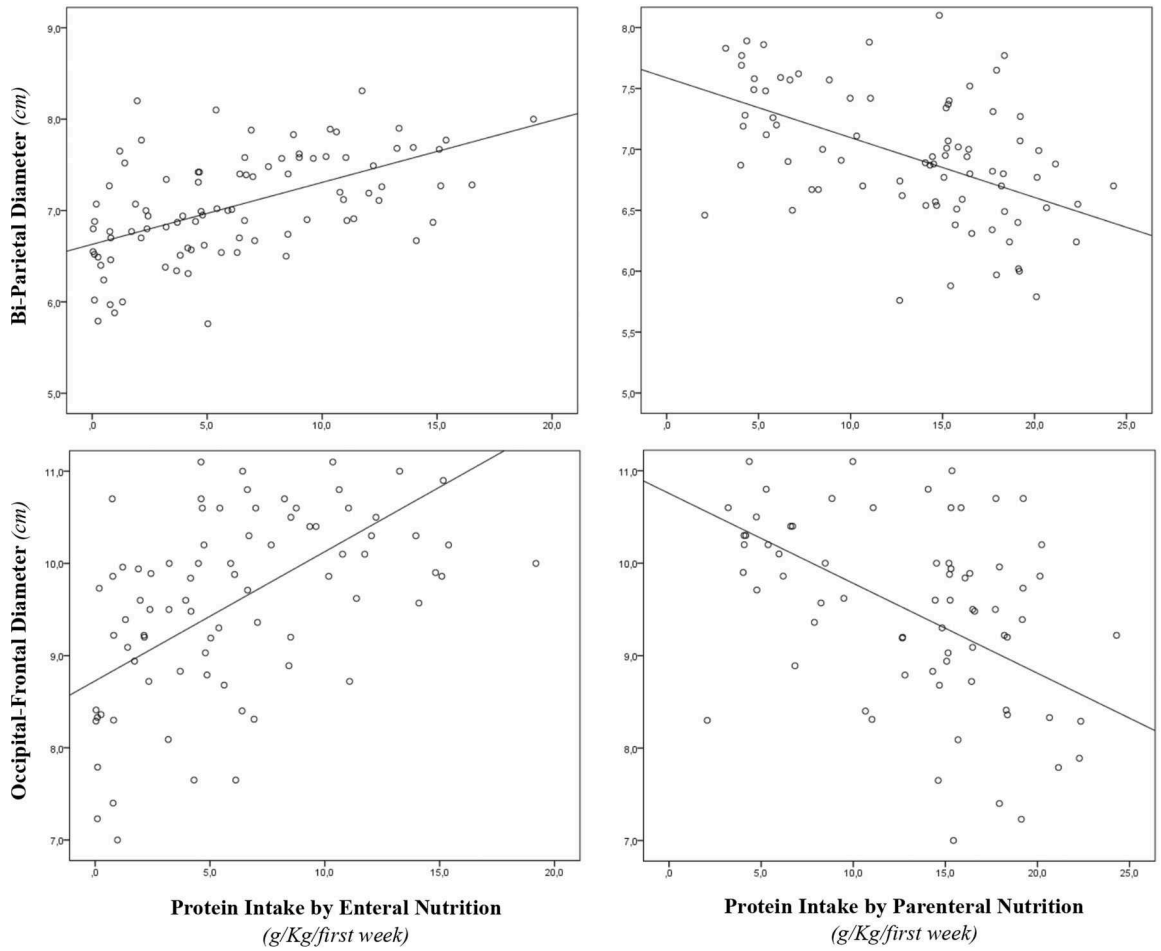

FIGURE 2 | Correlation between brain measures at 28 days of life and early protein intake. Enternal nutrition: Bi-Parietal Diameter ($r = 0.490$, $p < 0.001$), Occipital-frontal diameter ($r = 0.608$, $p < 0.001$). Parameter nutrition: Bi-parietal diameter ($r = -0.524$, $p < 0.001$), Occipital-frontal diameter ($r = -0.568$, $p < 0.001$).

extension of this area. Both height and width of the cerebellar vermis and transverse cerebellar diameter were measured in axial plane.

Statistical Analysis

Data analysis was performed using IBM the Statistical Package for the Social Sciences Statistics version 22.0 (SPSS Inc., Chicago, IL, USA). We checked for normality using Shapiro–Wilk test. The mean and standard deviation or median and interquartile range summarized continuous variables. We compared categorical variable using χ^2 test and paired and unpaired variables by *t* test or Mann-Whitney *U* test. Nutritional intake was related to the bidimensional measurements of the different brain structures and cerebral diameters collected during the first week of life (T0) and at 28 DOL (T1). We performed correlation between variables by Wilcoxon rank sum tests and by Pearson correlation. To evaluate the effects of protein intake given by PN in homogenous population, we selected newborns that were nourished mainly by PN in the first week of life. In particular, we analyzed separately patients receiving more than 70% of nutritional support by PN from 0 to 7 DOL. In this subpopulation, we calculated the percentile of total protein intake at the first week of life. Thus, we considered at high protein regimen intake patients receiving any value equal to or >50th percentile and at low protein regimen intake those receiving <50th centile of protein intake. To evaluate the effect of different protein intake on the size of cerebral structures, we compared newborns at high protein regimen intake with those at low protein regimen intake. Multivariable regression analysis was performed to study the possible influence of confounding variables (i.e., BW, gender, cord blood pH, nutritional intake, morbidity) on linear measurements of structures that were significantly correlated with protein intake at the first week of life. The level of significance for all statistical tests was two-sided ($p < 0.05$).

Ethics

The study was conducted in conformity with the World Medical Association Declaration of Helsinki for medical research involving human subjects. This article reports a part of the results of the study protocol that was approved by the ethics committee

of Policlinico Umberto I, University La Sapienza of Rome (with number 5089). We asked parents for consent, and we collected anonymized data in the database.

RESULTS

During the study period, we considered eligible 108 newborns. We enrolled 100 patients as shown in **Figure 1**. In **Table 1**, we reported the main demographic and clinical features of the study population. We observed a significant relation between head circumference and protein intake given by EN ($r = 0.467$, $p < 0.001$) and PN ($r = -0.478$, $p < 0.001$). We found a significant correlation between biparietal diameter, occipital–frontal diameter measured by cUS, and protein intake of the first week of life (**Figure 2**). Correlations between linear measurements of specific brain districts and early protein intake are reported in **Table 2**. In particular, length and genu of corpus callosum, caudate head (right and left), transverse diameter of cerebellum, and cerebellar vermis (height and width) were positively correlated with EN protein intake (**Table 2**). Body of corpus callosum, caudate head bilaterally, and cerebellum measures were negatively related with PN protein intake (**Table 2**). When we analyzed the total amount (EN + PN) of protein intake received in the first week of life, we observed a negative correlation with caudate head bilaterally and with vermis width (**Table 2**).

Multivariate regression analysis showed that many linear measurements of brain structures at 28 DOL (occipital–frontal diameter, caudate heads, and cerebellar vermis) depended on nutritional intake (**Table 3**). Of note, we observed a different relation with EN (positive) and PN (negative).

Biparietal diameter, corpus callosum, and cerebellum transverse diameter depended on covariates (i.e., BW, sex, pH at birth, morbidity), but not by protein intake (**Table 3**).

Forty-five newborns were nourished mainly by PN in the first week of life. In this subpopulation, we found that left caudate head and cerebellar vermis width were smaller in subjects receiving high protein intake compared with those receiving low protein intake at 28 DOL, but not at T0 (**Table 4**, **Table S2**). In **Table S3**, we reported the occurrence of PN complications according to protein regimen.

TABLE 2 | Correlations between cerebral structures linear measures and protein intake.

Measures[a]	Protein intake in the 1st week of life		
	By EN (g/kg first week)	By PN (g/kg first week)	Total (g/kg first week)
Corpus callosum			
Length	0.293*	−0.252	−0.059
Body	0.244	−0.276*	−0.198
Genu	0.301*	−0.252	0.047
Splenium	0.169	−0.177	−0.105
Caudate head			
Right	0.528**	−0.613**	−0.468**
Left	0.364**	−0.444**	−0.372**
Cerebellum			
Transverse diameter	0.440**	−0.403**	−0.148
Vermis height	0.356**	−0.274*	0.001
Vermis width	0.377**	−0.462**	−0.387**

[a]*Measured at 28 days of life. *p<0.05; **p<0.01.*

DISCUSSION

Brain development in neonatal life depends on early protein intake. We demonstrate that the route of protein administration may have different impact on cerebral measurements. Enteral intake has a positive effect, whereas high dose of amino acids

TABLE 3 | Multivariate analysis of covariate influencing cerebral measures at 28 days of life in preterm newborns.

Dependent variables[a]	Covariates (model 1)					Covariates (model 2)				
	Birth weight	Male sex	pH at birth	Morbidity[§]	EN protein intake 1st w	Birth weight	Male sex	pH at birth	Morbidity[§]	PN protein intake 1st w
Biparietal diameter	0.515*	−0.025	0.112	0.094	0.191	0.557*	0.039	0.130	0.091	−0.145
Occipital–frontal diameter	0.204	0.016	−0.023	−0.109	0.402*	0.319*	−0.051	−0.004	−0.139	−0.278*
Corpus callosum, length	0.106	0.080	−0.125	−0.213*	0.153	0.169	0.046	−0.141	−0.255*	−0.082
Corpus callosum, body	0.130	−0.082	0.235*	−0.106	0.036	0.062	−0.111	0.235*	−0.104	−0.121
Caudate head width, right	0.247*	0.076	0.079	0.080	0.305*	0.133	0.073	0.054	0.117	−0.488*
Caudate head width, left	0.238	−0.031	0.126	0.230*	0.210	0.072	−0.004	0.090	0.227*	−0.427*
Cerebellum transverse diameter	0.320*	0.233*	0.017	−0.004	0.164	0.468*	0.165	0.037	−0.003	−0.110
Cerebellar vermis, height	−0.073	0.209	−0.107	0.010	0.300*	0.070	0.117	−0.148	−0.078	−0.247
Cerebellar vermis, width	0.038	0.081	0.019	−0.083	0.271*	0.007	0.052	0.002	−0.171	−0.342*

[a]*Measured at 28 days of life.* [§]*Necrotizing enterocolitis and/or sepsis proven by positive cultures and/or bronchopulmonary dysplasia. *p < 0.05. 1st w, first week of life; EN, enteral nutrition; PN, parenteral nutrition.*

TABLE 4 | Effects of different protein intake in parenteral nutrition on cerebral measures.

General characteristics	High protein regimen	Low protein regimen	*p*
Number	23	22	
Gestational age at birth, weeks	27.6 ± 2.1	28.6 ± 2.5	0.161
Birth weight, g	1,014 ± 287	1,118 ± 320	0.763
Male sex, *n* (%)	13 (56.5)	14 (63.6)	1.000
Cesarean section, *n* (%)	21 (91.3)	18 (81.8)	0.311
Twins, *n* (%)	7 (30.4)	6 (27.3)	1.000
Antenatal steroids,[a] *n* (%)	15 (65.2)	19 (86.4)	0.165
1-min Apgar score	5 ± 2	5 ± 2	0.369
5-min Apgar score	8 ± 1	8 ± 1	0.859
pH at birth	7.2 ± 0.1	7.3 ± 0.1	0.387
Temperature at the 1st hour, °C	36.0 ± 0.4	36.2 ± 0.5	0.137
Invasive mechanical ventilation, *n* (%)	8 (34.8)	10 (45.5)	0.550
NEC, *n* (%)	0 (0)	1 (4.5)	0.489
Sepsis, *n* (%)	5 (21.7)	2 (9.1)	0.414
BPD, *n* (%)	3 (13.0)	0 (0)	0.233
IVH, *n* (%)	1 (4.3)	4 (18.2)	0.187
IVH stage ≥3, *n* (%)	0 (0)	3 (13.6)	0.109
PLV, *n* (%)	0 (0)	0 (0)	-
ROP, *n* (%)	3 (13.0)	13 (13.6)	0.646
Anemia of prematurity, *n* (%)	10 (43.5)	8 (36.4)	0.428
Mortality, *n* (%)	1 (4.3)	1 (4.5)	1.000
Full enteral feeding, days of life	22 ± 16	21 ± 11	0.893
Star of enteral nutrition, days of life	2 ± 2	2 ± 2	0.343
Duration of parenteral nutrition, days	21 ± 16	20 ± 11	0.807
Cerebral measures[b]			
Biparietal diameter	66 ± 6	68 ± 6	0.226
Occipital–frontal diameter	90 ± 14	89 ± 10	0.697
Head circumference	282 ± 29	295 ± 21	0.188
Corpus callosum			
Length	38 ± 5	39 ± 3	0.578
Body	2 ± 0	2 ± 0	0.186
Genu	3 ± 1	3 ± 1	0.883
Splenium	3 ± 1	3 ± 1	0.167
Caudate head			
Right	5 ± 1	5 ± 1	0.101
Left	5 ± 1	6 ± 1	0.037
Cerebellum			
Transverse diameter	42 ± 5	43 ± 5	0.624
Vermis height	10 ± 2	10 ± 2	0.975
Vermis width	7 ± 1	8 ± 2	0.049

Data were expressed as mean ± standard deviation, when not specified. After percentile calculation, we considered 19.4 g/kg per week (50°pc) the cutoff value to classify protein regimen intake as "high" or "low"; an intramuscular steroids cycle in two doses of 12 mg over a 24-h period. [a]Measured in mm at 28 days of life. [b]CRIB II: Clinical Risk Index for Babies, without temperature measures. NEC, necrotizing enterocolitis Bell stage ≥2; BPD, bronchopulmonary dysplasia; IVH, intraventricular hemorrhage; PLV, periventricular leukomalacia; ROP, retinopathy of prematurity.

by PN seems to affect the size of such brain structures during neonatal life.

Available evidences reported inconclusive results on the influence of early protein intake on the brain measurements (25). Differences between protein intake administered through either EN or PN have not been described in a recent meta-analysis including 21 randomized controlled trial (RCT) (25). In an RCT, comparing two groups of adolescents with a history of prematurity who were assigned to a standard- or high-EN protocol in the early postnatal life, those fed with preterm formula (protein 2 g/dL, 80 kcal/dL) showed significantly larger caudate volumes compared with babies fed by standard term formula (protein 1.4 g/dL, 68 kcal/dL) (26). The study is focused on the sole effect of enteral protein intake, whereas the role of PN was not investigated. Also, among cohort studies in this field, the relation between protein intake in PN and early cerebral growth was not clarified (5, 27, 28). Inconclusive results were also reported by studies that investigated the effects of early nutritional intake on brain maturation, instead of cerebral growth. Strømmen et al. (29) in an RCT reported a negative relation between aggressive nutrition and regional white matter mean diffusivity to TEA. No definite conclusions were drawn by Beauport et al. (30), which investigated the effects of total amounts of nutrients received in early life, without comparing the impact of protein intake given by PN separately by those of EN. To the best of our knowledge, we evaluate, for the first time, separately the role of route of administration of recommended protein intake on the brain in neonatal age. Our results underline the importance of protein intake on cerebral growth but, at the same time, suggest caution in the administration of high doses of amino acid in the first week of life through PN.

We hypothesize a number of mechanisms that may support the negative relation between PN intake and brain size. It is worth mentioning that newborns fed with higher PN are exposed to an environment, which limits infant's opportunity to develop their regulatory capacities (26). Furthermore, the side effects associated with aggressive PN (i.e., hyperglycemia, hypoglycemia, metabolic acidosis, elevated serum blood urea nitrogen, high plasma ammonia concentrations, hyperkalemia) may affect brain development (31). Recent studies have reported data on high protein intake delivered by PN leading to increased levels of specific amino acids, potentially toxic (e.g., glycine, phenylalanine, methionine) (32). It has also been described that insufficiency of amino acids, classified as essential, could represent a major limit for cerebral growth (33). Finally, an imbalance of amino acid levels may adversely affect neurotransmitters metabolism (32). In parallel, the positive effect of EN could be explained by the better composition of protein delivered through EN that may avoid the side effects PN related to the potential amino acids toxicity and by the balance of essential and non-essential amino acids.

We observed significant effects of protein intake mainly on caudate and cerebellar vermis, which are known to be a very vulnerable part of the brain in preterm infants (26). Preterm babies showing later neurological problems frequently present damage of these districts. We believe that protein intake

may affect the development of this district in a crucial phase of cerebral growth. Dopamine is a main neurotransmitter of neonatal brain (34). The caudate structure is highly innervated by dopamine neurons (35). The direct precursor of dopamine, L-DOPA, is synthesized from the nonessential amino acid tyrosine (36). Recently, Mayes et al. (37) reported that hyperalimentation by PN can result in a paradoxical fall of tyrosine levels. Low tyrosine levels, affecting dopamine synthesis, may impair the development of brain districts that directly depend by dopamine neurons. However, further studies are advocated to clarify the relation between protein intake and dopamine metabolism in cerebral growth.

Despite being interesting, the results of this study should be interpreted taking into account specific limitations. This is a single-center observational study. We know that the cUS is a highly operator-dependent imaging modality. In order to limit associated bias, two different physicians performed a series of scans using cUS, and each measurement was recorded only after an agreement between the two investigators. In addition, the physicians who performed the cUS were unaware of the nutritional intake received at the time of the cUS examination. To measure cerebral structures, we used cUS instead of MRI, considered the gold-standard technique for the study of brain volumes. To improve the accuracy, we collected and analyzed only measurements of the cerebral structures that were previously assessed in a comparative study between MRI and cUS (6). The use of cUS allowed us to perform serial measurements of brain structures, avoiding issues of transporting to the radiological service and the sedation during the scan session for critical babies. Finally, no data on long-term neurodevelopment were analyzed in this study. Thus, it is not possible to establish if the results observed at 28 DOL on brain measurements may have consequences on the long-term neurodevelopment. Finally, comparison between high and low protein intake regimen was performed on a subpopulation of newborns. This may affect the generalizability of the results.

In conclusion, we observed that the administration of high doses of protein by PN is harmful for premature babies, in line with recent studies on pediatric population, which suggest avoiding aggressive nutritional practice in critically ill subjects (38). Positive impact on brain development encourages the administration of recommended protein intake mainly by EN. When EN is not possible, a beneficial undernutrition by parenteral route could be considered as a safe option, particularly in the first DOL. A challenging issue that should be addressed by further research is to establish what are the nutritional strategies promoting growth and brain development without additional risk for preterm babies.

DATA AVAILABILITY STATEMENT

The raw data supporting the conclusions of this article will be made available by the authors, without undue reservation.

ETHICS STATEMENT

The studies involving human participants were reviewed and approved by the Ethics Committee of Policlinico Umberto I, University La Sapienza of Rome (with number 5089). Written informed consent to participate in this study was provided by the participants' legal guardian/next of kin.

AUTHOR CONTRIBUTIONS

GT, MCDN, GB, RC, and MDeC were responsible for the study design. GT, MCDN, GB, MDiC, and SC were responsible for the literature search and manuscript drafting. GT, MCDN, GB, MDiC, RC, SC, PP, MU, CG, BR, AR, GS, and MDeC were responsible for critical revision of the manuscript. All authors contributed to the article and approved the submitted version.

SUPPLEMENTARY MATERIAL

The Supplementary Material for this article can be found online at: https://www.frontiersin.org/articles/10.3389/fneur.2020.00885/full#supplementary-material

REFERENCES

1. Kumar RK, Singhal A, Vaidya U, Banerjee S, Anwar F, Rao S. Optimizing nutrition in preterm low birth weight infants—consensus summary. *Front Nutr.* (2017) 4:20. doi: 10.3389/fnut.2017.00020
2. Hay WW. Aggressive nutrition of the preterm infant. *Curr Pediatr Rep.* (2013) 1:229–39. doi: 10.1007/s40124-013-0026-4
3. van Goudoever JB, Carnielli V, Darmaun D, Sainz de Pipaon M, Braegger C, Bronsky J, et al. ESPGHAN/ESPEN/ESPR/CSPEN guidelines on pediatric parenteral nutrition: amino acids. *Clin Nutrit.* (2018) 37:2315–23. doi: 10.1016/j.clnu.2018.06.945
4. Senterre T, Terrin G, De Curtis M. Parenteral nutrition in premature infants In: *Pediatric Gastroenterology, Hepatology and Nutrition: A Comprehensive Guide To Practice.* Cham: Springer (2016). p. 73–86. doi: 10.1007/978-3-319-17169-2_7
5. Coviello C, Keunen K, Kersbergen KJ, Groenendaal F, Leemans A, Peels B, et al. Effects of early nutrition and growth on brain volumes, white matter microstructure, and neurodevelopmental outcome in preterm newborns. *Pediatr Res.* (2018) 83:102–110. doi: 10.1038/pr.2017.227
6. Leijser LM, Srinivasan L, Rutherford MA, Counsell SJ, Allsop JM, Cowan FM. Structural linear measurements in the newborn brain: accuracy of cranial ultrasound compared to MRI. *Pediatr Radiol.* (2007) 37:640–8. doi: 10.1007/s00247-007-0485-2
7. Dudink J, Jeanne Steggerda S, Horsch S, eurUS.brain group. State-of-the-art neonatal cerebral ultrasound: technique and reporting. *Pediatr Res.* (2020) 87:3–12. doi: 10.1038/s41390-020-0776-y
8. Beijst C, Dudink J, Wientjes R, Benavente-Fernandez I, Groenendaal F, Brouwer MJ, et al. Two-dimensional ultrasound measurements vs. magnetic resonance imaging-derived ventricular volume of preterm infants with germinal matrix intraventricular haemorrhage. *Pediatr Radiol.* (2020) 50:234–41. doi: 10.1007/s00247-019-04542-x
9. Horsch S, Bengtsson J, Nordell A, Lagercrantz H, Ådén U, Blennow M. Lateral ventricular size in extremely premature infants: 3D MRI confirms 2D ultrasound measurements. *Ultrasound Med Biol.* (2009) 35:360–6. doi: 10.1016/j.ultrasmedbio.2008.09.006

10. Benavente-Fernandez I, Lubián-Gutierrez M, Jimenez-Gomez G, Lechuga-Sancho AM, Lubián-López SP, Neonatal Neurology Foundation (Fundación Nene). Ultrasound lineal measurements predict ventricular volume in posthaemorrhagic ventricular dilatation in preterm infants. *Acta Paediatr.* (2017) 106:211–7. doi: 10.1111/apa.13645
11. Hintz SR, Barnes PD, Bulas D, Slovis TL, Finer NN, Wrage LA, et al. Neuroimaging and neurodevelopmental outcome in extremely preterm infants. *Pediatrics.* (2015) 135:e32–e42. doi: 10.1542/peds.2014-0898
12. Canani RB, Terrin G. Recent progress in congenital diarrheal disorders. *Curr Gastroenterol Rep.* (2011) 13:257–64. doi: 10.1007/s11894-011-0188-6
13. Salvia G, Cascioli CF, Ciccimarra F, Terrin G, Cucchiara S. A case of protein-losing enteropathy caused by intestinal lymphangiectasia in a preterm infant. *Pediatrics.* (2001) 107:416–7. doi: 10.1542/peds.107.2.416
14. Passariello A. Diarrhea in neonatal intensive care unit. *WJG.* (2010) 16:2664. doi: 10.3748/wjg.v16.i21.2664
15. Whitelaw A. Intraventricular haemorrhage and posthaemorrhagic hydrocephalus: pathogenesis, prevention and future interventions. *Semin Neonatol.* (2001) 6:135–46. doi: 10.1053/siny.2001.0047
16. Parry G, Tucker J, Tarnow-Mordi W. CRIB II: an update of the clinical risk index for babies score. *Lancet.* (2003) 361:1789–1791. doi: 10.1016/S0140-6736(03)13397-1
17. Terrin G, Boscarino G, Di Chiara M, Iacobelli S, Faccioli F, Greco C, et al. Nutritional intake influences zinc levels in preterm newborns: an observational study. *Nutrients.* (2020) 12:529. doi: 10.3390/nu12020529
18. Terrin G, Coscia A, Boscarino G, Faccioli F, Di Chiara M, Greco C, et al. Long-term effects on growth of an energy-enhanced parenteral nutrition in preterm newborn: a quasi-experimental study. *PLoS ONE.* (2020) 15:e0235540. doi: 10.1371/journal.pone.0235540
19. Terrin G, Passariello A, Canani RB, Manguso F, Paludetto R, Cascioli C. Minimal enteral feeding reduces the risk of sepsis in feed-intolerant very low birth weight newborns. *Acta Paediatrica.* (2009) 98:31–5. doi: 10.1111/j.1651-2227.2008.00987.x
20. Berni Canani R, Passariello A, Buccigrossi V, Terrin G, Guarino A. The nutritional modulation of the evolving intestine. *J Clin Gastroenterol.* (2008) 42:S197–200. doi: 10.1097/MCG.0b013e31817da155
21. Graça AM, Geraldo AF, Cardoso K, Cowan FM. Preterm cerebellum at term age: ultrasound measurements are not different from infants born at term. *Pediatr Res.* (2013) 74:698–704. doi: 10.1038/pr.2013.154
22. Davies MW, Swaminathan M, Betheras FR. Measurement of the transverse cerebellar diameter in preterm neonates and its use in assessment of gestational age. *Australas Radiol.* (2001) 45:309–12. doi: 10.1046/j.1440-1673.2001.00926.x
23. Imamoglu EY, Gursoy T, Ovali F, Hayran M, Karatekin G. Nomograms of cerebellar vermis height and transverse cerebellar diameter in appropriate-for-gestational-age neonates. *Early Hum Dev.* (2013) 89:919–23. doi: 10.1016/j.earlhumdev.2013.10.001
24. da Graça ALFM, Cardoso KRV, da Costa JMFP, Cowan FM. Assessment of gestational age using cerebellar measurements at cranial ultrasound: what is the best approach? *Early Hum Dev.* (2013) 89:1–5. doi: 10.1016/j.earlhumdev.2012.07.008
25. Osborn DA, Schindler T, Jones LJ, Sinn JK, Bolisetty S. Higher versus lower amino acid intake in parenteral nutrition for newborn infants. *Cochr Database System Rev.* (2018) 3:1465–858. doi: 10.1002/14651858.CD005949.pub2
26. Isaacs EB, Gadian DG, Sabatini S, Chong WK, Quinn BT, Fischl BR, et al. The effect of early human diet on caudate volumes and IQ. *Pediatr Res.* (2008) 63:308–14. doi: 10.1203/PDR.0b013e318163a271
27. Power VA, Spittle AJ, Lee KJ, Anderson PJ, Thompson DK, Doyle LW, et al. Nutrition, growth, brain volume, and neurodevelopment in very preterm children. *J Pediatrics.* (2019) 215:50–5.e3. doi: 10.1016/j.jpeds.2019.08.031
28. Schneider J, Fischer Fumeaux CJ, Duerden EG, Guo T, Foong J, Graz MB, et al. Nutrient intake in the first two weeks of life and brain growth in preterm neonates. *Pediatrics.* (2018) 141:e20172169. doi: 10.1542/peds.2017-2169
29. Strømmen K, Blakstad EW, Moltu SJ, Almaas AN, Westerberg AC, Amlien IK, et al. Enhanced nutrient supply to very low birth weight infants is associated with improved white matter maturation and head growth. *Neonatology.* (2015) 107:68–75. doi: 10.1159/000368181
30. Beauport L, Schneider J, Faouzi M, Hagmann P, Hüppi PS, Tolsa J-F, et al. Impact of early nutritional intake on preterm brain: a magnetic resonance imaging study. *J Pediatrics.* (2017) 181:29–36.e1. doi: 10.1016/j.jpeds.2016.09.073
31. Stensvold HJ, Strommen K, Lang AM, Abrahamsen TG, Steen EK, Pripp AH, et al. Early enhanced parenteral nutrition, hyperglycemia, and death among extremely low-birth-weight infants. *JAMA Pediatr.* (2015) 169:1003. doi: 10.1001/jamapediatrics.2015.1667
32. te Braake FWJ, van den Akker CHP, Riedijk MA, van Goudoever JB. Parenteral amino acid and energy administration to premature infants in early life. *Sem Fetal Neonatal Med.* (2007) 12:11–8. doi: 10.1016/j.siny.2006.10.002
33. Makrides M, Gibson RA, McPhee AJ, Collins CT, Davis PG, Doyle LW, et al. Neurodevelopmental outcomes of preterm infants fed high-dose docosahexaenoic acid: a randomized controlled trial. *JAMA.* (2009) 301:175. doi: 10.1001/jama.2008.945
34. Volpe JJ, Volpe JJ eds. *Volpe's Neurology of the Newborn.* Sixth edition. Philadelphia, PA: Elsevier (2018).
35. White NM. Some highlights of research on the effects of caudate nucleus lesions over the past 200 years. *Behav Brain Res.* (2009) 199:3–23. doi: 10.1016/j.bbr.2008.12.003
36. Musacchio JM. Chapter 1: enzymes involved in the biosynthesis degradation of catecholamines. In: *Inverson L. Biochemistry of Biogenic Amines.* Boston, MA: Springer (2013). p. 1–35. doi: 10.1007/978-1-4684-3171-1_1
37. Mayes K, Tan M, Morgan C. Effect of hyperalimentation and insulin-treated hyperglycemia on tyrosine levels in very preterm infants receiving parenteral nutrition. *JPEN J Parenter Enteral Nutr.* (2014) 38:92–8. doi: 10.1177/0148607112467036
38. Vanhorebeek I, Verbruggen S, Casaer MP, Gunst J, Wouters PJ, Hanot J, et al. Effect of early supplemental parenteral nutrition in the paediatric ICU: a preplanned observational study of post-randomisation treatments in the PEPaNIC trial. *Lancet Respir Med.* (2017) 5:475–83. doi: 10.1016/S2213-2600(17)30186-8

Conflict of Interest: The authors declare that the research was conducted in the absence of any commercial or financial relationships that could be construed as a potential conflict of interest.

frontiers in Neurology

ORIGINAL RESEARCH
published: 02 September 2020
doi: 10.3389/fneur.2020.00930

Intranasal IL-4 Administration Alleviates Functional Deficits of Periventricular Leukomalacia in Neonatal Mice

Lin-chao Yu[1,2,3,4,5], *Jing-kun Miao*[1,2,3,6], *Wei-bin Li*[7], *Na Chen*[1,2,3] *and Qi-xiong Chen*[1,2,3,4,7]*

[1] Department of Neonatology, Children's Hospital of Chongqing Medical University, Chongqing, China, [2] National Clinical Research Center for Child Health and Disorders, Chongqing, China, [3] Ministry of Education Key Laboratory of Child Development and Disorders, Chongqing, China, [4] Chongqing Key Laboratory of Pediatrics, Chongqing, China, [5] Chongqing Key Laboratory of Child Health and Nutrition, Chongqing, China, [6] Chongqing Health Center for Women and Children, Chongqing, China, [7] Chongqing Hospital of Traditional Chinese Medicine, Chongqing, China

Background: Periventricular leukomalacia (PVL) is the major form of brain injury in premature infants. Currently, there are no therapies to treat PVL. Several studies suggested that polarization of microglia, a resident macrophage-like immune cell in the central nervous system, plays a vital role in brain injury and recovery. As an important mediator of immunity, interleukin-4 (IL-4) has critical effects on many immune cells, such as astrocytes and microglia. Increasing evidence shows that IL-4 plays a well-established role in attenuating inflammation in neurological disorders. Additionally, as a noninvasive and highly effective method, intranasal drug administration is gaining increasing attention. Therefore, in our study, we hypothesized that intranasal IL-4 administration is a promising strategy for PVL treatment.

Methods: The therapeutic effects of IL-4 on neuroprotection were evaluated using a Control group, Hypoxia group, and Hypoxia + IL-4 treatment group. The PVL mouse model was established by a severe acute hypoxia (SAH) protocol. Exogenous IL-4 was intranasally administered to investigate its neuroprotective effects. A functional study was used to investigate neurological deficits, immunohistochemical technology and Western blotting were used to detect protein levels, and electron microscopy was used to evaluate myelination.

Results: The results suggested that hypoxia stimulated Iba1^{+} microglial activation, downregulated myelin-related gene (*NG2*, *MAG*, and *MBP*) expression, reduced MBP protein levels, and caused neurological deficits. However, the intranasal administration of exogenous IL-4 partially inhibited Iba1+ microglial activation, improved myelination, and alleviated neurological deficits. The mechanistic study showed that IL-4 improved myelination possibly through the IL-4Ra-mediated polarization of microglia from the M1 phenotype to the M2 phenotype.

OPEN ACCESS

Edited by:
Francisco J. Alvarez, Hospital de Cruces, Spain

Reviewed by:
Gavin John Clowry, Newcastle University, United Kingdom
Gulnaz Begum, University of Pittsburgh, United States

***Correspondence:**
Qi-xiong Chen
13193039866@126.com

Specialty section:
This article was submitted to Pediatric Neurology, a section of the journal Frontiers in Neurology

Received: *21 May 2020*
Accepted: *17 July 2020*
Published: *02 September 2020*

Citation:
Yu L-c, Miao J-k, Li W-b, Chen N and Chen Q-x (2020) Intranasal IL-4 Administration Alleviates Functional Deficits of Periventricular Leukomalacia in Neonatal Mice. Front. Neurol. 11:930. doi: 10.3389/fneur.2020.00930

Conclusion: In summary, our findings demonstrated that the intranasal administration of exogenous IL-4 improves myelination and attenuates functional deficits in a hypoxia-induced PVL model. Intranasal IL-4 administration may be a promising strategy for PVL treatment, for which further mechanistic studies are urgent.

Keywords: IL-4 administration, intranasally, periventricular leukomalacia, remyelination, microglia

INTRODUCTION

According to the WHO's estimates, births of very preterm infants (before 32 weeks of gestation) account for more than 2% of all live births, and the survival rates of these infants are more than 85% (1, 2), which is owing to advancements in obstetric and neonatal care (3). However, 25–50% of very preterm babies who survive still exhibit cognitive (4), visual (5), attention (3), and learning disabilities (6), such as cerebral palsy, which costs ∼1 million dollars per person in the United States (7). Diffuse white matter injury is the most common form of injury in preterm birth infants, especially in infants with very low birth weights, and it is a condition that leads to periventricular leukomalacia (PVL) (8, 9). Many studies have found that PVL is associated with disruptions in the normal progression of preoligodendrocytes, which leads to prominent hypomyelination (10–12). Consistent with the effects of hypoxia–ischemia, preterm WMI is also accompanied by significant oxidative damage (13, 14). Microglial cells are resident macrophage-like cells in the central nervous system that have vital roles during brain development (15, 16). To participate in injury responses, immune regulation, and cytotoxic effects, microglia are capable of acquiring complex phenotypes (17). M1-polarized phenotypes are related to the secretion of nitrogen species and pro-inflammatory cytokines (18); M2-polarized phenotypes are associated with the secretion of growth factors and anti-inflammatory cytokines (18). Some studies have found that activated microglia, at least in the initial phase after injury, are involved in injury to immature white matter. In the acute phase, activated microglia, such as those with M1 phenotypes, have harmful effects on neurons and glia by releasing inflammatory cytokines, generating free radicals, and enhancing excitotoxicity (19, 20). However, after acute injury, some microglia, such as those with M2 phenotypes (M2a and M2c), might promote injury repair by being involved in late anti-inflammatory responses (21, 22).

Interleukin-4 (IL-4), a cytokine secreted primarily by Th2 cells, eosinophils, basophils, and mast cells, is a critical regulator of immunity (23, 24). Some studies have shown that IL-4 plays a central role in the production of the anti-inflammatory factors IL-10 and IL-13 while suppressing the generation of pro-inflammatory cytokines, such as IL-1, INF-a, and TNF-a (25, 26). In a focal ischemia model, the administration of exogenous IL-4 improved the neurological score, increased the spontaneous polarization, reduced the infarction volume, and decreased the infiltration of macrophages/microglia (27, 28), especially those with M2 phenotypes. However, loss of IL-4 increased the number of cells with the M1 phenotype ($Iba1^+iNOS^+$) and decreased the number of cells with the M2 phenotype ($Iba1^+Arg^+$) (28).

In our previous study, the IL-4 concentrations were significantly lower in asphyxiated newborn mice than in normoxic mice. Considering that IL-4 is associated with reduced macrophage/microglia infiltration and altered microglia phenotype ratios during hypoxia–ischemia injury to the brain, we tested the hypothesis that IL-4 reduces the release of pro-inflammatory cytokines, increases the production of anti-inflammatory factors, and finally reduces injury in a PVL mouse model.

METHODS AND MATERIALS

Animals

Adult female C57BL/6 mice were purchased from Chongqing Medical University (Chongqing, China). The mice were housed under pathogen-free conditions. Water and food were available *ad libitum*. The female mice were crossed with age-matched male mice. Given that male preterm infants show more clinically relevant injuries and neurological impairments (29), only male pups were used. The mean anogenital distance from the caudal aspect of the genital area to the rostral aspect of the anus was used to assess neonatal gender (the mean distance is 1.9 ± 0.1 mm in males and 0.8 ± 0.1 mm in females) (30). The priori sample size was estimated by adequate statistical analysis. All the procedures were approved by the Experimental Animal Administration Committee of the university (followed the Chinese National Guidelines: GB/T 35892-20181) (31) and performed by qualified technicians following the 3R Principle: Reduction, Replacement, Refinement (32).

Establishment of the PVL Model

All the male pups were randomly divided into three groups: the normoxia group (Control), the hypoxia-induced saline-treated group (Hypoxia), and the hypoxia-induced IL-4-treated group (Hypoxia + IL-4 group). The PVL animal model was established according to Clayton et al. and Shen et al. with modification (33, 34). Given the unstable state of C57BL/6 mice under hypoxic environments, all the male pups were fostered to gestational age-matched lactating CD1 (ICR) dams at postnatal day 1 (P1). Briefly, at P3, pups were randomly placed in a sealed chamber with the mother, and the O_2 concentration was maintained at 7.5% by displacement with N_2. Hypoxia began at P3 for 24 h; after 24 h, the hypoxic pups were returned to room air. The control pups breathed room air during the experiment. Half of the hypoxic pups were randomly selected to be subjected to IL-4 administration. After exposure, all the pups were returned to lactating CD1 (ICR) dams until sacrifice or weaning.

Administration of Exogenous IL-4

IL-4 (mouse IL-4, 404-ML; R&D Systems) was prepared at a concentration of 100 ng μl^{-1} using a 0.45% normal saline solution and stored at −20°C. The pups in the Hypoxia group or the Hypoxia + IL-4 group were intranasally administered saline or IL-4 at a total dose of 80 ng g^{-1}. The IL-4 treatment started 6 h after PVL and was repeated at postnatal days 5–7. Briefly, the mouse heads were fixed vertically, and IL-4 was administered by a microliter syringe (Hamilton CO., Reno, Nevada) into one nostril. After administration, the pups were held for 2 min to allow the IL-4 to be absorbed. The control animals were also administered the same volume of saline using the same procedure.

Immunohistochemistry and Antibodies

At P4 and P11, mice were transcardially perfused with 4% paraformaldehyde, and white matter slices were sectioned with a microtome (Leica), as previously described (35, 36). Briefly, the slices were transferred to a slide, and fetal bovine serum was used to block the antigens. Then, the slices were incubated with primary antibodies for 12–16 h at 4°C; fluorescent-conjugated secondary antibodies were applied for 2–3 h at room temperature in the dark. To detect the maturity of oligodendrocytes, a human antibody against MBP was used. To detect the location of IL-4R, a rabbit antibody specific for phosphor-IL-4R was used. Microscopes (90I, Nikon, Japan) were used to detect the fluorescence values.

Western Immunoblotting

The white matter was dissected, and the total protein was extracted with RIPA lysis buffer (Beyotime, Harman, China; RIPA: protease inhibitors =1,000:1), as previously described. The same protein amount (20 μg) was loaded onto sodium dodecyl sulfate-polyacrylamide gels and separated by electrophoresis (Bio-Rad, CA, USA). The proteins were transferred onto 0.2-μm PVDF membranes, and the membranes were incubated with different primary antibodies (see **Table S1** for detail parameters) overnight at 4°C and with the appropriate secondary antibodies for 2 h at room temperature. An ECL kit (Millipore, USA) and an ECL Imaging System (Syngene G: BOX, UK) were used to detect protein expression. The images were analyzed using ImageJ software (NIH, Bethesda, Maryland).

Real-Time PCR

The total RNA was extracted from the white matter of the mice at P4 and P7 according to the procedure of the RNA Extraction Kit (LS1040, Promega). Real-time PCR was performed using a CFX96 real-time PCR detection system (Bio-Rad) with SYBR reagents (QuantiNova SYBR® Green RT-PCR Kit, Qiagen). The relative expression of cDNA fragments was normalized using the average expression value of GAPDH and analyzed using the comparative C^T method (37). Real-time PCR was performed using the primer sequences shown in **Table S2**.

ELISA

Whole brain tissues were collected at P7 to examine the concentration of IL-4 in the brain using a Mouse IL-4 ELISA kit [High Sensitivity; Neobioscience, EMC003(H)], according to the manufacturer's protocols. Briefly, the substrate was added to the plate and then placed directly in the spectrophotometer (462 nm wavelength, SpectraMax; Thermo, USA). The spectrophotometer and software (SoftMax, Release Pro 5) were programmed to shake the plate to homogenize the color in each well for 4 s before every reading, and the plate was read every 60 s until the end of the program. The sample levels were analyzed using a microtiter plate reader (Thermo, USA). Each sample was detected in duplicate, and the medians were used for analysis.

Electron Microscopy

Mice at P18 were deeply anesthetized with pentobarbital sodium (50 mg/kg) and transcardially perfused with ice-cold phosphate-buffered solution containing 4.0% glutaraldehyde (pH 7.4). The brains were coronally sliced, and the white matter was dissected and postfixed for 2 weeks. All the samples were examined with an FEI transmission electron microscope (Tecnai G2 20 TWIN) and processed for standard electron microscopy analysis. Briefly, the white matter was dissected and postfixed for 2 weeks at room temperature (20°C). The samples were then dehydrated in 50–70–80–90–95–100–100% alcohol for 15 min each. The samples were incubated with a mixture solution (acetone:embedding medium = 1:1) overnight to permeabilize them, and then the samples were polymerized for 48 h at 60°C. A microtome (Leica UC7) was used to slice the tissue into 60- to 80-nm sections. Finally, uranium-lead (uranium-saturated aqueous solution of 2% acetate, lead citrate, 80096180) was used for staining for 15 min each. The slices were observed under a transmission electron microscope, and images were collected to calculate the percentage of unmyelinated axons [axons <0.3 μm were excluded (38)] and the *g* ratio, which was calculated as the axon diameter divided by the entire myelinated fiber (38, 39).

FACS

Mice were deeply anesthetized and transcardially perfused with 100 ml of cold PBS, as described above. The M1 microglia and M2 microglia in the white matter were detected as previously described (40). The white matter in the mice in the Control, Hypoxia, and Hypoxia + IL-4 groups was harvested in FACS buffer (PBS with 1% FBS and 0.1% sodium azide) in a culture plate and homogenized with the rubber plunger of a 2-ml syringe on ice. Then, the cells were centrifuged at 3,000 rpm for 5 min at 4°C and resuspended in FACS buffer. Next, the cells were filtered through a 100-μm strainer, resuspended in 1 ml of FACS buffer and counted. The cells were stained with fluorochrome-labeled antibodies against CD45 (Biolegend, 368509, PE) and CD11b (Biolegend, 101211, APC) on ice for 40 min in the dark. The fluorescence threshold was set on the basis of the reactivity of the appropriate non-specific, fluorochrome-conjugated isotype controls. The data of the stained samples were acquired on a FACSCanto (a BD LSR II flow cytometer) using Diva software (v6.1.2; Institut Pasteur, Paris). The data were analyzed using FlowJo V10 software (v7.6.2; Tree Star, Ashland).

Functional Study

Rotarod testing was conducted as previously described (41, 42). The functional test was conducted at P30 and P60 with the ANY-Maze Video Tracking System (ANY-Maze, USA). On the day before the test, the animals were brought to the testing room and allowed to rest for 2 h before testing. After a training session of two consecutive trials before the testing day, the mice were subjected to test sessions with two speed modes: accelerating speeds (range, from 0 to 50 rpm) and fixed speeds (fixed, 40 rpm). Each test mode consisted of two trials on the rotarod, with a maximum of 300 s. Each trial interval lasted more than 1 h. The time each mouse spent on the rotarod was recorded, and the average time of each trial was used for analysis (43).

Statistics

In our study, 15–18 mice per group were analyzed in the functional study, and 4–6 mice per group were analyzed in the histochemical experiments. All the data are expressed as the mean ± S.E.M. and were analyzed by ANOVA (followed by Tukey's test) or unpaired Student's *t* test. GraphPad Prism (v.8.0.2) software and SPSS (v.20.0.0) software were used for all the statistical analyses, as appropriate. $P < 0.05$ was considered significant.

RESULTS

Severe Acute Hypoxia Causes PVL in Neonatal Mice

We established the preterm PVL model by placing mice in severe acute hypoxia or room air conditions, according to the methods described by Clayton et al. with brief modification (33). It was observed that reduced myelination due to a disrupted oligodendrocyte progenitor (preOL) pool contributes to PVL. Based on the images of the pathological brain specimens, diffuse, small hemorrhagic spots were clearly observed at the tissue surface at P4 in the Hypoxia group but were not observed at that in the Control group (**Figure 1A**). Regarding protein expression, hypoxia dramatically decreased the expression of myelin basic protein (MBP) in the white matter area of P4 mice compared to that in the white matter area of Control mice as determined by Western blotting (**Figure 1B**) and immunohistochemistry (**Figures 1C,E,F**). The expression of myelin-related mRNA (*Ng2*, *Mag*, and *Mbp*) in the white matter of hypoxic mice at P4 was obviously downregulated compared with that of the control mice (**Figure 1D**). These data showed that the PVL model had been successfully established.

Administration of Exogenous IL-4 Alleviates Functional Deficits in PVL

It is widely reported that IL-4 is closely associated with many brain injury diseases, such as cerebral infarction (44), transient focal cerebral ischemia (27, 28), neonatal asphyxia (45), and hypoxic–ischemic encephalopathy (46). First, we performed a dose-response experiment at the beginning of our research. We set the dose of IL-4 to be intranasally administered to a total of 0, 40, 80, and 120 ng g^{-1}, and functional assessments were conducted at P30, as shown in Figure S2. Functional differences were significantly detected in the mice administered 80 and 120 ng g^{-1} IL-4. Therefore, we reported the concentration of 80 ng g^{-1} in the study. To explore the effect of IL-4 on PVL in a mouse model, the concentration of IL-4 in the brain tissue and the expression of IL-4R in the white matter of the mice exposed to control and hypoxia conditions at P4 were detected. Obviously, decreased levels of IL-4 in the brain tissue and increased expression of IL-4R in the white matter were found in the mice exposed to hypoxia compared to those in the mice exposed to control conditions (**Figures 2A–D**). Exogenous IL-4 was intranasally administered to easily penetrate through the blood–brain barrier. To evaluate motor coordination and learning, rotarod testing was conducted with the mice in the Control, Hypoxia, and Hypoxia + IL-4 groups. At P30, the functional study showed that the hypoxic mice spent less time on the rotarod than the control mice. However, the administration of exogenous IL-4 caused the hypoxic mice to spend obviously more time on the rotarod than the mice exposed to hypoxia and administered saline (**Figure 2E**). Comparable results were observed in the mice at P60 (**Figure 2F**).

Administration of Exogenous IL-4 Improves Myelination

The improvements observed in the functional study urged us to examine the recovery of myelination in the mouse brain. The expression of MBP in the brain was measured by immunohistochemistry at P11 and by electron microscopy at P18. The mice exposed to hypoxia exhibited obviously delayed myelination in the brain compared to the mice exposed to control conditions. Interestingly, the intranasal administration of exogenous IL-4 to the mice exposed to hypoxia rescued myelination compared with the administration of saline to the hypoxic mice (**Figures 3A–C,G**). The *g* ratio (calculated as the axon diameter divided by the entire myelinated fiber) was used to assess the thickness of the myelin sheath. The microscopy results showed that the hypoxic mice had thinner myelination and a higher *g* ratio than the control mice. However, exogenous IL-4 administration to the hypoxic mice improved myelination and reduced the *g* ratio compared with the administration of saline to the hypoxic mice (**Figures 3D–F,H**). These data suggested that the intranasal administration of exogenous IL-4 rescued the expression of MBP and improved myelination.

Administration of Exogenous IL-4 Increases the Level of IL-4 in the Brain

To explore the role of IL-4 in the PVL model, the concentration of IL-4 in the brain at P7 was measured by ELISA. The level of IL-4 in the brains of mice exposed to hypoxia was lower than that in the brains of mice exposed to control conditions (**Figure 2D**). The intranasal administration of exogenous IL-4 increased the level of IL-4 in the hypoxic mouse brain (**Figure 2D**), indicating that the intranasal administration of IL-4 increased the concentration of IL-4 in the lesion area.

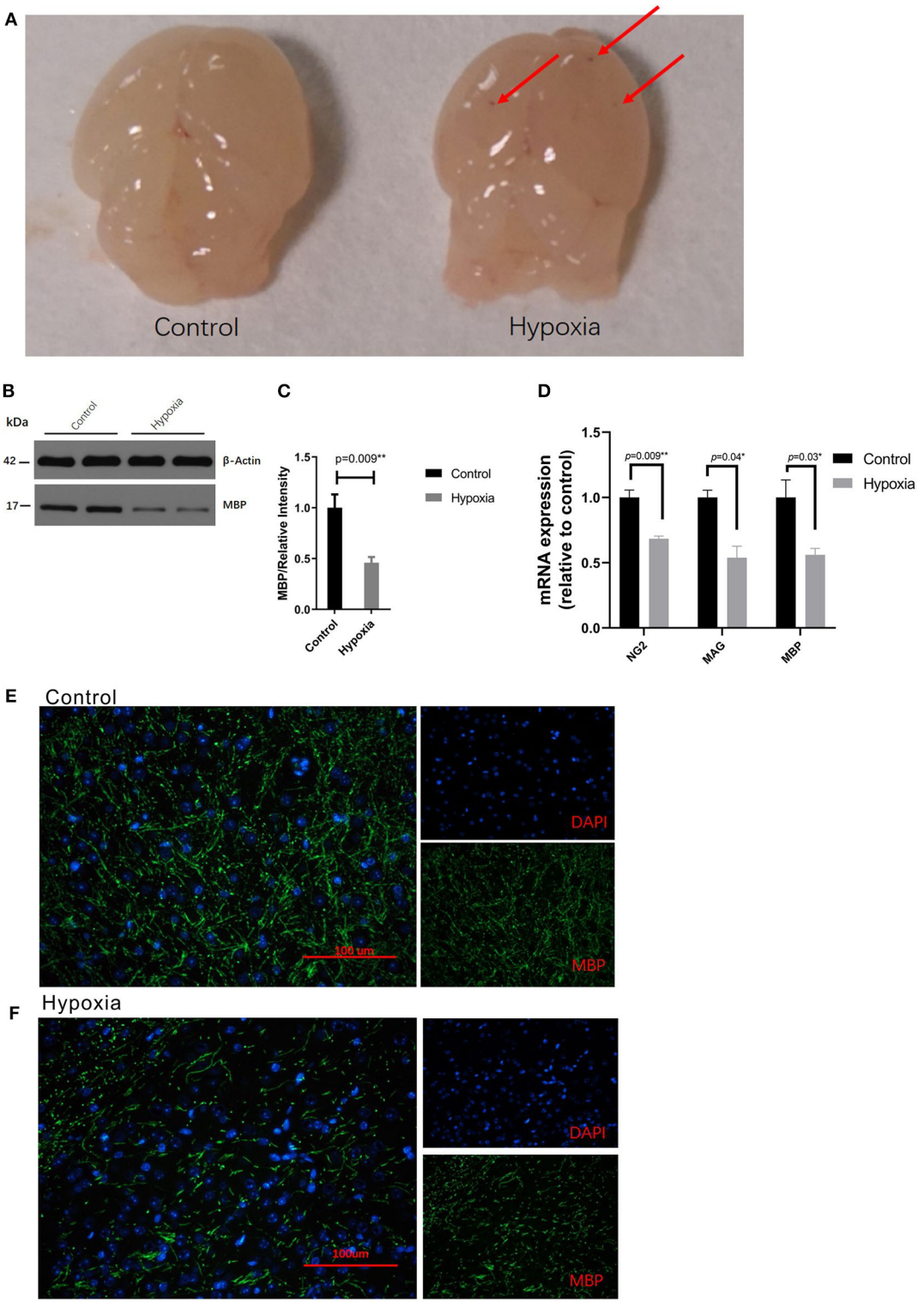

FIGURE 1 | Severe acute hypoxia causes diffuse white matter injury. **(A)** Images of pathological brain specimens from the mice in the Control (left) and Hypoxia (right) groups at P4. Diffuse, small hemorrhagic spots (red arrow) were observed in brain tissue in the Hypoxia group but not in that in the Control group ($n = 3$ brains for each group). **(B)** Western immunoblotting of MBP in the white matter from P4 mice exposed to control or hypoxic conditions. The expression level of MBP (top panel) in the Hypoxia group was significantly lower than that in the Control group ($n = 4$ brains for each group, $p = 0.01$ by unpaired two-tailed t test). The histograms represent the normalized relative quantitative values between the Control group and Hypoxia group. **(C)** Normalized relative quantitative values of the

(Continued)

FIGURE 1 | immunohistochemistry analysis of MBP between the Control group and Hypoxia group. **(D)** Gene expression analysis of myelin-related mRNA (Ng2, Mag, and Mbp) in the white matter of P4 mice exposed to control or hypoxic conditions. The gene expression levels of Ng2, Mag, and Mbp in the Hypoxia group were significantly downregulated compared to those in the Control group ($n = 4$–5 brains for each group, $p = 0.09$, 0.04, and 0.03, respectively, by unpaired two-tailed t test). GAPDH was used to normalize the gene expression levels. **(E,F)** Immunohistochemistry analysis of MBP in the white matter from the P4 mice exposed to control **(E)** or hypoxic **(F)** conditions. Reduced MBP (green) was shown in the Hypoxia group compared to that in the Control group. The exposure time was 50 ms in all the scopes ($n = 4$–5 brain per group, $p = 0.01$ by unpaired two-tailed t test). All the data are expressed as the mean ± S.E.M. MBP, myelin basic protein; Ng2, nerve-glia antigen 2; Mag, myelin-associated glycoprotein; Mbp, myelin basic protein.

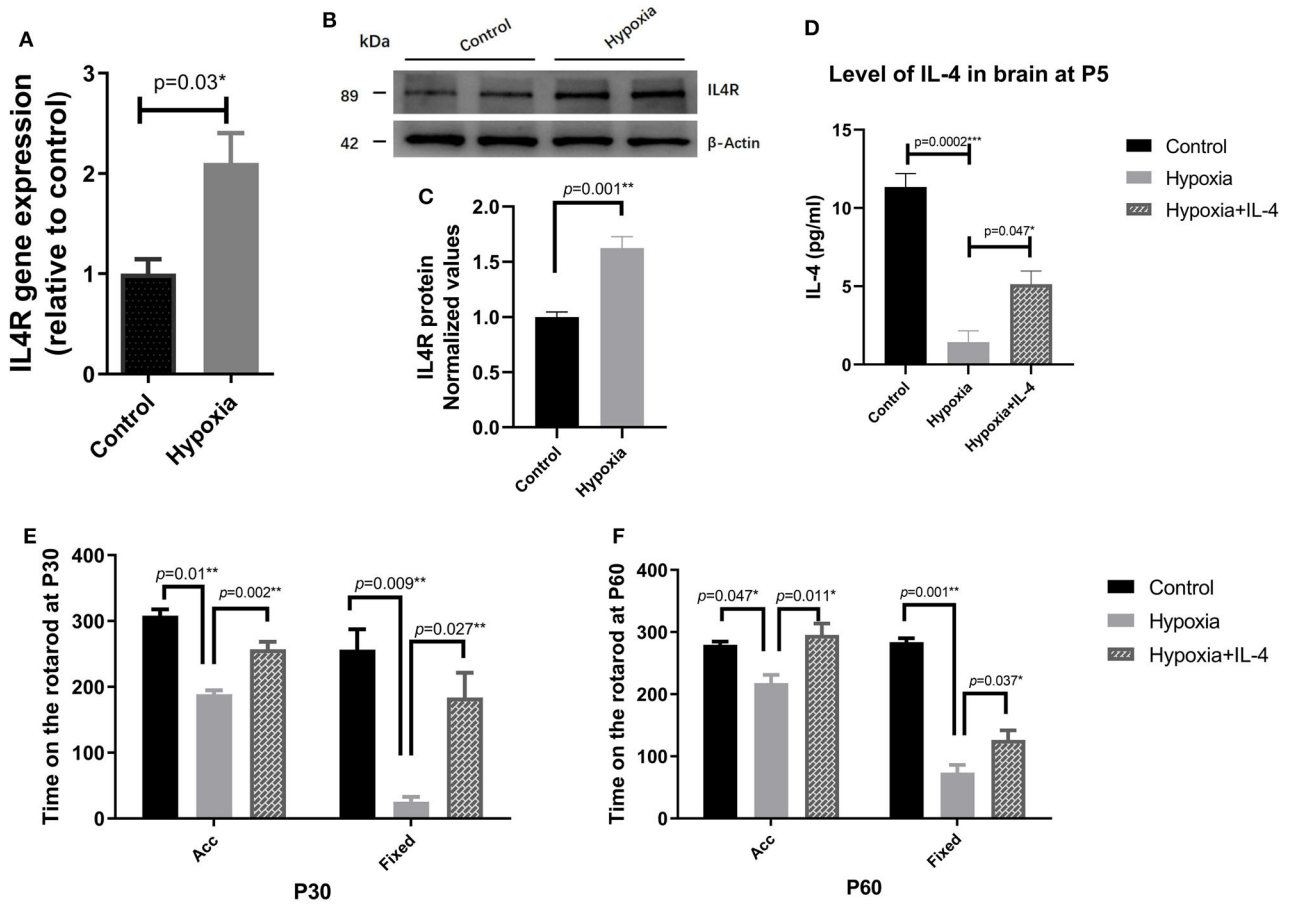

FIGURE 2 | The administration of exogenous IL-4 improves the functional deficits of PVL. **(A)** Gene expression analysis of the IL-4 receptor in the white matter of the P4 mice exposed to hypoxia or control conditions. The mRNA levels of the IL-4 receptor were significantly higher in the Hypoxia group than in the Control group ($n =$ 4–5 mice per group, $p = 0.008$ by ANOVA). **(B)** Western immunoblotting of IL-4R in the white matter of the P4 mice exposed to control or hypoxic conditions. The expression level of IL-4R (top panel) in the Hypoxia group was significantly higher than that in the Control group ($n = 5$ brains for each group, $p = 0.01$ by unpaired two-tailed t test). **(C)** The histograms represent the normalized relative quantitative values between the Control group and Hypoxia group. **(D)** Concentration of IL-4 in the P7 brains of the mice in the Control, Hypoxia, and Hypoxia + IL-4 groups ($n = 6$–7 mice per group, $p = 0.0002$ and 0.047, respectively, by ANOVA). **(E,F)**, Rotarod test of the mice in the Control, Hypoxia, and Hypoxia + IL-4 groups at P30 **(E)** and P60 **(F)**. The mice in the Hypoxia group exhibited shorter times on the rotarod than those in the Control group in different modes at P30 and P60 ($p = 0.01$, 0.009; 0.047, 0.001, respectively). However, the administration of IL-4 partially rescued the time on the rotarod compared to the administration of saline to the hypoxia mice in different modes at P30 and P60 ($n = 15$–18 mice per group, $p =$ 0.002, 0.027; 0.011, 0.037 by ANOVA). Acc, acceleration pattern; Fixed, fixed pattern.

Regulating the Effect of IL-4, Which Is Partially Dependent on Microglia Polarization

Many studies have found that microglia are involved in the neuroinflammation that protects against brain damage. To explore the role of microglial polarization in hypoxia, the microglia in the white matter zone were quantitatively analyzed by immunohistochemistry and Western blotting experiments. The quantitative results of the microglia in the white matter showed that exposure to hypoxia increased the numbers of Iba^+ microglia (**Figures 4A–C,G–I**). Interestingly, IL-4 administration slightly decreased the numbers of Iba^+ microglia (**Figures 4A–C,G**). In addition, microglial cells ($CD45^+CD11b^+$) were sorted by FACS (**Figure 4D**), and the

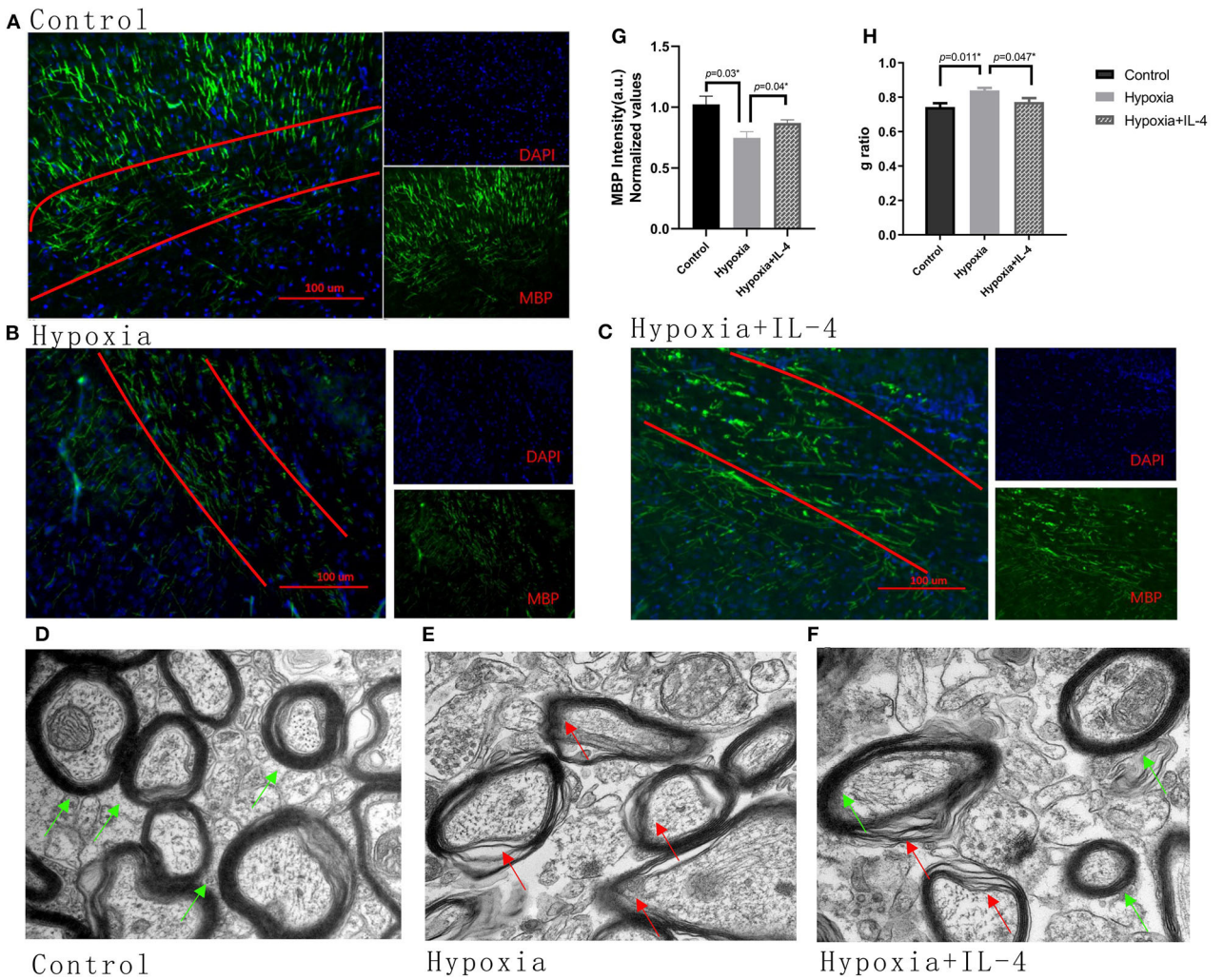

FIGURE 3 | Administration of exogenous IL-4 improves myelination. **(A–C)** Immunohistochemistry analysis of MBP at P11 in the white matter of the Control, Hypoxia, and Hypoxia + IL-4 groups. The level of MBP in the mice exposed to hypoxia **(B)** was significantly reduced compared with that in the mice exposed to control conditions **(A)** ($n = 4$–5 brains per group, $p = 0.03$ by ANOVA). However, the administration of exogenous IL-4 to the mice exposed to hypoxia **(C)** partly rescued myelination compared to the administration of saline to the mice exposed to hypoxia ($n = 4$–6 brains per group, $p = 0.04$ by ANOVA). The exposure time was 50 ms in all the scopes. **(G)** Normalized relative quantitative values of the immunohistochemistry analysis of MBP among the Control group, Hypoxia group, and Hypoxia + IL-4 group. **(D–F)** Electron microscopy images of the axons in the white matter of the P11 mice in the Control **(D)**, Hypoxia **(E)**, and Hypoxia + IL-4 **(F)** groups. **(H)** *g* ratio of axon myelination. There was an increased *g* ratio in the Hypoxia group compared with that in the Control group ($n = 3$ brains per group, more than 20 axons were calculated for each brain, $p = 0.011$ by ANOVA). However, the administration of IL-4 to the mice exposed to hypoxia decreased the *g* ratio compared to the administration of saline to the mice exposed to hypoxia ($p = 0.047$ by ANOVA).

gene and protein expression of iNOS, Arg1, and TNF-a were detected. Decreased iNOS and TNF-a expression and increased Arg1 expression were observed in the mice in the Hypoxia + IL-4 group compared with those in the Hypoxia group (**Figures 4E,F**), suggesting that the administration of IL-4 promotes microglial polarization from the M1 phenotype ($CD45^+CD11b^+$, high *iNOS* expression) to the M2 phenotype ($CD45^+CD11b^+$, high *Arg1* expression).

DISCUSSION

As the most common form of injury in infants with very low birth weights, PVL represents a large burden to the health system (7–9). Previous studies have revealed the potent neuroprotective effects of IL-4 in animal models (27, 28). Myelination is considered to be correlated with the manifestation of PVL (10, 11). Therefore, we performed the present study using the hypoxia model to investigate the effect of IL-4 in PVL. In the present study, we found that the intranasal administration of exogenous IL-4 improved the myelination of axons, and the improvement of myelination might partly depend on microglial polarization in the brain. These results show that IL-4 is important in modulating the improvement of myelination in PVL.

As the most potent immune cells in the CNS, microglial cells play an important role in CNS repair and regeneration

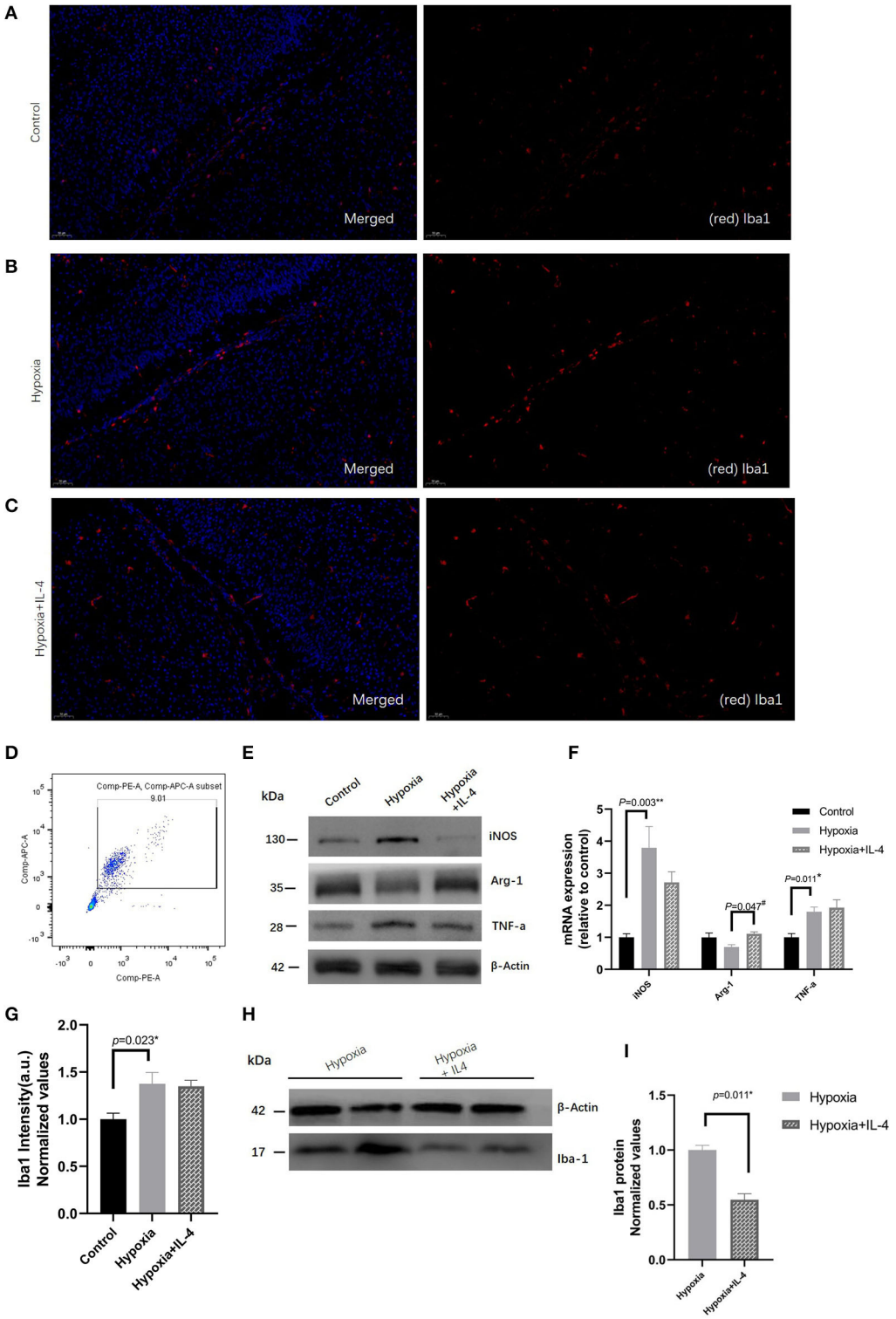

FIGURE 4 | Immunohistochemistry analysis of Iba1 in the white matter of P7 mice in the Control, Hypoxia, and Hypoxia + IL-4 groups. **(A–C)** Iba1+ cell staining at P7 in the white matter of the Control, Hypoxia, and Hypoxia + IL-4 groups. The numbers of microglia cells in the mice exposed to hypoxia **(B)** were significantly increased compared with those in the mice exposed to control conditions **(A)** ($n = 4$–5 brains per group, $p = 0.023$ by ANOVA). Additionally, the administration of exogenous IL-4 to mice exposed to hypoxia **(C)** slightly alleviated the activation of microglia compared to the administration of saline to the mice exposed to hypoxia ($n = 4$–5 brains per group, no significant difference, ANOVA). The exposure time was 50 ms in all the scopes. **(G)** Normalized relative quantitative values of

(Continued)

FIGURE 4 | immunohistochemistry analysis of Iba1 among the Control group **(A)**, Hypoxia group **(B)**, and Hypoxia + IL-4 **(C)** group. **(E)** mRNA expression of iNOS, Arg1, and TNF-a in the microglial cells sorted by FACS at P7 from the white matter of the mice in the Control, Hypoxia, and Hypoxia + IL-4 groups. **(F)** Western immunoblotting of iNOS, Arg-1, and TNF-a in the microglial cells sorted by FACS at P7 from the white matter of the mice in the Control, Hypoxia, and Hypoxia + IL-4 groups. Increased iNOS and TNF-a expression levels and decreased Arg-1 expression levels were observed in the Hypoxia group compared with the Control group. However, IL-4 administration reversed the expression of these proteins ($n = 4$ brains for each group). **(D)** Microglial cells sorted by FACS. **(H)** Western immunoblotting of Iba1 at P7 in the white matter of the mice in the Hypoxia and Hypoxia + IL-4 groups. The expression level of Iba1 in the Hypoxia + IL-4 group was significantly lower than that in the Hypoxia group ($n = 4$ brains for each group, $p = 0.011$ by unpaired two-tailed t test). **(I)** Normalized relative quantitative values of Western immunoblotting analysis of Iba1 in the P7 mice between the Hypoxia group and Hypoxia + IL-4 group. FACS, fluorescence-activated cell sorting.

(47, 48). Disruptions of myelination in early stages have deleterious consequences for the development of neuronal connectivity, such as in PVL, in both animal models and human specimens (13). The polarized phenotypes of microglial cells have distinct roles in the injury and recovery of white matter. Consistent with previous studies, our results suggested that hypoxia obviously increased the polarization of microglia (increased Iba1+ cell activation, increased iNOS expression, and decreased Arg1 expression) and caused a reduction in myelination (decreased MBP expression) in the mouse PVL model. In an *in vitro* model of inflammation, Chhor V et al. proved that stimulation with anti-inflammatory cytokines increased the expression of genes associated with the M2 microglial phenotype (such as Arg1); however, the expression of genes associated with the M1 phenotype (such as iNOS) was increased by stimulation with pro-inflammatory mediators (17). In our study, the gene and protein expression of iNOS, Arg1, and TNF-a were measured in FACS-sorted microglia by RT-PCR and Western blotting. In accordance with reported studies, our findings showed increased iNOS expression levels in $CD45^+CD11b^+$ cells and decreased Arg1 expression levels in $CD45^+CD11b^+$ cells. These results showed that microglial cells are closely related to myelination disturbances in the PVL mouse model.

As a T cell-derived mediator, IL-4 plays a critical role in several neurological disorders (49). Derecki N et al. reported that IL-$4^{-/-}$ mice exhibited severe learning abnormalities compared with wild-type mice. In addition, increased production of IL-4 was detected in mice training in the Morris water maze compared to that in untrained mice (50). In a focal ischemia mouse model, Xiong X et al. showed that IL-4 KO mice exhibited larger infarction volumes and worsened neurological scores than wild-type mice. In our study, our results showed that the administration of exogenous IL-4 improved myelination and reduced the polarization of microglia to the M1 phenotype. Furthermore, IL-4 alleviated the hypoxia-induced functional impairment in a PVL mouse model. As an immune cytokine, IL-4 has been reported to regulate the expression of MHC class II molecules and the enhancement of macrophage mannose receptor activity (51). In addition, Chhor V et al. found that stimulation with IL-4 increased the gene expression of M2 markers (such as Arg-1 and CD206) but did not increase the expression of M1 markers (such as TNF-a, IL-6, and IL-1b). Similarly, our results showed that the administration of exogenous IL-4 decreased iNOS expression in $CD45^+CD11b^+$ cells and increased Arg1 expression in $CD45^+CD11b^+$ cells. These results showed that IL-4 attenuates myelination disturbances and functional impairments by regulating microglia polarization in a PVL mouse model.

However, despite an increasing body of evidence supporting the beneficial effects of IL-4 in neurological diseases, the effect of IL-4 in hypoxia-induced brain injuries is under debate (44). Kim et al. reported that IL-4 levels were increased in patients with cerebral infarction (44). However, our results showed reduced IL-4 levels in the hypoxia-induced model. Many possibilities may explain this controversy. (1) Different tissues (serum and brain) exhibit different cytokine levels. Due to interference by the blood–brain barrier, the IL-4 levels in the brain may differ from those in serum. (2) Different experimental models (cerebral infarction and PVL models, human, and mouse models) may generate different IL-4 levels. The IL-4 receptor alpha chain (IL-4Ra) has been reported to mediate the effects of IL-4 signaling. When IL-4Ra binds its ligand, IL-4Ra can dimerize with the gamma chain or the IL-13 receptor alpha1, producing a type 1 complex or type 2 complex, respectively (52). In our results, we found increased IL-4Ra protein levels and decreased IL-4 concentrations in the PVL-induced mouse model. Part of the reason for these observations is probably because of compensatory mechanisms. A reduced ligand level would promote an increase in ligand receptors to reduce changes in the downstream signaling pathways. The mechanism of cerebral infarction in patients is obviously different from that in the PVL mouse model. However, the different effects observed in PVL models and infarction models remind us that IL-4 might play distinct roles in different diseases. In addition, our research only showed the correlation between the administration of exogenous IL-4 and the alleviation of functional deficits, and we did not include IL-$4^{-/-}$ transgenic mice in our study. Our team will address this limitation in our future work. Overall, intranasal IL-4 administration improved myelination and alleviated functional deficits, as presented in this study, which might be explained by the polarization of microglia, including the regulation of *iNOS* and *Arg1* expression in $CD45^+CD11b^+$ cells. These results might suggest the possibility of treating PVL by targeting the polarization of microglia.

CONCLUSION

Overall, our findings demonstrated that the intranasal administration of exogenous IL-4, at least in a hypoxia-induced PVL model, could improve myelination and attenuate functional deficits. These results show that intranasal IL-4 administration may be a new strategy for PVL treatment. Polarization of microglia is an important but not exclusive mechanism and needs to be further explored.

DATA AVAILABILITY STATEMENT

All datasets generated for this study are included in the article/**Supplementary Material**.

ETHICS STATEMENT

The animal study was reviewed and approved by the Experimental Animal Administration Committee of the University.

AUTHOR CONTRIBUTIONS

LY and QC were responsible for study concept and collated data and prepared manuscript. LY, NC, and JM carried out the studies and analyzed data. WL were responsible for working draft and ethical requirements concerning animal welfare. All authors contributed to the article and approved the submitted version.

FUNDING

This study was supported by the Major Project of Chongqing Health Committee (2019ZY013201 and 2017ZDXM29), the Chongqing Science and Technology Commission (cstc2018jxj1130006 and cstc2017shmsA130001), and the Innovation Program for People Studying Abroad in Chongqing (cx2017108).

ACKNOWLEDGMENTS

All authors would like to thank Xin Zhong for editing assistance.

SUPPLEMENTARY MATERIAL

The Supplementary Material for this article can be found online at: https://www.frontiersin.org/articles/10.3389/fneur.2020.00930/full#supplementary-material

REFERENCES

1. Als H, Behrman R, Checchia P, Denne S, Dennery P, Hall CB, et al. Preemie abandonment? Multidisciplinary experts consider how to best meet preemies needs at "preterm infants: a collaborative approach to specialized care" roundtable. *Modern Healthcare*. (2007) 37:17–24.
2. Horbar JD, Badger GJ, Carpenter JH, Fanaroff AA, Kilpatrick S, LaCorte M, et al. Trends in mortality and morbidity for very low birth weight infants, 1991–1999. *Pediatrics*. (2002) 110(1 Pt 1):143–51. doi: 10.1542/peds.110.1.143
3. Anderson PJ, De Luca CR, Hutchinson E, Spencer-Smith MM, Roberts G, Doyle LW. Attention problems in a representative sample of extremely preterm/extremely low birth weight children. *Dev Neuropsychol*. (2011) 36:57–73. doi: 10.1080/87565641.2011.540538
4. Soria-Pastor S, Padilla N, Zubiaurre-Elorza L, Ibarretxe-Bilbao N, Botet F, Costas-Moragas C, et al. Decreased regional brain volume and cognitive impairment in preterm children at low risk. *Pediatrics*. (2009) 124:e1161–70. doi: 10.1542/peds.2009-0244
5. Glass HC, Fujimoto S, Ceppi-Cozzio C, Bartha AI, Vigneron DB, Barkovich AJ, et al. White-matter injury is associated with impaired gaze in premature infants. *Pediatr Neurol*. (2008) 38:10–5. doi: 10.1016/j.pediatrneurol.2007.08.019
6. Litt J, Taylor HG, Klein N, Hack M. Learning disabilities in children with very low birthweight: prevalence, neuropsychological correlates, and educational interventions. *J Learn Disabil*. (2005) 38:130–41. doi: 10.1177/00222194050380020301
7. CfDCaP C. Economic costs associated with mental retardation, cerebral palsy, hearing loss and vision impairment–United States, 2003. *MMWR Morb Mortal Wkly Rep*. (2003) 53:7–9.
8. Loeliger M, Inder T, Cain S, Ramesh RC, Camm E, Thomson MA, et al. Cerebral outcomes in a preterm baboon model of early versus delayed nasal continuous positive airway pressure. *Pediatrics*. (2006) 118:1640–53. doi: 10.1542/peds.2006-0653
9. Buser JR, Maire J, Riddle A, Gong X, Nguyen T, Nelson K, et al. Arrested preoligodendrocyte maturation contributes to myelination failure in premature infants. *Anna Neurol*. (2012) 71:93–109. doi: 10.1002/ana.22627
10. Volpe JJ. Brain injury in premature infants: a complex amalgam of destructive and developmental disturbances. *Lancet Neurol*. (2009) 8:110–24. doi: 10.1016/S1474-4422(08)70294-1
11. Haynes RL, Billiards SS, Borenstein NS, Volpe JJ, Kinney HC. Diffuse axonal injury in periventricular leukomalacia as determined by apoptotic marker fractin. *Pediatr Res*. (2008) 63:656–61. doi: 10.1203/PDR.0b013e31816c825c
12. Riddle A, Maire J, Gong X, Chen KX, Kroenke CD, Hohimer AR, et al. Differential susceptibility to axonopathy in necrotic and non-necrotic perinatal white matter injury. *Stroke*. (2012) 43:178–84. doi: 10.1161/STROKEAHA.111.632265
13. Back SA. White matter injury in the preterm infant: pathology and mechanisms. *Acta Neuropathol*. (2017) 134:331–49. doi: 10.1007/s00401-017-1718-6
14. Back SA, Luo NL, Mallinson RA, O'Malley JP, Wallen LD, Frei B, et al. Selective vulnerability of preterm white matter to oxidative damage defined by F2-isoprostanes. *Annals Neurol*. (2005) 58:108–20. doi: 10.1002/ana.20530
15. Giulian D, Baker TJ. Characterization of ameboid microglia isolated from developing mammalian brain. *J Neurosci*. (1986) 6:2163–78. doi: 10.1523/JNEUROSCI.06-08-02163.1986
16. Glenn JA, Ward SA, Stone CR, Booth PL, Thomas WE. Characterisation of ramified microglial cells: detailed morphology, morphological plasticity and proliferative capability. *J Anatomy*. (1992) 180(Pt 1):109–18.
17. Chhor V, Le Charpentier T, Lebon S, Ore MV, Celador IL, Josserand J, et al. Characterization of phenotype markers and neuronotoxic potential of polarised primary microglia *in vitro*. *Brain Behav Immun*. (2013) 32:70–85. doi: 10.1016/j.bbi.2013.02.005
18. Edwards JP, Zhang X, Frauwirth KA, Mosser DM. Biochemical and functional characterization of three activated macrophage populations. *J Leukocyte Biol*. (2006) 80:1298–307. doi: 10.1189/jlb.0406249
19. Lehnardt S, Lachance C, Patrizi S, Lefebvre S, Follett PL, Jensen FE, et al. The toll-like receptor TLR4 is necessary for lipopolysaccharide-induced oligodendrocyte injury in the CNS. *J Neurosci*. (2002) 22:2478–86. doi: 10.1523/JNEUROSCI.22-07-02478.2002
20. Lehnardt S, Massillon L, Follett P, Jensen FE, Ratan R, Rosenberg PA, et al. Activation of innate immunity in the CNS triggers neurodegeneration through a Toll-like receptor 4-dependent pathway. *Proc Natl Acad Sci USA*. (2003) 100:8514–9. doi: 10.1073/pnas.1432609100
21. Butovsky O, Landa G, Kunis G, Ziv Y, Avidan H, Greenberg N, et al. Induction and blockage of oligodendrogenesis by differently activated microglia in an animal model of multiple sclerosis. *J Clin Invest*. (2006) 116:905–15. doi: 10.1172/JCI26836
22. Hagberg H, Mallard C, Ferriero DM, Vannucci SJ, Levison SW, Vexler ZS, et al. The role of inflammation in perinatal brain injury. *Nat Rev Neurol*. (2015) 11:192–208. doi: 10.1038/nrneurol.2015.13
23. Howard M, Farrar J, Hilfiker M, Johnson B, Takatsu K, Hamaoka T, et al. Identification of a T cell-derived b cell growth factor distinct from interleukin 2. *J Exp Med*. (1982) 155:914–23. doi: 10.1084/jem.155.3.914
24. Hu-Li J, Shevach EM, Mizuguchi J, Ohara J, Mosmann T, Paul WE. B cell stimulatory factor 1. (interleukin 4) is a potent costimulant for normal resting T lymphocytes. *J Exp Med*. (1987) 165:157–72. doi: 10.1084/jem.165.1.157

25. Hart PH, Vitti GF, Burgess DR, Whitty GA, Piccoli DS, Hamilton JA. Potential antiinflammatory effects of interleukin 4: suppression of human monocyte tumor necrosis factor alpha, interleukin 1, and prostaglandin E2. *Proc Natl Acad Sci USA*. (1989) 86:3803–7. doi: 10.1073/pnas.86.10.3803
26. Abbas AK, Murphy KM, Sher A. Functional diversity of helper T lymphocytes. *Nature*. (1996) 383:787–93. doi: 10.1038/383787a0
27. Xiong X, Barreto GE, Xu L, Ouyang YB, Xie X, Giffard RG. Increased brain injury and worsened neurological outcome in interleukin-4 knockout mice after transient focal cerebral ischemia. *Stroke*. (2011) 42:2026–32. doi: 10.1161/STROKEAHA.110.593772
28. Xiong X, Xu L, Wei L, White RE, Ouyang YB, Giffard RG. IL-4 Is required for sex differences in vulnerability to focal ischemia in mice. *Stroke*. (2015) 46:2271–6. doi: 10.1161/STROKEAHA.115.008897
29. Ment LR, Vohr B, Allan W, Katz KH, Schneider KC, Westerveld M, et al. Change in cognitive function over time in very low-birth-weight infants. *JAMA*. (2003) 289:705–11. doi: 10.1001/jama.289.6.705
30. Schneider J, Nyby J, Whitney G. Determining the sex of neonatal mice. (Mus musculus). *Behav Res Methods Instrum*. (1978) 10:105. doi: 10.3758/BF03205110
31. MacArthur Clark JA, Sun D. Guidelines for the ethical review of laboratory animal welfare People's Republic of China National Standard GB/T 35892–2018 [Issued 6 February 2018 Effective from 1 September 2018]. *Anim Models Exp Med*. (2020) 3:103–13. doi: 10.1002/ame2.12111
32. Lu J, Bayne K, Wang J. Current status of animal welfare and animal rights in China. *Alternat Lab Animals*. (2013) 41:351–7. doi: 10.1177/026119291304100505
33. Clayton BL, Huang A, Kunjamma RB, Solanki A, Popko B. The integrated stress response in hypoxia-induced diffuse white matter injury. *J Neurosci*. (2017) doi: 10.1523/JNEUROSCI.2738-16.2017
34. Shen Y, Plane JM, Deng W. Mouse models of periventricular leukomalacia. *J Visualized Exp*. (2010). 39:2738–16. doi: 10.3791/1951
35. Fritschy JM. Is my antibody-staining specific? How to deal with pitfalls of immunohistochemistry. *Eur J Neurosci*. (2008) 28:2365–70. doi: 10.1111/j.1460-9568.2008.06552.x
36. Liu HJ, Lai X, Xu Y, Miao JK, Li C, Liu JY, et al. alpha-asarone attenuates cognitive deficit in a pilocarpine-induced status epilepticus rat model via a decrease in the nuclear factor-kappab activation and reduction in microglia neuroinflammation. *Front Neurol*. (2017) 8:661. doi: 10.3389/fneur.2017.00661
37. Gao F, Yang YZ, Feng XY, Fan TT, Jiang L, Guo R, et al. Interleukin-27 is elevated in sepsis-induced myocardial dysfunction and mediates inflammation. *Cytokine*. (2016) 88:1–11. doi: 10.1016/j.cyto.2016.08.006
38. Furusho M, Dupree JL, Nave KA, Bansal R. Fibroblast growth factor receptor signaling in oligodendrocytes regulates myelin sheath thickness. *J Neurosci*. (2012) 32:6631–41. doi: 10.1523/JNEUROSCI.6005-11.2012
39. Liu J, Dietz K, DeLoyht JM, Pedre X, Kelkar D, Kaur J, et al. Impaired adult myelination in the prefrontal cortex of socially isolated mice. *Nat Neurosci*. (2012) 15:1621–3. doi: 10.1038/nn.3263
40. Xiong X, Gu L, Zhang H, Xu B, Zhu S, Zhao H. The protective effects of T cell deficiency against brain injury are ischemic model-dependent in rats. *Neurochem Int*. (2013) 62:265–70. doi: 10.1016/j.neuint.2012.11.016
41. Joo IS, Hwang DH, Seok JI, Shin SK, Kim SU. Oral administration of memantine prolongs survival in a transgenic mouse model of amyotrophic lateral sclerosis. *J Clin Neurol*. (2007) 3:181–6. doi: 10.3988/jcn.2007.3.4.181
42. Crawley JN. Behavioral phenotyping strategies for mutant mice. *Neuron*. (2008) 57:809–18. doi: 10.1016/j.neuron.2008.03.001
43. Kim SM, Kim H, Lee JS, Park KS, Jeon GS, Shon J, et al. Intermittent hypoxia can aggravate motor neuronal loss and cognitive dysfunction in ALS mice. *PLoS ONE*. (2013) 8:e81808. doi: 10.1371/journal.pone.0081808
44. Kim HM, Shin HY, Jeong HJ, An HJ, Kim NS, Chae HJ, et al. Reduced IL-2 but elevated IL-4, IL-6, and IgE serum levels in patients with cerebral infarction during the acute stage. *Journal of molecular neuroscience: MN*. (2000) 14:191–6. doi: 10.1385/JMN:14:3:191
45. Okazaki K, Nishida A, Kato M, Kozawa K, Uga N, Kimura H. Elevation of cytokine concentrations in asphyxiated neonates. *Biol Neonate*. (2006) 89:183–9. doi: 10.1159/000089180
46. Roka A, Beko G, Halasz J, Toldi G, Lakatos P, Azzopardi D, et al. Changes in serum cytokine and cortisol levels in normothermic and hypothermic term neonates after perinatal asphyxia. *Inflamm Res*. (2013) 62:81–7. doi: 10.1007/s00011-012-0554-3
47. Hu X, Leak RK, Shi Y, Suenaga J, Gao Y, Zheng P, et al. Microglial and macrophage polarization-new prospects for brain repair. *Nat Rev Neurol*. (2015) 11:56–64. doi: 10.1038/nrneurol.2014.207
48. Hanisch UK, Kettenmann H. Microglia: active sensor and versatile effector cells in the normal and pathologic brain. *Nat Neurosci*. (2007) 10:1387–94. doi: 10.1038/nn1997
49. Gadani SP, Cronk JC, Norris GT, Kipnis J. IL-4 in the brain: a cytokine to remember. *J Immunol*. (2012) 189:4213–9. doi: 10.4049/jimmunol.1202246
50. Derecki NC, Cardani AN, Yang CH, Quinnies KM, Crihfield A, Lynch KR, et al. Regulation of learning and memory by meningeal immunity: a key role for IL-4. *J Exp Med*. (2010) 207:1067–80. doi: 10.1084/jem.20091419
51. McInnes A, Rennick DM. Interleukin 4 induces cultured monocytes/macrophages to form giant multinucleated cells. *J Exp Med*. (1988) 167:598–611. doi: 10.1084/jem.167.2.598
52. Nelms K, Keegan AD, Zamorano J, Ryan JJ, Paul WE. The IL-4 receptor: signaling mechanisms and biologic functions. *Annual Rev Immunol*. (1999) 17:701–38. doi: 10.1146/annurev.immunol.17.1.701

Conflict of Interest: The authors declare that the research was conducted in the absence of any commercial or financial relationships that could be construed as a potential conflict of interest.

frontiers in Pediatrics

ORIGINAL RESEARCH
published: 18 September 2020
doi: 10.3389/fped.2020.00593

Exposure to Morphine and Caffeine Induces Apoptosis and Mitochondrial Dysfunction in a Neonatal Rat Brain

Sweatha Kasala[1†], Seema Briyal[2†], Preetha Prazad[1*], Amaresh K. Ranjan[2], Gospodin Stefanov[1], Ramona Donovan[3] and Anil Gulati[2,4]*

[1] Division of Neonatology, Department of Pediatrics, Advocate Children's Hospital, Park Ridge, IL, United States, [2] Chicago College of Pharmacy, Midwestern University, Downers Grove, IL, United States, [3] Advocate Aurora Research Institute, Park Ridge, IL, United States, [4] Pharmazz Inc. Research and Development, Willowbrook, IL, United States

OPEN ACCESS

Edited by:
Silvia Carloni, University of Urbino Carlo Bo, Italy

Reviewed by:
Giampaolo Morciano, University of Ferrara, Italy
Iraci Lucena da Silva Torres, Federal University of Rio Grande do Sul, Brazil

***Correspondence:**
Sweatha Kasala
Sweatha.kasala@gmail.com
Preetha Prazad
preetha.prazad@aah.org

[†] These authors have contributed equally to this work

Specialty section:
This article was submitted to Neonatology, a section of the journal Frontiers in Pediatrics

Received: *10 June 2020*
Accepted: *11 August 2020*
Published: *18 September 2020*

Citation:
Kasala S, Briyal S, Prazad P, Ranjan AK, Stefanov G, Donovan R and Gulati A (2020) Exposure to Morphine and Caffeine Induces Apoptosis and Mitochondrial Dysfunction in a Neonatal Rat Brain. Front. Pediatr. 8:593. doi: 10.3389/fped.2020.00593

Background: Preterm infants experience rapid brain growth during early post-natal life making them vulnerable to drugs acting on central nervous system. Morphine is administered to premature neonates for pain control and caffeine for apnea of prematurity. Simultaneous use of morphine and caffeine is common in the neonatal intensive care unit. Prior studies have shown acute neurotoxicity with this combination, however, little information is available on the mechanisms mediating the neurotoxic effects. The objective of this study was to determine the effects of morphine and caffeine, independently and in combination on mitochondrial dysfunction (Drp1 and Mfn2), neural apoptosis (Bcl-2, Bax, and cell damage) and endothelin (ET) receptors (ET_A and ET_B) in neonatal rat brain.

Methods: Male and female rat pups were grouped separately and were divided into four different subgroups on the basis of treatments–saline (Control), morphine (MOR), caffeine (CAFF), and morphine + caffeine (M+C) treatment. Pups in MOR group were injected with 2 mg/kg morphine, CAFF group received 100 mg/kg caffeine, and M+C group received both morphine (2 mg/kg) and caffeine (100 mg/kg), subcutaneously on postnatal days (PND) 3–6. Pups were euthanized at PND 7, 14, or 28. Brains were isolated and analyzed for mitochondrial dysfunction, apoptosis markers, cell damage, and ET receptor expression via immunofluorescence and western blot analyses.

Results: M+C showed a significantly higher expression of Bax compared to CAFF or MOR alone at PND 7, 14, 28 in female pups ($p < 0.05$) and at PND 7, 14 in male pups ($p < 0.05$). Significantly ($p < 0.05$) increased expression of Drp1, Bax, and suppressed expression of Mfn2, Bcl-2 at PND 7, 14, 28 in all the treatment groups compared to the control was observed in both genders. No significant difference in the expression of ET_A and ET_B receptors in male or female pups was seen at PND 7, 14, and 28.

Conclusion: Concurrent use of morphine and caffeine during the first week of life increases apoptosis and cell damage in the developing brain compared to individual use of caffeine and morphine.

Keywords: morphine, caffeine, mitochondrial function, apoptosis, neonatal rat model, brain

INTRODUCTION

Preterm neonates in the Neonatal Intensive Care Unit (NICU) are subjected to many essential but painful procedures (1). A growing focus on the comfort and pain control in the NICU has led to an exponential increase in opioid administration (2). Although opioid management for acute pain is thought to be evidence-based, prolonged use of opioids in neonates remains a concern secondary to its potential deleterious effects on the developing brain (3, 4). Caffeine citrate is a standard treatment for apnea of prematurity (AOP) in the extremely premature infants. The "Caffeine for Apnea of Prematurity (CAP)" trial demonstrated safety, tolerability, and efficacy of caffeine for treatment of apnea, with reduction in bronchopulmonary dysplasia (BPD) and improvement in survival of 18–21 month old preterm infants without neurodisability (5). Despite the widespread clinical use, effects of caffeine on the developing brain remained controversial. Morphine in association with caffeine is routinely used in the NICU (6, 7); however, there are conflicting reports surrounding morphine analgesia and its long-term neurologic effects in preclinical and clinical studies. Various *in vitro* (8, 9) and *in vivo* studies (10–12) have shown induced neuroapoptosis because of morphine treatment. Chronic morphine exposure has shown to cause a significant reduction in brain volume and dendritic growth (13), modification in synaptic neuroplasticity in limbic system and impairment in learning throughout adult life (14–16). It has also known to result in long-lasting neurochemical changes and affects hippocampal development (17, 18). Results from these studies suggest that morphine has neurotoxic effects; however, Zhaleh et al. has shown that use of a low-dose morphine could have suppressive effects on cytotoxicity (19). Moreover, a clinical study has shown an association between neonatal low-dose morphine analgesia and early alterations in cerebral structure as well as short-term neurobehavioral problems that did not persist into childhood (20). Conversely, several randomized trials have reported that short term or long-term morphine treatment in preterm neonates did not alter cognitive ability or motor development when measured at 5 and at 8–9 years of age (21–24).

Limited research exists on the safety and long-term consequences of caffeine on the developing brain. *In vivo* and *in vitro* studies have shown caffeine induced neuroapoptosis (25), alteration of astrogenesis (26), and transient motor impairment (27). Preclinical studies have shown that therapeutic doses of caffeine may significantly augment the neurotoxicity of sedative/anesthetic drugs (28), challenging the clinical assumption that caffeine is safe for premature infants when used in combination with sedative drugs.

Studies at the molecular level show that the developing rat brain from PND 1 to PND 7, closely correlates with the timing of synaptogenesis which is highly susceptible to neuroapoptosis (29, 30). The opioid and endothelin system modulate neuronal migration, differentiation and maturation during this period (31–34). Endothelin A (ET_A) and B (ET_B) receptors have been shown to play an important role in mitochondrial function in an adult stroke model. Blockage of ET_B receptors and activation of ET_A receptors appears to trigger apoptotic processes by modulating mitochondrial function (34). However, the involvement of ET receptors in relation to mitochondrial function in an animal model of drug-induced neurotoxicity is of interest and remained elusive.

Optimal mitochondrial function is crucial for brain development and function, including regulation of neurogenesis, neural stem cell differentiation (35, 36), and development of synapses (37, 38) which is controlled by mitochondrial fusion and fission (39). An abnormal increase in fission through dynamin-related protein 1 (Drp1), leads to mitochondrial insertion of pro-apoptotic proteins such as Bcl-2 associated × protein (Bax) triggering apoptosis. Anti- apoptotic proteins like Bcl-2 bind to Bax to prevent apoptosis, the balance between pro-apoptotic, and anti-apoptotic proteins on the mitochondrial membrane determine cell fate (40). Bcl-2 and Bax are present permanently on the mitochondrial and endoplasmic reticulum membranes controlling drug-induced mitochondria mediated apoptosis by regulating the calcium storage (41). Overexpression of mitofusin-2 (Mfn2) results in suppression of mitochondrial fragmentation leading to decreased apoptosis (42–44). Disturbance in fine balance between fusion/fission results in disturbed mitochondrial morphogenesis leading to altered development and function of immature synapses of nerves (37).

Since mitochondria may be the initial and one of the most vulnerable targets of drug-induced impairment of neuronal development, we hypothesized that caffeine in association with morphine would augment neuroapoptosis involving the activation of a mitochondria-dependent apoptotic cascade. This would manifest as an increase in the expression of ET_A, Drp1, Bax, cell damage, and decrease in the expression of ET_B, Mfn2, and Bcl-2. We also hypothesized that the central nervous system (CNS) protein expression would demonstrate gender-specific differences suggestive of female neuroprotective properties. The goal of the present study was to use a neonatal rat model to mimic clinical exposure to caffeine and morphine in the premature neonates and their effects on different stages of neurodevelopment through the specific CNS protein analyses.

MATERIALS AND METHODS

Animals

Twenty timed-pregnant Sprague–Dawley rats (Envigo, Indianapolis, IN) were housed in a room with controlled temperature (23 ± 1°C), humidity (50 ± 10%), and light (6:00 A.M−6:00 P.M). All animals were maintained on a 12-h light/dark schedule. Food and water were available *ad libitum*.

Experimental Procedures

On PND 3, male and female rat pups were grouped separately and were divided into four different subgroups on the basis of treatments–saline (Control), morphine (MOR), caffeine (CAFF), and morphine + caffeine (M+C) treatment. A total of 192 rat pups were used for the study. For western blot experiments: four animals per group (4 groups × 2 genders × 3 time-points = 96 animals (48 Male and 48 Female) and for immunofluorescence experiments: four animals per group (4 groups × 2 genders ×

3 time-point = 96 animals (48 Male and 48 Female) were used. Animal care and experimental procedures were performed in accordance with the guidelines for animal care and use following approval by the Institutional Animal Care and Use Committee (IACUC, MWU file # 3076) of Midwestern University.

Drugs

All drug doses were appropriately scaled keeping in mind the metabolic differences between rats and humans. All drugs were administered via a sterile filtered syringe with a 25-gauge needle. Each pup received treatments by subcutaneous injection with volumes adjusted as per body weight. Pups in control group were administered saline as per body weight with volumes ranging from 8 to 14 μl. The pups were recovered for 30 min following each injection in an incubator maintained at 34.5°C (nesting temperature) prior to being returned to their dams.

Caffeine Administration

In clinical practice, caffeine is administered as a bolus of 20 mg/kg followed by daily maintenance doses of 5–10 mg/kg/day for days to weeks. This standard dosing regimen achieves 6–50 μg/mL of blood caffeine levels which is considered safe for premature infants (45). Similar levels are reached in a mice model with 100 mg/kg of caffeine citrate subcutaneously (46, 47). Pups in CAFF, M+C groups were administered 100 mg/kg of caffeine citrate (Fisher Scientific, Hanover Park, IL) on PND 3 (30) and repeated every 24 h for a total of 4 days (PND 3–6).

Morphine Administration

In clinical practice, one method of administering morphine for acute pain is an intermittent bolus of 0.1 mg/kg morphine every 4 h intravenously. This dosing schedule attains a morphine level of 50–300 ng/ml in preterm infants to provide analgesic effects (48, 49). Comparable levels are closely achieved with a subcutaneous dose of 2 mg/kg/day in a neonatal rat pup model (50). Pups in MOR, M+C groups were administered 2 mg/kg of morphine sulfate (Henry Schein Animal Health, Dublin, OH, USA) on PND 3, repeated every 24 h for a total of 4 days (PND 3–6).

Euthanasia

On PND 7, 14, and 28, 8 pups from each group of same gender were euthanized by decapitation, and the brains were removed for western blot and immunofluorescence analysis. The brain of each pup was weighed and stored at −80°C for western blot and 4% paraformaldehyde (PFA) for immunofluorescence analyses.

Determination of CNS Proteins ET_A, ET_B, Drp1, Mfn2, Bcl-2, and Bax

Western Blot Analysis

Brain tissues were washed in chilled saline and homogenized in RIPA buffer (20 mM Tris-HCl pH 7.5, 120 mM NaCl, 1.0% Triton X-100, 0.1% SDS, 1% sodium deoxycholate, 10% glycerol, 1 mM EDTA, and 1× protease inhibitor, Roche). Proteins were isolated in solubilized form and concentration was determined using Folin-Ciocalteu's Reagent. Solubilized protein (60 μg) was denatured in Laemmli sample buffer (Bio-Rad, Hercules, CA), resolved in 10% SDS–PAGE and transferred on nitrocellulose membrane (Sigma-Aldrich, St. Louis, MO, USA). The membrane was then blocked with superblock solution for 1 h at room temperature. The membranes were probed for anti-ET_B, anti-ET_A, anti-Drp1, anti-Mfn2, anti-Bcl-2, and anti-Bax (1:1000; Abcam, Cambridge, MA) primary antibodies overnight at 4°C. Membranes were then incubated with goat anti-rabbit and anti-mouse IgG, horseradish peroxidase-conjugated (HRP) secondary antibody (1:2000; Santa Cruz Biotech., Santa Cruz, CA, USA) for 2 h at room temperature. β-actin (1:10,000; Sigma-Aldrich, St. Louis, MO, USA) was used as a loading control. The chemiluminescence of HRP was visualized with SuperSignal WestPico Chemiluminescent Substrate (Thermo Fisher Scientific, Bartlett, IL) using the Kodak Gel Logic 1,500 Imaging System (CarestreamHealth Inc., New Haven, CT). The protein band intensity indicating the protein expression was analyzed using ImageJ (NIH) software and graphs were plotted after normalizing the protein expression with β-actin expression.

Immunofluorescent Analysis

To confirm western blot data, immunofluorescence technique was used to detect expression of Drp1, Mfn2, Bcl-2, and Bax markers in rat brain tissues. Rat brains were fixed in 50 ml of 4% paraformaldehyde (PFA) in NaPO4 buffer solution for 2 h at room temperature, and then submerged in 20% sucrose/4% PFA solution and stored at 4°C for 48 h. Brains were sliced into 20 μm thick slices using a cryostat (Microtome cryostat HM 505E; Walldorf, Germany) at −20°C. Tissue sections were washed three times with 1× PBS and permeabilized with 1% Triton X-100 in PBS for 15 min at room temperature. Blocking with 5% BSA in 1× PBS for 1 h at room temperature was carried out. The brain sections were incubated with anti-Drp1, Mfn2, Bcl-2, and Bax antibody (1:200 diluted in 1× PBS) at 4°C overnight. Sections were washed twice in 1× PBS and incubated with Alexa Fluor 488-conjugated donkey anti-mouse secondary antibody and Alexa Fluor 555-conjugated donkey anti-rabbit secondary antibody (1:200, Abcam, Cambridge, MA) for 1 h at room temperature in the dark and mounted with prolong gold anti-fade reagent with DAPI (Cell Signaling Technology, Danvers, MA, USA). Fluorescence was detected using an inverted fluorescent microscope (Nikon Eclipse TiE, Melville, NY). All images for analysis were taken using the same exposure with a multi-channel ND acquisition using NIS Elements BR imaging software (Nikon Instruments, Inc., Melville, NY). Analyses were performed using NIS-Elements 3.01 imaging software from Nikon Instruments, Inc. (Melville, NY).

Assessment of Cell Damage

Cell damage, a measure of apoptosis, in brains of rat pups was evaluated using 7-amino actinomycin D (7AAD) assay on PND 7, 14, and 28. Rat pups brains were perfused with chilled 1× PBS and fixed with 50 ml of 4% paraformaldehyde (PFA) solution for 2 h. Fixed brains were incubated in 20% sucrose/4% PFA solution, pH 7.4 at 4°C for 48 h. Brain tissue was sliced into 20 μm thick slices at −20°C using a cryostat (Microtome cryostat HM 505E; Walldorf, Germany). Tissue sections were blocked with 4% BSA in 1× PBS for 30 min at 4°C. The brain sections

were incubated with fluorescent DNA binding agent, 7AAD (0.25 μg/mL; Thermo Fisher Scientific, Bartlett, IL) for 15 min at 4°C. Sections were washed thrice in 1× PBS and mounted with prolong gold anti-fade reagent with DAPI (Cell Signaling Technology, Danvers, MA, USA). Fluorescence was detected in a randomly fashion using inverted fluorescent microscope (Nikon Eclipse TiE, Melville, NY). Captured microscopic images were processed with NIS-Elements AR 4.13 software (Nikon, Melville, NY) and 7AAD positive nuclei were marked and counted. The data was represented as percent 7AAD positive cells normalized to the total number of nuclei in each field.

Statistical Analysis

Power analysis was conducted using GraphPad Instat-3.1 with a beta of 0.8 and alpha of 0.05. The sample size in each group was $N = 4$ based upon expected change determined from results published in literature using similar procedures. Data are presented as mean ± S.E.M. One-way ANOVA followed by Bonferroni's *post hoc* comparison test was used. A $P < 0.05$ was considered to be significant. The statistical analysis was processed with GraphPad Prism 8.00 (GraphPad, San Diego, CA, USA). All groups were compared against control and one another.

RESULTS

Effect of Treatment on Brain/Body Ratio

Brain/body weight ratio did not differ between different groups at different time points in both the genders.

Effect of Treatment on Apoptotic Markers (Bax and Bcl-2)

Western blot analyses showed a significant ($p < 0.01$) increase expression of Bax in both male and female in MOR, CAFF, and M+C groups compared to control group at PND 7, 14, and 28 (**Figure 1A**). M+C had a markedly increased Bax expression compared MOR and CAFF alone at PND 7, 14, and 28 in female group and at PND 7 and 14 in male group ($p < 0.01$, **Figure 1A**). MOR, CAFF, and M+C groups had a significant ($p < 0.01$) decrease in Bcl-2 expression in both male and female groups compared to control group at PND 7, 14, and 28 (**Figure 2A**). Expression of Bcl-2 remained unaltered in the M+C group compared to MOR or CAFF in both male and female groups at different time points. No significant differences in the expression of these markers were noted between male and female subgroups. Therefore, these results were further confirmed with immunofluorescence imaging only in male group. The qualitative immunofluorescence data of these markers showed higher expression of Bax (red, **Figure 1B**) and lower expression of Bcl-2 (red, **Figure 2B**) in MOR, CAFF, and M+C treated groups compared to control.

Effect of Treatment on Mitochondrial Function (Drp1 and Mfn2)

MOR, CAFF, and M+C groups had a significant ($p < 0.01$) increase in Drp1 expression in both male and female groups compared to control group at PND 7, 14, and 28 (**Figure 3A**). MOR, CAFF, and M+C groups had a significant ($p < 0.01$) decrease in Mfn2 expression compared to control group in both male and female groups at PND 7, 14, and 28 (**Figure 3B**) in western blot analyses. Expression of Drp1 and Mfn2 remained unaltered in the M+C group compared to MOR or CAFF group in both male and female groups at different time points. No significant differences in the expression of these markers were noted between male and female groups. Therefore, these results were further confirmed with immunofluorescence imaging only in male group. The immunofluorescence data of these markers showed higher expression of Drp1 (green, **Figure S1**) and lower expression of Mfn2 (green, **Figure S2**) in MOR, CAFF, and M+C treated groups.

Effect of Treatment on Cell Damage/Cell Death

No significant differences in the expression of apoptotic and mitochondrial dysfunction markers were noted between male and female subgroups, therefore, we assessed the DNA damage only in male group. Detection of apoptotic cell nuclei, was done using fluorescent DNA binding agent, 7-amino actinomycin D (7AAD). 7AAD is a membrane impermeant dye that binds to double stranded DNA and exhibit dramatic increase in fluorescence intensity. Apoptosis in cells is known to cause damage to cell membrane, which allows 7AAD dye enter into the damaged cells. After staining with 7AAD, apoptotic cells show red fluorescence, while undamaged cells showed no fluorescence. No signals of cell death were observed in the control group at PND 7, 14, and 28 (3.3, 2.5, and 3.0% 7AAD+ cells, respectively). Treatment with MOR, CAFF, and M+C, significantly ($p < 0.001$) increased the number of apoptotic cells on PND 7 (19.7, 18.5, and 22.3% 7AAD+ cells, respectively), PND 14 (24.6, 25.4, and 27.4% 7AAD+ cells, respectively), and PND 28 (24.4, 27.0, and 28.9% 7AAD+ cells, respectively) (**Figure 4**).

Effect of Treatment on Endothelin Receptors (ET_A and ET_B)

Expression of ET_A and ET_B did not differ between different groups at different time points in either gender (**Figure S3**).

DISCUSSION

This is the first study aimed to examine how morphine in association with caffeine, affect mitochondrial function, expression of ET receptors and apoptotic markers in a neonatal rat model. The results provide some insight into the role of mitochondria in neuroapoptosis induced from the drug combination. An important consideration in the study design was to mimic a NICU practice where extremely preterm neonates are treated with morphine for pain/agitation (1) in association with caffeine for AOP. The study targeted the peak synaptogenesis time window of PND 3–6 in a rat pup, which corresponds to a premature neonate at 26–32 week gestation (51, 52).

The results demonstrate that concurrent exposure to clinically relevant doses of morphine and caffeine trigger cell death in an immature brain that persist at various developmental stages

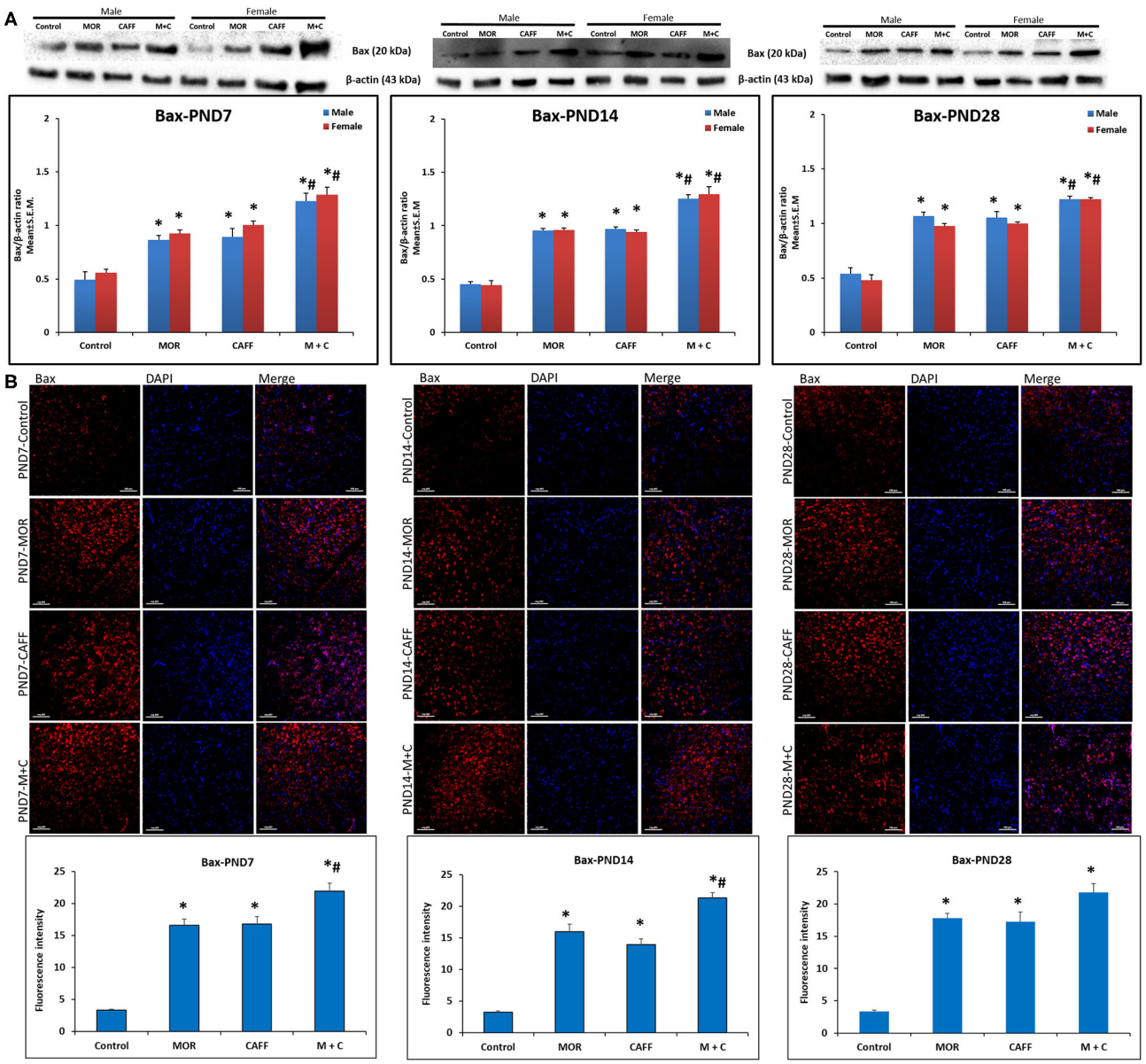

FIGURE 1 | Expression of pro-apoptosis marker Bax in rat pups brain. **(A)** Western blots and densitometry graphs, **(B)** immunofluorescence images in Control, MOR, CAFF, and M+C treated pups brain tissues at PND 7, PND 14, and PND 28. **(A)** All blots are representative of four different experiments with similar results. β-Actin was used as a loading control. **(B)** Representative Immunofluorescence microscopy images and fluorescence intensity graphs of Bax. MOR, CAFF, and M+C groups marked increase in the expression of the pro-apoptosis marker Bax (red) compared to control. Nuclei were stained with DAPI (blue). Bar scale = 100 μm. Values are expressed as mean ± S.E.M. *$P < 0.01$ vs. Control, #$P < 0.01$ Vs. MOR and CAFF alone.

(PND 7, 14, and 28) suggesting the potential for long-term debilitating neurological outcomes. Findings also confirm the previously reported higher cell death mediated via mitochondria dependent caspase-3 activation from moderate dose of caffeine and morphine (30). This is further supported by other studies where the addition of caffeine to other sedatives such as midazolam/ketamine/fentanyl/alcohol in PND 3 rat pups has shown a supra-additive effect, causing more neurotoxicity than expected (28, 47).

In our study, morphine caused a significant increase in apoptosis via Bax, possibly by an increase in mitochondrial fission (via Drp1) and a significant decrease in mitochondrial fusion (via Mfn2) at PND 7, 14, and 28 in male and female pups. This may suggest a disturbance in mitochondrial function from an imbalance in fission/fusion proteins resulting in cell death. These results are in agreement with previous studies which have indicated that chronic morphine induces up-regulation of the Bax and down-regulation of the Bcl-2 protein (8, 53–55).

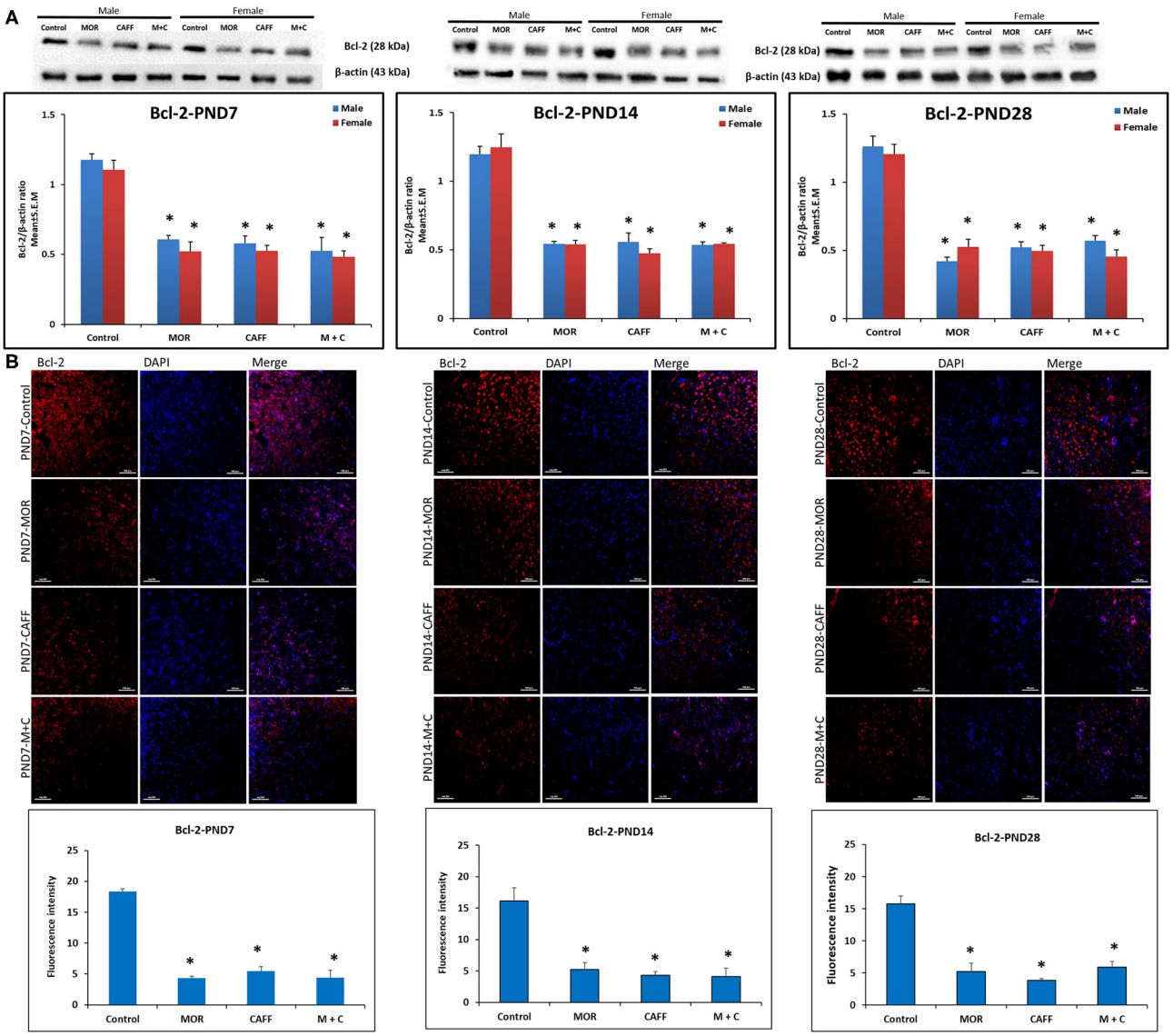

FIGURE 2 | Expression of anti-apoptosis marker Bcl-2 in rat pups brain. **(A)** Western blots and densitometry graphs, **(B)** immunofluorescence images in Control, MOR, CAFF, and M+C treated pups brain tissues at PND 7, PND 14, and PND 28. **(A)** All blots are representative of four different experiments with similar results. β-Actin was used as a loading control. **(B)** Representative Immunofluorescence microscopy images and fluorescence intensity graphs of Bcl-2 markers. MOR, CAFF, and M+C groups marked increase in the expression of the anti-apoptosis marker Bcl-2 (red) compared to control. Nuclei were stained with DAPI (blue). Bar scale = 100 μm. Values are expressed as mean ± S.E.M. *$P < 0.01$ vs. Control.

Further, these studies show that mitochondrial viability plays a key role in the cell apoptosis (8, 53, 56). While previous studies involving acute low dose morphine did not find an increase in cell death, the discriminating factor may be partly explained by different dosage use and inhibition of apoptosis by activation of opioid receptors via other pathways like phosphatidylinositol 3-kinase/protein kinase B (PI3K/Akt) (19).

Similar to morphine, our data suggest that caffeine increased apoptosis via Bax possibly by an increase in mitochondrial fission (via Drp1) and a significant decrease in mitochondrial fusion (via Mfn2) at PND 7, 14, and 28 in male and female pups. This suggests a potential role of mitochondria in the cell death. Consistent with our results, previous studies have shown that caffeine has a neurotoxic effect on the immature brain (25, 30, 47). Additionally, we also assessed cell damage with 7AAD assay and observed significantly increased cell damage in morphine and caffeine treated animals.

The exact mechanism involved with neurotoxicity from M+C combination remains unknown. Caffeine stimulates the respiratory center in the CNS via adenosine receptor inhibition at therapeutic doses, but at higher doses causes cellular changes via phosphodiesterase inhibition, Gamma amino butyric acid A receptor ($GABA_A$) inhibition and release of intracellular calcium (25, 57). On the other hand, morphine acts on the mu opioid receptor (MOR), the G protein coupled receptor, mediating pain and adverse effects, and at high concentrations can activate δ and

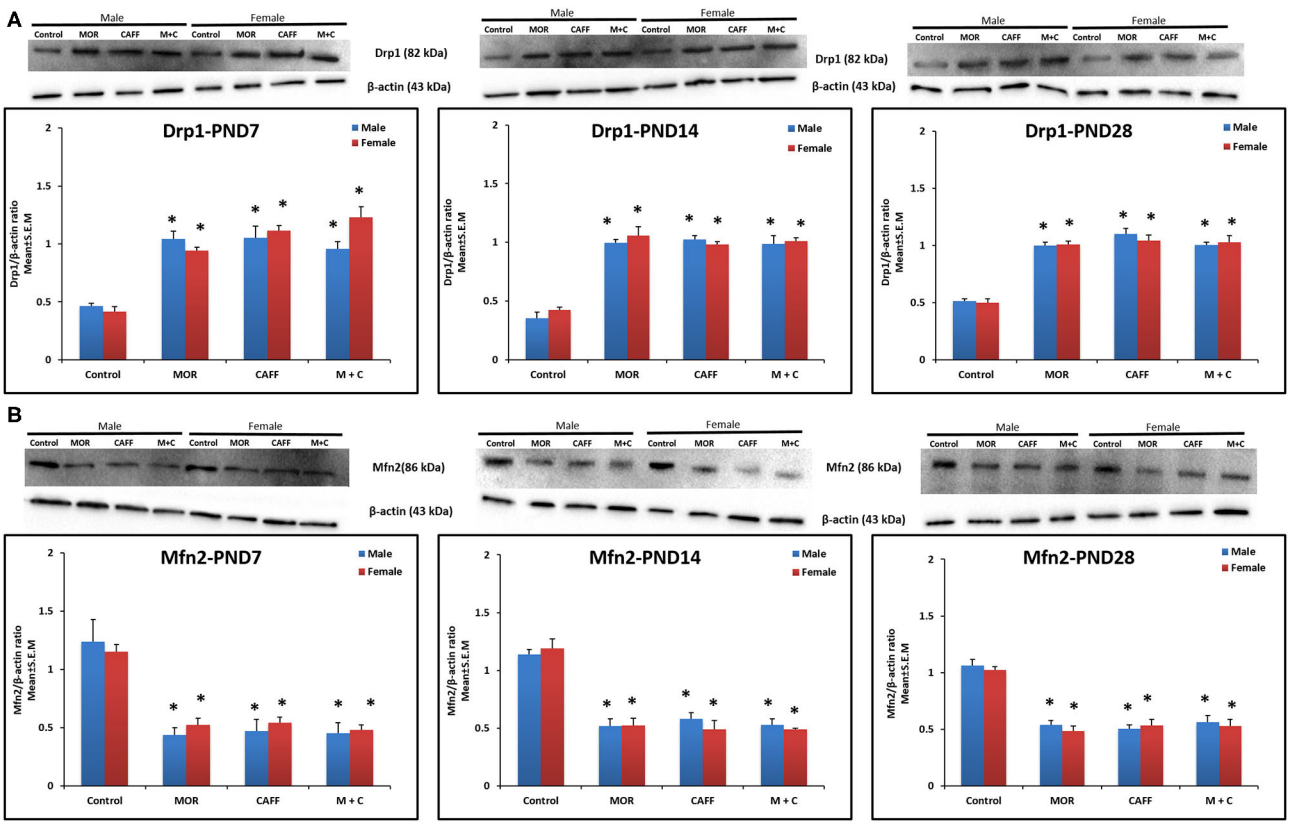

FIGURE 3 | Expression of mitochondrial fission protein Drp1 **(A)** and mitochondrial fusion protein Mfn2 **(B)** in rat pup's brain. Western blots and densitometry graphs of Control, MOR, CAFF, and M+C treated pups brain tissues at PND 7, PND 14, and PND 28. All blots are representative of four different experiments with similar results. β-Actin was used as a loading control. Values are expressed as mean ± S.E.M. *$P < 0.01$ vs. Control.

κ receptors (58). At a cellular level, morphine inhibits adenylate cyclase decreasing cyclic AMP (Adenosine Monophosphate) and thereby calcium ion entry into the cell. In theory, considering the opposite effects of morphine and caffeine on the calcium ion homeostasis, there should be minimal effect on apoptosis from this combination. This dysregulation of calcium equilibrium can be a possible mechanism to trigger apoptosis by increase in pro-apoptotic mediator via Bax (40) and decrease in anti-apoptotic mediator via Bcl-2.

Several intrinsic pathways mediating apoptosis signaling act on the mitochondria leading to release of pro-apoptotic proteins. In our study, the M+C group had a significant increase in expression of Drp1 protein and a decrease in expression of Mfn2 protein, suggesting this imbalance in the fission/fusion processes may play a causal role in the neuroapoptosis induced from this combination. However, the expression of Drp1 and Mfn2 protein expression did not differ in the M+C group in comparison to caffeine, morphine groups, suggesting that caffeine did not augment the neurotoxicity when used in association with morphine via the mitochondrial processes.

Research has shown the involvement of endothelin (ET) in CNS development during critical stages of neuronal migration, organization, and myelination (32, 33). ET receptors also have extensive involvement in the analgesic actions of opioids such as morphine (59–62). Mitochondria are important to ET's role in the molecular regulation of neurogenesis and angiogenesis in cerebral ischemia (34). However, the role of endothelin receptor expression and its relation to mitochondrial function in neuroapoptosis induced from drugs in a neonatal rat model was never explored. In our study, the expression of ET_A and ET_B did not differ in the M+C group in comparison to other groups. It can be interpreted that administration of morphine and caffeine does not affect the expression of brain ETA receptors and ET_B receptors.

Strengths of our Study

This is a pilot study to highlight the effects of morphine and caffeine, two most commonly used drugs in the NICU on central nervous system proteins. The study also provides evidence for the possible mitochondrial mechanism underlying morphine and caffeine induced neuronal damage. In future, this study will help in exploring the potential protective effect of selective Drp1 inhibitors in neurotoxicity induced from drug combinations routinely used in the NICU. Caution should be exerted when using caffeine with morphine in the NICU.

Our study has some important limitations: First, our neonatal rat model was used to model clinical practice of morphine and caffeine exposure in the absence of pain or other stress

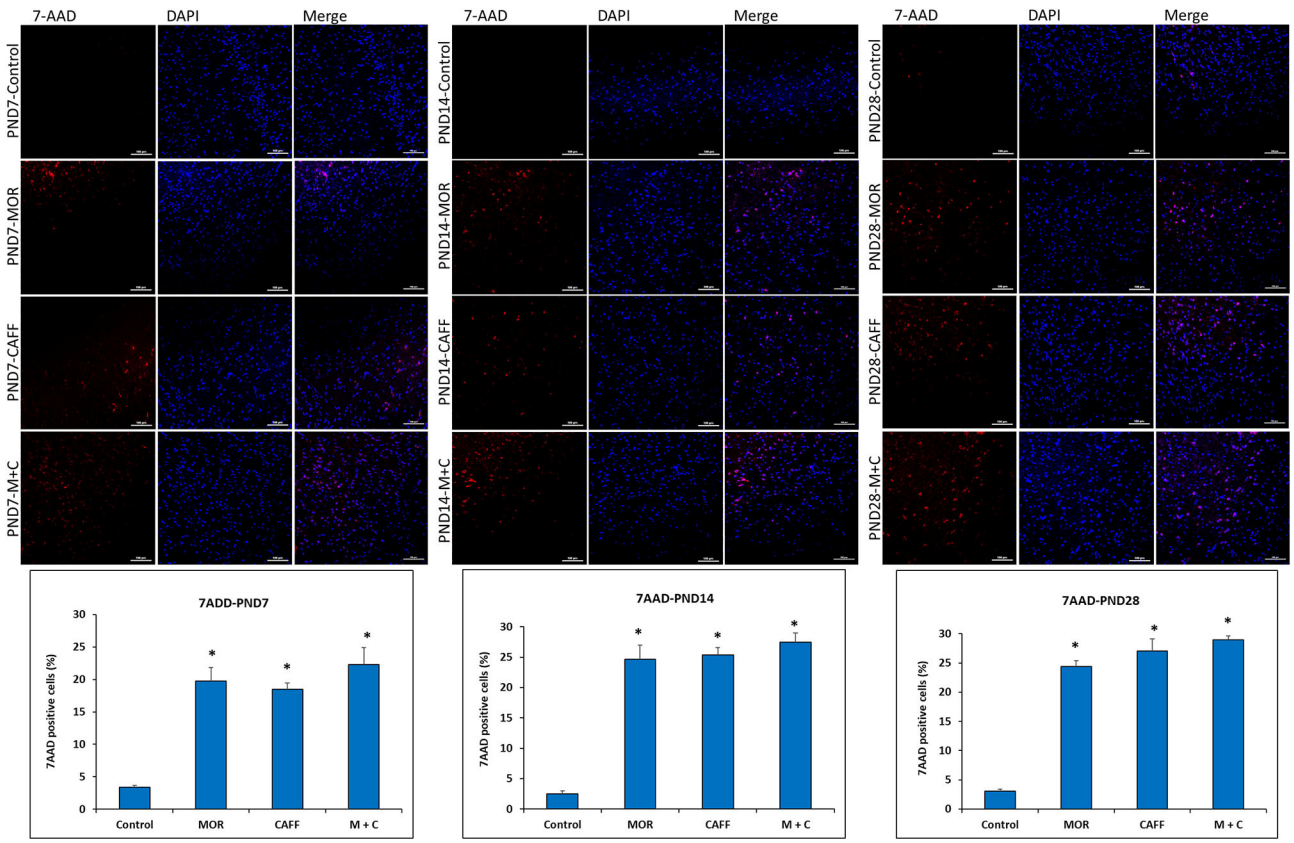

FIGURE 4 | DNA Damage: Representative fluorescence microscopy images of brain tissue sections of Control, MOR, CAFF, and M+C treated pups at PND 7, PND 14, and PND 28 and a graph of quantified 7AAD$^+$ cells. Scale bar = 100 μm. Values are expressed as mean ± S.E.M. *$P < 0.001$ vs. Control.

encountered in the NICU. While, some studies reported a model of neonatal stress and morphine treatment which produces long lasting neurobehavioral effects in adult rats (16), others showed that low doses of morphine may protect the brain from neurodegeneration in the presence of pain (63). Second, animal brain development is similar to humans, however, translating the findings from animal studies to humans is difficult and therefore, clinical studies are needed to address the long-term implications of morphine in association with caffeine in the preterm infants. Third, unlike previous studies, which noted specific regional brain damage based on receptor location, our study utilized the whole brain homogenates opposed to specific regions for CNS protein expression. A prior study has shown that caffeine in association with morphine caused greater cell death in thalamus than either drug alone at 24 h after drug administration (30). Further studies exploring thalamic areas for cell death at PND 7, 14 and 28 would be interesting. Additional studies looking into Drp1/Mfn2 localization and translocation from cytosol to mitochondria would be valuable.

In summary, we found that early exposure to morphine and caffeine alone and in association significantly induced apoptosis and caused disturbance in mitochondrial fission and fusion proteins suggesting involvement of mitochondrial dysfunction in apoptosis. Early exposure to morphine and caffeine combination induced greater apoptosis compared to morphine and caffeine alone. However, this combination did not demonstrate significant mitochondrial dysfunction compared to morphine and caffeine alone. Further molecular studies exploring other mechanisms of neurotoxicity may play a role in developing potential neuroprotective agents to minimize the neurotoxicity.

DATA AVAILABILITY STATEMENT

The raw data supporting the conclusions of this article will be made available by the authors, without undue reservation.

ETHICS STATEMENT

The animal study was reviewed and approved by Institutional Animal Care and Use Committee (IACUC, MWU file # 3076) of Midwestern University.

AUTHOR CONTRIBUTIONS

SK Development of hypotheses, research, and grant proposal. Performed laboratory experiments, data analysis, and interpretation. PP Research mentor and advisor. GS Research mentor and advisor. SB Oversight and carried out laboratory experiments, data generation, analysis, and

interpretation of results. AR Standardization of 7AAD assay and data analysis for cell death assay. RD Guidance with data analysis and manuscript preparation. AG Oversight of basic science laboratory at Midwestern University. All authors contributed to the article and approved the submitted version.

FUNDING

Financial support was provided by a grant from James R. and Helen D. Russell Institute for Research and Innovation Small Research Grants Program (Grant No. 2018–103), Advocate Lutheran General Hospital, Park Ridge, IL, Midwestern Univeristy, Chicago College of Pharmacy, Downer's Grove, IL.

ACKNOWLEDGMENTS

A special thank you to my research mentors and Midwestern University, Chicago College of Pharmacy.

SUPPLEMENTARY MATERIAL

The Supplementary Material for this article can be found online at: https://www.frontiersin.org/articles/10.3389/fped.2020.00593/full#supplementary-material

REFERENCES

1. Carbajal R, Rousset A, Danan C, Coquery S, Nolent P, Ducrocq S, et al. Epidemiology and treatment of painful procedures in neonates in intensive care units. *JAMA*. (2008) 300:60–70. doi: 10.1001/jama.300.1.60
2. Durrmeyer X, Vutskits L, Anand KJ, Rimensberger PC. Use of analgesic and sedative drugs in the NICU: integrating clinical trials and laboratory data. *Pediatr Res*. (2010) 67:117–27. doi: 10.1203/PDR.0b013e3181c8eef3
3. Borenstein-Levin L, Synnes A, Grunau RE, Miller SP, Yoon EW, Shah PS, et al. Narcotics and sedative use in preterm neonates. *J Pediatr*. (2017) 180:92–8.e1. doi: 10.1016/j.jpeds.2016.08.031
4. Carbajal R, Eriksson M, Courtois E, Boyle E, Avila-Alvarez A, Andersen RD, et al. Sedation and analgesia practices in neonatal intensive care units (EUROPAIN): results from a prospective cohort study. *Lancet Res Med*. (2015) 3:796–812. doi: 10.1016/S2213-2600(15)00331-8
5. Schmidt B, Roberts RS, Davis P, Doyle LW, Barrington KJ, Ohlsson A, et al. Long-term effects of caffeine therapy for apnea of prematurity. *N Engl J Med*. (2007) 357:1893–902. doi: 10.1056/NEJMoa073679
6. Anand KJS, Hall RW, Desai N, Shephard B, Bergqvist LL, Young TE, et al. Effects of morphine analgesia in ventilated preterm neonates: primary outcomes from the NEOPAIN randomised trial. *Lancet*. (2004) 363:1673–82. doi: 10.1016/S0140-6736(04)16251-X
7. Du W, Warrier I, Tutag Lehr V, Salari V, Ostrea E, Aranda JV. Changing patterns of drug utilization in a neonatal intensive care population. *Am J Perinatol*. (2006) 23:279–85. doi: 10.1055/s-2006-946719
8. Hu S, Sheng WS, Lokensgard JR, Peterson PK. Morphine induces apoptosis of human microglia and neurons. *Neuropharmacology*. (2002) 42:829–36. doi: 10.1016/S0028-3908(02)00030-8
9. Willner D, Cohen-Yeshurun A, Avidan A, Ozersky V, Shohami E, Leker RR. Short term morphine exposure *in vitro* alters proliferation and differentiation of neural progenitor cells and promotes apoptosis via mu receptors. *PLoS ONE*. (2014) 9:e103043. doi: 10.1371/journal.pone.0103043
10. Bajic D, Commons KG, Soriano SG. International journal of developmental neuroscience morphine-enhanced apoptosis in selective brain regions of neonatal rats. *Int J Dev Neurosci*. (2013) 31:258–66. doi: 10.1016/j.ijdevneu.2013.02.009
11. Emeterio EP, Tramullas M, Hurlé MA. Modulation of apoptosis in the mouse brain after morphine treatments and morphine withdrawal. *J Neurosci Res*. (2006) 83:1352–61. doi: 10.1002/jnr.20812
12. Katebi SN, Razavi Y, Alamdary SZ, Khodagholi F, Haghparast A. Morphine could increase apoptotic factors in the nucleus accumbens and prefrontal cortex of rat brain's reward circuitry. *Brain Res*. (2013) 1540:1–8. doi: 10.1016/j.brainres.2013.09.045
13. Seatriz JV, Hammer RPJr. Effects of opiates on neuronal development in the rat cerebral cortex. *Brain Res Bull*. (1993) 30:523–27. doi: 10.1016/0361-9230(93)90078-P
14. Beltran-Campos V, Silva-Vera M, Garcia-Campos ML, Diaz-Cintra S. Effects of morphine on brain plasticity. *Neurologia*. (2015) 30:176–80. doi: 10.1016/j.nrleng.2014.08.001
15. Miller EC, Zhang L, Dummer BW, Cariveau DR, Loh H, Law PY, et al. Differential modulation of drug-induced structural and functional plasticity of dendritic spines. *Mol Pharmacol*. (2012) 82:333–43. doi: 10.1124/mol.112.078162
16. Boasen JF, McPherson RJ, Hays SL, Juul SE, Gleason CA. Neonatal stress or morphine treatment alters adult mouse conditioned place preference. *Neonatology*. (2009) 95:230–9. doi: 10.1159/000165379
17. Rozisky JR, Laste G, de Macedo IC, Santos VS, Krolow R, Noschang C, et al. Neonatal morphine administration leads to changes in hippocampal BDNF levels and antioxidant enzyme activity in the adult life of rats. *Neurochem Res*. (2013) 38:494–503. doi: 10.1007/s11064-012-0941-8
18. Traudt CM, Tkac I, Ennis KM, Sutton LM, Daniel M. Development in rats. *J Neurosci Res*. (2013) 90:307–14. doi: 10.1002/jnr.22750
19. Zhaleh H, Azadbakht M, Pour AB, Zhaleh M. Morphine inhibits cell death in PC12 cells by activation of PI3K/Akt signal pathway morphine inhibits cell death in PC12 cells by activation of PI3K/Akt signal pathway. *EjarrCom*. (2012) 5:6–10.
20. Steinhorn R, McPherson C, Anderson PJ, Neil J, Doyle LW, Inder T. Neonatal morphine exposure in very preterm infants - cerebral development and outcomes. *J Pediatr*. (2015) 166:1200–7.e4. doi: 10.1016/j.jpeds.2015.02.012
21. de Graaf J, van Lingen RA, Simons SH, Anand KJ, Duivenvoorden HJ, Weisglas-Kuperus N, et al. Long-term effects of routine morphine infusion in mechanically ventilated neonates on children's functioning: five-year follow-up of a randomized controlled trial. *Pain*. (2011) 152:1391–7. doi: 10.1016/j.pain.2011.02.017
22. de Graaf J, van Lingen RA, Valkenburg AJ, Weisglas-Kuperus N, Groot Jebbink L, Wijnberg-Williams B, et al. Does neonatal morphine use affect neuropsychological outcomes at 8 to 9 years of age? *Pain*. (2013) 154:449–58. doi: 10.1016/j.pain.2012.12.006
23. Ferguson SA, Ward WL, Paule MG, Hall RW, Anand KJ. A pilot study of preemptive morphine analgesia in preterm neonates: effects on head circumference, social behavior, and response latencies in early childhood. *Neurotoxicol Teratol*. (2012) 34:47–55. doi: 10.1016/j.ntt.2011.10.008
24. Rozé JC, Denizot S, Carbajal R, Ancel PY, Kaminski M, Arnaud C, et al. Prolonged sedation and/or analgesia and 5-year neurodevelopment outcome in very preterm infants. *Arch Pediatr Adolesc Med*. (2008) 162:728–33. doi: 10.1001/archpedi.162.8.728
25. Kang SH, Lee YA, Won SJ, Rhee KH, Gwag BJ. Caffeine-induced neuronal death in neonatal rat brain and cortical cell cultures. *Neuropharmacol Neurotoxicol*. (2002) 13:5–10. doi: 10.1097/00001756-200210280-00023
26. Desfrere L, Olivier P, Schwendimann L, Verney C, Gressens P. Transient inhibition of astrocytogenesis in developing mouse brain following postnatal caffeine exposure. *Pediatr Res*. (2007) 62:604–9. doi: 10.1203/PDR.0b013e318156e425
27. Tchekalarova J, Kubova H, Mares P. Postnatal caffeine exposure : effects on motor skills and locomotor activity during ontogenesis. *Behav Brain Res*. (2005) 160:99–106. doi: 10.1016/j.bbr.2004.11.018
28. Cabrera OH, O'Connor SD, Swiney BS, Salinas-Contreras P, Manzella FM, Taylor GT, et al. Caffeine combined with sedative/anesthetic drugs triggers

widespread neuroapoptosis in a mouse model of prematurity. *J Mater Fetal Neonatal Med.* (2017) 30:2734–41. doi: 10.1080/14767058.2016.1261400
29. Yon JH, Daniel-Johnson J, Carter LB, Jevtovic-Todorovic V. Anesthesia induces neuronal cell death in the developing rat brain via the intrinsic and extrinsic apoptotic pathwaystle. *Neuroscience*. (2005) 135:815–27. doi: 10.1016/j.neuroscience.2005.03.064
30. Black AM, Pandya S, Clark D, Armstrong EA, Yager JY. Effect of caffeine and morphine on the developing pre-mature brain. *Brain Res*. (2008) 1219:136–42. doi: 10.1016/j.brainres.2008.04.066
31. Sargeant TJ, Miller JH, Day DJ. Opioidergic regulation of astroglial/neuronal proliferation: where are we now? *J Neurochem*. (2008) 107:883–97. doi: 10.1111/j.1471-4159.2008.05671.x
32. Jung KJ, Kim DW, Lee HN, Lee YS, Lee SJ, Che JH, et al. The role of endothelin receptor a during myelination of developing oligodendrocytes. *J Korean Med Sci*. (2011) 26:92–9. doi: 10.3346/jkms.2011.26.1.92
33. Gadea A, Aguirre A, Haydar TF, Gallo V. Endothelin-1 regulates oligodendrocyte development. *J Neurosci.* (2009) 29:10047–62. doi: 10.1523/JNEUROSCI.0822-09.2009
34. Gulati A. Endothelin receptors, mitochondria and neurogenesis in cerebral ischemia. *Curr Neuropharmacol*. (2016) 14:619–26. doi: 10.2174/1570159X14666160119094959
35. Wang W, Osenbroch P, Skinnes R, Esbensen Y, Bjørås M, Eide L. Mitochondrial DNA integrity is essential for mitochondrial maturation during differentiation of neural stem cells. *Stem Cells.* (2010) 28:2195–204. doi: 10.1002/stem.542
36. Khacho M, Slack RS. Mitochondrial dynamics in the regulation of neurogenesis: from development to the adult brain. *Dev Dyn.* (2018) 247:47–53. doi: 10.1002/dvdy.24538
37. Sanchez V, Feinstein SD, Lunardi N, Joksovic PM, Boscolo A, Todorovic SM, et al. General anesthesia causes long-term impairment of mitochondrial morphogenesis and synaptic transmission in developing rat brain. *Anesthesiology*. (2011) 115:992–1002. doi: 10.1097/ALN.0b013e3182303a63
38. Oklopcic A, Moy L, Ori CC, Erisir A, Jevtovic-todorovic V. Early exposure to general anesthesia disturbs rat brain. *Anesthesiology*. (2013) 118:1086–97. doi: 10.1097/ALN.0b013e318289bc9b
39. Chan DC. Mitochondrial fusion and fission in mammals. *Annu Rev Cell Dev Biol*. (2006) 22:79–99. doi: 10.1146/annurev.cellbio.22.010305.104638
40. Orrenius S, Gogvadze V, Zhivotovsky B. Calcium and mitochondria in the regulation of cell death. *Biochem Biophys Res Commun*. (2015) 460:72–81. doi: 10.1016/j.bbrc.2015.01.137
41. Tzifi F, Economopoulou C, Gourgiotis D, Ardavanis A, Papageorgiou S, Scorilas A. The role of BCL2 family of apoptosis regulator proteins in acute and chronic leukemias. *Adv Hematol.* (2012) 2012:524308. doi: 10.1155/2012/524308
42. Balog J, Mehta SL, Vemuganti R. Mitochondrial fission and fusion in secondary brain damage after CNS insults. *J Cereb Blood Flow Metab.* (2016) 36:2022–33. doi: 10.1177/0271678X16671528
43. Yoon Y, Pitts KR, McNiven MA. Mammalian dynamin-like protein DLP1 tubulates membranes. *Mol Biol Cell*. (2001) 12:2894–905. doi: 10.1091/mbc.12.9.2894
44. Smirnova E, Griparic L, Shurland DL, Van Der Bliek AM. Drp1 is required for mitochondrial division in mammalian cells. *Mol Biol the Cell*. (2001) 12:2245–56. doi: 10.1091/mbc.12.8.2245
45. Natarajan G, Botica ML, Thomas R, Aranda JV. Therapeutic drug monitoring for caffeine in preterm neonates: an unnecessary exercise? *Pediatrics*. (2007) 119:936–40. doi: 10.1542/peds.2006-2986
46. Kaplan GB, Greenblatt DJ, Kent MA, Cotreau-Bibbo MM. Caffeine treatment and withdrawal in mice : relationships between dosage, concentrations, locomotor activity and a, adenosine receptor binding. *J Pharmacol Exp Ther.* (1993) 266:1563–73.
47. Yuede CM, Olney JW, Creeley CE. Developmental neurotoxicity of alcohol and anesthetic drugs is augmented by co-exposure to caffeine. *Brain Sci.* (2013) 3:1128–52. doi: 10.3390/brainsci3031128
48. Carbajal R, Lenclen R, Jugie M, Paupe A, Barton BA, Anand KJ. Morphine does not provide adequate analgesia for acute procedural pain among preterm neonates. *Pediatrics*. (2005) 115:1494–500. doi: 10.1542/peds.2004-1425
49. Scott CS, Riggs KW, Ling EW, Fitzgerald CE, Hill ML, Grunau RV, et al. Morphine pharmacokinetics and pain assessment in premature newborns. *J Pediatr*. (1999) 135:423–9. doi: 10.1016/S0022-3476(99)70163-0
50. McPherson RJ, Gleason C, Mascher-Denen M, Chan M, Kellert B, Juul SE. A new model of neonatal stress which produces lasting neurobehavioral effects in adult rats. *Neonatology*. (2007) 92:33–41. doi: 10.1159/000100084
51. Back SA, Riddle A, McClure MM. Maturation-dependent vulnerability of perinatal white matter in premature birth. *Stroke*. (2007) 38:724–30. doi: 10.1161/01.STR.0000254729.27386.05
52. Craig A, Ling Luo N, Beardsley DJ, Wingate-Pearse N, Walker DW, Hohimer AR, et al. Quantitative analysis of perinatal rodent oligodendrocyte lineage progression and its correlation with human. *Exp Neurol*. (2003) 181:231–40. doi: 10.1016/S0014-4886(03)00032-3
53. Boronat MA, García-Fuster MJ, García-Sevilla JA. Chronic morphine induces up-regulation of the pro-apoptotic fas receptor and down-regulation of the anti-apoptotic Bcl-2 oncoprotein in rat brain. *Br J Pharmacol*. (2001) 134:1263–70. doi: 10.1038/sj.bjp.0704364
54. Liu LW, Lu J, Wang XH, Fu SK, Li Q, Lin FQ. Neuronal apoptosis in morphine addiction and its molecular mechanism. *Int J Clin Exp Med*. (2013) 6:540–5.
55. Motaghinejad M, Karimian SM, Motaghinejad O, Shabab B, Asadighaleni M, Fatima S. The effect of various morphine weaning regimens on the sequelae of opioid tolerance involving physical dependency, anxiety and hippocampus cell neurodegeneration in rats. *Fundam Clin Pharmacol.* (2015) 29:299–309. doi: 10.1111/fcp.12121
56. Yin D, Woodruff M, Zhang Y, Whaley S, Miao J, Ferslew K, et al. Morphine promotes jurkat cell apoptosis through pro-apoptotic FADD/P53 and anti-apoptotic PI3K/Akt/NF-?B pathways. *J Neuroimmunol.* (2006) 174:101–7. doi: 10.1016/j.jneuroim.2006.02.001
57. Daly JW, Fredholm BB. Caffeine - an atypical drug of dependence. *Drug Alcohol Depend*. (1998) 51:199–206. doi: 10.1016/S0376-8716(98)00077-5
58. Inturrisi CE. Clinical pharmacology of opiods for pain. *Clin J Pain*. (2002) 18:S3–13. doi: 10.1097/00002508-200207001-00002
59. Bhalla S, Zhang Z, Patterson N, Gulati A. Effect of endothelin-a receptor antagonist on mu, delta and kappa opioid receptor-mediated antinociception in mice. *Eur J Pharmacol.* (2010) 635:62–71. doi: 10.1016/j.ejphar.2010.03.003
60. Bhalla S, Rapolaviciute V, Gulati A. Determination of A2-adrenoceptor and imidazoline receptor involvement in augmentation of morphine and oxycodone analgesia by agmatine and BMS182874. *Eur J Pharmacol.* (2011) 651:109–21. doi: 10.1016/j.ejphar.2010.10.090
61. Bhalla S, Andurkar SV, Gulati A. Involvement of A2-adrenoceptors, imidazoline, and endothelin-A receptors in the effect of agmatine on morphine and oxycodone-induced hypothermia in mice. *Fundam Clin Pharmacol.* (2013) 27:498–509. doi: 10.1111/j.1472-8206.2012.01046.x
62. Bhalla S, Ali I, Lee H, Andurkar SV, Gulati A. Potentiation of oxycodone antinociception in mice by agmatine and BMS182874 via an imidazoline I2 receptor-mediated mechanism. *Pharmacol Biochem Behav*. (2013) 103:550–60. doi: 10.1016/j.pbb.2012.10.007
63. Dührsen L, Simons SH, Dzietko M, Genz K, Bendix I, Boos V, et al. Effects of repetitive exposure to pain and morphine treatment on the neonatal rat brain. *Neonatology*. (2012) 103:35–43. doi: 10.1159/000341769

Conflict of Interest: AG is founder and CEO of company Pharmazz Inc.

The remaining authors declare that the research was conducted in the absence of any commercial or financial relationships that could be construed as a potential conflict of interest.

NOMENCLATURE

Mitochondrial fission protein (Drp1)
Mitochondrial fusion protein (Mfn2)
Postnatal day (PND)
Bcl-2 associated x protein (BAX)
Endothelin A receptor (ET_A)
Endothelin B receptor (ET_B)
Neonatal Intensive Care Unit (NICU)
Central nervous system (CNS)
Apnea of Prematurity (AOP)
Caffeine for apnea of prematurity (CAP)
Bronchopulmonary dysplasia (BPD)
Endothelin (ET)
Institutional Animal Care and Use Committee (IACUC)
Midwestern University (MWU)
Paraformaldehyde (PFA)
Phosphate-buffered saline (PBS)
Bovine Serum Albumin (BSA)
Phosphatidylinositol 3-kinase (PI3K)
Protein kinase B (Akt)
Gamma amino butyric acid receptor ($GABA_A$)
7-amino actinomycin D (7AAD)

frontiers in Pediatrics

ORIGINAL RESEARCH
published: 25 September 2020
doi: 10.3389/fped.2020.576489

Cerebral Pulsed Arterial Spin Labeling Perfusion Weighted Imaging Predicts Language and Motor Outcomes in Neonatal Hypoxic-Ischemic Encephalopathy

Qiang Zheng[1], *Juan Sebastian Martin-Saavedra*[2], *Sandra Saade-Lemus*[2], *Arastoo Vossough*[2,3], *Giulio Zuccoli*[2], *Fabrício Guimarães Gonçalves*[2], *Colbey W. Freeman*[3], *Minhui Ouyang*[2], *Varun Singh*[4], *Michael A. Padula*[2,3], *Sara B. Demauro*[2,3], *John Flibotte*[2,3], *Eric C. Eichenwald*[2,3], *John A. Detre*[3], *Raymond Wang Sze*[2,3], *Hao Huang*[2,3] *and Misun Hwang*[2,3]*

[1] Yantai University, Yantai, China, [2] Children's Hospital of Philadelphia, Philadelphia, PA, United States, [3] University of Pennsylvania, Philadelphia, PA, United States, [4] Thomas Jefferson University, Philadelphia, PA, United States

OPEN ACCESS

Edited by:
Silvia Carloni,
University of Urbino Carlo Bo, Italy

Reviewed by:
Ana Carolina Coan,
Campinas State University, Brazil
Carlotta Spagnoli,
Santa Maria Nuova Hospital, Italy

***Correspondence:**
Misun Hwang
hwangm@email.chop.edu

Specialty section:
This article was submitted to Pediatric Neurology, a section of the journal Frontiers in Pediatrics

Received: 26 June 2020
Accepted: 21 August 2020
Published: 25 September 2020

Citation:
Zheng Q, Martin-Saavedra JS, Saade-Lemus S, Vossough A, Zuccoli G, Gonçalves FG, Freeman CW, Ouyang M, Singh V, Padula MA, Demauro SB, Flibotte J, Eichenwald EC, Detre JA, Sze RW, Huang H and Hwang M (2020) Cerebral Pulsed Arterial Spin Labeling Perfusion Weighted Imaging Predicts Language and Motor Outcomes in Neonatal Hypoxic-Ischemic Encephalopathy. Front. Pediatr. 8:576489. doi: 10.3389/fped.2020.576489

Rationale and Objectives: To compare cerebral pulsed arterial spin labeling (PASL) perfusion among controls, hypoxic ischemic encephalopathy (HIE) neonates with normal conventional MRI(HIE/MRI⊕), and HIE neonates with abnormal conventional MRI(HIE/MRI⊖). To create a predictive machine learning model of neurodevelopmental outcomes using cerebral PASL perfusion.

Materials and Methods: A total of 73 full-term neonates were evaluated. The cerebral perfusion values were compared by permutation test to identify brain regions with significant perfusion changes among 18 controls, 40 HIE/MRI⊖ patients, and 15 HIE/MRI⊕ patients. A machine learning model was developed to predict neurodevelopmental outcomes using the averaged perfusion in those identified brain regions.

Results: Significantly decreased PASL perfusion in HIE/MRI⊖ group, when compared with controls, were found in the anterior corona radiata, caudate, superior frontal gyrus, precentral gyrus. Both significantly increased and decreased cerebral perfusion changes were detected in HIE/MRI⊕ group, when compared with HIE/MRI⊖ group. There were no significant perfusion differences in the cerebellum, brainstem and deep structures of thalamus, putamen, and globus pallidus among the three groups. The machine learning model demonstrated significant correlation ($p < 0.05$) in predicting language($r = 0.48$) and motor($r = 0.57$) outcomes in HIE/MRI⊖ patients, and predicting language($r = 0.76$), and motor($r = 0.53$) outcomes in an additional group combining HIE/MRI⊖ and HIE/MRI⊕.

Conclusion: Perfusion MRI can play an essential role in detecting HIE regardless of findings on conventional MRI and predicting language and motor outcomes in HIE survivors. The perfusion changes may also reveal important insights into the reperfusion response and intrinsic autoregulatory mechanisms.

Our results suggest that perfusion imaging may be a useful adjunct to conventional MRI in the evaluation of HIE in clinical practice.

Keywords: arterial spin labeling, hypoxic ischemic encephalopathy, neonate, perfusion imaging, perfusion weighted imaging (PWI)

INTRODUCTION

Hypoxic-ischemic encephalopathy (HIE) represents a significant cause of mortality and chronic neurological disability in neonates with heterogeneous short- and long-term outcomes (1). HIE occurs in ∼2–3/1,000 births in the developed world (1). Therapeutic hypothermia has shown to reduce morbidity and mortality and improve neurodevelopmental outcomes in infants with moderate to severe HIE (2). Nevertheless, a substantial proportion of affected infants develop neurodevelopmental disorders. Further studies are therefore needed for early detection (3), injury assessment (4), injury pattern evaluation (5), and neurologic outcomes prediction (6).

HIE is currently evaluated with multimodality imaging, including magnetic resonance imaging (MRI) with T1-/T2-weighted imaging (T1WI/T2WI) (7), diffusion-weighted imaging (DWI) (8), diffusion tensor imaging (DTI) (9, 10), magnetic resonance spectroscopy (4), and arterial spin labeling (ASL) (11), and other modalities such as contrast-enhanced ultrasound (12). ASL is a noninvasive perfusion imaging technique that can assess regional cerebral blood flow (CBF) by magnetically labeling inflowing blood. Cerebral perfusion plays an essential role in the diagnosis and prognosis of neonatal HIE (13, 14). Cerebral perfusion changes may provide prognostic information with regard to monitoring reperfusion responses and ongoing injury (13).

Individualized neurodevelopmental outcome predictions in HIE survivors are critically important in assessing patient risk and ensuring proper neuroprotective and adjunctive interventions. Although classification trees have been developed to predict disability or death in infants with HIE (15), accurate prognostication remains challenging due to the broad spectrum of outcomes, ranging from survival with no neurodevelopmental sequelae to death (16).

Imaging may play a role in neurodevelopmental outcome prediction in HIE survivors, which could influence therapeutic decision-making and neuroprotective therapies. However, not all neonatal HIE patients with normal conventional MRI will have normal outcome (17, 18). In this regard, perfusion MRI may be more sensitive than conventional MRI in neonatal HIE. Cerebral perfusion has previously demonstrated value in predicting HIE outcomes, and both hypoperfusion (19) and hyperperfusion (20) may correlate with poor neurodevelopmental outcomes in HIE.

There is a literature gap regarding the evaluation of perfusion alterations in HIE neonates with normal conventional MRI, and the relationship between identified acute perfusion changes in the newborn and neurodevelopmental outcomes. In this study, our first major aim was to employ pulsed ASL (PASL) to explore cerebral perfusion changes in HIE neonates with normal and abnormal conventional brain MRI. We hypothesized that HIE results in cerebral perfusion changes, even in the absence of abnormal findings on conventional MRI. Building on this foundation, the second major aim of this study was to develop a machine learning (ML) model using cerebral PASL perfusion to predict neurodevelopmental outcomes.

MATERIALS AND METHODS

Participants and Data Acquisition

Seventy-three full term neonates were identified as a sample of convenience for a retrospective case-control study following an IRB-approved protocol, between January 2008 and July 2018. A waiver of consent/parental permission, assent and HIPAA authorization has been approved by our IRB. All neonates had T1WI, T2WI, DWI images and PASL of the brain. For clarity, T1WI, T2WI, and DWI sequences will be referred as conventional MRI.

The neonates were divided into three groups: control, HIE/MRI⊖, HIE/MRI⊕. The patients in HIE/MRI⊖ group were with clinical HIE and normal conventional MRI, while the patients from HIE/MRI⊕ group were with clinical HIE and abnormal conventional MRI. There was a fourth additional group combining all HIE patients from the HIE/MRI⊖ and HIE/MRI⊕ groups, called HIE/MRI± group.

The PASL images were acquired with perfusion model of PICORE Q2T from a Siemens 3T scanner using the following parameters: bolus time $Tl_1 = 700$ ms, inversion time $T_1 = 1{,}800$ ms, TR/TE = 2,600/14 ms, 14 slices, FOV = 200 × 200 mm, 64 × 64 matrix, voxel size=2.8 × 2.8 × 6.0 mm^3, flip angle = 90^0, 45 label/control image pairs. The reason for not using pseudo continuous arterial spin label (PCASL) is that only PASL is clinically available in our retrospective study.

Control Group Selection

Due to the challenge of finding completely healthy subjects in the context of the inpatient setting and subjects with a clinical indication for neuroimaging, the control cases were selected on the basis of not having any neurological alterations in the recorded neurological examinations (e.g., normal neurological exams, no seizures) during the length of their hospital stay, as well as a conventional brain MRI without neurological abnormalities, and no record of cardiopulmonary arrest, acidemia, or episodes of desaturation requiring intervention with invasive respiratory support. The non-neurological clinical indication for brain MRI was recorded (see Results for all indications).

HIE Cases Selection

HIE cases were preliminarily identified by clinical indication for brain MRI, including suspected or diagnosed HIE as well as indications potentially associated (e.g., meconium

TABLE 1 | The summarization of the outcome data.

		Cognitive composite		Language composite		Motor composite	
		>80	<80	>80	<80	>80	<80
HIE/MRI⊖ group	Patient number: 13	18	2	12	2	17	0
	Outcome records: 20						
HIE/MRI⊕ group	Patient number: 4	6	3	6	3	7	2
	Outcome records: 9						
HIE/MRI± group	Patient number: 17	24	5	23	5	24	2
	Outcome records: 29						

[a]*A proportion of patients had multiple time point outcomes, so outcome records > patient number.*
[b]*If the sum of (>80) and (<80) is smaller than outcome records, that means the data is missing.*

aspiration, cardiopulmonary arrest). Next, all cases were retrospectively reviewed, and only cases categorized as HIE as per the modified Sarnat criteria by the treating physicians were included. At our institution, neonatologists use a modified Sarnat stages scale including: level of consciousness (from stupor/coma to hyperalert/irritable), spontaneous activity, posture, tone, abnormalities of the primitive reflexes (e.g., weak suck or incomplete moro), and autonomic system alterations (e.g., deviated non-reactive pupils, variable heart rate).

The Bayley-III Scores Acquisition

Developmental assessments were performed using the Bayley Scales of Infant and Toddler Development, 3rd Edition (21), which provides cognitive, language, and motor composite scores at a mean age of 23 months, ranging from 12 to 30 months. Seventeen HIE neonates had 29 outcome data because a proportion of patients had multiple time point outcomes. The outcome data was summarized in **Table 1**.

Image Preprocessing

The ASL data processing toolbox (ASLtbx) was adopted for PASL image preprocessing (22). Motion correction by rigid registration was used to align PASL data to the mean PASL image, temporal-spatial smoothing was performed to prevent noise propagation, PASL perfusion difference images were computed by subtracting the time-averaged signal intensities of control and label images, and outlier cleaning was applied after perfusion subtraction to remove outlier PASL acquisition time points (23). The CBF map for PASL data was calculated by applying the single-compartment mode (24).

$$CBF = \frac{6000 \cdot \lambda \cdot (SI_{control} - SI_{label}) \cdot e^{\frac{TI}{T_{1b}}}}{2 \cdot \alpha \cdot TI_1 \cdot M_{0b}} \ [ml/100g/\min] \quad (1)$$

where $SI_{control}$ and SI_{label} were the time-averaged signal intensities of control and label images, respectively. the blood-brain partition coefficient $\lambda = 1.10\ mL/g$ for neonates (25, 26), $T_{1b} = 1,825ms$ for neonates was used for the longitudinal relaxation time of blood at 3.0 T MRI (27), labeling efficiency $\alpha = 0.98$ for PASL (24), the bolus time $TI_1 = 700\ ms$, and inversion time $TI = 1,800\ ms$. The factor of 6,000 converts the units from ml/g/s to the customary ml/100 g/min (28).

M_{0b} is the relaxed equilibrium magnetization of the arterial blood and calculated from the proton density-weighted image M_0 with fully relaxed blood spins as follows:

$$M_{0b} = R_i \cdot M_{0i} \cdot exp(TE/T_{2i} - TE/T_{2b}) \quad (2)$$

where $T_{2b} = 191ms$ for neonates (27). In our study, the M_{0b} was calculated on cerebrospinal fluid (CSF), white matter (WM), and gray matter (GM) separately with $i = CSF,\ WM\ or\ GM$ in Equation (2). Specifically, $R_{CSF} = 0.87$, $R_{WM} = 1.19$, $R_{GM} = 0.98$ (29) were the signal ratios of the tissue type used to blood from a proton density-weighted image, $T_{2CSF} = 250ms$, $T_{2WM} = 222ms$ and $T_{2GM} = 143ms$ (30) were used for neonates. To calculate M_{0CSF}, M_{0WM}, and M_{0GM}, we aligned the T2 image to M_0 space, and segmented the image into the CSF, WM and GM by thresholds 0.95 and 0.75. M_{0i} was the average signal intensity of CSF, WM or GM in M_0.

Statistical Analysis for Group Comparison

In part A of this study (**Figure 1**), a Penn-CHOP neonatal brain atlas (31) was adopted to identify brain regions by statistical comparison among the control, HIE/MRI⊖, HIE/MRI⊕, and HIE/MRI± groups. Four comparisons between groups were performed: (1) control vs. HIE/MRI⊖; (2) HIE/MRI⊕ vs. HIE/MRI⊕; (3) control vs. HIE/MRI⊕; (4) control vs. HIE/MRI±. CBF maps were aligned to the atlas space by the bridge of the subject native T2 space. Linear regression was performed to eliminate the effect of age and gender on the PASL data before statistical group comparison.

The averaged perfusion values in segmented brain structures were compared by permutation test to identify brain regions with statistically significant perfusion changes. The regional CBF map of each subject was normalized to their own averaged whole brain CBF value before group comparison. The normalization makes the CBF values more comparable across different subjects due to a big variation of the absolute CBF values. Therefore, the CBF values being quantified in this study are relative perfusion, not absolute perfusion.

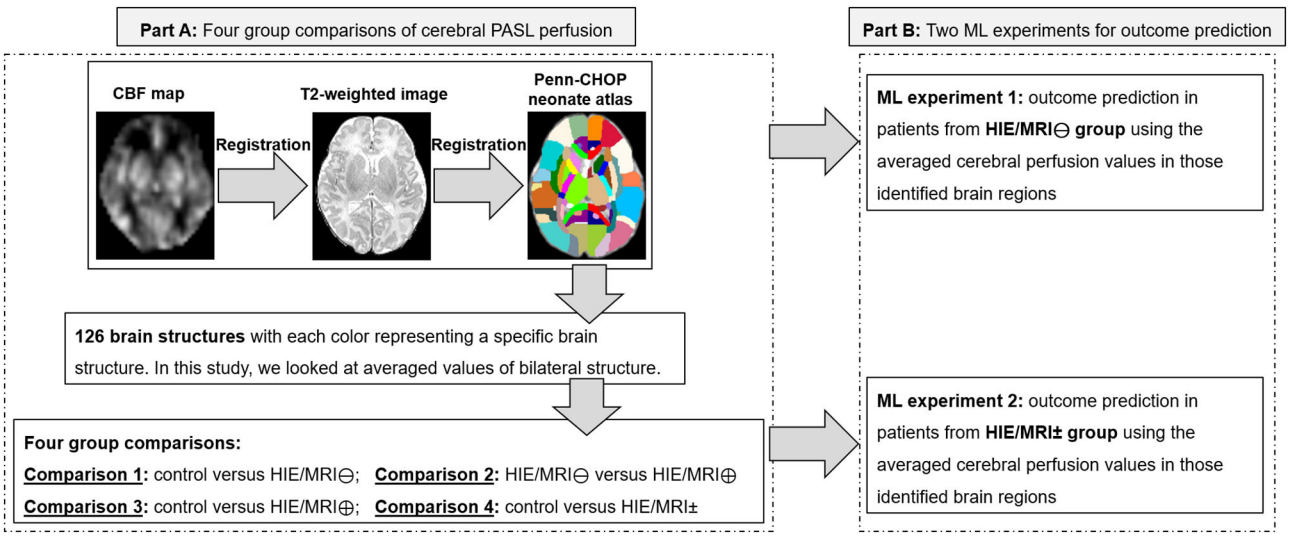

FIGURE 1 | Flow chart of the processing method. Part A: Four group comparisons of cerebral PASL perfusion. Part B: Two ML experiments for outcome prediction. In Part B, the ML experiment was not performed in patients from the HIE/MRI⊕ group separately due to limited patients having long-term outcomes in this group. ML, machine learning.

Machine-Learning-Assisted Outcome Prediction

In part B of this study (**Figure 1**), linear regression was used to predict the cognitive, language, and motor outcomes by leave-one-out cross-validation with feature dimensionality reduction by principal component analysis (PCA), where the optimal feature dimensionality was determined by grid search.

Two ML experiments were performed for predicting outcomes in patients from HIE/MRI⊖ and HIE/MRI± groups (Part B in **Figure 1**), respectively. The ML experiment was not performed in patients from the HIE/MRI⊕ group separately due to limited number of patients having long-term outcomes. The features fed into each ML experiment were slightly different when used for predicting outcomes.

For the experiment 1 (performed in the HIE/MRI⊖ group), the feature was a vector of averaged perfusion values from brain regions with significant perfusion changes obtained by comparison 1 (Part A in **Figure 1**).

For the experiment 2 (performed in the HIE/MRI ± group), the feature was a concatenated vector of averaged perfusion values from brain regions with significant intra- and inter-perfusion differences between the four groups. The intra- and inter perfusion differences were obtained by comparisons 2 and 4, respectively (Part A in **Figure 1**).

RESULTS

Subjects' Groups

Controls

A total of 18 neonates (10 males and eight females, age 16 ± 7.4 days at MRI, full term) were included as controls. The indications for brain MRI in these subjects were the following: facial hemangioma, assessment of congenital diaphragmatic hernia (in two cases), periodic breathing, subjective cyanotic episodes as reported by the caretakers (in four cases), poor feeding (in two cases), osteogenesis imperfecta, cardiac mass, cervical lymphangioma, follow-up of herpes simplex virus infection, follow-up of subdural hygromas, and periauricular scalp arteriovenous malformation.

HIE Cases

In the HIE/MRI⊖ group, there were 40 neonates (25 males and 15 females, age 8.7 ± 6.1 days at MRI, full term) with clinical HIE and normal conventional MRI. Thirty-two neonates underwent hypothermia therapy in this group. Besides, the HIE/MRI⊕ group consisted of nine mild cases, 11 moderate cases, 0 severe case, 20 cases with unknown severity.

In the HIE/MRI⊖ group, there were 15 neonates (six males and nine females, age 6.4 ± 4.5 days at MRI, full term) with clinical HIE and abnormal conventional MRI. Ten neonates underwent hypothermia therapy in this group. Besides, the HIE/MRI⊕ group consisted of one mild cases, five moderate cases, six severe cases, three cases with unknown severity.

The additional HIE/MRI± group is the combination of HIE/MRI⊖ and HIE/MRI⊕ groups.

Cerebral ASL Perfusion Changes in Both HIE/MRI⊖ and HIE/MRI⊕ Groups

Significantly decreased perfusion was found in the HIE/MRI⊖ group, when compared with controls (**Table 2A**). Decreased values were seen primarily in the anterior corona radiata, caudate, superior fronto-occipital fasciculus, superior frontal gyrus, precentral gyrus.

Both significantly increased and decreased PASL perfusion changes were detected in the HIE/MRI⊖ group, when compared with the HIE/MRI⊕ group. Decreased PASL perfusion

TABLE 2 | Brain regions with significant perfusion differences between control and HIE/MRI⊖ groups, and between HIE/MRI⊖ and HIE/MRI⊕ groups.

Brain regions	Normalized CBF (mean ± sd)		*p*-value
A: Control vs. HIE/MRI⊖	**Control**	**HIE/MRI⊖**	**($p < 0.05$)**
A.nterior corona radiate	0.96 ± 0.54	0.74 ± 0.29#	0.015
Caudate	1.31 ± 0.34	1.09 ± 0.41#	0.033
Superior fronto-occipital fasciculus	0.99 ± 0.44	0.86 ± 0.36#	0.046
Superior frontal gyrus	1.13 ± 0.34	1.02 ± 0.21#	0.043
Precentral gyrus	1.43 ± 0.25	1.38 ± 0.18#	0.009
B: HIE/MRI⊖ vs. HIE/MRI⊕	**HIE/MRI⊖**	**HIE/MRI⊕**	**($p < 0.05$)**
Cingulum hippocampal part	2.33 ± 0.60	1.98 ± 0.43#	0.015
Uncinate fasciculus	1.76 ± 0.65	1.41 ± 0.48#	0.032
Gyrus rectus	1.52 ± 0.52	1.15 ± 0.25#	0.034
Precentral gyrus	1.38 ± 0.18	1.58 ± 0.41*	0.028
Postcentral gyrus	1.40 ± 0.21	1.60 ± 0.36*	0.016
Superior parietal gyrus	1.01 ± 0.32	1.24 ± 0.32*	0.014
Precuneus	1.15 ± 0.42	1.44 ± 0.34*	0.016
Parahippocampal gyrus	2.22 ± 0.47	1.86 ± 0.45#	0.009
Superior occipital gyrus	1.02 ± 0.47	1.36 ± 0.58*	0.020
Middle occipital gyrus	1.04 ± 0.32	1.44 ± 0.48*	<0.001
Cuneus	1.43 ± 0.36	1.85 ± 0.54*	0.003
Hippocampus	2.09 ± 0.41	1.77 ± 0.40#	0.008

#*Decreased perfusion; *increased perfusion.*
Normalized CBF values of different brain regions and p-values for all groups.

TABLE 3 | Brain regions with significant perfusion differences between control and HIE/MRI⊖ groups, and between control and HIE/MRI ± groups.

Brain regions	Normalized CBF (mean ± sd)		*p*-value
A: Control vs. HIE/MRI⊕	**Control**	**HIE/MRI⊕**	**($p < 0.05$)**
Corpus callosum (body)	1.42 ± 0.24	1.27 ± 0.24#	0.017
Tapetum	1.08 ± 0.31	0.81 ± 0.33#	0.035
Gyrus rectus	1.52 ± 0.45	1.15 ± 0.25#	0.016
Superior parietal gyrus	1.05 ± 0.27	1.24 ± 0.32*	0.017
Precuneus	1.16 ± 0.36	1.44 ± 0.34*	0.008
Superior occipital gyrus	1.03 ± 0.43	1.36 ± 0.58*	0.020
Middle occipital gyrus	1.12 ± 0.40	1.44 ± 0.48*	0.008
Cuneus	1.42 ± 0.49	1.85 ± 0.54*	0.023
B: Control vs. HIE/MRI±	**Control**	**HIE reading ±**	**($p < 0{\cdot}05$)**
Anterior corona radiate	0.96 ± 0.54	0.73 ± 0.34#	0.020
Caudate	1.31 ± 0.34	1.08 ± 0.44#	0.026
Superior frontal gyrus	1.13 ± 0.34	1.00 ± 0.22#	0.017

#*Decreased perfusion; *increased perfusion.*
Normalized CBF values of different brain regions and p-values for all groups.

values were seen primarily in cingulum hippocampal part, uncinate fasciculus, gyrus rectus, parahippocampal gyrus, and hippocampus, while increased PASL perfusion values were seen primarily in the precentral gyrus, postcentral gyrus, superior parietal gyrus, superior occipital gyrus, middle occipital gyrus, and cuneus.

Further comparisons were performed between control and HIE/MRI⊖ groups (**Table 3A**) and between control and HIE/MRI± (**Table 3B**). Both significantly increased and decreased PASL perfusion changes were also detected in the HIE/MRI⊕ group, but only decreased PASL perfusion changes were detected in the HIE/MRI± group. The brain structures with significant perfusion changes have big overlaps between **Tables 3A**, **2B**, and between **Tables 2A**, **3B**.

There were no significant perfusion differences in the cerebellum, brainstem and deep structures such as the thalamus, putamen, and the globus pallidus among the control, HIE/MRI⊖ group, and HIE/MRI⊕ group.

Cerebral PASL Perfusion Predicts Language and Motor Outcomes in Both HIE/MRI⊖ and HIE/MRI± Groups

Following ML experiment 1 (Part B in **Figure 1**, HIE/MRI⊖ group) and using the feature vector of averaged perfusion values from brain regions with significant perfusion changes obtained by comparison 1 (Part A in **Figure 1**), the ML-assisted model demonstrated significant positive correlation values in predicting language ($r = 0.48$, $p = 0.03$) and motor ($r = 0.57$, $p = 0.01$) outcomes in the HIE/MRI⊖ group ($p < 0.05$), but not significant correlation in predicting cognitive outcome ($p = 0.33$). (First row in **Figure 2**).

Following ML experiment 2 (Part B in **Figure 1**, HIE/MRI± group) and using the concatenated feature vector of averaged perfusion values from brain regions with significant intra- and inter- perfusion differences obtained by comparisons 2 and 4 (Part A in **Figure 1**), the ML-assisted model demonstrated significant positive correlation values in predicting language ($r = 0.76$, $p < 0.001$) and motor ($r = 0.53$, $p = 0.005$) outcomes in the HIE/MRI± group ($p < 0.05$), but not significant correlation in predicting cognitive outcome ($p = 0.35$). (Second row in **Figure 2**).

DISCUSSION

HIE is a significant cause of morbidity and mortality in neonates (1). A considerable proportion of neonatal HIE survivors develop cognitive, language, and motor disorders. Cerebral perfusion has previously demonstrated value in predicting HIE outcomes, and both hypoperfusion (19) and hyperperfusion (20) may correlate with poor neurodevelopmental outcomes in HIE. ASL perfusion may play a role in the prediction of neurodevelopmental outcome in HIE survivors, which could influence therapeutic decision-making and implementation of neuroprotective therapies.

In this study, cerebral ASL perfusion changes were detected in different brain regions in HIE patients, regardless of findings on conventional MRI. Specifically, decreased cerebral ASL perfusions were detected in HIE/MRI⊖ group when compared with controls. The clinical significance of cerebral ASL perfusion changes is further evidenced by the predictive nature of these values to stratify language and motor outcomes in HIE patients, and those identified brain structures have been associated with

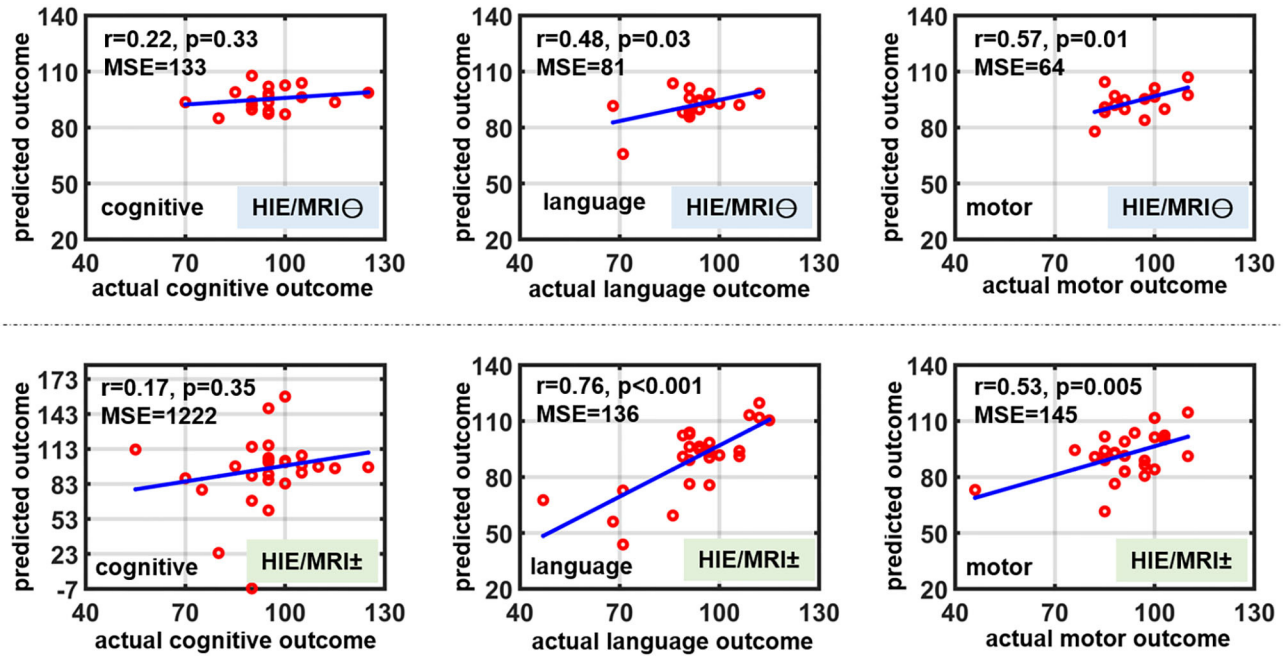

FIGURE 2 | Outcome prediction performance in HIE/MRI⊖ group (first line) and HIE/MRI ± group (second line). In the both groups, the predicted outcomes by machine learning model are significantly correlated with language and motor outcomes, but not with cognitive outcome.

language and motor functions. For instance, the precentral gyrus is the anatomical location of the primary motor cortex (32). Caudate nuclei, constituting the subcortical nuclei of basal ganglia, is responsible for motor control (33) and language (34). Superior frontal gyrus (35) and corona radiata (36) are also related to complex motor functions. These are evidences that ASL perfusion may be more sensitive than conventional MRI, including DWI, in the neuroimaging evaluation of neonatal HIE. Therefore, clinicians and radiologists should not rely solely on conventional MRI sequences in the neuroimaging evaluation of HIE.

There were no significant perfusion differences in the cerebellum, brainstem and deep structures such as the thalamus, putamen, and the globus pallidus among the control, HIE/MRI⊖ group, and HIE/MRI⊕ group. This may serve as an evidence that the intrinsic autoregulatory mechanisms are able to maintain perfusion to these areas of the brain and spare them from injury in mild to moderate hypoxic-ischemic insults (37) which constituted the majority of our retrospective cohort. Experiments performed in animal models have demonstrated that episodes of prolonged fetal hypoxia result in shunting of blood to vital brain structures, such as the brainstem, thalami, basal ganglia, and cerebellum, at the expense of less metabolically active structures, namely, the cerebral cortex and white matter (38). It should be noted, however, that prolonged, severe hypoxic ischemic event leads to permanent injury to the basal ganglia and thalami which is correlated with poor outcomes (39).

Both significantly increased and decreased PASL perfusion changes were detected in the HIE/MRI⊕ group, when compared with the HIE/MRI⊖ group or controls. Cortical structures are demonstrating increased perfusion in HIE/MRI⊕ group than HIE/MRI⊖ patients or controls with the exception of limbic structures including hippocampus, parahippocampal gyrus, cingulum hippocampal part and corpus callosum. The reason for cortical hyperperfusion could be due to ongoing reperfusion response and/or impaired autoregulation. With regard to decreased perfusion in the limbic system, it would be worthwhile to explore whether this represents progression to permanent injury given that these regions have been shown to be vulnerable to hypoxic ischemic insult (40, 41).

In the present study, we also found both hyperperfusion and hypoperfusion in those vital brain structures of cerebellum, brainstem and deep structures in both HIE/MRI⊖ and HIE/MRI⊕ groups. As shown in **Figure 3**, the patients with hypoperfusion in those vital brain structures had Bayley-III scores lower than 80 implying poor long-term outcomes, while the patients with hyperperfusion in those regions had good long-term outcomes with Bayley-III scores >80. This further demonstrated that hypoperfusion in those vital brain structures might progress to irreversible brain injury (42) and lead to poor long-term outcome.

A few limitations existed in the present study. (1) Accessing completely healthy subjects is challenging in the context of an inpatient and sick population, thus, subjects with other non-neurological abnormalities were included as controls. (2) The developmental assessments were carried out on a small data size with Bayley-III score in a relatively wide range of age in composite scores acquisition. (3) The selection of HIE cases was done on the basis of clinical diagnosis in real time by their treating physicians, using a fairly standardized clinical scale in

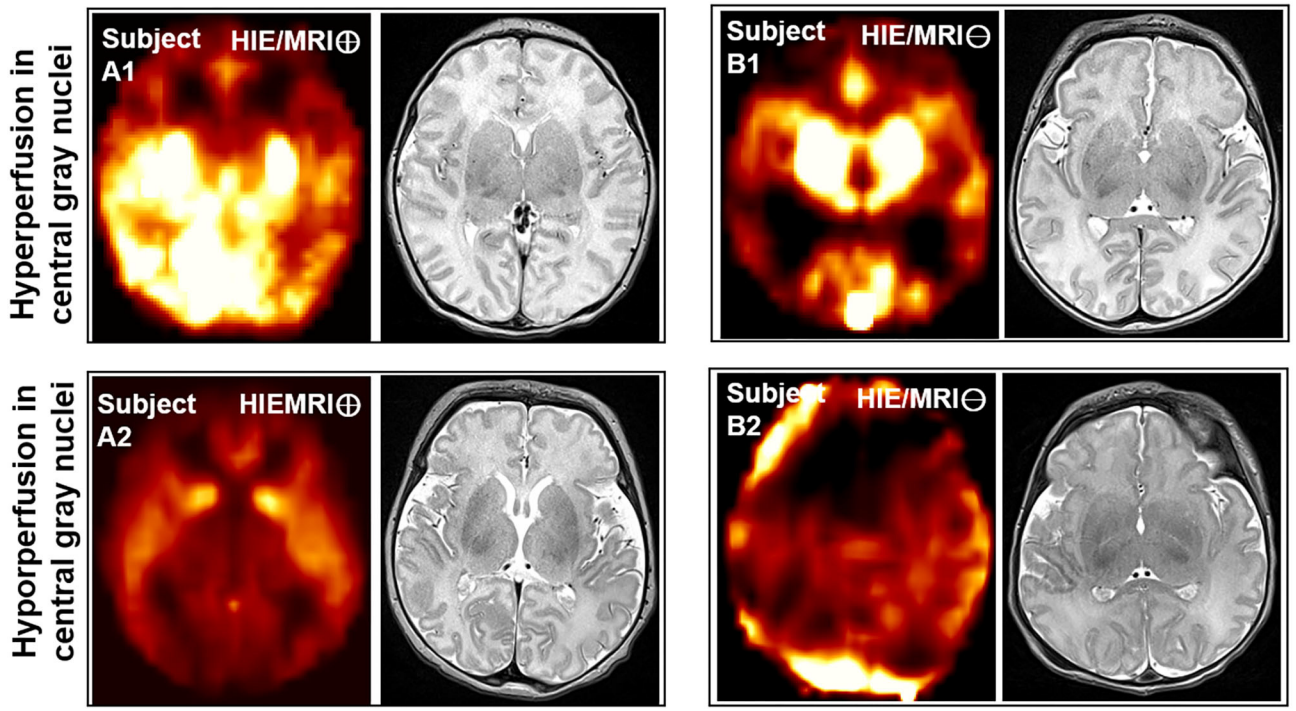

FIGURE 3 | Axial views of CBF map and T2WI image comparison of different HIE patients with good and poor outcome in the 1st and 2nd rows. Subject A1 is from HIE/MRI⊕ group, having hyperperfusion in those vital brain structures and Bayley-III scores of cognitive = 105(>80), language = 112(>80), and motor = 97(>80); Subject A2 is from HIE/MRI⊖ group, having hypoperfusion in those vital brain structures and Bayley-III scores of cognitive = 75(<80), language = 71(<80), and motor = 76(<80); Subject B1 is from HIE/MRI⊕ group, having hyperperfusion in those vital brain structures and Bayley-III scores of cognitive = 105(>80), language = 91(>80), and motor = 97(>80); Subject B2 is from HIE/MRI⊖ group, having hypoperfusion in those vital brain structures and Bayley-III scores of cognitive = 55(<80), language = 47(<80), and motor = 46(<80). The vital brain structures refer to cerebellum, brainstem and deep structures such as the thalamus, putamen, and the globus pallidus.

place at our institution (as described in the Methods section) that nonetheless may be subjective and introduces heterogeneity in the HIE cases. (4) ASL data of neonatal brain is low resolution, which may raise questions of the validity of perfusion values in small anatomic structures. In this regard, we believe that in the future, the robustness can further be improved with additional data.

Additionally, in the interpretation of our results, we acknowledge that the timing and degree of reperfusion is dependent on a wide spectrum of factors including selective vulnerability of brain regions, the severity of injury incurred, the extent of reperfusion response, the susceptibility of different brain regions to reperfusion injury, the timing of injury, the timing of imaging, and the presence or absence of subclinical seizures. For instance, brain MRI performed closer to the termination of therapeutic hypothermia may demonstrate increased perfusion as a sequelae of restorative perfusion. It would be interesting to assess in this regard whether the extent of reperfusion has implications on later outcomes, and whether this is dependent on gender, age, injury type or duration, and/or injury severity. Interpretation of brain perfusion also has inherent challenges, as it is difficult to discern restorative, beneficial reperfusion from reperfusion injury wherein marked metabolism perfusion uncoupling can result in high levels of reactive oxygen species and permanent brain damage. Despite the complexity of brain perfusion, our results show that it is indeed an important imaging marker for outcomes in HIE and that more carefully designed prospective studies are warranted to prospectively evaluate the spatiotemporal dynamics of brain perfusion.

In summary, we demonstrate that cerebral perfusion changes can be detected in HIE patients, including those with normal conventional MRI, highlighting the value of perfusion imaging in evaluating suspected HIE. The perfusion changes may reveal important insights into how individual's autoregulatory and reperfusion response to hypoxic insult influences outcomes. Moreover, these perfusion values significantly correlate with language and motor outcomes in HIE patients with normal and abnormal conventional MRI. Therefore, perfusion imaging is a promising tool for early risk stratification and prediction of language and motor outcomes in HIE survivors and may be a useful adjunct to conventional MRI in the evaluation of HIE in clinical practice.

DATA AVAILABILITY STATEMENT

The raw data supporting the conclusions of this article will be made available by the authors, without undue reservation.

ETHICS STATEMENT

The studies involving human participants were reviewed and approved by Children's Hospital of Philadelphia. Written informed consent to participate in this study was waived.

AUTHOR CONTRIBUTIONS

All authors have made substantial contributions to all of the following: (1) the conception and design of the study, or acquisition of data, or analysis and interpretation of data, (2) drafting the article or revising it critically for important intellectual content, (3) final approval of the version to be submitted.

FUNDING

This work was supported by National Institutes of Health (grant number KL2TR001879 to MH, MH092535, MH092535-S1, and HD086984 to HH) and National Natural Science Foundation of China (grant number 61802330, 61802331 to QZ).

REFERENCES

1. Vannucci RC. Hypoxic ischemic encephalopathy. *Amer J Perinatol.* (2000) 17:113–20. doi: 10.1055/s-2000-9293
2. Laptook AR, Shankaran S, Tyson JE, Munoz B, Bell EF, Goldberg RN, et al. Effect of therapeutic hypothermia initiated after 6 hours of age on death or disability among newborns with hypoxic ischemic encephalopathy: a randomized clinical trial. *JAMA*. (2017) 318:1550−60. doi: 10.1001/jama.2017.14972
3. Hwang M, Sridharan A, Darge K, Riggs B, Sehgal C, Flibotte J, et al. Novel quantitative contrast enhanced ultrasound detection of hypoxic ischemic injury in neonates and infants: pilot study 1. *J Ultrasound Med.* (2018) 38:2025–38. doi: 10.1002/jum.14892
4. Lally PJ, Montaldo P, Oliveira V, Soe A, Swamy R, Bassett P, et al. Magnetic resonance spectroscopy assessment of brain injury after moderate hypothermia in neonatal encephalopathy: a prospective multicenter cohort study. *Lancet Neurol.* (2019) 18:35–45. doi: 10.1016/S1474-4422(18)30325-9
5. Salas J, Tekes A, Hwang M, Northington FJ, Huisman T. AGM Head ultrasound in neonatal hypoxic ischemic injury and its mimickers for clinicians: a review of the patterns of injury and the evolution of findings over time. *Neonatology.* (2018) 114:185–97. doi: 10.1159/000487913
6. Hayes BC, Doherty E, Grehan A, Madigan C, McGarvey C, Mulvany S, et al. Neurodevelopmental outcome in survivors of hypoxic ischemic encephalopathy without cerebral palsy. *Eur J Pediatr.* (2018) 177:19–32. doi: 10.1007/s00431-017-3028-3
7. Kline-Fath BM, Horn PS, Yuan W, Merhar S, Venkatesan C, Thomas CW, et al. Conventional MRI scan and DTI imaging show more severe brain injury in neonates with hypoxic ischemic encephalopathy and seizures. *Early Hum Dev*. (2018) 122:8–14. doi: 10.1016/j.earlhumdev.2018.05.008
8. Maurya VK, Ravikumar R, Bhatia M, Rai R. Hypoxic ischemic brain injury in an adult: magnetic resonance imaging findings. *Med J Armed Forces India.* (2016) 72:75–7. doi: 10.1016/j.mjafi.2015.06.016
9. Salas J, Reddy N, Orru E, Carson KA, Chavez-Valdez R, Burton VJ, et al. The role of diffusion tensor imaging in detecting hippocampal injury following neonatal hypoxic ischemic encephalopathy. *J Neuroimaging.* (2018) 29:252–9. doi: 10.1111/jon.12572
10. Ouyang M, Dubois J, Yu Q, Mukherjee P, Huang H. Delineation of early brain development from fetuses to infants with diffusion MRI and beyond. *Neuroimage*. (2019) 185:836–50. doi: 10.1016/j.neuroimage.2018.04.017
11. Ho ML. Arterial spin labeling: clinical applications. *J Neuroradiol.* (2018) 45:276–89. doi: 10.1016/j.neurad.2018.06.003
12. Hwang M. Introduction to contrast enhanced ultrasound of the brain in neonates and infants: current understanding and future potential. *Pediatr Radiol.* (2019) 49:254–62. doi: 10.1007/s00247-018-4270-1
13. Proisy M, Mitra S, Uria-Avellana C, Sokolska M, Robertson NJ, Jeune FL, et al. Brain perfusion imaging in neonates: an overview. *AJNR Am J Neuroradiol.* (2016) 37:1766–73. doi: 10.3174/ajnr.A4778
14. Wintermark P. Injury and repair in perinatal brain injury: insights from non-invasive MR perfusion imaging. *Semin Perinatol.* (2015) 39:124–9. doi: 10.1053/j.semperi.2015.01.005
15. Ambalavanan N, Carlo WA, Shankaran S, Bann CM, Emich SL, Higgins RD, et al. Predicting outcomes of neonates diagnosed with hypoximic ischemic encephalopathy. *Pediatrics.* (2006) 118:2084–93. doi: 10.1542/peds.2006-1591
16. Perlman M, Shah PS. Hypoxic ischemic encephalopathy: challenges in outcome and prediction. *J Pediatr.* (2011) 158(2 Suppl.):e51–4. doi: 10.1016/j.jpeds.2010.11.014
17. Rollins N, Booth T, Morriss MC, Sanchez P, Heyne R, Chalak L. Predictive value of neonatal MRI showing no or minor degrees of brain injury after hypothermia. *Pediatr Neurol.* (2014) 50:447–51. doi: 10.1016/j.pediatrneurol.2014.01.013
18. Barnett E, Mercuri E, Rutherford M, Haataja L, Frisone MF, Henderson S, et al. Neurological and perceptual motor outcome at 5-6 years of age in children with neonatal encephalopathy: relationship with neonatal brain MRI. *Neuropediatrics.* (2002) 33:242–8. doi: 10.1055/s-2002-36737
19. Tortora D, Mattei PA, Navarra R, Panara V, Salomone R, Rossi A, et al. Prematurity and brain perfusion: arterial spin labeling MRI. *NeuroImage:Clinical.* (2017) 15:401–7. doi: 10.1016/j.nicl.2017.05.023
20. Vis JBd, Hendrikse J, Petersen ET, Vries LSd, Bel Fv, Alderliesten T, et al. Arterial spin labling perfusion MRI and outcome in neonates with hypoxic ischemic encephalopathy. *Eur Radiol.* (2015) 25:113–21. doi: 10.1007/s00330-014-3352-1
21. Bayley N. *Bayley Scales of Infant and Toddler Development*. 3rd ed. San Antonio, T:X Harcourt Assessment, Inc. (2006).
22. Wang Z, Aguirre GK, Rao H, Wang J, Fernandez-Seara MA, Childress AR, et al. Empirical optimization of ASL data analysis using an ASL data processing toolbox: ASLtbx. *Magn Reson Imaging.* (2008) 26:261–9. doi: 10.1016/j.mri.2007.07.003
23. Wang Z, Das SR, XIe SX, Arnold SE, Detre JA, Wolk DA. Arterial spin labeled MRI in prodromal Alzheimer's Disease: a multi-site study. *Neuroimage Clin.* (2013) 30:630–6. doi: 10.1016/j.nicl.2013.04.014
24. Alsop DC, Detre JA, Golay X, Gunther M, Hendrikse J, Hernandez-Garcia L, et al. Recommended implementation of arterial spin labeled perfusion MRI for clinical applications: a consensus of the ISMRM perfusion study group and the European consortium for ASL in dementia. *Magn Reson Med.* (2015) 73:102–16. doi: 10.1002/mrm.25197
25. Herscovitch P, Raichle ME. What is the correct value for the brain blood partition coefficient for water. *J Cereb Blood Flow Metab.* (1985) 5:65–9. doi: 10.1038/jcbfm.1985.9
26. Ouyang M, Liu P, Jeon T, Chalak L, Heyne R, Rollins NK, et al. Heterogeneous increases of regional cerebral blood flow during preterm brain development: preliminary assessment with pseudo-continuous arterial spin labeled perfusion MRI. *Neuroimage.* (2017) 147:233–42. doi: 10.1016/j.neuroimage.2016.12.034
27. Liu P, Chalak LF, Krishnamurthy LC, Mir I, Peng SL, Huang H, et al. T1 and T2 values of human neonatal blood at 3 Tesla: Dependence on hematocrit, oxygenation, and temperature. *Magn Reson Med.* (2016) 75:1730–5. doi: 10.1002/mrm.25775
28. Buxton RB. Quantifying CBF with arterial spin labeling. *J Magn Reson Imaging.* (2005) 22:723–6. doi: 10.1002/jmri.20462
29. Cavusoglu M, Pfeuffer J, Ugurbil K, Uludag K. Comparison of pulsed arterial spin labeling encoding schemes and absolute perfusion

quantification. *ScienceDirect*. (2009) 27:1039–45. doi: 10.1016/j.mri.2009.04.002
30. Counsell SJ, Kennea NL, Herlihy AH, Allsop JM, Harrison MC, Cowan FM, et al. T2 relaxation values in the developing preterm brain. *AJNR Am J Neuroradiol.* (2003) 24:1654–60.
31. Feng L, Li H, Oishi K, Mishra V, Song L, Peng, Q, et al. Age-specific gray and white matter DTI atlas for human brain at 33, 36 and 39 postmenstrual weeks. *Neuroimage*. (2019) 185:685–98. doi: 10.1016/j.neuroimage.2018.06.069
32. Banker L, Tadi P. *Neuroanatomy, Precentral Gyrus*. Treasure Island, FL: StatPearls (2019).
33. Lanciego JL, Luquin N, Obeso JA. Functional neuroanatomy of the basal gangli. *Cold Spring Harb Perspect Med.* (2012) 2:a009621. doi: 10.1101/cshperspect.a009621
34. Gronholm EO, Roll MC, Horne MA, Sundgren PC, Lindgren AG. Predominance of caudate nucleus lesions in acute ischaemic stroke patients with impairment in language and speech. *Eur J Neurol.* (2016) 23:148–53. doi: 10.1111/ene.12822
35. Martino J, Gabarros A, Deus J, Juncadella M, Acebes JJ, Torres A, et al. Intrasurgical mapping of complex motor function in the superior frontal gyrus. *Neuroscience.* (2011) 179:131–42. doi: 10.1016/j.neuroscience.2011.01.047
36. Misra UK, Kalita J. Central motor conduction studies in internal capsule and corona radiata infarction. *J neurol.* (1997) 244:579–85. doi: 10.1007/s004150050147
37. Huang BY, Castillo M. Hypoxic-ischemic brain injury: imaging findings from birth to adulthood. *Radiographics.* (2008) 28:417–39. doi: 10.1148/rg.282075066
38. Ashwal S, Majcher JS, Longo LD. Patterns of fetal lamb regional cerebral blood flow during and after prolonged hypoxia: studies during the posthypoxic recovery period. *Am J Obstet Gynecol.* (1981) 139:365–72. doi: 10.1016/0002-9378(81)90311-2
39. Vries LSd, Groenendaal F. Patterns of neonatal hypoxic-ischaemic brain injury. *Neuroradiology.* (2010) 52:555–66. doi: 10.1007/s00234-010-0674-9
40. Byeon JH, Kim GH, Kim JY, Sun W, Eun BL. Cognitive dysfunction and hippocampal damage induced by hypoxic-ischemic brain injury and prolonged febrile convulsions in immature rats. *J Korean Neurosurg Soc.* (2015) 58:22–9. doi: 10.3340/jkns.2015.58.1.22
41. Bubb EJ, Metzler-Baddeley C, Aggleton JP. The cingulum bundle: anatomy, function, and dysfunction. *Neurosci Biobehav Rev.* (2018) 92:104–27. doi: 10.1016/j.neubiorev.2018.05.008
42. Massaro AN, Bouyssi-Kobar M, Chang T, Vezina LG, Plessis AJd, Limperopoulos C. Brain perfusion in encephalopathic newborns after therapeutic hypothermia. *AJNR Am J Neuroradiol.* (2013) 34:1649–55. doi: 10.3174/ajnr.A3422

Conflict of Interest: The authors declare that the research was conducted in the absence of any commercial or financial relationships that could be construed as a potential conflict of interest.

frontiers in Neurology

ORIGINAL RESEARCH
published: 11 December 2020
doi: 10.3389/fneur.2020.586518

Multi-Slice Radiomic Analysis of Apparent Diffusion Coefficient Metrics Improves Evaluation of Brain Alterations in Neonates With Congenital Heart Diseases

Meijiao Zhu[1], Dadi Zhao[2], Ying Wang[1], Qinghua Zhou[3], Shujie Wang[1], Xuming Mo[4], Ming Yang[1]* and Yu Sun[5]*

[1] Department of Radiology, Children's Hospital of Nanjing Medical University, Nanjing, China, [2] Institute of Cancer and Genomic Sciences, University of Birmingham, Birmingham, United Kingdom, [3] Department of Informatics, University of Leicester, Leicester, United Kingdom, [4] Department of Cardio-Thoracic Surgery, Children's Hospital of Nanjing Medical University, Nanjing, China, [5] School of Biological Science and Medical Engineering, Southeast University, Nanjing, China

OPEN ACCESS

Edited by:
Francisco J. Alvarez, Hospital de Cruces, Spain

Reviewed by:
Maurizio Elia, Oasi Research Institute (IRCCS), Italy
Zhen Li, Huazhong University of Science and Technology, China

***Correspondence:**
Xuming Mo
mohsuming15@sina.com
Ming Yang
yangming19710217@163.com

Specialty section:
This article was submitted to Pediatric Neurology, a section of the journal Frontiers in Neurology

Received: *23 July 2020*
Accepted: *19 November 2020*
Published: *11 December 2020*

Citation:
Zhu M, Zhao D, Wang Y, Zhou Q, Wang S, Mo X, Yang M and Sun Y (2020) Multi-Slice Radiomic Analysis of Apparent Diffusion Coefficient Metrics Improves Evaluation of Brain Alterations in Neonates With Congenital Heart Diseases. Front. Neurol. 11:586518. doi: 10.3389/fneur.2020.586518

Apparent diffusion coefficients (ADC) can provide phenotypic information of brain lesions, which can aid the diagnosis of brain alterations in neonates with congenital heart diseases (CHDs). However, the corresponding clinical significance of quantitative descriptors of brain tissue remains to be elucidated. By using ADC metrics and texture features, this study aimed to investigate the diagnostic value of single-slice and multi-slice measurements for assessing brain alterations in neonates with CHDs. ADC images were acquired from 60 neonates with echocardiographically confirmed non-cyanotic CHDs and 22 healthy controls (HCs) treated at Children's Hospital of Nanjing Medical University from 2012 to 2016. ADC metrics and texture features for both single and multiple slices of the whole brain were extracted and analyzed to the gestational age. The diagnostic performance of ADC metrics for CHDs was evaluated by using analysis of covariance and receiver operating characteristic. For both the CHD and HC groups, ADC metrics were inversely correlated with the gestational age in single and multi-slice measurements ($P < 0.05$). Histogram metrics were significant for identifying CHDs ($P < 0.05$), while textural features were insignificant. Multi-slice ADC ($P < 0.01$) exhibited greater diagnostic performance for CHDs than single-slice ADC ($P < 0.05$). These findings indicate that radiomic analysis based on ADC metrics can objectively provide more quantitative information regarding brain development in neonates with CHDs. ADC metrics for the whole brain may be more clinically significant in identifying atypical brain development in these patients. Of note, these results suggest that multi-slice ADC can achieve better diagnostic performance for CHD than single-slice.

Keywords: radiomics, neonate, diffusion weighted imaging, congenital heart disease, neurodevelopment

1. INTRODUCTION

Congenital heart disease (CHD) leads to childhood morbidity, affecting six to eight births per million. Among the various types of CHD, non-cyanotic CHDs are relatively common (1). Although recent advancements in cardiac surgery have dramatically increased the survival rates among patients with CHD, the neurodevelopmental and cognitive features of such patients remain controversial (2–4). Clinical studies demonstrated altered pre-surgery brain development in more than half of neonates with CHD—a known a risk factor for neurodevelopmental impairment (5, 6). Long-term studies suggested that these deficits can persist until adolescence and young adulthood, potentially impacting the individual's ability to function in society. Early identification of altered brain development may aid in elucidating the potential mechanisms underlying brain dysmaturation in neonates with CHD, which may in turn allow for timely and appropriate protective treatments (7).

Functional imaging was used to study brain maturity and injury in neonates with CHD (8, 9). For example, magnetic resonance spectroscopy studies showed that neonates with cyanotic CHD exhibit characteristic decreased ratio of *N*-acteyl-aspartate to choline in the thalamus, basal ganglia, and corticospinal tracts (1). Unfortunately, children are often unable to tolerate the lengthy scan durations required for functional imaging, thus its clinical application in pediatric populations becomes less practical.

Conversely, diffusion weighted imaging (DWI) is routinely performed for the non-invasive assessment of tissue cellularity and cellular membrane integrity in clinical settings. DWI detects the random thermal motion of water molecules in living tissue (10–12). Diffusion coefficients of water are expressed as apparent diffusion coefficients (ADC), which reflect water diffusion and the development of membranes in neuronal and glial cells. However, further phenotypic information of lesions remains difficult to obtain through classic methods. Radiomics utilizes the full potential of the ADC to improve clinical diagnosis and prognosis through analysing quantitative factors in brain tissue (13–15). Histogram analysis can be used to quantify the distribution of signal intensity in voxels based on routinely acquired clinical ADC. Lesion heterogeneity is reflected by texture features that describe the statistical interrelationships between adjacent voxels. Recent clinical studies have highlighted the potential of radiomics in aiding the clinical diagnosis of pathologic subtypes of cervical cancer (16) and predicting the molecular characteristics of glioblastoma (17).

To our knowledge, very few studies have investigated radiomic ADC in brain development of neonates with CHDs. Classic methods normally select regions of interest (ROIs) from only representative slices, which may have resulted in underestimation of lesion heterogeneity (18). Alternatively, ROIs can be selected by covering the entire volume of the lesion, allowing for a complete assessment of tissue characteristics and heterogeneity in quantitative analysis (19). This study aimed to investigate the value of single-slice and multi-slice measurements by using ADC metrics and texture features for assessing brain alterations in neonates with CHD.

2. PATIENTS AND METHODS

2.1. Participants

This study retrospectively reviewed the preoperative ADC images of neonates with echocardiographically confirmed non-cyanotic CHDs treated at Children's Hospital of Nanjing Medical University from January 2012 to December 2016 (20). Neonates with mild neonatal pneumonia or scalp hematoma exhibiting normal intracranial MRI findings were enrolled as healthy controls (HCs). Seventy patients were excluded due to non-related neurological abnormalities or prematurity. All participants were followed up for 6 months, and those exhibiting typical development of the nervous system were enrolled as HCs. The present study was approved by the ethics committee of our institution (ethic number: 201603005-1).

2.2. Image Acquisition

MR images were acquired by using a Siemens Avanto 1.5T scanner (Siemens Healthcare, Erlangen, Germany) and a standard high-definition eight-channel surface head coil. Prior to scanning, participants received 5% chloral hydrate at a dose of 1 mL/kg via oral administration. MRI scans were obtained during sleep, with the patient in the supine position. Axial images were acquired orthogonally to the anterior-posterior commissure line in a standard fashion. Imaging protocols were as follows: multi-planar T_1-weighted spin-echo (SE) imaging (axial, repetition time (TR) 4,490 ms, echo time (TE) 7.5 ms; sagittal, TR 4,400 ms, TE 9 ms), axial T_2-weighted fast spin-echo (FSE) imaging (TR 5,570 ms, TE 117 ms), and axial fluid-attenuated inversion recovery (FLAIR) imaging (TR 6,000 ms, TE 92 ms). Axial DWIs were acquired in the Z, Y, and X directions (TR 3,200 ms, TE 99 ms) with b values of 0 and 1,000 s/mm^2. ADC images were automatically processed using a standard mono-exponential fit.

2.3. Feature Extraction

Single axial brain slices were selected at the level of periventricular white matter injury or periventricular leukomalacia, considering (punctate) white matter injury, periventricular leukomalacia, and stroke are the most commonly observed lesions on MRI (18, 21). All CHD patients were assessed through MR images by experienced neurologists to confirm having no obvious brain damages. Since the ROIs containing the entire tumor in each slice of the ADC image could provide overall information related to the tumor (22),

TABLE 1 | Demographic variables.

	Neonates with congenital Heart disease	Health Controls	*P*
Gender (female:male)	22:38	8:4	0.98
Age (days)	10.5 ± 2.9	8.6 ± 4.2	0.07
Gestational age (weeks)	40.6 ± 1.4	40.0 ± 1.3	0.11

ROIs were drawn on single-slice and multi-slice images by experienced neuro-radiologists for comparison after excluding cerebrospinal fluid outside the brain. ADC metrics and texture features were extracted for only regions of interest, which include average ADC, minimum ADC, maximum ADC, peak location of ADC (mode), ADC skewness (asymmetry), ADC kurtosis (flatness), ADC entropy (randomness), ADC variance, the 5th–95th percentiles ADC, contrast, dissimilarity, homogeneity, angular second moment (ASM), and energy (23–25). Computational feature extraction was performed by using Python (version 2.7, Python Software Foundation, Delaware, United States).

2.4. Statistical Analysis

The Kruskal-Wallis test was performed to compare the gender. The non-parametric unpaired *t*-test was performed to compare the ages and gestational ages. The Pearson correlation analysis was performed to evaluate the correlations between ADC metrics and gestational age. The independent-samples *t*-test was performed to compare group-specific ADC metrics and texture features. Receiver operating characteristic (ROC) analysis based on the empirical method was performed to evaluate the diagnostic performance of ADC metrics for CHDs (26), where both the area under the curve (AUC) and the Youden index value (YIV) were analyzed. All statistical analyses

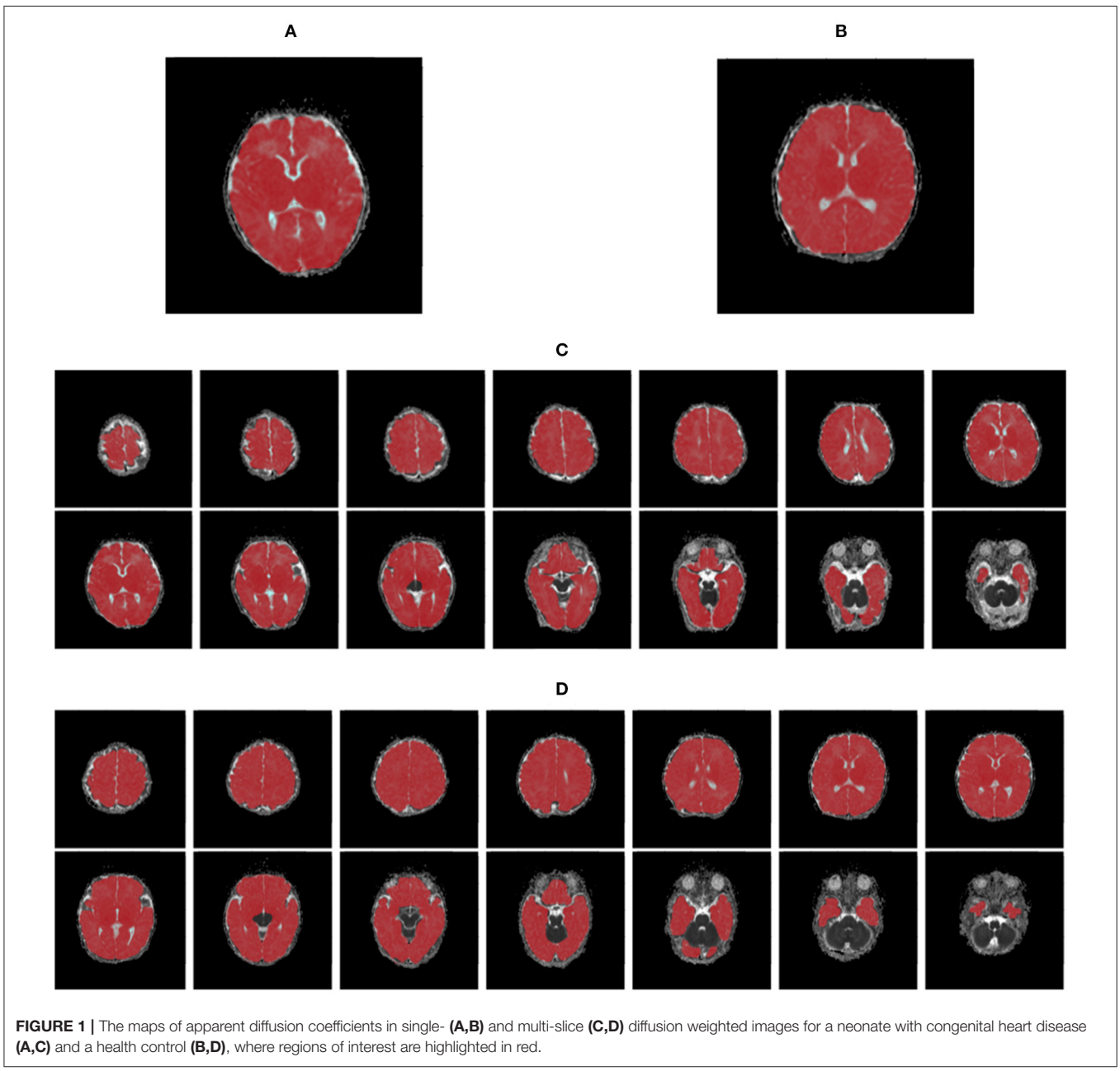

FIGURE 1 | The maps of apparent diffusion coefficients in single- **(A,B)** and multi-slice **(C,D)** diffusion weighted images for a neonate with congenital heart disease **(A,C)** and a health control **(B,D)**, where regions of interest are highlighted in red.

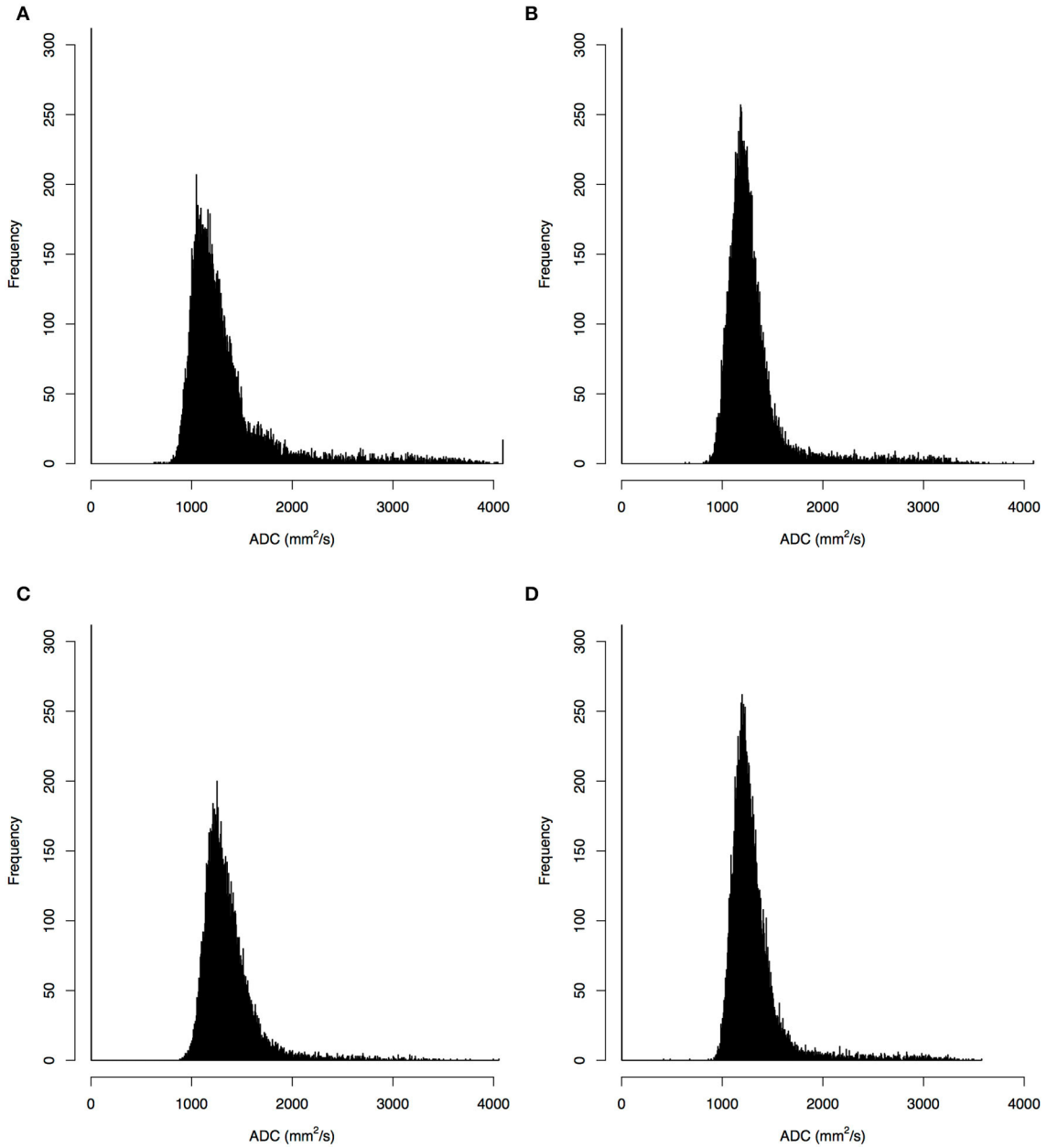

FIGURE 2 | Histograms of apparent diffusion coefficients (ADC) in the single- **(A,B)** and multi-slice **(C,D)** diffusion weighted images for a neonate with congenital heart diseases **(A,C)** and a health control **(B,D)**, where the histograms for multi-slice imaging were given by a selected slice.

were performed by using R (version 3.6.2, R Foundation, Vienna, Austria).

3. RESULTS

3.1. Demographic Characteristics

Sixty patients with CHDs [38 boys and 22 girls; age mean 10.5 days, standard deviation (SD) 2.91 days] and 22 HCs (14 boys and eight girls; age mean 8.6 days, SD 4.31 days) were enrolled in the cohort (**Table 1**). The malignant cohort included those with atrial septal defects ($N = 38$), patent ductus arteriosus ($N = 1$), both atrial and ventricular septal defects ($N = 2$), ventricular septal defect and patent ductus arteriosus ($N = 1$), atrial septal defects and patent ductus arteriosus ($N = 18$). The distribution of baseline epidemiological characteristics (gender $P = 0.98$, age $P = 0.07$, gestational age $P = 0.11$) was balanced between the CHD and HC groups. Representative ADC images and normalized histogram patterns for each group are presented in **Figures 1**, **2**. Visual assessment revealed differences in the skewness and kurtosis of the histograms for the CHD and NC

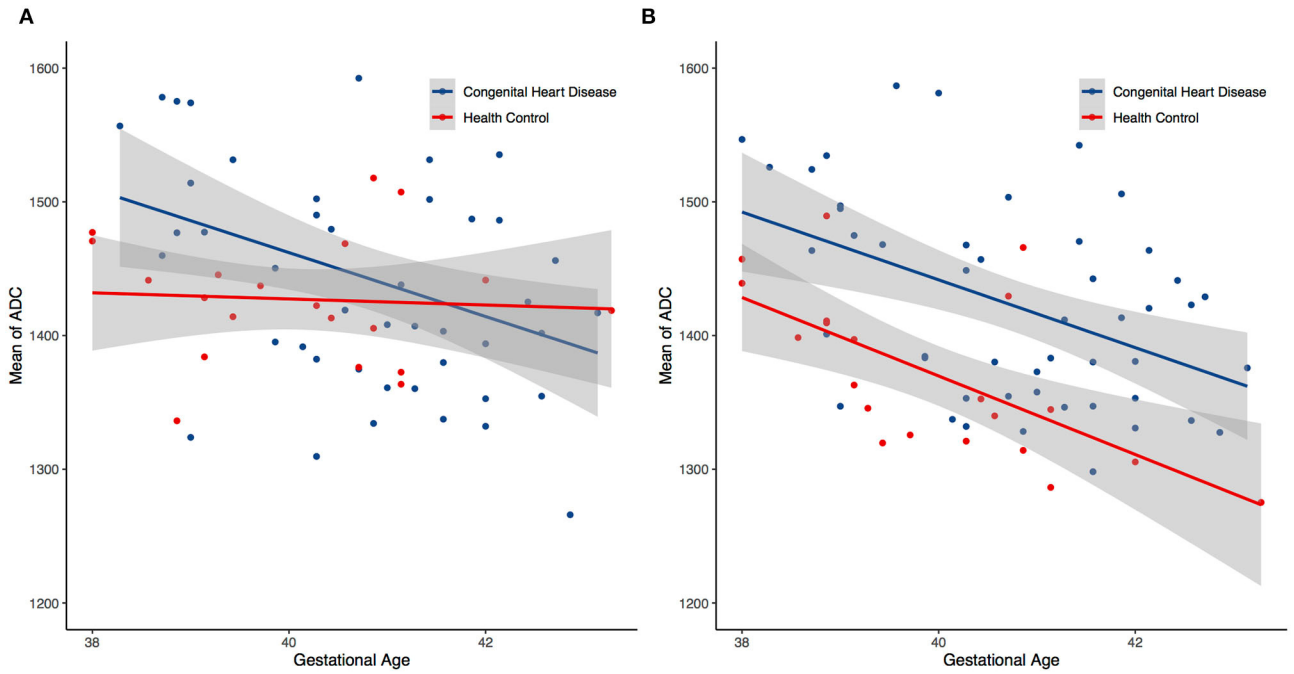

FIGURE 3 | Scatter plots showing negative trend between the gestational age and the mean apparent diffusion coefficients (ADC) for both single- **(A)** and multi-slice **(B)** diffusion weighted imaging.

groups. Skewness was greater in the HC group than in the CHD group, reflected by greater deviation from a normal distribution, while bias was greater among the cohort cases. Kurtosis, which reflects the sharpness of a frequency-distributed curve, more closely approximated a normal distribution in the CHD group than in the HC group.

3.2. Correlation Between Features and Gestational Age

All ADC of the CHD and HC groups were significantly and inversely correlated with gestational age ($r < 0$, $P < 0.05$) in both single- and multi-slice analyses (**Figure 3**). In the CHD group, all single- and multi-slice measurements exhibited a significant inverse correlation with gestational age ($r < 0$, $P < 0.05$), except for minimum ADC ($r > 0$, $P > 0.05$). However, in the HC group, no measurements exhibited a significant inverse correlation with gestational age ($r < 0$, $P > 0.05$), except for average ADC ($r < 0$, $P < 0.05$).

3.3. Comparison of Single and Multi-Slice Measurements

ADC metrics were higher in the CHD group than in the HC group. The significance of ADC metrics is shown in **Figure 4A**, which shows that certain ADC measurements allowed for significant discrimination of the CHD and HC groups. **Figure 4B** illustrates that a few ADC metrics show no significant differences between the two groups. Such measurements included the 70th–95th percentile ADC for the single-slice analyses as well as the 10th–95th percentile ADC for the multi-slice analyses. For both single- and multi-slice ADC analyses, kurtosis, variance, and skewness allowed for significant discrimination between the CHD and HC groups. Additional factors including ADC entropy and average ADC allowed for discrimination in the multi-slice analysis ($P < 0.05$, **Figure 4D**). Skewness and kurtosis were lower in the CHD group than in the HC group, in accordance with the results of the visual assessment. Multi-slice DWI revealed higher entropy and a more randomly distributed histogram in the HC group than in the CHD group, suggestive of greater ADC variability.

3.4. Comparison of ADC Metrics and Texture Features

Unlike the ADC metrics, most texture features showed no significance between the CHD and HC groups in either the single- or multi-slice analyses ($P > 0.05$), including contrast, dissimilarity, homogeneity, ASM, and energy. However, some texture features allowed for significant discrimination of the CHD and HC groups in single-slice measurements ($P < 0.05$, **Figure 4C**).

3.5. Diagnostic Performance

Among all ADC metrics and texture features, the 90th (single-slice: AUC = 0.70, YIV = 0.33, **Figure 5A**; multi-slice, AUC = 0.76, YIV = 0.39, **Figure 5B**) and 95th percentile ADC (single-slice: AUC = 0.67, YIV = 0.29, **Figure 5C**; multi-slice: AUC = 0.75, YIV = 0.40, **Figure 5D**) values allowed for the greatest discrimination between the CHD and HC

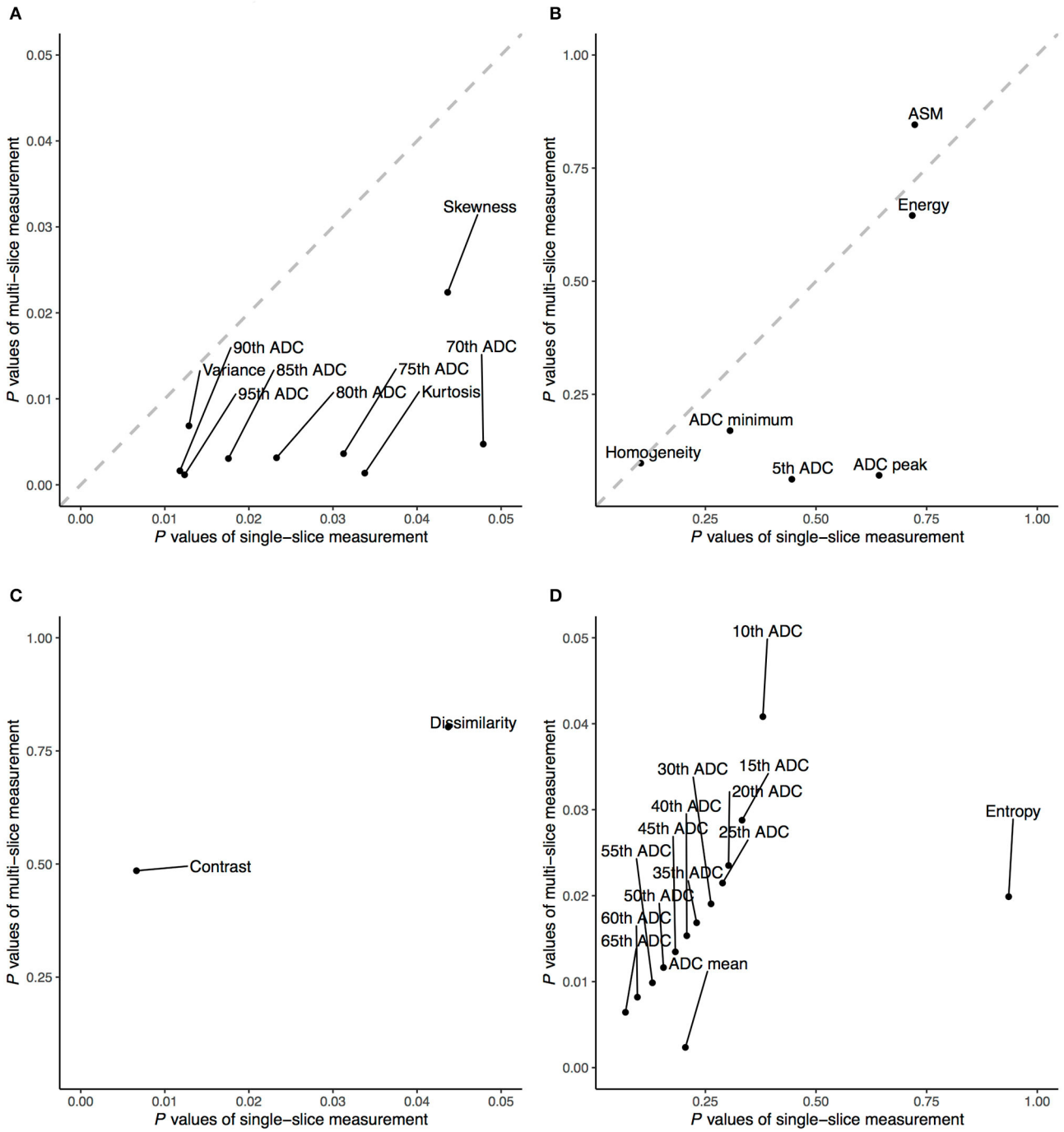

FIGURE 4 | Comparison of the significance level of apparent diffusion coefficients (ADC) and texture features between single- and multi-slice diffusion weighted imaging in evaluating neonates with congenital heart diseases compared to health controls, given as significant **(A)** and insignificant **(B)** in both single- and multi-slice measurements as well as significant for only single- **(C)** or multi-slice **(D)** measurements.

groups (**Figure 6**). ROC analysis of ADC metrics suggested that multi-slice measurements exhibited generally greater diagnostic capabilities than single-slice measurements, except for ADC entropy, skewness, and kurtosis as well as the 60th and 65th percentile ADC. ROC analysis also suggested that texture features were less significant for discrimination than most ADC metrics (**Figure 6**). ASM and homogeneity measurements were more significant for discrimination in multi-slice analyses than in single-slice analyses, while contrast and dissimilarity were less significant.

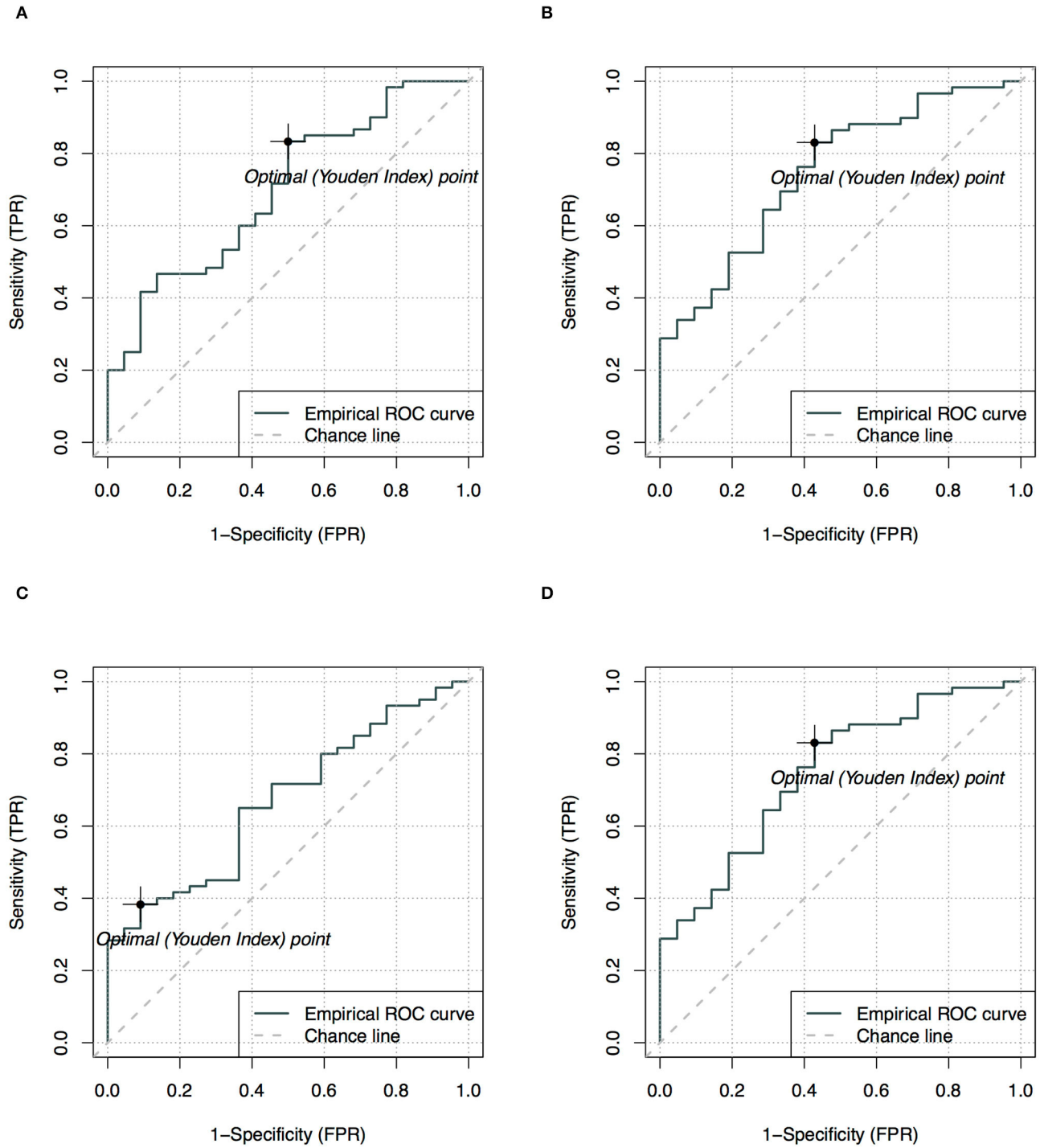

FIGURE 5 | Receiver operating characteristics analysis with optimal points for the 90th **(A,B)** and 95th **(C,D)** apparent diffusion coefficients (ADC), comparing single-slice measurement **(A,C)** and multi-slice measurement **(B,D)** in evaluating neonates with congenital heart diseases compared to health controls.

4. DISCUSSION

Changes in diffusion in the white matter of the perinatal brain (which may be related to myelination) could be a function of gestational age (27). This study showed similar univariate associations between several ADC metrics and the gestational age. Scatter plots of both measurements (**Figure 3**) revealed a linear decline in regional ADC metrics as a function of

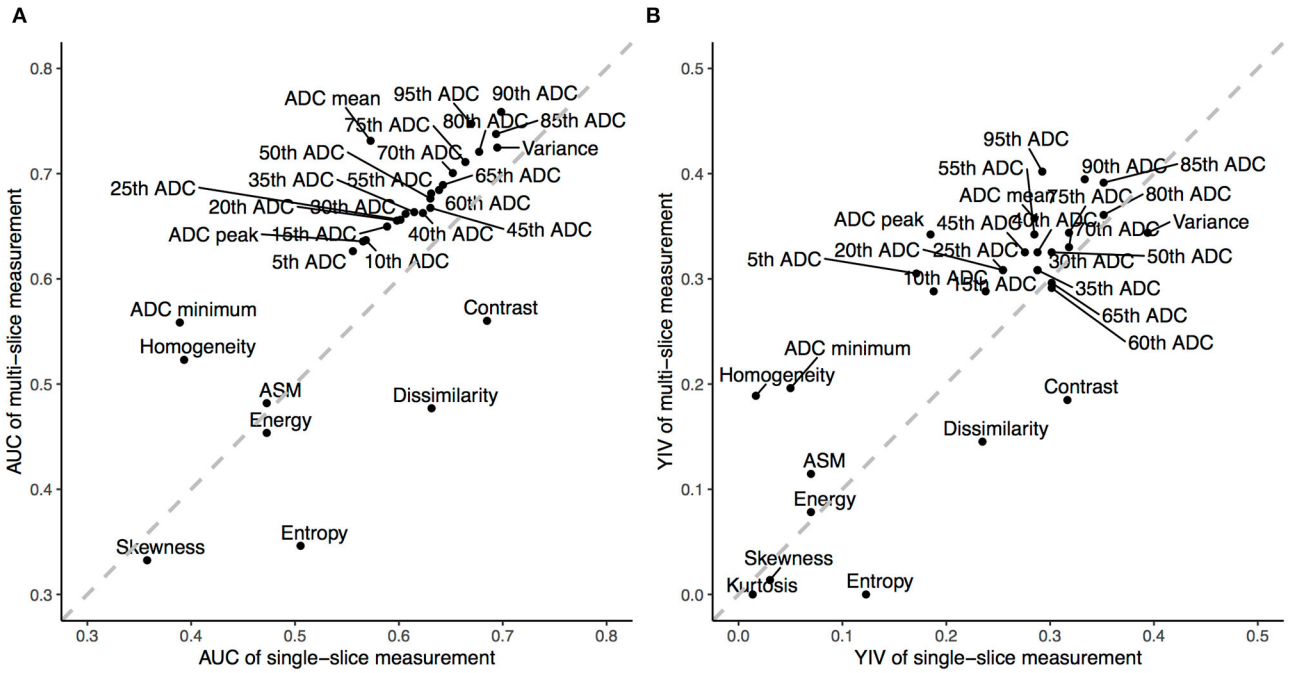

FIGURE 6 | The Area Under the Curve (AUC) and Youden Index Values (YIV) of the apparent diffusion coefficients (ADC) and texture features estimated through receiver operating characteristics for single- **(A)** and multi-slice **(B)** diffusion weighted imaging in evaluating neonates with congenital heart diseases compared to health controls.

the gestational age in both the CHD and HC groups. This corresponds to the negative correlation between brain diffusion measurements and gestational age reported before (28). These results indicate that radiomics can be used to quantitatively assess the extent of cerebral myelination in neonates.

In this study, ADC parameters were higher in the CSD group than in the HC group, suggestive of a regional increase in water diffusion and higher local free water content in the CSD group (29). Such differences may be caused by chronic hypoxic ischemic injury due to impaired circulation of oxygenated blood in the fetal and neonatal brain in the CHD group. Mild hypoxia-ischemia is reported to result in selective death and arrested maturation of oligodendrocyte progenitors, possibly leading to delays in brain myelination (21). In addition, delayed brain myelination in children with CHDs may lead to immature development of neurons and glial cells (30, 31). Taken together, these findings suggest that impaired myelination of axons in neonates with CHD can result in increased ADC parameters.

The analysis of ADC metrics demonstrated the heterogeneity of the CHD and HC groups. Indeed, ADC metrics revealed significant differences between the CHD and HC groups for single- and multi-slice analyses. Furthermore, values at the higher end of the cumulative ADC metrics significantly differed between the two groups, and the ADC histograms exhibited divergence toward the higher end, suggesting that the difference between the two groups is mostly observed at higher ADC. Ninetieth percentile ADC represented the most stable parameter for discriminating the CHD and HC groups, in accordance with the findings of a previous study that aimed to discriminate between radiological indeterminate vestibular schwannoma and meningioma in the cerebellopontine angle (32). Such phenomenons were suggested to be potentially caused by the greater frequency of necrotic or cystic components in high-grade or malignant tumors (18, 33). Similarly, the results in this study may be associated with increased water content in the brain, as reflected by higher ADC and delayed myelination, in children with CHD.

ADC histograms may be a potential biomarker of alterations of tissue structure. The lower skewness and kurtosis observed in the CHD group may reflect an abundance of cystic or edematous tissue, suggesting that lesions can be characterized physiologically by assessing the curvature of ADC histograms (13, 34). Further studies are required to clarify its classification performance between CHD and HC groups and validate its application in clinical settings.

This study indicated that the selected texture features were unable to achieve better diagnostic performance than ADC metrics. This may be due to substantial overlap in the regional ADCs for whole slices or whole brains that might lead to a lack of significant differences in texture features. Recent advances combined ADC metrics and texture features to perform classification for high-risk atypical meningiomas (35). Compared to ADC metrics that showed significance, texture features was suggested to have limited contribution to tumor classification. This finding indicates the limited ability of texture features for characterizing brain lesion. In summary, ADC metrics may

aid in the early assessment of brain alterations in neonates with CHD.

To the best of our knowledge, this is the first study comparing the diagnostic performance of ADC metrics between single-slice and multi-slice measurements. One of the most common types of brain injury seen in these neonates is white matter injury, which is similar to the pattern of injury observed in preterm neonates (36). Severe hypoxia-ischemia, presenting in the form of periventricular leukomalacia, results in neuronal death and could contribute to a reduction in axonal density (2). Single layers of periventricular white matter are therefore chosen and considered representative. Multi-slice measurements provided more statistically significant ADC parameters for diagnosis than single-slice measurements. Such multi-slice measurements may reflect the diffuse state of the brain in neonates with CHD more accurately than single-slice measurements, which is potentially due to the structural complexity of the brain and differences in the distribution of water molecule diffusion in the whole brain. ADC grayscale values and distributions derived from whole tumors could provide more quantitative information regarding the characteristics and heterogeneity of the tissue (15, 32), further supporting the potential clinical use of multi-slice measurements. Therefore, preoperative evaluation of the ADC using multiple slices may provide more useful information for differentiating patients with CHD from HCs. Meanwhile, given that single-slice measurements are easier to perform, the optimal technique should be determined based on individual patient needs in clinical settings. More detailed studies of functional areas will be carried out combined with following up.

The present study possesses some limitations of note. Firstly, performing MRI in healthy neonates is challenging because they are not normally included in clinical imaging studies. Consequently, few studies have reported ADC for healthy neonates, making it difficult to compare our findings with those of previous researchers (27). In addition, all neonates in our HC group were considered *healthy* based on MRI findings, but this grouping method also included patients with mild neonatal pneumonia or scalp hematoma. Nonetheless, all patients in the HC group were followed up for 6 months to confirm that no subsequent brain diseases occurred. Secondly, our study was also limited by its cross-sectional design, which did not allow us to obtain follow-up data regarding the relationship between ADC metrics and the development of advanced neural function. However, our preliminary results suggest that ADC metrics can be used to identify patients with CHDs, highlighting the need for additional validation studies. Lastly, the influence of genomic characteristics were not included due to the challenges associated with collecting such data. Future studies with extended follow-up periods should therefore assess the impact of genetic characteristics on neurodevelopmental disorders in children with CHDs.

5. CONCLUSION

Multi-slice analysis of the whole brain may provide more significant ADC metrics for the diagnosis of CHDs in neonates than single-slice analysis. Clinical application of multi-slice ADC may allow for more accurate diagnosis of CHDs than visual assessments based on single-slice measurements or structural imaging.

DATA AVAILABILITY STATEMENT

The original contributions presented in the study are included in the article/**Supplementary Materials**, further inquiries can be directed to the corresponding author/s.

ETHICS STATEMENT

The studies involving human participants were reviewed and approved by Ethics Committee, children's Hospital of Nanjing Medical University. Written informed consent to participate in this study was provided by the participants' legal guardian/next of kin.

AUTHOR CONTRIBUTIONS

MZ, YW, and SW prepared the data. MZ performed the literature search, analyzed the results, and drafted the manuscript. DZ analyzed the data, performed statistical analysis, and contributed substantially to manuscript revision. QZ preliminarily corrected the language. MY, XM, and YS supervised manuscript development and reviewed all sections. All authors reviewed and approved the final version of the manuscript.

FUNDING

This study was supported by the Research Project of Maternal and Child Health Care in Jiangsu (F201554), the Six Talent Peaks Project in Jiangsu Province (WSN-192), and the Research project of Jiangsu Provincial Health Commission (LGY2019009).

SUPPLEMENTARY MATERIAL

The Supplementary Material for this article can be found online at: https://www.frontiersin.org/articles/10.3389/fneur.2020.586518/full#supplementary-material

REFERENCES

1. Shedeed S, Elfaytouri E. Brain maturity and brain injury in newborns with cyanotic congenital heart disease. *Pediatr Cardiol.* (2011) 32:47–54. doi: 10.1007/s00246-010-9813-7
2. Morton P, Ishibashi N, Jonas R. Neurodevelopmental abnormalities and congenital heart disease: insights into altered brain maturation. *Circul Res.* (2017) 120:960–77. doi: 10.1161/CIRCRESAHA.116.309048
3. Marelli A, Ionescu-Ittu R, Mackie A, Guo L, Dendukuri N, Kaouache M. Lifetime prevalence of congenital heart disease in the general

population from 2000 to 2010. *Circulation*. (2014) 130:749–56. doi: 10.1161/CIRCULATIONAHA.113.008396
4. Marino B. New concepts in predicting, evaluating, and managing neurodevelopmental outcomes in children with congenital heart disease. *Curr Opin Pediatr*. (2013) 25:574–84. doi: 10.1097/MOP.0b013e328365342e
5. Miller S, McQuillen P, Hamrick S, Xu D, Glidden D, Charlton N, et al. Abnormal brain development in newborns with congenital heart disease. *N Engl J Med*. (2007) 357:1928–38. doi: 10.1056/NEJMoa067393
6. Mebius M, Kooi E, Bilardo C, Bos A. Brain injury and neurodevelopmental outcome in congenital heart disease: a systematic review. *Pediatrics*. (2017) 140:e20164055. doi: 10.1542/peds.2016-4055
7. Claessens N, Kelly C, Counsell S, Benders M. Neuroimaging, cardiovascular physiology, and functional outcomes in infants with congenital heart disease. *Dev Med Child Neurol*. (2017) 59:894–902. doi: 10.1111/dmcn.13461
8. Fontes K, Rohlicek C, Saint-Martin C, Gilbert G, Easson K, Majnemer A, et al. Hippocampal alterations and functional correlates in adolescents and young adults with congenital heart disease. *Hum Brain Mapp*. (2019) 40:3548–60. doi: 10.1002/hbm.24615
9. Schmithorst V, Votava-Smith J, Tran N, Kim R, Lee V, Ceschin R, et al. Structural network topology correlates of microstructural brain dysmaturation in term infants with congenital heart disease. *Hum Brain Mapp*. (2018) 39:4593–610. doi: 10.1002/hbm.24308
10. Kelly C, Makropoulos A, Cordero-Grande L, Hutter J, Price A, Hughes E, et al. Impaired development of the cerebral cortex in infants with congenital heart disease is correlated to reduced cerebral oxygen delivery. *Sci Rep*. (2017) 7:15088. doi: 10.1038/s41598-017-14939-z
11. Van Beers B, Vilgrain V. Biomarkers in abdominal imaging. *Abdom Imaging*. (2009) 34:663–7. doi: 10.1007/s00261-008-9480-9
12. Kilickesmez O, Bayramoglu S, Inci E, Cimilli T, Kayhan A. Quantitative diffusion-weighted magnetic resonance imaging of normal and diseased uterine zones. *Acta Radiol*. (2009) 50:340–7. doi: 10.1080/02841850902735858
13. Lin Y, Li H, Chen Z, Ni P, Zhong Q, Huang H, et al. Correlation of histogram analysis of apparent diffusion coefficient with uterine cervical pathologic finding. *Am J Roentgenol*. (2015) 204:1125–31. doi: 10.2214/AJR.14.13350
14. Gillies R, Kinahan P, Hricak H. Radiomics: images are more than pictures, they are data. *Radiology*. (2016) 278:563–77. doi: 10.1148/radiol.2015151169
15. Lambin P, Rios-Velazquez E, Leijenaar R, Carvalho S, van Stiphout R, Granton P, et al. Radiomics: extracting more information from medical images using advanced feature analysis. *Eur J Cancer*. (2012) 48:441–6. doi: 10.1016/j.ejca.2011.11.036
16. Xue H, Ren C, Yang J, Sun Z, Li S, Jin Z, et al. Histogram analysis of apparent diffusion coefficient for the assessment of local aggressiveness of cervical cancer. *Arch Gynecol Obstetr*. (2014) 290:341–8. doi: 10.1007/s00404-014-3221-9
17. Kickingereder P, Neuberger U, Bonekamp D, Piechotta P, Gtz M, Wick A, et al. Radiomic subtyping improves disease stratification beyond key molecular, clinical, and standard imaging characteristics in patients with glioblastoma. *Neuro-Oncol*. (2018) 20:848–57. doi: 10.1093/neuonc/nox188
18. Cauley K, Filippi C. Apparent diffusion coefficient histogram analysis of neonatal hypoxic-ischemic encephalopathy. *Pediatr Radiol*. (2014) 44:738–46. doi: 10.1007/s00247-013-2864-1
19. Kickingereder P, Bonekamp D, Nowosielski M, Kratz A, Sill M, Burth S, et al. Radiogenomics of glioblastoma: machine learning-based classification of molecular characteristics by using multiparametric and multiregional MR imaging features. *Radiology*. (2016) 281:907–18. doi: 10.1148/radiol.2016161382
20. Zhu M, Wang Y, Li H, Yang M, Mo X, Cheng R, et al. Brain alteration in neonates with congenital heart disease using apparent diffusion coefficient histograms. *Natl Med J China*. (2018) 98:3162–5. doi: 10.3760/cma.j.issn.0376-2491.2018.39.007
21. Easson K, Rohlicek C, Houde J, Gilbert G, Saint-Martin C, Fontes K, et al. Quantification of apparent axon density and orientation dispersion in the white matter of youth born with congenital heart disease. *Neuroimage*. (2020) 205:116255. doi: 10.1016/j.neuroimage.2019.116255
22. Kang Y, Choi S, Kim Y, Kim K, Sohn C, Kim J, et al. Gliomas: Histogram analysis of apparent diffusion coefficient maps with standard- or high-b-value diffusion-weighted MR imaging-correlation with tumor grade. *Radiology*. (2011) 261:882–90. doi: 10.1148/radiol.11110686
23. Murakami R, Hirai T, Sugahara T, Fukuoka H, Toya R, Nishimura S, et al. Grading astrocytic tumors by using apparent diffusion coefficient parameters: superiority of a one- versus two-parameter pilot method. *Radiology*. (2009) 251:838–45. doi: 10.1148/radiol.2513080899
24. Tozer D, Jger H, Danchaivijitr N, Benton C, Tofts P, Rees J, et al. Apparent diffusion coefficient histograms may predict low-grade glioma subtype. *NMR Biomed*. (2007) 20:49–57. doi: 10.1002/nbm.1091
25. Davnall F, Yip C, Ljungqvist G, Selmi M, Ng F, Sanghera B, et al. Assessment of tumor heterogeneity: an emerging imaging tool for clinical practice. *Insights Imaging*. (2012) 3:573–89. doi: 10.1007/s13244-012-0196-6
26. Ruopp M, Perkins N, Whitcomb B, Schisterman E. Youden Index and optimal cut-point estimated from observations affected by a lower limit of detection. *Biometr J*. (2008) 50:419–30. doi: 10.1002/bimj.200710415
27. Provenzale J, Liang L, DeLong D, White L. Diffusion tensor imaging assessment of brain white matter maturation during the first postnatal year. *Am J Roentgenol*. (2007) 189:476–86. doi: 10.2214/AJR.07.2132
28. Neil J, Shiran S, McKinstry R, Schefft G, Snyder A, Almli C, et al. Normal brain in human newborns: apparent diffusion coefficient and diffusion anisotropy measured by using diffusion tensor MR imaging. *Radiology*. (1998) 209:57–66. doi: 10.1148/radiology.209.1.9769812
29. Ou Y, Zllei L, Retzepi K, Castro V, Bates S, Pieper S, et al. Using clinically acquired MRI to construct age-specific ADC atlases: quantifying spatiotemporal ADC changes from birth to 6-year old. *Hum Brain Mapp*. (2017) 38:3052–68.
30. Beca J, Gunn J, Coleman L, Hope A, Reed P, Hunt R, et al. New white matter brain injury after infant heart surgery is associated with diagnostic group and the use of circulatory arrest. *Circulation*. (2013) 127:971–9. doi: 10.1161/CIRCULATIONAHA.112.001089
31. Shillingford A, Ittenbach R, Marino B, Rychik J, Clancy R, Spray T, et al. Aortic morphometry and microcephaly in hypoplastic left heart syndrome. *Cardiol Young*. (2007) 17:189–95. doi: 10.1017/S1047951107000248
32. Xu X, Li Y, Hong X, Wu F, Shi H. Radiological indeterminate vestibular schwannoma and meningioma in cerebellopontine angle area: differentiating using whole-tumor histogram analysis of apparent diffusion coefficient. *Int J Neurosci*. (2017) 127:183–90. doi: 10.3109/00207454.2016.1164157
33. Lim J, Kingdom T, Saini B, Chau V, Post M, Blaser S, et al. Cerebral oxygen delivery is reduced in newborns with congenital heart disease. *J Thorac Cardiovasc Surg*. (2016) 152:1095–103. doi: 10.1016/j.jtcvs.2016.05.027
34. McDonald K, Sebire NJ, Anderson J, Olsen Œ. Patterns of shift in ADC distributions in abdominal tumours during chemotherapy-feasibility study. *Pediatr Radiol*. (2011) 41:99–106. doi: 10.1007/s00247-010-1741-4
35. Kalasauskas D, Kronfeld A, Renovanz M, Kurz E, Leukel P, Krenzlin H, et al. Identification of high-risk atypical meningiomas according to semantic and radiomic features. *Cancers*. (2020) 12. doi: 10.3390/cancers12102942
36. Miller S, Ferriero D, Leonard C, Piecuch R, Glidden D, Partridge J, et al. Early brain injury in premature newborns detected with magnetic resonance imaging is associated with adverse early neurodevelopmental outcome. *J Pediatr*. (2005) 147:609–16. doi: 10.1016/j.jpeds.2005.06.033

Conflict of Interest: The authors declare that the research was conducted in the absence of any commercial or financial relationships that could be construed as a potential conflict of interest.

frontiers in Pediatrics

REVIEW
published: 12 January 2021
doi: 10.3389/fped.2020.599633

Abnormal Nutritive Sucking as an Indicator of Neonatal Brain Injury

Sabrina Shandley[1], Gilson Capilouto[2,3], Eleonora Tamilia[4], David M. Riley[5,6], Yvette R. Johnson[5,6,7] and Christos Papadelis[1,4,6,8]*

[1] Jane and John Justin Neurosciences Center, Cook Children's Health Care System, Fort Worth, TX, United States, [2] Department of Communication Sciences and Disorders, University of Kentucky, Lexington, KY, United States, [3] NFANT Labs, LLC, Marietta, GA, United States, [4] Division of Newborn Medicine, Department of Pediatrics, Boston Children's Hospital, Harvard Medical School, Boston, MA, United States, [5] Neonatal Intensive Care Unit, Cook Children's Health Care System, Fort Worth, TX, United States, [6] School of Medicine, Texas Christian University and University of North Texas Health Science Center, Fort Worth, TX, United States, [7] Neonatal Intensive Care Unit Early Support and Transition (NEST), Developmental Follow-Up Center, Neonatology Department, Cook Children's Health Care System, Fort Worth, TX, United States, [8] Department of Bioengineering, University of Texas at Arlington, Arlington, TX, United States

A term neonate is born with the ability to suck; this neuronal network is already formed and functional by 28 weeks gestational age and continues to evolve into adulthood. Because of the necessity of acquiring nutrition, the complexity of the neuronal network needed to suck, and neuroplasticity in infancy, the skill of sucking has the unique ability to give insight into areas of the brain that may be damaged either during or before birth. Interpretation of the behaviors during sucking shows promise in guiding therapies and how to potentially repair the damage early in life, when neuroplasticity is high. Sucking requires coordinated suck-swallow-breathe actions and is classified into two basic types, nutritive and non-nutritive. Each type of suck has particular characteristics that can be measured and used to learn about the infant's neuronal circuitry. Basic sucking and swallowing are present in embryos and further develop to incorporate breathing *ex utero*. Due to the rhythmic nature of the suck-swallow-breathe process, these motor functions are controlled by central pattern generators. The coordination of swallowing, breathing, and sucking is an enormously complex sensorimotor process. Because of this complexity, brain injury before birth can have an effect on these sucking patterns. Clinical assessments allow evaluators to score the oral-motor pattern, however, they remain ultimately subjective. Thus, clinicians are in need of objective measures to identify the specific area of deficit in the sucking pattern of each infant to tailor therapies to their specific needs. Therapeutic approaches involve pacifiers, cheek/chin support, tactile, oral kinesthetic, auditory, vestibular, and/or visual sensorimotor inputs. These therapies are performed to train the infant to suck appropriately using these subjective assessments along with the experience of the therapist (usually a speech therapist), but newer, more objective measures are coming along. Recent studies have correlated pathological sucking patterns with neuroimaging data to get a map of the affected brain regions to better inform therapies. The purpose of this review is to provide a broad scope synopsis of the research field of infant nutritive and non-nutritive feeding, their underlying neurophysiology, and relationship of abnormal activity with brain injury in preterm and term infants.

Keywords: sucking, brain injury, neuroimaging, nutritive, non-nutritive

OPEN ACCESS

Edited by:
Daniel Alonso-Alconada, University of the Basque Country, Spain

Reviewed by:
Ivan Leslie Hand, SUNY Downstate Medical Center, United States
Kevin Donald Broad, University College London, United Kingdom

****Correspondence:***
Sabrina Shandley
sabrina.shandley@cookchildrens.org

Specialty section:
This article was submitted to Neonatology, a section of the journal Frontiers in Pediatrics

Received: *27 August 2020*
Accepted: *24 November 2020*
Published: *12 January 2021*

Citation:
Shandley S, Capilouto G, Tamilia E, Riley DM, Johnson YR and Papadelis C (2021) Abnormal Nutritive Sucking as an Indicator of Neonatal Brain Injury. Front. Pediatr. 8:599633. doi: 10.3389/fped.2020.599633

HISTORICAL BACKGROUND

As early as the 1940's researchers began examining the sucking behavior of infants. Before this time, the milk ejection, or "let-down," reflex was regarded as the predominant method of breast milk transfer (1, 2). Sucking patterns of infants were differentiated based on the frequency and intensity of the sucking, which was found to correlate with whether or not fluid (breastmilk or formula) is present. These patterns became known as *nutritive* and *non-nutritive* sucking (1, 3–5). In the 1950's researchers started to deconstruct the infant suck into two different skills, *suction* and *expression/compression* (6–8). Based on this deconstruction, research in the 1960's focused on evaluating how an infant would modify these two skills to obtain nutrients using lab-made apparatus' that would control when nutrient was released based on the amount of suction or expression (6). These experiments demonstrated the incredible learning ability of an infant's brain to adapt to changing conditions in line with more recent ideas of brain neuroplasticity during the early years of life (9–11). Nurses also began noticing the relationship between feeding as an infant and speaking ability later in life (12). Concurrently, other groups began looking into the relationship between brain injury and sucking; they observed differences between non-nutritive sucking of normal, term infants, and those who experienced perinatal stress with or without neurological signs (3).

The 1970's brought the confirmation that the anatomy and physiology of the infant, feeding on a pure liquid diet, is profoundly different than the adult (13). This paved the way for the field of dysphagia in infants to be studied and treated differently than in adults. The following decade, dysphagia in infants and children became a focus of researchers and clinicians alike as medical care improved outcomes for preterm infants. Also, neuroscientists and speech therapists began to investigate the correlation between sucking pattern in infancy and fine motor skills around 6 months, speech-language delays at 18 months, and developmental delay at 24 months (14). In the 1990's the field broadened significantly to include molecular, developmental, and genetic biology (15, 16).

The new millennia began with trials that confirmed developmental enhancement interventions and physical therapy performed on infants with brain injury were not working well (11, 17, 18), even though success had been seen with older children (19–21). Another compounding factor was identification of infants with brain injury by MRI, which is unreliable as a sole predictor of clinical impairment or prognosis (22–24). Clearly, interventions need to be tailored to the term and preterm infants with brain injury and the injury itself needs other modalities for identification (25). During this time, the idea of neuroplasticity became the topic of numerous studies in cerebral palsy research which clearly demonstrates re-organization of the brain as a result of a prenatal or perinatal brain insult (26–31). Additionally, brain injury repair is being elucidated in both human and animal studies (32–36). These advancements have led to the current research field of identifying brain injury through evaluation of sucking as well as habilitation of sucking in infants to potentially repair brain injury.

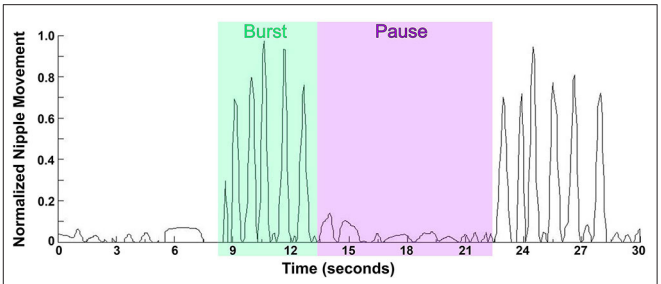

FIGURE 1 | Waveform pattern of NNS. Graph represents the extent of the movement of the lever inside the bottle nipple, measuring the expression component of sucking with 1.0 being the furthest the lever inside the nipple can move, and 0.5 being half the maximum distance. NNS occurs at up to two sucks per second in short, fast bursts lasting anywhere from 2 to 12 s with a pause between bursts of 3–13 s.

NUTRITIVE AND NON-NUTRITIVE SUCKING

Early in the investigations of infant's sucking it became clear that there are two distinct types, namely, *nutritive* and *non-nutritive* sucking. As an infant gains more experience, these sucking patterns mature in strength and efficiency. The variation within an individual is small, however there could be fairly significant interindividual variations. Non-nutritive sucking (NNS) is the primary pattern seen when an infant sucks on a pacifier, his/her thumb, or other objects. NNS occurs at up to two sucks per second (*frequency*) in short, fast bursts (1, 3, 14, 37). The bursts can last anywhere from 2 to 12 s (*burst duration*) with a rest period (pause) between bursts of 3–13 s [(3, 38); **Figure 1**]. The greatest predictors of a mature NNS pattern is post-menstrual age (PMA) and birth weight (39). As the infant ages, the *frequency* and *burst duration* may increase to a NNS pattern considered more mature, closer to two sucks per second with a duration between 2–8 s and less inter-burst duration and inter-rest period variations, hence a smoother, more regular NNS (38, 39). When breast-feeding, a newborn will begin with NNS until the milk ejection reflex occurs, then will switch to nutritive sucking (40). If NNS is not encouraged, by breast-feeding or pacifier use, for example, it will disappear by 4–5 months of age, however, fascinatingly it can be found in some adults with degenerative cerebral diseases (39).

There are several factors which may affect the different features of a NNS. For example, pacifier characteristics may impact the way an infant will suck on it. The thickness of the silicone of a pacifier, therefore, its stiffness, will affect the NNS pattern of infants. Stiffer pacifiers will elicit fewer sucks per burst, up to half as many, and also the strength, or amplitude, of each suck is decreased. The shape of the pacifier or any texture will also profoundly affect the NNS pattern (41–43).

Nutritive sucking (NS) occurs at a slower pace, about one suck per second (1, 3), and as the feed continues a burst–pause pattern emerges. The first minutes of NS are steady with none or very few short pauses, as the feed continues, bursts appear with a pause between bursts that gets longer toward the end of the feeding

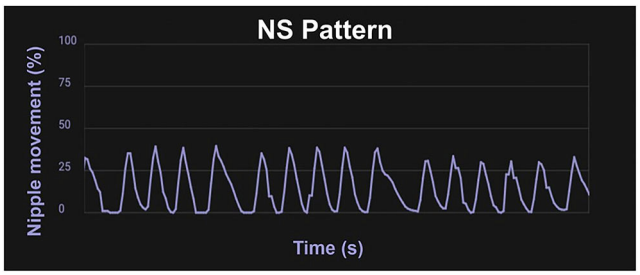

FIGURE 2 | Waveform pattern of NS. Graph from the infant Feeding Solution showing the extent of the movement of the lever inside the bottle nipple measuring the expression component of sucking with 100% being the furthest the lever inside the nipple can move, and 50% being half the maximum distance. A mature NS pattern demonstrates regular, smooth movement about one suck per second.

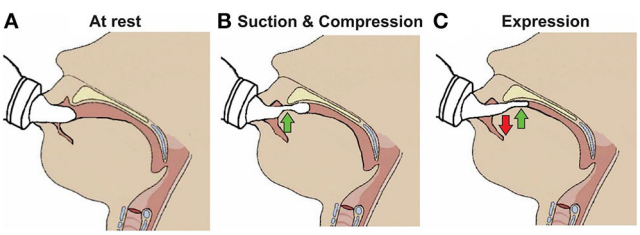

FIGURE 3 | Skills required for sucking in infants. **(A)** Infant at rest with the nipple inside the mouth. **(B)** Suction applied to the nipple to draw further into the mouth to form a teat and the tip of the tongue beginning to compress it. **(C)** Expression of the teat by the tongue movement against the hard palate.

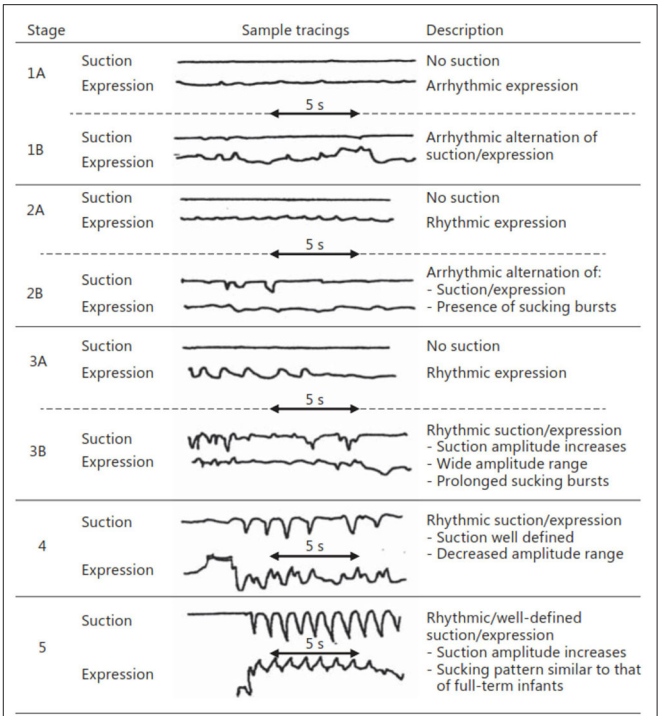

FIGURE 4 | Stages of NS. Early stages (1–3) are seen in preterm infants, while more mature stages (4 and 5) are seen in term infants as well as preterms after enough experience and maturation. Reprinted with permission from Lau (37).

[(14, 44); **Figure 2**]. The rooting reflex, which is the movement of an infant's head toward a touch on their cheek accompanied by mouth gapping, is present at birth for neurologically normal infants born at 32 weeks gestational age (GA) and older, and sometimes even very preterm infants will root before 32 weeks PMA (45). This reflex assists the infant in locating a food source and will disappear around 6 months old (1).

DEVELOPMENT OF NORMAL SUCKING ACTIVITY

Nutritive sucking is a highly coordinated activity between sucking, swallowing, and respiration (37, 46, 47). Sucking and swallowing skills develop *in utero* as the fetus regulates amniotic fluid levels (14, 16, 48, 49) and must be further developed *ex utero* to incorporate breathing. For both NS and NNS sucking, two skills are required, suction and expression/compression (1, 3, 6, 47, 50). Expression develops first and is the compression or stripping of the tongue against the hard palate to eject liquid (**Figure 3**). Expression/compression, without the suction component of oral feeding, appears to be present at birth as even very preterm infants as young as 26 weeks GA, have a coordinated 1:1 expression-swallow pattern, albeit slow, and the swallowing process is immature (37). Suction is intraoral negative pressure that draws liquid into the mouth. Suction also requires lowering the jaw to increase the volume of the mouth, closure of the nasal passage by the soft palate, and a tight seal by the lips to prevent air inflow. The development and coordination of these two skills can be measured in five stages: (i) stage 1, no suction and sporadic/arrhythmic expression; (ii) stage 2, no suction or weak, sporadic suction and more organized rhythmic expression pattern; (iii) stage 3, stronger expression, more organized suction/expression pattern emerging; (iv) stage 4, suction is well-defined, suction, and expression strength (amplitudes) becoming more consistent; and (v) stage 5, suction is stronger (increase amplitude), suction/expression has a defined, rhythmic pattern [(47, 51); **Figure 4**].

RELATIONSHIP TO BREATHING

For healthy adults swallowing is dominant to breathing, which prevents aspiration, and in 75–95% of adults swallowing is initiated during mid-expiration (52, 53). This pause in breathing to swallow is termed swallowing apnea, or deglutition apnea. Infants, however, vary considerably in their swallow-respiration patterns for inter-infant comparisons as well as inter- and intra-feeding comparisons. There are nine possible combinations of swallowing and breathing, with or without pauses: (i) inspiration (I)-swallow-I; (ii) I-swallow-expiration (E); (iii) E-swallow-I; (iv) E-swallow-E; (v) I-swallow-pause (P); (vi) P-swallow-I; (vii) E-swallow-P; (viii) P-swallow-E; and (ix) P-swallow-P. Some studies combine the swallow patterns with pauses into one

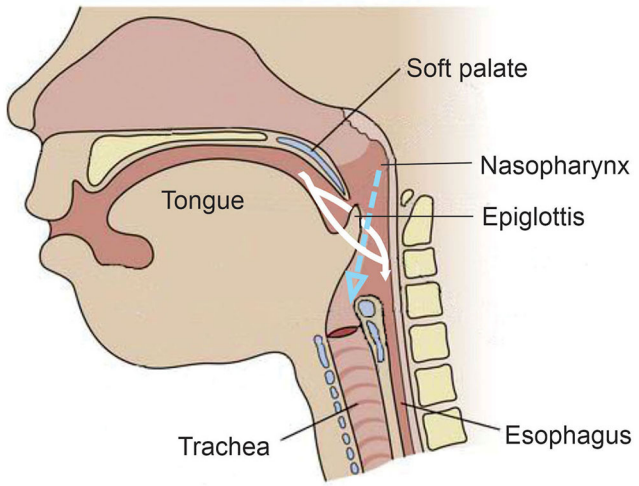

FIGURE 5 | Anatomy and physiology of the infant during feeding. Unlike the adult, the epiglottis moves upward toward the soft palate during feeding. The white indicates the fluid meal and demonstrates how it is made to go around the epiglottis and into the esophagus. The dotted blue arrow indicates the air coming from the nasal passage during the feeding and demonstrates its laminar flow into the trachea.

grouping as a "pause" group (54), others call it "apnea from multiple swallows (AMS)." In addition, some may group patterns by when the swallow occurs, type I having the swallow in-between phases (I-swallow-E and E-swallow-I), type II having the swallow within phases (I-swallow-I or E-swallow-E) and type III being AMS (55–57). As discussed in the next section, the anatomy and physiology of the infant is profoundly different than in the adult and allows feeding to be done simultaneously with breathing, which explains how an infant can have such variable patterns and not aspirate during feeding.

ANATOMY AND PHYSIOLOGY

The evolution from suckle to mastication as the infant matures into childhood develops and changes in anatomy, physiology, and neural networks (15, 16, 48, 52). Unlike adults, an infant's epiglottis moves upward to the soft palate, which allows the trachea to remain open to the nasopharynx to permit constant breathing during sucking. This has been described as the liquid being made to go around each side of the epiglottis and flow into the pharynx and esophagus while still allowing laminar flow of air through the nasopharynx into the trachea [(15, 52, 55, 58); **Figure 5**]. The brief pause (350–850 ms) in breathing by a sucking infant, deglutition apnea, has been attributed to neuronal control rather than an airway protection mechanism, perhaps in preparation for the more mature swallowing of an adult that requires aspiration prevention (15, 55).

The coordination of swallowing, breathing and sucking is an enormously complex sensorimotor process, requiring five cranial nerves, at least 26 pairs of muscles, the cervical and thoracic spinal cord as well as at least 10 discrete brain areas (48, 52, 53, 58). Due to the rhythmic nature of the suck-swallow-breathe process, these motor functions are controlled by central pattern generators (CPGs) (14, 15, 37, 48, 53, 58). The interneurons of these CPGs are found in the brainstem, specifically the upper medullary and pontine areas, and have been shown to be capable of generating a basic swallow without other input (14, 48, 53). CPGs are at the core of this complex system. A second level of controls includes subcortical structures including the basal ganglia, hypothalamus, cerebellum, amygdala, and tegmental area of the midbrain with a third level in the suprabulbar cortical swallowing center (48). **Figure 6** is a graphic representation of the brain network that coordinates sucking and swallowing. For a more in depth review the reader is directed to Hockman et al. (59), Diamant (60), Matsuo and Palmer (52), Mistry and Hamdy (48), Barlow (53), LaMantia et al. (16), Li-Jessen and Ridgway (61), and Maynard et al. (15).

The integration of these three levels of control in the brain are required to coordinate the three phases of NS: (i) oral; (ii) pharyngeal; and (iii) esophageal (15, 47, 48, 58). The oral phase requires cranial nerves (CN) V and VII to move the jaw and facial muscles (to latch onto either breast or bottle nipple) and CN XII for tongue movement to accomplish suction and expression/compression. The pharyngeal phase requires CN V, IX, and X for movement of the epiglottis anteriorly against the soft palate, expansion of the uvula and elevation of the hyoid bone and larynx to accomplish moving of liquid into the pharynx. The esophageal phase requires CN X for peristaltic movement of the esophageal muscles (15, 16, 52, 53, 55). Combined, the sensory and motor neurons that contribute to these five cranial nerves, sensory or motor relay nuclei in the brainstem, and their interconnections constitute the sucking neural circuit (15). This is a highly dynamic and constantly changing circuit based on chemosensory and experiential inputs.

SUCKING ACTIVITY IN PRETERM INFANTS

Healthy, term infants are, in general, born with the basic skills to perform NS, however, a preterm infant is denied the additional time *in utero* to develop. After gestational age of 28 weeks, it seems that sucking and swallowing are sufficient enough to begin oral feeding; however, they are not coordinated with breathing usually until 32 weeks PMA, with significant improvement around 34 weeks PMA (62, 63). In addition to age, clinicians look for signs of readiness to safely oral feed including, alert state, weight gain and stable respiration. However, age is not sufficient, preterm infants must develop in two aspects in order to attain a safe suck-swallow-breathe behavior for all three phase of the NS: (i) maturation (GA and PMA) and (ii) experience (14, 62, 64, 65).

During the oral phase, preterm infants have a lower frequency, volume, and negative pressure during NS compared to their term counterparts (41, 66). The preterm infant must experience oral feeding to learn and create the neuronal patterns required since maturation alone is not adequate. With sufficient maturation, preterm infants given training and oral feeding experiences as early as 32 weeks PMA, will progress to more mature sucking

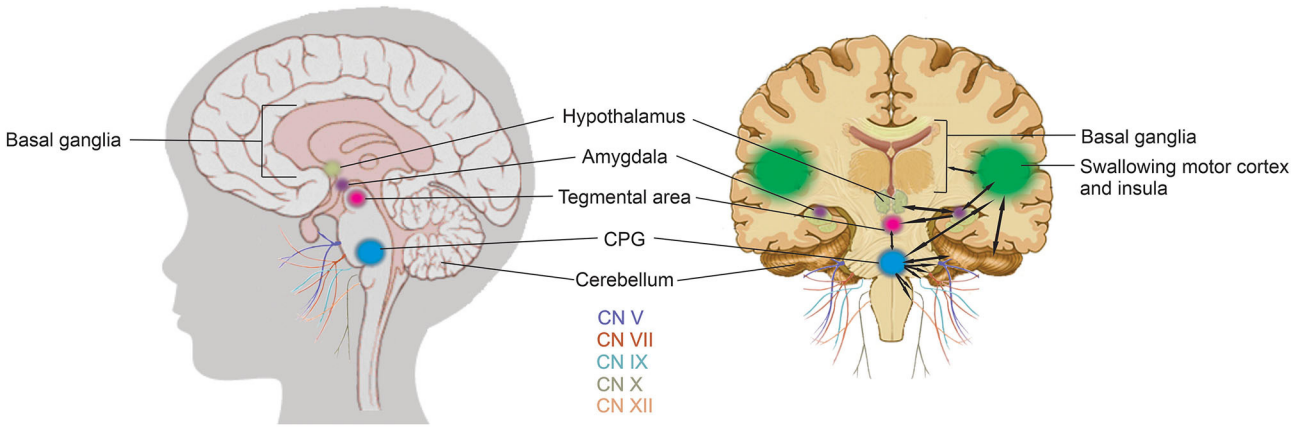

FIGURE 6 | Sucking and swallowing brain network. Sucking and swallowing is a bilateral process in the brain, each hemisphere has been shown to act both contralaterally and ipsilaterally, therefore, for simplicity, the black arrows on the right, coronal view of the brain indicate the complex integration and communication between the areas in only one hemisphere currently believed to be involved in the motor aspects of sucking. CPGs (blue), are at the core of this complex system. A second level of controls includes subcortical structures including the basal ganglia, hypothalamus (pale olive green), cerebellum, amygdala (purple), and tegmental area (pink) of the midbrain with a third level in the suprabulbar cortical swallowing center and insula (green). The cranial nerves (CN) required for the motor process of feeding and swallowing include CN V and VII to move the jaw and facial muscles, CN XII for tongue movement, CN V, IX, and X for movement of the epiglottis, expansion of the uvula and elevation of the hyoid bone and larynx, and CN X for peristaltic movement of the esophageal muscles.

stages of 3–5 around 34 weeks PMA, less experience will delay this progress (51, 64).

The preterm infant must also coordinate the pharyngeal and esophageal phases. The timing of pharyngeal peak pressure and the relaxation of the upper esophageal sphincter (UES) must evolve through both maturation and experience as well. Usually by the time a preterm infant is 34 weeks PMA, given enough experience, pharyngeal pressure is at its peak and the UES is able to fully and rapidly relax open. Younger preterm infants are at risk for dysphagia until this time because the pharyngeal pressure is lower and the UES is slower to relax open and does not open completely (67).

There is relatively little known about NNS in preterm infants in large part because it does not necessarily have an implication for NS performance until about 38 weeks PMA (44, 65, 68, 69). It is important, however, as a therapeutic action for the infant to help promote regulation of state (calm, sleepy, alert, fussy, crying, etc.) and lessen distress (39, 44). Similarly to NS, NNS is present around 28 weeks PMA and the frequency, volume, and negative pressure increases as the preterm infant ages (69). The pauses between bursts during NNS become shorter and more regular (less variation) and the bursts have increased frequency of sucks and longer duration with increasing PMA (39).

ASSESSMENTS

Routinely for many decades, clinicians, often speech therapists or nurse feeding specialists, have used a gloved finger and inserted it into the infant's mouth to gauge their sucking ability by considering the strength, rhythmicity, frequency and duration of sucks and bursts (14). This method is used to assess if an infant is ready to orally feed; whether they are able to get nutrition or if there is another issue causing clinical symptoms (such as failure-to-thrive). It is also used by lactation consultants to evaluate latch and sucking to aid in successful breast-feeding. Yet, this is a subjective judgement highly dependent upon the clinician's experience, tactile sensitivity, and how long the infant sucks on their finger. Going one step further, the Infant-Driven Feeding Scale was developed in an attempt to quantify the subjective assessments of the rater (70).

The Neonatal Oral-Motor Assessment Scale (NOMAS), developed in the mid-1980s, is a common observational tool used to assess jaw and tongue movement with qualitative results of normal sucking, disorganized sucking, or dysfunctional sucking pattern (71–74). A dysfunctional pattern is believed to be a sign of neurological impairment (75, 76), however it is controversial (71, 74). One problem lies in the NOMAS relying purely on the training and experience of the rater performing the scale because it is only an observation of how the infant feeds. A second problem arises when the NOMAS is compared to a later neurologic assessment. There are many different neurologic assessments done at different ages, and depending on which of them the NOMAS is compared to (BSID most commonly, early motor repertoire, or MOS, CRIB, Dubowitz, and NNNS to name a few), this can change how well the NOMAS score predicts the outcome of the neurologic assessment. A third problem comes from the variable chronological and gestational ages of the infants and/or preterms used in each study; there is not a routine age when the NOMAS is performed, nor are there consistent longitudinal scores taken for each infant in each study. Clinicians are in need for objective measures of the sucking pattern of each neonate in order to tailor therapies to improve primary measures along with improving secondary outcomes, such as weight gain or increase in feeding volume.

QUANTITATIVE MEASURES

One of the earliest known reports of quantifying neonatal sucking was published in 1865 by Herz, who measured negative intraoral pressure using a mercury manometer attached to a nipple (77). Other similar methods for quantifying early sucking can be found in the literature from the late 1800s through to the early 1900s [see (77) for review]. More recently, there has been an increasing number of technological solutions to advance the quantification of sucking activity (78).

Kron et al. published their seminal work for quantifying early sucking in 1963. Their interest in neonatal sucking was motivated by the desire to better understand the role of infant sucking in psychological development—specifically, personality formation (77). The researchers used a specially constructed nipple fused at the tip with rubber tubing that required active sucking (negative intraoral pressure) to release the flow of liquid. Continuous graphic output of the pressures within the mouth of the infant were recorded from a pressure transducer fixed between the flow device and the specialized nipple. Sucking variables included number of sucks per minute, volume consumed per minute and average pressure per suck, per minute. Based on results, the authors concluded that term infants altered their rate of sucking to increase the amount of liquid consumed on the second and third days of life. Further analyses suggested that infant sucking adaptations were a result of both maturation and a learning effect from the reinforcement of sucking at the breast or bottle. The instrumentation they used became known as the Kron Nutritive Sucking Apparatus (KNSA) (**Figure 7**).

Medoff-Cooper and colleagues used customized software to expand the sucking parameters that could be derived from the KNSA, in a 5 minute sucking session. These included number of sucks per session, sucking duration (interval from first to last suck in session), number of bursts in session (2-s pause defined separation of 2 bursts), mean burst duration, within-burst suck frequency, and mean maximum sucking pressure, among others (83). Following analyses, the authors concluded that for preterm infants, different aspects of sucking matured at different maturational ages. In a subsequent study by Bromiker et al. (84), suck rate, suck-to-burst ratio and time between bursts were used to investigate the influence of preterm infant feeding practice on feeding development at term. The authors found that earlier introduction of oral feeding resulted in greater feeding organization at term age; again highlighting the influence of learning and practice on the development of sucking skills.

Medoff-Cooper et al. went on to use the Nutritive Sucking Apparatus (NSA) (**Figure 7**), a modification of the KNSA, to investigate the relationship between preterm infant early sucking patterns and neurodevelopmental outcomes at 1 year corrected age (79). For this study, the researchers included a suck maturity index (SMI) to correlate sucking and developmental outcomes. The SMI was a composite score that included number of sucks, mean sucks per burst, and mean maximum pressure across all bursts. The authors found that sucking performance at 40 weeks PMA was significantly correlated to a standardized test of development at 1 year. They concluded that standardized assessment of neonatal sucking could serve as a means of early screening for the risk of developmental delay.

Ongoing modifications of the NSA have been published under the device name Medoff-Cooper Nutritive Sucking Apparatus (M-CNSA) (85). M-CNSA was used to investigate the effectiveness of a multi-sensory intervention on sucking organization of premature infants. The intervention group demonstrated significantly increased number of sucks, sucks per burst and maturity index by Day 7, as compared to premature infants receiving standard of care. The current evolution of the M-CNSA is now marketed under the device name Neonur (86), which houses a unit between a standard bottle and nipple that includes a pressure sensor, a signal processor and an on board flash memory drive. Following collection of sucking performance data, the memory drive data are downloaded to a PC and the data is processed via MATLAB® (MathWorks, Natick, Massachusetts). Sucking parameters recorded include those previously detailed in Bromiker et al. (84).

To better understand the relationship between sucking, swallowing and breathing, Mizuno and Ueda modified bottle nipples, routinely used in the nursery, to measure negative intraoral pressure (80). A silicone tube was inserted inside the nipple and connected to a microsemiconductor pressure transducer (**Figure 7**). Level of milk flow was dependent on the strength of the suction and expression component of the suck. They calculated sucking pressure, frequency, and duration as well as sucking efficiency. At the same time, they measured coordination of swallowing and respiration by recording pharyngeal pressure via an open silicone catheter placed transnasally at the oropharynx and connected to a transducer. Similar to Bromiker et al., they found that for healthy preterm infants, sucking pressure, frequency and duration matured with age. They also reported that the coordination of breathing and swallowing also matures with age.

In 2011, Lang et al. published work using the Orometer [(81); **Figure 7**]. The device they developed included an analytical system for analysis of suck data, the Suck Editor. They demonstrated the feasibility of their approach with a cohort of healthy term infants, confirming the work of others that specific aspects of sucking change with age. The authors concluded that quantitative measures of oral-motor function might serve as a proxy for neurodevelopment. In subsequent investigations using the Orometer and accompanying software, factor analysis of the more than 40 metrics collected by the system, identified seven factors that that best represent feeding skills as measured by the device: suck vigor, endurance, resting, irregularity, frequency, variability, and bursting (87). However, it is not clear the degree to which these specific measures might be sensitive to neurodevelopment.

Tamilia et al. advanced the field significantly by developing quantitative measures of sucking behavior that included indices reflective of motor coordination and control, which are particularly sensitive to neurological issues and overall neurodevelopmental status (88). Chief among these was a measure of movement smoothness. Smoothness is considered a characteristic of coordinated movement (89), and measures

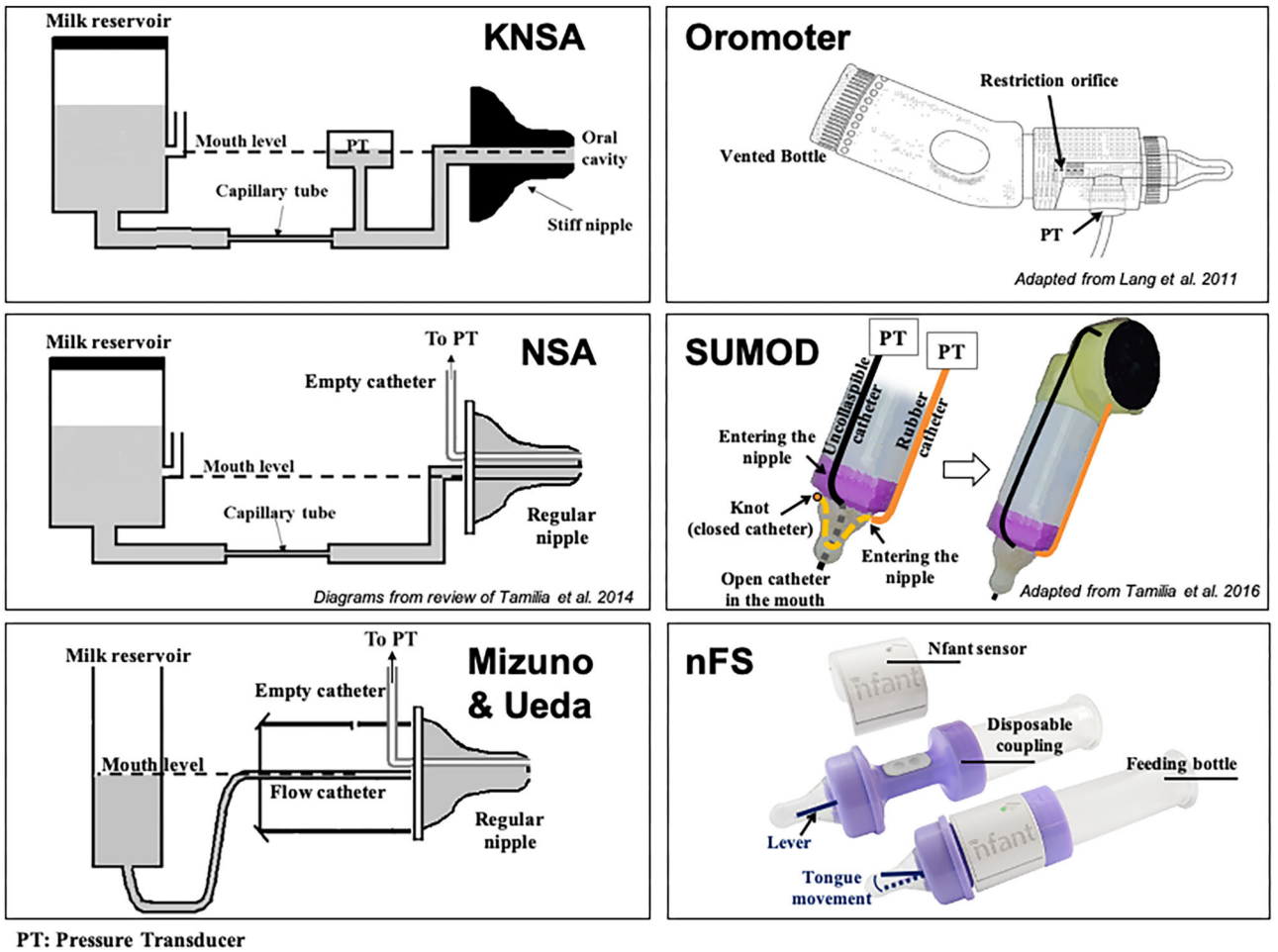

FIGURE 7 | Technological solutions to assess neonatal sucking. Schematic diagrams of some technological solutions used to measure sucking during bottle feeding in infants. **(Left)** Non-portable measuring apparatuses [KNSA (77), NSA (79), and Mizuno-Ueda system (80)]: pressure transducers (PTs) are used to measure sucking pressures exerted on a nipple, which is not connected to a regular feeding bottle, but to a reservoir containing milk via a flow-regulating capillary tube or regular catheter. The milk reservoir is always kept at the mouth level to eliminate net hydrostatic pressure (unlike in regular bottle-feeding sessions). Regular nipples were used in NSA and Mizuno & Ueda's systems, while a stiff nipple was used in KNSA. **(Right)** Portable measuring solutions: feeding bottles instrumented with pressure transducers (PTs) to measure different sucking pressures [Orometer (81) and SuMOD (82): via air-filled catheters] or tongue movement (nFS; via a lever). These solutions were designed to be attached to regular bottles for easy use in clinical settings. Orometer measures the suction component of sucking; nFS measures tongue movement (related to the expression component); while SuMOD measures suction and expression components separately (enabling coordination assessment). nFS is a wireless solution, while Orometer and SuMOD require wired connection to an acquisition system.

of smoothness have been used to quantify motor learning, development, and recovery in the reaching movements of healthy individuals, persons diagnosed with Parkinson's disease, and individuals post-stroke among others (90, 91). Smoothness is derived from the speed profile of a movement (88). Uncoordinated, immature movement is characterized by intermittent acceleration and deceleration—or multiple submovements—on the way to a target, therefore, the more intermittent accelerations and decelerations, the more "unsmooth" the movement (91). As with other cyclic and oscillating movements, Tamilia et al. emphasized the importance of analyzing and reporting the coefficient of variability of sucking parameters, rather than just the mean, since variability serves as a correlate of the organization and maturation of a motor skill (82). They also introduced novel measures to quantify the coordination between suction and expression movements by using a dynamic system approach, which allows investigation into the emergence of coordination patterns during infancy, and they showed how these measures may help characterize the feeding behavior of infants at risk for later neurodevelopmental delays. To measure both suction and expression, Tamilia et al. developed and used a portable sucking monitoring device (SuMOD), which was designed to be easily integrated on to any regular feeding bottle (**Figure 7**). Along with the device,

they developed an analytical automated system for the data analysis (82).

Capilouto et al. reported the use of sonomicrometry to measure the resultant compressive forces applied to the nipple during non-nutritive and nutritive sucking (92). Their work represented a shift from measurement of intraoral pressures to a focus on the role of the lingual musculature in driving safe and efficient feeding. The approach was grounded in animal models of tongue muscle disuse atrophy that documented multiple changes in rat tongue musculature between dam reared rat pups and intravenously fed (IV) rat pups from the same litter (93–96). Following sacrifice and excision of tongue muscle the IV fed group was found to have significantly fewer tongue muscle fibers, smaller fibers, and fewer motoneurons driving the muscle. The researchers concluded that same thing might be happening with infants non-orally fed for an extended period of time; such as preterm or sick term infants.

To test their aims, Capilouto et al. instrumented a standard pacifier and a flow through nipple with piezoelectric crystals strategically located to enable direct measurement of nipple deformation kinematics in response to forces of the tongue. After controlling for weight and PMA, they found significant differences in tongue force during NS and clinically significant differences in posterior tongue thickness between full term and preterm infants beginning to feed. Full term infants demonstrated greater tongue force and greater posterior tongue thickness as compared to healthy preterm infants (92, 97).

The use of sonomicrometry to examine sucking performance presented a number of challenges including the cumbersome nature of the computer equipment required to collect the data which required multiple people at bedside. The unsustainability of this approach took the team back into the lab to consider alternative ways to measure tongue movement on the nipple. The result was nfant® Feeding Solution (nFS; NFANT Labs, Marietta GA, USA) (**Figure 7**), a non-invasive device for quantifying neonatal and infant sucking performance cleared by the FDA for use in the NICU. nFS consists of a disposable nfant coupling that connects a standard bottle to a standard nipple. The coupling houses a cantilever mechanism for measuring tongue movement on the nipple. The nfant SSB Sensor connects to the coupling and wirelessly transmits real-time data on nipple movement to a tablet via the nfant Mobile App. nFS addresses a significant limitation of other devices as the real-time feedback of sucking performance allows the healthcare team to see the immediate impact of an intervention to improve feeding (98). Following a feeding, waveforms of NNS and NS nipple movement are transmitted to the HIPAA protected nfant Cloud Database and the signals converted via custom algorithms, to identify key features and measures that describe sucking performance.

Recently, Capilouto et al. compared objective metrics of nutritive sucking performance via nFS between preterm and full term infants at discharge (99). They found that suck frequency accounted for 28% of the variance in feeding-related length of stay (FRLOS) for preterm infants, while suck smoothness accounted for 34% of the variance in FRLOS for full term infants. The researchers concluded that suck frequency may be an important intervention target to consider for preterm infants having difficulty transitioning to full oral feeding. They concluded further, that suck smoothness might be a sensitive marker for identifying infants at risk for feeding difficulties. The utility of nFS for quantifying sucking performance pre- and post-intervention has also been demonstrated (100).

SUCKING ACTIVITY IN INFANTS WITH BRAIN INJURY

The location in the brain stem of the CPG that controls sucking and swallowing corroborates studies that have found brain stem injury results in feeding difficulties. Quattrocchi et al. found a strong association between infratentorial, specifically brain stem, lesions on MRI and a diagnosis of oral motor dysfunction in infants with a hypoxic-ischemic injury (101). Because sucking and swallowing is a highly organized process that requires several different areas of the brain, injuries in other areas result in feeding problems as well. Martinez-Biarge found an association between basal ganglia and thalamic (BGT) and mesencephalic injuries with feeding impairment. Infants with severe BGT and mesencephalic injuries had an 84% probability of having a feeding impairment and severe BGT injury with pontine involvement had a 91% probability of getting a gastrostomy or having a nasogastric tube for at least 6 months (102).

Some longer-term studies have found a relationship between feeding performance and better neurodevelopmental outcomes. Mizuno and Ueda found a significant correlation between improved NS patterns over two examinations performed 2 weeks apart and better neurodevelopmental outcome at 18 months of age (103). Medoff-Cooper et al. measured NS parameters at 34 and 40 weeks PMA and found a positive correlation between a more mature pattern and a better BSID-II score (both MDI and PDI subscales) at 12 months of age (79). These evaluations of feedings were over a short period, demonstrating not only the rapid ability of an infant to learn to feed which speaks to neuroplasticity, but it also implies there may be a very short window of opportunity to improve outcomes for infants.

Tamilia et al. demonstrated a correlation between microstructural abnormalities in the brain measured by MRI/DTI and sucking pattern variations. Specifically, motor tracts with poor integrity correlated with sucking patterns of lower smoothness and increased irregularity (31). This pilot study demonstrates the potential to identify brain injury through the analysis of nutritive sucking. Tamilia et al. used nFS to investigate the relationship between nutritive sucking and microstructural brain abnormalities (31). Using the accelerometer data captured via nFS, active feeding was analyzed using in-house software developed in MATLAB (82). Results indicated that specific sucking parameters were correlated with microstructural integrity of the sensorimotor tracts that control neonatal oral feeding (**Figure 8**). Specifically, low smoothness values as well as high sucking irregularity and low smoothness variability were associated with reduced microstructural

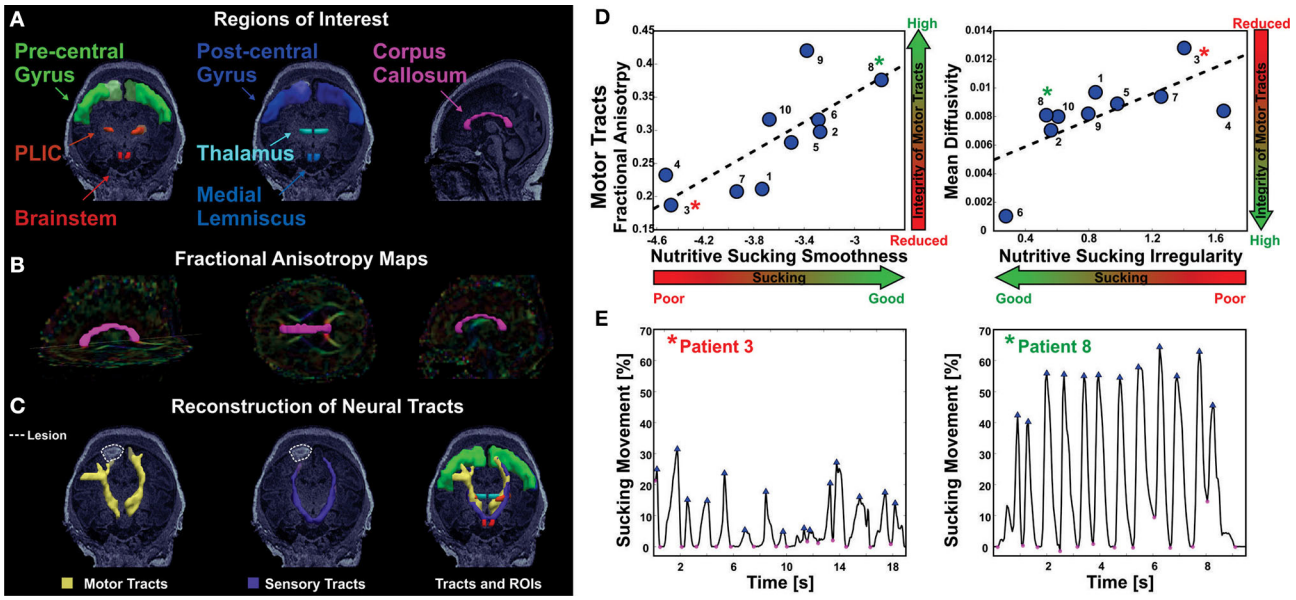

FIGURE 8 | Correlation of abnormal NS patterns with integrity of sensorimotor fibers in infants with established in infants with established brain injury [from Tamilia et al. (31)]. **(A)** Anatomically defined regions of interest overlaid on the T1 MRI of a female 4 day old preterm infant. On the left, regions of interest for the motor tracts; in the middle, regions of interest for the sensory tracts; on the right, regions of interest corresponding to the corpus callosum. **(B)** Corpus callosum (magenta) overlaid on the fractional anisotropy color-maps. **(C)** Axial view of the motor (in yellow) and sensory (in purple) tracts reconstructed via probabilistic diffusion imaging tractography, along with the regions of interest used for their delineation. Neural tracts and regions of interest are overlaid on the patient's MRI that shows ischemic injury in the right frontal lobe. **(D)** The values of nutritive sucking smoothness and irregularity are predictive of the fractional anisotropy and mean diffusivity values, respectively, for the motor tracts. High smoothness in the nutritive sucking pattern, which is indicative of good sucking skills, is associated with high-fractional anisotropy, which is indicative of intact neural tracts. High irregularity in nutritive sucking, which is indicative of poor sucking skills, is associated with high-mean diffusivity, which is indicative of low integrity of neural tracts. **(E)** Two bursts of nutritive sucking from patients 3* and 8*. The left waveform demonstrates a poor NS behavior of patient 3* characterized by low smoothness and high irregularity (i.e., presence of multiple peaks); while the right waveform demonstrates a good NS behavior of patient 8* characterized by the smooth and regular nutritive sucking pattern.

integrity. Researchers concluded that quantitative assessment of sucking at the bedside could potentially result in earlier diagnosis of diffuse white matter brain injuries. Identifying brain abnormalities while in the NICU could serve to inform NICU care and take advantage of neural plasticity when the benefits would be greatest.

THERAPIES

Infants that are unable to feed orally are deprived of the pleasurable oral sensation, instead they experience unpleasant sensations of a nasal-gastric tube, suctioning to prevent aspiration and/or tracheal intubation which makes them resistant, and even defensive, to oral feeding (58). Along with the motor restrictions this causes, the sensory inputs are detrimental to their oromotor development (14). It is vital to train infants to suck in order to feed orally and these are some examples of therapies applied: (i) *Kinesthetic:* a passive range of motion movement of the arms and/or legs during NNS. (ii) *Visual stimulation:* eye to eye contact during sucking. (iii) *Vestibular:* gentle horizontal rocking during sucking. (iv) *Auditory reinforcement*: an adapted pacifier is used to play soothing music (Pacifier Activated Lullaby, or PAL) or the mother's voice when the NNS reaches a threshold strength. The threshold can be increased as the infant gets stronger to further encourage development of a NNS (104). (v) *Sensorimotor stimulation*: A broad term that describes several techniques that can be used in various combinations to stimulate and/or reinforce an infant's suck. These techniques fall into one of three categories, oral/intraoral (O/IO), perioral (PO), or extraoral inputs and can vary between training times of 3–30 min, 2–4 times per day, for 10–14 days. O/IO includes gum and tongue stimuli ranging from a therapist's finger to a pulsating pacifier, PO consists of stroking or stimulating an infant's cheeks and/or lips, and extraoral entails tactile input to the head, neck, trunk, and/or limbs (54, 104). (vi) *Oral support*: The act of supporting the cheeks and chin during feeding. A novel example of this is using Kinesio Tape to apply a small force to a muscle by connecting the insertion and origin points to facilitate proper movement for sucking (105). (vii) *Swallowing program*: Placing a liquid bolus (either with a controlled flow nipple, a dropper or the like) on the tongue to stimulate a swallow response to encourage NS.

These therapies may be used in combination or sequentially to work toward the more advanced NS techniques. Fucile et al. found that oral (O) therapy for 15 minutes twice a day resulted in more mature sucking stages in both suction and expression components. However, tactile/kinesthetic (T/K) therapy of the same frequency and duration, did not improve sucking stages

but did improve the swallow-respiration pattern by decreasing apnea-inducing pauses and increasing the safer, more adult-like, intra-expiration swallow pattern. Interestingly, combining O and T/K did not result in compounding effects probably because the frequency and duration of therapy did not change, only the type of therapy, therefore, the combination therapy preterm infants received half the amount of O and T/K therapies as their single-therapy counterparts (54). It appears that NNS training alone does not have a significant effect on primary outcomes of sucking measures, which may have consequences later in life such as speech and developmental delay (104). However, it does result in clinically significant secondary outcomes of reduced hospital stay, transition from tube to bottle, and improved feeding performance (increased milk volume) (106–109).

A commercially available "pulsating" pacifier used for training an infant to non-nutritively suck, the NTrainer, has been shown to be effective (110, 111). The logic behind the device is to stimulate the nerves involved in NNS and, thus, the CPG, in order to form a functional, effective NNS pathway using the principle "neurons that fire together, will wire together." This therapy is effective in increasing the rates of NNS bursts, cycles, cycles per burst resulting in more daily oral feeds (110, 111). With the NTrainer, preterm infants showed an accelerated time to oral feed and time to discharge when it was used for 20 minutes up to four times per day until full oral feeding (112); however, in longer term follow up, NTrainer therapy did not result in improvement in cognition, language or motor skills (113). While NNS does accelerate the development of preterm infants while in the NICU, it does not appear to have any long term lasting effects on further brain development.

FUTURE DIRECTIONS

Development of the field of brain neuroimaging in correlation with sucking patterns needs further confirmation and advancement. The quantitative study of sucking in many abnormal conditions could provide valuable insights to advance our knowledge as well as inform therapies. For instance, oligohydramnios or esophageal atresia that may prevent a fetus from swallowing *in utero*; what affect does this have on their NS and NNS ability as neonates. Are their effective therapies and why are they effective or not within the context of what we know about the development of sucking. This would also apply to the study of the sucking activity of neonates and infants with other conditions, such as Prader-Willi, Down syndrome or Spinal Muscular Atrophy (SMA), to name a few.

Bromiker et al. compared nutritive sucking parameters in Israeli and American preterm infants and found American infants had more mature NS patterns (more sucks, a higher rate of sucks, more sucks per burst, and a shorter interburst width) at 34 weeks PMA which the authors attributed to oral feedings being initiated on average almost 2 weeks sooner (84). This supports the notion that oral feeding training should begin very early, while the infant is still in the NICU. The concept of using different imaging modalities such as magnetoencephalography (MEG) or high-density electroencephalography (HD-EEG) to identify brain abnormalities that might be missed using more routine imaging such as cranial ultrasound and MRI should be explored. The passive techniques of HD-EEG and MEG are safe and effective and may show promise in this fragile population.

There are currently animal studies that are using positron emission tomography (PET) imaging to localize metabolically deficient areas of the brain caused by neuroinflammation, hypoxic-ischemic encephalopathy (HIE), and endotoxin exposure (114–116). The drawback with PET is the radioactive isotope exposure, however, these studies have had exposures 8–12x less than a CT scan. A potential expansion of the use of PET, which could complement MRI data, could be in neonates with brain injury. There is currently no data correlating PET and sucking activity in neonates leaving this a large potential area for exploration.

A recent study by Badran et al. shows promise in using non-invasive vagus nerve stimulation (VNS) that targets the auricular branch, transcutaneous auricular VNS, or taVNS. Fifty-seven percent of the infants in their study that had previously failed oral feeding therapies attained full oral feeds after an average of 16 days of taVNS treatment (117). The idea that VNS along with motor activity can stimulate neuroplasticity, improve motor function, facilitate neurogenesis and reorganization as well as restoring brain function in both human and animal studies, makes this a promising line of inquiry.

Another major area requiring development is in training a neonate to suck correctly, using *both* expression/compression and suction. Feeding training in NICUs currently focuses on secondary outcomes; weight gain, hospital discharge time, etc., with little regard for the primary ability to use both suction and expression/compression in a rhythmic fashion for a mature NS pattern. The next step beyond this would be exploring whether the proper NS pattern aids in repairing the brain injury, or at least re-wire the circuitry around the damage. Neuroplasticity in infants is also still being elucidated, perhaps this advancement could lend insight there as well. Inconsistent results for developmental scales and the like may also improve with a focus on primary measures of NS.

CONCLUSION

The idea of a brain injury affecting the oral feeding of an infant has been around for decades. The flip side of that idea, the notion that we can identify a brain injury through analysis of how an infant sucks, could be instrumental in the identification of neonates in need of therapies and habilitation. Being able to do this very early in life, before any conventional scales or testing can be performed and even at the bedside while the neonate is still in the NICU, could take full advantage of neuroplasticity in early infancy and potentially guide clinicians in the repair of brain injury.

The window for training an infant to suck with a mature NS pattern is likely short, a few weeks, most of which could be done while still in the NICU. This concept of early oral feeding

training could likely greatly diminish or even eliminate the need for ongoing therapy and compliance after discharge home. Only time will tell if a mature NS pattern will lead to better long term neurocognitive, speech, and developmental outcomes for infants with brain injury; however, having an infant that can orally feed efficiently would be a great step forward to ease the stress on families taking their infant home.

AUTHOR CONTRIBUTIONS

SS contributed writing content and creating figures. GC, DR, and YJ contributed writing and editing content. ET and CP contributed writing, editing content, and creating figures. All authors contributed to the article and approved the submitted version.

REFERENCES

1. Woolridge M. The 'Anatomy' of infant sucking. *Midwifery*. (1986) 2:164–71. doi: 10.1016/S0266-6138(86)80041-9
2. Waller HK. A reflex governing the outflow of milk from the breast. *Lancet*. (1943) 241:69–72. doi: 10.1016/S0140-6736(00)89101-1
3. Wolff P. The serial organization of sucking in the young infant. *Pediatrics*. (1968) 42:943–56.
4. Yarrow LJ. The relationship between nutritive sucking experiences in infancy and non-nutritive sucking in childhood. *J Genet Psychol*. (1954) 84:149–62. doi: 10.1080/08856559.1954.10533672
5. Kron RE. Instrumental conditioning of nutritive sucking behavior in the newborn. In: Wortis J, editors. *Recent Advances in Biological Psychiatry, Vol. 9*. Boston, MA: Springer (1967). p. 295–300. doi: 10.1007/978-1-4684-8228-7_22
6. Sameroff A. The components of sucking in the human newborn. *J Exp Child Psychol*. (1968) 6:607–23. doi: 10.1016/0022-0965(68)90106-9
7. Ardran GM, Kemp FH, Lind JA. A cineradiographic study of bottle feeding. *Br J Radiol*. (1958) 31:11–22. doi: 10.1259/0007-1285-31-361-11
8. Colley JRT, Creamer B. Sucking swallowing in infants. *Br Med J*. (1958) 2:422–23. doi: 10.1136/bmj.2.5093.422
9. Raisman G. Neuronal plasticity in the septal nuclei of the adult rat. *Brain Res*. (1969) 14:25–48. doi: 10.1016/0006-8993(69)90029-8
10. Goldman P. Functional development of the prefrontal cortex in early life and the problem of neuronal plasticity. *Exp Neurol*. (1971) 32:366–87. doi: 10.1016/0014-4886(71)90005-7
11. Badr LK, Garg M, Kamath M. Interventions for infants with brain injury: results of a randomized controlled study. *Infant Behav Dev*. (2006) 29:80–90. doi: 10.1016/j.infbeh.2005.08.003
12. Blanchard I. Better feeding can mean better speaking. *Am J Nurs*. (1963) 63:94–5. doi: 10.1097/00000446-196363110-00018
13. Harding R. Function of the larynx in the fetus and newborn. *Ann Rev Physiol*. (1984) 46:645–59. doi: 10.1146/annurev.ph.46.030184.003241
14. Poore M, Barlow S. Suck predicts neuromotor integrity and developmental outcomes. *Perspect Speech Sci Orofacial Disord*. (2009) 19:44–51. doi: 10.1044/ssod19.1.44
15. Maynard T, Zohn I, Moody S, LaMantia A. Suckling, feeding, swallowing: behaviors. circuits, and targets for neurodevelopmental pathology. *Annu Rev Neurosci*. (2020) 43:315–35. doi: 10.1146/annurev-neuro-100419-100636
16. LaMantia A, Moody SA, Maynard T, Karpinski B, Zohn I, Mendelowitz D, et al. Hard to swallow: developmental biological insights into pediatric dysphagia. *Dev Biol*. (2016) 409:329–42. doi: 10.1016/j.ydbio.2015.09.024
17. Nelson MN, White-Traut RC, Vasan U, Silvestri J, Comiskey E, Meleedy-Rey P, et al. One-year outcome of auditory-tactile-visual-vestibular intervention in the neonatal intensive care unit: effects of severe prematurity and central nervous system injury. *J Child Neurol*. (2001) 16:493–8. doi: 10.2310/7010.2001.17044
18. Piper MC, Kunos VI, Willis DM, Mazer BL, Ramsay M, Silver KM. Early physical therapy effecdts onthe high-risk infant: a randomized controlled trial. *Pediatrics*. (1986) 78:216–24.
19. Kanda T, Pidcock FS, Hayakawa K, Yamori Y, Shikata Y. Motor outcome differences between two groups of children with spastic diplegia who received different intensities of early onset physiotherapy followed for. 5 years. *Brain Dev*. (2004) 26:118–26. doi: 10.1016/S0387-7604(03)00111-6
20. Liberty K. Developmental gains in early intervention based on conductive education by young children with motor disorders. *Int J Rehabil Res*. (2004) 27:17–25. doi: 10.1097/00004356-200403000-00003
21. Trahan J, Malouin F. Intermittent intensive physiotherapy in children with cerebral palsy: a pilot study. *Dev Med Child Neurol*. (2002) 14:233–9.
22. Ibrahim J, Mir I, Chalak L. Brain imaging in preterm infants <32 weeks gestation: a clinical review and algorithm for the use of cranial ultrasound and qualitative brain MRI. *Pediatr Res*. (2018) 84:799–806. doi: 10.1038/s41390-018-0194-6
23. Hinojosa-Rodriguez M, Harmony T, Carrillo-Prado C, Van Horn JD, Irimia A, Torgerson C, et al. Clinical neuroimaging in the preterm infant: diagnosis and prognosis. *Neuroimage Clin*. (2017) 16:355–68. doi: 10.1016/j.nicl.2017.08.015
24. Van't Hooft J, van der Lee JH, Opmeer BC, Aarnoudse-Moens CS, Leenders AG, Mol BW, et al. Predicting developmental outcomes in premature infants by term equivalent MRI: systematic review and meta-analysis. *Syst Rev*. (2015) 4:71. doi: 10.1186/s13643-015-0058-7
25. Blauw-Hospers CH, Hadders-Algra M. A systematic review of the effects of early intervention on motor development. *Dev Med Child Neurol*. (2005) 47:421–32. doi: 10.1017/S0012162205000824
26. Fiori S, Guzzetta A. Plasticity following early-life brain injury: insights from quantitative MRI. *Semin Perinatol*. (2015) 39:141–6. doi: 10.1053/j.semperi.2015.01.007
27. Cioni G, D'Acunto G, Guzzetta A. Perinatal brain damage in children: neuroplasticity, early intervention, and molecular mechanisms of recovery. *Prog Brain Res*. (2011) 189:139–54. doi: 10.1016/B978-0-444-53884-0.00022-1
28. Tillema, J.-M., Byars AW, Jacola LM, Schapiro MB, Schmithorst VJ, et al. Cortical reorganization of language functioning following perinatal left MCA stroke. *Brain Lang*. (2008) 105:99–111. doi: 10.1016/j.bandl.2007.07.127
29. Thickbroom GW, Byrnes ML, Archer SA, Nagarajan L, Mastaglia FL. Differences in sensory and motor cortical organization following brain injury early in life. *Ann Neurol*. (2001) 49:320–7. doi: 10.1002/ana.68
30. Staudt M, Braun C, Gerloff C, Erb M, Grodd W, Krageloh-Mann I. Developing somatosensory projections bypass periventricular brain lesions. *Neurology*. (2006) 67:522–5. doi: 10.1212/01.wnl.0000227937.49151.fd
31. Tamilia E, Parker MS, Rocchi M, Taffoni F, Hansen A, Grant PE, et al. Nutritive sucking abnormalities and brain microstructural abnormalities in infants with established brain injury: a pilot study. *J Perinatol*. (2019) 39:1498–508. doi: 10.1038/s41372-019-0479-6
32. Back SA. White matter injury in the preterm infant: pathology and mechanisms. *Acta Neuropathol*. (2017) 134:331–49. doi: 10.1007/s00401-017-1718-6
33. Rocha-Ferreira E, Hristova M. Plasticity in the neonatal brain following hypoxic-ischaemic injury. *Neural Plast*. (2016) 2016:4901014. doi: 10.1155/2016/4901014
34. Niimi Y, Levison SW. Pediatric brain repair from endogenous neural stem cells of the subventricular zone. *Rediatr Res*. (2018) 83:385–96. doi: 10.1038/pr.2017.261
35. Novak I, Morgan C. High-risk follow-up: early intervention and rehabilitation. In: Linda de Vries S, Hannah Glass C, editors. *Handbook of Clinical Neurology, Vol. 162*. Cambridge, MA: Elsevier (2019). p. 483–510. doi: 10.1016/B978-0-444-64029-1.00023-0
36. Wintermark P. Injury and repair in perinatal brain injury: insights from non-invasive MR perfusion imaging. *Semin Perinatol*. (2015) 39:124–9. doi: 10.1053/j.semperi.2015.01.005
37. Lau C. Development of suck and swallow mechanisms in infants. *Ann Nutr Metab*. (2015) 66:7–14. doi: 10.1159/000381361
38. Hafstrom M, Lundquist C, Lindecrantz K, Larsson K, Kjellmer I. Recording non-nutritive sucking in the neonate. *description of an*

automatized system for analysis. Acta Paediatr. (1997) 86:82–90. doi: 10.1111/j.1651-2227.1997.tb08838.x
39. Hafstrom M, Kjellmer I. Non-nutritive sucking in the healthy pre-term infant. *Early Hum Dev.* (2000) 60:13–24. doi: 10.1016/S0378-3782(00)00091-8
40. Mizuno K, Ueda A. Changes in sucking performance from nonnutritive sucking to nutritive sucking during breast- and bottle-feeding. *Pediatr Res.* (2006) 59:728–31. doi: 10.1203/01.pdr.0000214993.82214.1c
41. Zimmerman E, Barlow SM. Pacifier stiffness alters the dynamics of the suck central pattern generator. *J Neonatal Nurs.* (2008) 14:79–86. doi: 10.1016/j.jnn.2007.12.013
42. Zimmerman E, Forlano J, Gouldstone A. Not all pacifiers are created equal: a mechanical examination of pacifiers and their influence on suck patterning. *Am J Speech-Lang Pathol.* (2017) 26:1202–12. doi: 10.1044/2017_AJSLP-16-0226
43. Oder AL, Stalling DL, Barlow SM. Short-term effects of pacifier texture on NNS in neurotypical infants. *Int J Pediatr.* (2013) 26:168459. doi: 10.1155/2013/168459
44. Pickler RH, Reyna BA. Effects of non-nutritive sucking on nutritive sucking, breathing and behavior during bottle feeding of preterm infants. *Adv Neonatal Care.* (2004) 4:226–34. doi: 10.1016/j.adnc.2004.05.005
45. Meier P, Anderson GC. Responses of small preterm infants to bottle- and breast-feeding. *Am J Mater Child Nurs.* (1987) 12:97–105. doi: 10.1097/00005721-198703000-00006
46. Lau C. Interventions to improve oral feeding performance of preterm infants. *Perspect Swallow Swallow Disord.* (2014) 23:23–45. doi: 10.1044/sasd23.1.23
47. Lau C. Development of infant oral feeding skills: what do we know? *Am J Clin Nutr.* (2016) 103:616S–21. doi: 10.3945/ajcn.115.109603
48. Mistry S, Hamdy S. Neural control of feeding and swallowing. *Phys Med Rehabil Clin N Am.* (2008) 19:70–728. doi: 10.1016/j.pmr.2008.05.002
49. Festila D, Ghergie M, Muntean A, Matiz D, Serbanescu A. Suckling and non-nutritive sucking habit: what should we know? *Clujul Med.* (2014) 87:11–4.
50. Tamura Y, Yoko H, Yoshida S. Co-ordination of tongue movements and peri-oral muscle activities during nutritive sucking. *Develop Med Child Neurol.* (1996) 38:503–10. doi: 10.1111/j.1469-8749.1996.tb12111.x
51. Lau C, Alagugurusamy R, Schanler RJ, Smith EO, Shulman RJ. Characterization of the developmental stages of sucking in preterm infants during bottle feeding. *Acta Paediatr.* (2000) 89:846–52. doi: 10.1111/j.1651-2227.2000.tb00393.x
52. Matsuo K, Palmer J. Anatomy and physiology of feeding and swallowing - normal and abnormal. *Phys Med Rehabil Clin N Am.* (2008) 19:691–707. doi: 10.1016/j.pmr.2008.06.001
53. Barlow S. Central pattern generation involved in oral and respiratory control for feeding in the term infant. *Curr Opin Otolaryngol Head Neck Surg.* (2009) 17:187–93. doi: 10.1097/MOO.0b013e32832b312a
54. Fucile S, McFarland DH, Gisel EG, Lau C. Oral and nonoral sensorimotor interventions facilitate suck-swallow-respiration functions and their coordination in preterm infants. *Early Hum Dev.* (2012) 88:345–50. doi: 10.1016/j.earlhumdev.2011.09.007
55. Macias MER, Meneses GJS. Physiology of nutritive sucking in newborns and infants. *Bol Med Hosp Infant Mex.* (2011) 68:296–303.
56. Mizuno K, Ueda A, Takeuchi T. Effects of different fluids on the relationship between swallowing and breathing during nutritive sucking in neonates. *Biol Neonate.* (2002) 81:45–50. doi: 10.1159/000047183
57. Kelly BN, Huckabee M C,Frampton MA, Jones RD. Arousal has no effect on non-nutritive breathing-swallowing coordination during the first year of human life. *Int J Devl Neurosci.* (2008) 26:385–90. doi: 10.1016/j.ijdevneu.2008.03.006
58. Stevenson RD, Allaire JH. The development of normal feeding and swallowing. *Pediatric Clin North Am.* (1991) 38:1439–53. doi: 10.1016/S0031-3955(16)38229-3
59. Hockman CH, Bieger D, Weerasuriya A. Supranuclear pathways of swallowing. *Prog Neurobiol.* (1979) 12:15–32. doi: 10.1016/0301-0082(79)90009-1
60. Diamant NE. Firing up the swallowing mechanism. *Nat Med.* (1996) 2:1190–1. doi: 10.1038/nm1196-1190
61. Li-Jessen NYK, Ridgway C. Chapter 3: Neuroanatomy of voice and swallowing. In: Weissbrod P, Francis D, editors. *Neurologic and Neurodegenerative Diseases of the Larynx.* Cham: Springer International Publishing (2020). p. 21–40.
62. Cunha M, Barreiros J, Gonclaves I, Figueiredo H. Nutritive sucking pattern-from very low birth weight preterm to term newborn. *Early Hum Dev.* (2009) 85:125–30. doi: 10.1016/j.earlhumdev.2008.07.003
63. Bertoncelli N, Cuomo G, Cattani S, Mazzi C, Pugliese M, Coccolini E, et al. Oral feeding competences of healthy preterm infants: a review. *Int J Pediatrics.* (2012) 2012:896257. doi: 10.1155/2012/896257
64. Medoff-Cooper B. Nutritive sucking research: from clinical questions to research answers. *J Perinat Neonat Nurs.* (2005) 19:265–72. doi: 10.1097/00005237-200507000-00013
65. Mizuno K, Ueda A. Development of sucking behavior in infants who have not been fed for. 2 months after birth. *Pediatr Int.* (2001) 43:251–5. doi: 10.1046/j.1442-200x.2001.01388.x
66. Jain L, Sivieri E, Abbasi S, Bhutani V. Energetics and mechanics of nutritive sucking in the preterm and term neonate. *J Pediatr.* (1987) 111:894–8. doi: 10.1016/S0022-3476(87)80213-5
67. Rommel N, Van Wijk M, Boets B, Hebbard G, Haslam R, Davidson G, et al. Development of pharyngo-esophageal physiology during swallowing inthe preterm infant. *Neurogastroenterol Motil.* (2011) 23:401–8. doi: 10.1111/j.1365-2982.2011.01763.x
68. McCain GC. An evidence-based guideline for introducing oral feeding to healthy preterm infants. *Neonatal Netw.* (2003) 22:45–50. doi: 10.1891/0730-0832.22.5.45
69. Pineda R, Dewey K, Jacobsen A, Smith J. Non-nutritive sucking in the preterm infant. *Am J Perinatol.* (2018) 36:268–76. doi: 10.1055/s-0038-1667289
70. Ludwig SM, Waitzman KA. Changing feeding documentation to reflect infant-driven feeding practice. *Newborn Infant Nurs Rev.* (2007) 7:155–60. doi: 10.1053/j.nainr.2007.06.007
71. Zhang X, Xhou M, Yin H, Dai Y, Li Y. The predictive value of early oral motor assessments for neurodevelopmental outcomes of moderately and late preterm infants. *Medicine.* (2017) 96:50. doi: 10.1097/MD.0000000000009207
72. Braun MA, Palmer MM. A pilot study of oral-motor dysfunction in at-risk infants. *Phys Occup Ther Pediatr.* (1985) 5:13–26. doi: 10.1080/J006v05n04_02
73. Palmer MM, Crawley K, Blanco IA. Neonatal oral-motor assessment scale: a reliability study. *J Perinatol.* (1993) 13:28–35.
74. Zarem C, Kidokoro H, Neil J, Wallendorf M, Inder T. Psychometrics of the neonatal oral motor assessment scale. *Dev Med Child Neurol.* (2013) 55:1115–20. doi: 10.1111/dmcn.12202
75. Nieuwenhuis T, da Costa S, Bilderbeek E, Geven WC, van der Schans, Bos A. Uncoordinated sucking patterns in preterm infants are associated with abnormal general movements. *J Pediatr.* (2012) 161:792–8. doi: 10.1016/j.jpeds.2012.04.032
76. Palmer MM, Heyman MB. Developmental outcome for neonates with dysfunctional and disorganized sucking patterns: preliminary findings. *Infant-Toddler Intervent Transdiscipl J.* (1999) 299–308.
77. Kron RE, Stein M, Goddard KE. A method of measuring sucking behavior of newborn infants. *Psychosom Med.* (1963) 25:181–91. doi: 10.1097/00006842-196303000-00010
78. Tamilia E, Taffoni F, Formica D, Ricci L, Schena E, Keller F, et al. Technological solutions and main indices for the assessment of newborns' nutritive sucking: a review. *Sensors.* (2014) 14:634–58. doi: 10.3390/s140100634
79. Medoff-Cooper B, Shults J, Kaplan J. Sucking behavior of preterm neonates as a predictor of developmental outcomes. *J Dev Behav Pediatr.* (2009) 30:16–22. doi: 10.1097/DBP.0b013e318196b0a8
80. Mizuno K, Ueda A. The maturation and coordination of sucking, swallowing, and respiration in preterm infants. *J Pediatr.* (2003) 142:36–40. doi: 10.1067/mpd.2003.mpd0312
81. Lang WC N, Buist RM, Geary A, Buckley S, Adams E, et al. Quantification of intraoral pressures during nutritive sucking: methods with normal infants. *Dysphagia.* (2010) 26:277–86. doi: 10.1007/s00455-010-9305-1

82. Tamilia E, Formica D, Scaini A, Taffoni F. An automated system for the analysis of newborns' oral-motor behavior. *IEEE Trans Neurol Syst Rehabil Eng.* (2016) 24:1294–303. doi: 10.1109/TNSRE.2015.2496150
83. Medoff-Cooper B, Bilker WB, Kaplan JM. Suckling behavior as a function of gestational age: a cross-sectional study. *Infant Behav Dev.* (2001) 24:83–94. doi: 10.1016/S0163-6383(01)00063-7
84. Bromiker R, Arad I, Loughran B, Netzer D, Kaplan M, Medoff-Cooper B. Comparison of sucking patterns at introduction of oral feeding and at term in Israeli and American preterm infants. *Acta Paediatr.* (2005) 94:201–4. doi: 10.1111/j.1651-2227.2005.tb01891.x
85. Medoff-Cooper B, Rankin K, Li Z, Liu L, White-Traut R. Multisensory intervention for preterm infants improves sucking organization. *Adv Neonatal Care.* (2015) 15:142–9. doi: 10.1097/ANC.0000000000000166
86. Bromiker R, Medoff-Cooper B, Flor-Hirsch H, Kaplan M. Influence of hyperbilirubinemia on neonatal sucking. *Early Hum Dev.* (2016) 99:53–6. doi: 10.1016/j.earlhumdev.2016.04.008
87. Scherman A, Wiedrick J, Lang WC, Rdesinski RE, Lapidus J, McEvoy C, et al. Quantification of nutritive sucking among preterm and full-term infants. *Res Rep Neonatol.* (2018) 8:53–63. doi: 10.2147/RRN.S165421
88. Tamilia E, Delafield J, Fiore S, Taffoni F. An automated system for the assessment of nutritive sucking behavior in infants: a preliminary analysis on term neonates. In: *Conference Proceedings of the Annual International Conference of the IEEE Engineering in Medicine and Biology Society.* (2014). p. 5752–5.
89. Rohrer B, Fasoli S, Krebs HI, Hughes R, Volpe B, Frontera WR, et al. Movement smoothness changes during stroke recovery. *J Neurosci.* (2002) 22:8297–304. doi: 10.1523/JNEUROSCI.22-18-08297.2002
90. Balasubramanian S, Melendez-Calderon A, Burdet E. A robust and sensitive metric for quantifying movement smoothness. *IEEE Trans Biomed Eng.* (2012) 59:2126–36. doi: 10.1109/TBME.2011.2179545
91. Balasubramanian S, Melendez-Calderon A, Roby-Brami A, Burdet E. On the analysis of movement smoothness. *J Neuroeng Rehabil.* (2015) 12. doi: 10.1186/s12984-015-0090-9
92. Capilouto GJ, Cunningham TC, Frederick E, Dupont-Versteegden E, Desai N, Butterfield TA. Comparison of tongue muscle characteristics of preterm and full term infants during nutritive and nonnutritive sucking. *Infant Behav Dev.* (2014) 37:435–45. doi: 10.1016/j.infbeh.2014.05.010
93. Kinirons SA, Shall MS, McClung JR, Goldberg SJ. Effect of artificial rearing on the contractile properties and myosin heavy chain isoforms of developing rat tongue musculature. *J Neurophysiol.* (2003) 90:120–7. doi: 10.1152/jn.00809.2002
94. McClung JR, Goldberg SJ. Functional anatomy of the hypoglossal innervated muscles of the rat tongue: a model for elongation and protrusion of the mammalian tongue. *Anatom Rec.* (2000) 260:378–86. doi: 10.1002/1097-0185(20001201)260:4<378::AID-AR70>3.0.CO;2-A
95. Moore WA, Goldberg SJ, Shall MS. Effects of artificial rearing on contractile properties of genioglossus muscle in Sprague-Dawley rat. *Arch Oral Biol.* (2007) 52:133–41. doi: 10.1016/j.archoralbio.2006.09.004
96. Smith JC, McClung JR, Goldberg SJ. Effects of. 12 days of artificial rearing on morphology of hypoglossal motoneurons innervating tongue retrusors in rat. *Anat Rec A Discov Mol Cell Evol Biol.* (2006) 288A:280–5. doi: 10.1002/ar.a.20277
97. Capilouto GJ, Frederick E, Challa H. Measurement of infant tongue thickness using ultrasound: a technical note. *J Clin Ultrasound.* (2012) 40:364–7. doi: 10.1002/jcu.21933
98. Azuma D, Maron JL. Individualizing oral feeding assessment and therapies in the newborn. *Res Rep Neonatol.* (2020) 10:23–30. doi: 10.2147/RRN.S223472
99. Capilouto GJ, Cunningham TJ, Giannone PJ, Grider D. A comparison of the nutritive sucking performance of full term and preterm neonates at hospital discharge: a prospective study. *Early Hum Dev.* (2019) 134:26–30. doi: 10.1016/j.earlhumdev.2019.05.007
100. Capilouto GJ, Cunningham TJ, Desai N. Quantifying the impact of common feeding intervantions on nutritive sucking performance using a commercially available smart bottle. *J Perinatal Neonatal Nurs.* (2019) 33:331–9. doi: 10.1097/JPN.0000000000000435
101. Quattrocchi CC, Longo D, Delfino LN, Cilio MR, Piersigilli F, Capua MD, et al. Dorsal brain stem syndrome: MR imaging location of brain stem tegmental lesions in neonates with oral motor dysfunction. *Am J Neuroradiol.* (2010) 31:1438–42. doi: 10.3174/ajnr.A2103
102. Martinez-Biarge M, Diez-Sebastian, CJ J, Wusthoff, Lawrence S, Aloysius A, et al. Feeding and communication impairments in infants with central grey matter lesions following perinatal hypoxic-ischemic injury. *Eur J Paediatric Neurol.* (2012) 16:688–96. doi: 10.1016/j.ejpn.2012.05.001
103. Mizuno K, Ueda A. Neonatal feeding performance as a predictor of neurodevelopmental outcome at. 18 months. *Dev Med Child Neurol.* (2005) 47:299–304. doi: 10.1017/s0012162205000587
104. Grassi A, Sgherri G, Chorna O, Marchi V, Gagliardi L, Cecchi F, et al. Early intervention to improve sucking in preterm newborns. *Adv Neonatal Care.* (2018) 19:97–109. doi: 10.1097/ANC.0000000000000543
105. Lin CL, Wu WT, Chang KV, Lin HY, Chou LW. Application of Kinesio taping method for newborn swallowing difficultly. *Medicine.* (2016) 95:31–3. doi: 10.1097/MD.0000000000004458
106. Pinelli J, Symington AJ. Non nutritive sucking for promoting physiologic stability and nutrition in preterm infants. *Cochrane Database Syst Rev.* (2005) CD001071. doi: 10.1002/14651858.CD001071.pub2
107. Gaebler CP, Hanzlik JR. The effects of a prefeeding stimulation program on preterm infants. *Am J Occup Ther.* (1996) 50:184–92. doi: 10.5014/ajot.50.3.184
108. Fucile S, Gisel E, Lau C. Oral stimulation accelerates the transition from tube to oral feeding in preterm infants. *J Pediatr.* (2002) 141:230–6. doi: 10.1067/mpd.2002.125731
109. Tian X, Yi L, Zhang L, Zhou JG, Ma L, Ou YX, et al. Oral motor intervantino improved the oral feeding in preterm infants: evidence based on a meta-analysis with trial sequential analysis. *Medicine.* (2015) 94:e1310. doi: 10.1097/MD.0000000000001310
110. Barlow SM, Finan DS J, Lee, Chu S. Synthetic orocutaneous stimulation entrains preterm infants with feeding difficulties to suck. *J Perinatol.* (2008) 28:541–8. doi: 10.1038/jp.2008.57
111. Poore M, Zimmerman E, Barlow SM, Wang J, Gu F. Patterned orocutaneous therapy improves sucking and oral feeding in preterm infants. *Acta Paediatr.* (2008) 97:920–7. doi: 10.1111/j.1651-2227.2008.00825.x
112. Song D, Jegatheesan P, Nafday S, Ahmad KA, Nedrelow J, Wearden M, et al. Patterned frequency-modulated oral stimulation in preterm infants: a multicenter randomized controlled trial. *PLoS ONE.* (2019) *e*0212675. doi: 10.1371/journal.pone.0212675
113. Loeb DF, Imgrund CM, Lee J, Barlow SM. Preterm neurodevelopmental outcomes following orosensory entrainment intervention. *J Neonatal Nurs.* (2018) 24:203–7. doi: 10.1016/j.jnn.2017.11.001
114. Kannan S, Chugani HT. Applications of positron emission tomography in the newborn nursery. *Semin Perinatol.* (2010) 34:39–45. doi: 10.1053/j.semperi.2009.10.004
115. Kannan S, Balakrishnan B, Muzik O, Romero R, Chugani D. Positron emission tomography imaging of neuroinflammation. *J Child Neurol.* (2009) 24:443–52. doi: 10.1177/0883073809338063
116. Kannan S, Saadani-Makki F, Baladrishnan B, Chakraborty P, Janisse J, Lu X, et al. Magnitude of [(11)C]PK11195 binding is related to severity fo motor deficits in a rabbit model of cerebral palsy induced by intrauterine endotoxin exposure. *Dev Neurosci.* (2011) 33:231–40. doi: 10.1159/000328125
117. Badran BW, Jenkins DD, Cook D, Thompson S, Dancy M, DeVries WH, et al. Transcutaneous auricular vagus nerve stimulation-paired rehabilitation for oromotor feeding problems in newborns: an open-label pilot study. *Front Hum Neurosci.* (2020) 14:77. doi: 10.3389/fnhum.2020.00077

Conflict of Interest: GC is employed by the company NFANT Labs, LLC.

The remaining authors declare that the research was conducted in the absence of any commercial or financial relationships that could be construed as a potential conflict of interest.

frontiers in Neurology

BRIEF RESEARCH REPORT
published: 15 January 2021
doi: 10.3389/fneur.2020.618419

Acute Injection of Omega-3 Triglyceride Emulsion Provides Very Similar Protection as Hypothermia in a Neonatal Mouse Model of Hypoxic-Ischemic Brain Injury

Denny Joseph Manual Kollareth[1], *Hylde Zirpoli*[1], *Vadim S. Ten*[2] *and Richard J. Deckelbaum*[1,2]*

[1] *Institute of Human Nutrition, Columbia University Irving Medical Center, New York, NY, United States,* [2] *Department of Pediatrics, Vagelos College of Physicians and Surgeons, Columbia University Irving Medical Center, New York, NY, United States*

OPEN ACCESS

Edited by:
Daniel Alonso-Alconada, University of the Basque Country, Spain

Reviewed by:
Olatz Arteaga Cabeza, University of the Basque Country, Spain
Hélène Roumes, UMR5536 Centre de Resonance Magnetique des Systemes Biologiques (CRMSB), France

***Correspondence:**
Richard J. Deckelbaum
rjd20@cumc.columbia.edu

Specialty section:
This article was submitted to Stroke, a section of the journal Frontiers in Neurology

Received: *16 October 2020*
Accepted: *21 December 2020*
Published: *15 January 2021*

Citation:
Manual Kollareth DJ, Zirpoli H, Ten VS and Deckelbaum RJ (2021) Acute Injection of Omega-3 Triglyceride Emulsion Provides Very Similar Protection as Hypothermia in a Neonatal Mouse Model of Hypoxic-Ischemic Brain Injury. Front. Neurol. 11:618419. doi: 10.3389/fneur.2020.618419

Therapeutic hypothermia (HT) is a currently accepted treatment for neonatal asphyxia and is a promising strategy in adult stroke therapy. We previously reported that acute administration of docosahexaenoic acid (DHA) triglyceride emulsion (tri-DHA) protects against hypoxic-ischemic (HI) injury in neonatal mice. We questioned if co-treatment with HT and tri-DHA would achieve synergic effects in protecting the brain from HI injury. Neonatal mice (10-day old) subjected to HI injury were placed in temperature-controlled chambers for 4 h of either HT (rectal temperature 31–32°C) or normothermia (NT, rectal temperature 37°C). Mice were treated with tri-DHA (0.375 g tri-DHA/kg bw, two injections) before and 1 h after initiation of HT. We observed that HT, beginning immediately after HI injury, reduced brain infarct volume similarly to tri-DHA treatment (∼50%). Further, HT delayed 2 h post-HI injury provided neuroprotection (% infarct volume: 31.4 ± 4.1 vs. 18.8 ± 4.6 HT), while 4 h delayed HT did not protect against HI insult (% infarct volume: 30.7 ± 5.0 vs. 31.3 ± 5.6 HT). HT plus tri-DHA combination treatment beginning at 0 or 2 h after HI injury did not further reduce infarct volumes compared to HT alone. Our results indicate that HT offers similar degrees of neuroprotection against HI injury compared to tri-DHA treatment. HT can only be provided in tertiary care centers, requires intense monitoring and can have adverse effects. In contrast, tri-DHA treatment may be advantageous in providing a feasible and effective strategy in patients after HI injury.

Keywords: DHA, hypothermia, hypoxic-ischemic injury, neuroprotection, omega-3 fatty acids, stroke

INTRODUCTION

Hypoxic-ischemic (HI) brain injury is a serious occurrence that frequently results in death or significant long-term neurologic disability in both neonates and adults (1–3). Currently, therapeutic hypothermia (HT) is the only established treatment for neonates with HI encephalopathy (4). Selective head cooling with cooling caps or whole body cooling with passive cooling (turning radiant warmers/incubators off), cool packs and/or commercially available cooling

blankets are used for treatment in neonatal HI encephalopathy (5, 6). With regard to acute ischemic stroke in adults, tissue-type plasminogen activator (tPA) is the only drug approved by the U.S. Food and Drug Administration (FDA) (7). However, the narrow therapeutic window and the risk of hemorrhage are major limitations of tPA treatment, resulting in only 8–10% of adult stroke patients eligible for this drug (8). Preclinical studies and small scale clinical trials in adults after stroke have shown that HT substantially diminishes the degree of neural damage, reduces the rate of mortality and improves neurofunctional recovery (9–11).

The major molecular mechanisms affected by HT include decreased free-radical production, reduction of blood–brain barrier disruption, decreased excitatory amino acid release and attenuation of cell mediated inflammatory responses to cerebral ischemia (12, 13). Additionally, HT induces the inhibition of neuronal apoptosis through both mitochondrial based intrinsic pathways and receptor mediated extrinsic pathways (14). However, HT remains a complex medical approach, as it requires intense monitoring and is available only in tertiary care centers (15). Pilot studies on HT in stroke have shown that adult patients have less tolerance to cooling than neonates and HT may also induce unfavorable systemic effects, such as shivering, immune suppression, and pneumonia (16, 17). Combining HT with other treatment methods may help in reducing the adverse effects from HT as well as reaching multiple molecular targets in the setting of HI insult to obtain an increase in therapeutic time windows and an enhanced repair in long-term recovery (18).

As one of the major omega-3 polyunsaturated fatty acids (PUFA) in the brain, docosahexaenoic acid (DHA) is essential for development and function of the brain (19). DHA has been shown to reduce inflammation, excitotoxicity and to prevent brain volume loss in different animal models of HI injury (20–22). Studies from our laboratory showed that acute administration of triglyceride (TG) emulsions containing only DHA (tri-DHA) reduces brain injury and preserves short- and long-term neurological outcomes in neonatal mice (23, 24).

Based on these findings, we questioned if co-treatment with HT and tri-DHA would achieve synergic effects in protecting the brain from HI injury. We validated the neuroprotective efficacy of HT against HI injury in the neonatal model previously described by our laboratory (23, 25). Our results showed that tri-DHA provides similar degrees of neuroprotection as that of HT and combining HT with tri-DHA emulsion does not offer additional therapeutic benefit in HI injury.

MATERIALS AND METHODS

Ethics Statement

All research studies were carried out according to protocols approved by the Columbia University Institutional Animal Care and Use Committee (IACUC) in accordance with the Association for Assessment and Accreditation of Laboratory Animal Care guidelines (AAALAC).

Abbreviations: DHA, docosahexaenoic acid; h, hours; HT, hypothermia; NT, normothermia; TG, triglycerides; HI, hypoxic-ischemic; SPMs, specialized pro-resolving mediators; Tri-DHA, DHA TG emulsion.

Materials

DHA TG oil was purchased from Nu-Chek Prep, Inc. (Elysian, MN). Egg yolk phosphatidylcholine was obtained from Avanti Polar-Lipids, Inc. (Alabaster, AL). Radiolabeled [^{3}H]-cholesteryl hexadecyl ether was purchased from PerkinElmer (Boston, MA) ([^{3}H]CEt) (NET 85900).

Lipid Emulsions

Tri-DHA emulsions (10 g by TG weight/100 mL emulsion) were made in our laboratory with DHA TG oil and egg yolk phospholipids (PL) by sonication as previously detailed (23). The emulsions were analyzed for the amount of TG and PL using commercial kits (Wako Chemicals USA, Inc., Richmond, VA). The TG:PL mass ratio was 5.0 $\pm$ 1.0, similar to VLDL-sized particles. To prepare radiolabeled emulsions, [^{3}H]CEt was added to the TG-PL mixture before sonication (25).

Animal Procedures

Unilateral Cerebral Hypoxia-Ischemia Injury

Three-day-old C57BL/6J neonatal mice were purchased from Jackson Laboratories (Bar Harbor) with their birth mother. We used the Rice-Vannuci method of mild HI brain injury modified to 10-day old (p10) mice, as previously described (23). An initial pilot study on gender differences showed no significant changes in infarct volumes after HI injury between male and female mice. Hence, both male and female mice were used for these experiments and we did not separate our data by gender in the present study. Briefly, HI brain injury was induced by permanent ligation of the right common carotid artery. After 1.5 h of recovery, mice were exposed to hypoxic insult (humidified 8% O_2/92% N_2, Tech Air Inc., NY) for 15 min. Since HI brain injury in neonatal mice is associated with an endogenous drop in body core temperature (26), mice are kept at 37 $\pm$ 0.3°C during hypoxia to avoid hypothermia during the hypoxia period.

HT and Tri-DHA Treatments

Immediately after HI injury, pups were kept for 4 h in temperature controlled chambers with either HT or normothermia (NT), reaching rectal temperatures of 31–32°C or 37°C, respectively (23). We observed that pups placed in circulating air chambers set at 27°C maintained target rectal temperature 31–32°C. For the NT group, pups were placed in chambers set at 32°C, based on the protocol from our previous studies (23, 24). As the core temperature in neonatal rodents could be affected by distance from the dam (27), the pups were kept separately from the dam during the 4 h HT or NT treatment period. Sequential temperature measurements were obtained immediately after hypoxia (0 h) followed by 1, 2, 3, and 4 h during HT (probe type: RET-4; Physitemp Instruments, Clifton, NJ). Tri-DHA treatment [0.375 g tri-DHA/kg bw, intraperitoneal (i.p.), two injections, 1 h apart] was based on the protocol from our previous studies on tri-DHA neuroprotection against HI injury in neonatal mice (23, 24).

To investigate whether combined treatment of HT with tri-DHA emulsion enhances neuroprotection in HI damage, animals subjected to HT were administered with tri-DHA emulsion (0.375 g tri-DHA/kg bw, 2 injections, i.p.) at the beginning

of HT and at 1 h after initiation of HT. NT or HT control animals received saline injections. Following 4 h NT, pups in the control group were returned to the dam. Pups in the HT group underwent slow rewarming by increasing the chamber temperature at a rate of 0.1–0.2°C per minute till the pups reached a rectal temperature of 37°C, and were then returned to the dam.

Uptake and Distribution of Radiolabeled Tri-DHA Emulsion Particles in HT Mice

Using radiolabeled tri-DHA emulsion, we determined whether HT affects the absorption and distribution of emulsion particles after i.p. injection. Naïve neonatal mice injected with radiolabeled tri-DHA emulsion (0.375 g tri-DHA/kg bw, i.p., single injection) were immediately subjected to 4 h of either HT ($n = 3$) or NT ($n = 7$). The use of a single bolus injection to study emulsion distribution was based on previously established protocols from our laboratory (25, 28). Animals were sacrificed after 4 h of HT or NT and radioactivity in peritoneal fluid, blood, organs and tissues assessed by measuring the levels of [^{3}H]CEt.

Tissues and organs were homogenized using a Polytron Tissue Disruptor (Omni TH, Kenneswa, GA) and the radioactivity measured by liquid scintillation spectrometry (29). The samples were suspended in scintillation fluid (Ultima Gold scintillation fluid, PerkinElmer, Boston, MA), mixed and ^{3}H dpm assayed in a PerkinElmer Tri-Carb liquid scintillation spectrometer 5110 TR. Tissue uptake was expressed as percent of total recovered dose/organ for all the organs analyzed.

HT and Tri-DHA Therapeutic Time Windows

We determined the therapeutic window of HT after HI injury in mice: (1) 2 h delayed HT - pups placed with dam for 2 h after HI and then subjected to HT; (2) 4 h delayed HT - pups placed with dam for 4 h after HI and then subjected to HT. To investigate whether combined treatment of HT with tri-DHA emulsion prolongs the therapeutic window in HI injury, animals subjected to HT (2 or 4 h delayed after HI) were administered with tri-DHA emulsion (0.375 g tri-DHA/kg bw, 2 injections, i.p.) at the beginning of HT and at 1 h after initiation of HT. NT or HT control animals received saline injections. After the treatment period, pups in NT or HT groups were returned to the dam as described above.

Neuropathological Outcomes

At 24 h after HI insult, the animals were sacrificed and brains were harvested. Coronal slices of 1 mm were cut by using a brain slicer matrix. Slices were immersed in a PBS solution containing 2% triphenyltetrazolium chloride (TTC) at 37°C for 25 min. TTC is taken up into living mitochondria, which converts it to a red color. Unstained areas that appeared white were defined as infarct regions whereas viable regions appeared red. Using Adobe Photoshop and NIH Image J imaging applications, planar areas of infarction on serial sections were summed to obtain the volume (mm^3) of infarcted tissue. Infarct areas were expressed as % of the total area of the ipsilateral hemisphere (24). In a separate cohort of mice treated with HT or HT plus tri-DHA immediately after HI, brain atrophy at 7 days after HI injury was detected by Nissl staining, as previously described. The entire brain was sectioned every 200 μm and the thickness of each coronal slice was 50 μm. Sections were then incubated in a solution of 0.1% cresyl violet (Sigma-Aldrich, St. Louis, MO, USA) for 7 min. After a quick rinse in H_2O, slides were differentiated in 70% (v/v) ethanol with a few drops of acetic acid, followed by dehydration in graded ethanol and two changes of xylene. The sections were then mounted with Fisher Chemical™ Permount™ Mounting Media (30).

Statistical Analyses

Values are mean ± SEM. One-way ANOVA followed by *post hoc* Newman-Keuls multiple comparison test was applied to evaluate differences among the groups.

RESULTS

HT Does Not Affect Absorption or Organ Distribution of Tri-DHA Emulsion Particles

There was no mortality in animals subjected to NT or HT protocols. **Table 1** summarizes results of sequential temperature measurements in HT animals. Radiolabeled experiments showed that at 4 h after i.p. injection, ∼96% of the injected emulsion exited the peritoneal cavity in both NT and HT mice. Further, no significant differences were observed in the organ distribution of tri-DHA emulsion particles in NT vs. HT mice. The highest uptake of emulsion particles was in the liver (44–47% of recovered dose of radiolabeled emulsion), followed by muscle (20–23%) and heart (8–9%) in both NT and HT mice. The lowest uptake of emulsion particles was in the brain (<0.3% of recovered dose) in both NT and HT animals (data not shown).

HT or Tri-DHA Treatment After HI Injury Provides Similar Degrees of Neuroprotection

We evaluated neuroprotective effects of HT plus tri-DHA treatment beginning immediately after HI injury. HT or tri-DHA showed significant reduction (∼50%) in brain infarct volumes compared to saline treated NT animals (**Figures 1A,B**). Combination of treatments with HT and tri-DHA immediately after HI injury did not provide any additional benefits compared to HT treatment alone (**Figures 1A,B**).

TABLE 1 | Rectal temperature measurements immediately after hypoxia (0 h) and at 1, 2, 3, and 4 h during hypothermia (HT) in mice subjected to hypoxic-ischemic (HI) injury.

	HT	HT + tri-DHA
End of hypoxia (0 h)	35.2 ± 0.48	35.6 ± 0.41
1 h after HI	32.0 ± 0.16	32.2 ± 0.25
2 h after HI	31.4 ± 0.24	32.0 ± 0.17
3 h after HI	31.0 ± 0.19	32.1 ± 0.15
4 h after HI	31.6 ± 0.26	31.8 ± 0.28

Temperatures (°C) are expressed as mean ± SEM. n = 7–9.

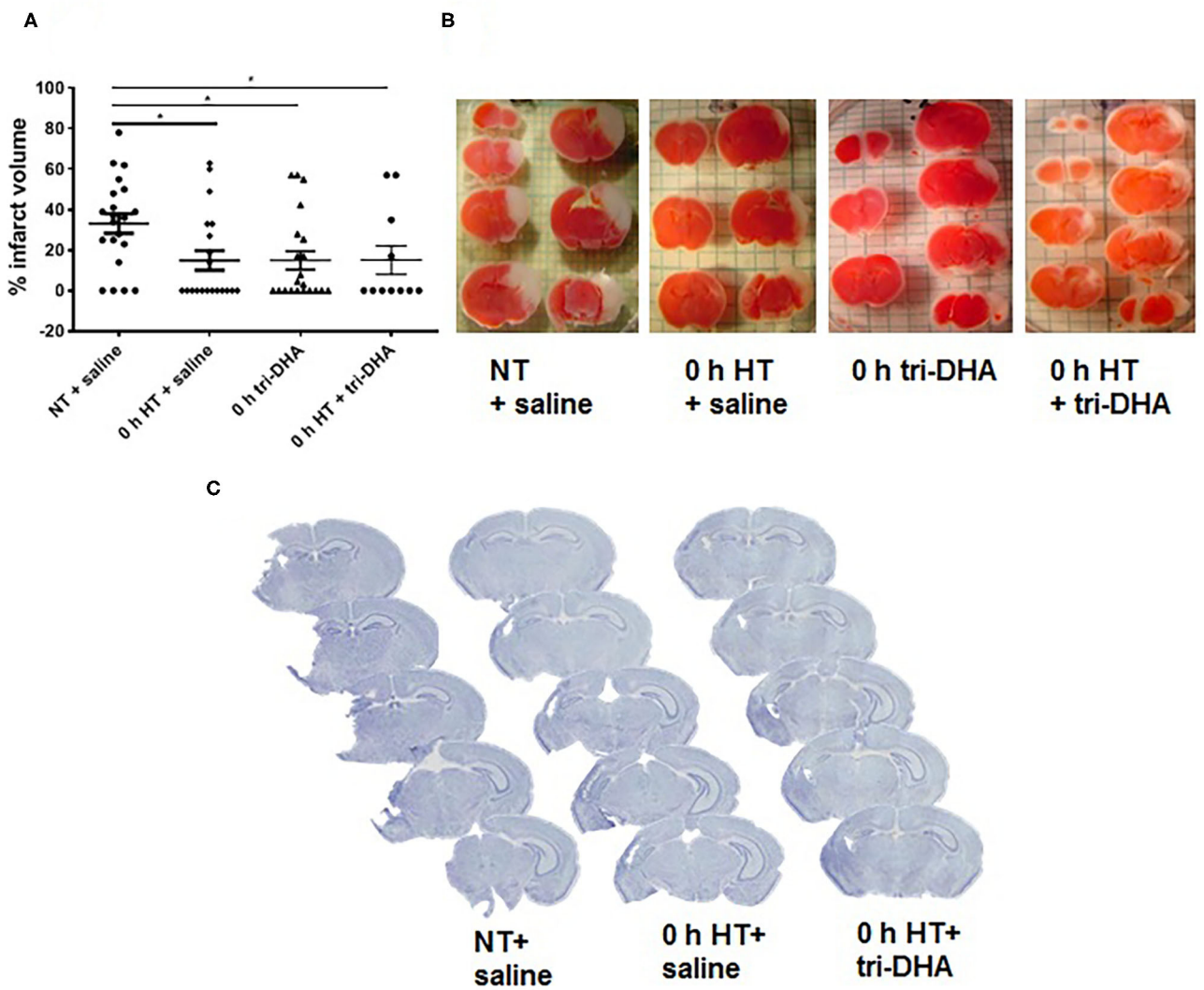

FIGURE 1 | Effect of hypothermia (HT) and tri-DHA on infarct volume: Infarct volume **(A)** and representative TTC stained cerebral sections **(B)** in mice treated with normothermia (NT) + saline ($n = 21$), HT + saline ($n = 20$), tri-DHA ($n = 21$) or HT + tri-DHA ($n = 11$) beginning immediately (0 h) after hypoxic-ischemic (HI) injury (% infarct volume: NT + saline- 33.2 ± 4.8, HT + saline- 14.9 ± 4.8, 0 h tri-DHA- 14.9 ± 4.5, 0 h HT + tri-DHA- 15.0 ± 7.0). Values are mean ± SEM. *$p < 0.05$; Representative Nissl-stained cerebral coronal sections from mice treated with NT + saline, HT + saline or HT + tri-DHA beginning immediately (0 h) after HI injury **(C)**.

Neuroprotection by HT plus tri-DHA administration beginning immediately after HI injury was maintained at 7 days after ischemic insult. Nissl staining demonstrated greater preservation of the ipsilateral hemisphere in HT or HT plus tri-DHA treated mice compared to the control group. However, the combination did not offer any therapeutic advantage compared to HT treatment alone. Representative Nissl stained sections are shown in **Figure 1C**.

HT Plus Tri-DHA Treatment After HI Injury Does Not Extend the Therapeutic Time Window

In the present study, we performed delayed HT treatment protocols to determine the therapeutic window for neuroprotection after ischemic injury. HT delayed 2 h post-HI showed reduced brain infarct volumes compared to NT animals. Further, HT plus tri-DHA treatment did not offer significant additional protection over that provided by HT alone beginning at 2 h after HI injury although there was a tendency for slightly more reduction in infarct size (% infarct volume: 31.4 ± 4.1 NT + saline vs. 18.8 ± 4.6 HT + saline vs. 12.7 ± 4.0 HT + tri-DHA) (**Figures 2A,B**). HT treatment delayed to 4 h after HI insult did not offer protection against ischemic injury. Combining HT and tri-DHA treatment with a delay of 4 h after HI injury did not extend the therapeutic window of HT. Although we observed an increase in infarct volume in animals treated with 4 h delayed HT + tri-DHA combination, the difference was not significant compared to NT or HT alone groups (**Figures 2C,D**). Thus, our results indicate that combined treatment of tri-DHA emulsion with HT does not provide additional significant benefit in neuroprotection in ischemic injury.

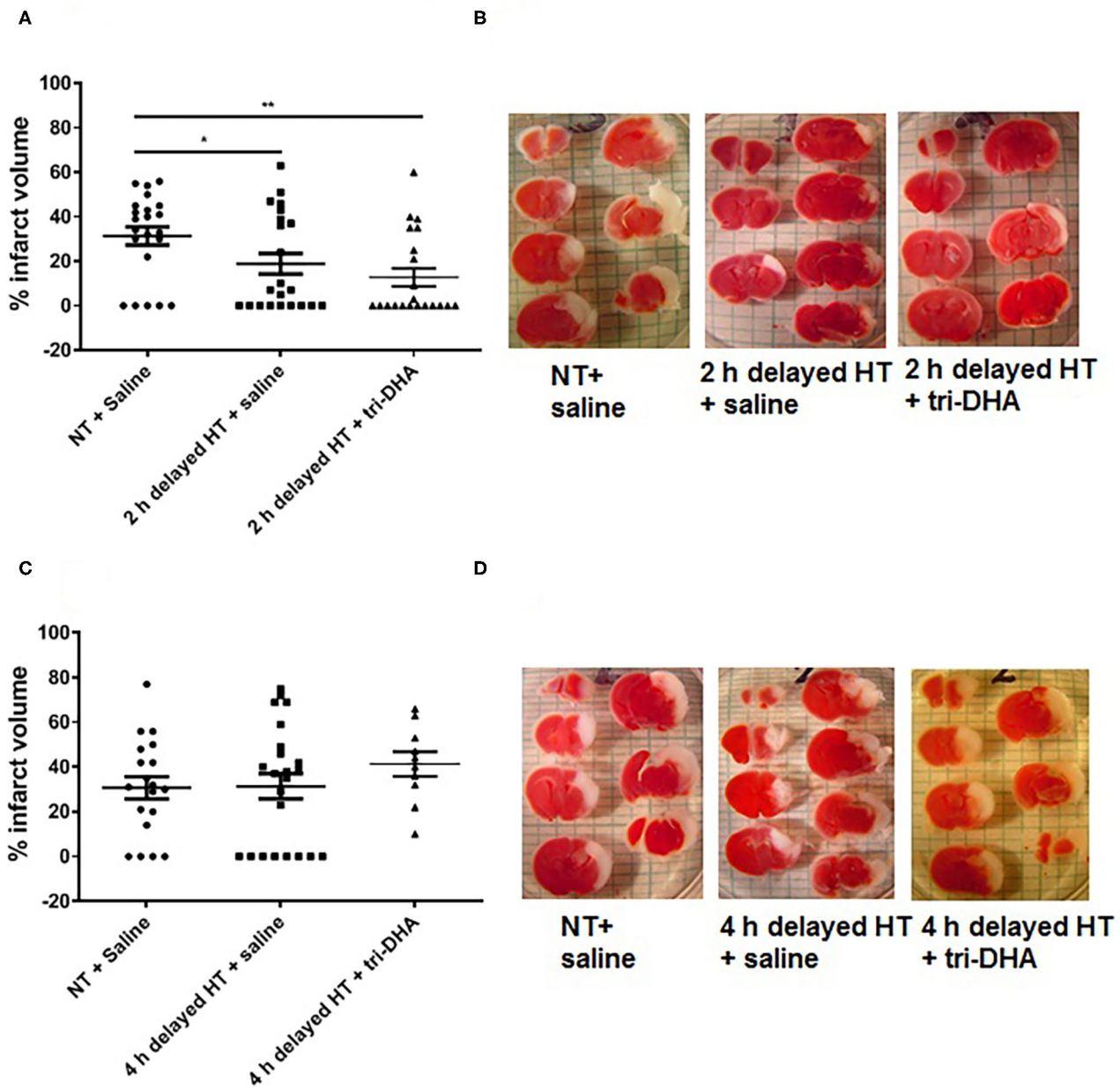

FIGURE 2 | Therapeutic windows of hypothermia (HT) and tri-DHA: Infarct volume **(A)** and representative TTC stained cerebral sections **(B)** in mice treated with normothermia (NT) + saline ($n = 22$), HT + saline ($n = 22$) or HT + tri-DHA ($n = 21$) beginning at 2 h after hypoxic-ischemic (HI) injury (% infarct volume: NT + saline- 31.4 ± 4.1, 2 h delayed HT + saline- 18.8 ± 4.6, 2 h delayed HT + tri-DHA- 12.7 ± 4.0); Infarct volume **(C)** and representative TTC stained cerebral sections **(D)** in mice treated with normothermia (NT) + saline ($n = 19$), HT + saline ($n = 23$) or HT + tri-DHA ($n = 10$) beginning at 4 h after hypoxic-ischemic (HI) injury (% infarct volume: NT + saline- 30.7 ± 5.0, 4 h delayed HT + saline- 31.3 ± 5.6, 4 h delayed HT + tri-DHA- 41.3 ± 5.5). Values are mean ± SEM. *$p < 0.05$, **$p < 0.01$.

DISCUSSION

In this study, our results show that HT administration exerts similar degrees of neuroprotection as that of tri-DHA. Further, combined treatment of HT with tri-DHA emulsion does not confer additional neuroprotection.

Therapeutic HT is a means of neuroprotection well established in the management of acute ischemic brain injuries such as anoxic encephalopathy after cardiac arrest and perinatal asphyxia (31). Randomized trials have shown that HT is also effective in improving neurological outcomes in traumatic brain injury patients (32). Neuroprotective benefits of systemic HT following ischemic stroke have been reported in clinical trials (9, 11). However, the use of HT for acute stroke treatment is still controversial and is limited by logistical challenges (9, 33).

HT initiated immediately after HI insult is neuroprotective and the degree of neuroprotection decreases linearly with the delay of initiation of cooling (34, 35). In neonatal mouse models of HI injury, HT beginning at 0 or 2 h after HI provides neuroprotection (26), while no studies have assessed the effect of HT when delayed by more than 2 h in mice. Our results showed that HT is neuroprotective up to 2 h after HI injury and the protection is lost with prolonged 4 h delay in treatment. In contrast, in a neonatal rat model, Sabir et al. (35) showed that HT delayed up to 6 h after HI insult provides neuroprotection. This may be related to differences in pathways of ischemic injury progression and neuroprotection in mice vs. rats (36). The basal metabolic rate per kg of body weight is seven times greater in mice than in humans (37) and this may play a major role in providing longer treatment windows for HT in humans in response to HI injury. Therefore, neuroprotection with 2 h delayed treatment in our protocol in mice may translate into longer time windows with HT in humans. Of relevant interest, after we reported a 2 h treatment window in neonatal mice (23), in pilot studies we documented a 6 h therapeutic window for omega-3 emulsion treatment in an adult stroke model (unpublished data). Since myelination is still occurring in the neonatal brain and the water content of the neonatal brain is greater than that of the mature brain, injury has a different appearance and time-course in the neonatal brain than in the adult brain. Cell death mechanisms have been shown to be different in the developing brain compared to that in the adult (38). The mechanisms of mitochondrial permeabilization are age-dependent and while Cyclophilin D is critical in the adult brain, B-cell lymphoma 2 (BCL-2) associated X (BAX)-related mechanisms dominate in the immature brain (39). Stroke triggers a robust inflammatory response in both adult and neonatal brain. Compared to the adult, microglial activation in neonates is much more rapid following ischemic injury. In the adult brain there is also a considerable contribution of infiltrating peripheral immune cells to the brain after stroke injury (40). In contrast, little infiltration of peripheral cells is seen acutely after neonatal stroke (41). Thus, these findings suggest differences in neonatal and adult central nervous system immune responses to injury (42, 43). We assume that these differences in ischemic injury pathophysiology and the efficacy of omega-3 fatty acids to act through these molecular pathways account for the differences in therapeutic windows observed between neonates and adults. Our present results also suggest that HT offers a very similar therapeutic window as tri-DHA treatment. A therapeutic window shorter than 6 h is recommended in neonates with HI encephalopathy (44, 45). However, few studies have demonstrated that HT initiated at 6–24 h after birth may also have benefits (46). The effective therapeutic window for HT in adult stroke patients is still not known (11, 14).

We tested whether DHA might add better neuroprotection as an adjuvant therapy to enhance the efficacy of HT after HI injury. Our results suggest that combining HT and tri-DHA does not enhance neuroprotection or extend the therapeutic window of treatment after HI injury. This is similar to recent findings from studies in newborn piglet models of HI injury, which showed that combined treatment of HT plus DHA had no additional benefits than HT alone or DHA alone treatment in reducing brain injury, oxidative stress, and inflammatory markers following HI insult (47, 48). However, another study in a neonatal rat model of HI injury reported that HT plus DHA synergistically reduced brain infarct volume and improved behavioral performances (49). Of interest, the inability to markedly enhance neuroprotection by HT plus tri-DHA treatment is not attributed to a reduction of absorption and distribution of tri-DHA emulsion particles, as demonstrated by our radiolabeled experiments. Additionally, low uptake of emulsion particles in the brain does not affect tri-DHA mediated neuroprotection in HI injury (25). Recent data from our laboratory have shown that injected tri-DHA emulsion is initially mainly taken up by the liver, which is then metabolized and secreted to plasma pools of lysophosphatidylcholine and non-esterified fatty acids, facilitating DHA brain transport (25). Further, we reported that tri-DHA administration increased DHA content in brain mitochondria and also induced a significant increase in DHA levels in blood and DHA derived specialized pro-resolving mediators (SPMs) in brain. Tri-DHA administration also increased blood levels of EPA and EPA derived SPMs in brain (24, 25). These rises in DHA, EPA, and SPMs derived from DHA and EPA might also contribute and explain the neuroprotective actions observed for DHA.

Both DHA and HT share common pathways of neuroprotection against HI injury. DHA or HT downregulate pro-apoptotic BAX and upregulate anti-apoptotic BCL-2, resulting in reduced cytochrome c release and decreased caspase activation (20, 50). DHA or HT promote activation of AKT that stimulates cell proliferation (51, 52). Further, it has been reported that in experimental stroke, DHA or HT treatment induce a decrease in microglial activation and pro-inflammatory cytokines such as interleukin 1β (IL-1β), IL-6 and tumor necrosis factor alpha (TNF-α) (53, 54). Additionally, both treatments inhibit nuclear factor kappa B (NF-κB), a transcription factor that activates many inflammatory signaling pathways (55, 56). DHA or HT have also been shown to prevent accumulation or release of excitotoxic amino acids such as glutamate (57, 58). Both DHA or HT limit reperfusion-driven acceleration in mitochondrial ROS release and protect against mitochondrial membrane permeabilization (24, 59). Thus, we speculate that overlapping neuroprotective mechanisms of DHA and HT render the combined treatment ineffective in providing enhanced neuroprotection in HI brain injury.

Previously, we reported a significant impairment in the behavioral outcomes of neonatal mice subjected to HI injury, while animals treated either with tri-DHA or neuroprotectin D1 (NPD1) had reduced infarct size with preservation of neurofunctional outcomes (24, 30). While in this study we did not measure neurofunctional outcomes following HI injury in the different groups, given the similar histological findings of HI injury and subsequent neuroprotection by HT or tri-DHA, we would predict similar levels of preservation of neurofunctional outcomes by both

treatments. Furthermore, we did not delineate the potential molecular mechanisms of DHA compared to HT (10, 20). Still these limitations do not negate the significance of our work, demonstrating that post-HI tri-DHA administration provides similar degree of neuroprotection as that of HT treatment.

Currently, HT is the only established treatment for moderate to severe encephalopathy in infants (60) and is a promising strategy still under investigation for stroke therapy in adults (61). Successful clinical translation of HT for stroke requires the control of different key parameters of HT therapy including onset time, duration, depth of HT and rewarming speed (14). Although cooling a patient is simple in concept, it is a complex medical procedure that involves coordination of efforts from specially trained health care staff along with preparedness for the management issues that may arise with HT (15, 62). Using HT as a treatment for stroke usually requires settings in a tertiary care hospital and is associated with high financial costs (63). Our findings show that HT or injection of tri-DHA emulsion reduce infarct volume and the degree of neuroprotection is similar for both treatments. Omega-3 fatty acids are safe and well tolerated in humans without major adverse effects (64–66). Intravenous injections are a common feasible procedure, which can be easily performed in primary care settings. Thus, if our results using omega-3 rich lipid emulsions prove effective in treating stroke in humans, acute omega-3 therapy could be considered as an alternative cost-effective therapy for HT after ischemic organ injuries such as stroke.

DATA AVAILABILITY STATEMENT

The original contributions presented in the study are included in the article/supplementary material, further inquiries can be directed to the corresponding author/s.

ETHICS STATEMENT

The animal study was reviewed and approved by Columbia University Institutional Animal Care and Use Committee.

AUTHOR CONTRIBUTIONS

DM performed all the experiments and wrote the first draft of the manuscript. HZ provided experimental assistance. RD, VT, and HZ advised on study design, on data analyses, and in revisions of the manuscript. RD, VT, HZ, and DM conceived the study, coordinated the experiments, and wrote the final version of the manuscript. All authors contributed to the article and approved the submitted version.

FUNDING

This work was supported by the National Institutes of Health grant R01 NS088197 (RD and VT).

ACKNOWLEDGMENTS

We thank Ms. Inge Hansen for her excellent technical support.

REFERENCES

1. Wu YW, Goodman AM, Chang T, Mulkey SB, Gonzalez FF, Mayock DE, et al. Placental pathology and neonatal brain MRI in a randomized trial of erythropoietin for hypoxic-ischemic encephalopathy. *Pediatr Res.* (2020) 87:879–84. doi: 10.1038/s41390-019-0493-6
2. Huang L, Zhang L. Neural stem cell therapies and hypoxic-ischemic brain injury. *Prog Neurobiol.* (2019) 173:1–17. doi: 10.1016/j.pneurobio.2018.05.004
3. Ye X, Shen T, Hu J, Zhang L, Zhang Y, Bao L, et al. Purinergic 2X7 receptor/NLRP3 pathway triggers neuronal apoptosis after ischemic stroke in the mouse. *Exp Neurol.* (2017) 292:46–55. doi: 10.1016/j.expneurol.2017.03.002
4. Aker K, Støen R, Eikenes L, Martinez-Biarge M, Nakken I, Håberg AK, et al. Therapeutic hypothermia for neonatal hypoxic-ischaemic encephalopathy in India (THIN study): a randomised controlled trial. *Arch Dis Child Fetal Neonatal Ed.* (2020) 105:405–11. doi: 10.1136/archdischild-2019-317311
5. Akula VP, Joe P, Thusu K, Davis AS, Tamaresis JS, Kim S, et al. A randomized clinical trial of therapeutic hypothermia mode during transport for neonatal encephalopathy. *J Pediatr.* (2015) 166:856–61.e2. doi: 10.1016/j.jpeds.2014.12.061
6. Peliowski-Davidovich A. Hypothermia for newborns with hypoxic ischemic encephalopathy. *Paediatr Child Health.* (2012) 17:41–3. doi: 10.1093/pch/17.1.41
7. Zhao Y, Wei ZZ, Lee JH, Gu X, Sun J, Dix TA, et al. Pharmacological hypothermia induced neurovascular protection after severe stroke of transient middle cerebral artery occlusion in mice. *Exp Neurol.* (2020) 325:113133. doi: 10.1016/j.expneurol.2019.113133
8. Zgavc T, Ceulemans A-G, Sarre S, Michotte Y, Hachimi-Idrissi S. Experimental and clinical use of therapeutic hypothermia for ischemic stroke: opportunities and limitations. *Stroke Res Treat.* (2011) 2011:689290. doi: 10.4061/2011/689290
9. Duan Y, Wu D, Huber M, Shi J, An H, Wei W, et al. New endovascular approach for hypothermia with intrajugular cooling and neuroprotective effect in ischemic stroke. *Stroke.* (2020) 51:628–36. doi: 10.1161/STROKEAHA.119.026523
10. Yenari MA, Han HS. Neuroprotective mechanisms of hypothermia in brain ischaemia. *Nat Rev Neurosci.* (2012) 13:267–78. doi: 10.1038/nrn3174
11. Kuczynski AM, Demchuk AM, Almekhlafi MA. Therapeutic hypothermia: applications in adults with acute ischemic stroke. *Brain Circ.* (2019) 5:43–54. doi: 10.4103/bc.bc_5_19
12. Jiang J, Yu M, Zhu C. Effect of long-term mild hypothermia therapy in patients with severe traumatic brain injury: 1-year follow-up review of 87 cases. *J Neurosurg.* (2000) 93:546–9. doi: 10.3171/jns.2000.93.4.0546
13. Berger C, Schabitz W-R, Wolf M, Mueller H, Sommer C, Schwab S. Hypothermia and brain-derived neurotrophic factor reduce glutamate synergistically in acute stroke. *Exp Neurol.* (2004) 185:305–12. doi: 10.1016/j.expneurol.2003.10.008
14. Wu L, Wu D, Yang T, Xu J, Chen J, Wang L, et al. Hypothermic neuroprotection against acute ischemic stroke: the 2019 update. *J Cereb Blood Flow Metab.* (2020) 40:461–81. doi: 10.1177/0271678X19894869
15. Lampe JW, Becker LB. State of the art in therapeutic hypothermia. *Annu Rev Med.* (2011) 62:79–93. doi: 10.1146/annurev-med-052009-150512
16. Kurisu K, Kim JY, You J, Yenari MA. Therapeutic hypothermia and neuroprotection in acute neurological disease. *Curr Med Chem.* (2019) 26:5430–55. doi: 10.2174/0929867326666190506124836
17. Yenari M, Kitagawa K, Lyden P, Perez-Pinzon M. Metabolic downregulation. *Stroke J Cereb Circ.* (2008) 39:2910–7. doi: 10.1161/STROKEAHA.108.514471

18. Cilio MR, Ferriero DM. Synergistic neuroprotective therapies with hypothermia. *Semin Fetal Neonatal Med.* (2010) 15:293–8. doi: 10.1016/j.siny.2010.02.002
19. Takeyama E, Islam A, Watanabe N, Tsubaki H, Fukushima M, Mamun MA, et al. Dietary intake of green nut oil or DHA ameliorates DHA distribution in the brain of a mouse model of dementia accompanied by memory recovery. *Nutrients*. (2019) 11:2371. doi: 10.3390/nu11102371
20. Mayurasakorn K, Williams JJ, Ten VS, Deckelbaum RJ. Docosahexaenoic acid: brain accretion and roles in neuroprotection after brain hypoxia and ischemia. *Curr Opin Clin Nutr Metab Care.* (2011) 14:158–67. doi: 10.1097/MCO.0b013e328342cba5
21. Eady TN, Khoutorova L, Obenaus A, Mohd-Yusof A, Bazan NG, Belayev L. Docosahexaenoic acid complexed to albumin provides neuroprotection after experimental stroke in aged rats. *Neurobiol Dis.* (2014) 62:1–7. doi: 10.1016/j.nbd.2013.09.008
22. Jiang X, Pu H, Hu X, Wei Z, Hong D, Zhang W, et al. A post-stroke therapeutic regimen with omega-3 polyunsaturated fatty acids that promotes white matter integrity and beneficial microglial responses after cerebral ischemia. *Transl Stroke Res.* (2016) 7:548–61. doi: 10.1007/s12975-016-0502-6
23. Williams JJ, Mayurasakorn K, Vannucci SJ, Mastropietro C, Bazan NG, Ten VS, et al. N-3 fatty acid rich triglyceride emulsions are neuroprotective after cerebral hypoxic-ischemic injury in neonatal mice. *PLoS ONE.* (2013) 8:e56233. doi: 10.1371/journal.pone.0056233
24. Mayurasakorn K, Niatsetskaya ZV, Sosunov SA, Williams JJ, Zirpoli H, Vlasakov I, et al. DHA but not EPA emulsions preserve neurological and mitochondrial function after brain hypoxia-ischemia in neonatal mice. *PLoS ONE.* (2016) 11:e0160870. doi: 10.1371/journal.pone.0160870
25. Manual Kollareth DJ, Deckelbaum RJ, Liu Z, Ramakrishnan R, Jouvene C, Serhan CN, et al. Acute injection of a DHA triglyceride emulsion after hypoxic-ischemic brain injury in mice increases both DHA and EPA levels in blood and brain. *Prostaglandins Leukot Essent Fatty Acids.* (2020) 162:102176. doi: 10.1016/j.plefa.2020.102176
26. Reinboth BS, Köster C, Abberger H, Prager S, Bendix I, Felderhoff-Müser U, et al. Endogenous hypothermic response to hypoxia reduces brain injury: implications for modeling hypoxic-ischemic encephalopathy and therapeutic hypothermia in neonatal mice. *Exp Neurol.* (2016) 283:264–75. doi: 10.1016/j.expneurol.2016.06.024
27. Galinsky R, Dean JM, Lear CA, Davidson JO, Dhillon S, Wassink G, et al. In the era of therapeutic hypothermia, how well do studies of perinatal neuroprotection control temperature? *Dev Neurosci.* (2017) 39:7–22. doi: 10.1159/000452859
28. Qi K, Al-Haideri M, Seo T, Carpentier YA, Deckelbaum RJ. Effects of particle size on blood clearance and tissue uptake of lipid emulsions with different triglyceride compositions. *J Parenter Enter Nutr.* (2003) 27:58–64. doi: 10.1177/014860710302700158
29. Manual Kollareth DJ, Chang CL, Hansen IH, Deckelbaum RJ. Radiolabeled cholesteryl ethers: a need to analyze for biological stability before use. *Biochem Biophys Rep.* (2018) 13:1–6. doi: 10.1016/j.bbrep.2017.10.007
30. Zirpoli H, Sosunov SA, Niatsetskaya ZV, Mayurasakorn K, Kollareth DJM, Serhan CN, et al. NPD1 rapidly targets mitochondria-mediated apoptosis after acute injection protecting brain against ischemic injury. *Exp Neurol.* (2020) 335:113495. doi: 10.1016/j.expneurol.2020.113495
31. van der Worp HB, Macleod MR, Kollmar R. Therapeutic hypothermia for acute ischemic stroke: ready to start large randomized trials? *J Cereb Blood Flow Metab.* (2010) 30:1079–93. doi: 10.1038/jcbfm.2010.44
32. Dietrich WD, Bramlett HM. Therapeutic hypothermia and targeted temperature management for traumatic brain injury: experimental and clinical experience. *Brain Circ.* (2017) 3:186–98. doi: 10.4103/bc.bc_28_17
33. Zhao H, Steinberg G. Limited therapeutic time windows of mild-to-moderate hypothermia in a focal ischemia model in rat. *Stroke Res Treat.* (2011) 2011:131834. doi: 10.4061/2011/131834
34. Gunn AJ. Cerebral hypothermia for prevention of brain injury following perinatal asphyxia. *Curr Opin Pediatr.* (2000) 12:111–5. doi: 10.1097/00008480-200004000-00004
35. Sabir H, Scull-Brown E, Liu X, Thoresen M. Immediate hypothermia is not neuroprotective after severe hypoxia-ischemia and is deleterious when delayed by 12 hours in neonatal rats. *Stroke.* (2012) 43:3364–70. doi: 10.1161/STROKEAHA.112.674481
36. Du Y, Deng W, Wang Z, Ning M, Zhang W, Zhou Y, et al. Differential subnetwork of chemokines/cytokines in human, mouse, and rat brain cells after oxygen-glucose deprivation. *J Cereb Blood Flow Metab.* (2017) 37:1425–34. doi: 10.1177/0271678X16656199
37. Demetrius L. Of mice and men. *EMBO Rep.* (2005) 6:S39–44. doi: 10.1038/sj.embor.7400422
38. Zhu C, Wang X, Xu F, Bahr BA, Shibata M, Uchiyama Y, et al. The influence of age on apoptotic and other mechanisms of cell death after cerebral hypoxia-ischemia. *Cell Death Differ.* (2005) 12:162–76. doi: 10.1038/sj.cdd.4401545
39. Wang X, Carlsson Y, Basso E, Zhu C, Rousset CI, Rasola A, et al. Developmental shift of cyclophilin D contribution to hypoxic-ischemic brain injury. *J Neurosci.* (2009) 29:2588–96. doi: 10.1523/JNEUROSCI.5832-08.2009
40. Iadecola C, Anrather J. The immunology of stroke: from mechanisms to translation. *Nat Med.* (2011) 17:796–808. doi: 10.1038/nm.2399
41. Denker SP, Ji S, Dingman A, Lee SY, Derugin N, Wendland MF, et al. Macrophages are comprised of resident brain microglia not infiltrating peripheral monocytes acutely after neonatal stroke. *J Neurochem.* (2007) 100:893–904. doi: 10.1111/j.1471-4159.2006.04162.x
42. Vexler ZS, Tang XN, Yenari MA. Inflammation in adult and neonatal stroke. *Clin Neurosci Res.* (2006) 6:293–313. doi: 10.1016/j.cnr.2006.09.008
43. Liu F, Mccullough LD. Inflammatory responses in hypoxic ischemic encephalopathy. *Acta Pharmacol Sin.* (2013) 34:1121–30. doi: 10.1038/aps.2013.89
44. Kendall GS, Kapetanakis A, Ratnavel N, Azzopardi D, Robertson NJ. Cooling on retrieval study group. Passive cooling for initiation of therapeutic hypothermia in neonatal encephalopathy. *Arch Dis Child Fetal Neonatal Ed* (2010) 95:F408–12. doi: 10.1136/adc.2010.187211
45. Gunn AJ, Groenendaal F. Delayed neuroprotection in the era of hypothermia: what can we add? *J Clin Neonatol.* (2016) 5:3. doi: 10.4103/2249-4847.173279
46. Laptook AR, Shankaran S, Tyson JE, Munoz B, Bell EF, Goldberg RN, et al. Effect of therapeutic hypothermia initiated after 6 hours of age on death or disability among newborns with hypoxic-ischemic encephalopathy. *JAMA.* (2017) 318:1550–60. doi: 10.1001/jama.2017.14972
47. Huun MU, Garberg H, Løberg EM, Escobar J, Martinez-Orgado J, Saugstad OD, et al. DHA and therapeutic hypothermia in a short-term follow-up piglet model of hypoxia-ischemia: effects on H+MRS biomarkers. *PLoS ONE.* (2018) 13:e0201895. doi: 10.1371/journal.pone.0201895
48. Huun MU, Garberg HT, Buonocore G, Longini M, Belvisi E, Bazzini F, et al. Regional differences of hypothermia on oxidative stress following hypoxia-ischemia: a study of DHA and hypothermia on brain lipid peroxidation in newborn piglets. *J Perinat Med.* (2018) 47:82–9. doi: 10.1515/jpm-2017-0355
49. Berman DR, Mozurkewich E, Liu Y, Shangguan Y, Barks JD, Silverstein FS. Docosahexaenoic acid augments hypothermic neuroprotection in a neonatal rat asphyxia model. *Neonatology.* (2013) 104:71–8. doi: 10.1159/000351011
50. An H, Duan Y, Wu D, Yip J, Elmadhoun O, Wright JC, et al. Phenothiazines enhance mild hypothermia-induced neuroprotection via PI3K/Akt regulation in experimental stroke. *Sci Rep.* (2017) 7:7469. doi: 10.1038/s41598-017-06752-5
51. Eady TN, Belayev L, Khoutorova L, Atkins KD, Zhang C, Bazan NG. Docosahexaenoic acid signaling modulates cell survival in experimental ischemic stroke penumbra and initiates long-term repair in young and aged rats. *PLoS ONE.* (2012) 7:e46151. doi: 10.1371/journal.pone.0046151
52. Zhao H, Shimohata T, Wang JQ, Sun G, Schaal DW, Sapolsky RM, et al. Akt contributes to neuroprotection by hypothermia against cerebral ischemia in rats. *J Neurosci.* (2005) 25:9794–806. doi: 10.1523/JNEUROSCI.3163-05.2005
53. Cai W, Liu S, Hu M, Sun X, Qiu W, Zheng S, et al. Post-stroke DHA treatment protects against acute ischemic brain injury by skewing macrophage polarity toward the M2 phenotype. *Transl Stroke Res.* (2018) 9:669–80. doi: 10.1007/s12975-018-0662-7
54. Lee JH, Wei ZZ, Cao W, Won S, Gu X, Winter M, et al. Regulation of therapeutic hypothermia on inflammatory cytokines, microglia polarization, migration and functional recovery after ischemic stroke in mice. *Neurobiol Dis.* (2016) 96:248–60. doi: 10.1016/j.nbd.2016.09.013
55. Zhang W, Hu X, Yang W, Gao Y, Chen J. Omega-3 polyunsaturated fatty acid supplementation confers long-term neuroprotection against neonatal hypoxic-ischemic brain injury through anti-inflammatory actions. *Stroke.* (2010) 41:2341–7. doi: 10.1161/STROKEAHA.110.586081

56. Yenari MA, Han HS. Influence of hypothermia on post-ischemic inflammation: role of nuclear factor kappa B (NFkappaB). *Neurochem Int.* (2006) 49:164–9. doi: 10.1016/j.neuint.2006.03.016
57. Moreira JD, Knorr L, Thomazi AP, Simão F, Battú C, Oses JP, et al. Dietary omega-3 fatty acids attenuate cellular damage after a hippocampal ischemic insult in adult rats. *J Nutr Biochem.* (2010) 21:351–6. doi: 10.1016/j.jnutbio.2009.01.013
58. Zhang H, Zhou M, Zhang J, Mei Y, Sun S, Tong E. Therapeutic effect of post-ischemic hypothermia duration on cerebral ischemic injury. *Neurol Res.* (2008) 30:332–6. doi: 10.1179/174313208X300279
59. Gong P, Hua R, Zhang Y, Zhao H, Tang Z, Mei X, et al. Hypothermia-induced neuroprotection is associated with reduced mitochondrial membrane permeability in a swine model of cardiac arrest. *J Cereb Blood Flow Metab.* (2013) 33:928–34. doi: 10.1038/jcbfm.2013.33
60. Oorschot DE, Sizemore RJ, Amer AR. Treatment of neonatal hypoxic-ischemic encephalopathy with erythropoietin alone, and erythropoietin combined with hypothermia: history, current status, and future research. *Int J Mol Sci.* (2020) 21:1487. doi: 10.3390/ijms21041487
61. Chen J, Liu L, Zhang H, Geng X, Jiao L, Li G, et al. Endovascular hypothermia in acute ischemic stroke: pilot study of selective intra-arterial cold saline infusion. *Stroke.* (2016) 47:1933–35. doi: 10.1161/STROKEAHA.116.012727
62. Li L, Yang R, Li P, Lu H, Hao J, Li L, et al. Combination treatment with methylene blue and hypothermia in global cerebral ischemia. *Mol Neurobiol.* (2018) 55:2042–55. doi: 10.1007/s12035-017-0470-1
63. Kim JJ, Buchbinder N, Ammanuel S, Kim R, Moore E, O'Donnell N, et al. Cost-effective therapeutic hypothermia treatment device for hypoxic ischemic encephalopathy. *Med Devices.* (2013) 6:1–10. doi: 10.2147/MDER.S39254
64. Zhang M-M, Zou Y, Li S-M, Wang L, Sun Y-H, Shi L, et al. The efficacy and safety of omega-3 fatty acids on depressive symptoms in perinatal women: a meta-analysis of randomized placebo-controlled trials. *Transl Psychiatry.* (2020) 10:193. doi: 10.1038/s41398-020-00886-3
65. Defilippis AP, Blaha MJ, Jacobson TA. Omega-3 Fatty acids for cardiovascular disease prevention. *Curr Treat Options Cardiovasc Med.* (2010) 12:365–80. doi: 10.1007/s11936-010-0079-4
66. Calder PC, Deckelbaum RJ. Intravenous fish oil in hospitalized adult patients: reviewing the reviews. *Curr Opin Clin Nutr Metab Care.* (2013) 16:119–23. doi: 10.1097/MCO.0b013e32835dbde9

Conflict of Interest: RD is a founding scientist and member of the scientific advisory board of DeckTherapeutics, Inc. (DT), a company that plans to use novel n-3 lipid emulsions to prevent tissue death after ischemic brain injury. The plans for DT do not overlap with any of the data presented in this paper.

The remaining authors declare that the research was conducted in the absence of any commercial or financial relationships that could be construed as a potential conflict of interest.

frontiers in Pediatrics

SYSTEMATIC REVIEW
published: 02 February 2021
doi: 10.3389/fped.2021.631258

Pathophysiology of Cerebral Hyperperfusion in Term Neonates With Hypoxic-Ischemic Encephalopathy: A Systematic Review for Future Research

*Dianne G. Kleuskens, Filipe Gonçalves Costa, Kim V. Annink, Agnes van den Hoogen, Thomas Alderliesten, Floris Groenendaal, Manon J. N. Benders and Jeroen Dudink**

Department of Neonatology, Wilhelmina Children's Hospital, University Medical Center Utrecht, Utrecht University, Utrecht, Netherlands

OPEN ACCESS

Edited by:
Francisco J. Alvarez, Hospital de Cruces, Spain

Reviewed by:
Raul Chavez-Valdez, Johns Hopkins Medicine, United States
Britt Nakstad, University of Oslo, Norway

***Correspondence:**
Jeroen Dudink
j.dudink@umcutrecht.nl

Specialty section:
This article was submitted to Neonatology, a section of the journal Frontiers in Pediatrics

Received: *19 November 2020*
Accepted: *07 January 2021*
Published: *02 February 2021*

Citation:
Kleuskens DG, Gonçalves Costa F, Annink KV, van den Hoogen A, Alderliesten T, Groenendaal F, Benders MJN and Dudink J (2021) Pathophysiology of Cerebral Hyperperfusion in Term Neonates With Hypoxic-Ischemic Encephalopathy: A Systematic Review for Future Research. Front. Pediatr. 9:631258. doi: 10.3389/fped.2021.631258

Worldwide neonatal hypoxic-ischemic encephalopathy (HIE) is a common cause of mortality and neurologic disability, despite the implementation of therapeutic hypothermia treatment. Advances toward new neuroprotective interventions have been limited by incomplete knowledge about secondary injurious processes such as cerebral hyperperfusion commonly observed during the first 1–5 days after asphyxia. Cerebral hyperperfusion is correlated with adverse neurodevelopmental outcome and it is a process that remains poorly understood. In order to provide an overview of the existing knowledge on the pathophysiology and highlight the gaps in current understanding of cerebral hyperperfusion in term animals and neonates with HIE, we performed a systematic research. We included papers scoping for study design, population, number of participants, study technique and relevant findings. Methodological quality was assessed using the checklist for cohort studies from The Joanna Briggs Institute. Out of 2,690 results, 34 studies were included in the final review—all prospective cohort studies. There were 14 studies of high, 17 moderate and 3 of low methodological quality. Data from the literature were analyzed in two main subjects: (1) Hemodynamic Changes subdivided into macro- and microscopic hemodynamic changes, and (2) Endogenous Pathways which was subdivided into N-methyl-D-aspartate/Mitogen activated protein kinase (NDMA/MAPK), Nitric Oxide (NO), prostanoids and other endogenous studies. Cerebral hyperperfusion in term neonates with HIE was found to be present 10–30 min after the hypoxic-ischemic event and was still present around day 10 and up to 1 month after birth. Cerebral hyperperfusion was also characterized by angiogenesis and cerebral vasodilation. Additionally, cerebral vasodilation was mediated by endogenous pathways such as MAPK through urokinase Plasminogen Activator (uPA), by neuronal NO synthase following NMDA and by prostanoid synthesis. Future research should elucidate the precise role of NMDA, MAPK and prostanoids in cerebral hyperperfusion.

Moreover, research should focus on possible interventions and the effect of hypothermia on hyperperfusion. These findings should be taken into account simultaneously with brain imagining techniques, becoming a valuable asset in assessing the impact in neurodevelopmental outcome.

Keywords: cerebral hyperperfusion, cerebral vasodilation, hyperemia, hypoxic-ischemic encephalopathy (HIE), neonatal encephalopathy, perinatal hypoxia-ischemia

HIGHLIGHTS

- What is already known? Cerebral hyperperfusion in term neonates with hypoxic-ischemic encephalopathy is often seen after the acute phase, occurring 6–15 h after the HI-event. Cerebral hyperperfusion is correlated with adverse neurodevelopmental outcome.
- What this review adds? Cerebral hyperperfusion is present 10–30 minutes after the hypoxic-ischemic event and persisted around day 10 and up to 1 month after birth. Cerebral hyperperfusion may be characterized by angiogenesis and cerebral vasodilation. A rise in prostanoids may contribute to vasodilatation trough MAPK. Another finding is that NMDA induces vasodilatation and the cerebroprotective effects of hypothermia therapy are not mediated by NMDA.
- What is still unknown? Future research needs to be developed about the precise role of NMDA, MAPK, prostanoids in cerebral vasodilation, and possible interventions.

INTRODUCTION

Hypoxic-ischemic encephalopathy (HIE) is one of the main causes of neonatal death and developmental psychomotor disorders in the pediatric population. The incidence of HIE is ∼1–8 per 1,000 live births in technically advanced countries and is up to 26 per 1,000 live births in less developed countries (1). Despite the widespread use of therapeutic hypothermia, a large proportion of infants will suffer from neurodevelopmental impairments, especially in the case of severe HIE (2). Therefore, new synergistic therapies need to be developed.

For clinicians, it is important to understand the pathophysiology of injury after the HI-event, due to its relevance in developing novel therapies and because neuroimaging has shown that subsequent brain injury evolves over the course of days, if not weeks (3). In the process of neonatal encephalopathy, a hypoxic-ischemic event, with intermitting anoxia or acute hypoxia, leads to a decreased cerebral perfusion, if the event occurs for long enough. This decreased perfusion sets a time-related pattern of injury pathways in motion, which is divided into distinct phases (4, 5). **Figure 1** provides a schematic overview of the phases of injury in HIE. After the hypoxic-ischemic event, there is the acute phase of injury, which is followed by a latent phase of injury. After ∼6–15 h, there is a secondary phase. A tertiary phase occurs weeks after the hypoxic-ischemic event. More extensive:

- The **acute phase**, also known as "primary energy failure," is characterized by anaerobic metabolism, oxidative stress, neuronal cell death, and excitotoxicity. In the process of excitotoxicity, a surplus in the amount of the excitatory amino acid glutamate leads to overstimulation of the 2-(aminomethyl)phenylacetic acid (AMPA), kainite (KA), and N-methyl-D-aspartate (NMDA) receptors. Overstimulation of AMPA and KA causes an influx of sodium (Na^+) and chloride (Cl^-), which leads to an increased cellular osmolality. Overstimulation of NMDA triggers the influx of calcium (Ca^{2+}), which leads to apoptosis and necrosis (4). The mitogen activated protein kinase (MAPK) signaling pathway is overactivated after the hypoxic-ischemic event, leading to neuronal apoptosis. Prostanoids also play a role in the hypoxic-ischemic event: stimulating prostanoid-receptors may be neuroprotective and prevent neuronal cerebellar injury (4). Depending on the duration of decreased perfusion and the presence or absence of medical intervention, a partial recovery with reperfusion occurs from 30 to 60 min after the hypoxic-ischemic event (6).

- The **latent phase** of injury follows after the acute phase, which may last from 1 to 6 h. This latent phase is characterized by neuroinflammation and the continuation of activated apoptotic cascades. In neonates with moderate to severe HIE, the latent phase is followed up by the secondary phase, also known as "secondary energy failure" (4).

- The **secondary phase** occurs within ∼6–15 h and is characterized by cytotoxic edema, excitotoxicity and cerebral hyperperfusion (7).

- The **tertiary phase** occurs in the weeks or months following primary energy failure. It involves remodeling of the injured brain, astrogliosis, and late cell death (8).

Abbreviations: AMPA, 2-(aminomethyl)phenylacetic acid; LRP, Lipoprotein-Related Protein; ASL, Arterial Spin Labeling; MABP, Mean Arterial Blood Pressure; BCAO, Bilateral Carotid Artery Occlusion; MAPK, Mitogen activated protein kinase; cAMP, Cyclic Adenosine Monophosphate; MCA, Middle Cerebral Artery; CBF, Cerebral Blood Flow; MRI, Magnetic Resonance Imaging; CFOE, Cerebral Fractional Oxygen Extraction; NIRS, Near-Infrared Spectroscopy; cGMP, Guanosine 3',5'-cyclic Monophosphate; NMDA, N-methyl-D-aspartate; CO, Cardiac Output; (n)NO, (neuronal) Nitric Oxide; CORM-A1, Carbon Monoxide Release Molecule-A1; PACAP, Pituitary Adenylate Cyclase-Activating Peptide; CrO2, Cerebral Oxygen Saturation; PRISMA, Preferred Reporting Items for Systematic Reviews and Meta-Analysis; CSF, Cerebral-Spinal Fluid; PRx, Pressure Reactivity; DWI, Diffusion-Weighted Imaging; RI, Resistance Index; GA, Gestational Age; uPA, Urokinase Plasminogen Activator; HIE, Hypoxic-Ischemic Encephalopathy; US, Ultrasound; HO/CO, Heme Oxylase/Carbon Monoxide; V_d, Diastolic Velocity; KA, Kainite; VEGF, Vascular Endothelial Growth Factor; KYNA, Kynurenine Acid; VTQ, Virtual Touch Quantification.

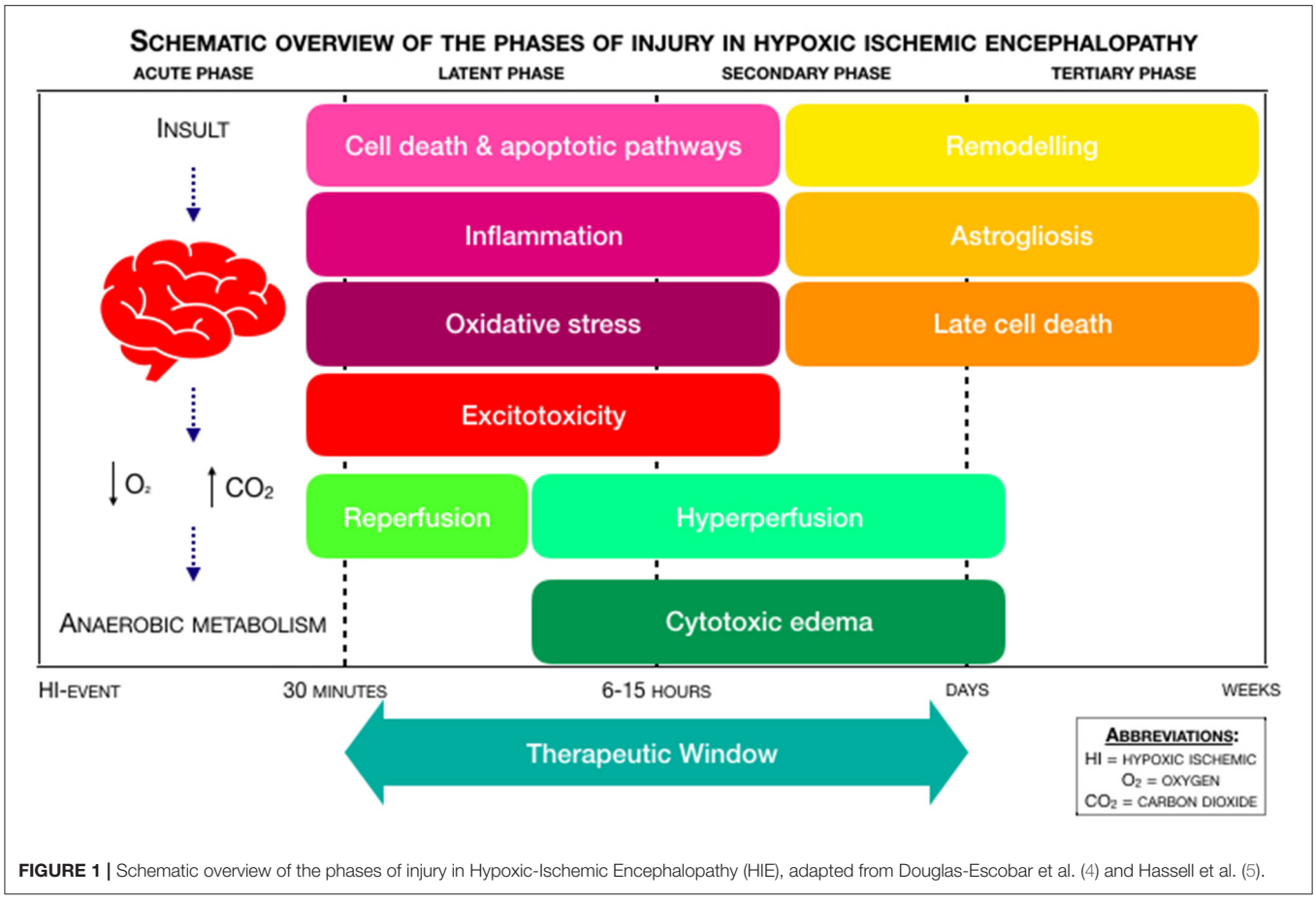

FIGURE 1 | Schematic overview of the phases of injury in Hypoxic-Ischemic Encephalopathy (HIE), adapted from Douglas-Escobar et al. (4) and Hassell et al. (5).

In this review, we focused on pathophysiology of cerebral hyperperfusion, often seen in the secondary phase of HI-injury, and not on the adverse outcome itself. Cranial ultrasound (cUS) and brain Magnetic Resonance Imaging (MRI) are the most used imaging techniques in neonates with HIE. Cerebral hyperperfusion seen on Arterial Spin Labeling (ASL) MRI is correlated with an adverse neurodevelopmental outcome (2, 9). To understand cerebral hyperperfusion, it is essential to elucidate when this phenomenon takes place and what the underlying mechanisms leading to hyperperfusion are. Understanding the pathophysiological mechanisms behind these observations will provide an insight into how cerebral hyperperfusion is associated with (adverse) outcome.

Given that this topic is prone to rapid changes in what is known to the scientific community, the review intents to provide a summary of the methods, models and studies already existing. With this paper we hope to create a platform that allows researchers to come up with novel ideas, using this review as a gateway for new research. This study aims to provide an overview of hemodynamic changes in cerebral hyperperfusion and endogenous pathways leading to cerebral hyperperfusion in term neonates with HIE.

METHODS

Study Design

A systematic review was performed following the steps of the Preferred Reporting Items for Systematic Reviews and Meta-Analysis (PRISMA) statement (10). Prior to initiation, the systematic review protocol was registered in PROSPERO (https:///www.crd.york.ac.uk/PROSPERO), registration number CRD42020152957. Because the studies in this systematic review were considered to be heterogeneous regarding study population, study technique and study outcome, we refrained from statistically pooling the data in a meta-analysis and performed a best evidence synthesis. The results of this systematic review will be described in a narrative manner.

Inclusion and Exclusion Criteria

To systematically review the pathophysiology of hyperperfusion in term neonates with hypoxic-ischemic encephalopathy, we conducted a search including papers in which term neonates (>36 weeks' GA) had a diagnosis of HIE caused by perinatal asphyxia, with or without hypothermia treatment. We also included animal studies with models of perinatal HIE at term equivalent age, because pathophysiology is more thoroughly studied in animal models. We excluded reviews, articles on

preterm neonates (<36 weeks' GA), articles with pooled data on both term and preterm neonates, articles on adults and articles on neonates with main pathology that alters the brain physiology (main cerebral hemorrhage, metabolic disorders, main cardiac abnormalities or chromosomic disorders). We also excluded articles with data on NIRS or MRI when they did not report effects on vascular resistance, (re)perfusion or cerebral blood volume. No date restrictions were applied. We limited the search to English articles only. When analyzing results, the authors considered rats and mouses as "small animals" and piglets and lambs as "large animals."

Since autoregulation is not the scope of this review, we did not include articles on this topic specifically. If the reader would like to have an in-depth overview of cerebral vascular autoregulation (CVAR) studies using NIRS in neonates and given that autoregulation is not the main focus of the review, we would like to refer to the paper of Thewissen et al. (11).

Search Strategy

The research question was defined according to the PICOTS system (**Supplementary Appendix 1**). The main search terms were Hypoxic-Ischemic Encephalopathy (HIE), Vasodilation and (Re-)perfusion. Besides title and abstract, MeSH-terms were used for all search terms (**Supplementary Appendixes 2**–**4**). A medical librarian with systematic review experience helped in developing the search strategy.

Data Sources, Studies Selections, and Data Extraction

Medline (PubMed) and Embase were searched from inception to December 12, 2018, with similar search strategies. Two researchers (D.K. and K.A.) independently analyzed all abstracts after removing duplicates while appraising the in- and exclusion criteria. The full text of potentially eligible studies was then assessed for inclusion using the same inclusion and exclusion criteria. If an inconsistency occurred during the abstract or full text analysis, a consensus was reached in a meeting or by the involvement of a third researcher (J.D.). Data were extracted and reviewed by D.K. and A.H. The characteristics of the included studies were recorded using data extraction forms, which included the following characteristics: study design, population, number of participants, study technique and relevant findings. Before submission of the review, the search was repeated in Medline and Embase for additional articles.

Methodological Quality

The Checklist for Cohort Studies from The Joanna Briggs Institute Critical Appraisal Tools was used to assess the methodological quality of the individual studies (12). The methodologic quality was assessed independently by two researchers (D.G.K. and A.H.), and disagreements were resolved in a meeting or by the consideration of a third researcher (J.D). We calculated the score and added up "Yes" as 1; "No" as 0 and "Unclear" as 0. Quality was calculated as the added up score, divided by the number of questions answered with "Yes," "No" or "Unclear." (Non-Applicable was not taken into account.) For example, 7 of 11 questions were answered with Yes and 1 question was answered with Non-Applicable. The calculated score is $7/(11-1) = 7/10 = 70\%$. A score of $\geq$80% was considered a study of high quality. A score between 60 and 80% was considered as moderate quality, whereas a score of $\leq$60% was considered to be of low quality. These cut-off values were agreed with the research team.

Best-Evidence Synthesis

A best-evidence synthesis was performed since the outcome measures of the included studies were too heterogeneous for a meta-analysis. We used the guidelines from Proper et al. (13) to synthesize the methodologic quality of the studies and to be able to reach conclusions regarding the pathophysiology of cerebral hyperperfusion. The guideline consists of the following three levels:

1. Strong evidence: consistent findings in multiple ($\geq$2) high-quality studies;
2. Moderate evidence: consistent findings in one high-quality study and at least one low-quality study, or consistent findings in multiple low-quality studies;
3. Insufficient evidence: only one study available or inconsistent findings in multiple ($\geq$2) studies.

Results were considered to be consistent when a minimum of 75% of the studies showed results in the same direction, which was defined according to significance ($p < 0.05$). If there were two or more high-quality studies, the studies of low methodologic quality were disregarded in the evidence synthesis.

RESULTS

The search in Medline and Embase provided 3,253 results. **Figure 2** provides a detailed overview of study screening and selection. The additional search in Medline and Embase before submission of the review did not provide further articles.

Data from the literature were analyzed and presented below in two main subjects: (1) Hemodynamic Changes subdivided into macro- and microscopic hemodynamic changes, and (2) Endogenous Pathways which was subdivided into NDMA/MAPK, NO, prostanoids, and other endogenous studies. This makes that the review has a total of six themes.

A total of 34 studies were eligible for the review; 12 hemodynamic changes studies and 22 endogenous pathway studies. In total, 44 human newborns and 334 animals (169 large animals; 165 small animals) were included in the hemodynamic changes studies. In the endogenous pathway studies, there were no human newborns studies included. A total of 775 animals (656 large animals; 119 small animals) in the endogenous pathway studies were studied; in five studies (14–18) the number of included animals in the study was unknown. All studies were prospective cohort studies. A separate subject about human studies was not made because there were not enough human studies for that. Characteristics, relevant findings and methodological quality of each study are summarized in **Tables 1**, **2**.

There were 14 studies of high, 17 studies of moderate and three studies of low methodological quality (**Tables 1**, **2**).

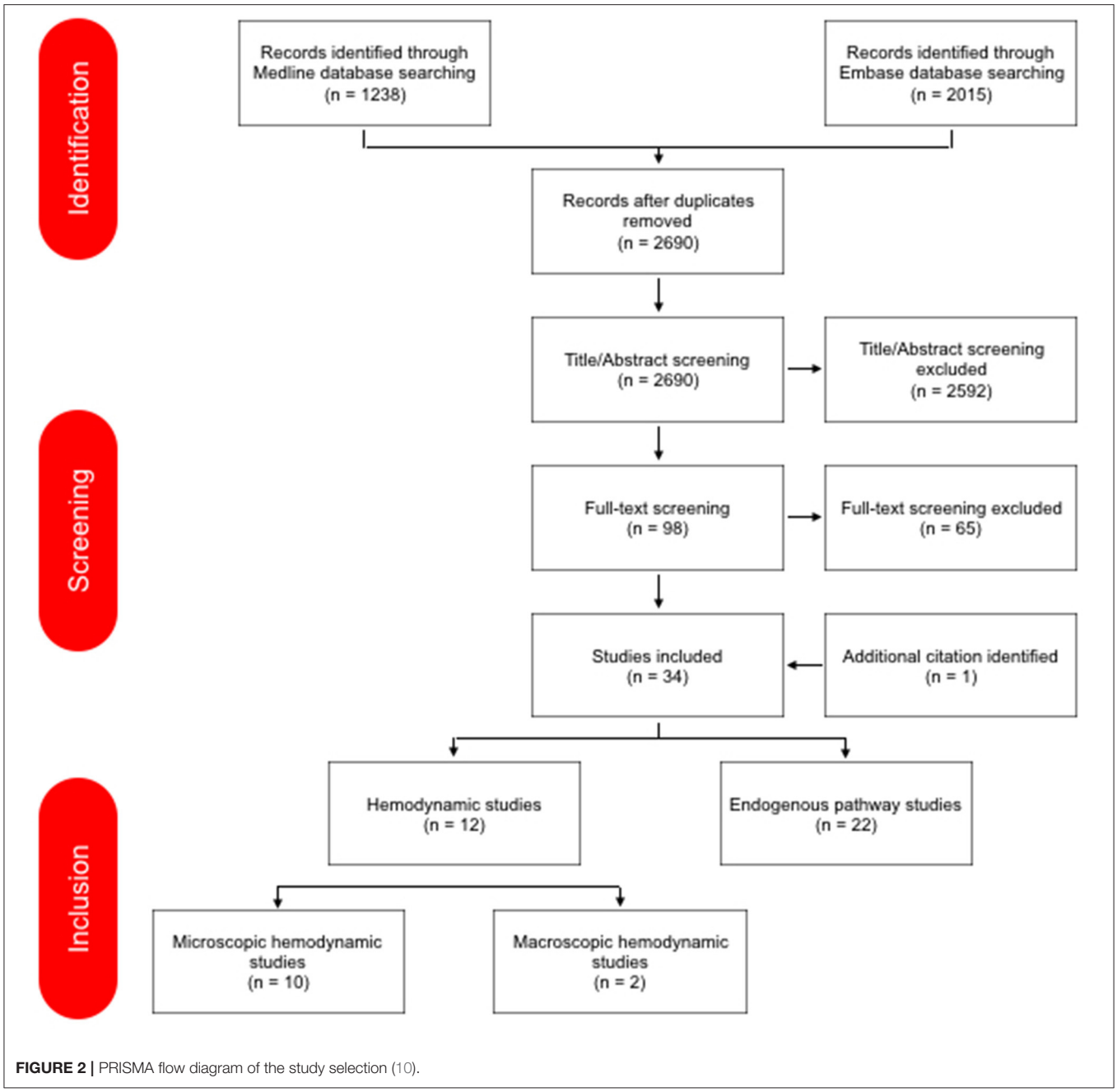

FIGURE 2 | PRISMA flow diagram of the study selection (10).

Table 3 shows the critical review of the studies, presenting the questions to assess methodological quality and the answers to these questions.

Macroscopic Hemodynamic Changes

Ten studies were included describing hemodynamic changes on a macrovascular level (**Figure 3**). Regarding small animal studies, Manole et al. (25), showed that after the hypoxic-ischemic (H-I) event cerebral blood flow (CBF) increases within 5 min and subsided after 10 min (studied with MRI). Wang et al. (23) used virtual touch tissue quantification (VTQ), histological staining and ultrasound to determine the severity of brain damage from HIE. In the asphyxia group, the diastolic velocity (Vd) was significantly increased 3 h post carotid ligation compared to the ischemia group, leading to a lower resistance index (RI) of the right MCA, indicating that the elasticity of the cerebral blood vessels decreases. This study suggests that there is a consistent correlation among histological and hemodynamic changes, VTQ values and neurodevelopmental outcome. Additionally, another small animal study showed in what regions hyperperfusion takes place. The study of Buckley et al. (21), showed hyperperfusion in both hemispheres, and more pronounced in the contralateral hemisphere (studied with diffuse correlation spectroscopy).

TABLE 1 | Study characteristics hemodynamic studies, relevant findings, and methodological quality.

References	Design	Population; no.	Technique	Relevant findings	Methodological quality
MACROSCOPIC HEMODYNAMIC STUDIES					
Jinnai et al. (19)	Prospective cohort	Piglets; *N* = 26	Near-infrared TRS	↓CBV within 24 h after the HI-insult, longer duration of LAEEG after insult is associated with a greater decrease in the HT group	High
Wu et al. (20)	Prospective cohort	Human newborns, gestational age 38,8 ± 2 weeks; *N* = 20	Electrical velocimetry, transcranial doppler	During the rewarming phase after HI: ↑CO due to ↑HR; ↑MCA peak systolic value; no changes in CrO_2 and CFOE, suggesting cerebral flow metabolism coupling remained intact during rewarming	High
Buckley et al. (21)	Prospective cohort	Rat pups; *N* = 46	Diffuse correlation spectroscopy	↑CBF after 5–10 min after the HI-insult in both hemispheres, more pronounced in the contralateral hemisphere	Moderate
Nakamura et al. (22)	Prospective cohort	Piglets; *N* = 21	Near-infrared TRS, Histologic staining	Increased CBV up to 6 h after HI insult indicated more marked histopathological brain damage	Moderate
Wang et al. (23)	Prospective cohort	Rat pups; *N* = 90	Color Doppler Ultrasound, VTQ, HE-staining	After asphyxia, ↑Vd of the MCA, ↓Vs and ↓RI of the MCA after 3 h; consistent with the pathological findings	Low
Chakkarapani et al. (24)	Prospective cohort	Piglets; *N* = 51	aEEG	Cerebrovascular Pressure Reactivity ([PRx; the correlation coefficient between intracranial and mean arterial blood pressure (MABP)]; PRx is impaired during HI, latent phase, secondary PRx peak (after 6 h) is correlated with severe neuropathology	Moderate
Manole et al. (25)	Prospective cohort	Rat pups; *N* = 17	ASL-MRI	After 8,5–9 min of asphyxial CA, subcortical hyperemia at 5 min was followed by a return of CBF to baseline values by 10 min, absence of cortical hyperemia after CA (cortical hypoperfusion)	High
Leffler et al. (26)	Prospective cohort	Piglets; *N* = 24	Radioactively labeled microspheres	Reactive hyperemia throughout the brain (except the cerebrum), peaking by 5 min and subsiding by 20 min of reperfusion	Moderate
Rosenberg et al. (27)	Prospective cohort	Neonatal lambs; *N* = 31	Radioactively labeled microspheres	2–5 h after asphyxia, ↑CBF, cerebral oxygen delivery ↓ and cerebral oxygen consumption remained stable due to a proportional increase in CFOE; impaired cerebral autoregulation. Second finding: postasphyxia cerebral vasodilation is not attributed to the evolution of gross cerebral edema	Moderate
Rosenberg et al. (28)	Prospective cohort	Neonatal lambs; *N* = 9	Radioactively labeled microspheres	↑CBF immediately after asphyxia, cerebral oxygen delivery ↑, cerebral oxygen consumption ↓, CFOE ↓	Moderate
MICROSCOPIC HEMODYNAMIC STUDIES					
Shaikh et al. (29)	Prospective cohort	Human newborns (*N* = 24); rat pups (*N* = 12)	ASL-MRI study	↑CBF around day 10 of life and up to 1 month of life; ↑VEGF expression 24-48 h after the HI-event, ↑endothelial cell count 7 and 11 days after the HI-event	High
Domoki et al. (30)	Prospective cohort	Piglets; *N* = 7, 1–2 days old	Closed cranial window, Laser-speckle imaging	Marked cortical hyperemia in 5/7 piglets, ↑pial artery diameters and arterial flow velocity	High

aEEG, amplitude-integrated electroencephalogram; ASL-MRI, arterial spin-labeled magnetic resonance imaging; CA, cardiac arrest; CBF, cerebral blood flow; CBV, cerebral blood volume; CFOE, cerebral fractional oxygen extraction; CO, cardiac output; CrSO2, regional cerebral oxygen saturation; HE, hematoxylin and eosin; HI, hypoxic ischemic; HT, hypothermia; HR, heart rate; LAEEG, low-amplitude electroencephalography; MCA, middle cerebral artery; MRI, magnetic resonance imaging; TRS, time resolved spectroscopy; Vd, diastolic velocity; VEGF, vascular endothelial growth factor; VTQ, virtual touch tissue quantification.

TABLE 2 | Study characteristics endogenous pathway studies, relevant findings, and methodological quality.

References	Design	Population; no.	Technique	Relevant findings	Methodological Quality
NMDA/MAPK					
Dang et al. (31)	Prospective cohort	Piglets; *N* = 25	H-MRS, DWI	The glutamate level in the basal ganglia underwent a "two-phase" change after HI: the first rise in glutamate after 0–6 h and second rise in glutamate after 24–30 h, due to reperfusion injury	High
Armstead et al. (32)	Prospective cohort	Rat pups; *N* = 65	Closed Cranial Window	Treatment with Plasminogen Activator Inhibitor peptide EEIIMD prevents the impairment of vasodilator responses to hypercapnia and hypotension after HI, by upregulating p38 MAPK	High
Kiessling et al. (33)	Prospective cohort	Piglets; *N* = 90	Closed Cranial Window	Inhibition of Urokinase Plasminogen Activator and Integrin prevents impairment of cerebrovasodilation after HI	Moderate
Armstead et al. (34)	Prospective cohort	Rat pups; *N* = 54	Closed Cranial Window	Urokinase Plasminogen Activator impairs cerebrovasodilation through LRP and MAPK	High
Bari et al. (35)	Prospective cohort	Piglets; *N* = 53	Closed Cranial Window	Kynurenine acid (KYNA) attenuates NMDA-induced pial artery dilatation; NMDA-induced arteriolar dilatation can be inhibited by KYNA	High
Philip et al. (36)	Prospective cohort	Newborn lambs; *N* = 42	Closed Cranial Window	Protein thyrosine kinase and MAPK impairs NMDA-induced cerebrovasodilation by nociceptin/orphanin FQ activation	Moderate
Jagolino et al. (37)	Prospective cohort	Newborn lambs; *N* = 119	Closed Cranial Window	Protein thyrosine kinase, MAPK and nociceptin/orphanin FQ impair hypercapnic cerebrovasodilation	Moderate
Perciaccante et al. (38)	Prospective cohort	Piglets; *N* = 60	Intravital microscopy	(1) Hypothermia fails to preserve cerebral arteriolar dilatation to NMDA during and following ischemia; (2) Cerebral vascular responsiveness to an excitatory neurotransmitter is intact despite the reduced metabolic rate during hypothermia	Moderate
Armstead et al. (39)	Prospective cohort	Piglets; *N* = 42	Closed Cranial Window	Nociceptin/Orphalin FQ and NMDA contribute to the impairment of hypotensive cerebrovasodilation	High
Taylor et al. (40)	Prospective cohort	Newborn lambs; *N* = 20	Microinjection into the brain, Doppler imaging	(1) Local microinjection with NMDA increases both local and global CBF within minutes of injection; (2) Most marked increases in the right midbrain, diencephalon and temporal lobe; (3) Alterations in echotexture are primarily due to intracellular cytoplasmic changes and microscopic hemorrhage	High
NO					
Hsu et al. (14)	Prospective cohort	Postpartum day-7 rat pups; *N* = ?	Electron microscopy, doppler imaging	Microvascular damage post HI is contributed by neurnal NOS, nNOS underwent a "two-phase" change after HI: first rise in nNOS directly after the HI-event (swollen nucleoli, CBF↓); second rise 3 h after reoxygenation (overactive microglia, ↑CBF)	Moderate
Domoki et al. (41)	Prospective cohort	Piglets; *N* = 45	Closed Cranial Window	NMDA-induced vasodilation is mediated by endothelium-independent nitric oxide release and activation of neuronal NOS positive neurons	Moderate
Dorrepaal et al. (42)	Prospective cohort	Newborn lambs; *N* = 16	unknown	Inhibition of NOS by N-nitro-L-arginine (NLA) restores autoregulation of cerebral bloodflow, suggesting a role for nitric oxide-induced vasodilation in the impairment of autoregulation	Moderate
Wilderman et al. (15)	Prospective cohort	Piglets; *N* = ?	Closed Cranial Window	Neuronally derived NO contributes to hypoxic pial artery dilatation, through the formation of cGMP and the subsequent release of methionine enkephalin and leucine enkephalin	Moderate

(Continued)

TABLE 2 | Continued

References	Design	Population; no.	Technique	Relevant findings	Methodological Quality
Armstead et al. (16)	Prospective cohort	Piglets, *N* = ?	Closed Cranial Window	Contribution of Kca channel activation to hypoxic cerebrovasodilation is not mediated by NO/cGMP	Low
PROSTANOID					
Taniguchi et al. (17)	Prospective cohort	Rat pups, cell-specific knockout mouse pups; *N* = ?	unknown	Prostaglandin E2 EP4 receptor is cerebroprotective, it improves cerebral perfusion in both the contralateral and ipsilateral hypoxic-ischemic hemispheres	Moderate
Pourcyrous et al. (43)	Prospective cohort	Piglets; *N* = 15	Radioactive microsphere CBF determination	(1) Brain stem bloodflow increases at 1 min of asphyxia, is maintained at 5 min of asphyxia and increases more during reventilation than bloodflow to cerebrum and cerebellum; (2) Inhibition of prostanoid production with indomethacin does not limit vasoconstriction	High
Leffler et al. (26)	Prospective cohort	Piglets; N-12	Radioactive microsphere CBF determination	The failure of hypercapnia to dilate pial arterioles after cerebral ischemia results from the inability of this stimulus to increase cerebral vasodilator prostanoid synthesis	Moderate
Leffler et al. (18)	Prospective cohort	Piglets; *N* = ?	Closed Cranial Window	(1) Prostanoid in cortical subarachnoid CSF increase during acute hypoxia combined with hypercapnia coincident with dilatation of the pial vessels; (2) Systemic indomethacin decreases pial artery dilatation in response to combined hypoxia and hypercapnia	Low
OTHER					
Parfenova et al. (44)	Prospective cohort	Piglets; *N* = 26	Intravital microscopy, closed cranial window	CO, produced by astrocytes, has antioxidant effects (HO/CO and CORM-A1) and is cerebroprotective in neonatal asphyxia	High
Wilderman et al. (45)	Prospective cohort	Piglets, *N* = 65	Closed Cranial Window	cAMP contributes to hypoxic pial artery dilatation; endogenous PACAP modulates cAMP-induced opioid release, thereby contributing to hypoxic pial artery dilatation	High
Rosenberg et al. (28)	Prospective cohort	Newborn lambs; *N* = 16	Radioactive microsphere CBF determination	(1) Immediately after 5 min of asphyxia, increased CBF up to 60 min of reperfusion; (2) Damage by oxygen free radicals during postasphyxia cerebral reperfusion is important to the genesis of late postasphyxia bloodflow and oxygen metabolism abnormalities (treatment with activated polyethylene glycol catalase increases the CBF significantly 5 min postasphyxia)	Moderate

cAMP, cyclic adenosine monophosphate; cGMP, cyclic guanosine monophosphate; CO, carbon monoxide; CORM-A1, CO-releasing molecule-A1; CSF, cerebrospinal fluid; DWI, diffusion-weighted imaging; HI, hypoxia ischemia; H-MRS, proton magnetic resonance imaging; HO, heme oxylase; Kca, calcium sensitive K-channel; LRP, lipoprotein-related protein; MAPK, mitogen-activated protein kinas; NMDA, n-methyl-d-aspartate, NO, nitric oxide, NOS, nitric oxide syntases; PACAP, pituitary adenylate cyclase-activating peptide.

TABLE 3 | Methodological analysis of the included studies.

Study	1. Were the two groups similar?	2. Were the exposures measured similarly to both groups?	3. Was the exposure measured reliably?	4. Were confounding factors identified?	5. Were strategies to deal with confounding factors stated?	6. Were the groups/ participants free of the outcome at the beginning?	7. Were the outcomes measured reliably?	8. Was the follow up time reported and long enough?	9. Was follow up complete?	10. Were strategies to address incomplete follow up utilized?	11. Was appropriate statistical analysis used?	
MACROSCOPIC HEMODYNAMIC STUDIES												
Jinnai et al. (19)	+	+	+	+	+	+	+	+	+	NA	+	10/10 = 100%
Wu et al. (20)	+	+	+	+	−	−	+	+	+	NA	+	8/10 = 80%
Buckley et al. (21)	+	+	−	+	−	+	+	+	?	−	+	7/11 = 63%
Nakamura et al. (22)	+	+	+	+	−	+	+	−	−	NA	?	6/10 = 60%
Wang et al. (23)	?	+	?	−	NA	+	?	+	−	NA	+	4/9 = 44%
Chakkarapani et al. (24)	+	+	+	−	NA	+	?	−	+	NA	+	6/9 = 67%
Manole et al. (25)	+	+	+	+	−	+	+	−	+	NA	+	8/10 = 80%
Leffler et al. (46)	+	−	−	−	−	+	+	+	+	NA	+	6/10 = 60%
Rosenberg et al. (27)	+	+	+	−	NA	+	+	−	+	NA	+	7/9 = 78%
Rosenberg et al. (28)	+	+	+	−	NA	+	+	−	+	NA	?	6/9 = 67%
MICROSCOPIC HEMODYNAMIC STUDIES												
Shaik et al. (29)	+	−	+	+	+	−	+	+	+	NA	+	8/10 = 80%
Domoki et al. (30)	+	+	+	+	−	+	+	+	+	NA	+	9/10 = 90%
ENDOGENOUS STUDIES—NMDA/MAPK												
Armstead et al. (32)	+	+	+	+	−	+	+	−	+	NA	+	8/10 = 80%
Kiessling et al. (33)	+	+	+	−	NA	+	+	−	+	NA	+	7/9 = 78%
Armstead et al. (34)	+	+	+	+	−	+	+	−	+	NA	+	8/10 = 80%
Bari et al. (35)	+	+	+	+	−	+	+	−	+	NA	+	8/10 = 80%
Philip et al. (36)	+	+	+	−	NA	+	+	−	+	NA	+	7/9 = 78%
Jagolino et al. (37)	+	−	+	+	−	+	+	?	+	NA	+	7/10 = 70%
Armstead et al. (39)	+	+	+	+	−	+	+	−	+	NA	+	8/10 = 80%
Taylor et al. (40)	+	+	+	+	+	+	+	−	+	NA	+	9/10 = 90%
ENDOGENOUS STUDIES—NO												
Hsu et al. (14)	−	?	+	−	NA	+	+	+	+	NA	+	6/9 = 67%
Domoki et al. (41)	+	+	+	−	NA	+	+	?	+	NA	+	7/9 = 78%
Dorrepaal et al. (42)	?	+	+	−	NA	+	+	−	+	NA	+	6/9 = 67%
Wilderman et al. (15)	−	?	+	+	−	+	+	−	+	NA	+	6/10 = 60%
Armstead et al. (16)	−	?	+	−	NA	+	+	−	+	NA	+	5/9 = 56%

(Continued)

TABLE 3 | Continued

Study	1. Were the two groups similar?	2. Were the exposures measured similarly to both groups?	3. Was the exposure measured reliably?	4. Were confounding factors identified?	5. Were strategies to deal with confounding factors stated?	6. Were the groups/ participants free of the outcome at the beginning?	7. Were the outcomes measured reliably?	8. Was the follow up time reported and long enough?	9. Was follow up complete?	10. Were strategies to address incomplete follow up utilized?	11. Was appropriate statistical analysis used?	
ENDOGENOUS STUDIES—PROSTANOID												
Taniguchi et al. (17)	–	?	+	+	–	+	+	+	+	NA	+	7/10 = 70%
Pourcyrous et al. (43)	+	+	+	+	+	+	+	–	+	NA	+	9/10 = 90%
Leffler et al. (46)	+	+	+	–	NA	+	+	–	+	NA	?	6/9 = 67%
Leffler et al. (18)	–	?	+	–	NA	+	+	–	+	NA	+	5/9 = 56%
ENDOGENOUS STUDIES—OTHER												
Parfenova et al. (44)	+	+	+	+	+	+	+	+	+	NA	+	10/10 = 100%
Dang et al. (31)	+	+	+	+	–	+	–	+	+	NA	+	8/10 = 80%
Perciaccante et al. (38)	?	+	+	+	–	+	+	–	+	NA	+	7/10 = 70%
Wilderman et al. (45)	+	?	+	+	+	+	+	–	+	NA	+	8/10 = 80%
Rosenberg et al. (28)	+	+	+	–	NA	+	+	–	+	NA	+	7/9 = 78%

+ Yes, – No, ? Unclear, NA Not Applicable.

The subsequent following items were assessed: (1). Were the two groups similar and recruited from the same population? (2). Were the exposures measured similarly to assign people to both exposed and unexposed groups? (3). Was the exposure measured in a valid and reliable way? (4). Were confounding factors identified? (5). Were strategies to deal with confounding factors stated? (6). Were the groups/participants free of the outcome at the start of the study (or at the moment of exposure)? (7). Were the outcomes measured in a valid and reliable way? (8). Was the follow up time reported and sufficient to be long enough for outcomes to occur? (9). Was follow up complete, and if not, were the reasons to loss to follow up described and explored? (10). Were strategies to address incomplete follow up utilized? (11). Was appropriate statistical analysis used?

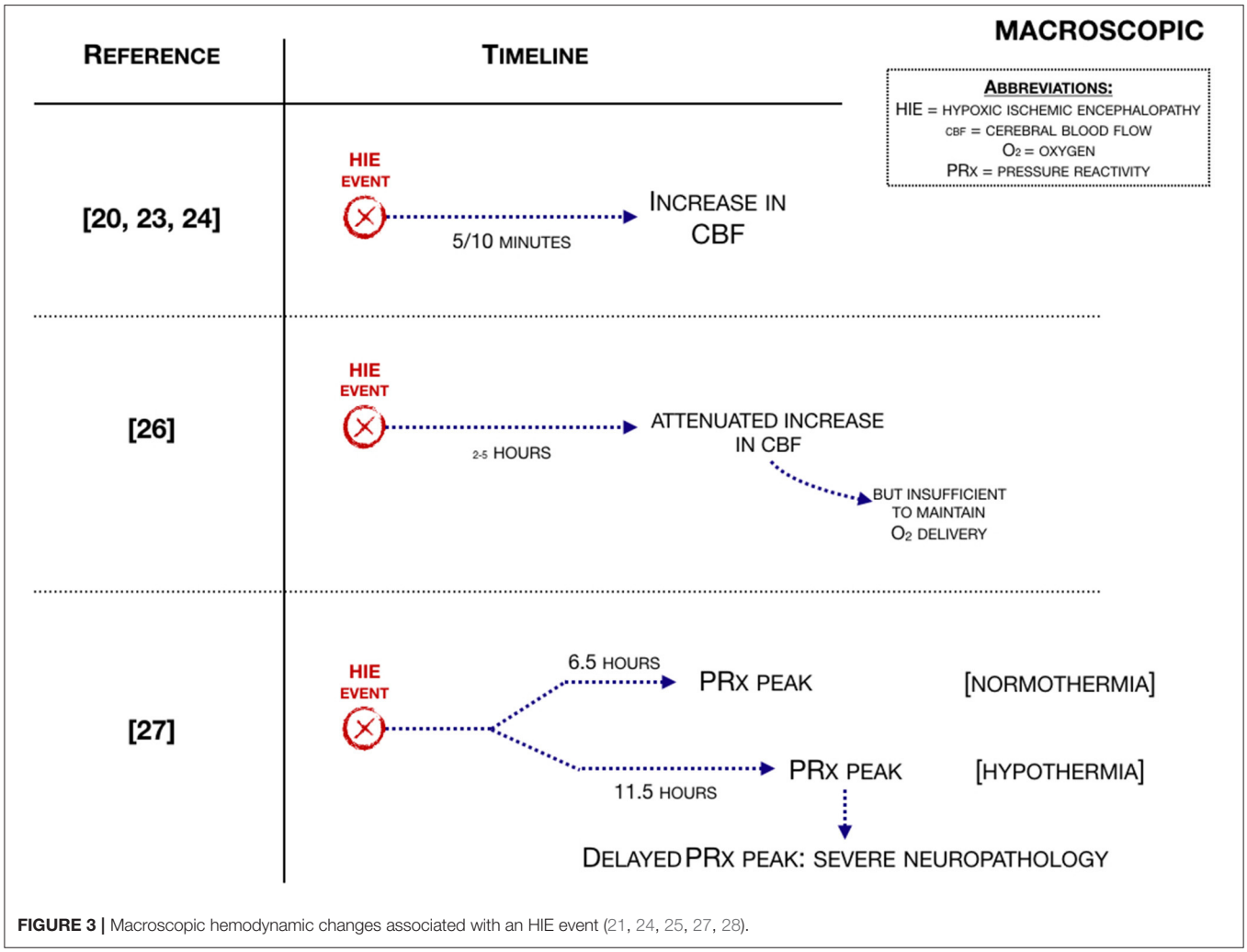

FIGURE 3 | Macroscopic hemodynamic changes associated with an HIE event (21, 24, 25, 27, 28).

Moving to large animal studies, Rosenberg studied cerebral blood flow (CBF) in 1986 (28) and in 1988 (27). Rosenberg et al. (27) showed that CBF was increased 2 h after the H-I event, although the increase was attenuated. The same group (28) demonstrated that reactive hyperemia was followed by a period of hypoperfusion. Cerebral oxygen delivery increased, while cerebral oxygen consumption was significantly decreased when compared to control, suggesting mitochondrial dysfunction. Additionally, cerebral fractional oxygen extraction (CFOE) decreased. CBF increased in response to induced hypoxia at 2–5 h after HI, but the increase is attenuated and is insufficient to maintain oxygen delivery. Cerebral oxygen consumption remained stable due to a proportional increase in CFOE (27). Another large animal study showed that an increased CBF subsided after 20 min of reperfusion (26) (studied with radiolabeled microspheres).

The study of Chakkarapani et al. (24) investigated cerebral perfusion by using cerebrovascular pressure reactivity (PRx). In this study, PRx was shown to be impaired during and after a H-I event. The study mentioned that a secondary PRx peak happened after 6.5 h in the normothermia group and after 11.5 h in the hypothermia group and that this was predictive of severe neuropathology and greater insult severity. Nakamura et al. (22), showed that an increased CBF within 6 h after the hypoxic-ischemic event indicates more marked histopathological damage [studied with near-infrared time-resolved spectroscopy (TRS)].

One large animal study investigated in what regions hyperperfusion takes place. Leffler et al. (26), studied hyperperfusion with radioactive-labeled microspheres. This study showed that hyperperfusion was present in the cerebellum, diencephalon, mesencephalon, medulla and spine.

Regarding human newborns, the study of Wu et al. (20) suggested reasons why CBF was increased. Wu et al. (20) used electrical velocimetry and transcranial doppler and indicated that there was an increased cardiac output (CO) in the rewarming phase after hypoxia-ischemia, which was due to an increase in heart rate. This study also showed an increase in the peak systolic velocity of the middle cerebral artery (MCA). The study of Shaikh et al. (29) studied both macroscopic and microscopic hemodynamic changes. This study included term asphyxiated newborns treated with hypothermia. In this study, regional CBF was studied around day 10 and around 1 month of life using MRI and ASL. They found that there was an

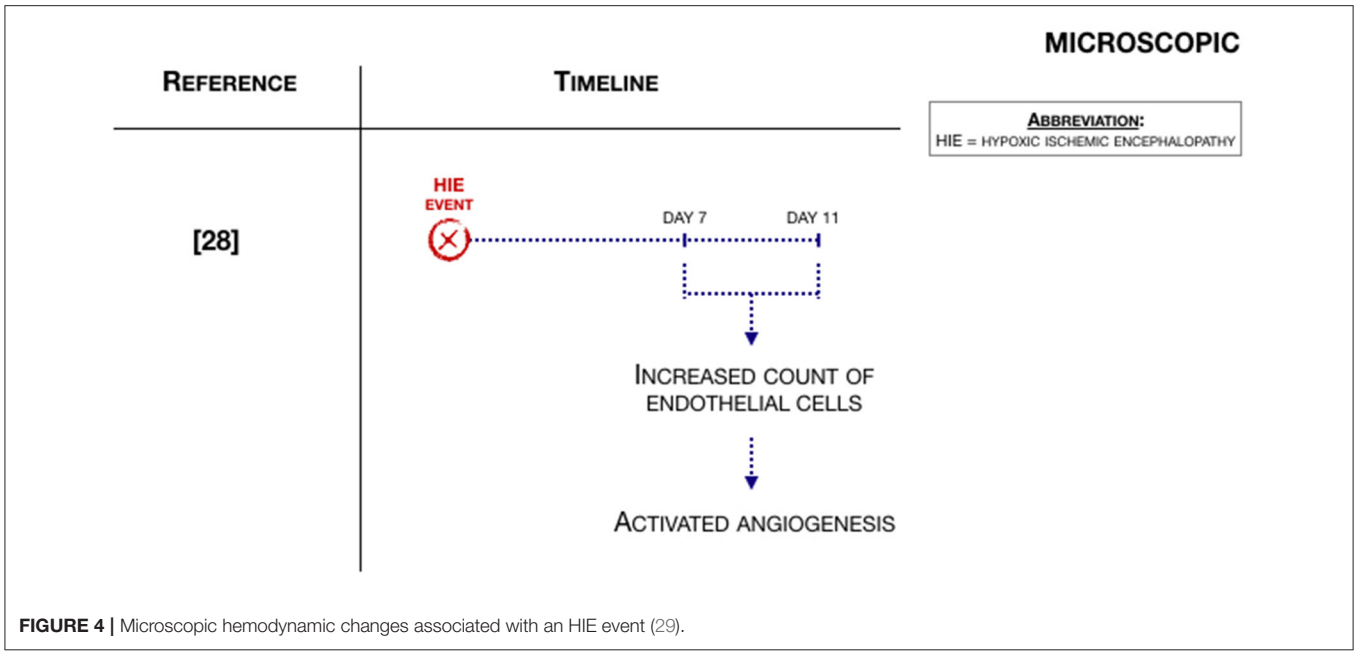

FIGURE 4 | Microscopic hemodynamic changes associated with an HIE event (29).

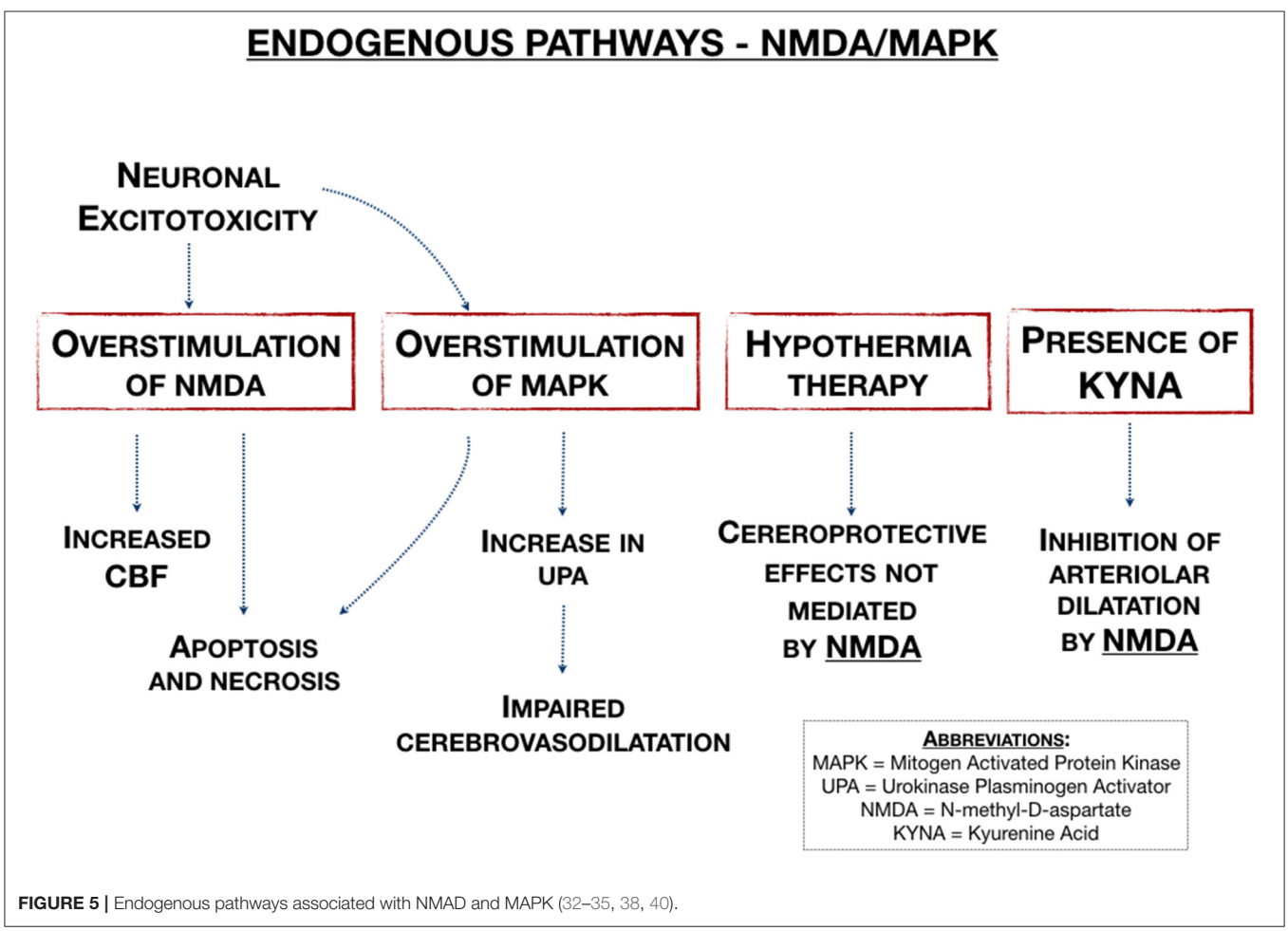

FIGURE 5 | Endogenous pathways associated with NMAD and MAPK (32–35, 38, 40).

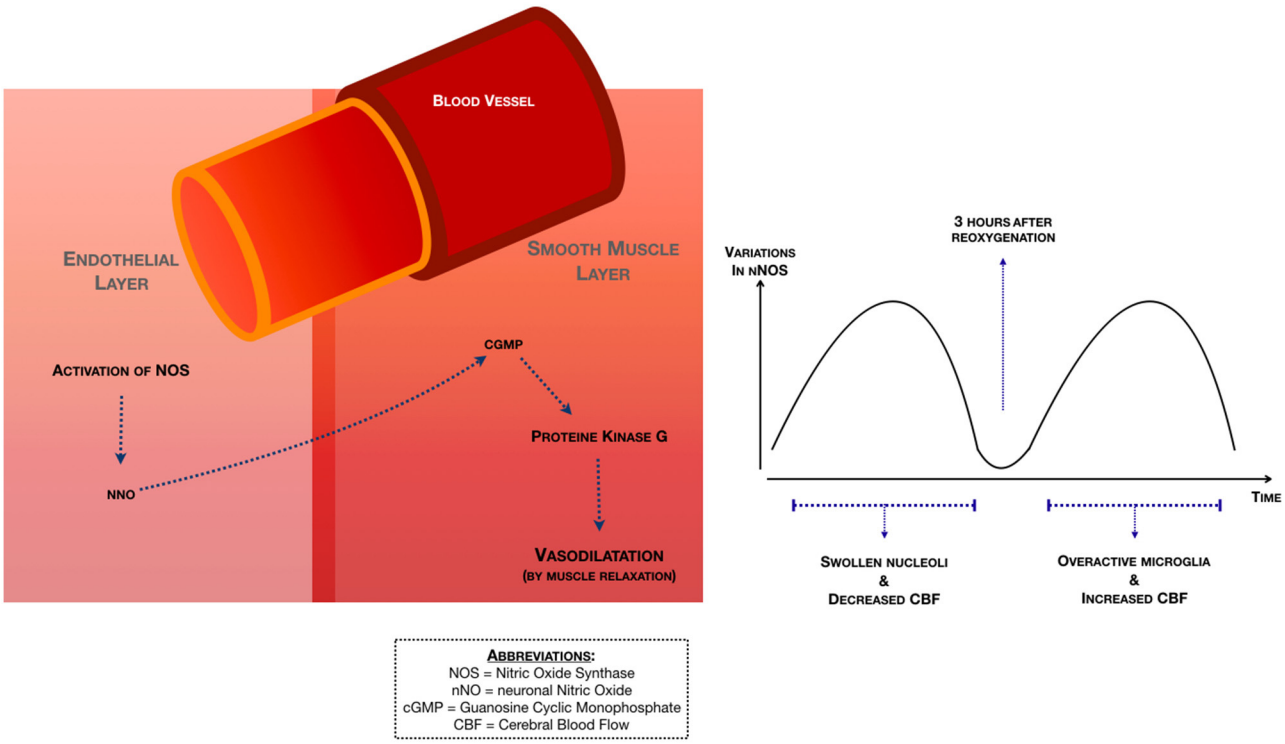

FIGURE 6 | Endogenous pathways associated with NO (14, 41, 42).

increased cerebral blood flow around day 10 in life and around 1 month of life, with no reported information between those two points.

Microscopic Hemodynamic Changes

Two articles also described hemodynamic changes on a microvascular level (29, 30). Shaikh et al. (29), the same study as in the macroscopic hemodynamic changes paragraph, studied angiogenesis in a small animal model of neonatal encephalopathy. They found that Vascular Endothelial Growth Factor (VEGF) was expressed in the first days of life of postmortem human brain tissue and rat pups after the hypoxic-ischemic event. Moreover, the count of endothelial cells was increased on 7 and 11 days after hypoxia-ischemia, indicating that there is active angiogenesis after hypoxia-ischemia (**Figure 4**).

Regarding large animals, Domoki et al. (30), studied microvascular hemodynamics with laser-speckle imaging. In five out of seven animals, marked cortical hyperemia was found 30 min after the initiation of hypoxia, with an increase in pial arteriolar diameters, simultaneously with arteriolar flow velocity. However, bilateral carotid artery occlusion (BCAO) could not elicit cortical ischemia and the data does not demonstrate a statistically significant effect.

Endogenous Pathways—NMDA/MAPK

In this section, we highlighted studies that described the effects of N-methyl-D-aspartate (NMDA) or mitogen activated protein kinase (MAPK). **Figure 5** is a graphical representation of these pathways. The current literature shows that in the process of neuronal excitotoxicity, overstimulation of the NMDA receptor by glutamate triggers the influx of calcium, which leads to apoptosis and necrosis. The MAPK-pathway plays also an important role in neonatal HIE because the overstimulation of this pathway also leads to apoptosis and necrosis. There were three studies (32–34) that all described that Urokinase Plasminogen Activator (uPA) impairs cerebral vasodilation.

Regarding small animal studies, Armstead et al. (34) described that uPA impairs cerebral vasodilation through lipoprotein-related protein (LRP) and the ERK isoform of MAPK. Additionally, Armstead et al. (32) confirms this with a uPA inhibitor and suggests that upregulation of p38 MAPK (a class of MAPK that reacts to stress stimuli) prevents cerebral vasodilation.

Moving to large animal studies, Kiessling et al. (33) described that inhibition of uPA could prevent vasodilatation, suggesting new therapeutic possibilities for clinical practice. On top of that, three other studies (36, 37, 39) described the effects of nociceptin/orphanin FQ and of Protein Tyrosine Kinase, showing that both can partially prevent hypotensive pial dilation impairment, when coadministred with the NMDA antagonist MK801.

The Doppler imaging study of Taylor et al. (40) described that local microinjection with NMDA resulted in increased local and global CBF within minutes of injection. Bari et al. (35) found that NMDA-induced arteriolar dilatation can

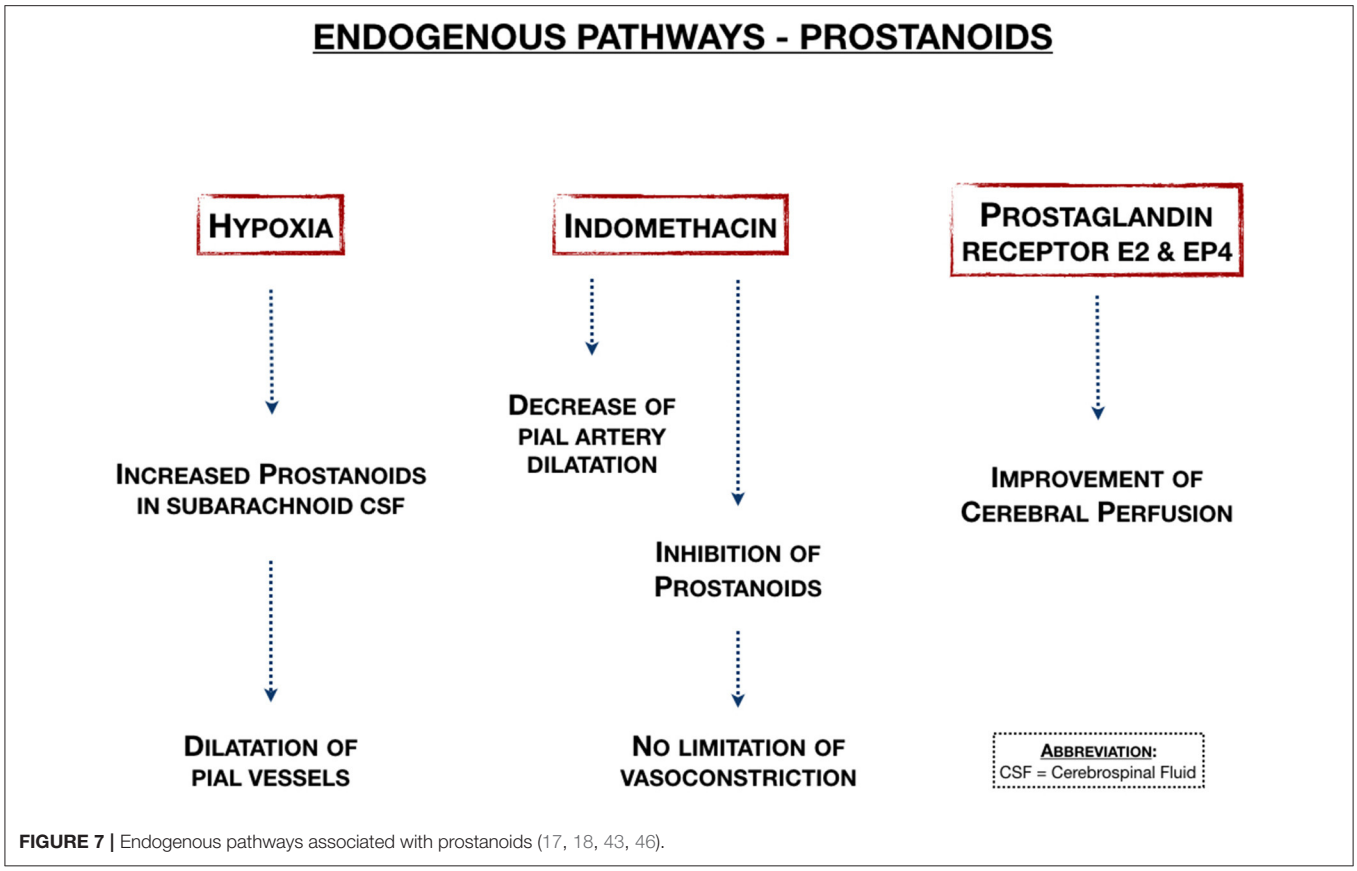

FIGURE 7 | Endogenous pathways associated with prostanoids (17, 18, 43, 46).

be inhibited by Kynurenine acid (KYNA). KYNA is a non-competitive antagonist to NMDA receptors and an antagonist to glutamate receptors, suggesting that KYNA attenuates NMDA-induced pial artery dilatation. The study of Perciaccante et al. (38), a study in which the population underwent intravital microscopy, suggests that hypothermia does not affect cerebral arteriolar dilatation to NMDA during and following ischemia, indicating that the cerebroprotective effects of hypothermia therapy are not mediated by NMDA. The study of Dang et al. (31), using proton magnetic resonance spectroscopy (^{1}H-MRS) and diffusion-weighted imaging (DWI), showed that the glutamate level in the basal ganglia underwent a "two-phase" change after HI: first a rise in glutamate after 0–6 h and secondly a rise in glutamate after 24–30 h, due to reperfusion injury.

Endogenous Pathways—NO

Nitric Oxide (NO) plays a major role in vessel dilatation. According to the study of Hsu et al. (14), a study with small animals that underwent Doppler imaging, neuronal NO synthase (nNOS) suffered a "two-phase" change after HI (**Figure 6**). The first rise in nNOS is directly after the HI-event and is characterized by swollen nuclei and a decreased CBF. The second rise in nNOS happens 3 h after reoxygenation and is characterized by overactive microglia and an increased CBF.

In large animal models, the study of Domoki et al. (41) described the relation between NO and NMDA. This study concluded that NMDA-induced vasodilation is mediated by endothelium-independent NO release and activation of nNOS positive neurons. Dorrepaal et al. (42) showed that neuronally derived NO contributes to hypoxic pial artery dilatation (**Figure 6**), through the formation of cGMP (cyclic guanosine monophosphate) and the subsequent release of methionine enkephalin and leucine enkephalin. The study of Armstead et al. (16) showed that the contribution of calcium-activated potassium channels to hypoxic cerebral vasodilation is not mediated by NO/cGMP.

Endogenous Pathways—Prostanoids

Prostanoids may be neuroprotective in neonatal HIE by stimulating the prostanoid E2 receptor (**Figure 7**). Four studies showed the effects of prostanoids on cerebral blood flow and vasodilation. Taniguchi et al. (17) showed that activation of the prostaglandin E2 EP4 receptor in small animals improved cerebral perfusion in both hemispheres and is therefore neuroprotective. In large animal studies that considered pial vessel mechanisms, Leffler et al. (18) showed that prostanoids were increased in subarachnoid CSF during acute hypoxia combined with hypercapnia, while Pourcyrous et al. (43) showed that inhibition of prostanoid production with indomethacin decreases pial artery dilation in response to combined hypoxia and hypercapnia. In another study from the same group,

Leffler et al. (46), they showed that hypercapnia didn't result in dilation of pial arterioles after cerebral ischemia, because of the inability of hypercapnia to increase cerebral vasodilator prostanoid synthesis.

Endogenous Pathways—Other

Three large animal studies did not fit the two main topics mentioned above. One study that focused on oxygen free radicals: Rosenberg et al. (47) showed that in damage by oxygen free radicals following hypoxia-ischemia, cerebral reperfusion plays a relevant role in the genesis of late postasphyxia blood flow and oxygen metabolism abnormalities. Treatment with polyethylene glycol catalase with oxygen free radicals increases the CBF significantly 5 min after the hypoxic-ischemic event, probably due to increased endothelial permeability. Another study focused on carbon monoxide (44). Carbon monoxide, produced by astrocytes, has antioxidants effects by heme oxylase/ carbon monoxide (HO/CO) and carbon monoxide release molecule-A1 (CORM-A1). HO/CO and CORM-A1 are neuroprotective in perinatal asphyxia, reducing brain oxidative stress and protecting against cerebrovascular dysfunction caused by prolonged neonatal asphyxia. The last study focused on cyclic adenosine monophosphate (cAMP): Wilderman et al. (45) concluded that cAMP contributes to hypoxic pial artery dilatation. Endogenous pituitary adenylate cyclase-activating peptide (PACAP) modulates cAMP-induced opioid release, thereby contributing to hypoxic pial artery dilatation.

Best-Evidence Synthesis

Overall, we found strong evidence in the studies regarding macroscopic and microscopic hemodynamic changes, the studies regarding NMDA/MAPK and the studies that did not fit the topics and were named in the "other" paragraph. We found moderate evidence in the studies with data on NO and prostanoids. There were no studies that reported insufficient evidence.

There were only two studies that reported data on human neonates (both high-quality studies): Wu et al. (20) and Shaikh et al. (29). Wu et al. (20) mentioned in the macroscopic hemodynamics paragraph, studied 20 human newborns that underwent electrical velocimetry and transcranial doppler. This study indicated that there was an increased cardiac output (CO) in the rewarming phase after hypoxia-ischemia, which was due to an increase in heart rate. This study also showed that the peak systolic velocity of the middle cerebral artery (MCA) was increased. Through NIRS measurements, Wu et al. (20) also mentioned that there were no changes in regional cerebral oxygen saturation (CrO_2) or cerebral fractional oxygen extraction (CFOE), suggesting that cerebral flow metabolism coupling remained intact during rewarming. Shaikh et al. (29), mentioned in the microscopic hemodynamics paragraph, included 24 term asphyxiated newborns treated with hypothermia. In this study, regional CBF was studied around day 10 and around 1 month of life using MRI and ASL. They found that there was an increased cerebral blood flow around day 10 in life and around 1 month of life, with no reported information between those two points (29).

DISCUSSION

Cerebral hyperperfusion seen in term neonates with hypoxic-ischemic encephalopathy (HIE) has been correlated with an adverse neurodevelopmental outcome (2, 9, 22–24). In order to understand how cerebral hyperperfusion is correlated with an adverse outcome, we must understand the pathophysiology. We reviewed current literature on the pathophysiology of cerebral hyperperfusion in term neonates with HIE.

Cerebral hyperperfusion may be increased up to 2–5 h after the hypoxic-ischemic event. Moreover, a secondary pressure reactivity peak may be predictive of severe neuropathology. Additionally, therapeutic hypothermia was shown to cause a 5-h delay in cerebral hyperperfusion (11.5 h instead of 6.5 h). Moreover, hyperperfusion is present in the cerebellum, diencephalon, mesencephalon, medulla and spine. Microscopic cerebral hyperperfusion was found to start 10–30 min after the initiation of hypoxia and was still observed around day 10 and around 1 month after birth. Moreover, after the hypoxic-ischemic event, VEGF is expressed and the endothelial cell count is increased, suggesting that angiogenesis is activated after hypoxia-ischemia. On the subject of NMDA and MAPK's endogenous pathway, we found that a rise in uPA can reduce cerebral vasodilation trough MAPK and that Nociceptin/Orphanin FQ contributes to the impairment of cerebral vasodilation. Moreover, NMDA induces vasodilation and hypothermia fails to preserve cerebral dilatation. Due to the reperfusion, there is a second rise in the excitatory amino acid glutamate after 24–30 h and it was also found that NMDA-induced vasodilation is mediated by nNOS through the formation of cGMP. Regarding prostanoids, they were found to be increased during hypoxia-ischemia and their synthesis' inhibition does not limit vasoconstriction. Lastly, prostanoid synthesis may contribute to vasodilation and improve perfusion by the prostaglandin E2 EP4 receptor.

This review suggests that cerebral hyperperfusion may be characterized by angiogenesis and cerebral vasodilation.

Cerebral vasodilation may be mediated by MAPK through uPA, by NMDA through nNOS and by prostanoid synthesis. Inhibition of prostanoid synthesis with indomethacin and inhibition of uPA may limit cerebral vasodilation and therefore may limit cerebral hyperperfusion. By understanding the pathophysiology, we can recognize and comprehend clinical patterns on diagnostic techniques earlier. Early diagnostics of cerebral hyperperfusion in neonates with HIE, can be beneficial for the development of new therapeutics.

There are several diagnostic techniques to detect cerebral hyperperfusion in neonates with HIE. Cranial Ultrasound (cUS) is a powerful and inexpensive alternative tool for MRI. cUS is widely available and can be repeated as often as necessary. cUS has no side effects, and, when performed by an experienced sonographer, provides a wealth of anatomical and functional information. According to Salas et al. (48), characteristic cUS findings of a term neonates with HIE are an increased echogenicity in the thalami, an enhanced gray-white matter differentiation and slit-like ventricles due to edema

from the cortical structures. Duplex Ultrasonography (DUS) typically shows decreased resistance index (RI) values (<0.60), as decreased RI values are highly predictive of poor prognosis with either death or severe disability. The study of Archer et al. (49) also described that a very low RI, corresponding to "luxury hyperperfusion," was correlated with an adverse outcome. One study in our search described a decreased RI of the right MCA in the asphyxia group, compared to the ischemia group (23). This study suggests that with hypoxic-ischemic injury, the elasticity of the brain tissue decreases, and these results are consistent with the pathological findings.

Brain Magnetic Resonance Imaging (MRI) is one of the most used techniques in neonates with HIE and is useful to predict long-term outcomes. In the study of Wintermark et al. (2), 18 asphyxiated neonates underwent MR imaging and ASL-PI (perfusion imaging by arterial spin labeling). In neonates treated with hypothermia, hyperperfusion occurred on day 2–3 in brain areas subsequently exhibiting injury. In neonates with normothermia, hyperperfusion occurred on days 1–6. This study also suggests that early hyperperfusion is correlated with later brain injury even in infants treated with induced hypothermia. Given that this study was not reviewing the pathophysiology but only hemodynamics, we excluded this study in the results. The finding that hypothermia delays the occurrence of hyperperfusion is also found in the study of Chakkarapani et al. (24). In this study, using cerebrovascular pressure reactivity (PRx) in piglets, a secondary PRx peak was associated with severe neuropathology and with greater insult severity and happened after 6.5 h in the normothermia group and after 11.5 h in the hypothermia group.

In the study of De Vis et al. (9), where 28 neonates diagnosed with HIE were assessed using MR imaging, ^{1}H-MRS, and ASL MRI, the main finding is that basal ganglia and thalami perfusion is higher in neonates with an adverse outcome. We have not found studies that investigated perfusion in the basal ganglia and the thalami specifically.

Limitations

There are several limitations in this systematic review. At first, when assessing the methodological quality of the included studies, we made several assumptions: we defined newborn animals as ≤7 days old, according to the Medline definition of "perinatal care." Studies with newborns >7 days old were excluded. When studies did not describe the age of the participated animals, we answered questions 1 and 2 in the critical appraisal as unknown. Additionally, when gender or weight was not described in the study, we assumed that this was a normal distribution of men and female animals and a normal weight. In most of the studies, there was no baseline table for the participating animals, so we assumed that they were healthy newborns without any outcome in the beginning of the study. In agreement with the research team, a follow-up time of ≥24 h was considered to be long enough for cerebral hyperperfusion to occur. Second, because the included studies were too heterogeneous for a meta-analysis, we narratively described the studies and used Proper guidelines for the best-evidence synthesis. For a systematic review, a meta-analysis would be favorable because the precision and accuracy of estimates can be optimized as more data is used, which also means that it may increase the statistical power to detect an effect. Only a few studies in our search were studies on human neonates. The aim of this review is to give an overview of the knowledge so far and make way for new research ideas, which can come from both human and animal populations. The fact that some of the studies considered in this review were related to animal models, means that age-estimation and correlations to human newborn models may pose as a challenge for future research. Moreover, one must consider the fact that small and large animals have different pathophysiologic mechanisms, and that should be taken into account when considering the different results. Finally, in five studies (14–18) the number of animals participated in the study is unknown, therefore generalization to other animal studies was impossible. Because of various limitations, the results have to be treated with caution.

CONCLUSION

The main findings are that cerebral hyperperfusion is present 10–30 min after the hypoxic-ischemic event and persisted around day 10 and up to 1 month of life. Cerebral hyperperfusion may be characterized by angiogenesis and cerebral vasodilation. We found that a rise in prostanoids can reduce cerebral vasodilation trough MAPK and that Nociceptin/Orphanin FQ contributes to the impairment of cerebral vasodilation. Moreover, NMDA induces vasodilation and the cerebroprotective effects of hypothermia therapy are not mediated by NMDA. Due to reperfusion, there is a second rise in the excitatory amino acid glutamate after 24–30 h and it was also found that NMDA-induced vasodilation is mediated by nNOS through the formation of cGMP. Regarding prostanoids, they were found to be increased during hypoxia-ischemia and their synthesis' inhibition does not limit vasoconstriction. Lastly, prostanoid synthesis may contribute to vasodilation and improve perfusion by the prostaglandin E2 EP4 receptor.

Implications and Suggestions for Future Research

The exact mechanism of cerebral hyperperfusion is not known yet, but we showed why it is clinically important. To develop new therapeutics for neonatal HIE, future research about the role of NMDA and MAPK and the implications of agents that can inhibit uPA or prostanoids, such as indomethacin in cerebral vasodilation needs to be developed. Given that there were only three studies (24, 29, 38) that described the effect of hypothermia therapy on cerebral hyperperfusion, evidence is limited and therefore, future research should also focus on this. Moreover, further research is required to translate these findings into clinical practice. These findings should be taken into account simultaneously with brain imagining techniques, as they present

themselves as a valuable asset in assessing the neurodevelopment throughout days/weeks after the hypoxic-ischemic event.

DATA AVAILABILITY STATEMENT

The original contributions presented in the study are included in the article/**Supplementary Material**, further inquiries can be directed to the corresponding authors.

AUTHOR CONTRIBUTIONS

DK contributed to the study concept, screened titles and abstracts, analyzed the data, and wrote the article. FC prepared the figures and contributed with writing the article. KA screened titles and abstracts and analyzed the data. AH, TA, and FG critically reviewed the article. MB and JD directed the project. All authors contributed to the article and approved the submitted version.

FUNDING

The authors acknowledged the financial support of EU H2020 MSCA-ITN-2018: INtegrating Functional Assessment measures for Neonatal Safeguard (INFANS), funded by the European Commission under Grant Agreement #813483.

ACKNOWLEDGMENTS

We thank Drs. Paulien Wiersma (P.W.), information specialist at Utrecht University Library, University Medical Center Utrecht, for helping with the search strategy.

SUPPLEMENTARY MATERIAL

The Supplementary Material for this article can be found online at: https://www.frontiersin.org/articles/10.3389/fped.2021.631258/full#supplementary-material

Supplementary Appendix 1 | Review question defined according to the PICOTS system.

Supplementary Appendix 2 | Summarized search strategy.

Supplementary Appendix 3 | Medline search strategy.

Supplementary Appendix 4 | Medline search string.

REFERENCES

1. Kurinczuk JJ, White-Koning M, Badawi N. Epidemiology of neonatal encephalopathy and hypoxic-ischaemic encephalopathy. *Early Hum Dev.* (2010) 86:329–38. doi: 10.1016/j.earlhumdev.2010.05.010
2. Wintermark P, Hansen A, Gregas MC, Soul J, Labrecque M, Robertson RL, et al. Brain perfusion in asphyxiated newborns treated with therapeutic hypothermia. *AJNR Am J Neuroradiol.* (2011) 32:2023–9. doi: 10.3174/ajnr.A2708
3. Ferriero DM. Neonatal brain injury. *N Engl J Med.* (2004) 351:1985–95. doi: 10.1056/NEJMra041996
4. Douglas-Escobar M, Weiss MD. Hypoxic-ischemic encephalopathy: a review for the clinician. *JAMA Pediatr.* (2015) 169:397–403. doi: 10.1001/jamapediatrics.2014.3269
5. Hassell KJ, Ezzati M, Alonso-Alconada D, Hausenloy DJ, Robertson NJ. New horizons for newborn brain protection: enhancing endogenous neuroprotection. *Arch Dis Child Fetal Neonatal Ed.* (2015) 100:F541–52. doi: 10.1136/archdischild-2014-306284
6. Bennet L, Roelfsema V, Pathipati P, Quaedackers JS, Gunn AJ. Relationship between evolving epileptiform activity and delayed loss of mitochondrial activity after asphyxia measured by near-infrared spectroscopy in preterm fetal sheep. *J Physiol.* (2006) 572 (Pt 1):141–54. doi: 10.1113/jphysiol.2006.105197
7. Lorek A, Takei Y, Cady EB, Wyatt JS, Penrice J, Edwards AD, et al. Delayed ("secondary") cerebral energy failure after acute hypoxia-ischemia in the newborn piglet: continuous 48-hour studies by phosphorus magnetic resonance spectroscopy. *Pediatr Res.* (1994) 36:699–706. doi: 10.1203/00006450-199412000-00003
8. Bennet L, Tan S, den Heuij L, Derrick M, Groenendaal F, van Bel F, et al. Cell therapy for neonatal hypoxia-ischemia and cerebral palsy. *Ann Neurol.* (2012) 71:589–600. doi: 10.1002/ana.22670
9. De Vis JB, Hendrikse J, Petersen ET, de Vries LS, van Bel F, Alderliesten T, et al. Arterial spin-labelling perfusion MRI and outcome in neonates with hypoxic-ischemic encephalopathy. *Eur Radiol.* (2015) 25:113–21. doi: 10.1007/s00330-014-3352-1
10. Liberati A, Altman DG, Tetzlaff J, Mulrow C, Gøtzsche PC, Ioannidis JPA, et al. The PRISMA statement for reporting systematic reviews and meta-analyses of studies that evaluate healthcare interventions: explanation and elaboration. *BMJ.* (2009) 339:b2700. doi: 10.1136/bmj.b2700
11. Thewissen L, Caicedo A, Lemmers P, Van Bel F, Van Huffel S, Naulaers G. Measuring near-infrared spectroscopy derived cerebral autoregulation in neonates: from research tool toward bedside multimodal monitoring. *Front Pediatr.* (2018) 6:117. doi: 10.3389/fped.2018.00117
12. Johanna Briggs Institute. *Critical Appraisal Tools: Checklist for Cohort Studies*. (2017). Available online at: https://joannabriggs.org/sites/default/files/2019-05/JBI_Critical_Appraisal-Checklist_for_Cohort_Studies2017_0.pdf
13. Proper KI, Singh AS, van Mechelen W, Chinapaw MJM. Sedentary behaviors and health outcomes among adults: a systematic review of prospective studies. *Am J Prev Med.* (2011) 40:174–82. doi: 10.1016/j.amepre.2010.10.015
14. Hsu Y-C, Chang Y-C, Lin Y-C, Sze C-I, Huang C-C, Ho C-J. Cerebral microvascular damage occurs early after hypoxia-ischemia via nNOS activation in the neonatal brain. *J Cereb Blood Flow Metab Off J Int Soc Cereb Blood Flow Metab.* (2014) 34:668–76. doi: 10.1038/jcbfm.2013.244
15. Wilderman MJ, Armstead WM. Role of endothelial nitric oxide synthase in hypoxia-induced pial artery dilation. *J Cereb Blood Flow Metab Off J Int Soc Cereb Blood Flow Metab.* (1998) 18:531–8. doi: 10.1097/00004647-199805000-00008
16. Armstead WM. Contribution of kca channel activation to hypoxic cerebrovasodilation does not involve NO. *Brain Res.* (1998) 799:44–8. doi: 10.1016/S0006-8993(98)00462-4
17. Taniguchi H, Anacker C, Wang Q, Andreasson K. Protection by vascular prostaglandin E2 signaling in hypoxic-ischemic encephalopathy. *Exp Neurol.* (2014) 255:30–7. doi: 10.1016/j.expneurol.2014.02.012
18. Leffler CW, Busija DW. Prostanoids in cortical subarachnoid cerebrospinal fluid and pial arterial diameter in newborn pigs. *Circ Res.* (1985) 57:689–94. doi: 10.1161/01.RES.57.5.689
19. Jinnai W, Nakamura S, Koyano K, Yamato S, Wakabayashi T, Htun Y, et al. Relationship between prolonged neural suppression and cerebral hemodynamic dysfunction during hypothermia in asphyxiated piglets. *Brain Dev.* (2018) 40:649–61. doi: 10.1016/j.braindev.2018.04.010
20. Wu T-W, Tamrazi B, Soleymani S, Seri I, Noori S. Hemodynamic changes during rewarming phase of whole-body hypothermia therapy in

neonates with hypoxic-ischemic encephalopathy. *J Pediatr.* (2018) 197:68–74.e2. doi: 10.1016/j.jpeds.2018.01.067
21. Buckley EM, Patel SD, Miller BF, Franceschini MA, Vannucci SJ. In vivo monitoring of cerebral hemodynamics in the immature rat: effects of hypoxia-ischemia and hypothermia. *Dev Neurosci.* (2015) 37:407–16. doi: 10.1159/000381704
22. Nakamura M, Jinnai W, Hamano S, Nakamura S, Koyano K, Chiba Y, et al. Cerebral blood volume measurement using near-infrared time-resolved spectroscopy and histopathological evaluation after hypoxic-ischemic insult in newborn piglets. *Int J Dev Neurosci Off J Int Soc Dev Neurosci.* (2015) 42:1–9. doi: 10.1016/j.ijdevneu.2015.02.009
23. Wang S-D, Liang S-Y, Liao X-H, Deng X-F, Chen Y-Y, Liao C-Y, et al. Different extent of hypoxic-ischemic brain damage in newborn rats: histopathology, hemodynamic, virtual touch tissue quantification and neurobehavioral observation. *Int J Clin Exp Pathol.* (2015) 8:12177–87.
24. Chakkarapani E, Dingley J, Aquilina K, Osredkar D, Liu X, Thoresen M. Effects of xenon and hypothermia on cerebrovascular pressure reactivity in newborn global hypoxic-ischemic pig model. *J Cereb Blood Flow Metab Off J Int Soc Cereb Blood Flow Metab.* (2013) 33:1752–60. doi: 10.1038/jcbfm.2013.123
25. Manole MD, Foley LM, Hitchens TK, Kochanek PM, Hickey RW, Bayir H, et al. Magnetic resonance imaging assessment of regional cerebral blood flow after asphyxial cardiac arrest in immature rats. *J Cereb Blood Flow Metab Off J Int Soc Cereb Blood Flow Metab.* (2009) 29:197–205. doi: 10.1038/jcbfm.2008.112
26. Leffler CW, Busija DW, Mirro R, Armstead WM, Beasley DG. Effects of ischemia on brain blood flow and oxygen consumption of newborn pigs. *Am J Physiol.* (1989) 257(6 Pt 2):H1917–26. doi: 10.1152/ajpheart.1989.257.6.H1917
27. Rosenberg AA. Regulation of cerebral blood flow after asphyxia in neonatal lambs. *Stroke.* (1988) 19:239–44. doi: 10.1161/01.STR.19.2.239
28. Rosenberg AA. Cerebral blood flow and O2 metabolism after asphyxia in neonatal lambs. *Pediatr Res.* (1986) 20:778–82. doi: 10.1203/00006450-198608000-00016
29. Shaikh H, Lechpammer M, Jensen FE, Warfield SK, Hansen AH, Kosaras B, et al. Increased brain perfusion persists over the first month of life in term asphyxiated newborns treated with hypothermia: does it reflect activated angiogenesis? *Transl Stroke Res.* (2015) 6:224–33. doi: 10.1007/s12975-015-0387-9
30. Domoki F, Zolei-Szenasi D, Olah O, Toth-Szuki V, Nemeth J, Hopp B, et al. Comparison of cerebrocortical microvascular effects of different hypoxic-ischemic insults in piglets: a laser-speckle imaging study. *J Physiol Pharmacol an Off J Polish Physiol Soc.* (2014) 65:551–8.
31. Dang Y-X, Shi K-N, Wang X-M. Early changes in glutamate metabolism and perfusion in basal ganglia following hypoxia-ischemia in neonatal piglets: a multi-sequence 3.0T MR study. *Front Physiol.* (2017) 8:237. doi: 10.3389/fphys.2017.00237
32. Armstead WM, Riley J, Cines DB, Higazi AA-R. PAI-1-derived peptide EEIIMD prevents hypoxia/ischemia-induced aggravation of endothelin- and thromboxane-induced cerebrovasoconstriction. *Neurocrit Care.* (2014) 20:111–8. doi: 10.1007/s12028-013-9906-2
33. Kiessling JW, Cines DB, Higazi AA-R, Armstead WM. Inhibition of integrin alphavbeta3 prevents urokinase plasminogen activator-mediated impairment of cerebrovasodilation after cerebral hypoxia/ischemia. *Am J Physiol Heart Circ Physiol.* (2009) 296:H862–7. doi: 10.1152/ajpheart.01141.2008
34. Armstead WM, Cines DB, Bdeir K, Kulikovskaya I, Stein SC, Higazi AA-R. uPA impairs cerebrovasodilation after hypoxia/ischemia through LRP and ERK MAPK. *Brain Res.* (2008) 1231:121–31. doi: 10.1016/j.brainres.2008.06.115
35. Bari F, Nagy K, Guidetti P, Schwarcz R, Busija DW, Domoki F. Kynurenic acid attenuates NMDA-induced pial arteriolar dilation in newborn pigs. *Brain Res.* (2006) 1069:39–46. doi: 10.1016/j.brainres.2005.11.033
36. Philip S, Armstead WM. Newborn pig nociceptin/orphanin FQ activates protein tyrosine kinase and mitogen activated protein kinase to impair NMDA cerebrovasodilation after ischemia. *Neuroreport.* (2003) 14:201–3. doi: 10.1097/00001756-200302100-00008
37. Jagolino AL, Armstead WM. PTK, MAPK, and NOC/oFQ impair hypercapnic cerebrovasodilation after hypoxia/ischemia. *Am J Physiol Heart Circ Physiol.* (2003) 284:H101–7. doi: 10.1152/ajpheart.00457.2002
38. Perciaccante JV, Domoki F, Puskar M, Busija DW. Effects of hypothermia on neuronal-vascular function after cerebral ischemia in piglets. *Am J Physiol Regul Integr Comp Physiol.* (2002) 283:R1362–7. doi: 10.1152/ajpregu.00134.2002
39. Armstead WM. NOC/oFQ and NMDA contribute to piglet hypoxic ischemic hypotensive cerebrovasodilation impairment. *Pediatr Res.* (2002) 51:586–91. doi: 10.1203/00006450-200205000-00007
40. Taylor GA, Trescher WA, Traystman RJ, Johnston M V. Acute experimental neuronal injury in the newborn lamb: US characterization and demonstration of hemodynamic effects. *Pediatr Radiol.* (1993) 23:268–75. doi: 10.1007/BF02010913
41. Domoki F, Perciaccante J V, Shimizu K, Puskar M, Busija DW, Bari F. N-methyl-D-aspartate-induced vasodilation is mediated by endothelium-independent nitric oxide release in piglets. *Am J Physiol Heart Circ Physiol.* (2002) 282:H1404–9. doi: 10.1152/ajpheart.00523.2001
42. Dorrepaal CA, Steendijk P, Baan J, van Bel F. Inhibition of nitric oxide synthesis following severe hypoxia-ischemia restores autoregulation of cerebral blood flow in newborn lambs. *Early Hum Dev.* (2001) 60:159–70. doi: 10.1016/S0378-3782(00)00104-3
43. Pourcyrous M, Leffler C, Busija D. Role of prostanoids in cerebrovascular responses to asphyxia and reventilation in newborn pigs. *Am J Physiol.* (1990) 259(3 Pt 2):H662–7. doi: 10.1152/ajpheart.1990.259.3.H662
44. Parfenova H, Pourcyrous M, Fedinec AL, Liu J, Basuroy S, Leffler CW. Astrocyte-produced carbon monoxide and the carbon monoxide donor CORM-A1 protect against cerebrovascular dysfunction caused by prolonged neonatal asphyxia. *Am J Physiol Heart Circ Physiol.* (2018) 315:H978–88. doi: 10.1152/ajpheart.00140.2018
45. Wilderman MJ, Armstead WM. Role of PACAP in the relationship between cAMP and opioids in hypoxia-induced pial artery vasodilation. *Am J Physiol.* (1997) 272(3 Pt 2):H1350–8. doi: 10.1152/ajpheart.1997.272.3.H1350
46. Leffler CW, Beasley DG, Busija DW. Cerebral ischemia alters cerebral microvascular reactivity in newborn pigs. *Am J Physiol.* (1989) 257(1 Pt 2):H266–71. doi: 10.1152/ajpheart.1989.257.1.H266
47. Rosenberg AA, Murdaugh E, White CW. The role of oxygen free radicals in postasphyxia cerebral hypoperfusion in newborn lambs. *Pediatr Res.* (1989) 26:215–9. doi: 10.1203/00006450-198909000-00012
48. Salas J, Tekes A, Hwang M, Northington FJ, Huisman TAGM. Head ultrasound in neonatal hypoxic-ischemic injury and its mimickers for clinicians: a review of the patterns of injury and the evolution of findings over time. *Neonatology.* (2018) 114:185–97. doi: 10.1159/000487913
49. Archer LN, Levene MI, Evans DH. Cerebral artery Doppler ultrasonography for prediction of outcome after perinatal asphyxia. *Lancet.* (1986) 2:1116–8. doi: 10.1016/S0140-6736(86)90528-3

Conflict of Interest: The authors declare that the research was conducted in the absence of any commercial or financial relationships that could be construed as a potential conflict of interest.

frontiers in Pediatrics

REVIEW
published: 04 February 2021
doi: 10.3389/fped.2021.618052

Impaired Oligodendrocyte Development Following Preterm Birth: Promoting GABAergic Action to Improve Outcomes

Julia C. Shaw[1,2]*, *Gabrielle K. Crombie*[1,2], *Hannah K. Palliser*[1,2] and *Jonathan J. Hirst*[1,2]

[1] School of Biomedical Sciences and Pharmacy, University of Newcastle, Newcastle, NSW, Australia, [2] Mothers and Babies Research Centre, Hunter Medical Research Institute, New Lambton Heights, NSW, Australia

Preterm birth is associated with poor long-term neurodevelopmental and behavioral outcomes, even in the absence of obvious brain injury at the time of birth. In particular, behavioral disorders characterized by inattention, social difficulties and anxiety are common among children and adolescents who were born moderately to late preterm (32–37 weeks' gestation). Diffuse deficits in white matter microstructure are thought to play a role in these poor outcomes with evidence suggesting that a failure of oligodendrocytes to mature and myelinate axons is responsible. However, there remains a major knowledge gap over the mechanisms by which preterm birth interrupts normal oligodendrocyte development. *In utero* neurodevelopment occurs in an inhibitory-dominant environment due to the action of placentally derived neurosteroids on the $GABA_A$ receptor, thus promoting GABAergic inhibitory activity and maintaining the fetal behavioral state. Following preterm birth, and the subsequent premature exposure to the *ex utero* environment, this action of neurosteroids on $GABA_A$ receptors is greatly reduced. Coinciding with a reduction in GABAergic inhibition, the preterm neonatal brain is also exposed to *ex utero* environmental insults such as periods of hypoxia and excessive glucocorticoid concentrations. Together, these insults may increase levels of the excitatory neurotransmitter glutamate in the developing brain and result in a shift in the balance of inhibitory: excitatory activity toward excitatory. This review will outline the normal development of oligodendrocytes, how it is disrupted under excitation-dominated conditions and highlight how shifting the balance back toward an inhibitory-dominated environment may improve outcomes.

Keywords: preterm (birth), oligodendrocyte, GABA, glutamate, neurosteroids

OPEN ACCESS

Edited by:
Silvia Carloni,
University of Urbino Carlo Bo, Italy

Reviewed by:
Justin Dean,
The University of Auckland, New Zealand
Lauren Jantzie,
Johns Hopkins University, United States

***Correspondence:**
Julia C. Shaw
Julia.c.shaw@newcastle.edu.au

Specialty section:
This article was submitted to Neonatology, a section of the journal Frontiers in Pediatrics

Received: *16 October 2020*
Accepted: *12 January 2021*
Published: *04 February 2021*

Citation:
Shaw JC, Crombie GK, Palliser HK and Hirst JJ (2021) Impaired Oligodendrocyte Development Following Preterm Birth: Promoting GABAergic Action to Improve Outcomes. Front. Pediatr. 9:618052. doi: 10.3389/fped.2021.618052

INTRODUCTION

The incidence of preterm birth has stubbornly remained at ∼8%, with the majority (∼74%) of these deliveries falling into the moderate to late preterm range (32–36 weeks of gestation) (1). Although short-term outcomes are good, these neonates have markedly disrupted brain development that persists into later life (2). In addition to major preterm birth related disorders, such as cerebral palsy and bronchopulmonary dysplasia, there is a well-established body of evidence supporting the notion that preterm infants born in the moderate to late range are also much more

likely to develop neurodevelopmental morbidities and learning disorders that become apparent at around school age (3–9). These disorders include internalizing disorders (such as anxiety and depression), inattentive attention deficit hyperactivity (ADHD) disorder and poor social skills (10). These disorders can be observed from pre-school age through to adulthood (10), but importantly, often occur in the absence of overt brain injury at the time of birth. Development of these disorders leads to significant socioeconomic burden for these individuals as well as for their families and the healthcare system (11). Thus, there is an urgent need to develop therapeutic strategies to reduce these negative effects of moderate to late preterm birth and we propose that this needs to be done in the early neonatal period.

Moderately to late preterm born neonates frequently already have, or will develop, subtle deficits in white matter tracts not visible on routine MRI (1, 12, 13) which persist beyond the time of full term, and despite further post-term development of myelination, behavioral disorders emerge in later life (1, 2, 7, 13). This review will examine the processes surrounding oligodendrocyte development, specifically in the late gestation fetus, and how premature exposure to the *ex utero* environment disrupts this process. We will also cover studies showing moderate to late gestation is characterized by an inhibitory tone in the developing brain that is subsequently lost following preterm birth. This inhibitory tone is maintained by the placentally derived neurosteroid, allopregnanolone (5α-pregnane-3α-ol-20-one) and its actions on the γ-aminobutyric acid a ($GABA_A$) receptor, which plays a key role in oligodendrocyte development *in utero* (14). Finally, we will also discuss some approaches that promote maturation of the oligodendrocyte lineage and myelination in the newborn brain resulting in improved neurodevelopmental outcomes.

OLIGODENDROCYTE DEVELOPMENT

Oligodendrocytes progress through a number of morphological and functional changes, from their origins as neural stem cells, to mature oligodendrocytes capable of myelin production (**Figure 1**). This is a highly regulated process that has already been described in detail elsewhere (15, 16). Briefly, neural stem cells commit to the oligodendrocyte lineage and become oligodendrocyte precursor cells (OPCs) under the influence of transcription factors including *Olig1/2*, *NKX2.2*, and *Sox10* (16, 17). From here, OPC expansion is heavily influenced by growth factors such as platelet derived growth factor (*PDGF*), which promote proliferation but inhibit differentiation (16, 18, 19). This ensures that a large pool of OPCs are created before they are committed to differentiation, which is an irreversible process. Thus, oligodendrocyte differentiation is driven by a loss of this "inhibition to differentiate" environment, likely by promoting expression of microRNAs that prevent transcription of differentiation inhibitors (16, 20, 21). Once OPCs have matured into pre-oligodendrocytes (pre-OLs) they differentiate under the control of a number of transcription factors, but one of the most crucial is known as myelin regulatory factor (*Myrf*) (16, 22). Expression of *Myrf*, and its interaction with *Sox10*, in differentiating oligodendrocytes induces the activation of genes encoding lipid structural proteins such as phosphodiesterase Enpp6, and thus enables the production of myelin (23). Deletion or inactivation of the *Myrf* gene prevents the generation of differentiated oligodendrocytes (23), without affecting pre-existing oligodendrocytes or myelin, and is associated with a subsequent impairment of learning ability, highlighting the integral role that this transcription factor, and oligodendrocyte development in general, plays in normal neurodevelopment.

Oligodendrocyte development is also driven by extracellular signals (16), such as endogenous glucocorticoids and neurotransmitters. A study in adult mice found that oligodendrocyte progenitors and mature oligodendrocytes express glucocorticoid receptors, leading the authors to suggest that glucocorticoids are involved in the differentiation processes of oligodendrocytes (24). Furthermore, the presence of steroid hormone cofactors that increase the transcriptional activity of glucocorticoid receptors is expressed in oligodendrocyte progenitor cells but not mature oligodendrocytes, thus strengthening the notion that glucocorticoids play a role in driving differentiation (24). It is important to note that whilst normal physiological levels of glucocorticoids, such as cortisol, are required for oligodendrocyte development, levels above normal may be detrimental due to the high expression of these receptors. Meanwhile, the neurotransmitter GABA is also involved in oligodendrocyte differentiation and myelination through activation of $GABA_A$ and $GABA_B$ receptors (25). In a hypoxic mouse study, addition of GABAergic drugs tiagabine and vigabatrin increased the number of mature oligodendrocytes, whilst addition of a $GABA_A$ receptor antagonist prevented this (26). Additionally, it was shown in a purified rat oligodendrocyte progenitor culture that addition of GABA accelerates oligodendrocyte differentiation by promoting branching and myelin protein expression (27). Importantly, these effects can be blocked by a $GABA_B$ receptor-specific antagonist (27). Furthermore, GABAergic neurons establish synaptic connections with oligodendrocytes to control differentiation and migration and ultimately induce the wrapping of axons (25).

The translation of myelin proteins such as myelin–associated glycoprotein (MAG), myelin oligodendrocyte glycoprotein (MOG), myelin basic protein (MBP), and myelin proteolipid protein (PLP) is reliant on contact with axons for the wrapping of myelin to occur (16, 28). Despite OPCs appearing in the fetal brain at ∼10 weeks of gestation, it is not until ∼30 weeks of gestation when the myelination of axons begins (16). Therefore, oligodendrocyte development may be markedly impacted by preterm birth during these final stages of maturation and myelination. Importantly, preclinical studies show that myelin proteins, such as MBP and PLP, are reduced in animals exposed to moderate to late gestation perinatal insults such as growth restriction and preterm delivery, whilst those expressed at earlier stages of the lineage are unaffected (29–34). This is to be expected given the developmental timeline, but critically, these relative reductions persist throughout life. The key question then becomes, how does preterm birth prevent this expansive pool of OPCs and pre-OLs from maturing and producing myelin? We propose the *ex utero* environment plays a crucial role in ongoing

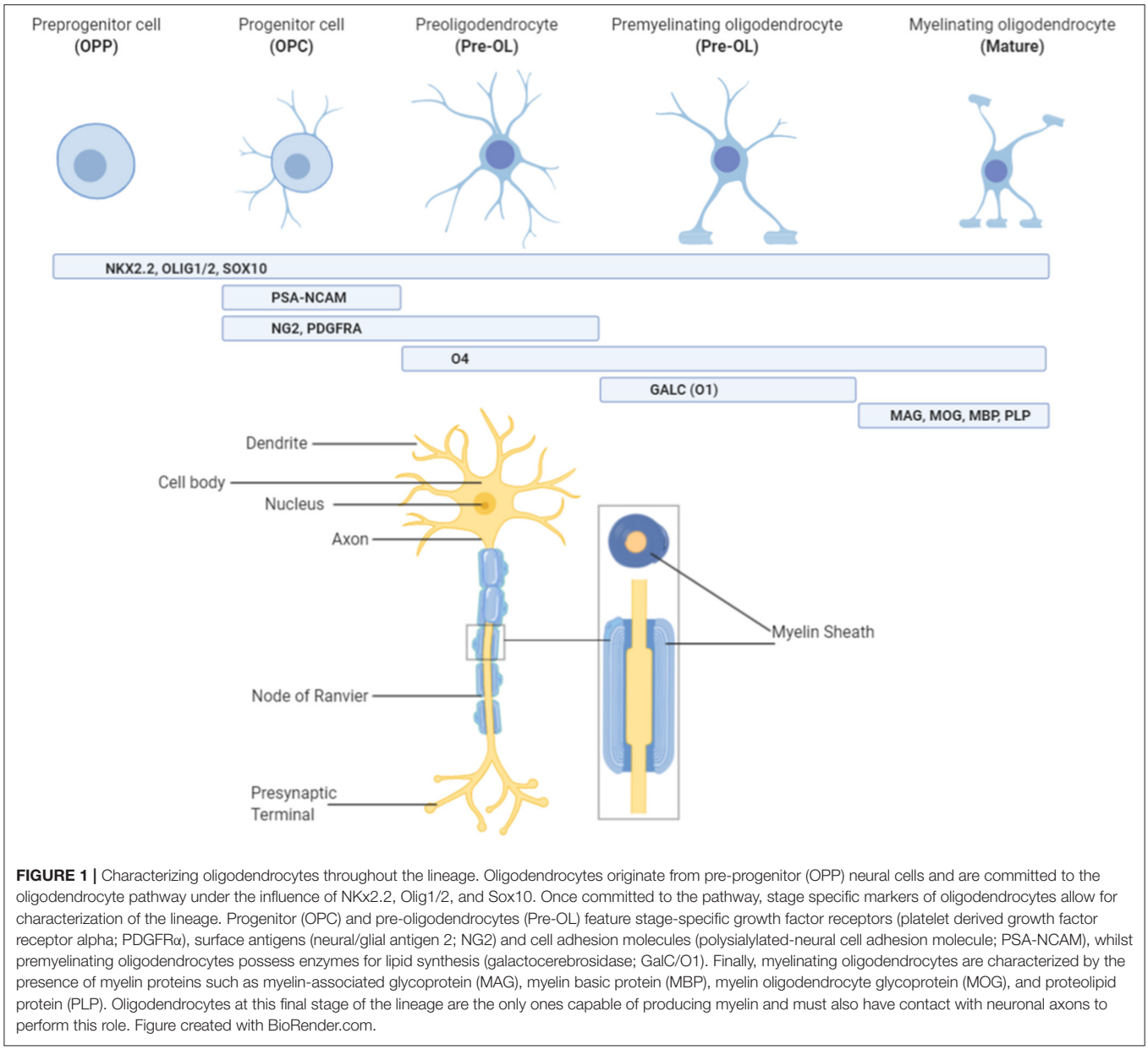

FIGURE 1 | Characterizing oligodendrocytes throughout the lineage. Oligodendrocytes originate from pre-progenitor (OPP) neural cells and are committed to the oligodendrocyte pathway under the influence of NKx2.2, Olig1/2, and Sox10. Once committed to the pathway, stage specific markers of oligodendrocytes allow for characterization of the lineage. Progenitor (OPC) and pre-oligodendrocytes (Pre-OL) feature stage-specific growth factor receptors (platelet derived growth factor receptor alpha; PDGFRα), surface antigens (neural/glial antigen 2; NG2) and cell adhesion molecules (polysialylated-neural cell adhesion molecule; PSA-NCAM), whilst premyelinating oligodendrocytes possess enzymes for lipid synthesis (galactocerebrosidase; GalC/O1). Finally, myelinating oligodendrocytes are characterized by the presence of myelin proteins such as myelin-associated glycoprotein (MAG), myelin basic protein (MBP), myelin oligodendrocyte glycoprotein (MOG), and proteolipid protein (PLP). Oligodendrocytes at this final stage of the lineage are the only ones capable of producing myelin and must also have contact with neuronal axons to perform this role. Figure created with BioRender.com.

deficits as the biological immaturity of the brain at the time of birth predisposes preterm neonates to respond poorly to *ex utero* insults such as increased cortisol, and periods of hypoxia, all in the absence of protective placental neurosteroid support. Furthermore, while oligodendrocyte development is heavily influenced by transcription factors and growth factors (16), it is also regulated by extracellular signals (16), hence a perturbation in these signals may affect the development of the lineage.

Perturbations to Oligodendrocyte Development After Preterm Birth

Following preterm birth, the newborn is exposed to the *ex utero* environment earlier than if it had remained *in utero* until term. Oligodendrocytes are highly sensitive to adverse conditions and are frequently injured by chemical and mechanical damage, which can occur following early delivery and the consequent premature exposure to the *ex utero* environment (35, 36). Substantive evidence indicates that ex-premature children experience impaired learning, and a loss of myelination is evident suggesting a causal pathway (13, 37–41). In infants born <27 weeks, diffuse microstructure alterations are observed on fractional anisotropy at term equivalence age in regions such as the corpus callosum and frontal cortex white matter when compared to term controls (38). Similarly, myelination deficits can be observed at term equivalence age in infants born <30 weeks and diagnosed with periventricular leukomalacia (PVL) (42). As the gestational age at the time of birth increases, these

white matter alterations become much harder to detect using routine imaging techniques whilst poor learning and behavioral outcomes remain evident (13, 43).

Post-mortem human studies have identified the relatively subtle effect of moderate to late preterm birth on the oligodendrocyte population, with the expression of Olig2-labeled cells significantly increased in areas with increased astrocytes, indicating injury (44). Additionally, myelination is sparse in these brains (44). Double-labeling of the Olig2 cells with stage-specific markers of the lineage revealed that the pre-oligodendrocyte population was increased in areas of injury, whilst the immature oligodendrocyte population was unaffected (44). This distinctive feature of moderate to late preterm birth-related white matter injury highlights that there is an imbalance in the oligodendrocyte lineage following preterm birth, with an increased percentage of pre-oligodendrocytes and a lower percentage of immature oligodendrocytes (44). In addition, whilst total neuron number is unaffected in areas indicative of white matter injury, the number of GABAergic neuronal cells is significantly decreased (45). It is possible that this loss of GABAergic neurons may contribute to the "arrest" in oligodendrocyte maturation due to a lack of the synaptic coupling with oligodendrocytes that induces myelin production and wrapping of axons, or due to the loss of GABA production which may lead to a shift away from an inhibitory dominant environment, and a shift toward an excitatory (glutamate) dominant environment. Thus, the primary characteristic of oligodendrocyte failure in the preterm brain is suggested to be an expansion of the pre-oligodendrocyte population, which is then unable to develop further, resulting in a net loss of ongoing myelination (39, 46, 47). There remains a major knowledge gap over the mechanisms that lead to this failure and how long it may persist for, and thus there is a current lack of effective therapies to combat preterm-birth related deficits in myelination. Below we present evidence to suggest that *ex utero* factors in the immediate postnatal period such as increased cortisol, periods of hypoxia, increases in excitability and loss of nurturing neurosteroids impact upon the overall biological immaturity of the preterm brain to result in a failure of oligodendrocytes to mature.

IMPORTANCE OF *IN UTERO* NEUROSTEROID CONCENTRATIONS

Neurosteroids are steroid hormones that not only protect the fetal brain but also form a key neuromodulatory system that regulates excitability and development during at least the second half of gestation in long gestation species including human, sheep and guinea pigs (14, 33, 48–50). In these species, progesterone production by the placenta provides precursors for the production of these neuroactive metabolites that influence the fetal brain (14, 50, 51). This placenta-brain interaction is critical in maintaining fetal brain excitability and development at least in late gestation. Allopregnanolone is the key neurosteroid during gestation with levels supported by the high level of placental progesterone production and metabolism (52, 53). This leads to allopregnanolone levels in the fetal circulation and brain that are markedly higher than in the neonate after birth and in the adult brain (33, 54). There is a marked decline in allopregnanolone levels following the fetal to neonatal transition in both preterm and term neonates (33). Therefore, preterm birth leads to a premature decline in allopregnanolone levels with animal studies showing this contributes to the reduced myelination that is associated with adverse patterns of behavior in the offspring (31, 33, 34). Importantly, although replacement with allopregnanolone analogs improves outcomes (55), progesterone treatment of neonates while raising allopregnanolone levels in the fetal circulation, does not appear to fully reverse the adverse effects of preterm birth on brain development (31). This may be because local levels in the brain are not adequately elevated or that progesterone may be metabolized to other steroids, in this instance cortisol (31), that are not effective in improving outcomes. These observations suggest that both progesterone production by the placenta and its metabolism to allopregnanolone is required to produce the nurturing steroid environment of the fetal brain.

Allopregnanolone Promotes Oligodendrocyte Development

Allopregnanolone is one of the major agonists of the $GABA_A$ receptor and elevated gestational levels in the fetal brain markedly increase the activity of inhibitory GABAergic pathways. Stimulation of the $GABA_A$ receptor in early gestation invokes an excitatory action, however this undergoes a switch to inhibitory (56). In species such as the guinea pig, non-human primate, and human this switch occurs at around 0.6 of gestation (57, 58), however in other rodent species, such as the rat and mouse, the switch occurs postnatally (59, 60). The switch is controlled by the developmentally regulated change in the expression of two co-transporters, the potassium chloride co-transporter (KCC2) and the sodium potassium chloride co-transporter (NKCC1), which control the influx and efflux of chloride (61, 62). In guinea pigs, non-human primates, and humans the marked decline in allopregnanolone after birth results in a consequent fall in GABAergic inhibition (33, 48). Therefore, it can be hypothesized that preterm birth leads to reduced GABA-mediated inhibitory tone, which may lead to reduced trophic drive for ongoing myelination. The sensitivity of $GABA_A$ receptors to allopregnanolone and other agonists is determined by the subunit composition of the receptors (63). The presence of α4–6 and δ-subunits in the $GABA_A$ receptor complex increases sensitivity to neurosteroid binding (50) and therefore receptors containing these subunits are important in driving trophic processes. Glial cells, and importantly oligodendrocytes, express $GABA_A$ receptors that are stimulated by extrasynaptic GABA released from nearby presynaptic terminals, with this stimulation strengthened by the co-binding of allopregnanolone (64). The $GABA_A$ receptor subtypes expressed in oligodendrocytes remains unclear and requires investigation, however allopregnanolone has been shown to stimulate both oligodendrocyte precursor and mature cells (65), supporting a gliotrophic interaction with $GABA_A$ receptors on these cells. Together these findings suggest that

the supportive effects attributed to GABAergic pathways in the fetus are mediated by extrasynaptic allopregnanolone-sensitive receptors (65–67), supporting the contention that GABAergic pathways have a major role in oligodendrocyte development that is prematurely lost following preterm birth. Thus, we suggest that $GABA_A$ receptor action has at least two key stimulatory roles in late gestation, (i) increasing maturation of oligodendrocytes and (ii) enhancing myelin production by mature cells.

ROLE OF ENVIRONMENTAL INSULTS IN FAILURE OF OLIGODENDROCYTES TO MATURE

Increased Cortisol

Neonatal intensive and special care units are inherently, but unavoidably, stressful for the preterm neonate. Repeated painful but necessary medical procedures, such as drug administration, heel prick blood collection, and respiratory management, as well as over-stimulation due to noise and light, have the potential to increase circulating cortisol concentrations in the preterm neonate (10, 68, 69). This increased cortisol in the neonatal period may be a key contributor to ongoing deficits in oligodendrocyte development, with evidence pointing to excess glucocorticoid-induced damage to oligodendrocytes that impedes their myelinating capability (70). Recently published embryonic rat spinal cord and cerebral cortex *in vitro* studies utilizing corticosterone, dexamethasone, and the glucocorticoid-receptor antagonist Mifepristone shows that prolonged exposure to glucocorticoids induces a dose-dependent reduction in myelination, which is prevented by Mifepristone (70). Interestingly, infection and chorioamnionitis associated utero-placental inflammation, a major cause of preterm birth, may also increase cortisol exposure. Placental cell culture studies have shown that infection-induced cytokines suppress placental 11β-hydroxysteroid dehydrogenase type 2 (HSD2) expression which would increase the passage of cortisol to the fetus (71). This increase in cortisol exposure may suppress allopregnanolone synthesis and potentiate the effects of inflammation on oligodendrocytes by lessening allopregnanolone-induced protection. Alternatively, some earlier studies have shown that neonatal treatment with lipopolysaccharide induced inflammation and raised allopregnanolone concentrations in the brain (72). The mechanism involved in this response is unclear and further studies of the potentially protective neurosteroid responses to infection are warranted.

We have also shown *in vivo* that increases in cortisol are associated with numerous other perinatal compromises, including intrauterine growth restriction, maternal stress exposure, pharmacological inhibition of allopregnanolone synthesis, and preterm birth (31, 32, 34, 73–79). In each of these cases there is a clear relationship between increased cortisol, decreased allopregnanolone, and mature myelin loss in vulnerable regions such as the hippocampus and cerebellum that are developing rapidly during the period of exposure. Furthermore, these stressful perinatal environments have long-lasting effects as we have also demonstrated that childhood-equivalent age behavior is affected by these *in utero* and immediate postnatal period exposures to abnormally high cortisol. Specifically, moderate to late gestation maternal stress exposure in guinea pigs increases maternal cortisol concentrations and reduces myelination in the fetal hippocampus (73). This deficit in myelination, as evidenced by reduced MBP immunostaining, persists until at least childhood-equivalent age, suggesting an ongoing loss of oligodendrocytes or a maturational arrest in their development (75, 76). Additionally, guinea pigs that are born preterm have increased salivary cortisol concentrations in the first 24 h of life, which remains elevated for males until at least childhood-equivalent age. This is associated with hyperactive behavior and deficits in hippocampal myelination (**Figure 2**) (34, 77).

Low neurosteroid environments, such as following preterm birth, and increased glucocorticoid action appear to have complex interactions. For example, in human hepatocyte cultures treatment with finasteride increased the action of cortisol on the glucocorticoid receptor, whilst overexpressing the enzyme responsible for neurosteroid synthesis (5α-Reductase type 1) dampened the effect of cortisol in these cultured cells (80). *In vivo* we have shown that pharmacologically increased plasma cortisol in preterm delivered male guinea pig neonates at term equivalence age is associated with an exacerbated reduction at the early and late stages of the oligodendrocyte lineage in the cerebellum. This was demonstrated by decreased Olig2, PDGFRα, and PLP protein expression (31). Furthermore, in prenatally stressed rats, exaggerated corticosterone responses to immune challenge with IL-1β were prevented with allopregnanolone pre-treatment, suggesting an attenuation of the stress response by neurosteroids (81). Repeated maternal betamethasone administration in late gestation guinea pigs also negates the protective effect of neurosteroids by reducing their synthesis in the placenta (82). A single course of betamethasone is standard clinical practice when there is a risk of preterm birth, as the glucocorticoid exposure is required to accelerate fetal lung development. Despite this finding in the guinea pig placenta, in humans exposure to a single course of betamethasone is not associated with an alteration in the neurosteroid synthesis enzymes 5α-reductase type 1 and 2 in the placenta (83), presumably due to the repeated vs. single course administration. Additionally, a study in rabbits using a single course of betamethasone based on the recommended human dose revealed no adverse effects of betamethasone on GABAergic and glutamatergic neurogenesis (84). However, a recent population-based retrospective cohort study in Finland has identified a significant increase in behavioral disorders in children that were exposed to a single course of betamethasone *in utero* (85). The significant increase was evident in both the preterm and term populations that were exposed to betamethasone, compared to age-equivalent children that were not exposed. This disconcerting finding highlights the detrimental effect that inappropriate glucocorticoid exposure in the perinatal period may have on later neurodevelopment.

These long-lasting impacts of glucocorticoids may be mediated by epigenetic changes in the immature preterm brain. Stress in pregnancy for example has been shown to increase

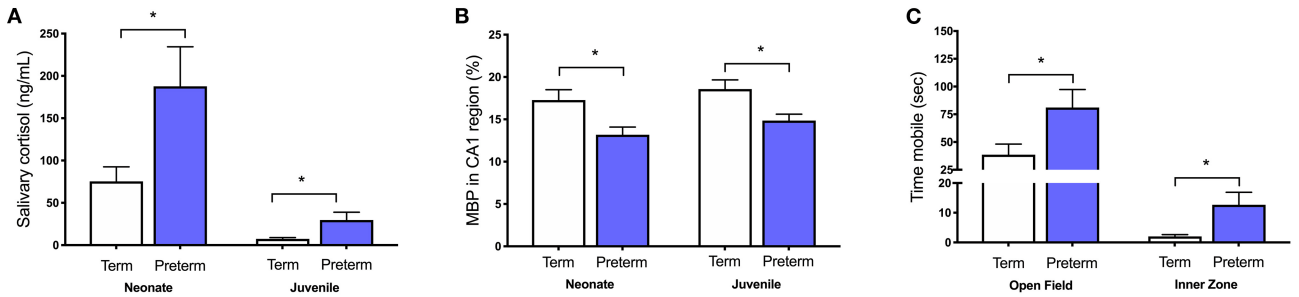

FIGURE 2 | Increased cortisol in the preterm neonate is associated with poor outcomes. Male guinea pigs born preterm (GA62; blue bars) have **(A)** higher salivary cortisol concentrations as a neonate (24 h old) and as a juvenile (corrected postnatal day 25), **(B)** decreased area coverage of myelin basic protein (MBP) in the CA1 region of the hippocampus, and **(C)** exhibit hyperactive behavior by spending more time mobile in the open field and inner zone when compared to term born (GA69; white bars) age-matched controls. Adapted from (34, 77). *$p < 0.05$, $n = 4$–10.

methylation of the *GAD1* gene, responsible for the conversion of glutamate to GABA, in hippocampal GABAergic neurons (86). A hyperactive phenotype was observed in these same mice at juvenile age but was prevented by Clozapine, an anti-psychotic but also a DNA-demethylation drug, supporting the link between stress-induced methylation changes in the brain and long-term behavior (87). Glucocorticoids have also been shown to affect histone acetylation, with synthetic glucocorticoid exposure in male guinea pig fetuses increasing acetylation in the hippocampus, suggesting that transcriptionally silenced genes are possibly becoming activated following inappropriate glucocorticoid exposure (88, 89). Furthermore, ill-timed glucocorticoid exposure in the fetal guinea pig induces permanent changes in functioning of the hypothalamic-pituitary-adrenal (HPA) axis and behavior that are passed down to the F1 offspring, again suggesting a role of epigenetic modifications (90, 91). However, whether these effects specifically target the transcription of regulators of the oligodendrocyte lineage or play a role in their failure to produce myelin following preterm birth is not clear and warrants investigation.

Periods of Hypoxia

Perinatal hypoxia, due to adverse events during labor or as a result of inadequate lung maturation for example, is relatively common in the preterm delivered population compared to term-born neonates (92). There is no doubt that hypoxia contributes to white matter injury in the preterm neonate (92). In particular, there is an extensive number of studies, in both human and animal models, supporting the notion that pre-OLs in particular are highly susceptible to hypoxic-related cell death following activation of caspase-3 (26, 47, 93, 94). Conversely, OPCs exhibit a robust response to hypoxia whereby the OPC pool is expanded as compared to the depletion of pre-OL cells (26, 39). This response means that a replenished population of pre-OL cells is created, but these new pre-OLs then fail to mature further, ultimately resulting in a net loss of myelin (39). Double labeling NG2 positive oligodendrocytes with the proliferation marker Ki67 in the neonatal rat cerebellum identifies the OPC pool of oligodendrocytes as those expanding in response to hypoxia, whilst the expression of mature oligodendrocyte markers was reduced for at least 20 days (26). Another neonatal rat model of hypoxia showed similar findings, with loss of the pre-OL pool by caspase-3 mediated cell death in the acute period, followed by a robust regeneration but a subsequent failure of this new cell population to mature (47). This type of oligodendrocyte injury is seen clinically in white matter lesions of deceased preterm neonates, where there is a lower percentage of immature oligodendrocytes compared to controls (94), and MRI assessment of myelination in children and adolescents born preterm. These studies have identified diffuse white matter microstructure deficits linking this acute loss of preOLs with a long-term reduction in myelin (41).

Damage due to hypoxic ischemic events is strongly linked with an increase in glutamate receptor activation, and a subsequent flow of excess calcium ions into the cell, leading to cell death *in vitro* (95–99). Decreased ATP during hypoxia leads to a reversal of glutamate transporters (100), with the result being an increase in extracellular glutamate release, primarily from astrocytes (99). Thus, there is increased glutamate which can then readily activate a-amino-3-hydroxy-5-methyl-isoxazolepropionic acid (AMPA) and kainate receptors located on oligodendrocytes (98, 101, 102), and N-methyl-D-aspartate (NMDA) receptors on myelin sheaths (102–104). In a sheep model of hypoxia, repeated umbilical cord occlusion resulted in marked glutamate efflux in the cerebral white matter where subjects with the greatest increases in extracellular glutamate following occlusion also had brain injury representative of PVL, suggesting a key role of glutamate (105). *In utero*, the fetus is protected from hypoxic periods by placentally-derived GABAergic agonist neurosteroids, such as allopregnanolone, which are much lower in the *ex utero* environment (106–108). The protective action of allopregnanolone has been demonstrated in late gestation fetal sheep following umbilical cord occlusion where allopregnanolone was increased in the fetal brain in response to asphyxia and, importantly, was shown to play a key role in protecting the fetal brain from asphyxia-induced cell death in vulnerable regions including the hippocampus and cerebellum (108). Infusion of finasteride (an inhibitor of allopregnanolone

synthesis), in addition to umbilical cord occlusion, significantly increased the amount of caspase-3 mediated cell death in neurons and astrocytes throughout the fetal brain, an effect that was lessened in the presence of normal gestational allopregnanolone concentrations (107). Interestingly, when a double infusion of finasteride and alfaxalone (an allopregnanolone analog) was performed, the effects of finasteride on behavioral activity and cell death were not seen, again highlighting the protective role of neurosteroids (109). Whilst these studies did not investigate the specific effect on oligodendrocytes, subsequent studies performed in the guinea pig show that inhibition of neurosteroid synthesis significantly decreases myelination in the subcortical white matter and experimentally induced growth restriction reduces myelination in the hippocampus (32). Altogether, these late gestation preclinical studies support the protective nature of allopregnanolone and therefore has implications for the preterm neonate where exposure to hypoxic periods often occurs in the relative absence of allopregnanolone.

Disruption to Sleep-Wake-Like Cycling

As oligodendrocytes produce myelin, their cell membrane expands to eventually support a membrane of 100 times their original size (15, 110). Understandably, this is a very high-energy demanding process, which under normal circumstances would take place whilst the fetus is *in utero* (1, 111, 112). In the case of preterm birth, this process takes place in the stimulating *ex utero* environment. Interestingly, oligodendrocytes of fetal origin are highly sensitive to glucose deprivation, exhibiting a failure to differentiate under these conditions, whilst oligodendrocytes of adult origin are relatively unaffected (113). Marked effects of glucose depletion are observed across the lineage *in vitro*, with low glucose concentrations inhibiting OPC differentiation and migration, reducing cell numbers across the lineage, and preventing myelination (114, 115). Glucose deprivation not only affects development and survival of oligodendrocytes, but also the morphology of surviving cells with reductions in branching and thinning of processes (116). Glucose levels are higher during sleep than wake (117) supporting the importance of the sleep-wake cycle during this period, and the contribution of fetal sleep-like states to promoting myelination.

Microarray results have identified subsets of genes that are differentially expressed in oligodendrocytes depending on sleep or wake state (118–120). During sleep, immature oligodendrocytes have a higher expression of genes associated with cell proliferation, including *Nrg2* (Neuregulin 2) which is essential for OPC proliferation through its activation of *ErbB* (Epidermal growth factor) family receptors (121, 122). Conversely, mature oligodendrocytes have a higher expression of genes related to phospholipid synthesis and myelination, such as *Pllp* (plasma membrane proteolipid) and *Opalin* (Oligodendrocytic myelin paranodal and inner loop protein) during sleep (121). Thus, the fetal sleep-like state, at least partially regulated by high levels of neurosteroids and GABAergic inhibitory activity (14), may be important for proliferation of OPCs and production of myelin by mature oligodendrocytes. Conversely, genes increased during periods of wakeful-like activity have roles in cell differentiation (121), which is consistent with the increase in glutamate during this state (123). Glutamate signaling through AMPA receptors promotes differentiation of oligodendrocytes whilst inhibiting OPC proliferation. This therefore has implications for the preterm neonate, where a loss of neurosteroid-GABA activity and exposure to the *ex utero* conditions interrupts the normal sleep-wake cycle, potentially affecting the expression of "sleep" genes, and contributing to the failure of mature oligodendrocytes to myelinate.

We have demonstrated that the neurosteroid-$GABA_A$ interaction regulates excitability in fetal life and has a major role in maintaining the fetal "sleep-like" states. In sheep, treatment with finasteride, an inhibitor of neurosteroid synthesis (5a-reductase type 1 and 2) at ∼0.88 of gestation (130 days out of a 147 day pregnancy) triggers an arousal-like and hyperactive state in fetal behavioral patterns (14, 49, 55). Similarly, fetal arousal behavior is also increased following treatment with trilostane, an inhibitor of progesterone synthesis (3β-hydroxysteroid dehydrogenase) and thus subsequent allopregnanolone synthesis (124, 125). Importantly, fetal behavior returns to normal following a subsequent infusion with progesterone (125). Therefore, when a neonate is born premature it is separated from this neurosteroid-rich environment, and the supportive fetal inhibition dominated "sleep-like" state is lost.

ENVIRONMENTAL INSULTS LEAD TO GLUTAMATE EXCITOTOXICITY

Glutamate, the main excitatory neurotransmitter of the CNS, is also involved in oligodendrocyte development, but this is limited to the proliferative stage of OPCs where glutamate guides migration through activation of AMPA receptors (65, 126). Conversely, increased glutamate present at the later stages of oligodendrocyte development promotes a rather hostile response. The expression of NMDA, AMPA and kainate receptors on oligodendrocytes makes them especially sensitive to increased extracellular glutamate and subsequent excitotoxic damage following excessive activation of the receptors *in vitro* (96–98, 103). In cultured oligodendrocytes, overactivation of ionotropic glutamate receptors results in an influx of calcium ions into the cell, the generation of reactive oxygen species (ROS) and activation of cell death pathways (95, 127). Interestingly, accumulation of ROS in oligodendrocytes following AMPA receptor overactivation is higher than in neurons (95), highlighting the increased susceptibility of oligodendrocytes to fluctuations in extracellular glutamate which is then further compounded by their inability to resist oxidative stress. Of the three receptor families, AMPA receptors (particularly those lacking the GluR2 subunit) may pose the greatest danger as activation of this receptor family results in the highest influx of calcium ions (95, 96). AMPA receptors undergo a developmental switch from highly calcium permeable GluR2-lacking receptors in early development, to GluR2-containing calcium impermeable receptors postnatally (128). However, it has been suggested that neurological insults can decrease the expression of the GluR2-subunit (129), for example global

ischemia increases the expression of genes that suppress GluR2 gene expression, thus increasing the permeability of AMPA receptors to calcium and the risk of excitotoxic cell death (130). Relative protein levels of the AMPA receptor subunits GluR1-GluR4 are differentially developmentally regulated in the human brain from mid gestation through to early childhood (131). Of note, the period where preterm birth may occur (between 25 and 37 weeks) shows low expression of the GluR2 subunit and thus highlights a vulnerable window for excitotoxic damage due to the increased potential for calcium influx (131). Furthermore, it has also been confirmed that AMPA receptors are expressed on developing human oligodendrocytes that populate fetal white matter within this preterm period of 23–32 weeks (132). These authors further demonstrated that addition of an AMPA-kainate receptor antagonist prevents calcium influx and glutamate excitotoxic cell death (132). Thus, these studies suggest that preOLs in particular are very susceptible to glutamate-induced oxidative stress due to the presence of GluR2-lacking AMPA receptors, which is exacerbated by their low expression of antioxidant enzymes and reduced capability to scavenge free radicals (133, 134). These observations are especially noteworthy given that human and animal studies suggest this stage of the lineage is the most adversely affected by preterm birth. Conversely, there is data to suggest mature oligodendrocytes are sensitive to glutamate excitotoxicity. Administration of glutamate in a rat model of spinal cord injury activated cell death pathways in mature oligodendrocytes, as evidenced by increased co-localized labeling of the mature oligodendrocyte cell marker CC1 [also known as adenomatous polyposis coli (APC)] with caspase-3 (135). Damage was most evident 6 h following administration but persisted for at least 1 week after the glutamate exposure.

It is interesting to note that each of the environmental insults discussed above is associated with a downstream increase in glutamate activity (**Figure 3**). Briefly, increased cortisol concentrations are linked with reductions in GABAergic neurosteroid interactions and a shift toward a glutamate dominated environment, increased wake and arousal periods are associated with raised glutamate concentrations, and hypoxia triggers a release of intracellular glutamate into the extracellular space. Currently available data regarding glutamate levels in the preterm infant are minimal and conflicting. In preterm infants without signs of brain injury, magnetic resonance imaging of the right frontal lobe at term equivalent age has shown that preterm birth at <27 weeks is associated with lower GABA and glutamate concentrations compared to term controls at 42 weeks post-menstrual age (136). Conversely, a recent prospective study involving preterm infants born <32 weeks showed that glutamate concentrations in the frontal lobe rises with increasing postnatal age, and furthermore that GABA concentrations correlated negatively with increasing gestational age at birth (137). The authors of this study speculated that preterm birth may therefore accelerate neurotransmitter production prematurely after early exposure to extra-uterine stresses (137). Thus, based on the most recent study increasing glutamate in the postnatal period may play a key role in the failure to myelinate following preterm birth.

Increasing GABAergic Action to Prevent Glutamate Excitotoxicity

The second half of gestation is a period of dramatic changes in the GABAergic system, with the density of GABAergic neurons peaking at full term and the migration of GABAergic neurons occurring throughout mid-gestation and into the early postnatal period. Therefore, preterm birth occurs at a vulnerable developmental window where the GABAergic system is not yet fully matured and ready for exposure to the *ex utero* environment. As discussed above, there is substantive evidence that overactivation of glutamate receptors on oligodendrocytes increases calcium ion flow into the cell, resulting in activation of cell death pathways. In the preterm neonate, we propose that targeting the immature GABAergic system by increasing action on $GABA_A$ receptors may prevent this damaging excitatory input and create a normal balance of inhibition:excitation. Organotypic cerebellar slice studies show that targeting the $GABA_A$ receptor using allopregnanolone or GABA itself promotes oligodendrocyte maturation and the production of myelin (26, 64, 65, 138, 139). Furthermore, drugs that act by increasing the available concentration of GABA either by preventing it's metabolism (Vigabatrin) or by inhibiting its' reuptake into astrocytes (Tiagabine) are able to increase the development of mature oligodendrocytes following hypoxia-mediated depletion (26). Seemingly, this restoration of the lineage is due to the action of GABA on oligodendrocyte $GABA_A$ receptors, as blocking these receptors using Bicuculline prevents the improvement in maturation (26). We have also demonstrated *in vivo* that increasing stimulation of $GABA_A$ receptors with $GABA_A$ receptor agonists following perinatal compromise is associated with an increase in myelination, and importantly a return to normal behavioral outcomes. In our model of prenatal stress, myelination deficits seen in juvenile guinea pigs exposed to stress *in utero* were restored by increasing neurosteroidogenic capacity in the week following spontaneous term birth (140). Furthermore, and highly pertinent to the search for potential therapies, we were also able to restore normal behavior and oligodendrocyte development in guinea pig offspring born premature. Moderately preterm (GA62; term = GA69) guinea pigs were administered the allopregnanolone analog Ganaxolone in the week following birth, resulting in increased myelination in the hippocampus and overlying subcortical white matter and a normal behavioral phenotype at childhood-equivalent age (**Figure 4**) (55). These data highlight how restoring inhibitory GABAergic action following insults such as hypoxia, excessive glucocorticoids, and early exposure to the *ex utero* environment can rectify or prevent perturbed oligodendrocyte maturation and ultimately increase the production of myelin. Thus, pharmacologically promoting GABAergic activity in the preterm neonatal brain warrants continued attention to determine feasibility for preventing myelination deficits and improving behavioral outcomes. Furthermore, approaches

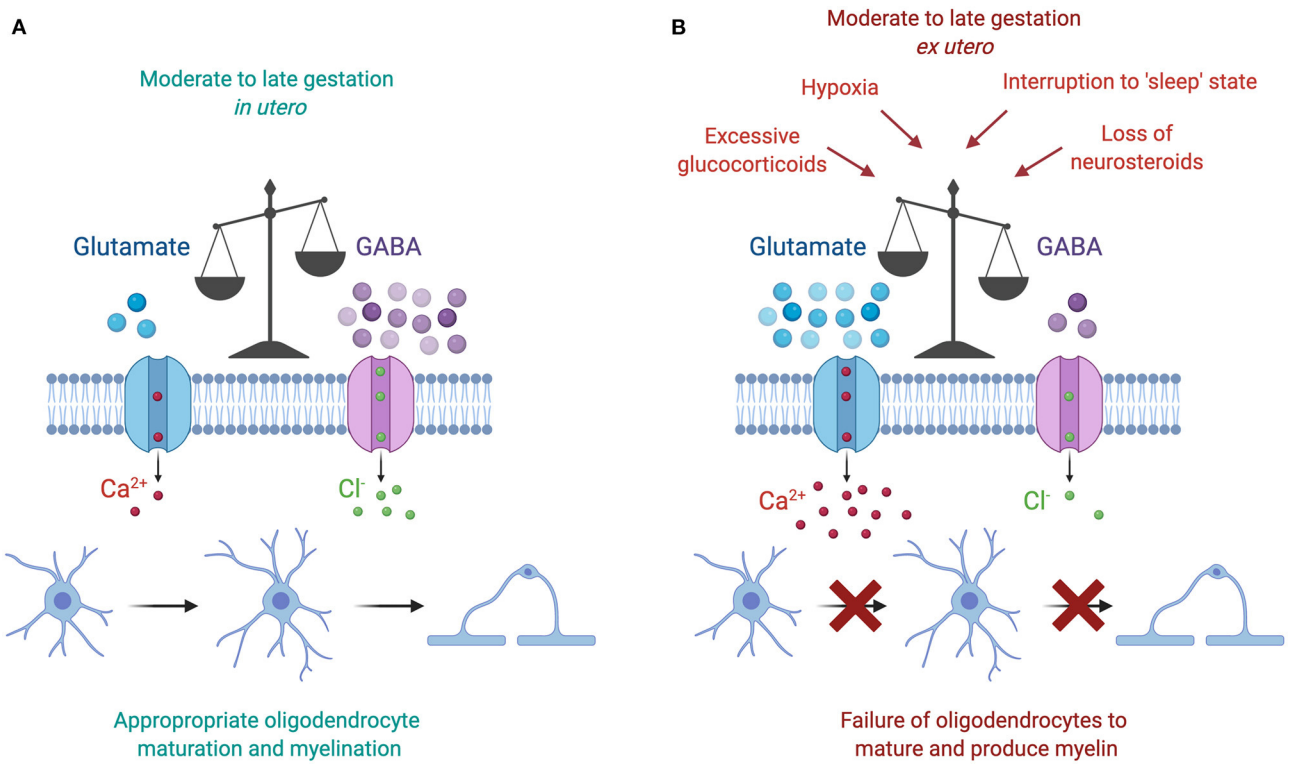

FIGURE 3 | (A) The moderate to late gestation *in utero* neural environment is characterized by a dominance of GABAergic activity, which plays a key role in promoting oligodendrocyte maturation and myelination. **(B)** The preterm *ex utero* environment is characterized by a loss of GABAergic activity following a reduction in placental neurosteroid supply. Subsequently, this loss disrupts the fetal "sleep" state, and may also coincide with additional adverse insults, including excessive glucocorticoid concentrations and periods of hypoxia. The resulting increase in glutamate action increases the amount of calcium ions flowing into the oligodendrocyte, thus preventing its normal development and production of myelin. Figure created with BioRender.com.

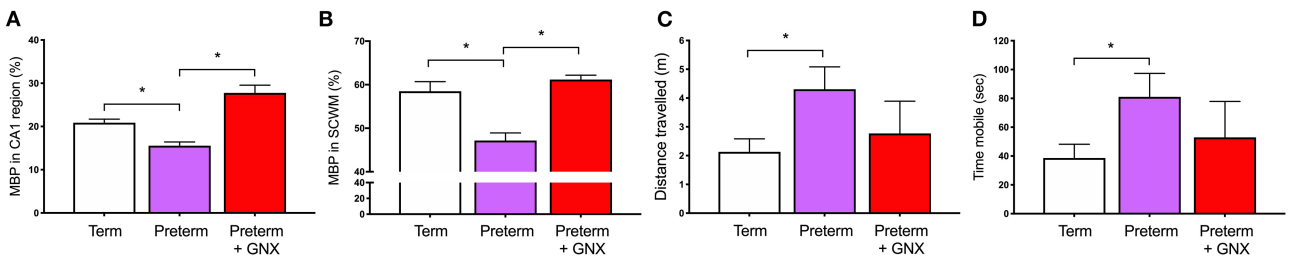

FIGURE 4 | Ganaxolone (GNX) 5 mg/kg by subcutaneous injection daily for 1 week following preterm birth restores mature myelin coverage in **(A)** the CA1 region of the hippocampus, and **(B)** the overlying subcortical white matter at childhood-equivalent age (corrected postnatal day 28). Behavior was also restored toward a term born phenotype for **(C)** the distance traveled, and **(D)** the time spent mobile in the open field arena. (*$p < 0.05$, $n = 4$–10). Adapted from (55).

targeting $GABA_A$ receptor specific subtype compositions may allow the selective targeting of appropriate stages of the oligodendrocyte lineage to improve myelination.

CONCLUSIONS

Moderate to late gestation preterm birth is associated with poor neurodevelopmental and behavioral outcomes. Diffuse deficits in myelination that persist into later life are relatively common among those born preterm. Post-mortem and animal studies identify an arrest in oligodendrocyte maturation in the neonatal preterm brain, highlighting a key role of the postnatal environment in oligodendrocyte dysfunction. Environmental insults in the immediate *ex utero* period, such as hypoxia and increased glucocorticoid exposure, have a compounding effect on biological immaturity of the preterm neonatal brain. The vulnerability of these neonates at disadvantage is further increased by the premature loss of neurosteroids that increase GABAergic action in the developing brain to

promote oligodendrocyte maturation and protect these cells from damaging insults. There appears to be a common downstream effect of these events that involves increases in extracellular glutamate and an overactivation of glutamate receptors on oligodendrocytes. This in turn results in a failure of oligodendrocytes to mature and produce myelin. Preclinical studies suggest that increasing GABAergic action, and thereby dampening the effect of glutamate, may enable oligodendrocytes to mature despite adverse events. Therefore, increasing GABAergic action in the immediate neonatal period may be a feasible avenue for targeted therapy following preterm birth to prevent myelination deficits and subsequent poor behavioral outcomes.

AUTHOR CONTRIBUTIONS

JS and JH were primary authors of the review. GC and HP assisted with writing and provided edits. All authors contributed to the article and approved the submitted version.

FUNDING

JS, GC, HP, and JH were supported by funding received from the NHMRC (Grant No. 1161981), the John Hunter Hospital Charitable Trust, and the Faculty of Health and Medicine (University of Newcastle).

REFERENCES

1. Kugelman A, Colin AA. Late preterm infants: near term but still in a critical developmental time period. *Pediatrics.* (2013) 132:741–51. doi: 10.1542/peds.2013-1131
2. Singh GK, Kenney MK, Ghandour RM, Kogan MD, Lu MC. Mental health outcomes in us children and adolescents born prematurely or with low birthweight. *Depress Res Treat.* (2013) 2013: 570743. doi: 10.1155/2013/570743
3. Cheong JL, Doyle LW. Increasing rates of prematurity and epidemiology of late preterm birth. *J Paediatr Child Health.* (2012) 48:784–8. doi: 10.1111/j.1440-1754.2012.02536.x
4. Chyi LJ, Lee HC, Hintz SR, Gould JB, Sutcliffe, TL. School outcomes of late preterm infants: Special needs and challenges for infants born at 32 to 36 weeks gestation. *J Pediatr.* (2008) 153:25–31. doi: 10.1016/j.jpeds.2008.01.027
5. Moster D, Lie RT, Markestad T. Long-term medical and social consequences of preterm birth. *N Engl J Med.* (2008) 359:262–73. doi: 10.1056/NEJMoa0706475
6. Loe IM, Lee ES, Luna B, Feldman HM. Behavior problems of 9-16 year old preterm children: biological, sociodemographic, and intellectual contributions. *Early Hum Dev.* (2011) 87:247–52. doi: 10.1016/j.earlhumdev.2011.01.023
7. Potijk MR, de Winter AF, Bos AF, Kerstjens JM, Reijneveld SA. Higher rates of behavioural and emotional problems at preschool age in children born moderately preterm. *Arch Dis Child.* (2012) 97:112–7. doi: 10.1136/adc.2011.300131
8. Baron IS, Litman FR, Ahronovich MD, Baker R. Late preterm birth: a review of medical and neuropsychological childhood outcomes. *Neuropsychol Rev.* (2012) 22:438–50. doi: 10.1007/s11065-012-9210-5
9. Petrini J, Dias T, McCormick M, Massolo M, Green N, Escobar G. Increased risk of adverse neurological development for late preterm infants. *J Pediatrics.* (2009) 154: 169–76. doi: 10.1016/j.jpeds.2008.08.020
10. Ream MA, Lehwald L. Neurologic consequences of preterm birth. *Curr Neurol Neurosci Rep.* (2018) 18:48. doi: 10.1007/s11910-018-0862-2
11. Beck S, Wojdyla D, Say L, Betran AP, Merialdi M, Requejo JH, et al. The worldwide incidence of preterm birth: a systematic review of maternal mortality and morbidity. *Bull World Health Organ.* (2010) 88:31–8. doi: 10.2471/BLT.08.062554
12. Spittle AJ, Walsh J, Olsen JE, McInnes E, Eeles AL, Brown NC, et al. Neurobehaviour and neurological development in the first month after birth for infants born between 32-42 weeks' gestation. *Early Hum Dev.* (2016) 96:7–14. doi: 10.1016/j.earlhumdev.2016.02.006
13. Brumbaugh JE, Conrad AL, Lee JK, DeVolder IJ, Zimmerman MB, Magnotta VA, et al. Altered brain function, structure, and developmental trajectory in children born late preterm. *Pediatr Res.* (2016) 80:197–203. doi: 10.1038/pr.2016.82
14. Hirst JJ, Kelleher MA, Walker DW, Palliser HK. Neuroactive steroids in pregnancy: key regulatory and protective roles in the foetal brain. *J Steroid Biochem Mol Biol.* (2014) 139:144–53. doi: 10.1016/j.jsbmb.2013.04.002
15. McLaurin JA, Yong VW. Oligodendrocytes and myelin. *Neurol Clin.* (1995) 13:23–49. doi: 10.1016/S0733-8619(18)30060-4
16. van Tilborg E, de Theije CGM, van Hal M, Wagenaar N, de Vries LS, Benders MJ, et al. Origin and dynamics of oligodendrocytes in the developing brain: implications for perinatal white matter injury. *Glia.* (2018) 66:221–38. doi: 10.1002/glia.23256
17. Emery B. Regulation of oligodendrocyte differentiation and myelination. *Science.* (2010) 330:779–82. doi: 10.1126/science.1190927
18. de Castro F, Bribian A, Ortega MC. Regulation of oligodendrocyte precursor migration during development, in adulthood and in pathology. *Cell Mol Life Sci.* (2013) 70:4355–68. doi: 10.1007/s00018-013-1365-6
19. Calver AR, Hall AC, Yu WP, Walsh FS, Heath JK, Betsholtz C, et al. Oligodendrocyte population dynamics and the role of PDGF *in vivo*. *Neuron.* (1998) 20:869–82. doi: 10.1016/S0896-6273(00)80469-9
20. Dugas JC, Cuellar TL, Scholze A, Ason B, Ibrahim A, Emery B, et al. Dicer1 and miR-219 are required for normal oligodendrocyte differentiation and myelination. *Neuron.* (2010) 65:597–611. doi: 10.1016/j.neuron.2010.01.027
21. Zhao X, He X, Han X, Yu Y, Ye F, Chen Y, et al. MicroRNA-mediated control of oligodendrocyte differentiation. *Neuron.* (2010) 65:612–26. doi: 10.1016/j.neuron.2010.02.018
22. Bujalka H, Koenning M, Jackson S, Perreau VM, Pope B, Hay CM, et al. MYRF is a membrane-associated transcription factor that autoproteolytically cleaves to directly activate myelin genes. *PLoS Biol.* (2013) 11:e1001625. doi: 10.1371/journal.pbio.1001625
23. Birey F, Kokkosis AG, Aguirre A. Oligodendroglia-lineage cells in brain plasticity, homeostasis and psychiatric disorders. *Curr Opin Neurobiol.* (2017) 47:93–103. doi: 10.1016/j.conb.2017.09.016
24. Matsusue Y, Horii-Hayashi N, Kirita T, Nishi M. Distribution of corticosteroid receptors in mature oligodendrocytes and oligodendrocyte progenitors of the adult mouse brain. *J Histochem Cytochem.* (2014) 62:211–26. doi: 10.1369/0022155413517700
25. Serrano-Regal MP, Bayon-Cordero L, Ordaz RP, Garay E, Limon A, Arellano RO, et al. Expression and function of GABA receptors in myelinating cells. *Front Cell Neurosci.* (2020) 14:256. doi: 10.3389/fncel.2020.00256
26. Zonouzi M, Scafidi J, Li P, McEllin B, Edwards J, Dupree JL, et al. GABAergic regulation of cerebellar NG2 cell development is altered in perinatal white matter injury. *Nat Neurosci.* (2015) 18:674–82. doi: 10.1038/nn.3990
27. Serrano-Regal MP, Luengas-Escuza I, Bayon-Cordero L, Ibarra-Aizpurua N, Alberdi E, Perez-Samartin A, et al. Oligodendrocyte differentiation and myelination is potentiated via GABAB receptor activation. *Neuroscience.* (2019 439:163–80. doi: 10.1016/j.neuroscience.2019.07.014
28. Nawaz S, Sanchez P, Schmitt S, Snaidero N, Mitkovski M, Velte C, et al. Actin filament turnover drives leading edge growth during myelin sheath formation in the central nervous system. *Dev Cell.* (2015) 34:139–51. doi: 10.1016/j.devcel.2015.05.013
29. Tolcos M, Petratos S, Hirst JJ, Wong F, Spencer SJ, Azhan A, et al. Blocked, delayed, or obstructed: what causes poor white matter development in intrauterine growth restricted infants? *Prog Neurobiol.* (2017) 154:62–77. doi: 10.1016/j.pneurobio.2017.03.009

30. Tolcos M, Bateman E, O'Dowd R, Markwick R, Vrijsen K, Rehn A, et al. Intrauterine growth restriction affects the maturation of myelin. *Exp Neurol.* (2011) 232:53–65. doi: 10.1016/j.expneurol.2011.08.002
31. Palliser HK, Kelleher MA, Tolcos M, Walker DW, Hirst JJ. Effect of postnatal progesterone therapy following preterm birth on neurosteroid concentrations and cerebellar myelination in guinea pigs. *J Dev Orig Health Dis.* (2015) 6:350–61. doi: 10.1017/S2040174415001075
32. Kelleher MA, Palliser HK, Walker DW, Hirst JJ. Sex-dependent effect of a low neurosteroid environment and intrauterine growth restriction on foetal guinea pig brain development. *J Endocrinol.* (2011) 208:301–9. doi: 10.1677/JOE-10-0248
33. Kelleher MA, Hirst JJ, Palliser HK. Changes in neuroactive steroid concentrations after preterm delivery in the Guinea pig. *Reprod Sci.* (2013) 20:1365–75. doi: 10.1177/1933719113485295
34. Shaw JC, Palliser HK, Dyson RM, Hirst JJ, Berry MJ. Long-term effects of preterm birth on behavior and neurosteroid sensitivity in the guinea pig. *Pediatr Res.* (2016) 80:275–83. doi: 10.1038/pr.2016.63
35. Antony J, Van Marle G, Opii W. Human endogenous retrovirus glycoprotein-mediated induction of redox reactants causes oligodendrocyte death and demyelination. *Nat Neurosci.* (2004) 7:1088–95. doi: 10.1038/nn1319
36. Blasko I, Humpel C, Grubeck-Loebenstein B. Astrocytes and oligodendrocytes during normal brain ageing. In: *Encyclopedia of Neuroscience.* ed LR Squire, Oxford: Academic Press (2009).
37. Rees S, Inder T. Fetal and neonatal origins of altered brain development. *Early Hum Dev.* (2005) 81:753–61. doi: 10.1016/j.earlhumdev.2005.07.004
38. Alexandrou G, Martensson G, Skiold B, Blennow M, Aden U, Vollmer B. White matter microstructure is influenced by extremely preterm birth and neonatal respiratory factors. *Acta Paediatr.* (2014) 103:48–56. doi: 10.1111/apa.12445
39. Back SA. White matter injury in the preterm infant: pathology and mechanisms. *Acta Neuropathol.* (2017) 134:331–49. doi: 10.1007/s00401-017-1718-6
40. Billiards SS, Haynes RL, Folkerth RD, Borenstein NS, Trachtenberg FL, Rowitch DH, et al. Myelin abnormalities without oligodendrocyte loss in periventricular leukomalacia. *Brain Pathol.* (2008) 18:153–63. doi: 10.1111/j.1750-3639.2007.00107.x
41. Caldinelli C, Froudist-Walsh S, Karolis V, Tseng CE, Allin MP, Walshe M, et al. White matter alterations to cingulum and fornix following very preterm birth and their relationship with cognitive functions. *Neuroimage.* (2017) 150:373–82. doi: 10.1016/j.neuroimage.2017.02.026
42. Rutherford MA, Supramaniam V, Ederies A, Chew A, Bassi L, Groppo M, et al. Magnetic resonance imaging of white matter diseases of prematurity. *Neuroradiology.* (2010) 52:505–21. doi: 10.1007/s00234-010-0700-y
43. Volpe JJ. Cerebral white matter injury of the premature infant-more common than you think. *Pediatrics.* (2003) 112 (1 Pt. 1):176–80. doi: 10.1542/peds.112.1.176
44. Buser JR, Maire J, Riddle A, Gong X, Nguyen T, Nelson K, et al. Arrested preoligodendrocyte maturation contributes to myelination failure in premature infants. *Ann Neurol.* (2012) 71:93–109. doi: 10.1002/ana.22627
45. Robinson S, Li Q, Dechant A, Cohen ML. Neonatal loss of gamma-aminobutyric acid pathway expression after human perinatal brain injury. *J Neurosurg.* (2006) 104 (6 Suppl):396–408. doi: 10.3171/ped.2006.104.6.396
46. Volpe JJ, Kinney HC, Jensen FE, Rosenberg PA. The developing oligodendrocyte: key cellular target in brain injury in the premature infant. *Int J Dev Neurosci.* (2011) 29:423–40. doi: 10.1016/j.ijdevneu.2011.02.012
47. Segovia KN, McClure M, Moravec M, Luo NL, Wan Y, Gong X, et al. Arrested oligodendrocyte lineage maturation in chronic perinatal white matter injury. *Ann Neurol.* (2008) 63:520–30. doi: 10.1002/ana.21359
48. Hirst JJ, Palliser HK, Shaw JC, Crombie G, Walker DW, Zakar T. Birth and neonatal transition in the guinea pig: experimental approaches to prevent preterm birth and protect the premature fetus. *Front Physiol.* (2018) 9:1802. doi: 10.3389/fphys.2018.01802
49. Nicol MB, Hirst JJ, Walker DW. Effect of finasteride on behavioural arousal and somatosensory evoked potentials in fetal sheep. *Neurosci Lett.* (2001) 306:13–6. doi: 10.1016/S0304-3940(01)01861-4
50. Belelli D, Herd MB, Mitchell EA, Peden DR, Vardy AW, Gentet L, et al. Neuroactive steroids and inhibitory neurotransmission: mechanisms of action and physiological relevance. *Neuroscience.* (2006) 138:821–9. doi: 10.1016/j.neuroscience.2005.07.021
51. Belelli D, Lambert JJ. Neurosteroids: endogenous regulators of the GABA(A) receptor. *Nat Rev Neurosci.* (2005) 6:565–75. doi: 10.1038/nrn1703
52. Brunton PJ, Russell JA, Hirst JJ. Allopregnanolone in the brain: protecting pregnancy and birth outcomes. *Prog Neurobiol.* (2014) 113:106–36. doi: 10.1016/j.pneurobio.2013.08.005
53. Hirst JJ, Palliser HK, Yates DM, Yawno T, Walker DW. Neurosteroids in the fetus and neonate: potential protective role in compromised pregnancies. *Neurochem Int.* (2008) 52:602–10. doi: 10.1016/j.neuint.2007.07.018
54. Gilbert Evans SE, Ross LE, Sellers EM, Purdy RH, Romach MK. 3alpha-reduced neuroactive steroids and their precursors during pregnancy and the postpartum period. *Gynecol Endocrinol.* (2005) 21:268–79. doi: 10.1080/09513590500361747
55. Shaw JC, Dyson RM, Palliser HK, Gray C, Berry MJ, Hirst JJ. Neurosteroid replacement therapy using the allopregnanolone-analogue ganaxolone following preterm birth in male guinea pigs. *Pediatr Res.* (2019) 85:86–96. doi: 10.1038/s41390-018-0185-7
56. Ganguly K, Schinder AF, Wong ST, Poo M. GABA itself promotes the developmental switch of neuronal GABAergic responses from excitation to inhibition. *Cell.* (2001) 105:521–32. doi: 10.1016/S0092-8674(01)00341-5
57. Coleman H, Hirst JJ, Parkington HC. The GABAA excitatory-to-inhibitory switch in the hippocampus of perinatal guinea-pigs. In: *The 40th Annual Meeting Fetal and Neonatal Physiological Society* Peurto Varas (2013).
58. Sedmak G, Jovanov-Milosevic N, Puskarjov M, Ulamec M, Kruslin B, Kaila K, et al. Developmental expression patterns of KCC2 and functionally associated molecules in the human brain. *Cereb Cortex.* (2016) 26:4574–89. doi: 10.1093/cercor/bhv218
59. Lysenko LV, Kim J, Madamba F, Tyrtyshnaia AA, Ruparelia A, Kleschevnikov AM. Developmental excitatory-to-inhibitory GABA polarity switch is delayed in Ts65Dn mice, a genetic model of down syndrome. *Neurobiol Dis.* (2018) 115:1–8. doi: 10.1016/j.nbd.2018.03.005
60. Scheyer AF, Borsoi M, Wager-Miller J, Pelissier-Alicot AL, Murphy MN, Mackie K, et al. Cannabinoid exposure via lactation in rats disrupts perinatal programming of the gamma-aminobutyric acid trajectory and select early-life behaviors. *Biol Psychiatry.* (2020) 87:666–77. doi: 10.1016/j.biopsych.2019.08.023
61. Rivera C, Voipio J, Payne JA, Ruusuvuori E, Lahtinen H, Lamsa K, et al. The K+/Cl– co-transporter KCC2 renders GABA hyperpolarizing during neuronal maturation. *Nature.* (1999) 397:251–5. doi: 10.1038/16697
62. Lee HH, Walker JA, Williams JR, Goodier RJ, Payne JA, Moss SJ. Direct protein kinase C-dependent phosphorylation regulates the cell surface stability and activity of the potassium chloride cotransporter KCC2. *J Biol Chem.* (2007) 282:29777–84. doi: 10.1074/jbc.M705053200
63. Lambert JJ, Cooper MA, Simmons RD, Weir CJ, Belelli D. Neurosteroids: endogenous allosteric modulators of GABA(A) receptors. *Psychoneuroendocrinology.* (2009) 34 (Suppl 1):S48–58. doi: 10.1016/j.psyneuen.2009.08.009
64. Kalakh S, Mouihate A. Enhanced remyelination during late pregnancy: involvement of the GABAergic system. *Sci Rep.* (2019) 9:7728. doi: 10.1038/s41598-019-44050-4
65. Habermacher C, Angulo MC, Benamer N. Glutamate versus GABA in neuron-oligodendroglia communication. *Glia.* (2019) 67:2092–106. doi: 10.1002/glia.23618
66. Mouihate A, Kalakh S. Ganaxolone enhances microglial clearance activity and promotes remyelination in focal demyelination in the corpus callosum of ovariectomized rats. *CNS Neurosci Ther.* (2020) 26:240–50. doi: 10.1111/cns.13195
67. Kalakh S, Mouihate A. Androstenediol reduces demyelination-induced axonopathy in the rat corpus callosum: impact on microglial polarization. *Front Cell Neurosci.* (2017) 11:49. doi: 10.3389/fncel.2017.00049
68. Peralta-Carcelen M, Schwartz J, Carcelen AC, Behavioral and socioemotional development in preterm children. *Clin Perinatol.* (2018) 45:529–46. doi: 10.1016/j.clp.2018.05.003
69. Milgrom J, Martin PR, Newnham C, Holt CJ, Anderson PJ, Hunt RW, et al. Behavioural and cognitive outcomes following an early stress-reduction intervention for very preterm and extremely preterm infants. *Pediatr Res.* (2019) 86:92–9. doi: 10.1038/s41390-019-0385-9

70. Miguel-Hidalgo JJ, Carter K, Deloach PH, Sanders L, Pang Y. Glucocorticoid-Induced reductions of myelination and connexin 43 in mixed central nervous system cell cultures are prevented by mifepristone. *Neuroscience.* (2019) 411:255–69. doi: 10.1016/j.neuroscience.2019.05.050
71. Chisaka H, Johnstone JF, Premyslova M, Manduch Z, Challis JR. Effect of pro-inflammatory cytokines on expression and activity of 11beta-hydroxysteroid dehydrogenase type 2 in cultured human term placental trophoblast and human choriocarcinoma JEG-3 cells. *J Soc Gynecol Investig.* (2005) 12:303–9. doi: 10.1016/j.jsgi.2005.02.003
72. Billiards SS, Walker DW, Canny BJ, Hirst JJ. Endotoxin increases sleep and brain allopregnanolone concentrations in newborn lambs. *Pediatr Res.* (2002) 52:892–9. doi: 10.1203/00006450-200212000-00014
73. Bennett GA, Palliser HK, Saxby B, Walker DW, Hirst JJ. Effects of prenatal stress on fetal neurodevelopment and responses to maternal neurosteroid treatment in Guinea pigs. *Dev Neurosci.* (2013) 35:416–26. doi: 10.1159/000354176
74. Bennett GA, Palliser HK, Shaw JC, Palazzi KL, Walker DW, Hirst JJ. Maternal stress in pregnancy affects myelination and neurosteroid regulatory pathways in the guinea pig cerebellum. *Stress.* (2017) 20:580–8. doi: 10.1080/10253890.2017.1378637
75. Bennett GA, Palliser HK, Shaw JC, Walker D, Hirst JJ. Prenatal stress alters hippocampal neuroglia and increases anxiety in childhood. *Dev Neurosci.* (2015) 37:535–45. doi: 10.1159/000437302
76. Bennett GA, Palliser HK, Walker D, Hirst J. Severity and timing: How prenatal stress exposure affects glial developmental, emotional behavioural and plasma neurosteroid responses in guinea pig offspring. *Psychoneuroendocrinology.* (2016) 70:47–57. doi: 10.1016/j.psyneuen.2016.04.011
77. Shaw J, Palliser H, Walker D, Hirst J. Preterm birth affects GABAA receptor subunit mRNA levels during the foetal-to-neonatal transition in guinea pigs. *J Dev Orig Health Dis.* (2015) 6:250–60. doi: 10.1017/S2040174415000069
78. Cumberland AL, Palliser HK, Rani P, Walker DW, Hirst JJ. Effects of combined IUGR and prenatal stress on the development of the hippocampus in a fetal guinea pig model. *J Dev Orig Health Dis.* (2017) 8:584–96. doi: 10.1017/S2040174417000307
79. Cumberland AL, Palliser HK, Walker DW, Hirst JJ. Cerebellar changes in guinea pig offspring following suppression of neurosteroid synthesis during late gestation. *Cerebellum.* (2017) 16:306–13. doi: 10.1007/s12311-016-0802-0
80. Nasiri M, Nikolaou N, Parajes S, Krone NP, Valsamakis G, Mastorakos G, et al. 5alpha-Reductase type 2 regulates glucocorticoid action and metabolic phenotype in human hepatocytes. *Endocrinology.* (2015) 156:2863–71. doi: 10.1210/en.2015-1149
81. Brunton PJ, Donadio MV, Yao ST, Greenwood M, Seckl JR, Murphy D, et al. 5alpha-Reduced neurosteroids sex-dependently reverse central prenatal programming of neuroendocrine stress responses in rats. *J Neurosci.* (2015) 35:666–77. doi: 10.1523/JNEUROSCI.5104-13.2015
82. McKendry AA, Palliser HK, Yates DM, Walker DW, Hirst JJ. The effect of betamethasone treatment on neuroactive steroid synthesis in a foetal guinea pig model of growth restriction. *J Neuroendocrinol.* (2010) 22:166–74. doi: 10.1111/j.1365-2826.2009.01949.x
83. Vu TT, Hirst JJ, Stark M, I.Wright MR, Palliser HK, Hodyl N, et al. Changes in human placental 5alpha-reductase isoenzyme expression with advancing gestation: effects of fetal sex and glucocorticoid exposure. *Reprod Fertil Dev.* (2009) 21:599–607. doi: 10.1071/RD08224
84. Vose LR, Vinukonda G, Diamond D, Korumilli R, Hu F, Zia MT, et al. Prenatal betamethasone does not affect glutamatergic or GABAergic neurogenesis in preterm newborns. *Neuroscience.* (2014) 270:148–57. doi: 10.1016/j.neuroscience.2014.04.009
85. Raikkonen K, Gissler M, Kajantie E. Associations between maternal antenatal corticosteroid treatment and mental and behavioral disorders in children. *JAMA.* (2020) 323:1924–33. doi: 10.1001/jama.2020.3937
86. Matrisciano F, Tueting P, Dalal I, Kadriu B, Grayson DR, Davis JM, et al. Epigenetic modifications of GABAergic interneurons are associated with the schizophrenia-like phenotype induced by prenatal stress in mice. *Neuropharmacology.* (2013) 68:184–94. doi: 10.1016/j.neuropharm.2012.04.013
87. Dong E, Tueting P, Matrisciano F, Grayson DR, Guidotti A. Behavioral and molecular neuroepigenetic alterations in prenatally stressed mice: relevance for the study of chromatin remodeling properties of antipsychotic drugs. *Transl Psychiatry.* (2016) 6:e711. doi: 10.1038/tp.2015.191
88. Crudo A, Petropoulos S, Suderman M, Moisiadis VG, Kostaki A, Hallett M, et al. Effects of antenatal synthetic glucocorticoid on glucocorticoid receptor binding, DNA methylation, and genome-wide mRNA levels in the fetal male hippocampus. *Endocrinology.* (2013) 154:4170–81. doi: 10.1210/en.2013-1484
89. Crudo A, Suderman M, Moisiadis VG, Petropoulos S, Kostaki A, Hallett M, et al. Glucocorticoid programming of the fetal male hippocampal epigenome. *Endocrinology.* (2013) 154:1168–80. doi: 10.1210/en.2012-1980
90. Liu L, Li A, Matthews SG. Maternal glucocorticoid treatment programs HPA regulation in adult offspring: sex-specific effects. *Am J Physiol Endocrinol Metab.* (2001) 280:E729–39. doi: 10.1152/ajpendo.2001.280.5.E729
91. Kapoor A, Petropoulos S, Matthews SG. Fetal programming of hypothalamic-pituitary-adrenal (HPA) axis function and behavior by synthetic glucocorticoids. *Brain Res Rev.* (2008) 57:586–95. doi: 10.1016/j.brainresrev.2007.06.013
92. Dhillon SK, Lear CA, Galinsky R, Wassink G, Davidson JO, Juul S, et al. The fetus at the tipping point: modifying the outcome of fetal asphyxia. *J Physiol.* (2018) 596:5571–92. doi: 10.1113/JP274949
93. Riddle A, Luo NL, Manese M, Beardsley DJ, Green L, Rorvik DA, et al. Spatial heterogeneity in oligodendrocyte lineage maturation and not cerebral blood flow predicts fetal ovine periventricular white matter injury. *J Neurosci.* (2006) 26:3045–55. doi: 10.1523/JNEUROSCI.5200-05.2006
94. Back SA, Han BH, Luo NL, Chricton CA, Xanthoudakis S, Tam J, et al. Selective vulnerability of late oligodendrocyte progenitors to hypoxia–ischemia. *J Neurosci.* (2002) 22:455–63. doi: 10.1523/JNEUROSCI.22-02-00455.2002
95. Ibarretxe G, Sanchez-Gomez MV, Campos-Esparza MR, Alberdi E, Matute C. Differential oxidative stress in oligodendrocytes and neurons after excitotoxic insults and protection by natural polyphenols. *Glia.* (2006) 53:201–11. doi: 10.1002/glia.20267
96. Sanchez-Gomez MV, Alberdi E, Ibarretxe G, Torre I, Matute C. Caspase-dependent and caspase-independent oligodendrocyte death mediated by AMPA and kainate receptors. *J Neurosci.* (2003) 23:9519–28. doi: 10.1523/JNEUROSCI.23-29-09519.2003
97. Yoshioka A, Bacskai B, Pleasure D. Pathophysiology of oligodendroglial excitotoxicity. *J Neurosci Res.* (1996) 46:427–37. doi: 10.1002/(SICI)1097-4547(19961115)46:4<427::AID-JNR4>3.0.CO;2-I
98. Alberdi E, Sanchez-Gomez MV, Marino A, Matute C. Ca(2+) influx through AMPA or kainate receptors alone is sufficient to initiate excitotoxicity in cultured oligodendrocytes. *Neurobiol Dis.* (2002) 9:234–43. doi: 10.1006/nbdi.2001.0457
99. Rinholm JE, Vervaeke K, Tadross MR, Tkachuk AN, Kopek BG, Brown TA, et al. Movement and structure of mitochondria in oligodendrocytes and their myelin sheaths. *Glia.* (2016) 64:810–25. doi: 10.1002/glia.22965
100. Li S, Mealing GA, Morley P, Stys PK. Novel injury mechanism in anoxia and trauma of spinal cord white matter: glutamate release via reverse Na+-dependent glutamate transport. *J Neurosci.* (1999) 19:RC16. doi: 10.1523/JNEUROSCI.19-14-j0002.1999
101. McDonald JW, Althomsons SP, Hyrc KL, Choi DW, Goldberg MP. Oligodendrocytes from forebrain are highly vulnerable to AMPA/kainate receptor-mediated excitotoxicity. *Nat Med.* (1998) 4:291–7. doi: 10.1038/nm0398-291
102. Salter MG, Fern R. NMDA receptors are expressed in developing oligodendrocyte processes and mediate injury. *Nature.* (2005) 438:1167–71. doi: 10.1038/nature04301
103. Fu Y, Sun W, Shi Y, Shi R, Cheng JX. Glutamate excitotoxicity inflicts paranodal myelin splitting and retraction. *PLoS ONE.* (2009) 4:e6705. doi: 10.1371/journal.pone.0006705
104. Karadottir R, Cavelier P, Bergersen LH, Attwell D. NMDA receptors are expressed in oligodendrocytes and activated in ischaemia. *Nature.* (2005) 438:1162–6. doi: 10.1038/nature04302
105. Loeliger M, Watson CS, Reynolds JD, Penning DH, Harding R, Bocking AD, et al. Extracellular glutamate levels and neuropathology in cerebral white matter following repeated umbilical cord

occlusion in the near term fetal sheep. *Neuroscience.* (2003) 116:705–14. doi: 10.1016/S0306-4522(02)00756-X
106. Yawno T, Hirst JJ, Castillo-Melendez M, Walker DW. Role of neurosteroids in regulating cell death and proliferation in the late gestation fetal brain. *Neuroscience.* (2009) 163:838–47. doi: 10.1016/j.neuroscience.2009.07.009
107. Yawno T, Yan E, Walker D, Hirst J. Inhibition of neurosteroid synthesis increases asphyxia-induced brain injury in the late gestation fetal sheep. *Neuroscience.* (2007) 146:1726–33. doi: 10.1016/j.neuroscience.2007.03.023
108. Nguyen PN, Yan EB, Castillo-Melendez M, Walker DW, Hirst JJ. Increased allopregnanolone levels in the fetal sheep brain following umbilical cord occlusion. *J Physiol.* (2004) 560:593–602. doi: 10.1113/jphysiol.2004.069336
109. Yawno T, Yan EB, Hirst JJ, Walker DW. Neuroactive steroids induce changes in fetal sheep behavior during normoxic and asphyxic states. *Stress.* (2011) 14:13–22. doi: 10.3109/10253890.2010.504789
110. Bradl M, Lassmann H. Oligodendrocytes: biology and pathology. *Acta Neuropathol.* (2010) 119:37–53. doi: 10.1007/s00401-009-0601-5
111. Herschkowitz N. Brain development in the fetus, neonate and infant. *Neonatology.* (1988) 54:1–19. doi: 10.1159/000242818
112. de Graaf-Peters VB, Hadders-Algra M. Ontogeny of the human central nervous system: what is happening when? *Early Hum Dev.* (2006) 82:257–66. doi: 10.1016/j.earlhumdev.2005.10.013
113. Baldassarro VA, Marchesini A, Giardino L, Calza L. Differential effects of glucose deprivation on the survival of fetal versus adult neural stem cells-derived oligodendrocyte precursor cells. *Glia.* (2020) 68:898–917. doi: 10.1002/glia.23750
114. Yan H, Rivkees SA. Hypoglycemia influences oligodendrocyte development and myelin formation. *Neuroreport.* (2006) 17:55–9. doi: 10.1097/01.wnr.0000192733.00535.b6
115. Rinholm JE, Hamilton NB, Kessaris N, Richardson WD, Bergersen LH, Attwell D. Regulation of oligodendrocyte development and myelination by glucose and lactate. *J Neurosci.* (2011) 31:538–48. doi: 10.1523/JNEUROSCI.3516-10.2011
116. Zhou P, Guan T, Jiang Z, Namaka M, Huang QJ, Kong JM. Monocarboxylate transporter 1 and the vulnerability of oligodendrocyte lineage cells to metabolic stresses. *CNS Neurosci Ther.* (2018) 24:126–34. doi: 10.1111/cns.12782
117. Poggiogalle E, Jamshed H, Peterson CM. Circadian regulation of glucose, lipid, energy metabolism in humans. *Metabolism.* (2018) 84:11–27. doi: 10.1016/j.metabol.2017.11.017
118. Cirelli C. The genetic and molecular regulation of sleep: from fruit flies to humans. *Nat Rev Neurosci.* (2009) 10:549–60. doi: 10.1038/nrn2683
119. Cirelli C, Gutierrez CM, Tononi G. Extensive and divergent effects of sleep and wakefulness on brain gene expression. *Neuron.* (2004) 41:35–43. doi: 10.1016/S0896-6273(03)00814-6
120. Mongrain V, Hernandez SA, Pradervand S, Dorsaz S, Curie T, Hagiwara G, et al. Separating the contribution of glucocorticoids and wakefulness to the molecular and electrophysiological correlates of sleep homeostasis. *Sleep.* (2010) 33:1147–57. doi: 10.1093/sleep/33.9.1147
121. Bellesi M, Pfister-Genskow M, Maret S, Keles S, Tononi G, Cirelli C. Effects of sleep and wake on oligodendrocytes and their precursors. *J Neurosci.* (2013) 33:14288–300. doi: 10.1523/JNEUROSCI.5102-12.2013
122. Canoll PD, Musacchio JM, Hardy R, Reynolds R, Marchionni MA, Salzer JL. GGF/neuregulin is a neuronal signal that promotes the proliferation and survival and inhibits the differentiation of oligodendrocyte progenitors. *Neuron.* (1996) 17:229–43. doi: 10.1016/S0896-6273(00)80155-5
123. Dash MB, Douglas CL, Vyazovskiy VV, Cirelli C, Tononi G. Long-term homeostasis of extracellular glutamate in the rat cerebral cortex across sleep and waking states. *J Neurosci.* (2009) 29:620–9. doi: 10.1523/JNEUROSCI.5486-08.2009
124. Nicol M, Hirst J, Walker D, Thorburn G. Effect of alteration of maternal plasma progesterone concentrations on fetal behavioural state during late gestation. *J Endocrinol.* (1997) 152:379–86. doi: 10.1677/joe.0.1520379
125. Crossley KJ, Nicol MB, Hirst JJ, Walker DW, Thorburn GD. Suppression of arousal by progesterone in fetal sheep. *Reprod Fertil Dev.* (1997) 9:767–73. doi: 10.1071/R97074
126. Pitman KA, Young KM. Activity-dependent calcium signalling in oligodendrocyte generation. *Int J Biochem Cell Biol.* (2016) 77 (Pt A):30–4. doi: 10.1016/j.biocel.2016.05.018
127. Kim UJ, Lee BH, Lee KH. Neuroprotective effects of a protein tyrosine phosphatase inhibitor against hippocampal excitotoxic injury. *Brain Res.* (2019) 1719:133–9. doi: 10.1016/j.brainres.2019.05.027
128. Wright A, Vissel B. The essential role of AMPA receptor GluR2 subunit RNA editing in the normal and diseased brain. *Front Mol Neurosci.* (2012) 5:34. doi: 10.3389/fnmol.2012.00034
129. Pellegrini-Giampietro DE, Zukin RS, Bennett MV, Cho S, Pulsinelli WA. Switch in glutamate receptor subunit gene expression in CA1 subfield of hippocampus following global ischemia in rats. *Proc Natl Acad Sci U.S.A.* (1992) 89:10499–503. doi: 10.1073/pnas.89.21.10499
130. Calderone A, Jover T, Noh KM, Tanaka H, Yokota H, Lin Y, et al. Ischemic insults derepress the gene silencer REST in neurons destined to die. *J Neurosci.* (2003) 23:2112–21. doi: 10.1523/JNEUROSCI.23-06-02112.2003
131. Talos DM, Follett PL, Folkerth RD, Fishman RE, Trachtenberg FL, Volpe JJ, et al. Developmental regulation of alpha-amino-3-hydroxy-5-methyl-4-isoxazole-propionic acid receptor subunit expression in forebrain and relationship to regional susceptibility to hypoxic/ischemic injury. II. Human cerebral white matter and cortex. *J Comp Neurol.* (2006) 497:61–77. doi: 10.1002/cne.20978
132. Follett PL, Deng W, Dai W, Talos DM, Massillon LJ, Rosenberg PA, et al. Glutamate receptor-mediated oligodendrocyte toxicity in periventricular leukomalacia: a protective role for topiramate. *J Neurosci.* (2004) 24:4412–20. doi: 10.1523/JNEUROSCI.0477-04.2004
133. Folkerth RD, Haynes RL, Borenstein NS, Belliveau RA, Trachtenberg F, Rosenberg PA, et al. Developmental lag in superoxide dismutases relative to other antioxidant enzymes in premyelinated human telencephalic white matter. *J Neuropathol Exp Neurol.* (2004) 63:990–9. doi: 10.1093/jnen/63.9.990
134. Yap V, Perlman JM. Mechanisms of brain injury in newborn infants associated with the fetal inflammatory response syndrome. *Semin Fetal Neonatal Med.* (2020) 25:101110. doi: 10.1016/j.siny.2020.101110
135. Xu GY, Liu S, Hughes MG, McAdoo DJ. Glutamate-induced losses of oligodendrocytes and neurons and activation of caspase-3 in the rat spinal cord. *Neuroscience.* (2008) 153:1034–47. doi: 10.1016/j.neuroscience.2008.02.065
136. Kwon SH, Scheinost D, Lacadie C, Benjamin J, Myers EH, Qiu M, et al. GABA, resting-state connectivity and the developing brain. *Neonatology.* (2014) 106:149–55. doi: 10.1159/000362433
137. Basu SK, Pradhan S, Jacobs MB, Said M, Kapse K, Murnick J, et al. Age and sex influences gamma-aminobutyric acid concentrations in the developing brain of very premature infants. *Sci Rep.* (2020) 10:10549. doi: 10.1038/s41598-020-67188-y
138. Ghoumari AM, Baulieu EE, Schumacher M. Progesterone increases oligodendroglial cell proliferation in rat cerebellar slice cultures. *Neuroscience.* (2005) 135:47–58. doi: 10.1016/j.neuroscience.2005.05.023
139. Ghoumari AM, Ibanez C, El-Etr M, Leclerc P, Eychenne B, O'Malley BW, et al. Progesterone and its metabolites increase myelin basic protein expression in organotypic slice cultures of rat cerebellum. *J Neurochem.* (2003) 86:848–59. doi: 10.1046/j.1471-4159.2003.01881.x
140. Crombie GK, Palliser HK, Shaw JC, Hodgson DM, Walker DW, Hirst JJ, Behavioural deficits induced by chronic perinatal stress is ameliorated by Xbd173 administration in male guinea pig offspring. *J Paediatr Child Health.* (2018) 54:15. doi: 10.1111/jpc.13882_31

Conflict of Interest: The authors declare that the research was conducted in the absence of any commercial or financial relationships that could be construed as a potential conflict of interest.

frontiers in Pediatrics

ORIGINAL RESEARCH
published: 08 February 2021
doi: 10.3389/fped.2020.556216

Neonatal Encephalopathy Is Associated With Altered IL-8 and GM-CSF Which Correlates With Outcomes

*Deirdre U. Sweetman[1,2,3], Tammy Strickland[4,5], Ashanty M. Melo[4,5], Lynne A. Kelly[2,4,5], Chike Onwuneme[1,6], William R. Watson[6], John F. A. Murphy[1,3], Marie Slevin[1], Veronica Donoghue[7], Amanda O'Neill[6] and Eleanor J. Molloy[2,4,5,8,9,10]**

[1] Neonatology, National Maternity Hospital, Dublin, Ireland, [2] National Children's Research Centre, Dublin, Ireland, [3] Paediatrics, Royal College of Surgeons in Ireland, Dublin, Ireland, [4] Discipline of Paediatrics, Trinity College Dublin, Dublin, Ireland, [5] Trinity Translational Medicine Institute, St James Hospital, Dublin, Ireland, [6] UCD School of Medicine and Medical Sciences, University College Dublin, Dublin, Ireland, [7] Radiology Department, Children's University Hospital, Dublin, Ireland, [8] Childrens University Hospital (CHI) at Tallght, Tallaght University Hospital, Dublin, Ireland, [9] Paediatrics, Coombe Women's and Infant's University Hospital, Dublin, Ireland, [10] Neonatology, Children's Health Ireland at Crumlin, Dublin, Ireland

OPEN ACCESS

Edited by:
Francisco J. Alvarez, Hospital de Cruces, Spain

Reviewed by:
L. S. De Vries, Independent Researcher, Utrecht, Netherlands
Hector Lafuente Echevarría, Biodonostia Health Research Institute (IIS Biodonostia), Spain

***Correspondence:**
Eleanor J. Molloy
eleanor.molloy@tcd.ie

Specialty section:
This article was submitted to Neonatology, a section of the journal Frontiers in Pediatrics

Received: *27 April 2020*
Accepted: *21 December 2020*
Published: *08 February 2021*

Citation:
Sweetman DU, Strickland T, Melo AM, Kelly LA, Onwuneme C, Watson WR, Murphy JFA, Slevin M, Donoghue V, O'Neill A and Molloy EJ (2021) Neonatal Encephalopathy Is Associated With Altered IL-8 and GM-CSF Which Correlates With Outcomes. Front. Pediatr. 8:556216. doi: 10.3389/fped.2020.556216

Aim: To investigate the relationship between cytokines associated with innate immune cell activation and brain injury and outcome in infants with NE compared to neonatal controls.

Methods: Serum and CSF biomarkers associated with activated neutrophils and monocytes [Interleukin-8 (IL-8) and Granulocyte-Macrophage-Colony-Stimulating-Factor (GM-CSF)] were serially measured using duplex immunoassays on days 1, 3 and 7 in term newborns with NE and controls. Results were compared to grade of encephalopathy, seizures, MRI brain imaging, mortality and Bayley Score of Infant and Toddler Development (Bayley-III) at 2 years of age.

Results: Ninety-four infants had serum samples collected with 34 CSF samples. NE Grade II/III was significantly associated with elevated on day 2 serum IL-8. Mortality was best predicted by elevated day 1 IL-8. GM-CSF was initially elevated on day 1 and abnormal MRI imaging was associated with decreased day 2 GM-CSF. Elevated GM-CSF at day of life 6–7 correlated negatively with composite cognitive, language and motor Bayley-III scores at 2 years.

Conclusion: Moderate or severe NE and mortality was associated with elevated IL-8. Day 2 GM-CSF could predict abnormal MRI results in NE and Bayley-III. Therefore, these cytokines are altered in NE and may predict early outcomes and further implicate inflammatory processes in NE.

Keywords: outcomes, cytokines, therapeutic hypothermia, neonatal brain injury, perinatal asphyxia, hypoxic-ischemic encephalopathy

INTRODUCTION

Neonatal encephalopathy (NE) can result in long-term neurodevelopmental impairment in term infants. Therapeutic hypothermia (TH) is the only standard treatment but morbidity remains elevated at 50% (1–3). Systemic inflammation and a dysregulated immune response are features of NE (4, 5). Elevated leukocytes are associated with adverse neurodevelopmental outcome in infants with NE (6). We have previously reported the alteration of vascular endothelial growth factor (VEGF) and erythropoietin (Epo), two cytokines associated with hypoxia in NE infants, and the use of these cytokines as markers of severity of hypoxia-ischemia and brain injury (7).

Infants with NE also present systemic inflammation, therefore we were interested in cytokines associated with innate immune cell activation such as Interleukin-8 (IL-8) and granulocyte-macrophage colony-stimulating factor (GM-CSF). IL-8 and GM-CSF stimulate neutrophils and monocytes in both adults and neonates (8). IL-8 is a chemotactic cytokine that mainly facilitates neutrophil recruitment and activation during immunological responses at the site of inflammation (9). IL-8 concentrations in the serum of neonates with perinatal asphyxia are significantly higher than levels in control newborns on day 1 of life and has been suggested as a suitable candidate biomarker in NE (10–12).

GM-CSF is a member of the βc family of glycoprotein cytokines that has potent effects in stimulating the proliferation, maturation and function of haematopoietic cells as well as regulating multiple biological processes such as native and adaptive immunity, inflammation, normal and autoimmunity but is also thought to exert biological effects on non-haematopoietic cells (13). Imbalance of GM-CSF may induce chronic inflammation and brain inflammation (14, 15). Spath et al. described that the excess production of GM-CSF induces reactive oxygen species (ROS) by brain-infiltrating phagocytes leading to spontaneous brain inflammation and neurological disease (14).

We hypothesized that infants with NE may have altered serum and cerebrospinal fluid (CSF) cytokines associated with leukocyte activation (GM-CSF and IL-8) and may reflect severity of brain injury in NE. The objective of this study was to investigate the relationship between serum biomarkers and outcome suh as severity of encephalopathy, seizures, MRI brain, mortality and neurodevelopment in infants with NE.

MATERIALS AND METHODS

Ethical Approval

Ethical committee approval was received from the National Maternity Hospital, Dublin, a tertiary referral, University-affiliated Maternity hospital in 2011. In all cases written informed consent was taken from parents of infants enrolled in the study.

Abbreviations: NE, neonatal encephalopathy; CP, cerebral palsy; VEGF, vascular endothelial growth factor; Epo, erythropoietin; IL-8, interleukin-8; GM-CSF, granulocyte-macrophage colony-stimulating factor; CSF, cerebrospinal fluid; TH, therapeutic hypothermia; BG, basal ganglia; W, watershed; BG/W, combined basal ganglia/watershed.

Patient Groups

We prospectively recruited infants with NE and neonatal controls as previously described (7, 16). The following study groups were enrolled: **Neonatal Controls:** Serum samples from term healthy control infants following normal delivery with normal Apgar scores, normal neurological examination and postnatal course; **Neonatal Encephalopathy:** Infants were divided into subgroups according to the grade of clinical encephalopathy according to the classification of Sarnat and Sarnat as follows: (a) **NE 0/I**: infants who required resuscitation following delivery with no neurological signs or mild encephalopathy; (b) **NE II/III**: moderate/severe encephalopathy (17). Infants with congenital abnormalities or evidence of maternal substance abuse were excluded.

All infants had serial cranial ultrasounds performed within the first 24 h of life and those with NE had an MRI brain within the first 10 days of life. MRIs were scored and reported independently by a pediatric radiologist as either "normal" or "abnormal" and classified with the Barkovich score (18). Seizures were diagnosed clinically based on recognition by nursing/medical staff of abnormal paroxysmal, repetitive and stereotypical events. Infants with NE also had continuous video EEG monitoring or aEEG monitoring over the first 3 days of life and were graded in a blinded fashion as having a "normal" or "abnormal" EEG by the electrophysiologist (GB) (19).

NE infants were followed up at 18–24 months of age and had a Bayleys Score of Infant Development III performed by a developmental psychologist (MS). Composite cognitive, language and motor developmental scores were grouped as normal (>90 in each category) or at risk or abnormal (<90 in each category).

Magnetic Resonance Imaging

All infants with NE were examined on a 1.5T scanner and all were examined before day 10 of life. The sequences used were: Diffusion with ADC Map, T1 in axial and sagittal planes, T2 in axial plane, gradient echo and spectroscopy.

Serum and CSF Sampling

Serum samples were collected from infants at risk of NE at 1, 2, 3, and 7 days of life. At each time point 1.2 mL of serum were collected either from a peripheral venous or arterial catheter sample and were centrifugated (3,000 rpm at 4°C × 5 min) and the supernatant was stored at −80°C until batch cytokine analysis was carried out. CSF samples were similarly centrifugated and the supernatant stored at −80°C. Frozen serum and CSF samples were thawed at room temperature, then kept on ice until ready to assay (7).

Cytokine Analysis

Interleukin-8 and GM-CSF were determined by immunoassay using commercial kits (Human Ultra-Sensitive IL-8 and Human Ultra-Sensitive GM-CSF®, Meso Scale Diagnostic, MA, USA). All blockers and wash buffers were prepared and validated according to manufacturer's guidelines. The assays employed a sandwich immunoassay format where capture antibodies were coated in a patterned array on the bottom of the wells of

a singleplex plate. The samples were analyzed on these pre-coated plates according to the manufacturer's instructions using a SECTOR® Imager where a voltage applied to the plate electrodes causes the captured labels to emit light and the intensity of emitted light provides a quantitative measure of analytes in the sample. Reproducibility was good with calculated concentration %CV < 5% for standards in the quantitative range of the assays (7).

Statistical Analysis

Statistical analysis was carried out using the PASW statistical package version 18 (www.ibm.com/SPSS_Statistics). Significance was assumed for values of $p < 0.05$. We divided the timing of biomarker sampling into 5 blocks; day 1 (D1), day 2 (D2), day 3 (D3), days 4 and 5 (D4–5) and days 6, 7, and 8 (D6–8). The majority of the serum samples were taken over days 1–3 of life. A score of 3 or 4 for the combined Basal Ganglia/Watershed Barkovich score was coded as severe brain injury. Histogram analysis of the serum and CSF biomarker data revealed a non-normal distribution. Therefore medians (IQRs) were employed to describe the data and non-parametric tests, the Mann-Whitney *U* and Kruskal-Wallis test were used for comparative analysis with outcomes of TH, seizure occurence, grade of NE, MRI brain result, mortality. Bayley-III outcomes at 18–24 months of age were correlated with serum and CSF biomarker concentrations in the first week of life via Spearman correlation. Receiver Operating Characteristic (ROC) curves and cut-off values were calculated for all outcomes.

RESULTS

Clinical Outcomes

The study enrolled a total of 94 term neonates including controls ($n = 12$) and infants exposed to perinatal asphxia with NE 0-III ($n = 82$). There were serum samples from 94 neonates ($n = 247$ total serum samples) and 34 neonates with NE had CSF samples collected during their NICU admission. The neonatal controls had a mean gestational age of 39.4 ± 1.2 weeks and birth weight of 3.5 ± 0.4 kg with 6 males. All were born by spontaneous vaginal delivery with Apgar scores at both 1 and 5 min of 9 ± 1 and had normal neurological examinations. There were no significant differences between controls and NE cases with regard to gestational age, birth weight, gender or outborn status. Infants with NE were significantly more likely to be delivered by lower segment cesarean section or instrumental delivery and had significantly lower Apgar scores at 1 and 5 min compared to controls.

The decision to perform a lumbar puncture was made by the treating neonatologist based on a clinical suspicion of sepsis/meningitis. Thirty-nine infants required TH in accordance with the TOBY (Total Body Hypothermia for Neonatal Encephalopathy) criteria (20) and were treated for 72 h duration and 4 infants died. The grades of encephalopathy according to Sarnat and Sarnat (17) were as follows: Infants exposed to perinatal asphyxia but with no neurological signs (denoted as grade 0, $n = 6$); Mild NE (grade I, $n = 23$); Moderate NE (grade II, $n = 42$); Severe NE (grade III, $n = 11$). The NE group II/III were significantly more likely to be outborn, have lower 1, 5, and 10 min Apgar scores, have clinical seizures, undergo TH, have abnormal MRI brain imaging and had significantly lower admission pH, admission bicarbonate and larger base excess values compared to NE group 0/I. However, there were no significant differences between the NE groups 0/I and II/III with regard to gestational age, birth weight, gender, mode of delivery, multiplicity, mortality, cord pH, cord base excess and cord lactate values, as previously described (7).

Serum Biomarker Data

GM-CSF and IL-8 concentration were measured on serum samples from NE infants and controls. GM-CSF levels were not significantly different in NE patients vs. controls during first week of life. On the contrary, IL-8 was significantly higher on day 1 ($p = 0.0017$), 2 ($p = 0.0048$), and 3 ($p = 0041$) in NE patients compared to controls. IL-8 concentration in NE infants serum was significantly lower on day 7 compared to day 1 ($p = 0.0005$), day 2 ($p = 0.0012$), and day 3 ($p = 0.0017$) of life (**Table 1**).

Infants who underwent TH had significantly elevated IL-8 levels on day 3 ($p = 0.008$) (**Table 2a**). GM-CSF concentration was not altered. Grade II/III NE was significantly associated with elevated serum IL-8 levels on days 2 and 6–8 ($p = 0.02$, cut-off level 34.23 pg/mL) (**Table 2a**). Seizures were not significantly associated with any of the serum or CSF biomarkers investigated, whereas mortality was associated with high concentration of GM-CSF ($p = 0.035$) and IL-8 ($p = 0.01$) on day 1 (**Table 2b**).

Magnetic Resonance Imaging Findings

MRI brain scans were performed on 66 infants (patients with normal MRI $n = 35$). Barkovich scores were available for the MRI brain scans of 64 infants with NE with the following results: Basal Ganglia (BG) score: 1 ($n = 3$);2 ($n = 2$); 3 ($n = 2$); 4 ($n = 6$). Watershed (W) score=1 ($n = 7$);2 ($n = 3$); 4 ($n = 3$); 5 ($n = 3$). Combined Basal Ganglia/Watershed (BG/W) score=1 ($n = 5$); 2 ($n = 10$); 3 ($n = 6$); 4 ($n = 1$). There were significantly higher levels of serum GM-CSF on day 3 in infants with BG/W scores of 3/4 compared to those who scored 1/2 [1 (0.5–2.8) vs. 0.4 (0.2–0.7) pg/mL; $p = 0.03$]. GM-CSF levels increased over time in neonates with normal MRI brain. Abnormal MRI brain imaging was significantly associated with decreased GM-CSF levels on day 2 ($p = 0.001$) and day 3 ($p = 0.01$) compared to normal MRI brain image, whereas IL-8 concentration was not altered (**Table 2b**).

Neurodevelopmantal Followup (Bayley-III)

Neurodevelopmental assessments at 18–24 months of age were performed on 43 infants of the 53 infants with NE II/III originally recruited. Composite cognitive, language and motor Bayley-III scores were calculated and divided into normal (Bayley III>90) and abnormal (Bayley III < 90) categories. 21, 30, and 12% demonstrated cognitive, language and motor delay, respectively. The diagnoses were as follows: 7 (16%) were diagnosed with a disability, including cerebral palsy (CP. $n = 1$) and autism ($n = 2$). Bayley scores < 90 in either cognition, motor, or language were detected in 17 (40%): 14 (32%) language, 7 (16%) cognitive, and 6 (14%) motor domain. Infants with disability had more

TABLE 1 | GM-CSF and IL-8 concentrations in controls and NE infants over the first week of life.

Cytokine	Control	NE D1	NE D2	NE D3	NE D6–8
GM-CSF (pg/mL)	0.56 (0.08)	0.59 (0.05)	0.62 (0.06)	1.06 (0.17)	0.65 (0.09)
IL8 (pg/mL)	35.86 (7.0)	133.81** (23.3)	137.53** (29.2)	149.07** (30.2)	49.86** (10.1)

*Serum concentrations of GM-CSF and IL-8 in NE patients (n = 82) expressed as pg/mL (day 1–7) vs. controls (n = 12) were measured by duplex cytokine analysis in the first week of life. (**p < 0.01 using the Mann–Whitney test).*

TABLE 2 | Associations between serum biomarker values of cases infants and outcome measures of (a) TH and NE grade and (b) MRI brain and mortality.

Biomarker	Day of life	TH			NE Grade		
		Yes	No	*p*	0/I	II/III	*p*
(a)							
IL-8	**2**	65.7 (47.3–142.2)	37.7 (21.8–267.5)	0.12	33.5 (21.8–59.6)	75.3 (44.4–232.6)	0.02
	3	68.4 (46.5–153.2)	32.5 (17.7–85.9)	0.008	32.5 (18.3–59.1)	66 (36.7–145)	0.07
	6–8	30.5 (21.8–45.9)	44.9 (28.3–124.4)	0.26	9.1 [x]	35.7 (25.2–49.3)	0.01
(b)							
Biomarker	**Day of life**	**MRI**			**Survival**		
		Abnormal	**Normal**	***p***	**No**	**Yes**	***p***
GM-CSF	**1**	0.48 (0.29–0.67)	0.36 (0.26–0.73)	0.63	1.21 (0.54–1.56)	0.41 (0.29–0.74)	0.035
	2	0.39 (0.2–0.63)	0.7 (0.41–1.19)	0.001	0.31 (0.19–0.48)	0.54 (0.35–0.81)	0.13
	3	0.56 (0.36–0.97)	1.21 (0.64–1.47)	0.01	0.54[x]	0.69 (0.45–1.23)	0.33
IL−8	**1**	74.8 (27–444.5)	86 (40.6–154.2)	0.91	1834.2 (283.2–4932.3)	72.3 (35.6–181.7)	0.01
	3	81.6 (23.7–253.3)	56.1 (38.9–94.6)	0.69	300 [x]	55.6 (32.7–112.8)	0.05

Medians and IQRs of (a) TH vs. no TH and grade of NE and (b) normal vs. abnormal MRI and survival in NE are listed in each column, followed by a p-value for each comparison; Days without significant results excluded; x = no interquartile range available due to small sample numbers. All analysis used the Mann-Whitney U-test for comparisons of non-parametric data.

abnormalities on discharge examination and brain MRI, with longer hospital stay ($p < 0.001$).

GM-CSF and IL-8 concentration did not correlate with cognitive and motor Bayley III scores. Elevated GM-CSF, but not IL8 concentration on days 4–5 of life correlated negatively with composite language ($p = 0.0242$) Bayley III scores at 2 years (**Figure 1**).

Cerebrospinal Fluid Biomarker Data

Thirty-four infants had CSF samples collected with the following grades of encephalopathy: NE 0/I ($n = 5$); NE II/III ($n = 29$). CSF samples were taken on median (IQR) day 4 (1.8–5.0). Seventeen infants in this group required TH, 22 infants developed clinical seizures and 1 infant died. The median (IQR) for GM-CSF was 0.096 (0.06–0.28) pg/mL and for IL-8 was 236.02 (58.94–545.56) pg/mL. There were no significant associations found between either of the CSF biomarkers and TH, seizure occurence, NE grade, MRI result, Bayley-III score or mortality. There was no significant association between CSF biomarkers and the presence of severe brain injury on MRI imaging (grade 3 or 4 BG/W Barkovich Score).

DISCUSSION

In this study we found a significant association between decreased levels of GM-CSF on days 2 and 3 and abnormal MRI brain imaging. GM-CSF regulates cell growth and promotes proliferation of granulocytes and monocytes/macrophages (21). It has been previously reported that preterm infants who later develop CP have significantly lower levels of GM-CSF compared to controls (22) while term infants who are later diagnosed with CP have significantly higher levels of GM-CSF in their newborn heelprick samples compared to matched controls (23).

Marlow et al. (24) found that there was no detrimental effect of GM-CSF treatment on 2-year neurodevelopmental outcomes in a randomized control trial of preterm infants in which prophylactic GM-CSF was used to prevent sepsis. Similar to our cohort, Okazaki et al. (25) found no difference between levels of serum GM-CSF in severe NE infants who had TH ($n = 5$) compared to mild NE infants, who did not have TH ($n = 5$) and to controls ($n = 4$). In a previous cohort of infants with NE from our group we found increased GM-CSF on day 1 was associated with adverse outcomes (5). Despite the small numbers of infants who died in our current cohort, we found a significant association between elevated GM-CSF and IL-8 on day 1 of life with mortality. Spath et al. (14) have recently demonstrated that excess production of GM-CSF induced spontaneous brain inflammation and neurological dysfunction in an animal model by the production of ROS. We have previously found that neonatal neutrophils derived from umbilical cord blood had increased ROS and activation following GM-CSF treatment *in vitro* compared

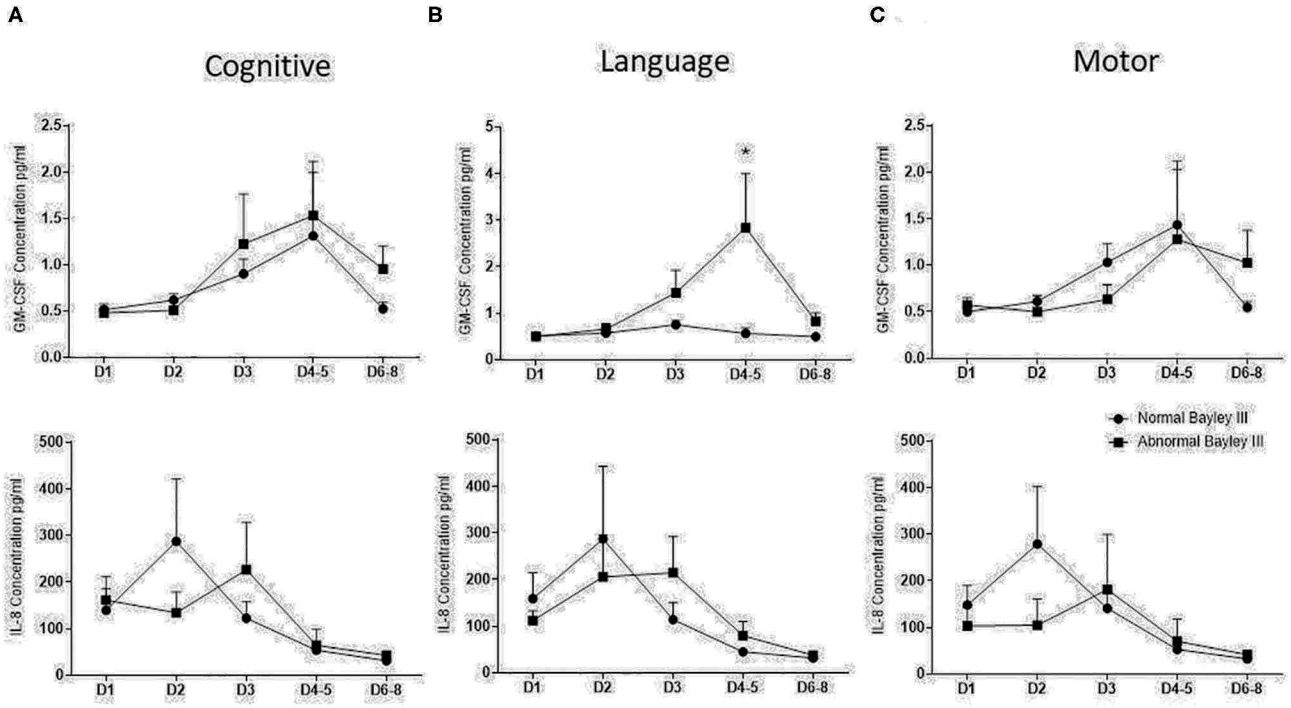

FIGURE 1 | Correlation between GM-CSF and IL8 and neurodevelopmental outcome. Bayley developmental score was performed on NE infants at 2 years of age and correlated with GM-CSF and IL-8 concentrations obtained by duplex cytokine analysis. Graphs showing mean (± SEM) GM-CSF, at the top, and IL-8, at the bottom, concentration values between normal (circles) and abnormal (squares) Bayley score from NE neonates divided by cognitive **(A)**, language **(B)**, and motor **(C)** (*$p < 0.05$ using the Mann-Whitney test).

with either granulocyte colony-stimulating factor (G-CSF) or lipolysaccharide (8).

We found significant association between elevated day 2 IL-8 levels and grade II/III NE. This is in keeping with previous research showing elevation of IL-8 levels in asphyxiated term infants compared to healthy control infants on day 1 with levels equilibrating by day 4 of life (10, 11). In the first days of life in healthy newborns cytokines are stable and not significantly altered (26). Opposite to Bartha et al. (27) findings where IL-8 production in the brain was associated with abnormal neurodevelopmental outcomes in NE, we found that levels of IL-8 are not associated with abnormal neurodevelopmental outcomes, this discrepancy can be explained because in the Bartha study neurodevelopmental outcome was considered abnormal if the infant died, whereas in the present study these patients were excluded. High concentration of IL-8 in the CSF of term infants have been correlated with severe encephalopathy (27, 28). Term infants with abnormal outcomes in the short (11) and long-term using MRI-defined neuroabnormalities and adverse neurological outcome (27) have been reported to have significantly higher postnatal serum and newborn heelprick IL-8 levels compared to infants with normal outcomes. Nelson et al. (23) found significantly higher levels of IL-8 in the newborn heelprick samples of 31 infants who subsequently developed spastic CP compared to 65 term controls. IL-8 also appeared to correlate significantly with NE-induced seizures and may serve as a biomarker for earlier detection of brain damage in neonatal seizures (29). However, these studies were all done in the pre-TH era.

In this study, infants who underwent TH had significantly elevated serum and IL-8 levels on day 3 compared to those who did not receive TH. Our findings are supported by previous work by Jenkins et al. who found significantly higher levels of IL-8 in TH compared to normothermic infants with NE at most time points over the first 80 h of life. Infants following TH with better outcomes at 12 months showed uniform down regulation of IL-8 from their peak levels observed at 24 h to their nadir at 36 h (30).

GM-CSF and IL-8 are markers of brain injury in situations like stroke and neurodegenerative disorder. In this study we showed the association of serum GM-CSF and IL-8 levels with survival and brain damage, and the importance of the follow up of these cytokines in the first days of life in neonatal encephalopathy.

DATA AVAILABILITY STATEMENT

The raw data supporting the conclusions of this article will be made available by the authors, without undue reservation.

ETHICS STATEMENT

The studies involving human participants were reviewed and approved by The Research Ethics Committee (REC) of The National Maternity Hospital. Written informed consent to

participate in this study was provided by the participants' legal guardian/next of kin.

AUTHOR CONTRIBUTIONS

DS, AM, LK, and TS conceived the study and prepared the manuscript. DS and TS performed the laboratory experiments and analyzed the data. CO, WW, JM, and AO'N reviewed the final data analyses and contributed to the writing of the manuscript. MS performed the Bayley's assessments. VD is the radiologist who reported all cranial ultrasound and MRIs. EM supervised the design and execution of the study, performed the final data analyses, and contributed to the writing of the manuscript.

FUNDING

This work was supported by the National Children's Research Centre, Crumlin, Dublin, Ireland 2009 (EM); Children's University Hospital, Temple Street, Dublin, Ireland 2011 (EM).

ACKNOWLEDGMENTS

We wish to thank all of the parents, babies, laboratory, and hospital staff who generously participated in this project. In addition, we wish to thank Dr. Ricardo Segurado for all the support and assistance with statistical analysis and Prof. Geraldine Boylan for her help with the EGGs.

REFERENCES

1. Ferriero DM. Neonatal brain injury. *New Engl J Med.* (2004) 351:1985–95. doi: 10.1056/NEJMra041996
2. Edwards AD, Brocklehurst P, Gunn AJ, Halliday H, Juszczak E, Levene M, et al. Neurological outcomes at 18 months of age after moderate hypothermia for perinatal hypoxic ischaemic encephalopathy: synthesis and meta-analysis of trial data. *BMJ.* (2010) 340:c363. doi: 10.1136/bmj.c363
3. Aslam S, Strickland T, Molloy EJ. Neonatal encephalopathy: need for recognition of multiple etiologies for optimal management. *Front Pediatr.* (2019) 7:142. doi: 10.3389/fped.2019.00142
4. O'Hare FM, Watson RW, O'Neill A, Blanco A, Donoghue V, Molloy EJ. Persistent systemic monocyte and neutrophil activation in neonatal encephalopathy. *J Matern Fetal Neonatal Med.* (2016) 29:309–16. doi: 10.3109/14767058.2014.1000294
5. O'Hare FM, Watson RW, O'Neill A, Segurado R, Sweetman D, Downey P, et al. Serial cytokine alterations and abnormal neuroimaging in newborn infants with encephalopathy. *Acta Paediatr.* (2017) 106:561–7. doi: 10.1111/apa.13745
6. Morkos AA, Hopper AO, Deming DD, Yellon SM, Wycliffe N, Ashwal S, et al. Elevated total peripheral leukocyte count may identify risk for neurological disability in asphyxiated term neonates. *J Perinatol.* (2007) 27:365–70. doi: 10.1038/sj.jp.7211750
7. Sweetman DU, Onwuneme C, Watson WR, Murphy JF, Molloy EJ. Perinatal asphyxia and erythropoietin and VEGF: serial serum and cerebrospinal fluid responses. *Neonatology.* (2017) 111:253–9. doi: 10.1159/000448702
8. Molloy EJ, O'Neill AJ, Grantham JJ, Sheridan-Pereira M, Fitzpatrick JM, Webb DW, et al. Granulocyte colony-stimulating factor and granulocyte-macrophage colony-stimulating factor have differential effects on neonatal and adult neutrophil survival and function. *Pediatr Res.* (2005) 57:806–12. doi: 10.1203/01.PDR.0000156500.13600.B5
9. Mackay CR. Chemokines: immunology's high impact factors. *Nat Immunol.* (2001) 2:95–101. doi: 10.1038/84298
10. Fotopoulos S, Mouchtouri A, Xanthou G, Lipsou N, Petrakou E, Xanthou M. Inflammatory chemokine expression in the peripheral blood of neonates with perinatal asphyxia and perinatal or nosocomial infections. *Acta Paediatr.* (2005) 94:800–6. doi: 10.1080/08035250510026526
11. Okazaki K, Nishida A, Kato M, Kozawa K, Uga N, Kimura H. Elevation of cytokine concentrations in asphyxiated neonates. *Biol Neonate.* (2006) 89:183–9. doi: 10.1159/000089180
12. Ramaswamy V, Horton J, Vandermeer B, Buscemi N, Miller S, Yager J. Systematic review of biomarkers of brain injury in term neonatal encephalopathy. *Pediatr Neurol.* (2009) 40:215–26. doi: 10.1016/j.pediatrneurol.2008.09.026
13. Baldwin GC. The biology of granulocyte-macrophage colony-stimulating factor: effects on hematopoietic and nonhematopoietic cells. *Dev Biol.* (1992) 151:352–67. doi: 10.1016/0012-1606(92)90175-G
14. Spath S, Komuczki J, Hermann M, Pelczar P, Mair F, Schreiner B, et al. Dysregulation of the cytokine GM-CSF induces spontaneous phagocyte invasion and immunopathology in the central nervous system. *Immunity.* (2017) 46:245–60. doi: 10.1016/j.immuni.2017.01.007
15. Lotfi N, Thome R, Rezaei N, Zhang GX, Rezaei A, Rostami A, et al. Roles of GM-CSF in the pathogenesis of autoimmune diseases: an update. *Front Immunol.* (2019) 10:1265. doi: 10.3389/fimmu.2019.01265
16. Sweetman D, Kelly LA, Zareen Z, Nolan B, Murphy J, Boylan G, et al. Coagulation profiles are associated with early clinical outcomes in neonatal encephalopathy. *Front Pediatr.* (2019) 7:399. doi: 10.3389/fped.2019.00399
17. Sarnat HB, Sarnat MS. Neonatal encephalopathy following fetal distress. A clinical and electroencephalographic study. *Arch Neurol.* (1976) 33:696–705. doi: 10.1001/archneur.1976.00500100030012
18. Barkovich AJ, Hajnal BL, Vigneron D, Sola A, Partridge JC, Allen F, et al. Prediction of neuromotor outcome in perinatal asphyxia: evaluation of MR scoring systems. *AJNR Am J Neuroradiol.* (1998) 19:143–9.
19. Murray DM, Boylan GB, Ryan CA, Connolly S. Early EEG findings in hypoxic-ischemic encephalopathy predict outcomes at 2 years. *Pediatrics.* (2009) 124:e459–67. doi: 10.1542/peds.2008-2190
20. Azzopardi DV, Strohm B, Edwards AD, Dyet L, Halliday HL, Juszczak E, et al. Moderate hypothermia to treat perinatal asphyxial encephalopathy. *New Engl J Med.* (2009) 361:1349–58. doi: 10.1056/NEJMoa0900854
21. Sun L, Rautela J, Delconte RB, Souza-Fonseca-Guimaraes F, Carrington EM, Schenk RL, et al. GM-CSF quantity has a selective effect on granulocytic vs. monocytic myeloid development and function. *Front Immunol.* (2018) 9:1922. doi: 10.3389/fimmu.2018.01922
22. Kaukola T, Satyaraj E, Patel DD, Tchernev VT, Grimwade BG, Kingsmore SF, et al. Cerebral palsy is characterized by protein mediators in cord serum. *Ann Neurol.* (2004) 55:186–94. doi: 10.1002/ana.10809
23. Nelson KB, Dambrosia JM, Grether JK, Phillips TM. Neonatal cytokines and coagulation factors in children with cerebral palsy. *Ann Neurol.* (1998) 44:665–75. doi: 10.1002/ana.410440413
24. Marlow N, Morris T, Brocklehurst P, Carr R, Cowan F, Patel N, et al. A randomised trial of granulocyte-macrophage colony-stimulating factor for neonatal sepsis: childhood outcomes at 5 years. *Arch Dis Child Fetal Neonatal Ed.* (2015) 100:F320-6. doi: 10.1136/archdischild-2014-307410
25. Okazaki K, Kusaka T, Kondo M, Kozawa K, Yoshizumi M, Kimura H. Temporal alteration of serum G-CSF and VEGF levels in perinatal asphyxia treated with head cooling. *Cytokine.* (2012) 60:812–4. doi: 10.1016/j.cyto.2012.08.001
26. Lusyati S, Hulzebos CV, Zandvoort J, Sauer PJ. Levels of 25 cytokines in the first seven days of life in newborn infants. *BMC Res Notes.* (2013) 6:547. doi: 10.1186/1756-0500-6-547
27. Bartha AI, Foster-Barber A, Miller SP, Vigneron DB, Glidden DV, Barkovich AJ, et al. Neonatal encephalopathy: association of cytokines with MR spectroscopy and outcome. *Pediatr. Res.* (2004) 56:960–6. doi: 10.1203/01.PDR.0000144819.45689.BB

28. Savman K, Blennow M, Gustafson K, Tarkowski E, Hagberg H. Cytokine response in cerebrospinal fluid after birth asphyxia. *Pediatr Res.* (1998) 43:746–51. doi: 10.1203/00006450-199806000-00006
29. Ellison VJ, Mocatta TJ, Winterbourn CC, Darlow BA, Volpe JJ, Inder TE. The relationship of CSF and plasma cytokine levels to cerebral white matter injury in the premature newborn. *Pediatr Res.* (2005) 57:282–6. doi: 10.1203/01.PDR.0000148286.53572.95
30. Jenkins DD, Rollins LG, Perkel JK, Wagner CL, Katikaneni LP, Bass WT, et al. Serum cytokines in a clinical trial of hypothermia for neonatal hypoxic-ischemic encephalopathy. *J Cereb Blood Flow Metabolism.* (2012) 10:1888–96. doi: 10.1038/jcbfm.2012.83

Conflict of Interest: The authors declare that the research was conducted in the absence of any commercial or financial relationships that could be construed as a potential conflict of interest.

frontiers in Cellular Neuroscience

ORIGINAL RESEARCH
published: 09 April 2021
doi: 10.3389/fncel.2021.633185

Human Cord Blood Derived Unrestricted Somatic Stem Cells Restore Aquaporin Channel Expression, Reduce Inflammation and Inhibit the Development of Hydrocephalus After Experimentally Induced Perinatal Intraventricular Hemorrhage

Deepti Purohit[1], Dina A. Finkel[1], Ana Malfa[1], Yanling Liao[2], Larisa Ivanova[2], George M. Kleinman[3], Furong Hu[2], Shetal Shah[1], Carl Thompson[4], Etlinger Joseph[5], Michael S. Wolin[4], Mitchell S. Cairo[2,6†], Edmund F. La Gamma[1,2,7†] and Govindaiah Vinukonda[2,5†]*

[1]The Regional Neonatal Center, Maria Fareri Children's Hospital at Westchester Medical Center, New York Medical College, Valhalla, NY, United States, [2]Department of Pediatrics, New York Medical College, Valhalla, NY, United States, [3]Department of Pathology, Westchester Medical Center, New York Medical College, Valhalla, NY, United States, [4]Department of Physiology, New York Medical College, Valhalla, NY, United States, [5]Department of Cell Biology and Anatomy, New York Medical College, Valhalla, NY, United States, [6]Departments of Medicine, Pathology, Microbiology and Immunology, New York Medical College, Valhalla, NY, United States, [7]Department of Biochemistry and Molecular Biology, New York Medical College, Valhalla, NY, United States

Intraventricular hemorrhage (IVH) is a severe complication of preterm birth associated with cerebral palsy, intellectual disability, and commonly, accumulation of cerebrospinal fluid (CSF). Histologically, IVH leads to subependymal gliosis, fibrosis, and disruption of the ependymal wall. Importantly, expression of aquaporin channels 1 and 4 (AQP1 and AQP4) regulating respectively, secretion and absorption of cerebrospinal fluids is altered with IVH and are associated with development of post hemorrhagic hydrocephalus. Human cord blood derived unrestricted somatic stem cells (USSCs), which we previously demonstrated to reduce the magnitude of hydrocephalus, as having anti-inflammatory, and beneficial behavioral effects, were injected into the cerebral ventricles of rabbit pups 18 h after glycerol-induced IVH. USSC treated IVH pups showed a reduction in ventricular size when compared to control pups at 7 and 14 days (both, $P < 0.05$). Histologically, USSC treatment reduced cellular infiltration and ependymal wall disruption. In the region of the choroid plexus, immuno-reactivity for AQP1 and ependymal wall AQP4 expression were suppressed after IVH but were restored following USSC

Abbreviations: IVH, Intraventricular hemorrhage; PHH, Post-hemorrhagic hydrocephalus; USSC, Unrestricted somatic stem cells; SVZ, Sub-ventricular zone; AQP1, Aquaporin 1; AQP4, Aquaporin 4; TGF-β, Transforming growth factor beta; IL-10, Interleukin-10; MMP-9, Matrix-metalloproteinase-9.

OPEN ACCESS

Edited by:
Daniel Alonso-Alconada, University of the Basque Country, Spain

Reviewed by:
Qianwei Chen, Army Medical University, China
Magnus Gram, Lund University, Sweden

***Correspondence:**
Edmund F. La Gamma
edmund_lagamma@nymc.edu

[†]These authors share senior authorship

Specialty section:
This article was submitted to Cellular Neuropathology, a section of the journal Frontiers in Cellular Neuroscience

Received: *24 November 2020*
Accepted: *22 March 2021*
Published: *09 April 2021*

Citation:
Purohit D, Finkel DA, Malfa A, Liao Y, Ivanova L, Kleinman GM, Hu F, Shah S, Thompson C, Joseph E, Wolin MS, Cairo MS, La Gamma EF and Vinukonda G (2021) Human Cord Blood Derived Unrestricted Somatic Stem Cells Restore Aquaporin Channel Expression, Reduce Inflammation and Inhibit the Development of Hydrocephalus After Experimentally Induced Perinatal Intraventricular Hemorrhage. Front. Cell. Neurosci. 15:633185. doi: 10.3389/fncel.2021.633185

administration. Effects were confirmed by analysis of mRNA from dissected choroid plexus and ependymal tissue. Transforming growth factor beta (TGF-β) isoforms, connective tissue growth factor (CTGF) and matrix metalloprotease-9 (MMP-9) mRNA, as well as protein levels, were significantly increased following IVH and restored towards normal with USSC treatment ($P < 0.05$). The anti-inflammatory cytokine Interleukin-10 (IL-10) mRNA was reduced in IVH, but significantly recovered after USSC injection ($P < 0.05$). In conclusion, USSCs exerted anti-inflammatory effects by suppressing both TGF-β specific isoforms, CTGF and MMP-9, recovered IL-10, restored aquaporins expression towards baseline, and reduced hydrocephalus. These results support the possibility of the use of USSCs to reduce IVH consequences in prematurity.

Keywords: unrestricted somatic stem cells, intraventricular hemorrhage, hydrocephalus, aquaporin (AQP), choroid plexus, ependymal wall, cerebral palsy, white matter injury

INTRODUCTION

Intraventricular hemorrhage (IVH) arises from rupture of immature and developing blood vessels in the germinal matrix of premature infants. IVH occurs in up to 25% of preterm neonates where 10% of events are further complicated by hydrocephalus (Campos-Ordonez et al., 2014; Koschnitzky et al., 2018). A recent NIH workshop on post-hemorrhagic hydrocephalus (PHH) reported that IVH affected neonates develop somatic growth impairment, white matter damage, motor dysfunction and neurocognitive deficiency (Koschnitzky et al., 2018). Moreover, IVH is associated with prolonged neonatal hospitalization and increased lifelong medical care costs (Christian et al., 2016). Presently, since only palliative therapies exist, mitigation of IVH related co-morbidities would reduce patient mortality and significantly reduce health care costs due to late effects of IVH on preterm newborns.

The magnitude of ventricular dilation correlates with morphological and functional damage proportional to the degree of subependymal gliosis, fibrosis and disruption of the ependymal lining (Karimy et al., 2017). Mechanistically, post hemorrhagic hydrocephalus (PHH) arises from either over secretion or impaired absorption of cerebrospinal fluid (CSF). The latter is due in part to blood obstructing arachnoid villi associated with fibro-proliferative responses, inflammation and sub-ependymal gliosis. Subtypes of ungated aquaporin water channels represent another important pathway governing CSF homeostasis, as does the glymphatic drainage system (Gunnarson et al., 2004; Zelenina, 2010; Verkman et al., 2017). AQP1 and AQP4 are associated with CSF hypersecretion and reduced absorption respectively (Verkman et al., 2017). AQP1 is expressed primarily along the choroid plexus epithelial lining and, in knockout studies using mice, the loss of AQP1 function reduced CSF production and intraventricular pressure (Oshio et al., 2005; Trillo-Contreras et al., 2019).

AQP4 channels are predominantly expressed on the surface of ependymal cells lining the lateral and third ventricles and along astrocyte foot processes surrounding capillaries (glia limitans). AQP4 channels function primarily to absorb CSF and interstitial fluid (ISF) of the brain parenchyma (Amiry-Moghaddam and Ottersen, 2003; Lehmann et al., 2004; Papadopoulos and Verkman, 2013). AQP4 knockout mice develop ventricular enlargement and increased intracranial pressure (ICP) suggesting a protective role of AQP4 in maintaining normal ventricular volume (Bloch et al., 2005; Filippidis et al., 2012). In a recent study on double-knockout mice for both AQP1 and AQP4, the preponderance of CSF accumulation was attributed to failure of AQP4 mediated CSF resorption rather than excessive AQP1 mediated CSF production (Igarashi et al., 2014; Trillo-Contreras et al., 2019). Taken together, these observations underscore the importance of aquaporin channels in CSF homeostasis.

In PHH, free hemoglobin and iron contribute to inflammation and result in increased toll-like receptor (TLR) expression which correlates with hypersecretion of CSF (Gao et al., 2014; Gram et al., 2014; Karimy et al., 2017). Further, studies with CSF show up-regulation of TGFβ isoforms (Cherian et al., 2004a) which in turn stimulate production of extracellular matrix (Whitelaw et al., 2002). However, few studies have examined the changes in TGF-β isoforms relative to the progression of subependymal gliosis and fibrosis (Kitazawa and Tada, 1994; Douglas et al., 2009; Kaestner and Dimitriou, 2013). Therefore, experiments correlating changes in TGF-β isoforms and CNS scarring after PHH would be informative.

Currently, there are no effective clinical treatments for PHH except removal of CSF by surgical diversion. Nonsurgical cell based therapies represent an emerging opportunity to prevent acute and long-term morbidity associated with PHH in the preterm neonate. Preclinical investigations of PHH created by injection of exogenous blood into the ventricles, evaluated the effects of mesenchymal stem cells (MSCs). These reports showed improved myelination, neuroprotection and less apoptosis (Liu et al., 2010; Ahn et al., 2014; Mukai et al., 2017). To expand upon these observations, our group investigated unrestricted somatic stem cells (USSCs) from human cord blood that were engineered to express the luciferase reporter gene, confirmed a stable non-teratogenic phenotype and successfully tracked USSC *in vivo* migration in a rabbit model of intraventricular hemorrhage IVH (Vinukonda et al., 2019). We selected USSCs because they release growth

factors and cytokines with known neuroprotective and axonal growth promoting functions at higher levels than MSCs and for their anti-inflammatory and immunomodulatory properties. Released peptides include leukemia inhibitory factor (LIF), vascular endothelial growth factor (VEGF; Jin et al., 2000; Sun et al., 2003) and stromal cell-derived factor-1, which induces homing of neural stem cells to ischemic brain regions (Imitola et al., 2004; Kogler et al., 2005) and stimulates axonal sprouting after spinal cord injury (Opatz et al., 2009).

On the basis of USSC functions and our prior report (Vinukonda et al., 2019), we hypothesized that USSC administration would stabilizes the aquaporin water channels in the choroid plexus and ependymal wall resulting in reduced hydrocephalus after IVH. Further, we hypothesized that USSC administration would also suppress inflammation in the choroid plexus (TLR2, TLR4 and NF-kB) as well as ventricular wall matrix reorganization (TGF-β isoforms, matrix metalloproteinase-9, MMP-9), and promote anti-inflammatory cytokine (Interleukin-10; IL-10) expression which collectively would contribute to the attenuation of PhH after IVH.

MATERIALS AND METHODS

Human Cord Blood Derived Unrestricted Somatic Stem Cell Isolation

USSCs were isolated from human umbilical cord blood mononuclear cells according to the methods of Kogler and colleagues as we have previously described (Kogler et al., 2004; Liao et al., 2014; Vinukonda et al., 2019). USSCs were transduced with a lentivirus carrying GFP-luciferase gene prepared using the lenti-viral construct, pSico PolII-eGFP-Luc2 (generously provided by Dr. Glenn Merlino at the National Cancer Institute) to enable *in vivo* identification while enabling the cells to retain their functionality (Liao et al., 2014). To ensure the rigor, reproducibility, and authentication of this biological reagent, we created multiple vials of frozen USSC stock from one batch of this isolated reagent and characterized the cells for cell-specific expression markers using microarray gene expression analysis to reconfirm fidelity with the parent USSC phenotype (Liao et al., 2014).

Glycerol-Induced Interventricular Hemorrhage Followed by the Development of Post Hemorrhagic Hydrocephalus in Premature Rabbit Kits

Timed pregnant New Zealand white rabbits (Oryctolagus cuniculus) were purchased from Charles River Laboratories Incorporation (Wilmington, MA, USA) and premature rabbit pups were delivered by cesarean-section at E29 gestational age (term *gestation* = 32 days). Newborn pups were maintained and fed according to our previously published methods (Georgiadis et al., 2008; Chua et al., 2009). At 3–4 h of postnatal age, newborn pups were treated with 50% intraperitoneal glycerol: water (6.5 g/kg) which induced IVH in approximately 70% of all treated pups (Georgiadis et al., 2008; Chua et al., 2009; Vinukonda et al., 2019). Head ultrasound was performed at the 24 h postnatal age to determine the presence and severity of IVH [Acuson Sequoia C256, ultra-sonographic Imaging System (Siemens Corp., Washington, DC, USA)]. The grades of IVH were defined based on the ventricular volume (length, breadth and depth in coronal and sagittal views) and pups were classified as: (i) no gross IVH; (ii) moderate, gross IVH (70–150 mm^3); or (iii) severe IVH (151–250 mm^3) filling both ventricles completely. In our model the severe grade of IVH pups are at high risk for the development of hydrocephalus. Therefore, we included only moderate and severe IVH pups in the USSC treatment group and IVH saline group (Chua et al., 2009; Dohare et al., 2019). Hydrocephalus was defined as a ventricle area that measures more than three standard deviations (SD) above the mean for age in pups without IVH. The New York Medical College Institutional Animal Care and Use Committee (IACUC) approved all interventions.

Anatomical Localization of Intracerebral Ventricular (ICV) Administered USSCs

USSCs were administered into the cerebral ventricle using the following coordinates from the Bregma: 1 mm posterior, 4 mm lateral and 3 mm deep (1×10^6 cells in 10 μl normal saline to each ventricle) as we previously published (Vinukonda et al., 2019). We confirmed the presence and anatomical location of migrated USSCs in rabbit tissues at different postnatal ages using methods published previously (Vinukonda et al., 2019). Representative live animal bioluminescence imaging (BLI), coronal slice BLI and USSC specific immunostaining images are shown in **Supplementary Figures 3G–L**. Briefly, the sections were stained to identify the USSCs using anti-human nuclei (hNuc) antibody (Cat #MAB 1218, EMD Millipore, USA) and counter stained with diamidino-phenylindole (DAPI). We confirmed USSC survival and migration as previously described in our recent publication (Vinukonda et al., 2019). To determine whether USSCs could migrate from the point of administration, we tested for the presence or absence of USSCs in other organs: liver, spleen, heart and lung using USSC bioluminescence as well as specific immunostaining on representative sections made from each organ. The data confirmed no immune reactivity indicating no sustained trapping of exogenously administered USSCs in other organs (Vinukonda et al., 2019).

Assignment of Rabbit Pups to Experimental Groups, Initial Tissue Collection and Processing for Endpoint Studies

At 24 h after birth, pups with moderate or severe IVH littermates were alternately assigned to either IVH-saline or IVH-USSC administration in birth order from each litter; the cycle was repeated until all affected pups were accounted for. Similarly, the no IVH control pups were assigned as unaffected control pups. Replicate animal experiments were conducted until the sample size for each treatment category was achieved for all assays performed. Each intervention group was targeted to receive five to six pups for analysis except for animals sacrificed solely for

laser dissection of the lining of the choroid plexus. In laser dissected tissue, we used four pups per group for mRNA analysis (sp. aquaporins, TLR4, TLR2 and NF-kB) to avoid excessive wastage of animals using this technique.

We collected rabbit forebrain tissue samples from the three experimental groups of rabbit pups at postnatal days 3, 7 and 14 (Georgiadis et al., 2008; Vinukonda et al., 2010, 2019). Soon, after rabbit pups were put to death, their brains were quickly removed and cut into a single 3 mm coronal slice at the mid-septal nucleus (using a brain matrix slicer, Cat #BSRAS001-1, Zivic Instruments, Pittsburg, PA, USA) starting from the cranial end of the frontal lobe. The sub-ventricular zone (SVZ) was manually dissected under a microscope (described below) or the entire 3 mm coronal slice was directly snap-frozen on dry ice and stored in −80°C until tissues were used for RNA isolation or lysates for Western blot or ELISA analyses. The remaining part of the forebrain was directly processed, fixed and mounted as a coronal block for immunohistochemistry (IHC), cresyl violet or H&E staining described below. **Supplementary Figure 1** illustrates the protocol timeline and the process of tissue harvesting.

Hematoxylin-Eosin (H&E) Staining and Ventricle Cross Sectional Area

To measure the ventricular cross sectional area, coronal brain sections were stained by either Hematoxylin-Eosin (H&E) or cresyl violet methods as previously described (Chua et al., 2009; Gram et al., 2014; Ley et al., 2016; Vinukonda et al., 2019). After staining the images were created using an EOVS microscope with a measuring graticule using a digital scanning camera attached to the microscope (Life-Technology-Thermo Fisher Scientific, Waltham, MA, USA). To measure the cross-sectional area of the ventricles, and whole forebrain parenchyma in the three experimental groups, we used Image-J software following our previously published methods (Chua et al., 2009; Vinukonda et al., 2019). As shown in **Supplementary Figure 1C**, we first measured total brain area and then measured each ventricle area. To calculate brain parenchymal area, we subtracted the mean ventricular area of both ventricles from the total region. The final data are presented as mean ± SEM.

Immunohistochemistry (IHC) and Image Analysis for AQP1 Expression

Immunohistochemical staining was performed as we previously described (Braun et al., 2007; Vinukonda et al., 2010). Briefly, the tissue was fixed in 4% paraformaldehyde in phosphate buffered saline (0.1 M PBS; pH: 7.4) for 18 h followed by cryoprotection by immersing slices in 15% sucrose in 0.1 M PBS for 24 h and then another 24 h in 30% sucrose. Finally, the cryoprotected tissues were frozen into optimum cutting temperature compound (Sakura, Japan; Cat #23-730-571, Thermo Fisher Scientific) for 20 μm sectioning and staining. The fixed sections were hydrated in 0.01 M phosphate buffered saline (PBS) and incubated with the primary antibodies overnight at 4°C followed by a secondary antibody for 1 h at room temperature. After washing, the sections were mounted with mounting media—slow fade Light Anti-fade reagent (Molecular probes, Invitrogen, CA, USA) and then visualized microscopically. AQP1 staining was performed using mouse monoclonal antibody (Cat #NB600-749, Novus Biologicals, Littleton, CO, USA) and AQP4 immunostaining was done using mouse monoclonal antibodies (Cat #ab9512, Abcam, Cambridge, UK[1]). The sections were counter stained with diamidino-phenylindole (DAPI) to identify nuclei density to facilitate structural boundaries of the brain. The fluorescence signals for immunoreactivity were imaged at 4×, 10× and 20× objectives, using a Nikon Eclipse 90i microscope a Nikon DS-Qi1Mc camera, and NISE elements AR 4.20 software (Nikon Instruments, Japan).

Multiple images of the entire choroid plexus were obtained in the lateral ventricle for AQP1 expression in all experimental groups. Each image was analyzed for AQP1 pixel intensity using Image-J software (Rasband WS, USA; NIH, Bethesda, MD, USA[2], 1997–2016). To quantify pixel fluorescence intensity of AQP1, the image was opened in the Image-J window and a region of interest was drawn around the choroid epithelium using the software tool (**Supplementary Figure 1E**). The integrated pixel density was normalized to the area measured and compared across experimental groups. To calculate the mean AQP1 intensity, we averaged two to three serial sections from each rabbit pup (six pups per group). This data are presented as mean ± SEM. The investigator was blinded to the group until the analysis was completed.

Enzyme-Linked Immunosorbent Assay for MMP-9 Expression in the Dissected Tissue Lysate

Using the coronal brain slices at the level of the mid-septal nucleus (Vinukonda et al., 2010, 2019), approximately 200 mg of frozen tissue was homogenized in 500 μl of 1× lysis buffer from 2× stock buffer provided by manufacturer (CODE #EL-lysis, Ray Biotech). The tissue homogenates were made using Minilys homogenizer (Bertin Technologies, MD, USA) and Precellys lysing kit for soft tissue homogenizing ceramic beads (1.4 mm, part #91-PCS-CK14; Bertin Technologies, MD, USA). The lysed samples were incubated for 30 min by shaking at 4°C, following spin down in a microfuge at 10,000 rpm speed for 5 min at (4°C) and the clear supernatant was transferred into a clean tube. The total protein concentration was determined using the BCA protein assay kit (Cat #23227, Pierce, Thermo Fisher Scientific, Waltham, MA, USA). Each sample was diluted into a final concentration of 250 ng/μl. Finally, 100 μl aliquots were created and stored at −80°C to avoid repeated freeze-thaw cycles until performing antibody array/ELISA testing. The assay was performed using 100 μl aliquots according to the manufacturer's protocol for the three experimental groups at postnatal day 14. Matrix-metalloproteinase-9 (MMP-9) quantification was assessed using the manufactures protocol (Cat #QAL-CYT-1, Ray Biotech, Norcross, GA, USA); quantification was determined using the software program provided in the kit protocol. Data were presented as mean ± SD after being normalized to protein concentration.

[1]www.abcam.com
[2]http://imagej.nih.gov/ij/

Quantification of Normal and Reactive Astrocyte Cell Density

To investigate the effect of USSC infusion on astrocyte cell density in coronal brain sections, we used a primary antibody (mouse monoclonal GFAP; Cat #G6171, St. Louis, MO, USA) and counter-stained sections with DAPI nuclear staining at postnatal day 14. Since the brain hemorrhage and resultant reactive gliosis is non-uniform around the ventricle (subventricular and periventricular white matter) we counted all positive cells in the entire subventricular zone SVZ and periventricular zone (PVZ) area. The cell counting on fixed sections was done as described previously (Vinukonda et al., 2010). Two investigators (blinded for experimental groups) determined the cell density using Image-J software with grid. We counted four sections in each pup and five pups from each group. Data was presented in scatter plot as mean cell count (mean ± SEM).

Sample Preparation for RNA Isolation From Laser Microdissection of Choroid Plexus

Real-time TaqMan gene expression assays for AQP1 were performed on postnatal day 3 using laser micro-dissected choroid plexus tissue sections. Briefly, the sample was embedded in optimal cutting temperature (OCT) compound, snap frozen in liquid nitrogen and stored at −80°C. Serial coronal sections were made at the level of mid-septal nucleus (18–20 μm thickness) containing the choroid plexus in the lateral ventricles cut at −20°C using a cryostat (Leica-Germany). The sections were mounted on polyethylene naftelato (PEN) membrane slides (2.0 μm Leica Microsystems 3P, Germany). Laser capture microdissection was performed using a LMD6500 Leica laser microdissector (Leica-Germany). The CP was viewed on its monitor using a 20× objective and microsamples of the CP were selected using the software tool. Laser dissected CP from both lateral cerebral ventricles are shown in **Supplementary Figure 1D**. The collection tube caps were preloaded with 50 μl of RLT plus buffer and immediately processed for RNA extraction.

Microscopic Dissection of Ependymal Wall SVZ Tissue for RNA Isolation

SVZ tissue samples were harvested at the level of the mid-septal nucleus from 3 mm thick coronal slice on postnatal days 3, 7 and 14. We chose this level because the germinal matrix is noticeable at this location and is a useful landmark to reproducibly dissect homogenous tissues from all experimental groups. Slices were separated into wax-coated petri dishes containing sterile cold PBS and stabilized with sterile head pins so that the lateral ventricle could be viewed under a dissecting microscope. As shown in the **Supplementary Figures 1F,G**, we dissected a region of 0.5–1 mm size reflecting the ependymal wall using fine microdissection scissors along the lateral side of both lateral ventricle walls. Immediately after dissection of the tissue, samples were snap frozen in liquid nitrogen and stored it at −80°C, until further processing.

Total RNA Isolation and cDNA Synthesis

Total RNA extraction was performed using three different isolation procedure kits to optimize extraction from various tissues quantities obtained after microdissections. Briefly, after homogenization, RNA was precipitated with 70% alcohol and purified total RNA was collected using a spin column following the manufacturer's protocol. We have used three specific RNA isolation kits based on the types and amount of sample used for the isolation: (i) the "RNeasy-plus micro kit" (Cat #74034, Qiagen) specific for micro-dissected cryosections, was used for extraction of RNA from the laser dissected sample collected into RLT-plus buffer containing sterile Eppendorf tube. (ii) The "RNeasy micro kit" (Cat #74004, Qiagen) was used for RNA extraction tissue samples collected using microscope from the SVZ; and (iii) we used the "RNeasy mini kit" (Cat #74104) for the larger 3 mm thick total coronal slice. RNA was eluted into RNase free water, the quality and quantity were assessed using a Nano-Drop® Spectrophotometer ND-2000C (Thermo Fisher Scientific, Waltham, MA, USA). The first-strand complementary DNA (cDNA) was synthesized by using 1 μg of total RNA with oligo-dT primers using the transcriptor high fidelity cDNA synthesis kit (Cat #05081955001, Roche Diagnostics, Indianapolis, IN, USA). In the case of RNA extracted from laser-dissected samples, quantity was not measured, and the total amount was used to make cDNA due to the lower quantity of total RNA from this tissue.

TaqMan Gene Expression Assay

The TaqMan gene expression was performed using ABI quanta studio (Thermo Fisher Scientific, Waltham, MA, USA) as previously described (Vinukonda et al., 2010, 2019). The mRNA transcript levels were determined by two-step quantitative real time TaqMan PCR using the TaqMan chemistry reaction mix purchased from Roche (Cat #04913850001, Roche, Indianapolis, IN, USA). The following single tube TaqMan probe-primer mixes were used: Oc03395705_m1 (AQP4), Oc04096741_m1 (AQP1), Oc03395687_g1 (CTGF), Oc03397520_m1 (MMP-9), Oc03824728_s1 (TLR2), Oc03398503_m1 (TLR4), Oc03398424_m1 (TGFb2), Hs01086000_m1 (TGFb3), Oc03396940_m1 (IL-10), Oc03823402_g1 (GAPDH; Thermo Fisher Scientific, Waltham, MA, USA) as described previously (Vinukonda et al., 2010). Analysis was completed using the efficiency corrected ΔΔCT method and the data was presented in percentages (Livak and Schmittgen, 2001; Schmittgen, 2001).

Statistical Methods

To determine differences in cell counts between the three groups, we used one-way ANOVA to compare treatments. Comparisons between groups on day 3, 7 and 14 were conducted using one way ANOVA using GraphPad Prism-6 (GraphPad Software, CA, USA). All *post hoc* comparisons were done using Tukey multiple comparison testing and P-values < 0.05 were considered significant. While gender differences are an important component of biological variation, since there is no published evidence of gender difference causing IVH and in an effort to minimize animal exploitation, we did not perform a gender-specific analysis of our data sets.

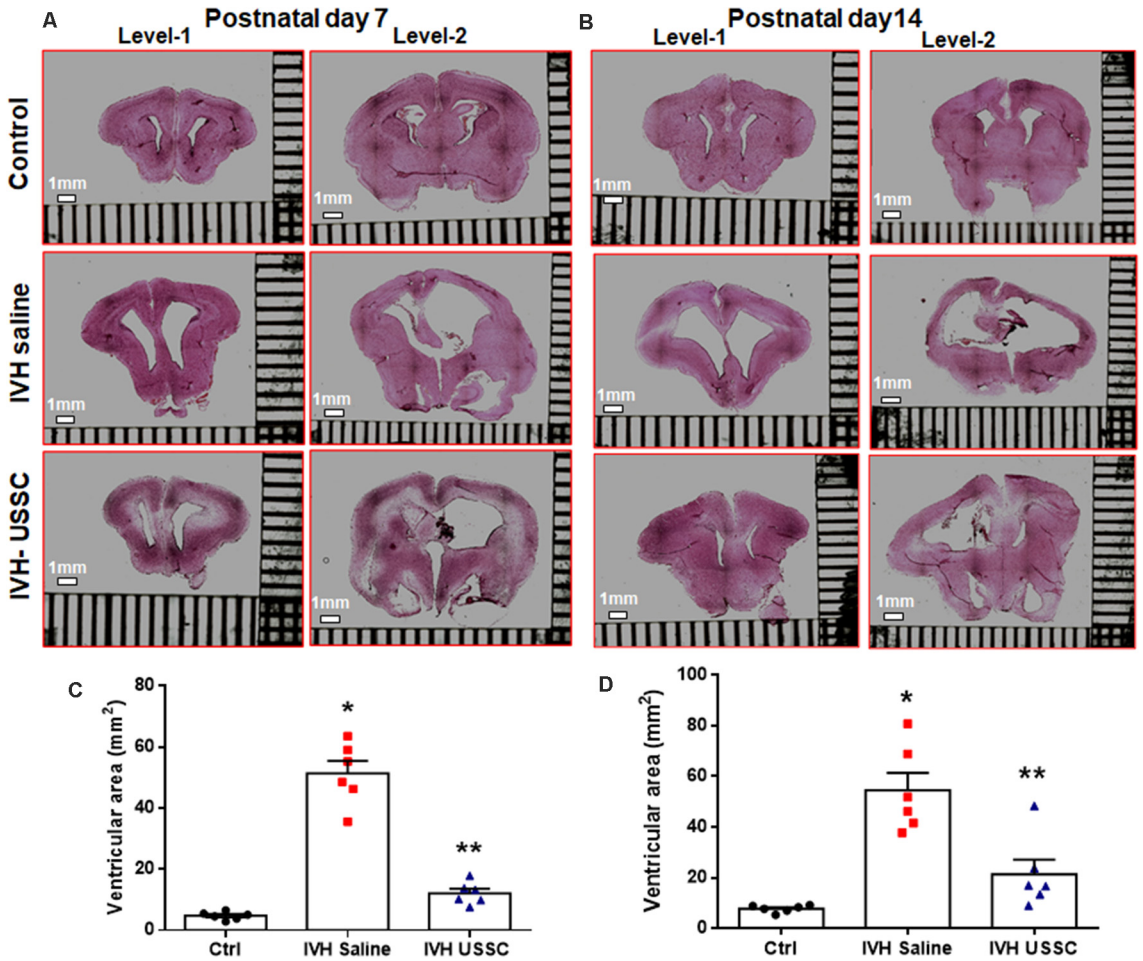

FIGURE 1 | Intracerebroventricular unrestricted somatic stem cells (USSC) administration reduced cross sectional area of lateral ventricles in post-hemorrhagic hydrocephalus (PHH). **(A)** Representative Hematoxylin and Eosin (H&E) stained coronal section on postnatal day 7 at two levels (rostral forebrain: level-1 and caudal forebrain: level-2) with and without USSC administration, showing ventricular size in normal healthy control, intraventricular hemorrhage (IVH) saline control and single dose USSC (2×10^6 cells/dose) injected (left panel **A**). **(B)** Ventricular area on postnatal day 14 in normal healthy control, IVH saline control and single dose USSC (2×10^6 cells/dose) injected (right panel **B**). The stitched images are taken at low power for both postnatal ages from 20 μm sections. The scale bar in all images is 1 mm. Images were scanned using EVOS® FL Auto Imaging System (Thermo Fisher Scientific, Waltham, MA, USA). **(C,D)** Scatter plots with bar graphs showing cross-sectional area of lateral ventricles measurement on postnatal day 7 **(C)** and 14 **(D)**. The mean cross sectional measured on two alternate sections taken from hippocampus towards the rostral side of the coronal block made at the level of mid-septal nucleus (total ventricular area is the sum of the left and right values at level-2 that are averaged from two alternate section for each pup). Each symbol in the experimental groups represent one rabbit pup (*$P < 0.05$ for control vs. IVH and **$P < 0.05$ for IVH vs. USSCs; the values represent mean ± SEM; $n = 6$ in each group for both postnatal days 7 and 14). *P*-values were derived by one-way ANOVA with Tukey's multiple comparisons test.

RESULTS

USSCs Significantly Reduced Ventricular Enlargement After Intraventricular Hemorrhage

We assessed the cross-sectional area of the lateral ventricles and the brain parenchymal area on coronal sections taken at the level of the mid-septal nucleus on postnatal days 7 and 14. Representative H&E images are depicted in **Figure 1A** for day 7 and in **Figure 1B** for day 14; the mean ventricular area is presented as shown in **Figures 1C,D**. We found a significantly higher mean ventricular area in IVH pups with PHH when compared with the no IVH controls at postnatal days 7 and 14 (mean ventricular area for day 7 was 5 ± 0.5 mm^2 in control vs. 51 ± 10 mm^2 in IVH; and for day 14 was 8 ± 0.6 mm^2 in control vs. 54 ± 7 mm^2 in IVH, $P < 0.05$ for both). Importantly, USSC administration *via* the ICV route attenuated the ventricular enlargement caused by hemorrhage at both postnatal ages 7 and 14 days (mean ventricular area was 51 ± 10 mm^2 in IVH vs. 12 ± 4 mm^2 in USSC injected IVH pups at postnatal day 7 and for day 14 was 54 ± 7 mm^2 in IVH vs. 21 ± 6 IVH + USSC injected pups; **Figures 1C,D**, $P < 0.05$ for both). USSC-treated IVH pups showed a reduction in ventricular area (~60%) when compared to non-treated animals at 7 and 14 days. To confirm that the attenuated ventricular area was the

functional effect of USSCs rather than the glycerol injected in the peritoneal cavity, we assessed ventricular cross-sectional area measurements among healthy controls (no glycerol injected, no IVH) vs. glycerol injected but no IVH rabbit pups on postnatal day 14 (**Supplementary Figures 3A–D**). There was no significant difference between two groups for either total brain area or for mean ventricular area on postnatal day 14 (**Supplementary Figures 3C,D**).

The mean total brain area (parenchyma + ventricles) was comparable across the experimental groups, whereas the brain parenchymal area alone was significantly reduced after IVH on postnatal day 14 (**Supplementary Figures 2A,B**, $P < 0.05$ for brain parenchyma Ctrl vs. IVH). Taken together, this data indicated that the reduction in the ventricular area after USSC injection in IVH pups is mediated by USSC stem cells and does not arise as a primary result of changes in brain parenchymal volume after PHH.

Morphological and Histological Changes of the Lateral Ventricle Ependymal Wall and Choroid Plexus Epithelium in PHH

The morphological damage is dependent on massive RBC extravasation into the parenchyma and the lateral ventricles (physical damage) followed by subsequent secondary toxicants released by RBC degradation (cellular and molecular damage). Since the area and gross damage is variable, for consistency of comparisons, we specifically focused on the ventricle wall around the GM, CPE and CP at level-2 (multiple sections starting from hippocampus towards rostral side) with anatomically matched sections taken from the mid-septal nucleus. H&E stained coronal sections of the lateral ventricles were used to evaluate epithelial cell changes and ependymal wall integrity in the lateral ventricle walls and the choroid plexus epithelial (CPE) border. Representative images around the germinal matrix of the lateral ventricles and CPE in the lateral ventricle are depicted in **Figure 2**. As shown in panel **A**, low power (4×) and **B** high power (20×; top to bottom), the control pups with no IVH showed an intact multicellular dense ependymal layer and preserved CSF brain parenchymal barrier (**Figures 2A,B**, top panel). Whereas, in IVH pups with PHH, this ependymal layer was disrupted and detached indicating damaged CSF and brain parenchymal barriers (**Figures 2A,B**, middle panel). Importantly, with USSC treatment, this damage was partially recovered, and some areas showed less ependymal cell damage (**Figures 2A,B**, bottom panel). Further, we assessed histopathological changes on H&E stained coronal sections in CPE, as shown in **Figure 2C**. The choroid plexus (CP) sections from IVH pups showed prominent structural damage when compared with no IVH pups who had well-organized and preserved blood CSF barrier. The epithelial cell lining of the CP was intact in the controls (**Figure 2C**, top), whereas in IVH pups, the cells were reduced in number, disorganized and undergoing cell death. The cells were also flattened and lost their normal layered appearance (**Figure 2C**, middle). The CP was also filled with blood at multiple areas of fibrosis surrounded by histiocytes (inflammatory cells). Importantly, after USSC administration, we noted partial recovery of the integrity of the CPE border (**Figure 2C**, bottom).

USSC Administration Significantly Improved Homeostasis of Aquaporin-1 Expression in the Choroid Plexus Following Experimentally Induced PHH

AQP1 is a non-gated membrane transport protein primarily expressed in the choroid plexus epithelium (CPE) facing the ventricular cavities where it secrets 80% of the total CSF. We investigated whether IVH causes changes in AQP1 expression in the CPE during the progression of PHH. We performed AQP1 immunostaining on fixed coronal section on postnatal day 7 and 14 (**Figure 3**). AQP1 immunoreactivity decreased in early injury on day 7 when compared with no IVH controls, whereas USSC administration improved it towards normal (**Figure 3A**) and significantly restored levels to near normal by day 14 (**Figure 3B**). We also show sections with AQP1 staining (not merged with DAPI) in the CP to illustrate reduced and discontinuous AQP1 expression in IVH pups compared to control and USSC treated pups (**Figure 3C**); on Image-J measurements of the integrated AQP1, pixel density was reduced ($P < 0.05$, **Supplementary Figure 2C**). The secondary antibody Alexa-594 alone was used as negative control for AQP1 expression and showed no immunoreactivity in the CP (**Supplementary Figure 2F**). Pathological conditions such as IVH mediated injury can enhance short-term vulnerability of other aquaporins as well. To this end, we also examined immunostained coronal sections from IVH pups with AQP4 antibody and found weak to no immune-reactivity for AQP4 staining in this region (**Supplementary Figures 2D,E**).

To test whether AQP1 mRNA expression in the CP would also change in IVH pups with and without USSC treatment, we performed real time TaqMan assays using rabbit-specific probes on cDNA made from laser dissected CP sections from coronal slices (Karimy et al., 2017). Consistent with our observation in AQP1 immunoreactivity, the AQP1 mRNA levels were also reduced (**Figure 4A**) in IVH pups on postnatal day 3 (100 ± 14 in control vs. 27 ± 10 in IVH) but were significantly improved by USSC administration (83 ± 14; **Figure 4A**, $P < 0.05$). Taken together, these results demonstrated that AQP1 expression on the choroid plexus progressively decreased in early postnatal age after IVH but was significantly restored toward normal levels after USSC administration. Importantly, the AQP4 mRNA expression in real time PCR showed high Ct (cycle threshold) detection values in CP and was not measurable after IVH.

USSC Administration Increases Toll-Like Receptors (TLRs) and NF-KB Expression in Choroid Plexus Epithelium Following Experimentally Induced PHH

Recent studies have demonstrated that IVH derived metabolites can cause CPE inflammation resulting in CSF hypersecretion and the development of PHH. Prior studies had shown that this hypersecretion was mediated by activated TLR-NF-kB pathways

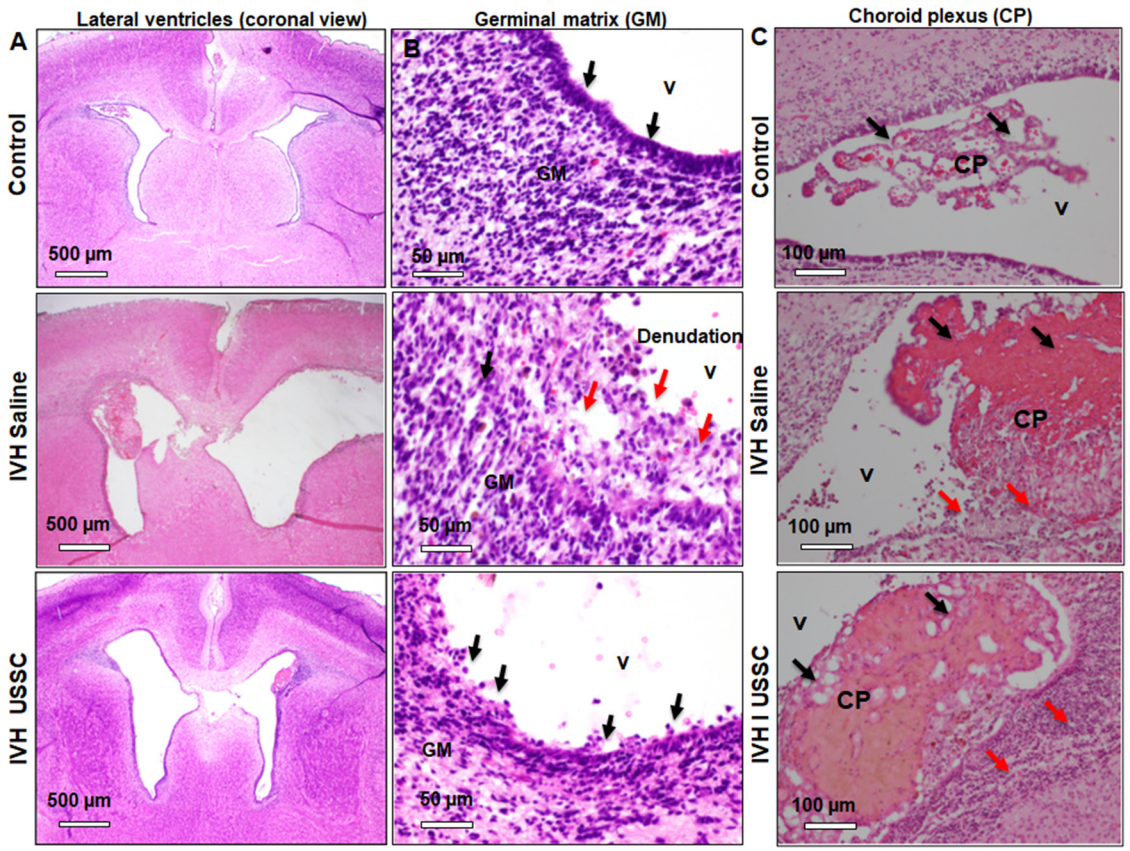

FIGURE 2 | Histopathological recovery after USSC administration in germinal matrix and choroid plexus in the lateral ventricles after PHH. **(A,B)** Representative H&E stained coronal sections at the level of mid-septal nucleus after USSC administration. Note: the normal intact ependymal wall in control low power (black arrow, top panel-**A**; 4×) and high power (top panel-**B**; 20×) vs. the damaged wall after IVH (red arrow middle panel **A**; 4× and panel-**B**; 20×). Compare effects after USSC injection showing recovered germinal matrix (bottom panel **A** and **B**; 4× and 20× images). The arrow shows normal and damaged areas. The Scale bar for panel **(A)** 500 μm and for panel **(B)** is 50 μm. **(C)** Representative H&E stained coronal section with choroid plexus showing normal intact choroid epithelium in control shown in black arrow (top panel-**C**; 20×), damaged choroid plexus (CP) filled with blood shown in black arrow, histiocytic and damaged epithelium in IVH (middle image panel–**C**; 20×) compare to effects of USSC injection showing partial recovery in the CP (panel-**C**; 20× image). The arrow shows normal vs. damaged areas. The scale bar for all images is 100 μm, USSC: 2×10^6 cells/dose. All images were taken using Olympus microscope model BX43F (Olympus Corporation-Life Sciences).

(Gram et al., 2014; Karimy et al., 2017). Therefore, we tested whether IVH alters expression of TLRs and whether USSCs affected TLR levels as an index of inflammation. We performed real time TaqMan gene expression assay using rabbit specific mRNA probes for TLR2, TLR4, NF-kB using cDNA made with laser dissected CP from day 3 IVH pups with and without USSC and compared them with naïve controls (**Figures 4B,D**). We found significantly increased levels of TLR2 (100 ± 4 in control vs. 207 ± 24 in IVH, $P < 0.05$) and a trend toward increased TLR4 after early injury in IVH pups. With USSC administration at the early time point, both TLR mRNAs as well as the levels of the proinflammatory marker NF-kB were unaffected, Taken together the laser dissected CP mRNA expression data suggests that during the early injury phase, IVH activates TLR-NF-kB inflammation cascades. It is also evident, that a single dose of USSCs was not sufficient to suppress the TLRs' action at an early stage of therapy and may require multiple doses of USSCs and later study time points (7–14 day) to fully characterize changes.

USSCs' Administration Significantly Enhanced Aquaporin-4 Expression in the Ependymal Lining of the Lateral Ventricles Following Experimentally Induced PHH

AQP4 is expressed in brain parenchyma and ependymal cells lining the lateral ventricles and facilitates the transport of excess water out of the ventricle. Increased expression of AQP4 is reported in various disease states, such as stroke and hydrocephalus (Mao et al., 2006; Paul et al., 2011). Up-regulated AQP4 is associated with excess water in the interstitial spaces, as a compensatory response to ease CSF elimination. To test whether AQP4 expression is altered in the ependymal layer lining the lateral ventricles and brain parenchyma, we first immune-stained the coronal sections using an AQP4 specific antibody on postnatal day 7 and 14. This was followed by quantification of AQP4 mRNA expression, from dissected SVZ tissue and from coronal slices at the level of the mid-septal nucleus on postnatal days 3, 7 and 14 in all the three

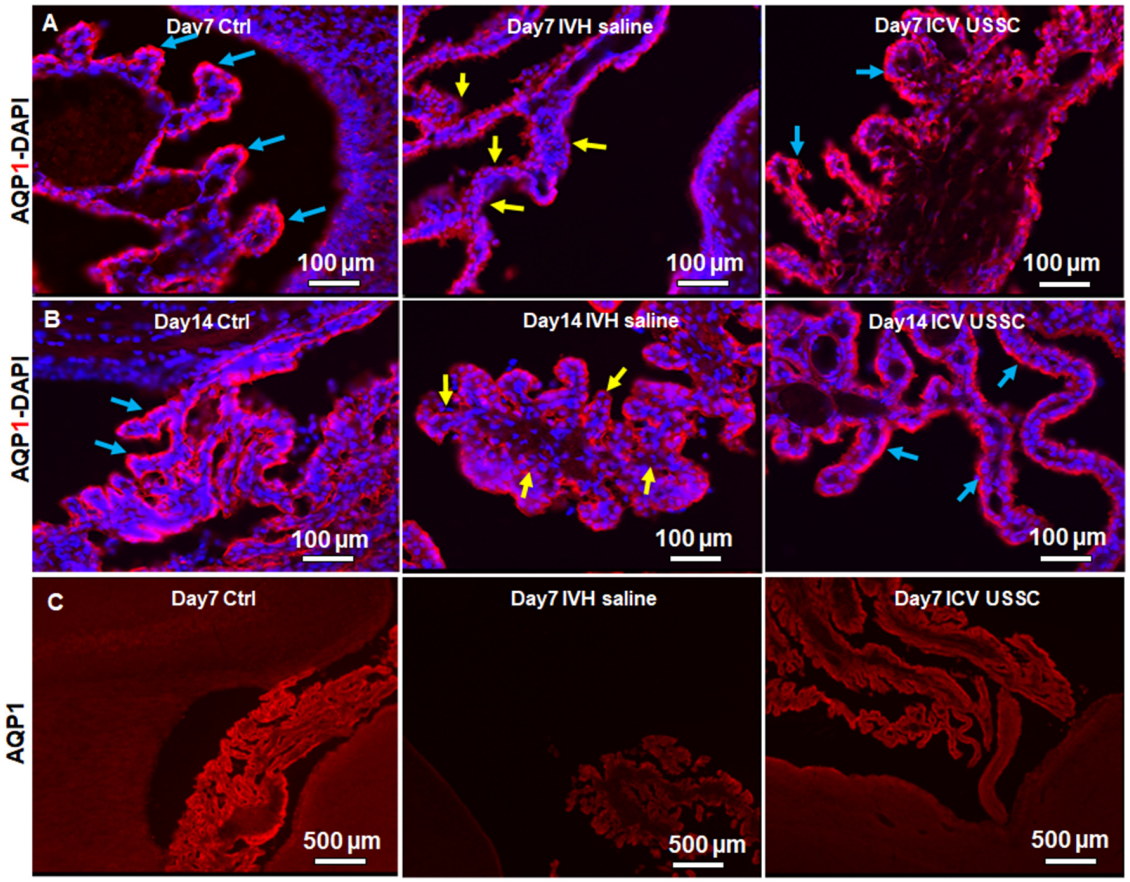

FIGURE 3 | USSC administration recovered aquaporin1 (AQP1) expression in the choroid plexus after PHH. **(A)** Representative immunofluorescence image of cryosections labeled with AQP1 specific antibody (arrows showing choroid epithelium immunoreactivity) on postnatal days 7. Strong AQP1 immunoreactivity in the control (blue arrows), reduced signal (yellow arrows) in IVH followed by recovered expression (blue arrows), and images from left to right respectively at postnatal day 7. CPE (Choroid plexus epithelial cells). Images were taken at 20× objective; blue = DAPI stain, 20 µm sections. Scale bar 100 µm. **(B)** Strong AQP1 immunoreactivity in the control (blue arrows), reduced signal (yellow arrows) in IVH followed by recovered expression (blue arrows), and the images from left to right respectively at day 14. Images were taken at 20× objective; blue = DAPI stain, 20 µm sections. Scale bar 100 µm. **(C)** Representative immunofluorescence image of cryosections labeled with aquaporin1. As seen in the high power image (panel-**B** above), the strong AQP1 immunoreactivity is evident over the entire choroid plexus in the control, reduced signal in IVH followed by recovered strong AQP1 expression observed in images from left to right respectively at day 14. Images were taken at 4× objective; 20 µm sections. The scale bar is 500 µm. Fluorescence images were taken using "Nikon Eclipse 90i microscope" (Nikon Instruments, Japan).

experimental groups. The immune-reactivity for AQP4 in the lateral ventricle ependymal layer was reduced in IVH on both postnatal days 7 and 14 when compared with healthy controls (**Figures 5A,B**), whereas USSC administration partially improved the AQP4 immuno-reactivity (**Figures 5A,B**). We also observed reduced AQP4 expression on the lateral ventricular ependymal wall in IVH pups compared to control and USSC treated pups over the entire ventricular wall at low power image with single staining with AQP4 and not merged with DAPI (**Figure 5C**). The secondary antibody Alexa-594 alone was used as negative control for AQP4 expression. As shown in **Supplementary Figures 3E,F**, the ventricular wall in the lateral side and in GM region showed no immunoreactivity. It has been reported that under pathological conditions, AQP1 is also expressed in the ventricular ependymal wall as well as in the brain parenchyma. To this end, we immune-stained coronal sections for AQP1 expression in three experimental groups. We found AQP1 immuno-signals in the ependymal wall and brain parenchyma in IVH pups compared to a sparse to no expression in control and USSC treated rabbit pups on postnatal day 7 (**Supplementary Figure 2G**).

To confirm our immunostaining data, we evaluated samples for AQP4 mRNA expression in ependymal wall tissue (from dissected SVZ) and total coronal brain slices to see the regional and time dependent expression of AQP4 during critical periods of progression of hydrocephalus. In IVH pups, AQP4 mRNA was significantly reduced in both ependymal wall tissue and brain parenchyma on postnatal day 3 (100 ± 14 in control vs. 54 ± 7 in IVH for SVZ and 100 ± 18 in control vs. 49 ± 4 in IVH for parenchyma), whereas USSC administration partially improved it (113 ± 15 for USSC treated SVZ and 89 ± 7 in parenchyma; **Figures 6A,B**, $P < 0.05$ all pairwise comparisons). Similar trends were seen on postnatal day 7, in both dissected SVZ and brain parenchyma RNA. By postnatal day 14, AQP4 expression

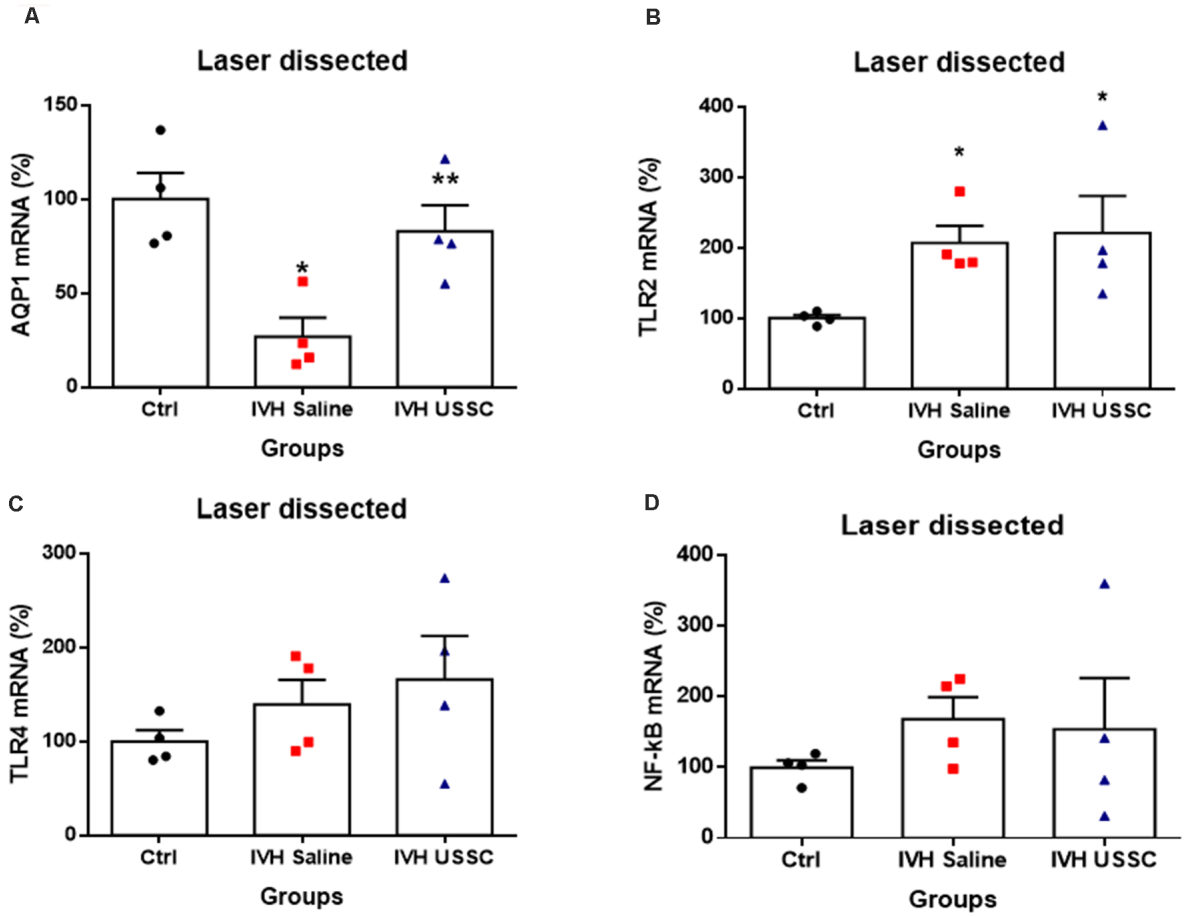

FIGURE 4 | USSC administration mitigates AQP1 expression and does not suppress toll like receptors (TLRs) in choroid plexus epithelium during early IVH injury at postnatal day 3. **(A–D)** Scatter plot bar graphs showing TaqMan gene expression assay using laser dissected choroid plexus RNA at postnatal day 3. **(A)** Reduced AQP1 mRNA expression in IVH compared with healthy controls in laser dissected tissue region; after the USSC treatment, expression was recovered to normal (*$P < 0.05$ for Ctrl vs. IVH, **$P < 0.05$ for IVH vs. USSCs; $n = 4$ in each group). **(B)** Increased mRNA levels for TLR-2 after IVH independent of USSC treatment (*$P < 0.05$ for Ctrl vs. IVH and Ctrl vs. USSC; $n = 4$ in each group). **(C–D)** For both TLR4 and NF-kB mRNA, levels were comparable between the three interventional groups. (p –ns). The data represent mean ± SEM; for postnatal day 3. *P*-values were derived by one-way ANOVA with Tukey's multiple comparisons test.

was significantly reduced in dissected SVZ in IVH pups but was partially improved by USSC administration (**Figure 6A**, $P < 0.05$).

AQP1 is mainly expressed on the choroid plexus epithelial lining and is involved in CSF secretion but under certain pathological conditions, it can also be expressed in the brain parenchyma. We next investigated AQP1 mRNA expression in the dissected SVZ and found increased levels on postnatal day 7 and 14, whereas USSC administration diminished this increase at both time points and was significant by postnatal day 14 (for day 7: 118 ± 16 control, 293 ± 45 in IVH and 197 ± 57 in USSC; for day 14: 147 ± 12 in control, 280 ± 50, 156 ± 26 in USSC treated pups; **Figure 6C**, $P < 0.05$). Similar results in mRNA expression were seen in coronal brain slices on day 3, the AQP1 levels decreased in IVH and improved partially by USSC infusion (for day 3: 100 ± 26 in control, 29 ± 4 in IVH and 83 ± 9 in USSC; **Figure 6D**, $P < 0.05$ for both). In general, for the one AQP1 expression, the CT (cycle threshold) level was 75% higher than for AQP4.

USSC Administration Suppressed Gliosis and Fibrosis in SVZ After PHH

The subventricular zone astrocytes and the lateral ventricular wall ependymal cells arise from radial glial progenitor cells. Radial glial progenitor cell proliferation and maturation continues from early postnatal ages through maturity. An early inflammatory reaction due to hemorrhagic blood, blood components and altered TGF-β isoforms contribute to astrocytosis and scar formation, which are thought to adversely affect astrocyte lineage differentiation and proliferation during PHH. To evaluate the effects of USSC treatment, we assessed normal vs. reactive astrocyte cell counts in healthy controls and hemorrhagic pups with and without USSC administration on postnatal day 14. We found a significantly increased number of normal and reactive astrocytes (GFAP + astrocyte cell density)

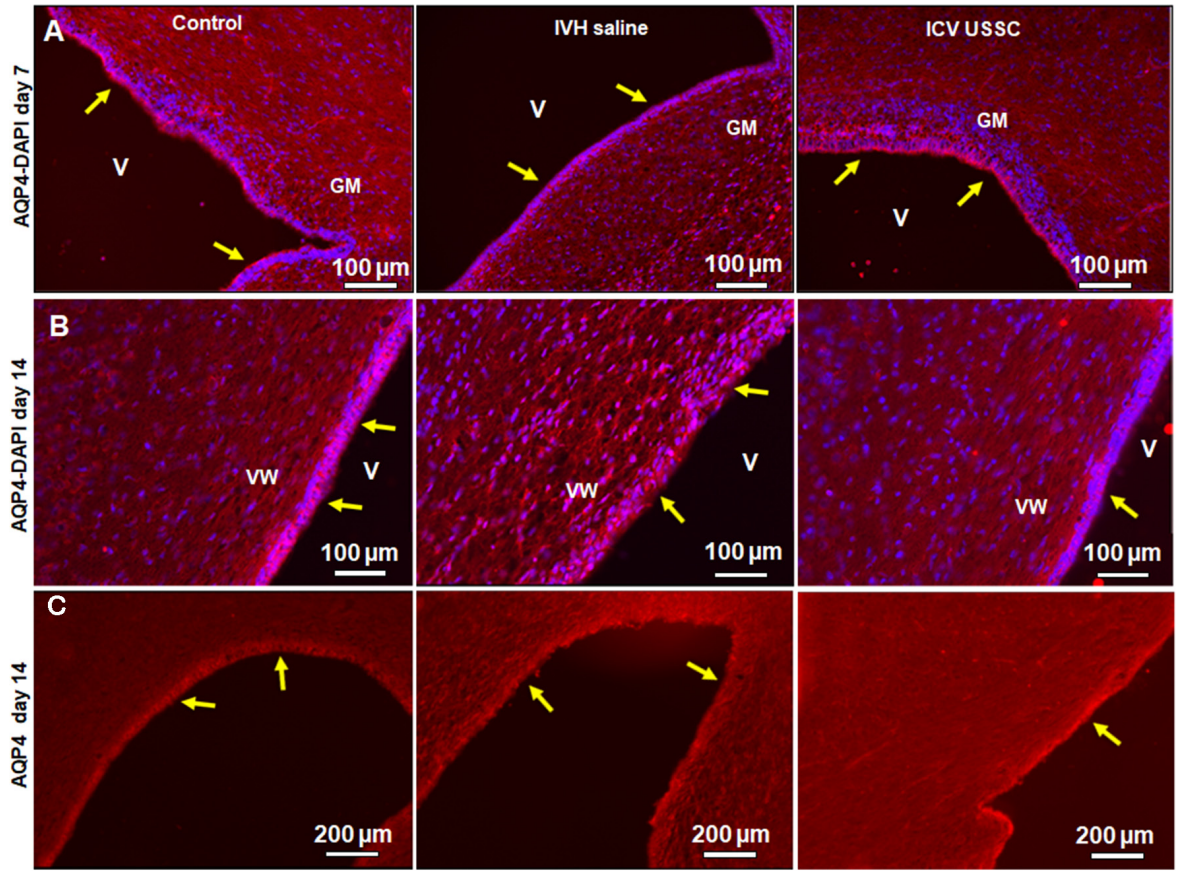

FIGURE 5 | USSC administration improved aquaporin4 (AQP4) expression in the ependymal-lining layer of the ventricle after PHH. **(A)** Immunofluorescence image of cryosections labeled with AQP4 specific antibody (arrows showing immunoreactivity along the ventricular wall) at postnatal days 7. Strong AQP4 immunoreactivity was observed on postnatal day 7 in the control, reduced signal in IVH followed by recovered intensify of expression in USSC treated pups around the germinal matrix (GM); images from left to right respectively (panel **A**). Images were taken at GM region (20× objective; $n = 5$ in each group); 20 µm sections. V, ventricle; VW, ventricle wall; GM, germinal matrix. The scale bar is 100 µm. **(B)** Strong AQP4 immuno-reactivity on day 14 in the control, reduced signal after IVH followed by recovery of intensity of expression after USSC treatment and increased cellularity (blue = DAPI); images from left to right respectively. Images were taken at lateral ventricular wall (20× objective; $n = 5$ in each group); 20 µm sections. V, ventricle; VW, ventricle wall; GM, germinal matrix. The scale bar is 100 µm. **(C)** Immunofluorescence images of cryosections labeled for AQP4. The AQP4 in the ventricle wall was higher as seen in panel **(B)** in the control group and showed reduced and discontinuous signal after IVH followed by recovered to strong AQP4 expression after USSC treatment. The images were from left to right for control, IVH and IVH USSC injected pups respectively at day 14. Images were taken covering the major ventricular area at 10× objective ($n = 5$ in each group) 20 µm sections. V, ventricle; VW, ventricle wall, GM, germinal matrix. The scale bar is 200 µm. Fluorescence images were obtained using "Nikon Eclipse 90i microscope" (Nikon Instruments, Japan).

in IVH pups compared with controls on postnatal day 14 (for normal astrocytes in control 164.2 ± 2 vs. 305 ± 63 in IVH and reactive astrocytes in control 252 ± 41 vs. 743 ± 144 in IVH; **Figure 8D**, $P < 0.05$ for both). USSC administration resulted in significantly suppressed reactive astrocytosis on postnatal day 14 (mean cell density 743 ± 144 in IVH vs. 334 ± 47 in USSC treated pups; **Figure 8D**, $P < 0.05$).

Transforming growth factor-beta (TGF-β) is a multi-potent growth factor and cytokine. Altered expression of TGF-β isoforms are associated with astrocyte differentiation, scar formation and extracellular matrix tissue remodeling (Gomes et al., 2005; Hsieh et al., 2010). TGF-β dependent mechanisms are implicated in CNS fibrotic pathologies and subependymal gliosis in post hemorrhagic animal models. To investigate the changes in TGF-β expression in the SVZ, we dissected the lateral ventricle wall from the brain parenchyma and assessed mRNA levels of TGF-β isoforms (TGF-β2 and TGF-β3) including connective tissue growth factor (CTGF). CTGF, also known as CCN2, is a modular matricellular protein of the CCN family of extracellular matrix-associated heparin-binding proteins and is critically involved in wound repair and fibrotic disease (Hall-Glenn and Lyons, 2011).

After PHH, the TGF-β2 isoforms mRNA levels were increased on postnatal days 7 and 14 (for day 7: 109 ± 21 control, 209 ± 16 in IVH and 136 ± 25; **Figure 7A**, $P < 0.05$ for day 7) while TGF-β3 isoforms were elevated in both USSC and PHH groups on day 3 (**Figure 7B**, $P < 0.05$). In contrast, by postnatal day 14, TGF-β3 levels significantly increased in IVH pups but were reduced after USSC treatment (for day 3: 100 ± 11 control, 199 ± 31 in IVH and 260 ± 33 in USSC; for day 14: 168 ± 19 in control, 321 ± 47 and 187 ± 34 in USSC treated pups; **Figure 7B**, $P < 0.05$). Further, CTGF

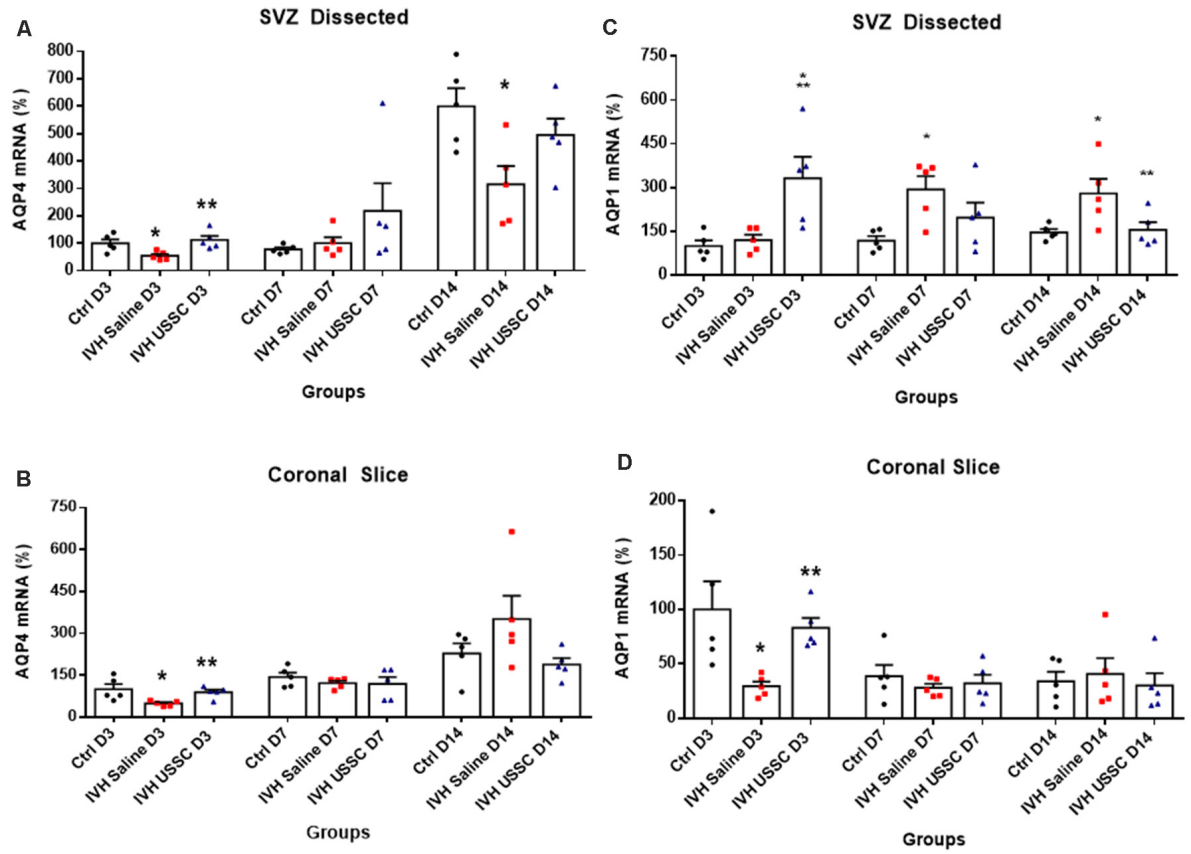

FIGURE 6 | USSC administration altered the expression of the AQP4 and AQP1 mRNA in Sub-ventricular zone (SVZ) and brain parenchyma in PHH. **(A,B)** Scatter plot with bar graphs showing TaqMan gene expression assay in microscopic dissected SVZ and coronal slice tissue mRNA for AQP4 expression. **(A)** SVZ dissected tissue mRNA showed reduced expression in IVH pups compared with controls at days 3 and 14 for AQP4, whereas after USSC treatment, the AQP4 expression was elevated to normal or above IVH group at both postnatal ages (*$P < 0.05$ for Ctrl vs. IVH, **$P < 0.05$ IVH vs. USSCs, $n = 5$ in each group). The data represent mean ± SEM; for each group for three postnatal days 3, 7 and 14. *P*-values were derived by one-way ANOVA with Tukey's multiple comparisons test. **(B)** Similar comparisons in coronal slice mRNA showed reduced AQP4 expression in IVH on day 3 that recovered to normal levels after USSCs at all time points (*$P < 0.05$ for Ctrl vs. IVH, **$P < 0.05$ IVH vs. USSCs, $n = 5$ in each group). The data represent mean ± SEM; for each group for three postnatal days 3, 7 and 14. *P*-values were derived by one-way ANOVA with Tukey's multiple comparisons test. **(C,D)** Scatter plot with bar graphs showing TaqMan gene expression assay in dissected SVZ and coronal slice tissue mRNA for AQP1 expression. **(C)** SVZ dissected tissue mRNA on postnatal day 3 for AQP1 showed increased expression in USSC treated pups compared with controls and IVH pups (*$P < 0.05$ for Ctrl and **$P < 0.05$ IVH vs. USSCs, $n = 6$ in each group). Significantly, increased AQP1 expression occurred in IVH pups on day 7 and 14 compared to controls. After USSC, this increase was significantly reduced on day 14 (*$P < 0.05$ for Ctrl vs. IVH, **$P < 0.05$ IVH vs. USSCs, $n = 5$ in each group). The data represent mean ± SEM; for each group for three postnatal days 3, 7 and 14. *P*-values were derived by one-way ANOVA with Tukey's multiple comparisons test. **(D)** AQP1 mRNA expression in the coronal slice RNA showed reduced AQP1 expression in IVH on day 3 and recovered levels after USSC administration (*$P < 0.05$ for Ctrl vs. IVH, **$P < 0.05$ IVH vs. USSCs, $n = 5$ in each group). Comparable AQP1 expression was observed on postnatal day 7 and 14. The data represent mean ± SEM; for each group for three postnatal days 3, 7 and 14. *P*-values were derived by one-way ANOVA with Tukey's multiple comparisons test.

mRNA in the SVZ at day 3 was also significantly increased in IVH pups compared with healthy controls but was reduced in PHH after USSC treatment (for day 3: 100 ± 23 in control vs. 250 ± 90 in IVH and 135 ± 19 in USSC; **Figure 7C**, $P < 0.05$). While in the brain parenchymal, RNA was reduced for CTGF expression on postnatal day 3 (100 ± 16 control, 47 ± 6 in IVH and 117 ± 17 in USSC (**Figure 7D**, $P < 0.05$). Immune-reactivity for CTGF around the lateral ventricle showed similar patterns and was reduced after USSC treatment (data not shown). This data suggests early fibrosis after post injury in the ependymal wall rather than brain parenchymal area.

Further, we also evaluated whether USSC administration had any effect on the expression of extracellular matrix (ECM) inflammatory scar protein MMP-9. MMPs are primary components of neuro-inflammation, tissue reorganization and blood-brain barrier (BBB) disruption proteins (Rosell et al., 2006; Vella et al., 2015). Therefore, we assessed the expression of MMP-9 in the coronal lysate from healthy controls and hemorrhagic pups with and without USSC treatment at postnatal day 14, using a cytokine array assay. We found a significant increase in MMP-9 protein expression in IVH pups compared to normal healthy controls, whereas USSC administration significantly reduced MMP-9 protein expression (**Figures 8A,B**,

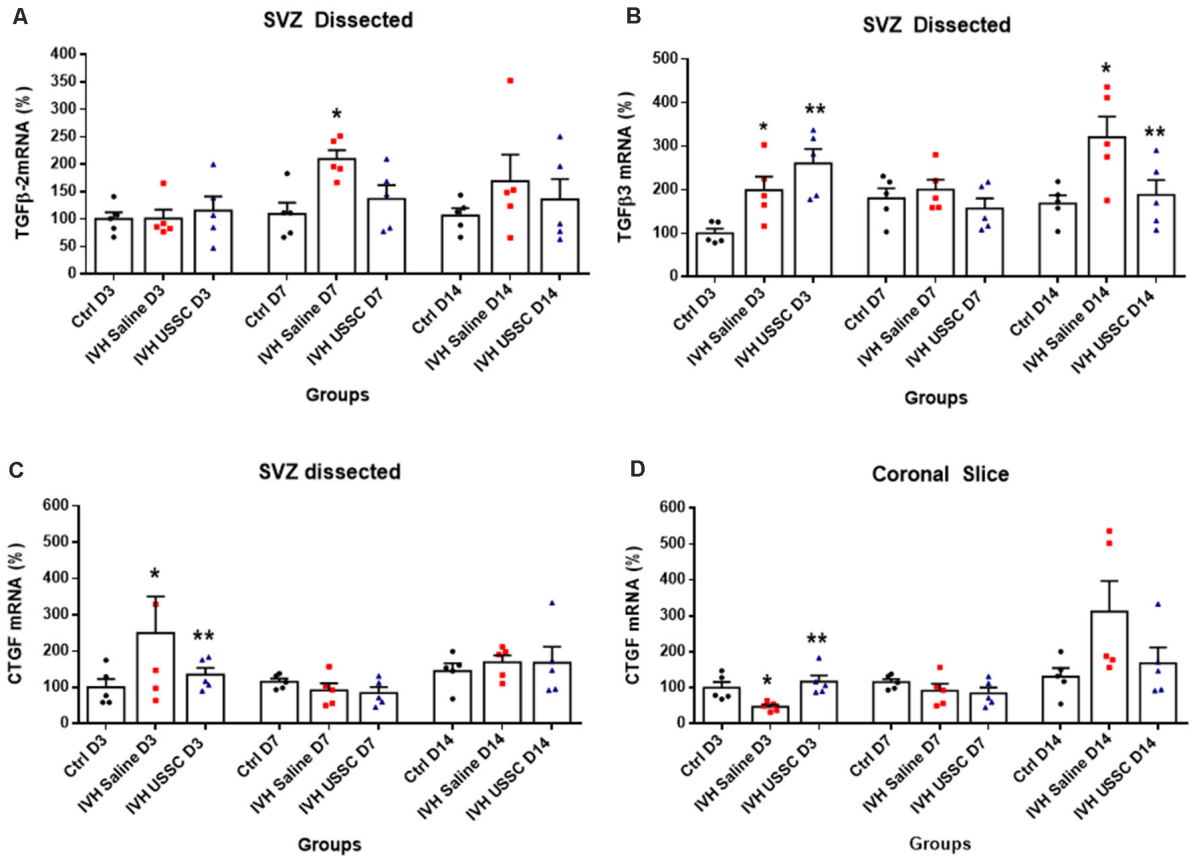

FIGURE 7 | USSC administration suppressed the expression of TGF-β isoforms and connective tissue growth factor (CTGF) mRNA in SVZ in PHH. **(A,B)** Scatter plot with bar graphs showing TaqMan gene expression assay in microscopic dissected SVZ tissue for TGF-β isoforms 2 and 3 mRNA. **(A)** Increased TGF-β2 isoform mRNA was observed in IVH pups on postnatal 7th day, whereas it reduced after USSC treatment (*$P < 0.05$, Ctrl vs. IVH, $n = 5$ in each group). **(B)** Increased TGF-β3 expression was observed on day 3 in IVH pups with and without USSC treatment (*$P < 0.05$, Ctrl vs. IVH, **$P < 0.05$ for Ctrl vs. USSC, IVH vs USSC, Ctrl vs. USSC, $n = 5$ in each group). On postnatal day 14, TGF-β3 significantly increased in IVH pups compared to control and was reduced to normal levels after USSC treatment (*$P < 0.05$, IVH vs. USSC, **$P < 0.05$ for IVH vs. USSC, $n = 5$ in each group). The data represent mean ± SEM; for each group for three postnatal days 3, 7 and 14. *P*-values were derived by one-way ANOVA with Tukey's multiple comparisons test. **(C,D)** Scatter plot with bar graphs showing TaqMan gene expression assay in microscopic dissected SVZ tissue and total coronal slice for CTGF mRNA levels. **(C)** CTGF mRNA was increased in IVH pups on day 3 in SVZ and suppressed to normal levels after USSC treatment and was comparable on 7th and 14th day (*$P < 0.05$ for Ctrl vs. IVH and **$P < 0.05$ for IVH vs. USSC at day 3, $n = 5$ in each group). **(D)** CTGF mRNA was increased in coronal slice on day 14 after IVH while USSC administration reduced CTGF after IVH on day 14 (*$P < 0.05$ for Ctrl vs. IVH and **$P < 0.05$ for IVH vs. USSC on day 3, $n = 5$ in each group). The data represent mean ± SEM; for each group for three postnatal days 3, 7 and 14. *P*-values were derived by one-way ANOVA with Tukey's multiple comparisons test.

$P < 0.05$). Of note, the elevation in MMP-9 mRNA expression in SVZ on postnatal day 3 was comparable in IVH pups whether they received USSC treatment or not (100 ± 6 in control, 401 ± 95 in IVH and 491 ± 98 IVH USSC; **Figure 8C**, $P < 0.05$ vs. control). This early response can be attributed to ependymal and parenchymal damage as well as an immediate response of exogenous USSCs to the new pathological environment. In contrast, on postnatal day 14, the increase of MMP-9 was significantly reduced after USSC treatment compared with IVH saline controls (**Figure 8B**). Taken together, the MMP-9 data suggests that active ECM remodeling exists early in hemorrhage and that USSCs produce an anti-inflammatory effect by day 14 which may contribute to less structural remodeling.

To further evaluate anti-inflammatory activity of USSCs, we investigated steady-state levels of the anti-inflammatory cytokine IL-10 mRNA in the three experimental groups on postnatal days 3, 7 and 14. We observed significantly reduced IL-10 mRNA levels in hemorrhagic pups compared to normal healthy controls on postnatal day 3. After ICV USSC administration, there was a significant increase on postnatal day 3 above control and IVH groups (100 ± 11 in control, 24.59 ± 7 in IVH and 165 ± 41 IVH USSC; **Figure 8E**, $P < 0.05$).

DISCUSSION

This is the first study evaluating the effects of USSCs on the density of aquaporin water channels 1 and 4 in the choroid plexus epithelium and lateral ventricular ependymal wall after IVH-induced hydrocephalus. We demonstrated that after experimentally induced IVH, USSC administration attenuated

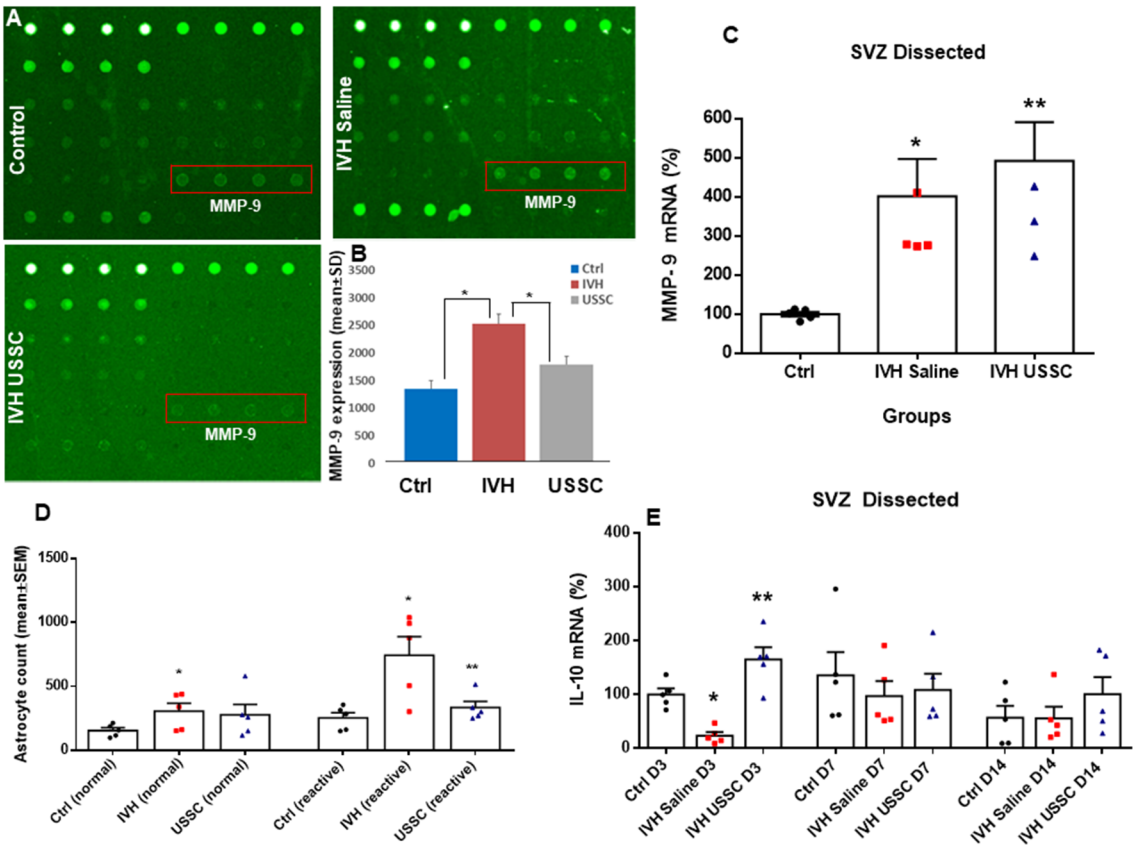

FIGURE 8 | USSC administration suppressed inflammation and enhanced anti-inflammatory cytokine IL-10 mRNA expression in SVZ after PHH. **(A)** Rabbit cytokine array laser scanned images showing reduced MMP-9 expression after USSC treatment. The representative images are for MMP-9 expression in control, IVH pups with and without USSCs (boxed area = sample loaded as quadruplicates at postnatal day 14). **(B)** Bar graph shows increased MMP-9 protein expression in IVH pups compared to control pups, whereas USSC treated pups showed significantly reduced expression on postnatal day 14 (*$P < 0.05$ Ctrl vs. IVH as well as IVH vs. USSC pups, $n = 5$ pups in each group). The data represent mean ± SD. Assay using rabbit cytokine Array (Ray Biotech., Cat #QAL_CYT-1). **(C)** Scatter plot with bar graph for TaqMan gene expression assay in microscopic dissected SVZ tissue for MMP-9 mRNA was higher in IVH pups with and without USSC treatment on postnatal day 3 (*$P < 0.05$ for Ctrl vs. IVH and **$P < 0.05$ for IVH vs. USSC group, $n = 5$ pups in each group). The data represent mean ± SEM; for postnatal day 3. *P*-values were derived by one-way ANOVA with Tukey's multiple comparisons test. **(D)** Total astrocyte cell count showing that normal and reactive astrocytes increased in IVH whereas after USSC treatment, a reduction in reactive astrocyte cell density was observed on day 14 (*$P < 0.01$ Ctrl vs. IVH and Ctrl vs. USSC for normal astrocytes and *$P < 0.05$ for IVH vs. Ctrl, **$P < 0.05$ for IVH vs. USSC both groups for reactive, $n = 5$ pups in each group). **(E)** Bar graphs show TaqMan gene expression assay in microscopic dissected SVZ tissue for IL-10 mRNA. IL-10 mRNA reduced in IVH pups compared to no IVH controls on day 3; whereas USSC injected pups with IVH showed significantly enhanced IL-10 mRNA expression (*$P < 0.05$ Ctrl vs. IVH, **$P < 0.05$ for IVH vs. USSC, $n = 5$ pups in each group). USSC treated pups showed elevated IL-10 mRNA levels on day 14 (*$P < 0.05$ USSC vs. other two groups, $n = 5$ pups in each group), The data represent mean ± SEM; for each group for three postnatal days 3, 7 and 14. *P*-values were derived by one-way ANOVA with Tukey's multiple comparisons test.

ventricular cross sectional area dimensions on postnatal ages 7 and 14 days, reduced cell infiltration and reduced denudation of ependymal cells from the lateral ventricle walls and choroid plexus (**Figures 2B,C**). Moreover, USSCs restored the reduced AQP1 immunoreactivity of the choroid plexus back up towards baseline (**Figure 3**). By comparison, in the SVZ, the converse pattern occurred where USSCs lowered the elevated AQP1 mRNA on days 7 and 14 after PHH back down toward normal (**Figure 6C**). After PHH, reduced levels of AQP4 immunoreactivity increased along the ependymal wall lining of the lateral ventricles and in the SVZ to nearly normal by day 14 after USSC treatment (**Figures 5A,B** and **Figure 6A**). Viewed together, our AQP1 and AQP4 data correlates with a reduced magnitude of hydrocephalus after USSC treatment consistent with improved CSF fluid homeostasis. This is significant as aquaporin's are ungated transporters that function passively moving water in proportion to their cell surface density. Our observations do not preclude other mechanisms of CSF resorption *via* the glymphatic system or *via* arachnoid villi. Evaluation of those processes will be conducted in future work.

Inflammation is a key determinant of CNS injury where PHH is associated with generalized neuroinflammation (Del Bigio et al., 2003; Deren et al., 2009). PHH is characterized as a nonspecific reactive proliferation of astrocytes and microglia arising in part from lysis of RBCs followed by release of heme and iron (Strahle et al., 2014). PHH-induced inflammation is associated with subependymal gliosis, fibrosing arachnoiditis

and meningeal fibrosis (Cherian et al., 2004a,b). We found that mRNA expression of TGF-β2 and TGF-β3 increased in the SVZ after PHH and that USSC infusion attenuated the expression of these inflammatory isoforms compared to untreated PHH controls (day 14; **Figures 7A,B**). USSCs also reduced the ECM inflammatory scar protein MMP-9 but not its mRNA (**Figures 8B,C**) and the density of reactive astrocytes (**Figure 8D**). The elevation of the anti-inflammatory cytokine IL-10 in both the SVZ and CP following USSC administration (**Figure 8E**) was consistent with this moderating pattern.

CTGF can cooperate with TGF-β to induce sustained fibrosis (Mori et al., 1999) and to exacerbate extracellular matrix production in association with other fibrosis-inducing conditions (Brigstock, 2010). The anti-inflammatory effects of USSCs were also evident as a reduction in CTGF mRNA in the SVZ on day 3 (**Figure 7C**) and in coronal slices of the brain parenchyma on day 14 (**Figure 7D**) as compared to elevated levels after IVH, respectively. TLR and NF-kB pathway mediated inflammation were not significantly altered by USSCs on day 3 (**Figures 4C,D**) suggesting an absent or time-dependent effect or perhaps, an insufficient quantify of cells. Taken together, our observations support an interpretation that USSCs contribute to an anti-inflammatory and regenerative process after injury.

USSCs are novel stem cell that possess significant highly anti-inflammatory and immunomodulatory capacities that have not been investigated in any IVH models of PHH. The earliest preclinical animal studies with PHH focused on mesenchymal stem cells (MSCs) in neonatal and adult models where, unlike our endogenous blood model, the injury was established by injection of exogenous blood (Ahn et al., 2013, 2014; Zhu et al., 2014). Human cord blood derived USSCs are more primitive than MSCs and do not express HLA phenotypic markers that will cause rejection in xenographic transplantation. Putative additional advantages over MSCs are that USSCs possess a higher regenerative and neuroprotective potential as shown in multiple CNS injury models (Kogler et al., 2004; Vinukonda et al., 2019). Beyond these findings, we selected USSCs because they release multiple growth factors and cytokines (Kogler et al., 2005; Mukai et al., 2017). These factors are likely to be involved in cell lineage and differentiation of multiple CNS progenitor cells in the subventricular zone both during development and in the CNS repair after injury (Hatzistergos et al., 2010; Ko et al., 2018). The current report extended our prior observations that demonstrated migration of USSCs to areas of injury and less severe hydrocephalus plus improved motor function (Vinukonda et al., 2019).

Our choice of a rabbit model of PHH was based on a range of pragmatic considerations. Rabbits have a gyrencephalic brain with a perinatal growth plan similar to newborn infants. Moreover, both are vulnerable to vascular injury immediately after birth leading to IVH and development of PHH (Ballabh, 2010, 2014). The pups are large and easy to work with and most conveniently, show glycerol-induced spontaneous rupture of the germinal matrix vasculature creating a reproducible form of IVH (Georgiadis et al., 2008; Chua et al., 2009). Significantly, PHH injury in the CNS of rabbit pups mimics cellular and behavioral effects analogous to observations in human infants including reduced myelination, ventricle dilation and subsequent behavioral deficits and motor impairments (Chua et al., 2009; Vinukonda et al., 2010).

The limitations of this study include the fact that we did not directly measure the rate of CSF turnover and so, could not parse the contributions of the other routes of CSF elimination/production in homeostasis. An additional limitation is that we identified beneficial correlations, yet, we do not know precisely what factors are induced or released by USSCs to produce the observed effects or what mechanism of release exist or how they are activated. Lastly, due to the complexities of the mechanisms examined, we elected only one dose of cells and one timing of the intervention to enable a discovery focused on putative pathways; optimized dosing will be examined in future works as the current report is clearly encouraging as a potential therapy. Other long-term transplant safety concerns, such as tumor formation, chronic rejection, etc. have not been reported thus far but will also be addressed in the future. Finally, AQ5 plays a role primarily in the generation of saliva, tears and pulmonary secretions (Sveinsdottir et al., 2014). To maintain focus in this report, it was neither studied by us in the context of CSF production nor were other channels: AQ0, AQ2, or AQ6 but are now considerations for future work on this topic.

The development of PHH is a common problem in premature infants and remains a major public health concern in the United States and around the world due to its catastrophic impact on long-term neurodevelopmental outcomes. Cell-based therapy is a promising therapeutic modality. USSCs may someday prove to be an alternative as a therapeutic approach in preterm neonates with IVH.

In conclusion, this is the first mechanistic report using human cord blood derived USSCs in the treatment of experimentally induced IVH and PHH. USSCs demonstrated anti-inflammatory effects, restored aquaporin channel expression, and mitigated the severity of PHH. Overall, these results support the continued investigation of the reparative qualities of human cord blood derived USSCs as therapy for severe IVH and for attenuation of PHH that may someday lead to clinical use.

DATA AVAILABILITY STATEMENT

The raw data supporting the conclusions of this article will be made available by the authors, without undue reservation.

ETHICS STATEMENT

The animal study was reviewed and approved by the New York Medical College Institutional Animal Care and Use Committee (IACUC) approved all interventions.

AUTHOR CONTRIBUTIONS

GV: conception, design, performed experiments, assembly, analysis, interpretation of the data, and wrote the manuscript. EL and MC: conception, data interpretation, manuscript writing, financial support, and approval of the manuscript. SS, GK,

CT, EJ, and MW: experimental and statistical methods, review the manuscript. YL and LI: USSC isolation, labeling and BLI imaging. FH, DP, AM, and DF: animal care, sample collection, immunostaining, cell count, neurobehavioral study, cell count, and imaging. All authors contributed to the article and approved the submitted version.

FUNDING

This study was supported by the Boston Children's Health Physicians' Neonatal Division pilot grant for stem cell research (GV and EL) and in part by the Pediatric Cancer Research Foundation (MC).

ACKNOWLEDGMENTS

We thank Rita Daly for proofreading the manuscript and thank Joanne Abraham for technical assistance with images from Cell Biology, New York Medical College.

SUPPLEMENTARY MATERIAL

The Supplementary Material for this article can be found online at: https://www.frontiersin.org/articles/10.3389/fncel.2021.633185/full#supplementary-material.

SUPPLEMENTARY FIGURE 1 | Diagrammatic representation of methods and samples collection procedures. **(A)** The image showing premature rabbit pups delivered from New Zealand, white rabbit (at E29 gestational age, term 32 days). Image showing eight healthy and similar size premature rabbit pups. **(B)** Diagrammatic representation of experimental protocols performed at different postnatal ages. At 3–4 h of postnatal age, newborn pups were treated with 50% intraperitoneal glycerol: water (6.5 g/kg) to induce cerebral hemorrhage. At 24 h of age single dose USSC was injected (1×10^6 cells/dose in each lateral ventricle. The samples for immunohistochemistry (IHC), PCR and lysate preparation were collected on postnatal days 3, 7 and 14. The ventricular cross sectional area was measured on postnatal day 7 and 14. **(C)** Representative of cresyl violet stained coronal section used for measuring total brain area (dotted lines) and ventricle area (marked with continuous line). The coronal sections were scanned using EVOS imaging microscope system (XL core 1000 auto scanner, Thermo Fisher Scientific, Waltham, MA, USA). The mean cross sectional was measured at the level of mid-septal nucleus. The mean cross sectional area was measured on two alternate sections taken from the hippocampus towards the rostral side from the coronal block made at the level of the mid-septal nucleus (total ventricular area is sum of the left and right at level-2 and then averaged for two alternate sections for each pup); 20 μm coronal sections. LV, left ventricle; RV, right ventricle. **(D)** H&E stained representative coronal section showing both lateral ventricles with choroid plexus. The choroid plexus was laser dissected for RNA isolation. **(E)** Immunofluroscence stained coronal section on slide showing choroid plexus immune-signal (selected with yellow dotted lines) stained for AQP1 expression and measured for pixel intensity using image-J software. The mean pixel intensity was normalized with area measured for each image. **(F–H)** Representative images for thick coronal slice and section on slide stained with H&E and AQP4 antibody. The direct measurements of thick coronal slice **(F)** and H&E stained section labeled ependymal wall dissected (dotted lines in red **(G)** represents 0.5–1 mm thick microscopic, dissected tissue) and dense AQP4 expression on the ependymal wall **(H)**.

SUPPLEMENTARY FIGURE 2 | (A,B) Scatter plot with bar graph showing total brain area and parenchymal area at postnatal day 14. **(A)** Comparable total brain area in experimental groups on postnatal day 14 in normal healthy control, IVH saline control and IVH USSC injected pups (single dose USSC (2×10^6 cells/dose). Scatter plot with bar graphs shows total brain area measured on two alternate sections taken from the hippocampus towards the rostral side from the coronal block made at the level of mid-septal nucleus. **(B)** Reduced brain parenchymal area in IVH pups on postnatal day 14. Scatter plot with bar graphs shows total brain parenchymal area that was derived by subtraction of lateral ventricular cross sectional area from total brain area (ventricular cross sectional area data from **Figure 1B** and total brain area data from supplement **Figure 2A**). Both the total brain area and the ventricular cross sectional area are measured on two alternate sections taken from the hippocampus towards the rostral side from the coronal block made at the level of mid-septal nucleus). Each symbol in the experimental groups represent a rabbit pup (*$P < 0.05$ for control vs. IVH; the values represent mean ± SEM; $n = 6$ in each group for both postnatal day 14). *P*-values were derived from one-way ANOVA with Tukey's multiple comparisons test. **(C)** Scatter plot showing mean expression for AQP1 pixel intensity measured using Image-J software (*$P < 0.05$ for control vs. IVH and IVH vs. USSCs; the data represent mean ± SEM, $n = 6$ controls, 4 IVH saline and 4 IVH USSC). Each symbol in the experimental groups represent a single rabbit pup. *P*-values were derived by one-way ANOVA with Tukey's multiple comparisons test. **(D,E)** Representative immunofluorescence images of cryosections labeled with AQP4. Weak to no AQP4 expression in the choroid plexus (CP); 20 μm sections. The scale bar is 100 μm. **(F)** Representative immunofluorescence image of cryosections labeled with negative control Donkey anti-mouse secondary antibody in CP. No AQP1 signal is seen with secondary antibody alone. Secondary antibody, Alexa-Flour 594, donkey anti-mouse (Cat #A21203, Invitrogen Thermo Fisher Scientific, Waltham, MA, USA). Highly cross-adsorbed secondary antibody with minimal cross reactivity to rabbit tissue20 μm sections. The scale bar is 100 μm. **(G)** Representative immunofluorescence image of cryosections labeled with AQP1 in lateral ventricular ependymal wall. Weak to no AQP1 expression in the lateral ventricular wall around the germinal matrix (GM). All images were taken at 20× objective; blue = DAPI stain; 20 μm sections. The scale bar is 100 μm.

SUPPLEMENTARY FIGURE 3 | (A,B) Representative hematoxylin and eosin (H&E) stained coronal section on postnatal day 14 at forebrain level-2 with and without glycerol injected no IVH pups. The total brain area and ventricular area was comparable in normal healthy control vs. glycerol injected no IVH control. The stitched images taken at low power for both postnatal ages; 20 μm sections. The scale bar is 1 mm. **(C,D)**. Representative scatter plot with bar graphs shows cross-sectional area of lateral ventricles measurement **(C)** and total brain area **(D)** on postnatal day 14. The mean cross sectional measured on two alternate sections taken from the hippocampus towards the rostral side from the coronal block made at the level of the mid-septal nucleus (total ventricular area is sum of the left and right at level-2 and averaged for two alternate section for each pup). Each symbol in the experimental groups represent a rabbit pup (no significant differences in healthy control vs. glycerol no IIVH control; the values represent mean ± SEM; $n = 4$ in each group). **(E,F)** Representative immunofluorescence image of cryosections labeled with negative control for AQP4 Donkey anti-mouse secondary antibody in lateral ventricle wall. No AQP4 signal with secondary antibody alone cryosections stained on the lateral ventricle on the lateral side **(E)** and ventricle wall around the GM **(F)**. Secondary antibody, Alexa-Flour 594, donkey anti-mouse (Cat #A21203, Invitrogen Thermo Fisher Scientific, Waltham, MA, USA). Highly cross-adsorbed secondary antibody with minimal cross reactivity to rabbit tissue. 20 μm sections. The scale bar is 100 μm. **(G–J)** Bioluminescence live image (BLI) of USSC administration by intracerebroventricular injection in IVH premature rabbit pups. **(G)** Representative BLI live image for IVH pup after single dose of USSC (right image) and no USSC injected negative control pup (left image). The strong red fluorescence signal indicates highest USSC density at postnatal day 3 (2×10^6 cells/dose). **(H)** BLI image showing dispersed USSC over postnatal day 7 and day 14 **(H)**. **(I,J)** Bioluminescence (BLI) and anatomical structures. **(I)** Image of brain coronal slice from day 3 IVH USSC injected pups, showing strong BLI signal **(I)**, and the IVH-saline control pup no USSC injected coronal slice show no BLI signals. **(J)** Coronal thick slices of brain showing blood in the ventricles. **(K,L)** Representative Immunofluroscence images of cryosections for tracking intracerebral ventricular (ICV) delivered USSC stem cells. **(K)** Using a human-specific nuclear antibody the illustration shows the USSCs (green) and rabbit cells (DAPI—blue in **L**). The data indicates healthy live cells in the rabbit brain parenchyma. Note: DAPI stains both rabbit and Human cells whereas human-nuclear antibody stains only human USSC cells. All images were taken at 20× objective; blue = DAPI stain; 20 μm sections. The scale bar is 100 μm.

REFERENCES

Ahn, S. Y., Chang, Y. S., and Park, W. S. (2014). Mesenchymal stem cells transplantation for neuroprotection in preterm infants with severe intraventricular hemorrhage. *Korean J. Pediatr.* 57, 251–256. doi: 10.3345/kjp.2014.57.6.251

Ahn, S. Y., Chang, Y. S., Sung, D. K., Sung, S. I., Yoo, H. S., Lee, J. H., et al. (2013). Mesenchymal stem cells prevent hydrocephalus after severe intraventricular hemorrhage. *Stroke* 44, 497–504. doi: 10.1161/STROKEAHA.112.679092

Amiry-Moghaddam, M., and Ottersen, O. P. (2003). The molecular basis of water transport in the brain. *Nat. Rev. Neurosci.* 4, 991–1001. doi: 10.1038/nrn1252

Ballabh, P. (2010). Intraventricular hemorrhage in premature infants: mechanism of disease. *Pediatr. Res.* 67, 1–8. doi: 10.1203/PDR.0b013e3181c1b176

Ballabh, P. (2014). Pathogenesis and prevention of intraventricular hemorrhage. *Clin. Perinatol.* 41, 47–67. doi: 10.1016/j.clp.2013.09.007

Bloch, O., Papadopoulos, M. C., Manley, G. T., and Verkman, A. S. (2005). Aquaporin-4 gene deletion in mice increases focal edema associated with staphylococcal brain abscess. *J. Neurochem.* 95, 254–262. doi: 10.1111/j.1471-4159.2005.03362.x

Braun, A., Xu, H., Hu, F., Kocherlakota, P., Siegel, D., Chander, P., et al. (2007). Paucity of pericytes in germinal matrix vasculature of premature infants. *J. Neurosci.* 27, 12012–12024. doi: 10.1523/JNEUROSCI.3281-07.2007

Brigstock, D. R. (2010). Connective tissue growth factor (CCN2, CTGF) and organ fibrosis: lessons from transgenic animals. *J. Cell Commun. Signal.* 4, 1–4. doi: 10.1007/s12079-009-0071-5

Campos-Ordonez, T., Herranz-Perez, V., Chaichana, K. L., Rincon-Torroella, J., Rigamonti, D., Garcia-Verdugo, J. M., et al. (2014). Long-term hydrocephalus alters the cytoarchitecture of the adult subventricular zone. *Exp. Neurol.* 261, 236–244. doi: 10.1016/j.expneurol.2014.05.011

Cherian, S., Thoresen, M., Silver, I. A., Whitelaw, A., and Love, S. (2004a). Transforming growth factor-betas in a rat model of neonatal posthemorrhagic hydrocephalus. *Neuropathol. Appl. Neurobiol.* 30, 585–600. doi: 10.1111/j.1365-2990.2004.00588.x

Cherian, S., Whitelaw, A., Thoresen, M., and Love, S. (2004b). The pathogenesis of neonatal post-hemorrhagic hydrocephalus. *Brain Pathol.* 14, 305–311. doi: 10.1111/j.1750-3639.2004.tb00069.x

Christian, E. A., Jin, D. L., Attenello, F., Wen, T., Cen, S., Mack, W. J., et al. (2016). Trends in hospitalization of preterm infants with intraventricular hemorrhage and hydrocephalus in the United States, 2000–2010. *J. Neurosurg. Pediatr.* 17, 260–269. doi: 10.3171/2015.7.PEDS15140

Chua, C. O., Chahboune, H., Braun, A., Dummula, K., Chua, C. E., Yu, J., et al. (2009). Consequences of intraventricular hemorrhage in a rabbit pup model. *Stroke* 40, 3369–3377. doi: 10.1161/STROKEAHA.109.549212

Del Bigio, M. R., Wilson, M. J., and Enno, T. (2003). Chronic hydrocephalus in rats and humans: white matter loss and behavior changes. *Ann. Neurol.* 53, 337–346. doi: 10.1002/ana.10453

Deren, K. E., Forsyth, J., Abdullah, O., Hsu, E. W., Klinge, P. M., Silverberg, G. D., et al. (2009). Low levels of amyloid-beta and its transporters in neonatal rats with and without hydrocephalus. *Cerebrospinal Fluid Res.* 6:4. doi: 10.1186/1743-8454-6-4

Dohare, P., Kidwai, A., Kaur, J., Singla, P., Krishna, S., Klebe, D., et al. (2019). GSK3beta inhibition restores impaired neurogenesis in preterm neonates with intraventricular hemorrhage. *Cereb. Cortex* 29, 3482–3495. doi: 10.1093/cercor/bhy217

Douglas, M. R., Daniel, M., Lagord, C., Akinwunmi, J., Jackowski, A., Cooper, C., et al. (2009). High CSF transforming growth factor beta levels after subarachnoid hemorrhage: association with chronic communicating hydrocephalus. *J. Neurol. Neurosurg. Psychiatry* 80, 545–550. doi: 10.1136/jnnp.2008.155671

Filippidis, A. S., Kalani, M. Y., and Rekate, H. L. (2012). Hydrocephalus and aquaporins: the role of aquaporin-4. *Acta Neurochir. Suppl.* 113, 55–58. doi: 10.1007/978-3-7091-0923-6_12

Gao, C., Du, H., Hua, Y., Keep, R. F., Strahle, J., and Xi, G. (2014). Role of red blood cell lysis and iron in hydrocephalus after intraventricular hemorrhage. *J. Cereb. Blood Flow Metab.* 34, 1070–1075. doi: 10.1038/jcbfm.2014.56

Georgiadis, P., Xu, H., Chua, C., Hu, F., Collins, L., Huynh, C., et al. (2008). Characterization of acute brain injuries and neurobehavioral profiles in a rabbit model of germinal matrix hemorrhage. *Stroke* 39, 3378–3388. doi: 10.1161/STROKEAHA.107.510883

Gomes, F. C., Sousa Vde, O., and Romao, L. (2005). Emerging roles for TGF-beta1 in nervous system development. *Int. J. Dev. Neurosci.* 23, 413–424. doi: 10.1016/j.ijdevneu.2005.04.001

Gram, M., Sveinsdottir, S., Cinthio, M., Sveinsdottir, K., Hansson, S. R., Morgelin, M., et al. (2014). Extracellular hemoglobin—mediator of inflammation and cell death in the choroid plexus following preterm intraventricular hemorrhage. *J. Neuroinflammation* 11:200. doi: 10.1186/s12974-014-0200-9

Gunnarson, E., Zelenina, M., and Aperia, A. (2004). Regulation of brain aquaporins. *Neuroscience* 129, 947–955. doi: 10.1016/j.neuroscience.2004.08.022

Hall-Glenn, F., and Lyons, K. M. (2011). Roles for CCN2 in normal physiological processes. *Cell. Mol. Life Sci.* 68, 3209–3217. doi: 10.1007/s00018-011-0782-7

Hatzistergos, K. E., Quevedo, H., Oskouei, B. N., Hu, Q., Feigenbaum, G. S., Margitich, I. S., et al. (2010). Bone marrow mesenchymal stem cells stimulate cardiac stem cell proliferation and differentiation. *Circ. Res.* 107, 913–922. doi: 10.1161/CIRCRESAHA.110.222703

Hsieh, H. L., Wang, H. H., Wu, W. B., Chu, P. J., and Yang, C. M. (2010). Transforming growth factor-beta1 induces matrix metalloproteinase-9 and cell migration in astrocytes: roles of ROS-dependent ERK- and JNK-NF-kB pathways. *J. Neuroinflammation* 7:88. doi: 10.1186/1742-2094-7-88

Igarashi, H., Tsujita, M., Kwee, I. L., and Nakada, T. (2014). Water influx into cerebrospinal fluid is primarily controlled by aquaporin-4, not by aquaporin-1: 17O JJVCPE MRI study in knockout mice. *Neuroreport* 25, 39–43. doi: 10.1097/WNR.0000000000000042

Imitola, J., Raddassi, K., Park, K. I., Mueller, F. J., Nieto, M., Teng, Y. D., et al. (2004). Directed migration of neural stem cells to sites of CNS injury by the stromal cell-derived factor 1alpha/CXC chemokine receptor 4 pathway. *Proc. Natl. Acad. Sci. U S A* 101, 18117–18122. doi: 10.1073/pnas.0408258102

Jin, K. L., Mao, X. O., and Greenberg, D. A. (2000). Vascular endothelial growth factor: direct neuroprotective effect in *in vitro* ischemia. *Proc. Natl. Acad. Sci. U S A* 97, 10242–10247. doi: 10.1073/pnas.97.18.10242

Kaestner, S., and Dimitriou, I. (2013). TGF beta1 and TGF beta2 and their role in posthemorrhagic hydrocephalus following SAH and IVH. *J. Neurol. Surg. A Cent. Eur. Neurosurg.* 74, 279–284. doi: 10.1055/s-0033-1342929

Karimy, J. K., Zhang, J., Kurland, D. B., Theriault, B. C., Duran, D., Stokum, J. A., et al. (2017). Inflammation-dependent cerebrospinal fluid hypersecretion by the choroid plexus epithelium in posthemorrhagic hydrocephalus. *Nat. Med.* 23, 997–1003. doi: 10.1038/nm.4361

Kitazawa, K., and Tada, T. (1994). Elevation of transforming growth factor-beta 1 level in cerebrospinal fluid of patients with communicating hydrocephalus after subarachnoid hemorrhage. *Stroke* 25, 1400–1404. doi: 10.1161/01.str.25.7.1400

Ko, H. R., Ahn, S. Y., Chang, Y. S., Hwang, I., Yun, T., Sung, D. K., et al. (2018). Human UCB-MSCs treatment upon intraventricular hemorrhage contributes to attenuate hippocampal neuron loss and circuit damage through BDNF-CREB signaling. *Stem Cell Res. Ther.* 9:326. doi: 10.1186/s13287-018-1052-5

Kogler, G., Radke, T. F., Lefort, A., Sensken, S., Fischer, J., Sorg, R. V., et al. (2005). Cytokine production and hematopoiesis supporting activity of cord blood-derived unrestricted somatic stem cells. *Exp. Hematol.* 33, 573–583. doi: 10.1016/j.exphem.2005.01.012

Kogler, G., Sensken, S., Airey, J. A., Trapp, T., Muschen, M., Feldhahn, N., et al. (2004). A new human somatic stem cell from placental cord blood with intrinsic pluripotent differentiation potential. *J. Exp. Med.* 200, 123–135. doi: 10.1084/jem.20040440

Koschnitzky, J. E., Keep, R. F., Limbrick, D. D., Jr., Mcallister, J. P., 2nd, Morris, J. A., Strahle, J., et al. (2018). Opportunities in posthemorrhagic hydrocephalus research: outcomes of the hydrocephalus association posthemorrhagic hydrocephalus workshop. *Fluids Barriers CNS* 15:11. doi: 10.1186/s12987-018-0096-3

Lehmann, G. L., Gradilone, S. A., and Marinelli, R. A. (2004). Aquaporin water channels in central nervous system. *Curr. Neurovasc. Res.* 1, 293–303. doi: 10.2174/1567202043362081

Ley, D., Romantsik, O., Vallius, S., Sveinsdottir, K., Sveinsdottir, S., Agyemang, A. A., et al. (2016). High presence of extracellular hemoglobin

in the periventricular white matter following preterm intraventricular hemorrhage. *Front. Physiol.* 7:330. doi: 10.3389/fphys.2016.00330

Liao, Y., Itoh, M., Yang, A., Zhu, H., Roberts, S., Highet, A. M., et al. (2014). Human cord blood-derived unrestricted somatic stem cells promote wound healing and have therapeutic potential for patients with recessive dystrophic epidermolysis bullosa. *Cell Transplant.* 23, 303–317. doi: 10.3727/096368913X663569

Liu, A. M., Lu, G., Tsang, K. S., Li, G., Wu, Y., Huang, Z. S., et al. (2010). Umbilical cord-derived mesenchymal stem cells with forced expression of hepatocyte growth factor enhance remyelination and functional recovery in a rat intracerebral hemorrhage model. *Neurosurgery* 67, 357–365. doi: 10.1227/01.NEU.0000371983.06278.B3

Livak, K. J., and Schmittgen, T. D. (2001). Analysis of relative gene expression data using real-time quantitative PCR and the $2^{-\Delta\Delta\ CT}$ method. *Methods* 25, 402–408. doi: 10.1006/meth.2001.1262

Mao, X., Enno, T. L., and Del Bigio, M. R. (2006). Aquaporin 4 changes in rat brain with severe hydrocephalus. *Eur. J. Neurosci.* 23, 2929–2936. doi: 10.1111/j.1460-9568.2006.04829.x

Mori, T., Kawara, S., Shinozaki, M., Hayashi, N., Kakinuma, T., Igarashi, A., et al. (1999). Role and interaction of connective tissue growth factor with transforming growth factor-beta in persistent fibrosis: a mouse fibrosis model. *J. Cell. Physiol.* 181, 153–159. doi: 10.1002/(SICI)1097-4652(199910)181:1<153::AID-JCP16>3.0.CO;2-K

Mukai, T., Mori, Y., Shimazu, T., Takahashi, A., Tsunoda, H., Yamaguchi, S., et al. (2017). Intravenous injection of umbilical cord-derived mesenchymal stromal cells attenuates reactive gliosis and hypomyelination in a neonatal intraventricular hemorrhage model. *Neuroscience* 355, 175–187. doi: 10.1016/j.neuroscience.2017.05.006

Opatz, J., Kury, P., Schiwy, N., Jarve, A., Estrada, V., Brazda, N., et al. (2009). SDF-1 stimulates neurite growth on inhibitory CNS myelin. *Mol. Cell. Neurosci.* 40, 293–300. doi: 10.1016/j.mcn.2008.11.002

Oshio, K., Watanabe, H., Song, Y., Verkman, A. S., and Manley, G. T. (2005). Reduced cerebrospinal fluid production and intracranial pressure in mice lacking choroid plexus water channel aquaporin-1. *FASEB J.* 19, 76–78. doi: 10.1096/fj.04-1711fje

Papadopoulos, M. C., and Verkman, A. S. (2013). Aquaporin water channels in the nervous system. *Nat. Rev. Neurosci.* 14, 265–277. doi: 10.1038/nrn3468

Paul, L., Madan, M., Rammling, M., Chigurupati, S., Chan, S. L., and Pattisapu, J. V. (2011). Expression of aquaporin 1 and 4 in a congenital hydrocephalus rat model. *Neurosurgery* 68, 462–473. doi: 10.1227/NEU.0b013e3182011860

Rosell, A., Ortega-Aznar, A., Alvarez-Sabin, J., Fernandez-Cadenas, I., Ribo, M., Molina, C. A., et al. (2006). Increased brain expression of matrix metalloproteinase-9 after ischemic and hemorrhagic human stroke. *Stroke* 37, 1399–1406. doi: 10.1161/01.STR.0000223001.06264.af

Schmittgen, T. D. (2001). Real-time quantitative PCR. *Methods* 25, 383–385. doi: 10.1006/meth.2001.1260

Strahle, J. M., Garton, T., Bazzi, A. A., Kilaru, H., Garton, H. J., Maher, C. O., et al. (2014). Role of hemoglobin and iron in hydrocephalus after neonatal intraventricular hemorrhage. *Neurosurgery* 75, 696–705. doi: 10.1227/NEU.0000000000000524

Sun, Y., Jin, K., Xie, L., Childs, J., Mao, X. O., Logvinova, A., et al. (2003). VEGF-induced neuroprotection, neurogenesis and angiogenesis after focal cerebral ischemia. *J. Clin. Invest.* 111, 1843–1851. doi: 10.1172/JCI17977

Sveinsdottir, S., Gram, M., Cinthio, M., Sveinsdottir, K., Mörgelin, M., Ley, D., et al. (2014). Altered expression of aquaporin 1 and 5 in the choroid plexus following preterm intraventricular hemorrhage. *Dev. Neurosci.* 36, 542–551. doi: 10.1159/000366058

Trillo-Contreras, J. L., Toledo-Aral, J. J., Echevarria, M., and Villadiego, J. (2019). AQP1 and AQP4 Contribution to cerebrospinal fluid homeostasis. *Cells* 8:197. doi: 10.3390/cells8020197

Vella, J., Zammit, C., Di Giovanni, G., Muscat, R., and Valentino, M. (2015). The central role of aquaporins in the pathophysiology of ischemic stroke. *Front. Cell. Neurosci.* 9:108. doi: 10.3389/fncel.2015.00108

Verkman, A. S., Tradtrantip, L., Smith, A. J., and Yao, X. (2017). Aquaporin water channels and hydrocephalus. *Pediatr. Neurosurg.* 52, 409–416. doi: 10.1159/000452168

Vinukonda, G., Csiszar, A., Hu, F., Dummula, K., Pandey, N. K., Zia, M. T., et al. (2010). Neuroprotection in a rabbit model of intraventricular hemorrhage by cyclooxygenase-2, prostanoid receptor-1 or tumour necrosis factor-alpha inhibition. *Brain* 133, 2264–2280. doi: 10.1007/s00011-021-01455-0

Vinukonda, G., Liao, Y., Hu, F., Ivanova, L., Purohit, D., Finkel, D. A., et al. (2019). Human cord blood-derived unrestricted somatic stem cell infusion improves neurobehavioral outcome in a rabbit model of intraventricular hemorrhage. *Stem Cells Transl. Med.* 8, 1157–1169. doi: 10.1002/sctm.19-0082

Whitelaw, A., Thoresen, M., and Pople, I. (2002). Posthemorrhagic ventricular dilatation. *Arch. Dis. Child. Fetal Neonatal Ed.* 86, F72–F74. doi: 10.1136/fn.86.2.F72

Zelenina, M. (2010). Regulation of brain aquaporins. *Neurochem. Int.* 57, 468–488. doi: 10.1016/j.neuint.2010.03.022

Zhu, W., Gao, Y., Chang, C. F., Wan, J. R., Zhu, S. S., and Wang, J. (2014). Mouse models of intracerebral hemorrhage in ventricle, cortex and hippocampus by injections of autologous blood or collagenase. *PLoS One* 9:e97423. doi: 10.1371/journal.pone.0097423

Conflict of Interest: The authors declare that the research was conducted in the absence of any commercial or financial relationships that could be construed as a potential conflict of interest.

frontiers | Frontiers in Pediatrics

ORIGINAL RESEARCH
published: 28 April 2022
doi: 10.3389/fped.2022.793189

Neurogenesis Is Reduced at 48 h in the Subventricular Zone Independent of Cell Death in a Piglet Model of Perinatal Hypoxia-Ischemia

Daniel Alonso-Alconada[1], Pierre Gressens[2], Xavier Golay[3] and Nicola J. Robertson[4,5]*

[1] Department of Cell Biology and Histology, School of Medicine and Nursing, University of the Basque Country (UPV/EHU), Leioa, Spain, [2] NeuroDiderot, Inserm, Université de Paris, Paris, France, [3] Department of Brain Repair and Rehabilitation, Institute of Neurology, University College London, London, United Kingdom, [4] Institute for Women's Health, University College London, London, United Kingdom, [5] Edinburgh Neuroscience, Centre for Clinical Brain Sciences, The University of Edinburgh, Edinburgh, United Kingdom

Cellular and tissue damage triggered after hypoxia-ischemia (HI) can be generalized and affect the neurogenic niches present in the central nervous system. As neuroregeneration may be critical for optimizing functional recovery in neonatal encephalopathy, the goal of the present work was to investigate the neurogenic response to HI in the neurogenic niche of the subventricular zone (SVZ) in the neonatal piglet. A total of 13 large white male piglets aged <24 h were randomized into two groups: i) HI group (n = 7), animals submitted to transient cerebral HI and resuscitation; and ii) Control group (n = 6), non-HI animals. At 48 h, piglets were euthanized, and the SVZ and its surrounding regions, such as caudate and periventricular white matter, were analyzed for histology using hematoxylin-eosin staining and immunohistochemistry by evaluating the presence of cleaved caspase 3 and TUNEL positive cells, together with the cell proliferation/neurogenesis markers Ki67 (cell proliferation), GFAP (neural stem cells processes), Sox2 (neural stem/progenitor cells), and doublecortin (DCX, a marker of immature migrating neuroblasts). Hypoxic-ischemic piglets showed a decrease in cellularity in the SVZ independent of cell death, together with decreased length of neural stem cells processes, neuroblast chains area, DCX immunoreactivity, and lower number of Ki67 + and Ki67 + Sox2 + cells. These data suggest a reduction in both cell proliferation and neurogenesis in the SVZ of the neonatal piglet, which could in turn compromise the replacement of the lost neurons and the achievement of global repair.

Keywords: newborn, neonatal brain, hypoxia-ischemia, neurogenesis, subventricular zone

OPEN ACCESS

Edited by:
Graeme R. Polglase, Monash University, Australia

Reviewed by:
Vladimir Riljak, Charles University, Czechia
Robert Galinsky, The Ritchie Centre, Hudson Institute of Medical Research, Australia

****Correspondence:***
Daniel Alonso-Alconada
daniel.alonsoa@ehu.eus

Specialty section:
This article was submitted to Neonatology, a section of the journal Frontiers in Pediatrics

Received: *11 October 2021*
Accepted: *04 April 2022*
Published: *28 April 2022*

Citation:
Alonso-Alconada D, Gressens P, Golay X and Robertson NJ (2022) Neurogenesis Is Reduced at 48 h in the Subventricular Zone Independent of Cell Death in a Piglet Model of Perinatal Hypoxia-Ischemia. Front. Pediatr. 10:793189. doi: 10.3389/fped.2022.793189

INTRODUCTION

During embryonic development, the formation of the central nervous system (CNS) results from a tightly regulated balance between the processes of apoptosis and neurogenesis, which occurs accomplished in time and space (1, 2). At the time of birth, however, the human brain is not yet fully developed [almost 2/3 of the cells are produced after birth; (3)], so intrapartum-related insults like hypoxia-ischemia (HI) may disbalance the apoptosis-neurogenesis equilibrium, obstructing the

proper maturational process and leading to life-long sequelae (4). Neonatal HI triggers a series of complex and harmful metabolic cascades that lead to generalized cellular and tissue damage and affect numerous gray and white matter brain regions, but less is known about the effect of HI on the neurogenic niches.

In the CNS, the two neurogenic niches that retain neural stem cells and progenitors with regenerative potential are the subgranular zone of the hippocampal dentate gyrus and the subventricular zone (SVZ) of the lateral ventricle (5). To date, controversy exists around how HI modifies the neurogenic response of the newborn brain. While some reports indicate that HI suppresses the endogenous genesis of neural stem cells and progenitors (6, 7), other studies point out in the opposite direction, suggesting that neurogenesis is increased in the SVZ after HI (8, 9).

Post-injury neurogenesis is a complex process that can be affected by a number of factors, including the duration, type, location, and intensity of damage (10). For instance, the SVZ has shown to be stricken after severe HI (6), whereas in moderate brain injury, neurogenesis was stimulated (9, 11). The period of time since the insult also modulates the neurogenic response to damage: after an initial phase of decreased cell proliferation accompanied by extensive cell death in the rodent SVZ (6, 12), the morphology of the ipsilateral SVZ has shown to increase its size, a phenomenon attributed to augmented cell proliferation (8, 9, 11). Since HI typically occurs at a time when these niches are actively generating new brain cells, we hypothesize that the endogenous neurogenic capability of the SVZ contributing to the plasticity of the newborn brain and/or to tissue remodeling could be compromised if this area is affected.

As described, most of the work on neural stem cells and progenitors of the SVZ has been conducted in rodents. The newborn piglet SVZ shares many anatomical similarities with the SVZ in the human infant, and the SVZ persists beyond fetal development serving as a source of piglet new cells (13). The aim of this study was to investigate if HI affects the SVZ of the neonatal piglet by evaluating its possible changes in cellularity, cell death, cell proliferation, and neurogenesis early after a quantified global cerebral hypoxic-ischemic insult.

MATERIALS AND METHODS

All experimentation was in accordance with UK Home Office Guidelines [Animals (Scientific Procedures) Act 1986] and approved by the Animal Care and Use Committee of University College London Biological Services and Institute of Neurology.

Animal Experiments and Surgical Preparation

Thirteen large white male piglets aged <24 h were included in this study. Briefly, piglets were sedated with intramuscular midazolam (0.2 mg/kg), and arterial O_2 saturation was monitored (Nonin Medical). Isoflurane anesthesia (4% vol/vol) was applied *via* a facemask during tracheostomy and intubation and was maintained (3% during surgery, 2% otherwise). Piglets were mechanically ventilated to maintain arterial partial pressures of O_2 (PaO_2; 8–13 kPa) and CO_2 ($PaCO_2$; 4.5–6.5 kPa) allowing for temperature correction of the arterial blood sample.

An umbilical venous catheter was inserted to infuse maintenance fluids (10% dextrose, 60 ml/kg/day), fentanyl (3–6 μg/kg/h), and antibiotics (benzylpenicillin 50 mg/kg and gentamicin 2.5 mg/kg, every 12 h). An umbilical arterial catheter was inserted for continuous heart rate (HR) and mean arterial blood pressure (MABP) monitoring and 6-h blood sampling to measure PaO_2, $PaCO_2$, pH, electrolytes, glucose (3–10 mmol/L), and lactate (Abbott Laboratories). Bolus infusions of colloid (Gelofusin, B Braun Medical Ltd.) and inotropes maintained MABP >40 mmHg. Arterial lines were maintained by infusing 0.9% saline solution (Baxter, 1 ml/h) with heparin sodium (1 IU/ml) to prevent line blockage. Both common carotid arteries were surgically isolated at the level of the fourth cervical vertebra and encircled by remotely controlled vascular occluders (OC2A, *In Vivo* Metric). After surgery, piglets were positioned prone in a plastic pod with their heads immobilized.

Cerebral Hypoxia-Ischemia

Before insult, piglets were randomized into two groups, using a computer-generated randomization sequence and opaque sequentially numbered envelopes. The hypoxic-ischemic (HI, $n = 7$) insult was performed according to the original hypoxia-ischemia protocol with transient carotid artery occlusion and contemporaneous hypoxia (14–16). Non-HI animals were not positioned in the scanner nor were subjected to hypoxia or ischemia, serving as controls (Control, $n = 6$).

A magnetic resonance spectroscopy (MRS) surface coil was secured to the cranium, and the animal was positioned in a 9.4 Tesla Agilent MRI scanner, while in the MRI scanner, transient HI was induced by remote occlusion of both common carotid arteries, using inflatable vascular occluders, and reducing the fraction of inspired oxygen (FiO_2) to 12% (vol/vol).

During HI ($n = 7$), cerebral energetics were monitored every 2 min by phosphorus (31P) MRS, and the β-nucleotide triphosphate (β-NTP; mainly ATP) peak height was automatically measured. When β-NTP peak height had fallen to 40% of baseline, FiO_2 was adjusted in order to stabilize β-NTP at that level for 12.5 min. At the end of this 12.5-min period, the occluders were deflated and FiO_2 was normalized; 31P spectra were acquired for a further 1 h to monitor recovery from HI. The time integral of the decrement of β-NTP/EPP [EPP = exchangeable phosphate pool = inorganic phosphate + phosphocreatine + (2γ + β)-NTP] during HI and the first 1 h of resuscitation quantified the acute energy depletion. Piglets were maintained normothermic (rectal temperature 38.5°C) throughout the entire experiment by using a warmed water mattress (Tecotherm) above and below the animal. All animals received continuous physiological monitoring (SA instruments) and intensive life support throughout experimentation.

Histology and Immunohistochemistry

At 48 h, piglets were euthanized with pentobarbital, and the brain was fixed by cardiac perfusion with cold 4% paraformaldehyde, dissected out, and post-fixed at 4°C in 2% paraformaldehyde

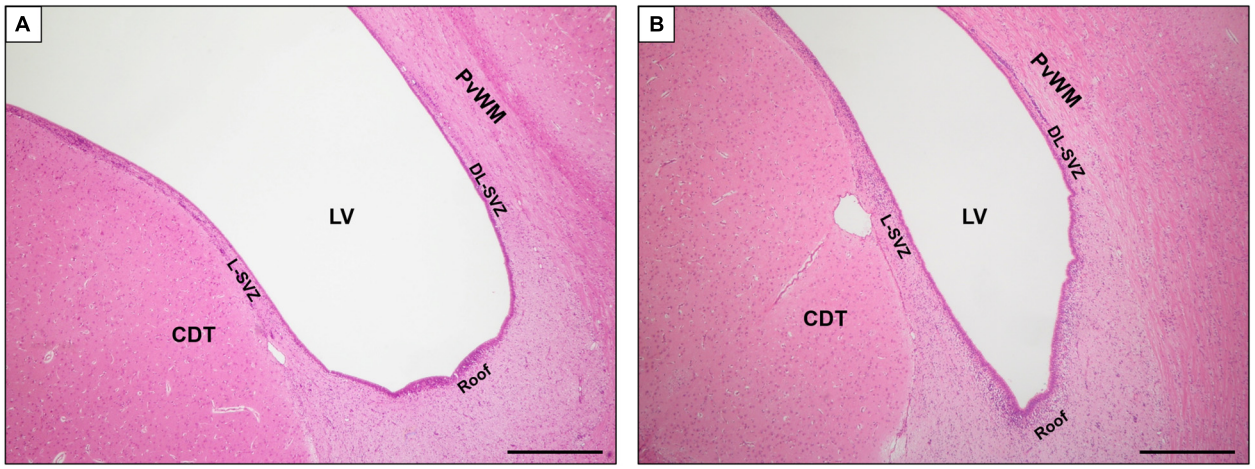

FIGURE 1 | Magnified image of coronal section of the SVZ at bregma –2.0 **(A)** and –4.0 **(B)** brain levels sampled in this study. H&E staining. LV, lateral ventricle; SVZ, subventricular zone; DL-SVZ, dorsolateral-SVZ; L-SVZ, lateral-SVZ. Original magnification 40×. Scale bar: 500 μm.

for 7 days; 5-mm-thick coronal slices of the right hemisphere, starting from anterior to the optic chiasma, were embedded in paraffin, sectioned to 5 μm thickness, and stained with H&E to validate the bregma for analysis.

For each animal, 2 levels (bregma −2.0 and −4.0) were evaluated. There were five regions of interest, namely, the SVZ, which was in turn divided into 3 subareas (**Figure 1**): roof, dorsolateral-SVZ (DL-SVZ, close to the periventricular white matter), and lateral-SVZ (L-SVZ, apposed to the caudate nucleus); and the caudate nucleus and the periventricular white matter, both being SVZ-surrounding regions (**Figure 1**).

Hematoxylin-Eosin Staining

Paraffin-embedded brain samples were stained following the automated procedure corresponding to Hematoxylin-Eosin (H&E) staining by a Shandon Varistain V24-4 (Thermo Electron Corporation, United States) using Harris hematoxylin (Shandon Gill 2 Hematoxylin, Thermo Scientific, United States) and eosin Y (Shandon Eosin-Y Alcoholic, Thermo Scientific, United States).

Histological Examination of Cell Death in Hematoxylin-Eosin Samples

Histological changes were evaluated in the SVZ (roof, DL-SVZ, and L-SVZ), caudate nucleus, and periventricular white matter brain regions at both bregma −2.0 and −4.0 levels (**Supplementary Figures 1, 2**) by using H&E staining and analyzed with Fiji/ImageJ image software. For each animal, level, and section, a total of fifteen non-overlapping microphotographs (3 from each area) were taken at 400 × magnification in a light field optical microscope (Olympus BX50F4, Japan). A blinded histologist counted morphologically well-preserved cells (undamaged), together with cells with apoptotic or necrotic features. Apoptotic-like cells were characterized by the presence of nuclear karyorrhexis and low cytoplasmic change, whereas necrotic cells were identified by a pyknotic nucleus or no nucleus, along with a swollen, eosinophilic cytoplasm (17). We did not count apoptotic nor necrotic profiles that were within or adjacent to blood vessels to avoid including apoptotic/necrotic endothelial and white blood cells. The undamaged, apoptotic and necrotic cell count was averaged from 3 high-power fields from 3 slides from the same region in each animal, and values are given as cells per mm^2.

Transferase-Mediated Incorporation of Digoxigenin-Labeled Nucleotide

DNA fragmentation was revealed by using the terminal deoxynucleotidyl transferase-mediated incorporation of digoxigenin-labeled nucleotide (TUNEL) assay (Roche, Burgess Hill, United Kingdom). Briefly, *in situ* end-labeling of fragmented DNA was carried out on brain slices that were first deparaffinated, hydrated, pretreated in 3% H_2O_2, and subjected to a protease-K digestion (Promega, Southampton, United Kingdom). TUNEL was visualized using avidin-biotinylated horseradish complex (ABC, Vector Laboratories, Peterborough, United Kingdom) and diaminobenzidine/H_2O_2 (DAB, Sigma, Poole, United Kingdom) enhanced with $CoSO_4$ and $NiCl_2$. Finally, TUNEL sections were dehydrated and cover-slipped with DPX (VWR, Leighton Buzzard, United Kingdom).

Caspase 3 Immunohistochemistry

After deparaffination, antigen retrieval was performed using a pH 6 solution of 10 mM sodium citrate + 0.05% Tween20 in distilled water where samples were boiled 3 times before being kept for 20 min at 95–98°C. After cooling at room temperature, the endogenous peroxidase was blocked, and samples were incubated in 5% bovine serum albumin blocking buffer. Brain slices were then incubated with primary antibody rabbit anti-Caspase 3 (1:100, 9661 L, Cell Signaling, United States) overnight. The next day, samples were incubated with a biotin-conjugated secondary antibody (1:500, goat anti-rabbit, 65-6140, Invitrogen, United States) for 1 h at room temperature followed

by horseradish peroxidase-streptavidin conjugate (1:500, 43-4323, Thermo Fisher, United States) plus diaminobenzidine. Right after, sections were counterstained with hematoxylin and mounted with DPX.

An investigator blind to the treatment group performed the quantitative analyses of caspase 3 expression. For each level, section, and brain region, caspase-3 positive cells were counted in three fields (at 40 × magnification, with an area of 0.077 mm^2) and the average was converted into counts per mm^2.

Fluorescent Immunohistochemistry

Brain slices for fluorescence immunohistochemistry were managed as detailed in the "Immunohistochemistry" section until incubation with primary antibody. For single labeling, radial-glia/neural stem cells were identified using an anti-glial fibrillary acidic protein (GFAP) antibody to assess neurogenic activity close to the ventricular wall (mouse anti-GFAP, 1:100, MA5-12023, Thermo Fisher, United States); an anti-doublecortin (DCX) antibody was used to identify young neurons/neuroblasts (mouse anti-DCX, 1:50, sc-271390, Santa Cruz Biotechnology, United States); cell proliferation was identified by an anti-Ki67 antibody (mouse anti-Ki67; 1:50, STJ96966, St Johns Labs, United Kingdom). Double immunohistochemical staining was used to detect the cellular co-localization of Ki67 with Sox2 (neural stem/progenitor cells; 1:100, Santa Cruz Biotechnology, United States). Immunoreactivity was revealed using Alexa Fluor 488 and Texas Red (1:300, Thermo Fisher, United States) secondary antibodies incubated in the dark for 1 h at room temperature. After final washes, fluoromount aqueous mounting medium (F4680, Sigma) was added, and each section was covered by a cover slip. Negative controls received identical treatment except for the omission of primary antibodies and showed no specific staining.

Histological Evaluation of Markers of Neurogenesis

Sections were examined using Fiji/ImageJ image software, and analyses and quantifications were performed by two independent investigators blinded to the treatment group. We extended the analysis including the cell-dense band of DCX + young neurons along the walls of the lateral ventricle levels (**Supplementary Figure 3**). The SVZ is further subdivided into roof, dorsolateral-SVZ (DL-SVZ, close to the periventricular white matter), and lateral-SVZ (L-SVZ, apposed to the caudate nucleus). For each animal, level, and section, a total of nine non-overlapping microphotographs (3 from each area) were taken at 200 × or 400 × magnification.

The length of the GFAP positive cells processes lining the SVZ was measured and averaged using Fiji/ImageJ software in three separate microscopic fields at 40 × in the roof, DL-SVZ, and L-SVZ areas with a fluorescence laser microscope. The software was previously calibrated, and the mean length of the processes was obtained after 6 random measurements (**Supplementary Figure 4**) for each photograph (18). Values are given as μm.

Quantification of Ki67 + and Sox2 + Ki67 + cells was performed in three non-adjacent fields of view at 20 × magnification along the DL-SVZ and L-SVZ edges of the lateral ventricle (18, 19). In each case, the mean of Ki67 + and Sox2 + Ki67 + cells were divided by the area to obtain a measurement of cells per mm^2.

From sections stained with H&E, photomicrographs were obtained, and the area of neuroblast chains in the SVZ [high density of cells that take up hematoxylin that corresponds to DCX, (20)] was traced and measured in square millimeters.

For DCX fluorescent immunohistochemical evaluation, all the immuno-positive areas along the SVZ were digitalized, and whole fluorescence was obtained because of the confluence of the expression (21). Neuroblasts generated from type 2 progenitors express markers of the neuronal lineage like DCX from their first expression of neuronal lineage and during migration, well before they mature as neurons, so DCX thus is a good early marker in human fetal brain and also in animal studies of neural cell lineage in neurepithelium (22).

Statistical Analysis

A two-tailed, unpaired Student's *t*-test was performed for comparisons; data were considered significantly different if $p < 0.05$. Bar graphs appear as mean with 95%CI. Statistical analysis was performed using the Graphpad Prism 8 software package (GraphPad Software, Inc., La Jolla, CA, United States).

RESULTS

Hypoxia-Ischemia Induced a Decrease in Cellularity in the Neonatal Piglet Subventricular Zone, Caudate Nucleus, and Periventricular White Matter

In the sagittal section, the SVZ can be easily identified using conventional histological stains as an aggregation of small darkly stained cells located immediately adjacent to the ventricles and descending along the length of the dorsolateral (DL, close to the periventricular white matter) and lateral (L-SVZ, close to the caudate nucleus) walls of the lateral ventricle (**Figure 1**).

We first evaluated the cellularity of the SVZ, caudate nucleus, and periventricular white matter quantifying the number of morphologically well-preserved (undamaged) cells. After a HI event, the cellularity of the SVZ of the neonatal piglet was reduced. The roof ($p < 0.01$), the L-SVZ ($p < 0.01$), and the DL-SVZ ($p < 0.05$) subareas showed significantly lower counts of morphologically well-preserved cells after neonatal HI (**Figure 2**, upper graph). Quantitative evaluation of the caudate nucleus ($p < 0.05$) and periventricular white matter's cellularity ($p < 0.001$) confirmed the decrease in well-preserved cells in the asphyctic piglet in both SVZ-surrounding regions (**Figure 2**, lower graph).

The Neonatal Piglet Subventricular Zone Is Resistant to Hypoxia-Ischemia-Induced Cell Death

Although the SVZ appeared swollen at 48 h of recovery from HI, H&E-stained samples revealed less death in this area, suggesting

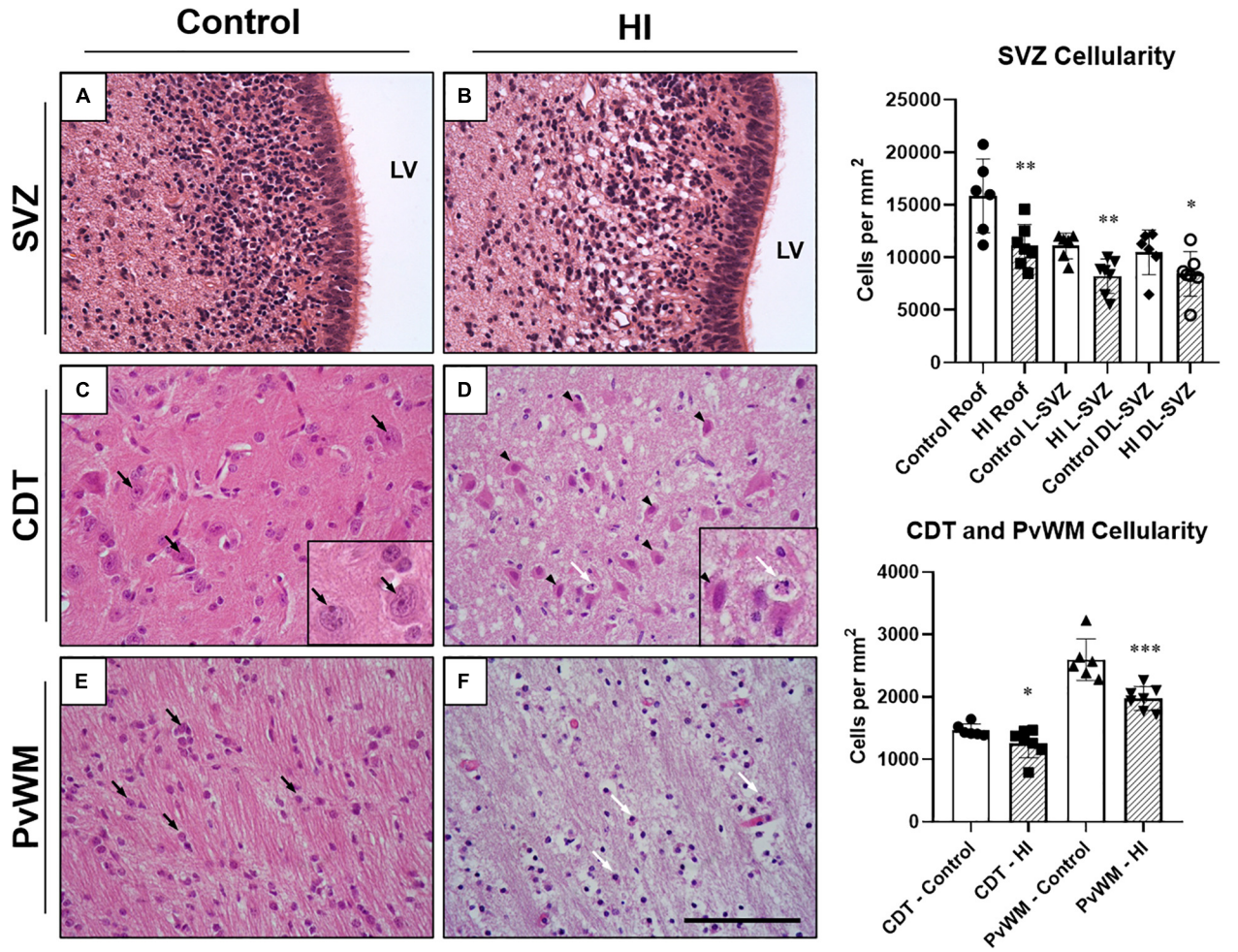

FIGURE 2 | Representative microphotographs of the subventricular zone (SVZ), caudate nucleus (CDT), and periventricular white matter (PvWM) brain regions from control and HI piglets. The piglet SVZ is a highly cellular area with small and closely situated to each other round cells **(A)**. SVZ appeared swollen at 48 h after HI but with very less or absent necrotic or apoptotic features **(B)**. In CDT, well-demarcated cells (black arrows) with well-defined nucleolus (seen in the inset at 630 × magnification), and dense neuropil were observed in control piglets **(C)**. In contrast, in HI animals **(D)** cells with necrotic (black arrowheads) and apoptotic (white arrow) features were present (seen in the inset at 630 × magnification), with diffuse edematous matrix and hypodense neuropil. In PvWM, black arrows identify examples of morphologically undamaged oligodendrocytes **(E)**. **(F)** Shows damaged cells (white arrows) together with diffuse edema and disrupted neuropil from an HI-injured piglet. Graphs: HI reduced the cellularity of the roof (**$p < 0.01$), L-SVZ (**$p < 0.01$), and DL-SVZ (*$p < 0.05$) subareas of the SVZ, an effect also observed in CDT (*$p < 0.05$) and PvWM (***$p < 0.001$) cell counts. LV, lateral ventricle; SVZ, Subventricular zone; CDT, caudate nucleus; PvWM, periventricular white matter. H&E staining. Original magnification 400×. Scale bar: 100 μm.

that these cells are relatively resistant to damage. A quantitative evaluation later revealed that damaged cells (either with necrotic or apoptotic features) were rarely observed in the SVZ of control (**Figure 2A**) or HI group (**Figure 2B**): values were very low for necrotic- (0–0.8 cells per mm^2) or apoptotic-like cells (0.7–1.2 cells per mm^2) for both experimental groups, with no differences between control and HI in the three SVZ subareas evaluated (roof, DL-SVZ, or L-SVZ). The absence of cell death in the SVZ was further confirmed when studying TUNEL immune-stained slices from both control and HI piglets (**Figures 3A,B**).

Later, we focused on the caudate nucleus and periventricular white matter. In H&E-stained samples, we observed extensive cell death in both the caudate nucleus (**Figure 2D**) and periventricular white matter (**Figure 2F**) after HI. Caudate nucleus and periventricular white matter of HI piglets showed increased perivascular and pericellular space suggesting edema. Additional changes in the surrounding neuropil included swelling of endothelial cells. Damaged cells appeared necrotic in appearance (nuclear pyknosis with a swollen, eosinophilic cytoplasm) and also apoptotic (fragmented, rounded, dense chromatin with minimal cytoplasmic change) (**Figures 2D,F**). Quantification of characteristic morphologically altered cell nuclei and cytoplasm revealed notorious necrotic and apoptotic processes in the caudate nucleus and periventricular white matter after HI: caudate nucleus showed high counts of necrotic (Control:2.3 ± 12.6 vs. HI: 99.31 ± 77.4 cells per mm^2; $p < 0.01$) and apoptotic (Control:1.9 ± 11.2 vs. HI: 6.8 ± 11.0 cells per mm^2; $p < 0.002$) cell death, and an increase was observed

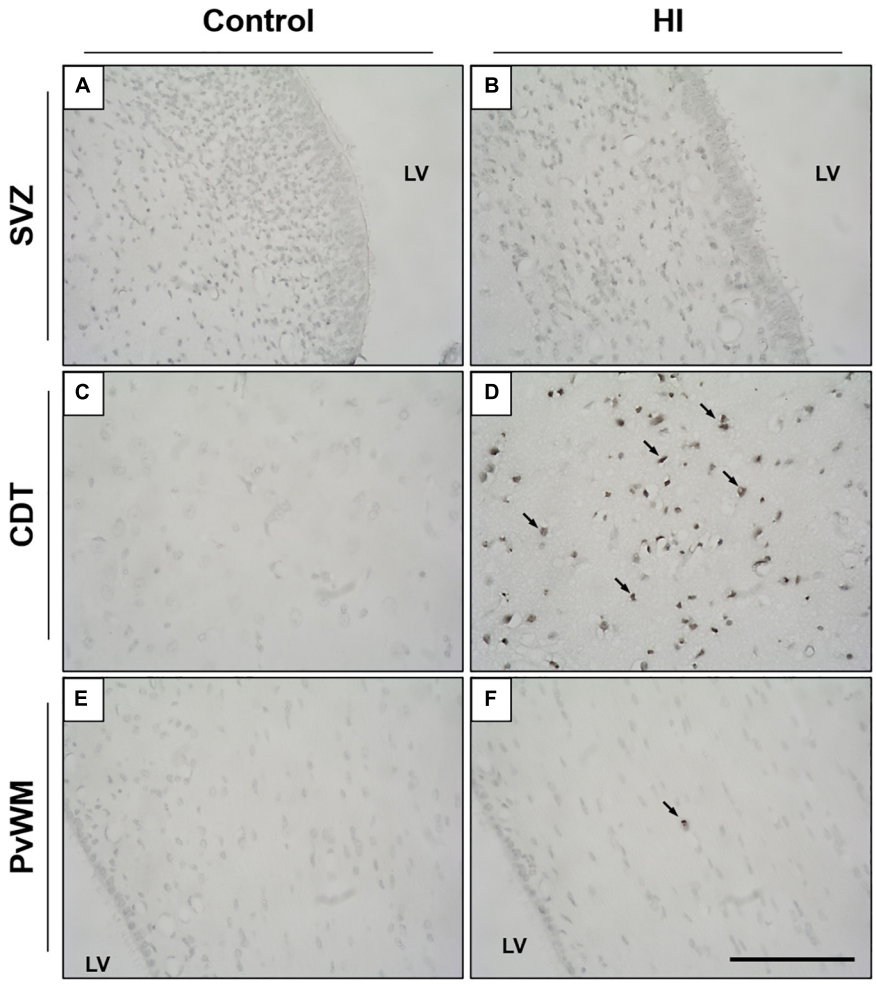

FIGURE 3 | Representative microphotographs of TUNEL immunostaining in the SVZ, caudate nucleus (CDT), and periventricular white matter (PvWM) brain regions from control **(A,C,E)** and HI **(B,D,F)** piglets. SVZ from both experimental groups showed no signs of cell death, as no TUNEL positive nuclei were observed **(A,B)**. In CDT and PvWM, however, immunoreactive cells are observed after HI, especially in the former [black arrows, **(D)**]. LV, lateral ventricle; SVZ, subventricular zone; CDT, caudate nucleus; PvWM, periventricular white matter. Original magnification 400×. Scale bar, 100 μm.

for periventricular white matter for necrosis (2.9 ± 11.4 vs. 99.5 ± 52.2 cells per mm^2; $p < 0.05$) or apoptosis (2.6 ± 10.4 vs. 1.2 ± 3.5 cells per mm^2; $p < 0.05$). The lack of DNA fragmentation described above for the SVZ (**Figures 3C,E**) contrasted with the obvious presence in the caudate nucleus and periventricular white matter after HI (**Figures 3D,F**) using TUNEL immunohistochemistry.

Caspase 3 Expression in the Subventricular Zone Is Maintained After Hypoxia-Ischemia

Immunohistochemical staining showed that caspase-3 was present in the SVZ of both control and HI animals (**Figure 4**). In the ependymal layer, most of the cells appear positively stained. Ependymal cells can be distinguished by their location, larger nuclei, ciliated apical domain, and organization in a simple epithelium. These cells were not included in the counts.

Caspase-3 + cells were also observed in the zone immediately subjacent to the ependymal layer of control and HI piglets (**Figures 4A,B**), but the quantitative analysis did not reveal differences in the counts per mm^2 in the three SVZ subareas (**Figure 4**, graph). Further, caspase-3 + nuclei were from non-pyknotic cells. Caudate nucleus and periventricular white matter from control piglets showed a low presence of caspase-3, contrasting with extensively labeled HI samples.

Hypoxia-Ischemia Reduced the Length of Glial Fibrillary Acidic Protein + Cells Processes

The process length of GFAP + cells (radial-glia like cells or type 1 or neural stem cells) in the SVZ was measured in the three SVZ subareas (i.e., roof, DL-SVZ, and L-SVZ) to assess the neurogenic activity close to the ventricular wall. GFAP + cells showed a large cytoplasm with thin processes that can extend

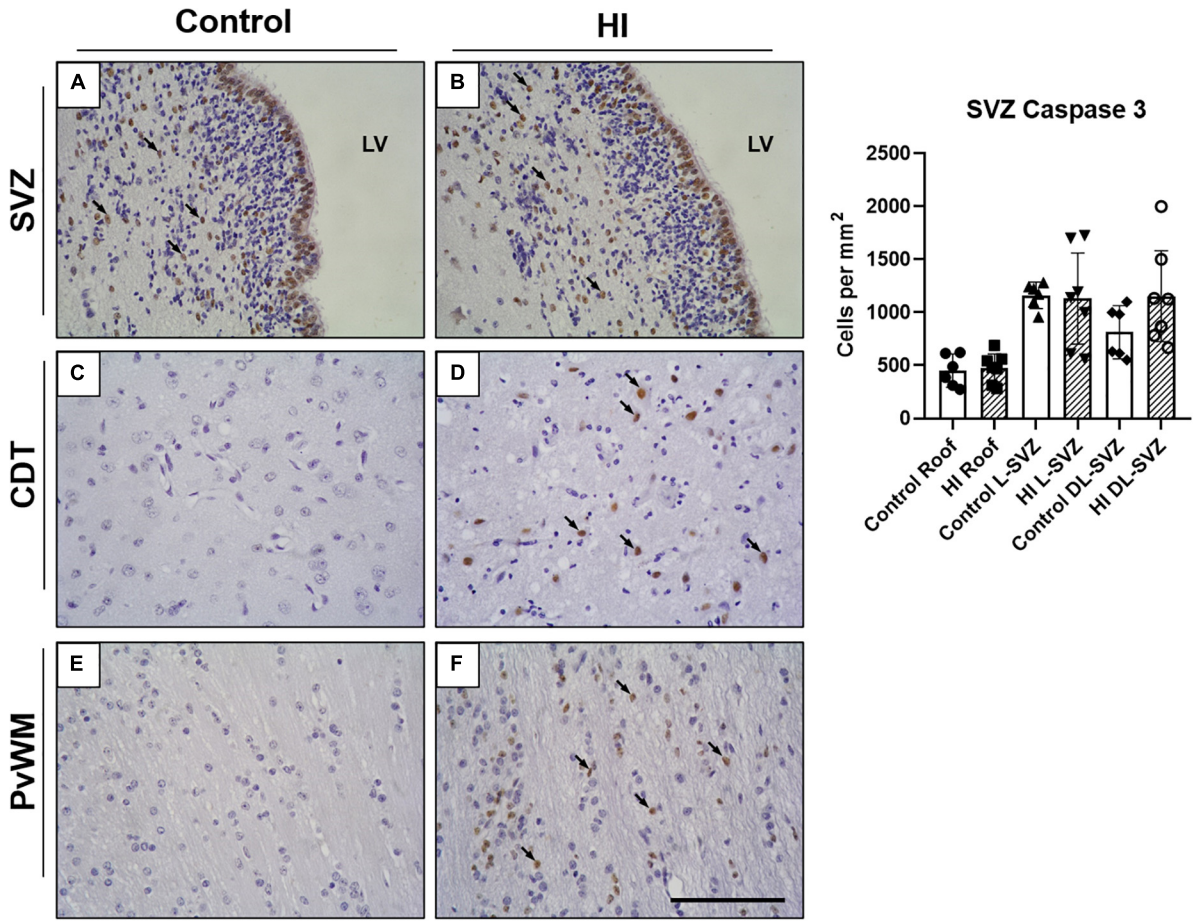

FIGURE 4 | Representative microphotographs of Caspase-3 immunostaining in SVZ, caudate nucleus (CDT), and periventricular white matter (PvWM) brain regions from control **(A,C,E)** and HI **(B,D,F)** piglets. Caspase 3 positive cells can be observed in the SVZ of both experimental groups (black arrows), including the ependymal layer and the underneath SVZ **(A,B)**. Caspase-3 immunoreactivity was also evident in CDT **(D)** and PvWM **(F)** from HI animals. Graph: no differences were observed in caspase-3 positive cell counts in the roof, L-SVZ, or DL-SVZ subareas of the SVZ between control and HI piglets. LV, lateral ventricle; SVZ, subventricular zone; CDT, caudate nucleus; PvWM, periventricular white matter. Original magnification 400×. Scale bar: 100 μm.

several micrometers away from the ependyma lining the lateral ventricle toward the inner brain parenchyma (**Figure 5**). The length of GFAP + processes differed from each SVZ subarea being longer in the roof and decreasing its size when getting away from this area along the DL- and L-SVZs. When comparing control and HI groups, HI significantly ($p < 0.01$ for roof and DL-SVZ; $p < 0.05$ for L-SVZ) reduced the length of GFAP + processes in the three subareas of the SVZ (**Figure 5**, graph).

Hypoxia-Ischemia Diminished Cell Proliferation in the Subventricular Zone

Ki67-positive cells were present as individual or small clusters of cells in the SVZ of both control and HI piglets, extending several cells thick from the ependymal layer along the DL-SVZ and L-SVZ edges of the lateral ventricle (**Figure 6A**). Control animals showed slightly higher values of Ki67 + cells in the L-SVZ (63.89 ± 19.01 cells per mm^2) than in the DL-SVZ (44.13 ± 9.33 cells per mm^2). HI reduced cell proliferation by half in both L-SVZ (31.94 ± 6.98 cells per mm^2; $p < 0.001$ vs. control) and DL-SVZ (19.44 ± 8.65 cells per mm^2; $p < 0.001$ vs. Control) regions (**Figure 6**, upper graph).

Consistent with this finding, we also observed a significant decrease in the number of Sox2 + Ki67 + cells in the same regions after HI. Neural stem/progenitor cells (Sox2 +) appeared in control (**Figure 6C**) and HI (**Figure 6D**) piglets, with more presence in the L-SVZ. Its proliferation, determined by Sox2 and Ki67 double labeling, was also affected after HI, with a significant decrease in the number of Sox2 + Ki67 + cells in both L-SVZ ($p < 0.0001$ vs. control) and DL-SVZ ($p < 0.0001$ vs. control) subareas (**Figure 6**, lower graph).

Neuroblast Chain Area and Doublecortin Staining Are Reduced After Hypoxia-Ischemia

Control animals showed an abundance of neuroblast chains (assessed by H&E staining; **Figures 7A,B**) and DCX + neuroblasts (immunofluorescence; **Figures 7C,D**). Both techniques gave us a

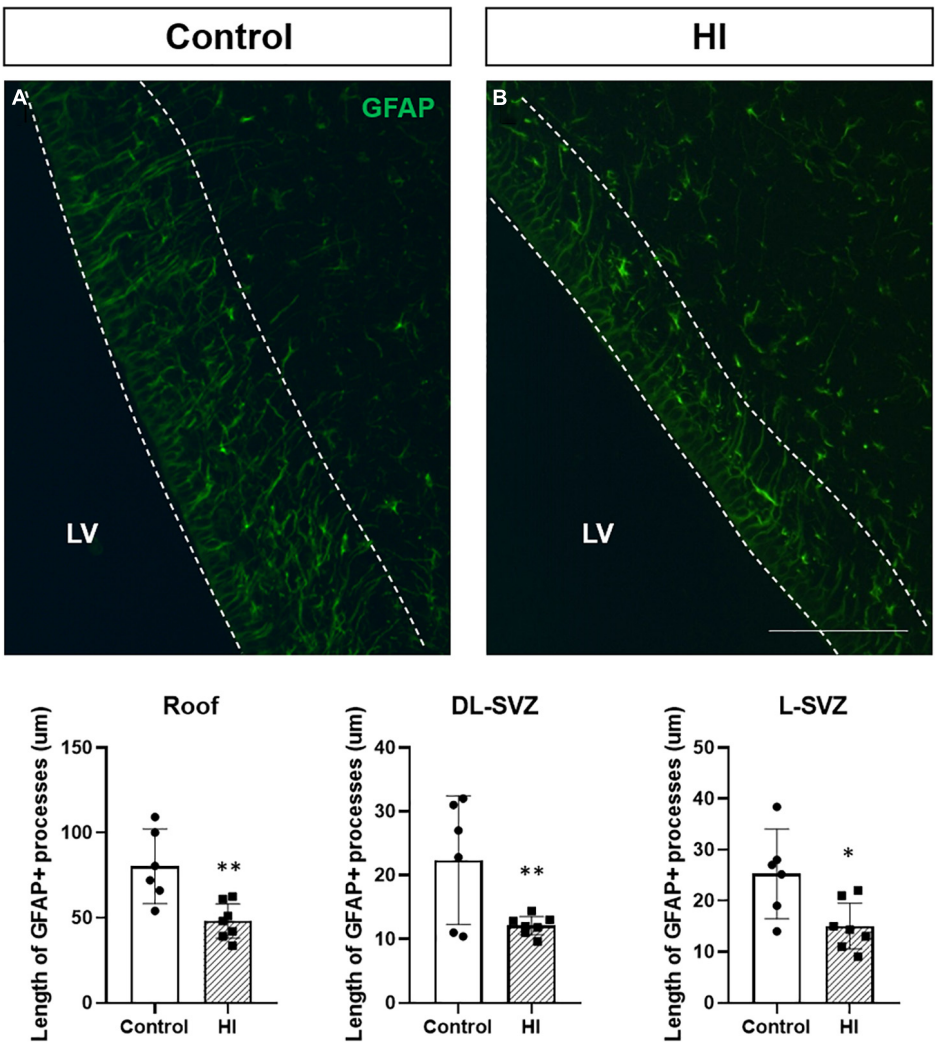

FIGURE 5 | Fluorescent microphotographs of GFAP immune-stained samples from control and HI piglets. GFAP reveals the length of the processes of radial-glia/neural stem cells in the SVZ **(A)**. HI [**(B)** and graph] significantly reduced the length of GFAP + processes in the three subareas of the SVZ: roof (**$p < 0.01$), DL-SVZ (**$p < 0.01$), and L-SVZ (*$p < 0.05$). LV, lateral ventricle; SVZ, subventricular zone; CDT, caudate nucleus; PvWM, periventricular white matter. Original magnification 400×. Scale bar: 100 μm.

strong positive correlation between the area of neuroblast chains and DCX immunofluorescence ($R^2 = 0.6447$, $p < 0.0001$). HI displayed a significant reduction in the area of neuroblast chains (H&E, $p = 0.0003$) and DCX immunofluorescence ($p = 0.0044$) compared with control animals (**Figure 7**, graph).

DISCUSSION

In this study, hypoxic-ischemic piglets showed a decrease in cellularity in the SVZ independent of cell death at 48 h. Furthermore, HI decreased the length of GFAP + processes, the neuroblast chains area, DCX immunoreactivity, and the number of Ki67 + and Ki67 + Sox2 + cells, thus suggesting that, early after the HI event, a reduction in both cell proliferation and neurogenesis occurs.

Cellular and tissue damage triggered after HI can be generalized and affect the neurogenic niches present in the central nervous system. Levison et al. (6) described that moderate-to-severe HI reduced 20% of the total cells from the SVZ in rodents, so we first wanted to explore if HI could reduce the cellularity in the SVZ of the newborn piglet. The porcine SVZ is structurally similar to its human counterpart, made up of a crowd of small cells closely situated to each other, adjacent to the ependyma of the lateral ventricles and extending toward the inner brain parenchyma. In our model, HI reduced the number of cells in the piglet SVZ without increasing cell death, as the quantification of necrotic or apoptotic profiles was minimal or absent, later confirmed by the rare presence of TUNEL-positive cells. In the same manner, Morton et al. (18) found no differences in cell death within the SVZ in hypoxic brains using a porcine model of hypoxia-only injury, thus indicating that cell death is not

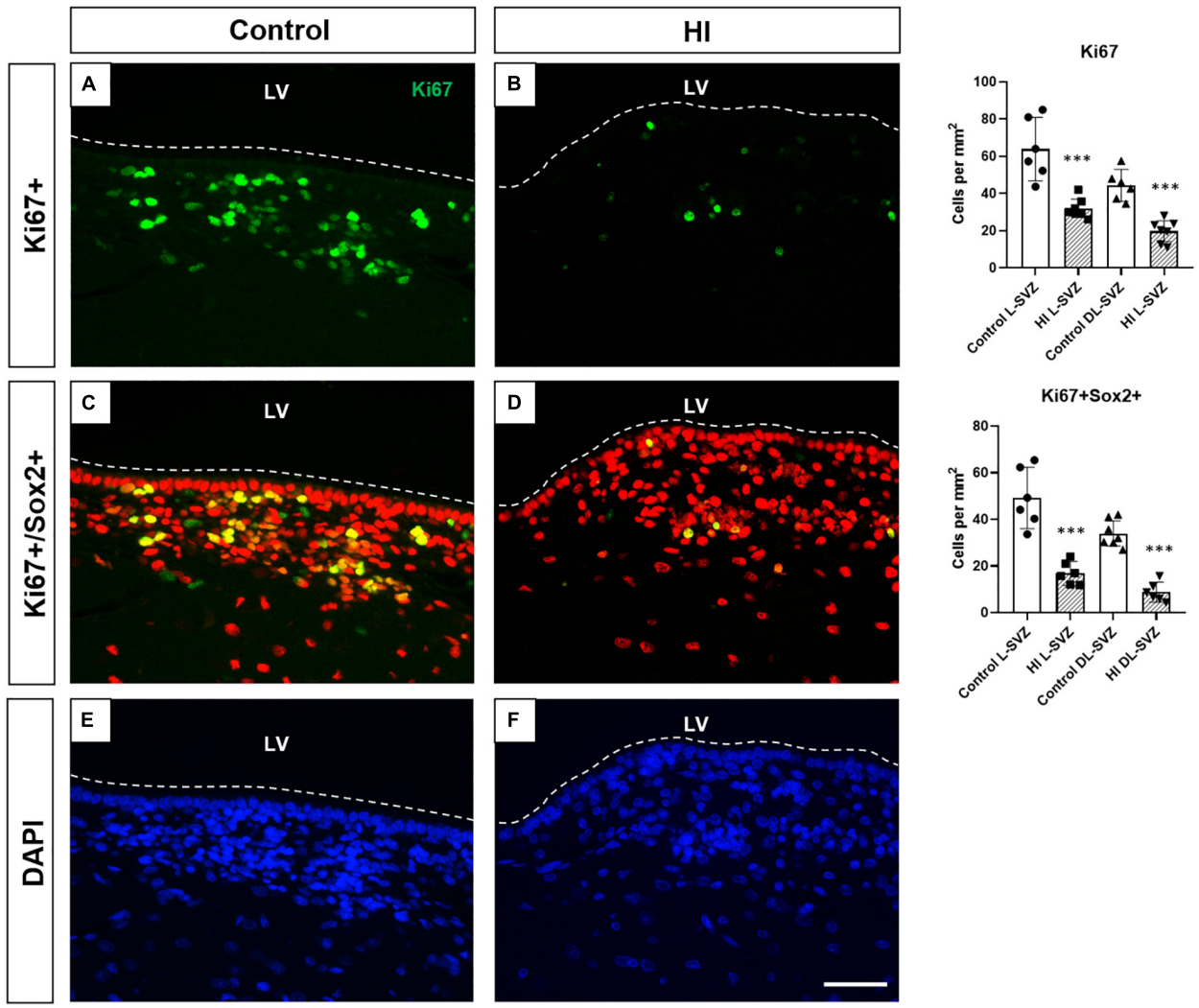

FIGURE 6 | Fluorescent microphotographs of Ki67 [cell proliferation, **(A,B)**], Sox2/Ki67 [neural stem/progenitor cell proliferation, **(C,D)**], and DAPI [nuclei, **(E,F)**] immune-stained samples from control and HI piglets. Ki67 positive cells (green) are abundant in the control piglet **(A)**, whereas HI **(B)** significantly reduced its counts by half in L-SVZ and DL-SVZ (both ***$p < 0.001$). Double Sox2 (red) + /Ki67 (green) + cells are observed in control animals; again, HI reduced neural stem/progenitor cell counts in L-SVZ and DL-SVZ (both ***$p < 0.001$). DAPI immunostaining reveals total nuclei. LV, lateral ventricle; SVZ, subventricular zone; CDT, caudate nucleus; PvWM, periventricular white matter. Original magnification 400×. Scale bar: 100 μm.

a major underlying mechanism in the reduction of cellularity in the piglet SVZ.

Similarly, the rodent SVZ became swollen during recovery from perinatal HI (as seen here), but few of those cells died (7, 23), with cell death values of approximately 0.3% of the total SVZ cells. The same authors also evaluated caspase 3 activation, describing no differences in the percentage of active caspase-3-positive cells in either the ipsilateral or contralateral SVZs after HI in rodents (7, 23). In our work, control animals showed abundant immunoreactivity for caspase-3 in the SVZ neurogenic niche, but HI did not affect the cell counts. Indeed, caspase-3 positive nuclei were observed in non-pyknotic cells, so we cannot rule out a possible non-apoptotic role of this enzyme (24, 25) in the piglet SVZ. Despite the most recognized role of caspase-3, i.e., its capacity of inducing DNA fragmentation, its activation modulates a number of biological processes that do not cause cell death, including dendritic pruning, cell differentiation, and cell proliferation (26, 27).

Whereas the piglet SVZ could be a brain region resilient to HI-induced cell death, SVZ-surrounding regions like the periventricular white matter and caudate nucleus appeared vulnerable to HI. As previously reported by our group in piglets (16) and by other authors in rodents (23), in this study we show cellular degenerative changes in both brain regions at 48 h after HI, with low counts of morphologically well-preserved cells and high values of apoptotic and necrotic profiles, confirmed with immunohistochemical techniques. Unlike "mature tissues" like the caudate nucleus or periventricular white matter, those containing neuronal precursors like the SVZ have their particular architecture, functions, and

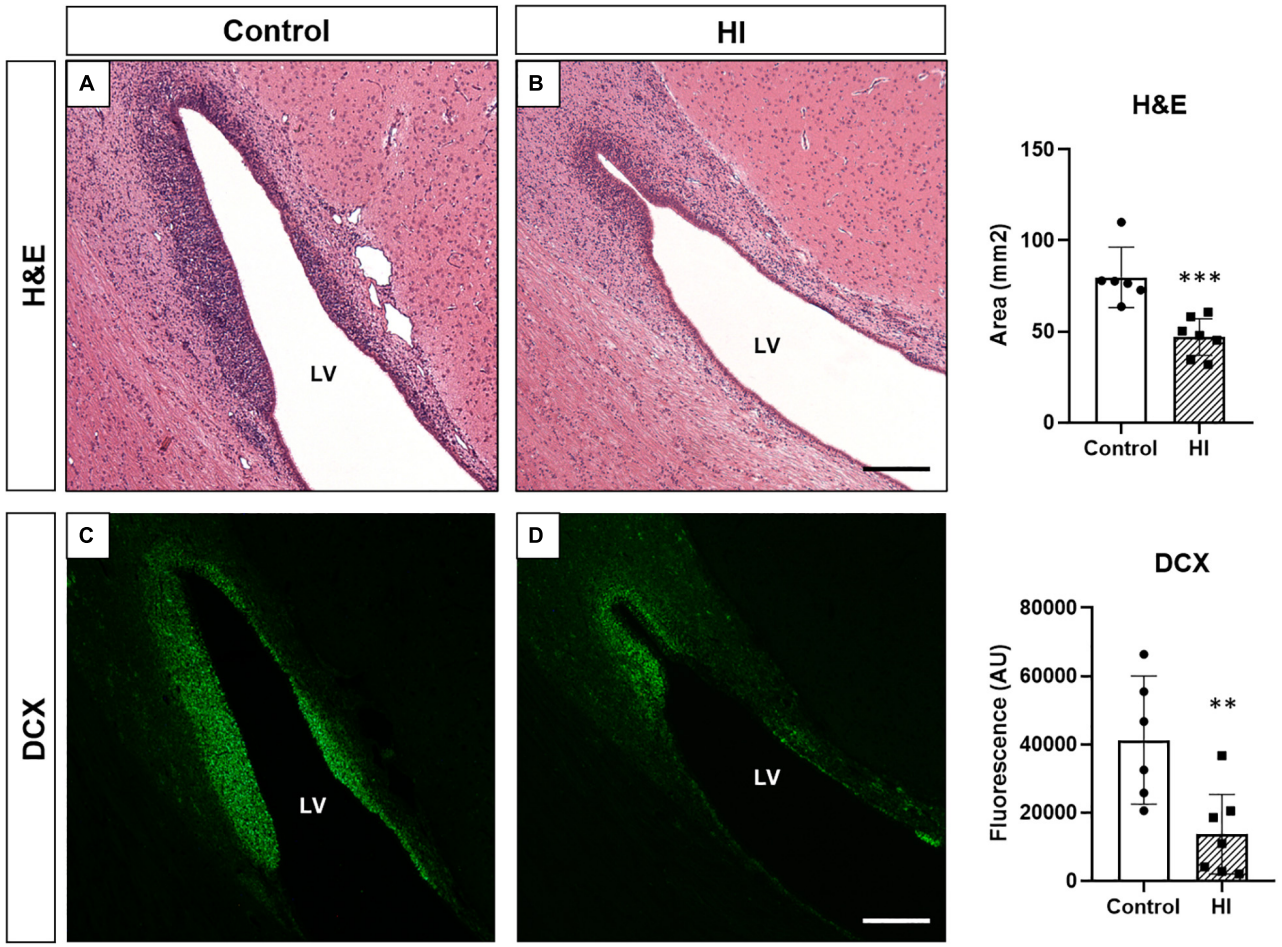

FIGURE 7 | Neuroblast evaluation through hematoxylin and eosin staining [H&E, **(A,B)**] and doublecortin immunohistochemistry [DCX, **(C,D)**] from control and HI piglets. The abundant presence of neuroblasts in control animals **(A,C)** is reduced after HI **(B,D)**. Graphs: the average neuroblast chains area (***$p < 0.001$) and fluorescent intensity of DCX expression (**$p < 0.01$) in the SVZ was significantly reduced after HI. LV, lateral ventricle; H&E, hematoxylin and eosin staining; DCX, doublecortin; AU, arbitrary units Original magnification 100×. Scale bar: 500 μm.

fates (12). Together with the presence of large blood vessels affording rapid reperfusion after HI (28), neurogenic tissues often have lower oxygen levels compared with others, and their cells considerably rely upon anaerobic respiration (29), thus providing resistance to hypoxic phenomena. *In vitro* studies support the evidence for strong homeostatic controls over SVZ cells (30) and their resistance to pro-death stimuli after brain injury (23), especially when compared with the vulnerability of mature cells located in adjacent gray and white matter brain regions. These special features of SVZ cells could be partially attributed to their high levels of cytoplasmic glycogen (31) and antiapoptotic proteins (32), which could act as substrate during HI and ameliorate cell death cascades, respectively.

If cell death was not a prominent mechanism in the piglet SVZ after HI, we wondered if the reduction in SVZ cellularity could be related to a decrease in its neurogenic potential. In the SVZ, neurogenesis originates from a primary progenitor with morphological and functional characteristics of a glial cell, which expresses glial fibrillary acidic protein (GFAP) (33). GFAP was used as a surrogate for radial glia, and these GFAP + cells appeared in control animals showing a triangular shape and exhibiting long and thin processes toward the brain parenchyma. As radial glia can give rise to neural stem cells, among other cell types, we wanted to assess the neurogenic activity close to the ventricular wall, showing that HI significantly reduced the average length of the processes of GFAP + radial-glia like cells when compared with control animals, an observation also described in piglets submitted to hypoxia only (18).

Neural stem cells give rise to type 2 progenitors that undergo rapid proliferation responsible for most of the expansion of the pool of newly generated cells. The piglet SVZ exhibits high postnatal cell proliferation potency even at 6–7 or 32 weeks of age (34). This capacity was also observed in our samples from control animals, showing noticeable Ki67 + cell counts in both L- and DL-SVZ areas. However, HI induced a significant reduction in cell proliferation in the SVZ of animals post-HI, whose

counts diminished by half compared with control. Consistent with this finding, we also found a reduction in the number of Sox2 + Ki67 + cells. As stated in the introduction, previous works in rodents have described that HI can either decrease (6, 7) or increase the regenerative capacity of the SVZ (9, 11). Later works suggested a possible sequential pattern in which asphyxia decreased SVZ cell proliferation at 24 h after HI, followed by an increase in cell division 7 days after the injury in the neonatal rat (35). The other neurogenic niche, the hippocampal subgranular zone, displayed a similar behavior after HI, presenting an initial decrease in cell proliferation continued by a subsequent increase after the injury (36). As a limitation of this work, we assessed only the short-term effects of HI in the neonatal piglet SVZ: the long-term effects are unknown, including a potential increase in cell proliferation or in neurogenesis in the SVZ after the initial decrease observed in this work.

In this study, the relative high abundance of neuroblasts revealed by H&E and DCX immunostaining in the SVZ of control animals was drastically reduced after HI. DCX is considered a marker of neuronal lineage/migrating neuroblasts. Its expression is thought to be specific for newly generated neurons, since nearly all DCX-positive cells express early neuronal antigens but lack antigens specific for glial, undifferentiated, or apoptotic cells (22, 37). The described biphasic pattern has also been described for DCX after traumatic brain injury: normothermic animals showed a reduction in DCX at 72 h after the injury, with subsequent recovery to their basal values at 7 days (38).

Altogether, these results suggest that neurogenesis is reduced early after neonatal HI in the SVZ of the postnatal piglet, when HI-induced cell death is still ongoing in certain regions of the brain, which could compromise the replacement of the lost neurons and the achievement of global repair.

DATA AVAILABILITY STATEMENT

The raw data supporting the conclusions of this article will be made available by the authors, without undue reservation.

ETHICS STATEMENT

The animal study was reviewed and approved by Animal Care and Use Committee of University College London Biological Services and Institute of Neurology.

AUTHOR CONTRIBUTIONS

DA-A, XG, PG, and NR contributed to the acquisition, analysis, and interpretation of data. DA-A contributed to the conception and design, analysis, and interpretation of data. DA-A and NR wrote the article. All authors revised the original manuscript and agreed on its contents.

FUNDING

This work was supported by the United Kingdom Medical Research Council (G0501259), Basque Government Postdoctoral Program (POS_2013_1_191), EITB Maratoia-BIOEF (BIO18/IC/003), and the Spanish Ministry of Science and Innovation (MINECOR20/P66/AEI/10.13039/501100011033). This study was undertaken at University College London Hospitals/University College London, which received a proportion of funding from the UK Department of Health's National Institute for Health Research Biomedical Research Centers funding scheme.

ACKNOWLEDGMENTS

We thank the research team involved in these studies at UCL over the past 20 years.

SUPPLEMENTARY MATERIAL

The Supplementary Material for this article can be found online at: https://www.frontiersin.org/articles/10.3389/fped.2022.793189/full#supplementary-material

REFERENCES

1. Oppenheim RW. Cell death during development of the nervous system. *Annu Rev Neurosci.* (1991) 14:453–501. doi: 10.1146/annurev.ne.14.030191.002321
2. Blaschke AJ, Staley K, Chun J. Widespread programmed cell death in proliferative and postmitotic regions of the fetal cerebral cortex. *Development.* (1996) 122:1165–74. doi: 10.1242/dev.122.4.1165
3. Dobbing J, Sands J. Quantitative growth and development of human brain. *Arch Dis Child Fetal Neonat Ed.* (1973) 48:757. doi: 10.1136/adc.48.10.757
4. Donega V, van Velthoven CT, Nijboer CH, Kavelaars A, Heijnen CJ. The endogenous regenerative capacity of the damaged newborn brain: boosting neurogenesis with mesenchymal stem cell treatment. *J Cereb Blood Flow Metab.* (2013) 33:625–34. doi: 10.1038/jcbfm.2013.3
5. Breunig JJ, Arellano JI, Macklis JD, Rakic P. Everything that glitters isn't gold: a critical review of postnatal neural precursor analyses. *Cell Stem Cell.* (2007) 1:612–27. doi: 10.1016/j.stem.2007.11.008
6. Levison SW, Rothstein RP, Romanko MJ, Snyder MJ, Meyers RL, Vannucci SJ. Hypoxia/ischemia depletes the rat perinatal subventricular zone of oligodendrocyte progenitors and neural stem cells. *Dev Neurosci.* (2001) 23:234–47. doi: 10.1159/000046149
7. Romanko MJ, Rothstein RP, Levison SW. Neural stem cells in the subventricular zone are resilient to hypoxia/ischemia whereas progenitors are vulnerable. *J Cereb Blood Flow Metab.* (2004) 24:814–25. doi: 10.1097/01.WCB.0000123906.17746.00
8. Plane JM, Liu R, Wang TW, Silverstein FS, Parent JM. Neonatal hypoxic-ischemic injury increases forebrain subventricular zone neurogenesis in the mouse. *Neurobiol Dis.* (2004) 16:585–95. doi: 10.1016/j.nbd.2004.04.003
9. Yang Z, Levison SW. Hypoxia/ischemia expands the regenerative capacity of progenitors in the perinatal subventricular zone. *Neuroscience.* (2006) 139:555–64. doi: 10.1016/j.neuroscience.2005.12.059
10. Yu TS, Washington PM, Kernie SG. Injury-induced neurogenesis: mechanisms and relevance. *Neuroscientist.* (2016) 22:61–71. doi: 10.1177/1073858414563616

11. Ong J, Plane JM, Parent JM, Silverstein FS. Hypoxic-ischemic injury stimulates subventricular zone proliferation and neurogenesis in the neonatal rat. *Pediatr Res.* (2005) 58:600–6. doi: 10.1203/01.PDR.0000179381.86809.02
12. Brazel CY, Rosti RT III, Boyce S, Rothstein RP, Levison SW. Perinatal hypoxia/ischemia damages and depletes progenitors from the mouse subventricular zone. *Dev Neurosci.* (2004) 26:266–74. doi: 10.1159/000082143
13. Costine BA, Missios S, Taylor SR, McGuone D, Smith CM, Dodge CP, et al. The subventricular zone in the immature piglet brain: anatomy and exodus of neuroblasts into white matter after traumatic brain injury. *Dev Neurosci.* (2015) 37:115–30. doi: 10.1159/000369091
14. Lorek A, Takei Y, Cady EB, Wyatt JS, Penrice J, Edwards AD, et al. Delayed ("secondary") cerebral energy failure after acute hypoxia-ischemia in the newborn piglet: continuous 48-hour studies by phosphorus magnetic resonance spectroscopy. *Pediatr Res.* (1994) 36:699–706. doi: 10.1203/00006450-199412000-00003
15. Robertson NJ, Faulkner S, Fleiss B, Bainbridge A, Andorka C, Price D, et al. Melatonin augments hypothermic neuroprotection in a perinatal asphyxia model. *Brain.* (2013) 136(Pt 1):90–105. doi: 10.1093/brain/aws285
16. Alonso-Alconada D, Broad KD, Bainbridge A, Chandrasekaran M, Faulkner SD, Kerenyi A, et al. Brain cell death is reduced with cooling by 3.5 degrees C to 5 degrees C but increased with cooling by 8.5 degrees C in a piglet asphyxia model. *Stroke.* (2015) 46:275–8. doi: 10.1161/STROKEAHA.114.007330
17. Ditsworth D, Priestley MA, Loepke AW, Ramamoorthy C, McCann J, Staple L, et al. Apoptotic neuronal death following deep hypothermic circulatory arrest in piglets. *Anesthesiology.* (2003) 98:1119–27. doi: 10.1097/00000542-200305000-00014
18. Morton PD, Korotcova L, Lewis BK, Bhuvanendran S, Ramachandra SD, Zurakowski D, et al. Abnormal neurogenesis and cortical growth in congenital heart disease. *Sci Transl Med.* (2017) 9:eaah7029. doi: 10.1126/scitranslmed.aah7029
19. Tolcos M, Markwick R, O'Dowd R, Martin V, Turnley A, Rees S. Intrauterine growth restriction: effects on neural precursor cell proliferation and angiogenesis in the foetal subventricular zone. *Dev Neurosci.* (2015) 37:453–63. doi: 10.1159/000371344
20. Doetsch F, García-Verdugo JM, Alvarez-Buylla A. Cellular composition and three-dimensional organization of the subventricular germinal zone in the adult mammalian brain. *J Neurosci.* (1997) 17:5046–61. doi: 10.1523/JNEUROSCI.17-13-05046.1997
21. Koob AO, Harris BT, Duhaime AC. Cellular genesis in the postnatal piglet. *Int J Dev Neurosci.* (2008) 26:641–6. doi: 10.1016/j.ijdevneu.2008.04.001
22. Sarnat HB. Clinical neuropathology practice guide 5-2013: markers of neuronal maturation. *Clin Neuropathol.* (2013) 32:340–69. doi: 10.5414/NP300638
23. Rothstein RP, Levison SW. Damage to the choroid plexus, ependyma and subependyma as a consequence of perinatal hypoxia/ischemia. *Dev Neurosci.* (2002) 24:426–36. doi: 10.1159/000069052
24. Kennedy NJ, Kataoka T, Tschopp J, Budda RC. Caspase activation is required for T cell proliferation. *J. Exp Med.* (1999) 190:1891–6. doi: 10.1084/jem.190.12.1891
25. Zermati Y, Garrido C, Amsellem S, Fishelson S, Bouscary D, Valensi F, et al. Caspase activation is required for terminal erythroid differentiation. *J Exp Med.* (2001) 193:247–54. doi: 10.1084/jem.193.2.247
26. D'Amelio M, Cavallucci V, Cecconi F. Neuronal caspase-3 signaling: not only cell death. *Cell Death Differ.* (2010) 17:1104–14. doi: 10.1038/cdd.2009.180
27. Fan W, Dai Y, Xu H, Zhu X, Cai P, Wang L, et al. Caspase-3 modulates regenerative response after stroke. *Stem Cells.* (2014) 32:473–86. doi: 10.1002/stem.1503
28. Towbin A. *Brain Damage in the Newborn and its Neurologic Sequels: Pathological and Clinical Correlation*. Danvers, MA: PRM Publishing Company (1998).
29. Chatzi C, Schnell E, Westbrook GL. Localized hypoxia within the subgranular zone determines the early survival of newborn hippocampal granule cells. *Elife.* (2015) 4:e08722. doi: 10.7554/eLife.08722
30. Dizon ML, Shin L, Sundholm-Peters NL, Kang E, Szele FG. Subventricular zone cells remain stable in vitro after brain injury. *Neuroscience.* (2006) 142:717–25. doi: 10.1016/j.neuroscience.2006.06.050
31. Blakemore WF. The ultrastructure of the subependymal plate in the rat. *J Anat.* (1969) 104:423–33.
32. Brazel CY, Romanko MJ, Rothstein RP, Levison SW. Roles of the mammalian subventricular zone in brain development. *Prog Neurobiol.* (2003) 603:1–21. doi: 10.1016/s0301-0082(03)00002-9
33. von Bohlen und Halbach O. Immunohistological markers for proliferative events, gliogenesis, and neurogenesis within the adult hippocampus. *Cell Tissue Res.* (2011) 345:1–19. doi: 10.1007/s00441-011-1196-4
34. Guidi S, Bianchi P, Alstrup AK, Henningsen K, Smith DF, Bartesaghi R. Brain Postnatal neurogenesis in the hippocampal dentate gyrus and subventricular zone of the Göttingen minipig. *Brain Res Bull.* (2011) 85:169–79. doi: 10.1016/j.brainresbull.2011.03.028
35. Iwai M, Ikeda T, Hayashi T, Sato K, Nagata T, Nagano I, et al. Temporal profile of neural stem cell proliferation in the subventricular zone after ischemia/hypoxia in the neonatal rat brain. *Neurol Res.* (2006) 28:461–8. doi: 10.1179/016164105X49283
36. van Velthoven CT, Kavelaars A, van Bel F, Heijnen CJ. Mesenchymal stem cell treatment after neonatal hypoxic-ischemic brain injury improves behavioral outcome and induces neuronal and oligodendrocyte regeneration. *Brain Behav Immun.* (2010) 24:387–93. doi: 10.1016/j.bbi.2009.10.017
37. Rao MS, Shetty AK. Efficacy of doublecortin as a marker to analyse the absolute number and dendritic growth of newly generated neurons in the adult dentate gyrus. *Eur J Neurosci.* (2004) 19:234–46. doi: 10.1111/j.0953-816x.2003.03123.x
38. Bregy A, Nixon R, Lotocki G, Alonso OF, Atkins CM, Tsoulfas P, et al. Posttraumatic hypothermia increases doublecortin expressing neurons in the dentate gyrus after traumatic brain injury in the rat. *Exp Neurol.* (2012) 233:821–8. doi: 10.1016/j.expneurol.2011.12.008

Conflict of Interest: The authors declare that the research was conducted in the absence of any commercial or financial relationships that could be construed as a potential conflict of interest.

Advantages of publishing in Frontiers

OPEN ACCESS
Articles are free to read for greatest visibility and readership

FAST PUBLICATION
Around 90 days from submission to decision

HIGH QUALITY PEER-REVIEW
Rigorous, collaborative, and constructive peer-review

TRANSPARENT PEER-REVIEW
Editors and reviewers acknowledged by name on published articles

Frontiers
Avenue du Tribunal-Fédéral 34
1005 Lausanne | Switzerland

Visit us: www.frontiersin.org
Contact us: frontiersin.org/about/contact

REPRODUCIBILITY OF RESEARCH
Support open data and methods to enhance research reproducibility

DIGITAL PUBLISHING
Articles designed for optimal readership across devices

FOLLOW US
@frontiersin

IMPACT METRICS
Advanced article metrics track visibility across digital media

EXTENSIVE PROMOTION
Marketing and promotion of impactful research

LOOP RESEARCH NETWORK
Our network increases your article's readership